Electrostatically Enhanced Phosphoric Acids and Their Applications in Brønsted Acid Catalysis

A DISSERTATION

SUBMITTED TO THE FACULTY OF THE

UNIVERSITY OF MINNESOTA

BY

Jie Ma

IN PARTIAL FULFILLMENT OF THE REQUIREMENTS

FOR THE DEGREE OF

DOCTOR OF PHILOSOPHY

Steven R. Kass, Adviser

June 2018

Acknowledgement

I would like to first express my sincere gratitude to my adviser, Prof. Steven Kass, for providing me the precious opportunity to conduct my PhD research under his instruction. His guidance, support and encouragement are valuable treasures for me to grow up as a scientist and build up confidence in my career.

I would also like to thank all the members in the Department of Chemistry for creating the excellent academic environment. The support and assistance I received from faculty members, facility staffs and other students are priceless experiences in my research career.

Thanks to Prof. Thomas Hoye, Prof. Marc Hillmyer and Prof. Gunda Georg for being willing to serve on my committee.

Last but not least, I would like to express my special appreciation to my family and my girlfriend, Hui Tian, for their selfless love, support and patience, which make the long way of career, as well as of life, not lonely for me.

Abstract

Different types of Brønsted acid catalysts are commonly used in a wide variety of organic transformations and are of continuing interest because there is a general need to carry out reactions in a faster and higher yielding manner with greater selectivities. Phosphoric acid derivatives, with their fairly strong acidity and structural flexibility that enables them to be incorporated into rigid organic frameworks, are one of the most efficient and versatile classes of Brønsted acids. Herein, a novel type of electrostatically enhanced phosphoric acids that contain positively charged ion centers are synthesized and studied. The activities of achiral phosphoric acids with alkylated pyridinium ion moieties were examined in a variety of organic transformations. In addition, the activities and enantioselectivities of a series of chiral phosphonium ion tagged phosphoric acids were also evaluated in several different organic reactions. The study of electrostatically enhanced phosphoric acids was found to provide promising avenues for developing novel Brønsted acid catalysts.

Table of Contents

List of Tables vi

List of Figures viii

List of Schemes xv

List of Abbreviations xvii

Chapter 1: Background and Introduction 1

1.1. Organocatalysts 1

1.2. Asymmetric Catalysis 4

1.3. Brønsted Acid Catalysts 7

1.4. Catalytic Functionalities 9

1.5. Phosphoric Acid Catalysts 11

1.5.1. Background 11

1.5.2. Activation Modes of Phosphoric Acids in Catalysis 20

1.5.3. Reactivity of Phosphoric Acid Catalysts 21

1.5.3.1. Early Strategies of Reactivity Enhancement for Phosphoric Acid Catalysts 21

1.5.3.2. Electrostatically Enhanced Acid Catalysts 26

1.5.4. Enantioselectivity with Phosphoric Acid 31

1.6. Focus of This Work 34

Chapter 2: Electrostatically Enhanced Phosphoric Acids: A Tool in Brønsted Acid Catalysis 36

2.1. Background 36

2.2. Results and Discussion 37

2.3. Conclusion 43

2.4. Experimental Section 44

2.4.1. General Information 44

2.4.2. Synthesis Procedures 45

2.4.3. Kinetic Studies 48

2.4.4. Catalyst Titration 50

Chapter 3: Asymmetric Arylation of 2,2,2-Trifluoroacetophenones Catalyzed by Chiral Electrostatically-Enhanced Phosphoric Acids 51

3.1. Background 51

3.2. Results and Discussion 52

3.3. Conclusion 59

3.4. Experimental Section 59

3.4.1. General Information 59

3.4.2. General Procedure for the Friedel-Crafts Reaction 60

3.4.3. Synthesis Procedures 61

3.4.4. Characterizations of Friedel-Crafts Adducts from Reactions Run at 0 ˚C 68

Chapter 4: Electrostatically Enhanced Phosphoric Acids and Their Applications in Asymmetric Friedel-Crafts Alkylations 78

4.1. Introduction 78

4.2. Results and Discussion 79

4.3. Conclusion 88

4.4. Experimental 88

4.4.1. Materials and General Methods 88

4.4.2. Synthesis Procedures. 89

4.4.3. General Procedure for the Friedel-Crafts Alkylations 96

4.4.4. Analytical Data for the Friedel-Crafts Products 96

Bibliography 100

References for Chapter 1 100

References for Chapter 2 105

References for Chapter 3 106

References for Chapter 4 109

Appendices 112

Appendix for Chapter 2 112

Appendix for Chapter 3 132

Appendix for Chapter 4 217

List of Tables

Chapter 1

Table 1. Influence of 3,3’-substituents on reaction rates. 23

Table 2. Rate acceleration by electron-withdrawing groups. 24

Table 3. Reaction yields of a phosphoric acid and *N*-phosphoramide catalyzed radical addition. 24

Table 4. Rate enhancement of 5,5’-bitetralone-based chiral phosphoric acid. 25

Table 5. Reactivity enhancement by a strong Lewis acid additive. 26

Table 6. Kinetic study of a Friedel-Crafts alkylation catalyzed by phenol derivatives. 28

Table 7. Kinetic study of a Friedel-Crafts alkylation catalyzed by thioureas. 29

Table 8. Kinetic study of a Friedel-Crafts alkylation catalyzed by chiral thioureas. 30

Chapter 2

Table 1. Kinetic data of Friedel-Crafts reactions. 39

Table 2. Kinetic data of Diels-Alder reactions. 42

Table 3. Kinetic data of polymerizations. 43

Chapter 3

Table 1. Optimization of reaction conditions. 54

Table 2. Screening of reaction solvents. 55

Table 3. Reaction scope. 57

Table 4. Catalyst comparisons. 58

Chapter 4

Table 1. Optimizations of catalysts and reaction conditions. 80

Table 2. Counteranion screening results. 82

Table 3. Reaction medium screening. 83

Table 4. Comparison of charged and noncharged catalysts. 84

Table 5. Substrate scope. 86

Appendix for Chapter 2

Table S1. Kinetic data of Friedel-Crafts reactions of indole and *β*-nitrostyrene. 112

Table S2. Kinetic data of Friedel-Crafts reactions of *N*-methylindole and *β*-nitrostyrene. 114

Table S3. Kinetic data of Diels-Alder reactions. 115

Table S4. Kinetic data of polymerizations. 117

Appendix for Chapter 4

Table S1. Kinetic data for the Friedel-Crafts alkylation of indole with *trans*-*β*-nitrostyrene. 218

List of Figures

Chapter 1

Figure 1. Covalent and non-covalent organocatalysis. 2

Figure 2. Catalytic cycles of organocatalysts. 3

Figure 3. Common base and acid organocatalysts. 3

Figure 4. Different types of molecular chirality. 4

Figure 5. Strategies of asymmetry induction. 6

Figure 6. Lewis acid catalysis and Brønsted acid catalysis. 7

Figure 7. Common hydrogen bond and Brønsted acid catalysts. 8

Figure 8. General and specific Brønsted acid catalysis. 8

Figure 9. Common activation modes for hydrogen bond and strong acid catalysts. 9

Figure 10. Representative catalytic functionalities and their roles in mechanisms. 10

Figure 11. Examples of bifunctional chemical motifs. 10

Figure 12. Bifunctional thioureas. 10

Figure 13. General features of 3,3'-BINOL-derived phosphoric acid catalysts. 11

Figure 14. Mono activation by a phosphoric acid. 20

Figure 15. Dual activation modes of a phosphoric acid. 21

Figure 16. Bifunctional activation brought about by a phosphoric acid. 21

Figure 17. Plot of reaction rates for a Nazarov cyclization versus catalyst acidities. 22

Figure 18. IR study of a series of phenol derivatives with known gas-phase acidities. 27

Figure 19. Relationship between catalyst bulkiness and reaction selectivity. 31

Figure 20. Relationship between AREA(θ) and bulkiness of 3,3'-substituents. 32

Figure 21. Relationship between AREA(θ) and enantiomeric excess for a Mannich reaction. 32

Chapter 2

Figure 1. Charged phosphoric acids reported in this study. 37

Chapter 3

Figure 1. Catalysts involved in this work. 52

Chapter 4

Figure 1. Catalysts used in this work; different counteranions for **2a** were also studied. 79

Figure 2. Linear least squares fit of second-order rate constants vs the catalyst (**2b**) mol %; 87
k (M^{-1} h^{-1}) = 0.016 x **2b** mol % – 0.0040, r^2 = 1.00. Inset is for the normalized time scale analysis.

Figure 3. Proposed Friedel-Crafts alkylation transition state. 88

Appendix for Chapter 2

Figure S1. Observed rate constants versus catalyst mol % loadings for the Friedel-Crafts 120
reactions of β-nitrostyrene with indole (top) and *N*-methylindole (bottom).

Figure S2. Number-average molecular weight ($M_{n,NMR}$) versus conversion plots in 121
toluene-d_8 (a), benzene-d_6 (b), CD_2Cl_2 (c) and $CDCl_3$ (d).

Figure S3. ^{1}H and ^{13}C NMR spectra of **3**. 122

Figure S4. ^{1}H, ^{13}C and ^{31}P NMR spectra of **4**. 123

Figure S5. ^{1}H, ^{13}C, ^{19}F and ^{31}P NMR spectra of **1**. 124

Figure S6. ^{1}H, ^{13}C and ^{31}P NMR spectra of **5**. 126

Figure S7. ^{1}H, ^{13}C, ^{19}F and ^{31}P NMR spectra of **2**. 128

Figure S8. ^{1}H, ^{13}C and ^{31}P NMR spectra of di(3-nitrophenyl)phosphate (DPP*). 130

Appendix for Chapter 3

Figure S1. ^{1}H, ^{13}C and ^{31}P NMR of tris(*p*-ethylphenyl)phosphine (**7c**). 133

Figure S2. ^{1}H, ^{13}C and ^{31}P NMR of tris(*p*-n-propylphenyl)phosphine (**7d**). 134

Figure S3. ^{1}H, ^{13}C and ^{31}P NMR of (*R*)-(2,2'-dihydroxy-[1,1'-binaphthalene]-3,3'-diyl)bis(triphenylphosphonium) iodide (**9a**). 136

Figure S4. ^{1}H, ^{13}C and ^{31}P NMR of (*R*)-(2,2'-dihydroxy-[1,1'-binaphthalene]-3,3'-diyl)bis(tri-*p*-tolylphosphonium) iodide (**9b**). 137

Figure S5. ^{1}H, ^{13}C and ^{31}P NMR of (*R*)-(2,2'-dihydroxy-[1,1'-binaphthalene]-3,3'-diyl)bis(tris(4-ethylphenyl)phosphonium) iodide (**9c**). 139

Figure S6. ^{1}H, ^{13}C and ^{31}P NMR of (*R*)-(2,2'-dihydroxy-[1,1'-binaphthalene]-3,3'-diyl)bis(tris(4-propylphenyl)phosphonium) iodide (**9d**). 140

Figure S7. ^{1}H, ^{13}C and ^{31}P NMR of (*R*)-(2,2'-dihydroxy-[1,1'-binaphthalene]-3,3'-diyl)bis(diphenyl-(*p*-tolyl)phosphonium) iodide (**9e**). 142

Figure S8. ^{1}H, ^{13}C and ^{31}P NMR of (*R*)-(4-hydroxy-4-oxidodinaphtho[2,1-*d*:1',2'-*f*][1,3,2]dioxaphosphepine-2,6-diyl)bis(triphenylphosphonium) chloride (**10a**). 143

Figure S9. ^{1}H, ^{13}C and ^{31}P NMR of (*R*)-(4-hydroxy-4-oxidodinaphtho[2,1-*d*:1',2'-*f*][1,3,2]dioxaphosphepine-2,6-diyl)bis(tri-*p*-tolylphosphonium) chloride (**10b**). 145

Figure S10. ^{1}H, ^{13}C and ^{31}P NMR of (*R*)-(4-hydroxy-4-oxidodinaphtho[2,1-*d*:1',2'-*f*][1,3,2]dioxaphosphepine-2,6-diyl)bis(tris(4-ethylphenyl)phosphonium) chloride (**10c**). 146

Figure S11. ^{1}H, ^{13}C and ^{31}P NMR of (*R*)-(4-hydroxy-4-oxidodinaphtho[2,1-*d*:1',2'-*f*][1,3,2]dioxaphosphepine-2,6-diyl)bis(tris(4-propylphenyl)phosphonium) chloride (**10d**). 148

Figure S12. ^{1}H, ^{13}C and ^{31}P NMR of (*R*)-(4-hydroxy-4-oxidodinaphtho[2,1-*d*:1',2'-*f*][1,3,2]dioxaphosphepine-2,6-diyl)bis-(diphenyl(*p*-tolyl)phosphonium) chloride (**10e**). 149

Figure S13. ^{1}H, ^{13}C, ^{19}F and ^{31}P NMR of (*R*)-(4-hydroxy-4-oxidodinaphtho[2,1-*d*:1',2'-*f*][1,3,2]dioxaphosphepine-2,6-diyl)bis(triphenylphosphonium) tetrakis[3,5-bis(trifluoromethyl)phenyl]borate (**2a**). 151

Figure S14. ^{1}H, ^{13}C, ^{19}F and ^{31}P NMR of (*R*)-(4-hydroxy-4-oxidodinaphtho[2,1-*d*:1',2'-*f*][1,3,2]di-oxaphosphepine-2,6-diyl)bis(tri-*p*-tolylphosphonium) tetrakis[3,5-bis(trifluoromethyl)phenyl]borate (**2b**). 153

Figure S15. ^{1}H, ^{13}C, ^{19}F and ^{31}P NMR of (*R*)-(4-hydroxy-4-oxidodinaphtho[2,1-*d*:1',2'-*f*][1,3,2]dioxaphosphepine-2,6-diyl)bis(tris(4-ethylphenyl)phosphonium) tetrakis[3,5-bis(trifluoromethyl)phenyl]borate (**2c**). 155

Figure S16. ^{1}H, ^{13}C, ^{19}F and ^{31}P NMR of (*R*)-(4-hydroxy-4-oxidodinaphtho[2,1-*d*:1',2'-*f*][1,3,2]dioxaphosphepine-2,6-diyl)bis(tris(4-propylphenyl)phosphonium) tetrakis[3,5-bis(trifluoromethyl)phenyl]borate (**2d**). 157

Figure S17. ^{1}H, ^{13}C, ^{19}F and ^{31}P NMR of (*R*)-(4-hydroxy-4-oxidodinaphtho[2,1-*d*:1',2'-*f*][1,3,2]dioxaphosphepine-2,6-diyl)bis(diphenyl(*p*-tolyl)phosphonium) tetrakis[3,5-bis(trifluoromethyl)phenyl]borate (**2e**). 159

Figure S18. ^{1}H, ^{13}C and ^{19}F NMR of 2,2,2-trifluoro-1-(1H-indole-3-yl)-1-phenylethanol (**5a**). 161

Figure S19. ^{1}H, ^{13}C and ^{19}F NMR of 3-(2,2,2-trifluoro-1-(1H-indole-3-yl)-1-phenylyl)-1H-indole (**6**). 162

Figure S20. ^{1}H, ^{13}C and ^{19}F NMR of 2,2,2-trifluoro-1-(5-fluoro-1H-indole-3-yl)-1-phenylethanol (**5b**). 164

Figure S21. ^{1}H, ^{13}C and ^{19}F NMR of 2,2,2-trifluoro-1-(5-bromo-1H-indole-3-yl)-1-phenylethanol (**5c**). 165

Figure S22. ^{1}H, ^{13}C and ^{19}F NMR of 2,2,2-trifluoro-1-(5-methoxyl-1H-indole-3-yl)-1-phenylethanol (**5d**). 167

Figure S23. ^{1}H, ^{13}C and ^{19}F NMR of 2,2,2-trifluoro-1-(6-methyl-1H-indole-3-yl)-1-phenylethanol (**5e**). 168

Figure S24. ^{1}H, ^{13}C and ^{19}F NMR of 2,2,2-trifluoro-1-(7-chloro-1H-indole-3-yl)-1-phenylethanol (**5f**). 170

Figure S25. ^{1}H, ^{13}C and ^{19}F NMR of 2,2,2-trifluoro-1-(7-bromo-1H-indole-3-yl)-1-phenylethanol (**5g**). 171

Figure S26. ^{1}H, ^{13}C and ^{19}F NMR of 2,2,2-trifluoro-1-(7-methyl-1H-indole-3-yl)-1-phenylethanol (**5h**). 173

Figure S27. ^{1}H, ^{13}C and ^{19}F NMR of 2,2,2-trifluoro-1-(7-ethyl-1H-indole-3-yl)-1-phenylethanol (**5i**). 174

Figure S28. ^{1}H, ^{13}C and ^{19}F NMR of 2,2,2-trifluoro-1-(4-fluorophenyl)-1-(1H-indole-3-yl)ethanol (**5j**). 176

Figure S29. ^{1}H, ^{13}C and ^{19}F NMR of 1-(4-chlorophenyl)-2,2,2-trifluoro-1-(1H-indole-3-yl)ethanol (**5k**). 177

Figure S30. ^{1}H, ^{13}C and ^{19}F NMR of 1-(4-bromophenyl)-2,2,2-trifluoro-1-(1H-indole-3-yl)ethanol (**5l**). 179

Figure S31. ^{1}H, ^{13}C and ^{19}F NMR of 2,2,2-trifluoro-1-(1H-indole-3-yl)-1-*p*-tolylethanol (**5m**). 180

Figure S32. ^{1}H, ^{13}C and ^{19}F NMR of 2,2,2-trifluoro-1-(4-trifluoromethylphenyl)-1-(1H-indole-3-yl)ethanol (**5n**). 182

Figure S33. ^{1}H, ^{13}C and ^{19}F NMR of 1-(3-chlorophenyl)-2,2,2-trifluoro-1-(1H-indole-3-yl)ethanol (**5o**). 183

Figure S34. ^{1}H, ^{13}C and ^{19}F NMR of 2,2,2-trifluoro-1-(1H-indole-3-yl)-1-3,5-difluorophenylethanol (**5p**). 185

Figure S35. ^{1}H, ^{13}C and ^{19}F NMR of 1-(3-chloro-5-fluorophenyl)-2,2,2-trifluoro-1-(1H-indole-3-yl)ethanol (**5q**). 186

Figure S36. ^{1}H, ^{13}C and ^{19}F NMR of 1-(3.5-dichlorophenyl)-2,2,2-trifluoro-1-(1H-indole-3-yl)ethanol (**5r**). 188

Figure S37. ^{1}H, ^{13}C and ^{19}F NMR of 2,2,2-trifluoro-1-(1H-indole-3-yl)-1-2,3,4,5,6-pentafluorophenylethanol (**5s**). 189

Figure S38. ^{1}H, ^{13}C and ^{19}F NMR of 2-chloro-2,2-difluoro-1-(1H-indole-3-yl)-1-phenylethanol (**5t**). 191

Figure S39. ^{1}H, ^{13}C and ^{19}F NMR of 2,2,2-trifluoro-1-(1-methyl-indole-3-yl)-1-phenylethanol (**5u**). 192

Appendix for Chapter 4

Figure S1. ^{1}H and ^{13}C NMR of (*R*)-2,2'-bis(ethoxymethoxy)-1,1'-binaphthyl (**7**). 219

Figure S2. ^{1}H and ^{13}C NMR of (*R*)-3,3'-dibromo-2,2'-bis(ethoxymethoxy)-1,1'-binaphthyl (**8**). 220

Figure S3. ^{1}H and ^{13}C NMR of (*R*)-3,3'-di(3-pyridyl)-2,2'-di(ethoxymethoxy)-1,1'-binaphthyl (**9a**). 221

Figure S4. ^{1}H and ^{13}C NMR of (*R*)-3,3'-di[3-(5-methyl)pyridyl]-2,2'-di(ethoxymethoxy)-1,1'-binaphthyl (**9b**). 222

Figure S5. ^{1}H and ^{13}C NMR of (*R*)-3,3'-di(3-*N*-octylpyridinium)-2,2'-dihydroxyl-1,1'-binaphthyl iodide (**10a**). 223

Figure S6. ^{1}H and ^{13}C NMR of (*R*)-3,3'-di(3-(*N*-octyl-5-methyl)pyridinium)-2,2'-dihydroxyl-1,1'-binaphthyl iodide (**10b**). 224

Figure S7. ^{1}H, ^{13}C and ^{31}P NMR of (*R*)-3,3'-(4-hydroxy-4-oxidodinaphtho[2,1-*d*:1',2'-*f*][1,3,2]dioxaphosphepine-2,6-diyl)bis(1-octylpyridin-1-ium) chloride (**11a**). 225

Figure S8. ^{1}H, ^{13}C and ^{31}P NMR of (*R*)-5,5'-(4-hydroxy-4-oxidodinaphtho[2,1-*d*:1',2'-*f*][1,3,2]dioxaphosphepine-2,6-diyl)bis(3-methyl-1-octylpyridin-1-ium) chloride (**11b**). 226

Figure S9. ^{1}H, ^{13}C, ^{19}F and ^{31}P NMR of (*R*)-3,3'-(4-hydroxy-4-oxidodinaphtho[2,1-*d*:1',2'-*f*][1,3,2]dioxaphosphepine-2,6-diyl)bis(1-octylpyridin-1-ium) tetrakis[3,5-bis(trifluoromethyl)phenyl]borate (**1a**). 228

Figure S10. ^{1}H, ^{13}C, ^{19}F and ^{31}P NMR of (*R*)-5,5'-(4-hydroxy-4-oxidodinaphtho[2,1-*d*:1',2'-*f*][1,3,2]dioxaphosphepine-2,6-diyl)bis(3-methyl-1-octylpyridin-1-ium) tetrakis[3,5-bis(trifluoromethyl)phenyl]borate (**1b**). 230

Figure S11. ^{1}H, ^{13}C, ^{19}F and ^{31}P NMR of (*R*)-(4-hydroxy-4-oxidodinaphtho[2,1-d:1',2'-f][1,3,2]dioxaphosphepine-2,6-diyl)bis(triphenylphosphonium) tetrafluoroborate (**2f**). 232

Figure S12. ^{1}H, ^{13}C, ^{19}F and ^{31}P NMR of (*R*)-(4-hydroxy-4-oxidodinaphtho[2,1-d:1',2'-f][1,3,2]dioxaphosphepine-2,6-diyl)bis(triphenylphosphonium) hexafluorophosphate (**2g**). 234

Figure S13. ^{1}H, ^{13}C, ^{19}F and ^{31}P NMR of (*R*)-(4-hydroxy-4-oxidodinaphtho[2,1-d:1',2'-f][1,3,2]dioxaphosphepine-2,6-diyl)bis(triphenylphosphonium) tetrakis(pentafluorophenyl)borate (**2h**). 236

Figure S14. ^{1}H and ^{13}C NMR of 3-(2-nitro-1-phenylethyl)-1H-indole (**6a**). 238

Figure S15. ^{1}H and ^{13}C NMR of 7-chloro-3-(2-nitro-1-phenylethyl)-1H-indole (**6e**). 239

Figure S16. ^{1}H and ^{13}C NMR of 6-methoxy-3-(2-nitro-1-phenylethyl)-1H-indole (**6h**). 240

Figure S17. ^{1}H and ^{13}C NMR of 6-methyl-3-(2-nitro-1-phenylethyl)-1H-indole (**6i**). 241

Figure S18. ^{1}H and ^{13}C NMR of 3-(2-nitro-1-phenylethyl)-1-methyl-indole (**6q**). 242

List of Schemes

Chapter 1

Scheme 1. Early reports of amine and proline catalyzed reactions. 1

Scheme 2. Energy diagram for uncatalyzed and enantioselectively catalyzed reactions. 6

Scheme 3. Mannich-type reactions by Akiyama et al. (2004). 12

Scheme 4. Direct Mannich reactions by Uraguchi and Tereda (2004). 12

Scheme 5. Hydrophosphonylation of imines by Akiyama et al. (2005). 13

Scheme 6. Transfer hydrogenation by Hoffmann et al. (2005). 13

Scheme 7. Reductive aminations by Storer et al. (2006). 14

Scheme 8. Biginelli reactions by Chen et al. using hydrogenated BINOL-derived phosphoric acids (2006). 14

Scheme 9. Vinylogous Mannich-type reactions by Akiyama et al. (2008). 15

Scheme 10. Kinetic resolution of secondary alcohols by Harada et al. (2013). 15

Scheme 11. A recyclable phosphoric acid catalyst for Friedel-Crafts reactions by Hermeke and Toy (2011). 16

Scheme 12. Mannich-type reactions catalyzed by a biphenol-derived phosphoric acid (2011). 16

Scheme 13. Imine amidation reactions catalyzed by a VAPOL-derived phosphoric acid (2005). 17

Scheme 14. Fischer indolizations catalyzed by a spirocyclic phosphoric acid (2011). 17

Scheme 15. Mannich-type reactions catalyzed by a TADDOL-derived phosphoric acid (2005). 18

Scheme 16. 1,3-Dipolar cycloadditions catalyzed by a bisphosphoric acid (2008). 18

Scheme 17. Diels-Alder reactions catalyzed by a bisphosphoric acid (2011). 19

Scheme 18. Mukaiyama–Mannich reactions catalyzed by a bulky phosphoric acid (2016). 19

Scheme 19. Friedel-Crafts alkylation emphasizing the hydrogen bond formed between 33

the phosphoryl oxygen and indole.

Scheme 20. Mannich-type reaction emphasizing the role of the acidic hydrogen in a phosphoric acid catalyst. 34

Chapter 2

Scheme 1. Synthetic Route for Catalyst **1** and **2**. 38

Appendix for Chapter 2

Scheme S1. Plausible transition states for the Friedel-Crafts reaction of *β*-nitrostyrene with indole and *N*-methylindole. 112

Appendix for Chapter 3

Scheme S1. Synthetic scheme of **2a-2e**. 132

Appendix for Chapter 4

Scheme S1. Synthetic route for pyridinium ion-containing phosphoric acids **1a** and **1b**. 217

List of Abbreviations

Å	Angstrom
ACN	acetonitrile
AcOH	acetic acid
AN	acrylonitrile
AREA(θ)	a remote environment angle
BAr^F_4	tetrakis(3,5-bis(trifluoromethyl)phenyl)borate
BINOL	1,1'-bi-2-naphthols
^oC	degree in Celsius
cat.	catalyst
δ	chemical shift in part per million
DFT	density functional theory
DMSO	dimethyl sulfoxide
DPP	diphenyl phosphate
E_A	activation energy
ee	enantiomeric excess
er	enantiomeric ratio
ESI	electrospray ionization
FT-IR	Fourier transform infrared
g	gram(s)
h	hour(s)
H8-BINOL	5,5',6,6',7,7',8,8'-octahydro-1,1'-bi-2-naphthol
HOMO	highest occupied molecular orbital
HRMS	high resolution mass spectrometry
IR	infrared
JINGLE	1,1'-binaphthyl-2,2'-bis(sulfuryl)imides

kcal	kilocalorie
LUMO	lowest unoccupied molecular orbital
m/z	mass to charge ratio
µL	microliter
min (m)	minute(s)
mM	millimolar
M_n	number-average molecular weight
mol	mole
MPLC	medium pressure liquid chromatography
MS	molecular sieves
MVK	methyl vinyl ketone
nd	not determined
NLS	nonlinear least square
NMR	nuclear magnetic resonance
PEG	polyethylene glycol
Ph	phenyl
PPG	polypropylene glycol
ppm	parts per million
PTFE	polytetrafluorethylene
RT	room temperature
SPINOL	1,1’-spirobiindane-7,7’-diol
t	time
TADDOL	α,α,α,α-tetraaryl-1,3-dioxolane-4,5-dimethanols
THF	tetrahydrofuran
TiPSY	3,3’-bis(triphenylsilyl)-1,1’-binaphthyl-2,2’-diyl hydrogenphosphate
TLC	thin layer chromatography
TOF	time of flight

TRIP	3,3’-bis(2,4,6-triisopropylphenyl)-1,1’-binaphthyl-2,2’-diyl hydrogenphosphate
TS	transition state
TsOH	*p*-toluenesulfonic acid
TTMSSH	tris(trimethylsilyl)silane
UV-Vis	ultraviolet-visible spectroscopy
VAPOL	2,2’-diphenyl-(4-biphenanthrol)

Chapter 1: Background and Introduction

1.1. Organocatalysts

Organocatalysts refer to metal-free organic molecules that in substoichiometric amounts accelerate chemical reactions.[1] Though occasional reports of metal-free species, such as amine **1** and proline **2**,[2] appeared in the early literature during the twentieth century (Scheme 1), the significance of organocatalysis was not recognized until recently. This term was formally introduced in the early 2000s, and this area has witnessed rapid growth and become a well-established research field.[1a,1c,1d,3]

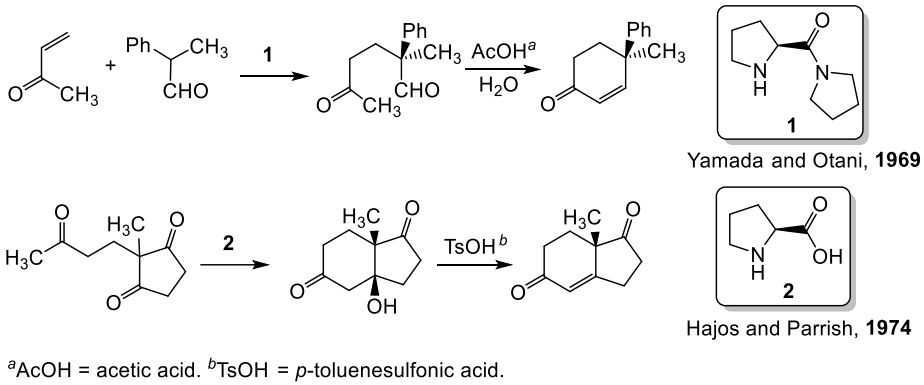

[a]AcOH = acetic acid. [b]TsOH = *p*-toluenesulfonic acid.

Scheme 1. Early reports of amine and proline catalyzed reactions.

Compared to organometallic catalysts, metal-free species are generally non-toxic, inexpensive, and robust to air and moisture.[3a,4] Moreover, they are particularly useful in applications where metals cannot be tolerated such as pharmaceutical production.[5] In addition, in some reactions substrates, products or impurities may poison metal catalysts, whereas organocatalysts offer a potential solution to this problem.[6] All of these features make organocatalysts attractive alternatives to organometallic systems.

Interactions between catalysts and substrates can be divided into two general categories: one where covalent bonds are formed and the other involves the formation of non-covalent complexes. In the former case, the catalyst and substrate form a covalent adduct structure within the catalytic cycle. Typical examples include enamine formation with amines to elevate the highest occupied molecular

orbital (HOMO) of the amine substrate,[7] and iminium ion generation with imidazolidinones to lower the lowest unoccupied molecular orbital (LUMO) of the reactant (Figure 1(a)).[8] In comparison, the latter case includes exclusively non-covalent interactions such as hydrogen bonding or ion pairing to lower the LUMO of the substrates. Most Brønsted acid catalysts belong to this latter category (Figure 1(b)).[9]

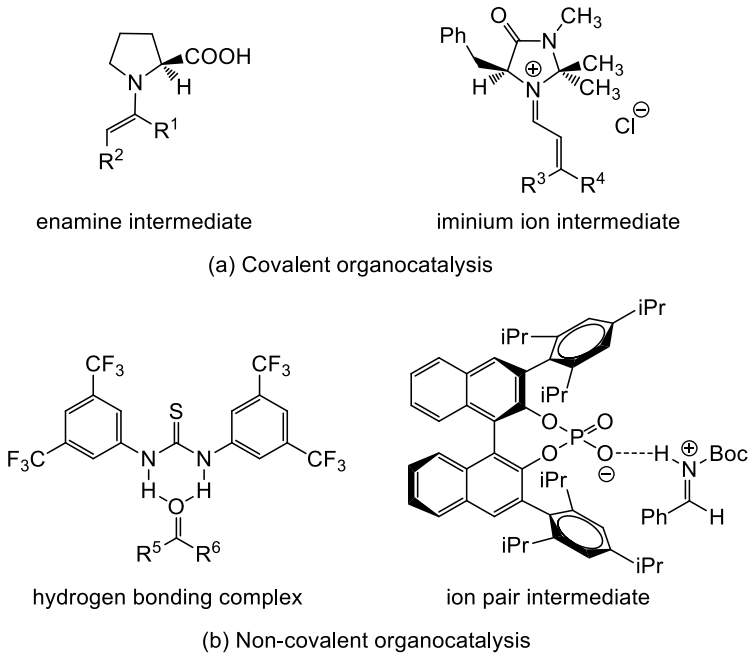

Figure 1. Covalent and non-covalent organocatalysis.

Seayad and List introduced a broad classification of organocatalysts based upon their mechanisms of reactions: Lewis acids, Lewis bases, Brønsted acids and Brønsted bases. The four categories are illustrated in Figure 2.[10] Lewis base catalysis is initiated by the nucleophilic addition of the catalyst (LB:) to the substrate (S). Lewis acid catalysis is initiated by the nucleophilic addition of the substrate (S:) to the catalyst (LA). In contrast, Brønsted base (BB) or acid (BA) catalysis is initiated by deprotonation or protonation of the substrate by the catalyst. In all cases, subsequent product formation and catalyst regeneration complete the catalytic cycle. A multifunctional organocatalyst may promote more than one type of interaction in the mechanistic pathway. Obviously, this classification cannot be applied to reactions with obscure mechanisms.[3b,10]

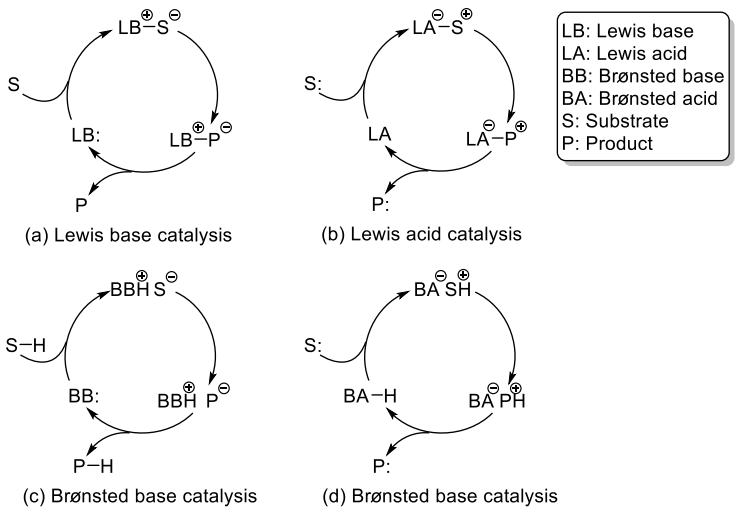

Figure 2. Catalytic cycles of organocatalysts.

A number of metal-free molecules have proved themselves as successful organocatalysts. As summarized in Figure 3, common bases used in this regard include phosphines (**3**),[11] amines (**4**),[12]

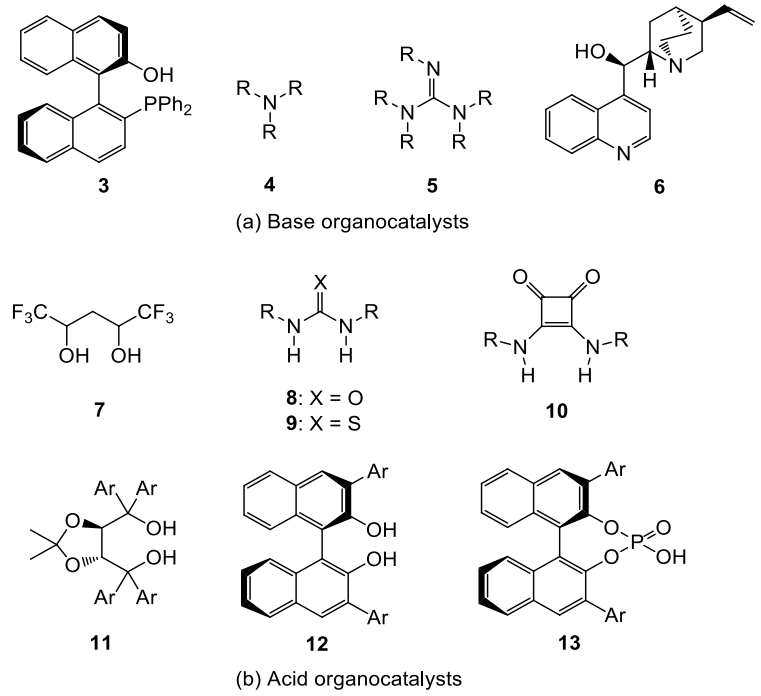

Figure 3. Common base and acid organocatalysts.

guanidines (**5**),[13] cinchonidines (**6**),[14] etc. and common acids are diols (**7**),[15] ureas (**8**),[16] thioureas (**9**),[17] squaramides (**10**),[18] α,α,α,α-tetraaryl-1,3-dioxolane-4,5-dimethanols (TADDOLs) (**11**),[19] 1,1'-bi-2-naphthols (BINOLs) (**12**),[19] phosphoric acids (**13**),[19-20] etc. Currently, combinations of different functional groups are also prevalent in organocatalyst studies as they can promote unique synergistic activation behaviors.[21]

1.2. Asymmetric Catalysis

Chirality is a primary property of a molecule that makes it non-superimposable on its mirror image. This is a structurally well-defined feature that differentiates a chiral molecule with its mirror-inverted molecule, known as its enantiomer.[22] Different structural features may cause point, axial or planar chirality of a molecule (Figure 4). The construction of point chirality, which can be caused by four

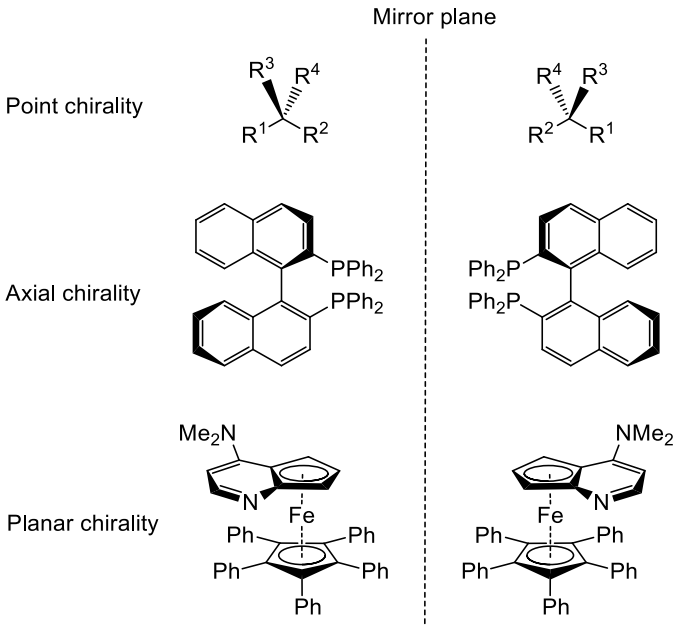

Figure 4. Different types of molecular chirality.

different groups at a tetrasubstituted carbon, is a major focus of this study, and is an area of great interest in the organic chemistry community.[23] A pair of enantiomers in an achiral environment are not

distinguishable in terms of physical properties such as melting point, solubility, etc. However, in the chiral environment of living things, they may have completely different properties in biochemistry and pharmaceuticals.[24] For this reason, the control of absolute configuration is crucial in the pharmaceutical industry and has become an essential part of modern organic synthesis.[23b,25]

Several common methods are used to access enantiomerically pure compounds: (1) A racemic mixture can be separated by resolution. The enantiomers are reacted with a chiral resolving agent to form a pair of diastereomers, which enables the two compounds to be separated by conventional techniques before being converted back to their original structures.[26] (2) A pair of enantiomers can be separated by chiral chromatography.[27] (3) A synthesis can be performed with pre-existing chiral molecules, which are often naturally occurring products and which will become incorporated into the final product.[28] (4) A chiral auxiliary can be applied to assist the formation of a chiral center.[29] (5) A chiral catalyst can be used to generate a product enantioselectively directly from racemic materials.[30] All of these methods have advantages and drawbacks. Chiral resolutions and chromatographic separations are not efficient methods if one enantiomer is desired over the other since at least half of the product may be unused. Synthesis with naturally occurring chiral compounds is generally not ideal either because there are only a limited number of such available species. The major disadvantage of the chiral auxiliary method is the need for extra synthetic steps to introduce and remove the chiral templates.

Chiral catalysis provides an attractive alternative strategy in that a broad range of reactions and substrates can be targeted and the products can be formed in high yields and good enantioselectivities without adding additional reaction steps. Given the asymmetry of chiral catalysts, two prochiral transition states with different activation energies typically are formed in the rate-determining step. The lower barrier pathway leads to the major enantiomer and the difference in the activation energies dictates the observed enantiomeric ratio of the product (Scheme 2).[31]

In chiral catalysis, a well-organized transition state is required for successful enantiomer discriminations. And the stereochemical outcome is controlled by the chiral environment of the catalyst.[21a,30,32] For hydrogen-bonding catalysts, the asymmetry is introduced by incorporating a chiral scaffold that often bears a secondary functional group. In this way not only does a hydrogen bond form

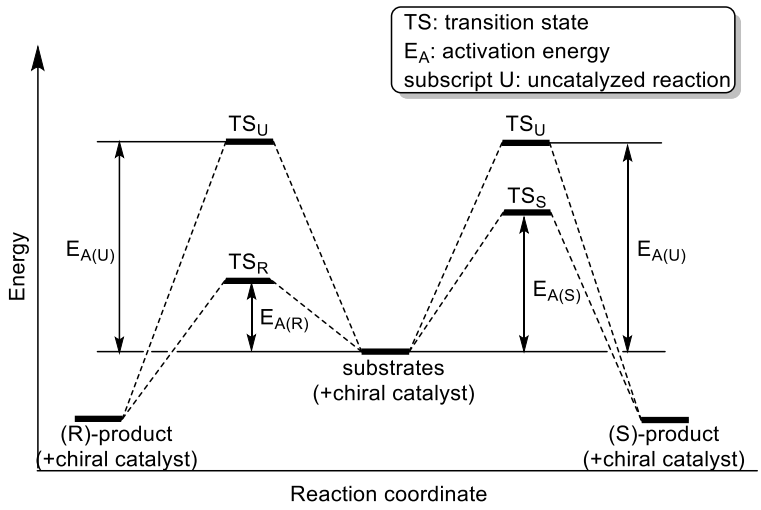

Scheme 2. Energy diagram for uncatalyzed and enantioselectively catalyzed reactions.

between the catalyst and the substrate, but additional interactions arise from the secondary functional group resulting in three-dimensional preorganization of the transition state (Figure 5(a)).[21c,33] Phosphoric acid catalysts, on the other hand, tend to completely protonate substrates and form contact ion pairs along with a secondary hydrogen bond between the phosphoryl oxygen and the substrate. Both of these interactions promote the catalyst bound complex to organize in the "chiral channel" formed by bulky substituents and lead to the observed product enantioselectivity (Figure 5(b)).[20a,34]

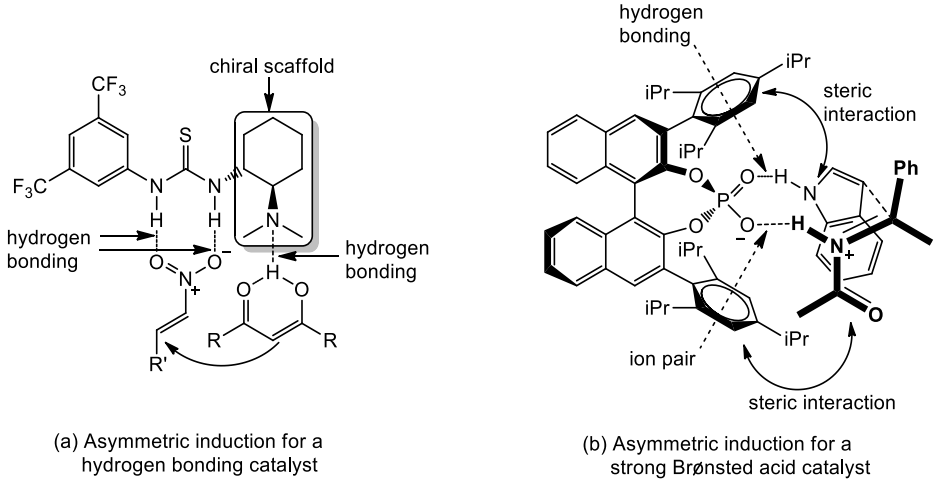

Figure 5. Strategies of asymmetry induction.

1.3. Brønsted Acid Catalysts

A proton can be regarded as the smallest Lewis acid, though this term usually refers to boron, aluminum and transition metal containing compounds. The source of the proton can act as a hydrogen bond donor or a Brønsted acid, both of which are important activation modes in organocatalysis.[9a,35] Brønsted acid catalysts were traditionally employed only for the formation and cleavage of carbon-oxygen bonds, but their activity for carbon-carbon bond formation has gradually been recognized over the past decade.[34]

Lewis acid catalysts are usually generated *in situ* with a metal-centered compound and chiral ligands, and they activate substrates with the metal center (Figure 6(a)). In comparison, Brønsted acid catalysts are typically used directly and employ their acidic hydrogen to lower the LUMO of C=O, C=NR or $C=CR_2$ containing compounds via a hydrogen bond or protonation. This electrophilically activates the substrate and facilitates nucleophilic attack (Figure 6(b)).[34]

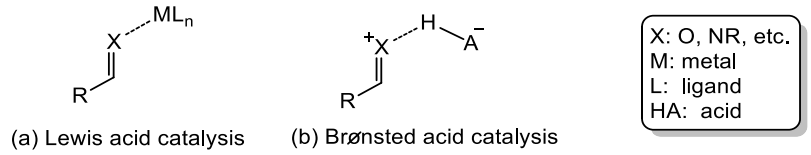

Figure 6. Lewis acid catalysis and Brønsted acid catalysis.

Brønsted acids can be classified into two categories according to their acidities: (1) Hydrogen bonding catalysts. Diols (**7**), ureas (**8**), thioureas (**9**), squaramides (**10**), TADDOLs (**11**), and BINOL derivatives (**12**) belong to this type due to their relatively weak acidities (Figure 7(a)). (2) Strong acid catalysts. Phosphoric acids (**13**), phosphoramides (**14**), dicarboxylic acids (**15**), disulfonic acids (**16**), and 1,1'-binaphthyl-2,2'-bis(sulfuryl)imides (JINGLEs) (**17**) are examples in this category (Figure 7(b)).[9a,19,36]

Hydrogen bonding catalysts always promote general Brønsted acid catalysis, in which partial or complete protonation of the substrate occurs in the rate-determining step of the reaction. In contrast, strong acid catalysts usually undergo specific Brønsted acid catalysis in which a reversible protonation of the reactant occurs in a pre-equilibrium step (Figure 8).[19,37]

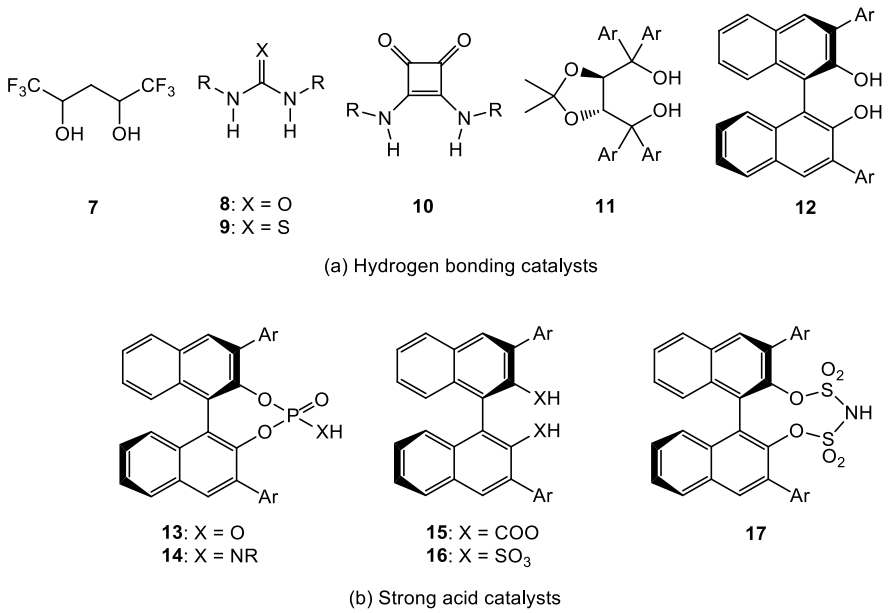

Figure 7. Common hydrogen bond and Brønsted acid catalysts.

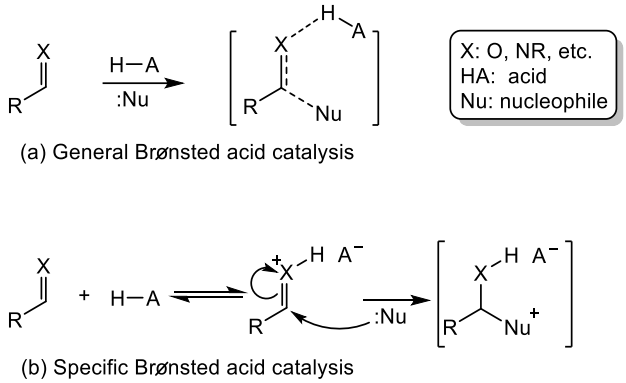

Figure 8. General and specific Brønsted acid catalysis.

For hydrogen bonding catalysts, depending on the number and geometry of the active hydrogens they possess, they can activate substrates by forming one (Figure 9(a)), two (Figure 9(b)) or more hydrogen bonds.[38] In contrast, strong acid catalysts usually activate reactants by protonation and formation of contact ion pairs (Figure 9(c)).[19] It is worth noting that although this is a broad classification scheme,

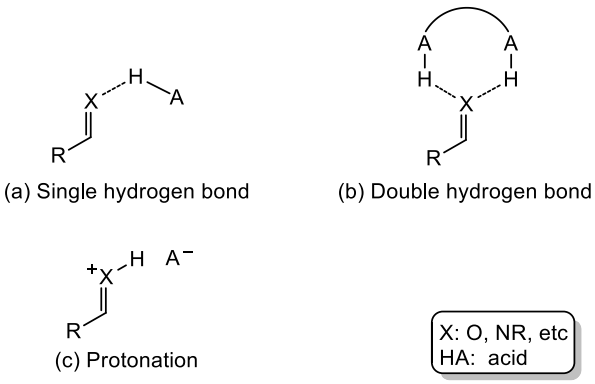

Figure 9. Common activation modes for hydrogen bond and strong acid catalysts.

there is no clear boundary between these two modes of activation. For example, strong acids can hydrogen bond to a substrate if it is a weak base, or if the catalyst acidity is diminished by the reaction conditions.[20a]

1.4. Catalytic Functionalities

A catalytic functional component refers to the basic unit in the catalyst structure that plays a distinct role in the operating reaction mechanism.[39] The number and type of these functionalities typically determine the activation behavior of the catalyst.[40] For non-redox reactions, four major types of functionalities have been identified: Lewis and Brønsted bases which increase the HOMO energies of a nucleophile by serving as a source of electron density, and Lewis and Brønsted acids which decrease the LUMO energy of an electrophile by using the empty orbitals of a metal, proton or hydrogen bond donor.[21d,39] Typical groups and the roles they serve are summarized in Figure 10.[39] It is worth adding that in many cases one chemical motif represents one functional component in a catalyst, but this need not be the case. That is, some chemical functionalities are bifunctional and can perform more than one role in a transition structure.[39] For instance, a phosphoric acid (-POOH) can serve as a Brønsted acid using its OH group and simultaneously act as a Lewis base by exploiting the phosphoryl oxygen atom.[34] Another common example is a primary or secondary amine, which serve as a Brønsted or Lewis base and as a hydrogen bond donor at the same time (Figure 11).[12b,41]

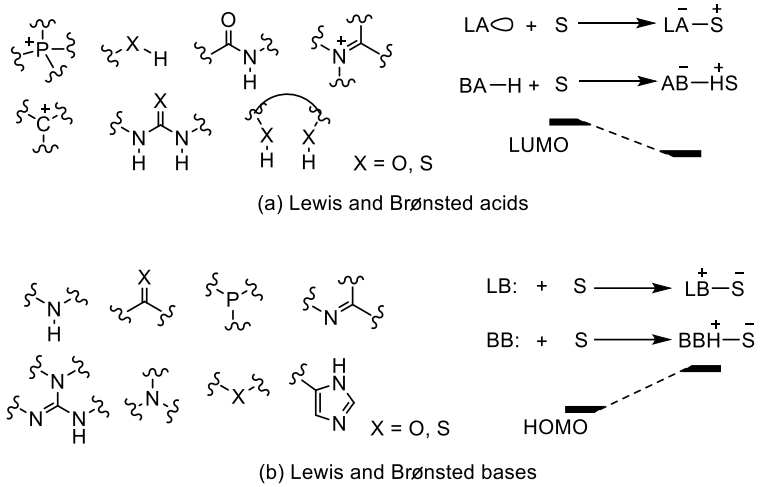

Figure 10. Representative catalytic functionalities and their roles in mechanisms.

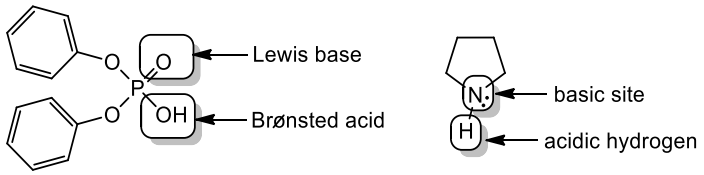

Figure 11. Examples of bifunctional chemical motifs.

Aside from employing these motifs that are naturally bifunctional, a more prevalent modification method for organocatalysts is the introduction of extra functionalities into the scaffold. This enables synergistic activation to occur and can result in enhanced reactivity and selectivity.[21b,33,40a] For example, thioureas can have amine, phosphine or hydroxyl containing side chains on their chiral scaffold to bind the substrate and organize the transition state so as to induce enantiomeric discrimination in the products (Figure 12).[42]

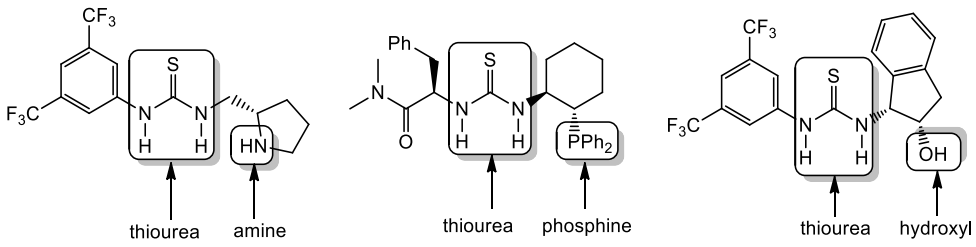

Figure 12. Bifunctional thioureas.

1.5. Phosphoric acid catalysts

1.5.1. Background

Since the first discovery of axially chiral BINOL-derived phosphoric acids as catalysts by Akiyama and Terada, there has been a rapidly increasing number of reports based on these species and their derivatives.[20a] This research area is particularly intriguing because these phosphoric acids have the following attributes (Figure 13): [9a,20a,34,43]

(1) They are much stronger acids than neutral hydrogen bonding catalysts, typically making them more active and capable of promoting higher energy processes.

(2) The phosphoryl oxygen can function as a Lewis base providing for the possibility of bifunctional catalysis.

(3) The extent of steric hindrance is readily tunable by coupling different substituents at the 3,3'-positions of the BINOL backbone.

(4) Electronic effects are adjustable through modifications of the 3,3'-groups or by partial hydrogenation of the BINOL backbone.

(5) Alternative axially chiral scaffolds, such as biphenyl, vaulted biaryl, TADDOL or 1,1'-spirobiindane-7,7'-diol (SPINOL) backbones can be employed.

(6) Phosphoric acid derivatives such as phosphoramides, thiophosphoric acids, imidodiphosphoric acids, and thiophosphoramides readily can be prepared.

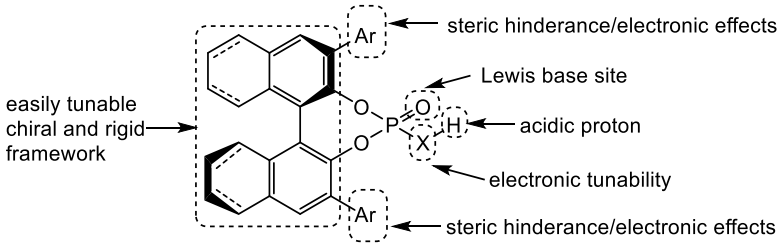

Figure 13. General features of 3,3'-BINOL-derived phosphoric acid catalysts.

One of the two earliest reports on phosphoric acid catalysts was disclosed by Akiyama et al. In this study, an array of phenyl-based substituents at the 3,3'-positions of (*R*)-BINOL were examined in

Mannich-type reactions. Catalyst reactivity and enantioselectivity was found to be greatly influenced by the 3,3'-substituent. The parent compound gave racemic products in low yields, while 3,3'-phenyl-derived substituents showed markedly improved reactivities and enantioselectivities. Among these latter catalysts, the 4-nitrophenyl substituent gave excellent yields and high enantiomeric excess (ee) values in reduced reaction times (Scheme 3).[44]

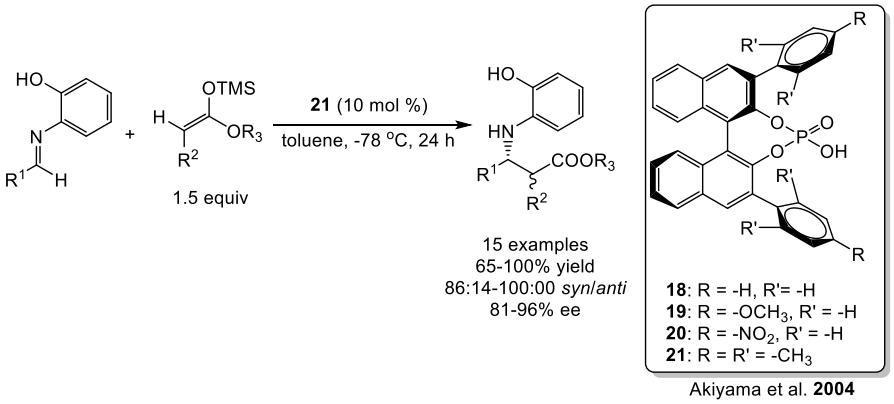

Scheme 3. Mannich-type reactions by Akiyama et al. (2004).

At almost the same time, Uraguchi and Tereda independently noticed that phenyl substituents with additional bulky functional groups at the 3,3'-positions of (*R*)-BINOL contributed to a dramatic increase in the enantiopurity of the product from a Mannich reaction. The bulkiest group examined (i.e., R = 4-(2-naphthyl)phenyl, Scheme 4) was found to give the highest ee and yield.[45]

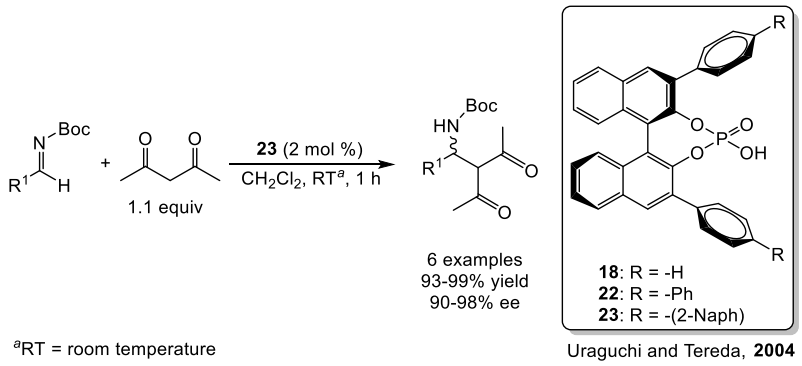

Scheme 4. Direct Mannich reactions by Uraguchi and Tereda (2004).

Later, Akiyama et al. developed a similar catalyst with two trifluoromethyl groups at the meta positions of the 3,3'-phenyl substituents, and it outperformed the previous catalysts with 4-nitrophenyl groups in terms of both reactivity and enantioselectivity in a hydrophosphonylation reaction (i.e., 90% versus 99% yields and 23% versus 43% ee in 24 h, Scheme 5).[46]

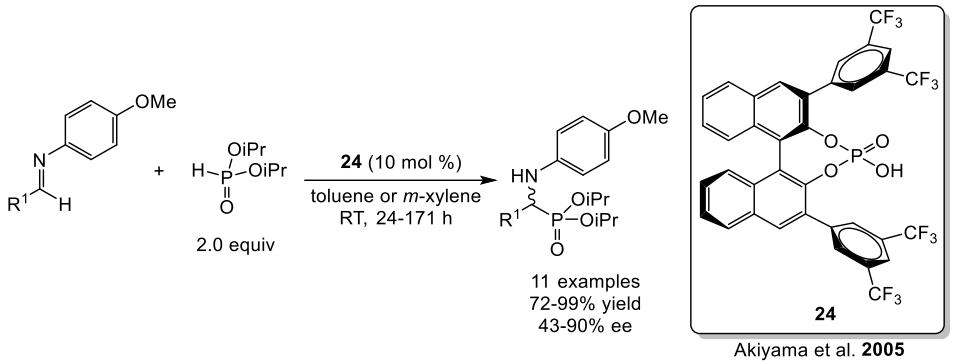

Scheme 5. Hydrophosphonylation of imines by Akiyama et al. (2005).

These early studies focused on relatively simple phenyl-based substituents at the 3,3'-position of BINOL, but bulkier phosphoric acids were subsequently found to be more successful catalysts. Hoffmann et al. reported the application of 3,3'-bis(2,4,6-triisopropylphenyl)-1,1'-binaphthyl-2,2'-diyl hydrogenphosphate (TRIP) in the transfer hydrogenation of imines. This new catalyst gave the best ee of all of the phosphoric acids that were examined and did so in excellent yields (Scheme 6).[47] TRIP has proved to be one of the most versatile and efficient phosphoric acid catalysts to date.[48]

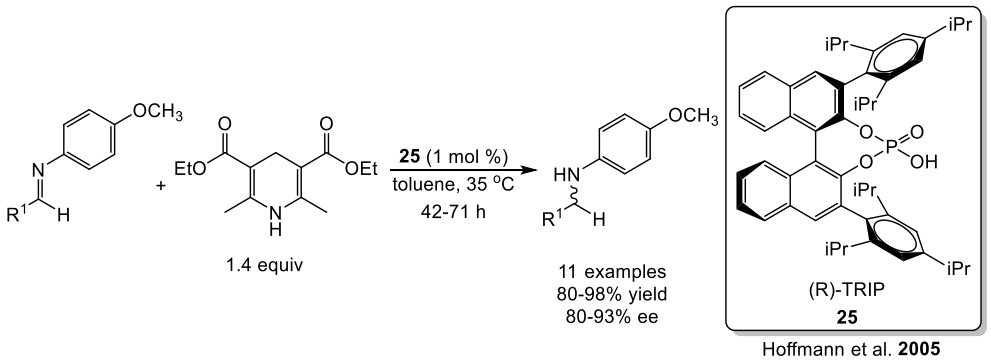

Scheme 6. Transfer hydrogenation by Hoffmann et al. (2005).

Storer et al. later reported the successful utility of another bulky phosphoric acid catalyst, 3,3'-bis(triphenylsilyl)-1,1'-binaphthyl-2,2'-diyl hydrogenphosphate (TiPSY), in a reductive amination reaction. Compared with other previously developed phenyl-based substituents, the 3,3'-triphenylsilyl substituted (*R*)-BINOL backbone was more successful in achieving high yields and enantioselectivities (Scheme 7).[49]

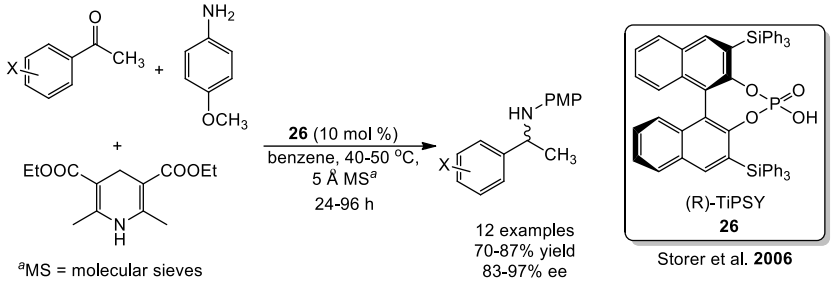

Scheme 7. Reductive aminations by Storer et al. (2006).

In some organic transformations, BINOL-derived phosphoric acids give only moderate outcomes, but the partially hydrogenated analogue (i.e., 5,5',6,6',7,7',8,8'-octahydro-1,1'-bi-2-naphthol, H8-BINOL) obtained by adding 4 equivalents of H_2 to the 5,5' to 8,8' positions of the BINOL backbone, provided greatly improved catalyst performance. Chen et al. reported an enantioselective Biginelli reaction using a variety of BINOL- and H8-BINOL-derived phosphoric acids, and the latter species provided higher enantioselectivities (Scheme 8).[50] Additional H8-BINOL-derived phosphoric acids with different 3,3'-substituents subsequently were developed and applied to a variety of reactions.[51]

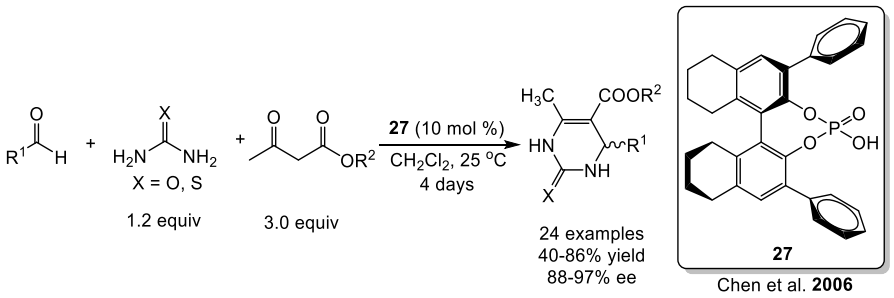

Scheme 8. Biginelli reactions by Chen et al. using hydrogenated BINOL-derived phosphoric acids (2006).

An alternative method to tune the electronic effects of BINOLs is to introduce extra substituents at the 6,6'-positions. Akiyama et al. disclosed their study of an (*R*)-TRIP derivative with iodine atoms at the 6,6'-positions, and this new species outperformed TRIP by increasing the ee by 8% in a vinylogous Mannich-type reaction (Scheme 9). Computations revealed that the iodine atoms do not alter the dihedral angle of the BINOL, indicating that the improved performance is probably due to electronic effects.[52]

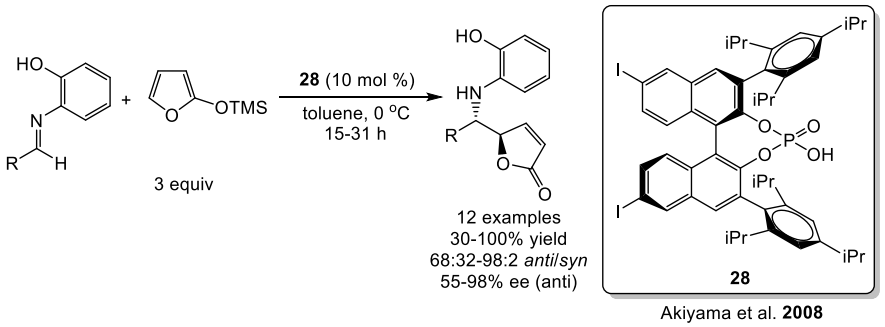

Scheme 9. Vinylogous Mannich-type reactions by Akiyama et al. (2008).

A similar (*R*)-TRIP derivative with nitro groups at the 6,6'-positions was reported by Harada et al. This new catalyst led to a significant 4.6-fold increase in the s factor for the kinetic resolution of secondary alcohols (Scheme 10).[53]

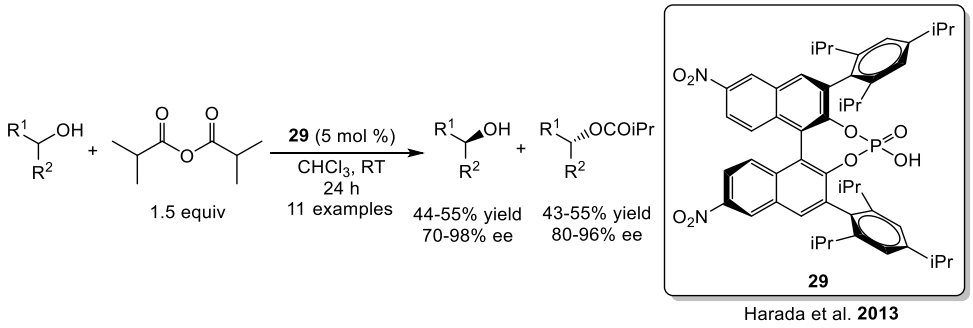

Scheme 10. Kinetic resolution of secondary alcohols by Harada et al. (2013).

Hermeke and Toy synthesized a 6,6'-phosphonium ion tagged (*R*)-TRIP catalyst and achieved

moderate to good enantioselectivity for two Friedel-Crafts reactions of indole and alkenes. Moreover, the catalyst can readily be recovered from solution by precipitation leading to limited reusability (Scheme 11).[54]

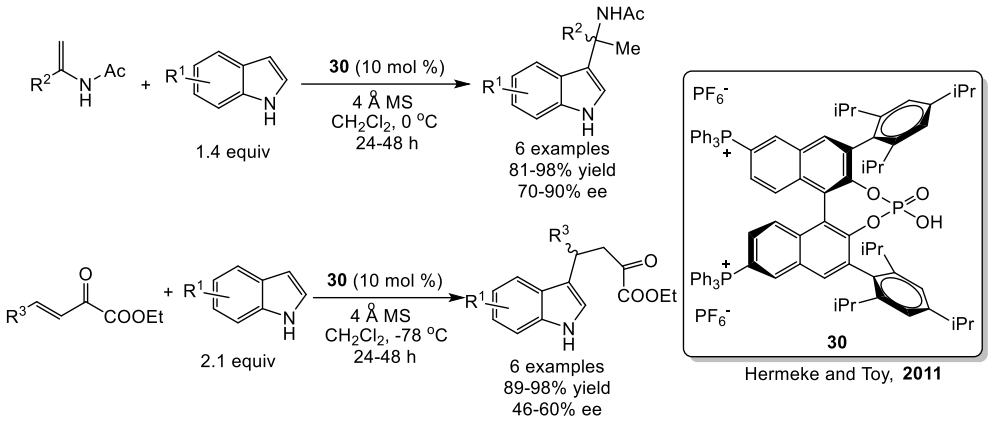

Scheme 11. A recyclable phosphoric acid catalyst for Friedel-Crafts reactions by Hermeke and Toy (2011).

The development of alternative BINOL backbones is a continuing area of research.[20a] For example, Kashikura et al. reported a (*S*)-biphenol-derived phosphoric acid bearing bulky 9-anthryl groups. It was found to lead to faster reactions and greater enantioselectivities in a Mannich-type transformation compared to the analogous BINOL and H8-BINOL derivatives (Scheme 12).[55]

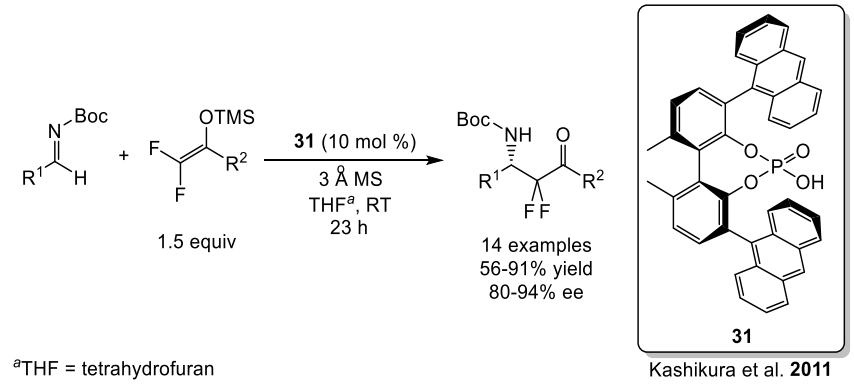

Scheme 12. Mannich-type reactions catalyzed by a biphenol-derived phosphoric acid (2011).

A phosphoric acid with a 2,2'-diphenyl-(4-biphenanthrol) (VAPOL) backbone also proved its utility in an imine amidation reaction reported by Rowland et al. Compared with BINOL-derived phosphoric acids, the VAPOL-derivative **32** was found to give excellent enantioselectivity without sacrificing reactivity (Scheme 13).[56]

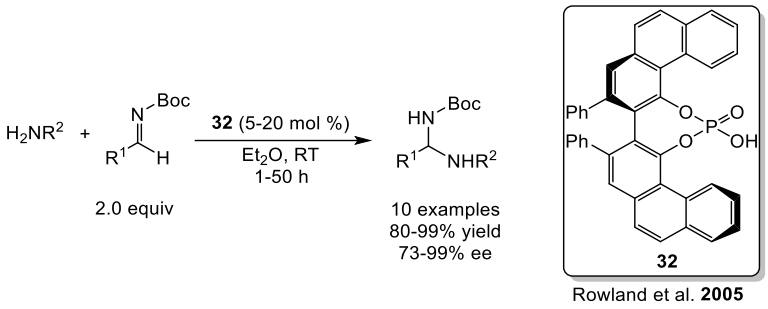

Scheme 13. Imine amidation reactions catalyzed by a VAPOL-derived phosphoric acid (2005).

As a novel chiral scaffold, spirocyclic phosphoric acids are advantageous in a number of reactions. Muller et al. reported their application in an asymmetric Fischer indolization, and they proved to be advantageous over other VAPOL, BINOL and H8-BINOL derivatives both in terms of reactivity and enantioselectivity (Scheme 14).[57]

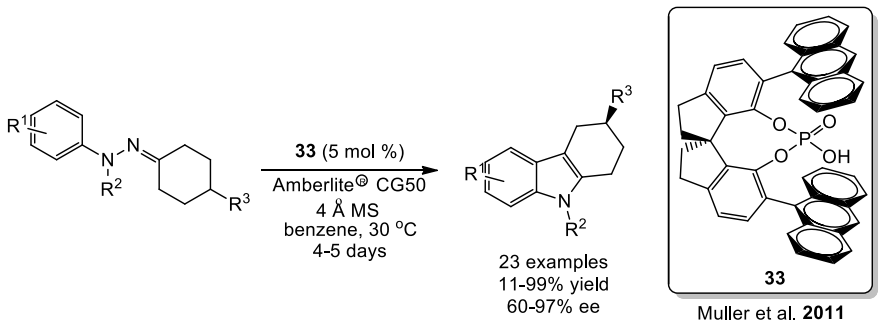

Scheme 14. Fischer indolizations catalyzed by a spirocyclic phosphoric acid (2011).

TADDOL is a double hydrogen bond donor and Akiyama et al. developed a chiral phosphoric acid derived from it. This species (**34**) was tested in a Mannich-type reaction and provided excellent results.

Other aryl groups were examined and a 4-trifluoromethylphenyl substituent was found to give the best results (Scheme 15).[58]

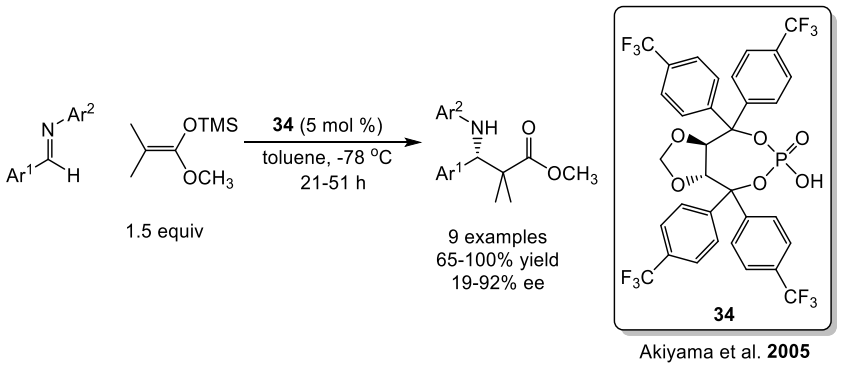

Scheme 15. Mannich-type reactions catalyzed by a TADDOL-derived phosphoric acid (2005).

New phosphoric acid catalysts with further innovative designs have been reported in the last decade. Chen et al. demonstrated the synthesis and application of a chiral diphosphoric acid with two linked BINOL skeletons in a 1,3-dipolar cycloaddition reaction. Excellent yields and enantioselectivities were achieved in this study, whereas commonly used monophosphoric acids only gave poor to moderate ee values (Scheme 16).[59] A density functional theory (DFT) computational study was able to rationalize the importance of simultaneous activation of dipole and dipolarophile by the bifunctional chiral bisphosphoric acids.[60]

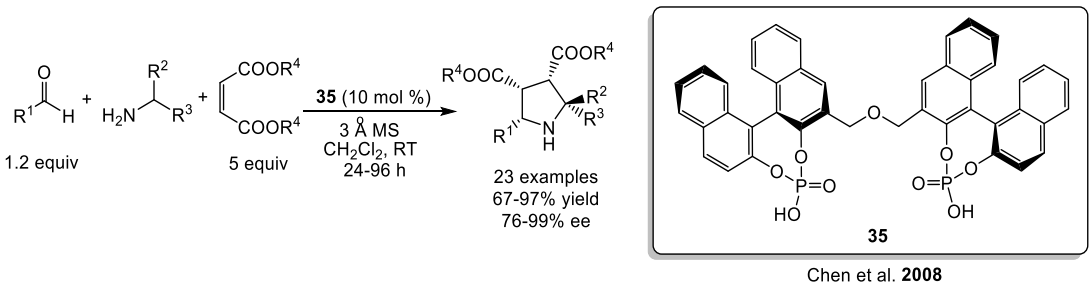

Scheme 16. 1,3-Dipolar cycloadditions catalyzed by a bisphosphoric acid (2008).

Momiyama et al. synthesized another diphosphoric acid with only a single BINOL skeleton and it

displayed excellent reactivity and enantioselectivity in a Diels-Alder reaction with only a 2.5 mol % catalyst loading. In comparison, the bulky monophosphoric acid TRIP gave poor yields and lower ee values even with a 5.0 mol % loading (Scheme 17).[61]

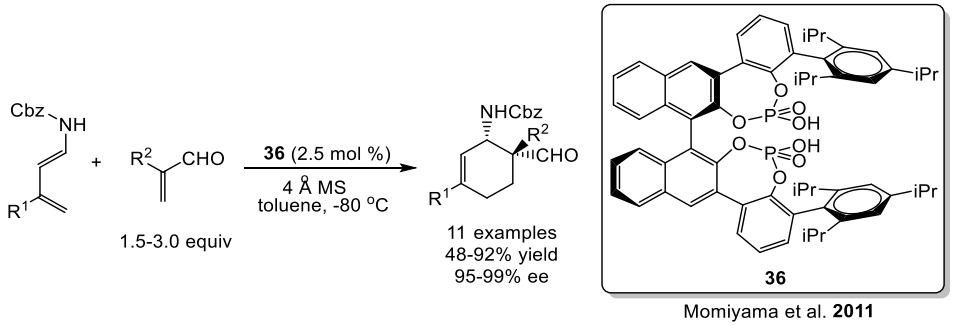

Scheme 17. Diels-Alder reactions catalyzed by a bisphosphoric acid (2011).

Zhou and Yamamoto applied a phosphoric acid bearing 2,4,6-trimethyl-3,5-dinitrophenyl substituents at the 3,3'-positions of (*R*)-BINOL in Mukaiyama–Mannich reactions and achieved excellent yields as well as enantioselectivities. In this new catalytic structure, the electronic effects of the NO_2 groups endowed high reactivity, and the crowded environment created by the methyl and nitro substituents led to a strong chiral induction. The absence of the *o*-methyl groups or all three methyl substituents undermined the observed enantioselectivity (Scheme 18).[62]

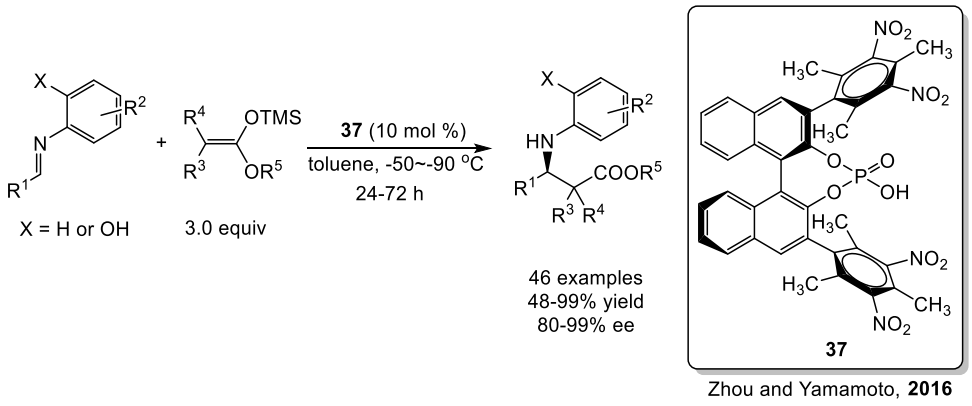

Scheme 18. Mukaiyama–Mannich reactions catalyzed by a bulky phosphoric acid (2016).

1.5.2. Activation Modes of Phosphoric Acids in Catalysis

Investigating the mechanism of a catalyzed reaction can be beneficial since it elucidates the key points of a catalyst and may suggest a means for carrying out structural improvements. Three activation modes of phosphoric acids were proposed by Parmar et al.: Mono activation, dual activation and bifunctional activation.[20a]

Mono activation promoted by the acidic hydrogen in a phosphoric acid is the most obvious and simplified mode of activation. This pathway was proposed for substrates that contain only one Lewis basic site. In this case the acidic site of the phosphoric acid protonates or hydrogen bonds to the most basic position of the substrate, electrophilically activating it and facilitating nucleophilic attack (Figure 14).[63]

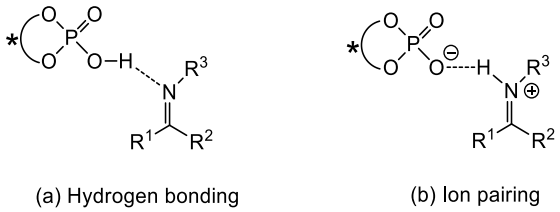

Figure 14. Mono activation by a phosphoric acid.

Dual activation is the least common of the three pathways, but it can be a powerful activating mechanism. In this mode, two hydrogen bonds form between the catalyst and the substrate. They can consist of a bidentate hydrogen bond between the acidic site of the catalyst and two basic positions in the substrate (Figure 15 (a)). Alternatively, if the substrate has both acidic and basic sites they can interact with the phosphoryl oxygen atom and the acidic hydrogen leading to the formation of two hydrogen bonds (Figure 15 (b)).[34]

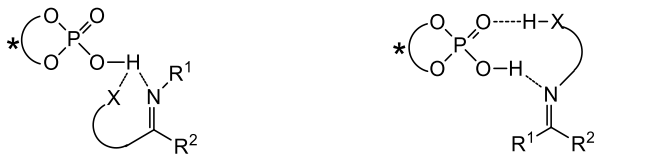

Figure 15. Dual activation modes of a phosphoric acid.

Bifunctional activation covers the majority of reactions catalyzed by phosphoric acids. In this pathway, the phosphoric acid uses its acidic site to form a hydrogen bond with a Lewis basic site in one substrate (i.e., the electrophile) and its phosphoryl oxygen to interact with the nucleophile. In this way, both substrates are simultaneously activated (Figure 16).[64]

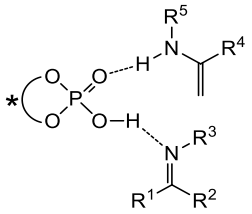

Figure 16. Bifunctional activation brought about by a phosphoric acid.

1.5.3. Reactivity of Phosphoric Acid Catalysts

1.5.3.1. Early Strategies of Reactivity Enhancement for Phosphoric Acid Catalysts

A study by Kaupmees et al. chose a series of Brønsted acids and measured their acidities by ultraviolet-visible spectroscopy (UV-Vis) in acetonitrile (ACN). A first-order Nazarov cyclization was chosen as a model reaction and these Brønsted acids were tested as catalysts for this transformation. A clear relationship was found between the observed reaction rate and the catalyst acidities, and higher catalyst acidity resulted in a larger reaction rate (Figure 17).[65]

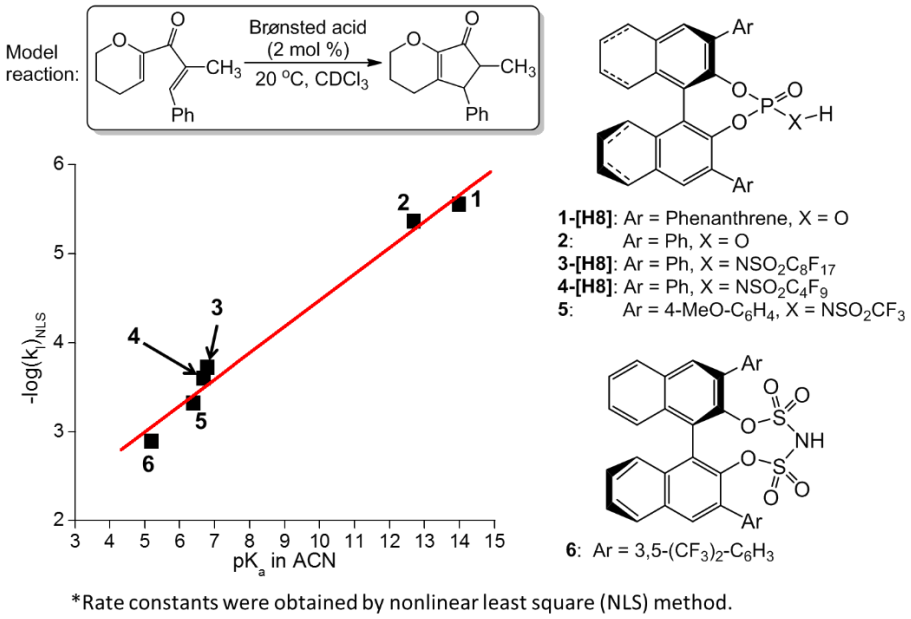

Figure 17. Plot of reaction rates for a Nazarov cyclization versus catalyst acidities.

As early as the first report of the BINOL derived phosphoric acids by Akiyama et al., the rate acceleration of electron-withdrawing groups was noticed. By introducing a nitro group onto the para-position of the 3,3'-phenyl substituents, the reaction time for a Mannich-type transformation could be shortened from 20 h to 4 h. In contrast, the introduction of electron-donating 2,4,6-trimethyl or *p*-methoxy groups led to extended reaction times. In addition, the enantiomeric excess of products generated with the 4-nitrophenyl substituted BINOL-derived phosphoric acid also outperformed the other derivatives (Table 1).[44]

Later, Akiyama et al. disclosed the results of an enantioselective hydrophosphonylation of imines catalyzed by phosphoric acids. In this study, the 3,5-$(CF_3)_2$ substituents on 3,3'-phenyl groups provided better rate accelerations than a 4-nitro substituent and gave complete conversion of the reactants in 24 h, while the analogous catalyst without electron-withdrawing groups led to only a 70% yield in the same period of time. Moreover, the enantioselectivity of the 3,5-$(CF_3)_2$-phenyl substituted BINOL phosphoric acid was the best among all of the catalysts that were examined (Table 2).[46]

Table 1. Influence of 3,3'-substituents on reaction rates.[a]

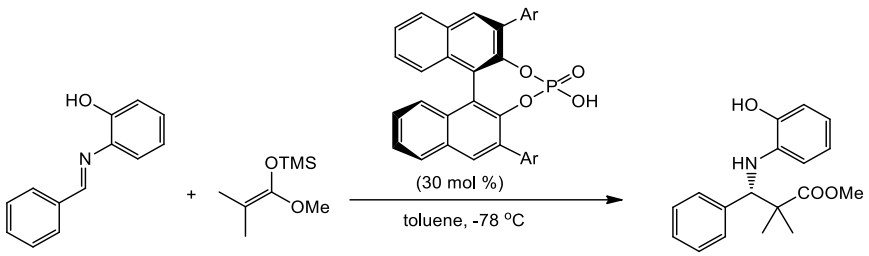

entry	Ar	t (h)	yield (%)	ee (%)
1	H	22	57	0
2	Ph	20	100	27
3	2,4,6-$Me_3C_6H_2$	27	100	60
4	4-$MeOC_6H_4$	46	99	52
5	**4-$NO_2C_6H_4$**	**4**	**96**	**87**

[a]Reactions performed with 0.162 mmol aldimine, 0.486 mmol ketene silyl acetal and 0.0486 mmol catalyst in toluene at -78 °C.

Converting phosphoric acids to *N*-phosphoramides is another strategy to improve their reactivity since the latter species are more acidic. In a study by Lee and Kim, a comparison was done between a 3,3'-(2-naphthyl)-BINOL based phosphoric acid and its *N*-phosphoramide derivative in a radical addition reaction. While the phosphoric acid only gave a 37% yield after 12 hours, the phosphoramide was found to give an improved yield (61%), indicating that the latter catalyst is more efficient. An improved ee was observed too, but in both cases the enantioselectivity was poor (Table 3).[66]

Table 2. Rate acceleration by electron-withdrawing groups.[a]

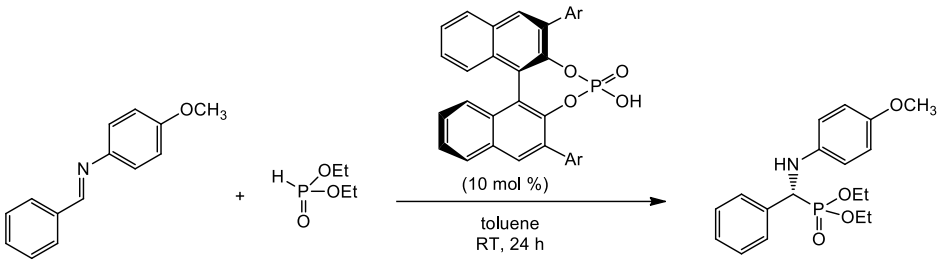

entry	Ar	yield (%)	ee (%)
1	Ph	70	23
2	4-$NO_2C_6H_4$	90	23
3	4-$CF_3C_6H_4$	69	35
4	**3,5-$(CF_3)_2C_6H_3$**	**99**	**43**

[a]Reactions performed with 0.135 mmol *N*-benzylidene-*p*-anisidine, 0.270 mmol diethyl phosphite and 0.0135 mmol catalyst in toluene at 20 °C.

Table 3. Reaction yields of a phosphoric acid and *N*-phosphoramide catalyzed radical addition.[a]

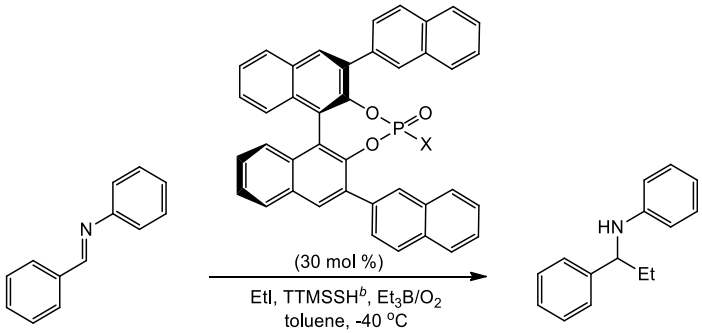

entry	X	t (h)	yield (%)	ee (%)
1	OH	12	37	3
2	**$NHSO_2CF_3$**	**12**	**61**	**21**

[a]Reactions performed with 0.05 mmol imine, 0.25 mmol ethyl iodide, 0.15 mmol TTMSSH, 0.10 mmol Et_3B and 0.15 mmol catalyst in toluene at -40 °C. [b]TTMSSH = tris(trimethylsilyl)silane.

Modification of the BINOL backbone is another method for reactivity enhancement. Wang et al. developed a phosphoric acid bearing a 5,5'-bitetralone scaffold. The acidity of the catalyst was increased by the introduction of electron-withdrawing carbonyl groups. This novel catalyst was found to outperform its BINOL and H8-BINOL analogues in terms of reactivity without harming the enantioselectivity (Table 4).[67]

Table 4. Rate enhancement of 5,5'-bitetralone-based chiral phosphoric acid.[a]

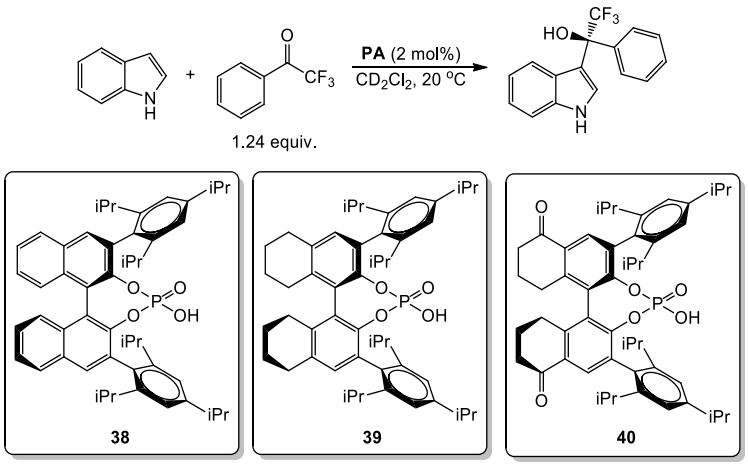

entry	cat.	k (M^{-1} h^{-1})[b]	k_{rel}	ee (%)
1	38	0.242	1.00	92
2	39	0.134	0.554	92
3	**40**	**0.385**	**1.59**	**93**

[a]Reactions performed with 0.17 mmol indole, 0.21 mmol 2,2,2-trifluoroacetophenone and 0.0034 mmol catalyst in 0.6 mL of CD_2Cl_2 at 20 °C. [b]Calculated from a second-order fit of the original conversion data.

Though not commonly studied, additives that can enhance the acidity of the phosphoric acid also should accelerate reactions. In a study by Hatano et al., 5 mol % of BINOL phosphoric acid was found to give no product for the Diels-Alder reaction between cyclopentadiene and methacrolein. In contrast, when an equivalent amount to the phosphoric acid of boron tribromide was added, a good yield was

obtained through the interaction of BBr_3 and the phosphoryl oxygen. As a control, 5 mol % of BBr_3 without the phosphoric acid led to a significantly lower yield. In addition, BBr_3 was found to influence the *endo*/*exo* ratio and the observed enantioselectivity suggesting the importance of an *in situ* generated 1:1 phosphoric acid/BBr_3 complex (Table 5).[68]

Table 5. Reactivity enhancement by a strong Lewis acid additive.[a]

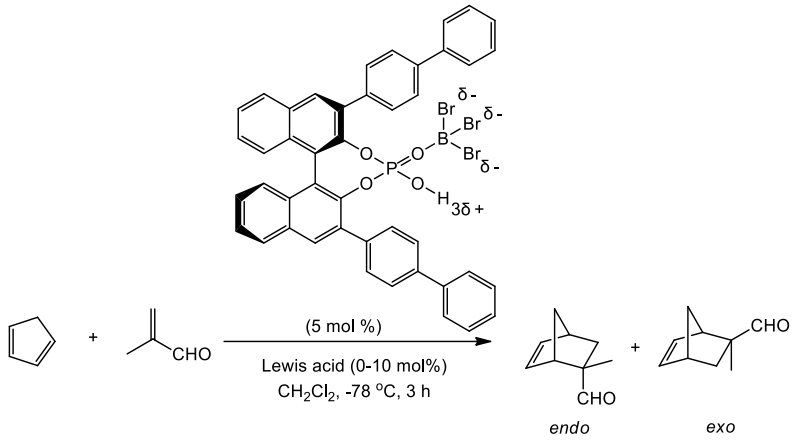

entry	Lewis acid (mol %)	yield (%)	*endo*/*exo*	ee of *exo*-product (%)
1	-	0	nd[c]	nd
2	BBr_3 (2.5)	92	3:97	61
3	**BBr_3 (5.0)**	**99**	**2:98**	**89**
4	BBr_3 (7.5)	78	2:98	85
5	BBr_3 (10)	64	8:92	18
6[b]	BBr_3 (5.0)	66	10:90	nd

[a]Reactions performed with 2.5 mmol cyclopentadiene, 0.50 mmol methacrolein, 0.025 mmol catalyst, and 0-0.05 mmol boron tribromide in 2 mL of CH_2Cl_2 at -78 °C. [b]The reaction was performed without phosphoric acid catalyst. [c]nd = not determined.

1.5.3.2. Electrostatically Enhanced Acid Catalysts

In a recent study by Samet et al., a series of phenol derivatives with different substituents were examined using infrared (IR) techniques. The O-H stretches of phenol in CCl_4 and CCl_4 with 1% (v/v)

CD_3CN were measured, and a red shift in the latter solvent was observed (Figure 18(a)). This was attributed to the formation of a $ArOH\cdots NCCD_3$ hydrogen bond. Moreover, the red shift was found to be correlated to the acidity of the phenol. That is, weaker acids with electron-donating groups (e.g., CH_3 and OCH_3) have smaller IR shifts while stronger acids with electron-withdrawing groups (e.g., NO_2 and CF_3, etc.) display larger red shifts. As a result, phenols with positively charged centers were observed to have even larger red shifts of the O-H stretch indicating that these species are much stronger acids than all of the noncharged analogues that were examined (Figure 18(b)).[69]

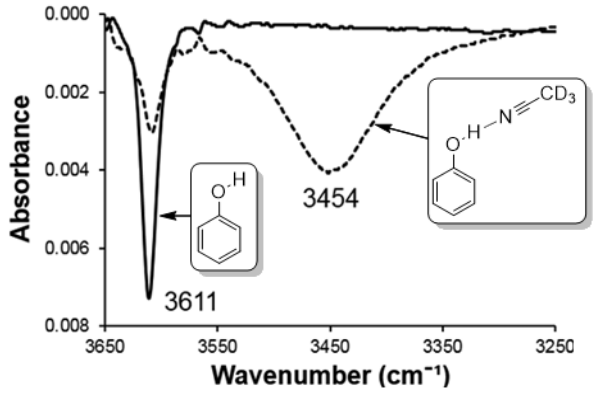

(a) Red shift of phenol OH peak upon addition of CD_3CN.

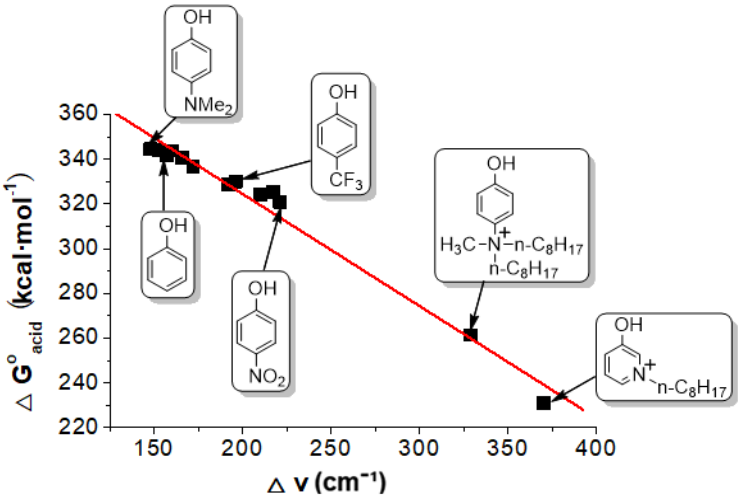

(b) Relationship between gas-phase acidities and the IR shifts of the O-H absorption.

Figure 18. IR study of a series of phenol derivatives with known gas-phase acidities.

The strong acidities of charged phenols were verified by using them as acid catalysts in a Friedel-Crafts reaction of *N*-methylindole and *trans*-*β*-nitrostyrene. As shown in Table 6, when this transformation was performed in a non-polar solvent the positively charged phenols were found to lead to reactions rates that are several orders of magnitudes higher than for *p*-nitrophenol. These results, just like the IR shifts, are in much better accord with the gas-phase acidities of the phenols as opposed to the dimethyl sulfoxide (DMSO) pK_a values (entry 1 and 3-4). The non-coordinating counteranion, tetrakis(3,5-bis(trifluoromethyl)phenyl)borate ($BAr^F{}_4^-$), was also found to be crucial in this study since I^- formed a hydrogen bond with the OH group and undermined the reactivity (entry 2). Dilute solutions in this case have lower polarities, so while the Friedel-Crafts occurred more slowly, the differences between charged and noncharged catalysts are larger (entry 5-7).[69]

Later, Fan and Kass applied the charge-enhancement strategy to thiourea catalysts. In this work, mono- (**47**) and di-*N*-methylpyridinium thioureas (**48**) were synthesized and examined as catalysts for the reaction of *N*-methylindole with *trans*-*β*-nitrostyrene. Compared to their neutral analogues, *N,N'*-diphenylthiourea (**45**) and Schreiner's thiourea (**46**), the charged catalysts led to reaction rates that are orders-of-magnitude larger. These results indicate that the incorporation of charged centers into hydrogen bond donors can improve their catalytic performance (Table 7).[70]

Table 6. Kinetic study of a Friedel-Crafts alkylation catalyzed by phenol derivatives.[a]

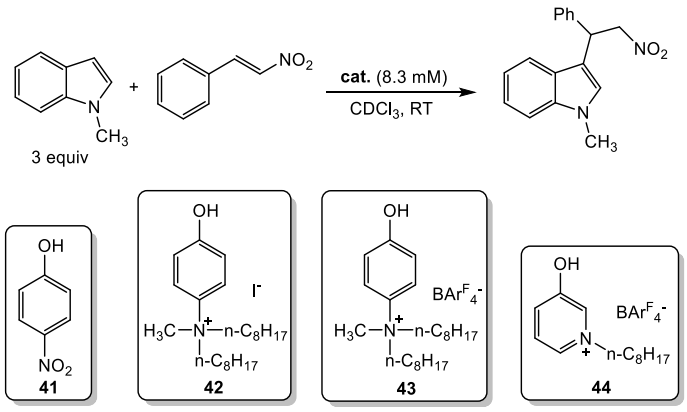

Continued Table 6.

entry	catalyst	[β-NS] (mM)	pK_a (DMSO)	$\triangle G^o_{acid}$ (kcal mol^{-1})[b]	$t_{1/2}$ (h)	k_{rel}
1	41	83	10.8	320.9 ± 2.0	1200	1
2	42	83	12.5 ± 1.0[c]	261.4[d]	8400	0.14
3	43	83	12.5 ± 1.0[c]	261.4[d]	42	29
4	44	83	12.4 ± 1.1[c]	231.1[e]	1.6	750
5	41	29	10.8	320.9 ± 2.0	4100	1
6	43	29	12.5 ± 1.0[c]	261.4[d]	64	64
7	44	29	12.4 ± 1.1[c]	231.1[e]	2.1	2000

[a]Reactions performed with 29 or 83 mM *trans*-β-nitrostyrene, 3 equiv of indole and 8.3 mM catalyst in $CDCl_3$ at 20 °C. [b]Equilibrium values are from ref 71 unless otherwise noted; some values are the average of two similar results. [c]Measured in DMSO by bracketing using two colored indicators. [d]B3LYP/6-31+G(d,p) computations on the ammonium cation. [e]Calculated value is for 3-methylpyridinium phenol.

This past year (2017), Fan and Kass expanded the above study to chiral thioureas. They synthesized a series of *N*-alkylated pyridinium containing thioureas with a chiral 2-indanol substituent and applied them in the Friedel-Crafts reaction of indole and *trans*-β-nitrostyrene. The analogous noncharged

Table 7. Kinetic study of a Friedel-Crafts alkylation catalyzed by thioureas.[a]

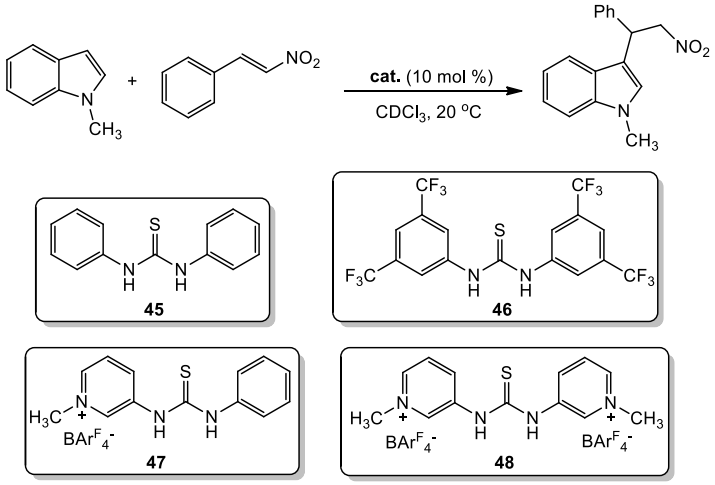

Continued Table 7.

entry	cat.	k (M^{-1} h^{-1})	$t_{1/2}$ (h)	k_{rel}
1	-	2.8×10^{-3}	1100	-
2	45	3.9×10^{-3}	820	0.035
3	46	1.1×10^{-1}	29	1.0
4	**47**	**7.1×10^{-1}**	**4.5**	**6.5**
5	**48**	**45**	**0.071 (4.3 m)**	**410**

[a]Reactions performed with 239 mM *N*-methylindole, 80 mM *trans-β*-nitrostyrene and 8.3 mM catalyst in $CDCl_3$ at 20 °C.

bis(3,5-trifluoromethyl)phenyl substituted thiourea gave only trace conversion after 48 hours whereas the charged species led to good conversions and enantiomeric ratio (er) values (Table 8).[72]

Table 8. Kinetic study of a Friedel-Crafts alkylation catalyzed by chiral thioureas.[a]

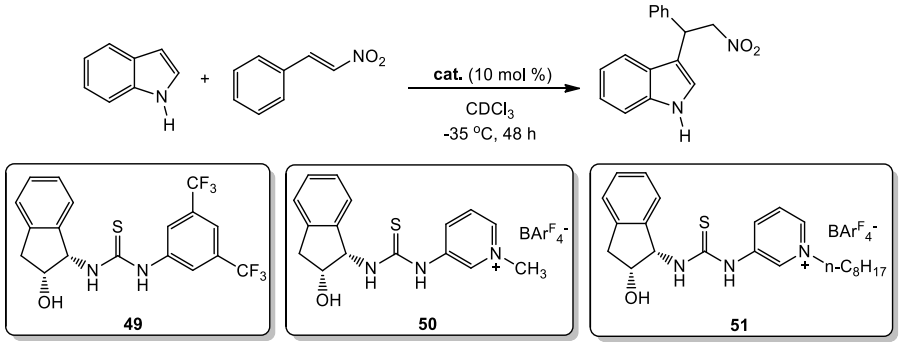

entry	cat.	conversion (%)	er
1	49	trace	-
2	**50**	**76**	**91:9**
3	**51**	**41**	**93:7**

[a]Reactions performed with 250 mM indole, 83 mM *trans-β*-nitrostyrene and 8.3 mM catalyst in $CDCl_3$ at -35 °C.

1.5.4. Enantioselectivity with Phosphoric Acids

The stereoselectivity of BINOL derived phosphoric acid catalysts rely primarily on structures with substituents at the 3,3'-positions to create a narrow chiral channel for the substrates to reach the acid center.[20a,34] In most cases, increasing the size of the 3,3'-substituents is beneficial for strong asymmetric induction and high enantioselectivity (Figure 19 (a) and (b)). For this reason, most of the successful and widely used catalysts bear bulky groups at the 3,3'-positons of the BINOL backbone.[43,73] Typical examples include 2,4,6-triisopropylphenyl, triphenylsilyl, and 9-anthracenyl, among others. On occasion, however, too much bulkiness (or particularly large substrates) can prevent the reaction from occurring (Figure 19 (c))[74] or lead to reversed enantioselectivities.[75] Thus in designing phosphoric acid catalysts, the Goldilocks approach needs to be adopted. That is, the substituents at the 3,3'-positions need to be not too large or too small, but just right, this is typically determined experimentally by trial and error.[48b,76]

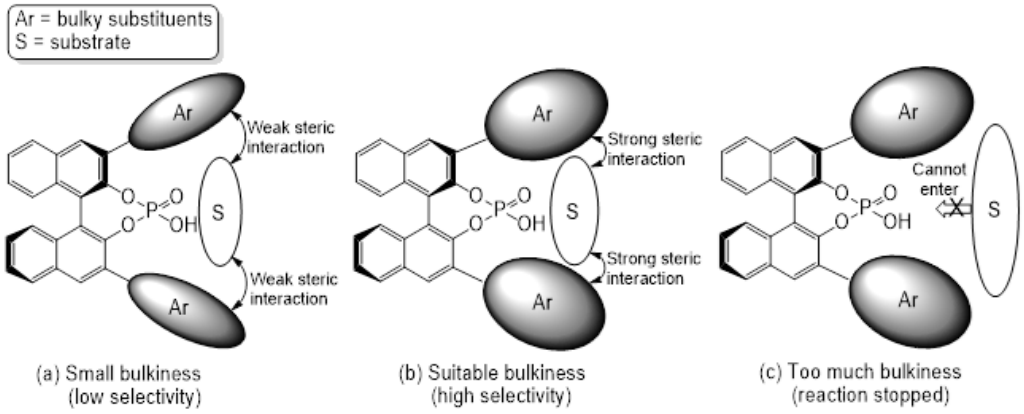

Figure 19. Relationship between catalyst bulkiness and reaction selectivity.

Reid and Goodman introduced the idea of a remote environment angle (AREA(θ)) as a steric parameter to evaluate the size of the chiral cavity in BINOL-derived phosphoric acid catalysts. AREA(θ) was defined as the smallest angle between the center of a 3,3'-substituent atom and the vector from the center of the phosphorus atom to the midpoint of the two adjacent oxygen atoms. Obviously, small 3,3'-substituents provide a large AREA(θ), and big groups correspond to a small AREA(θ) (Figure 20).

Accurate AREA(θ) values are most easily obtained by computations.[76]

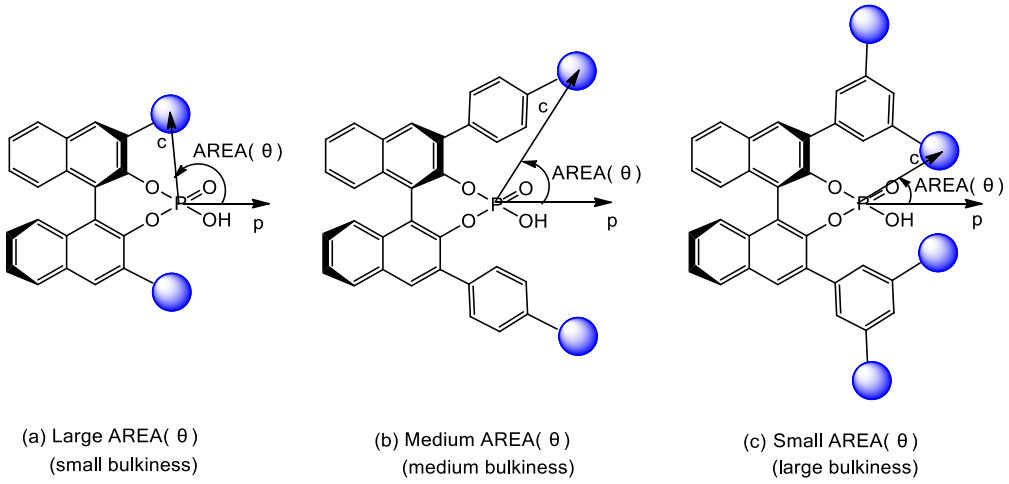

Figure 20. Relationship between AREA(θ) and bulkiness of 3,3'-substituents.

In Uraguchi and Tereda's study, a Mannich reaction was catalyzed by a series of chiral phosphoric acids with different 3,3'-substituents on the BINOL scaffold. A good correlation between computed AREA(θ) values and experimental enantioselectivity data was found. Apparently, a decreasing AREA(θ), which corresponds to a larger sized substituent, led to an improved ee (Figure 21).[45,76]

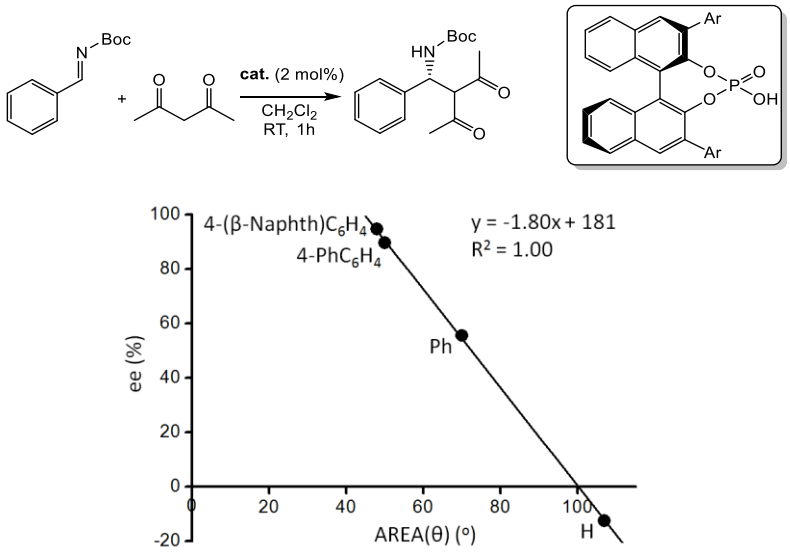

Figure 21. Relationship between AREA(θ) and enantiomeric excess for a Mannich reaction.

Besides the bulkiness of substituents at the 3,3'-positions of the BINOL scaffold, the promotion of appropriate activation modes is also crucial for high enantioselectivity. The lack of appropriate functionality usually leads to little or no product selectivity.[34,77] For example, Itoh et al. investigated the Friedel-Crafts alkylation of indole and *trans*-*β*-nitrostyrene. At -35 °C, after 48 h, the alkylation of indole gave a 76% yield and 91% ee whereas the reaction with *N*-methylindole gave an 11% yield of racemic product (Scheme 19). This difference was attributed to the presence or absence of an interaction between the phosphoryl oxygen and N-H group of indole. The difference in the results between indole and *N*-methylindole emphasizes the importance of the secondary functional group in the catalyst (i.e., the phosphoryl oxygen).[78]

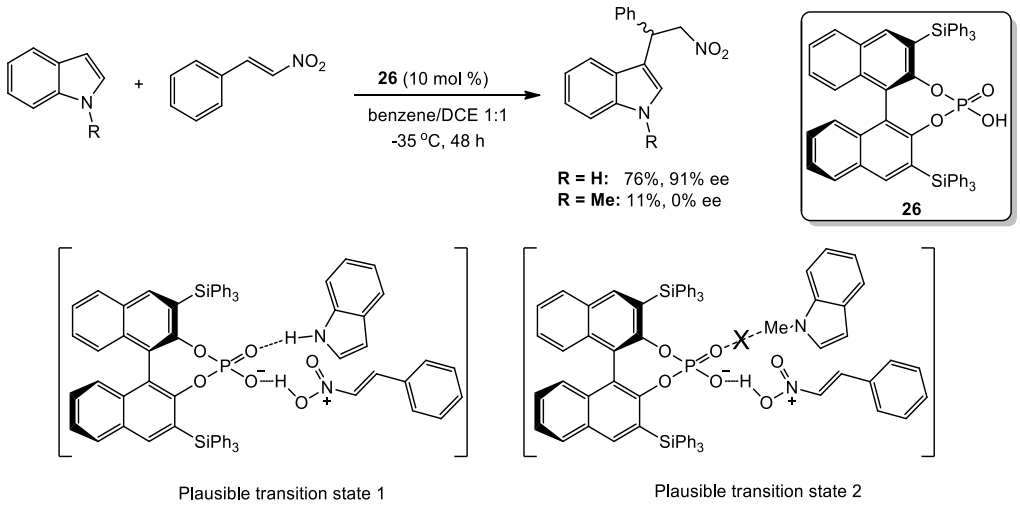

Scheme 19. Friedel-Crafts alkylation emphasizing the hydrogen bond formed between the phosphoryl oxygen and indole.

Hatano et al. presented their investigation into the impact of salt impurities on phosphoric acid catalysts. The replacement of the acidic proton by a metal cation leads to the disappearance of hydrogen bonding between the catalyst and substrate, and this had a substantial impact on the reactivity of a Mannich-type reaction (Scheme 20). Interestingly, a metal cation can lead to improved enantioselectivities in some cases due to Lewis acid interactions.[79]

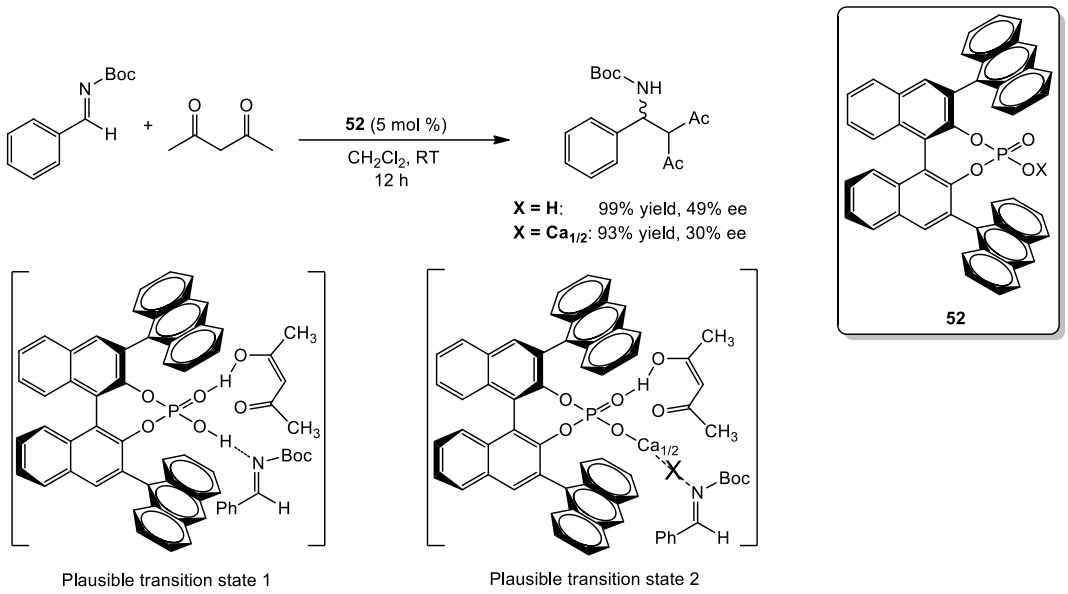

Scheme 20. Mannich-type reaction emphasizing the role of the acidic hydrogen in a phosphoric acid catalyst.

1.6. Focus of This Work

In this dissertation, the powerful acidity enhancement strategy of introducing cationic groups to a catalyst structure is employed in the design of highly activated phosphoric acids. Chapter 2 demonstrates the synthesis of the simplest charge-containing phosphoric acids by replacing one or both of the phenyl groups in diphenyl phosphate (DPP) with 3-*N*-octylpyridinium rings. These species were then compared to DPP in several different transformations. Chapter 3 presents the expansion of this strategy to chiral BINOL-derived phosphoric acids. The procedures for incorporating triaryl phosphonium groups into the catalyst scaffold are introduced, followed by the application of these species in the Friedel-Crafts reactions between indoles and trifluoroacetophenone derivatives. Screening of catalysts, temperatures, solvents and substrates is presented, and a comparison to noncharged analogues is described. A mechanism based on experimental data is also proposed in this chapter. Chapter 4 reports on the application of phosphonium ion tagged phosphoric acids in a different Friedel-Crafts alkylation of indole by *trans*-*β*-nitrostyrene. A new pyridinium ion containing species was also introduced, which turned out to be not as good as phosphonium ion containing analogues. Further screenings of the reaction conditions using the optimized catalyst led to excellent enantioselectivities, and a subsequent

comparison to conventional noncharged chiral phosphoric acids that have proven to be highly successful is presented. In addition, the mechanism of this transformation is also addressed.

Chapter 2: Electrostatically Enhanced Phosphoric Acids: A Tool in Brønsted Acid Catalysis*

2.1. Background

Brønsted acids are among the most commonly employed catalysts and are used to promote a wide variety of chemical transformations.[1,2] They provide an excellent alternative to transition-metal-containing catalysts in that they tend to be tolerant of water and air and generally are environmentally friendlier.[2,3] Substrate activation commonly takes place by proton transfer or hydrogen bonding, both of which lower the energy of the lowest unoccupied molecular orbitals (LUMO) and facilitate nucleophilic attack.[4,5] Different types of Brønsted acid catalysts with a range of acidities have been developed including thioureas,[6] α,α,α,α-tetraaryl-1,3-dioxolane-4,5-dimethanols (TADDOLs),[7] 1,1'-bi-2-naphthol (BINOL) derivatives,[8] and phosphoric acids,[9] and their utility has been amply demonstrated. Of these compounds, phosphoric acids are inherently the strongest acids, and their structural flexibility enables them to be introduced into rigid organic frameworks. The presence of a phosphoryl oxygen also can serve as a hydrogen bond accepting site, enabling dual or bifunctional activation modes that increase their catalytic potential.[1,9a,10]

Diphenyl phosphate [$(PhO)_2P(O)OH$, DPP] is widely used and can catalyze a variety of transformations such as Friedel-Crafts and Diels-Alder reactions[11,12] and ring-opening polymerizations.[13] Its reactivity is limited due to its modest acidity but can be enhanced by the presence of strong electron-withdrawing groups on the two aromatic rings.[14] More acidic derivatives are of interest given Rueping et al.'s recent report demonstrating the relationship between catalyst acidity and activity.[15] That is, more acidic catalysts led to faster rates of a Nazarov cyclization test reaction.

The incorporation of a positively charged center into phenols and thioureas recently was found to

---

*Reprinted adapted with permission from: Ma, J.; Kass, S. R. *Org. Lett.* **2016**, *18*, 5812-5815. Copyright 2016 American Chemical Society.

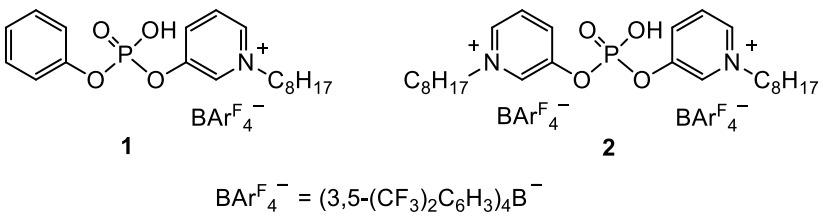

Figure 1. Charged phosphoric acids reported in this study.

enhance their acidities and catalytic reactivities.[16,17] We therefore decided to investigate charge-containing phosphoric acid derivatives of DPP (**1** and **2**, Figure 1) and report the results herein.

2.2. Results and Discussion

Two electrostatically enhanced phosphoric acids **1** and **2** were envisioned in which one or both of the phenyl groups in DPP are replaced by *N*-alkylated pyridinium ions.[18] The positively charged substituents should act as powerful electron-withdrawing groups in low polarity media, but not in polar solvents, and the long-chain octyl groups were selected to enhance the solubility of these salts in solvents such as dichloromethane, chloroform, and toluene. A noncoordinating counteranion is required to avoid deactivating hydrogen bonds with the phosphoryl hydroxyl group, and tetrakis(3,5-bis(trifluoromethyl)phenyl)borate (BAr$^{F}_{4}{}^{-}$) was chosen for this purpose since it also has good solubility and reactivity characteristics.[19-21]

Both catalysts were synthesized as illustrated in Scheme 1 starting with commercially available 3-hydroxypyridine. Its *N*-alkylation with 1-iodooctane afforded the pyridinium iodide salt (**3**) in a reasonable yield (66%) as previously described.[16] Upon reaction of **3** with phenyl dichlorophosphate or phosphorus oxychloride followed by an aqueous hydrolysis, the halide salts corresponding to **1** and **2** were produced (**4** and **5**). Ion exchange with NaBAr$^{F}_{4}$ in CH_2Cl_2 occurred readily since the sodium halide salts are not soluble and precipitate out of solution. A sulfuric acid wash was subsequently carried out to ensure that the target compounds were produced in their protonated form (HCl is not suitable; presumably, it leads to loss of the octyl group) and this was verified via titration.

Scheme 1. Synthetic route for catalysts **1** and **2**.

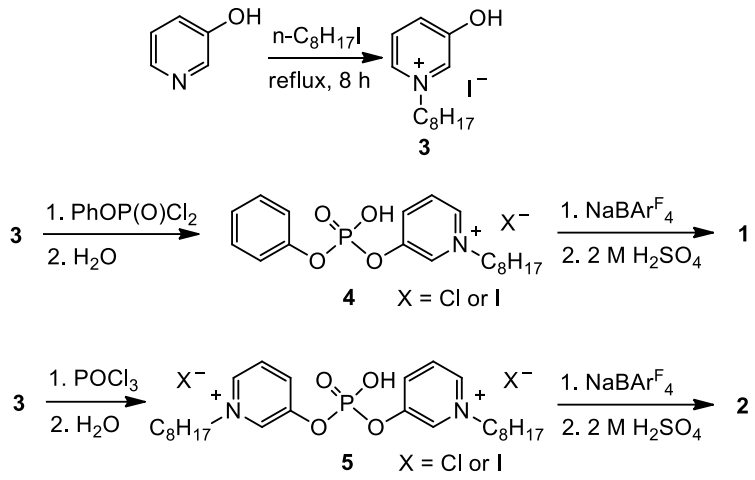

To evaluate the catalytic reactivity of **1** and **2**, the room-temperature Friedel-Crafts alkylation of indole and *N*-methylindole with *β*-nitrostyrene were examined at various catalyst loadings in dichloromethane and chloroform (eq 1). These transformations were monitored by ^{1}H NMR, and the

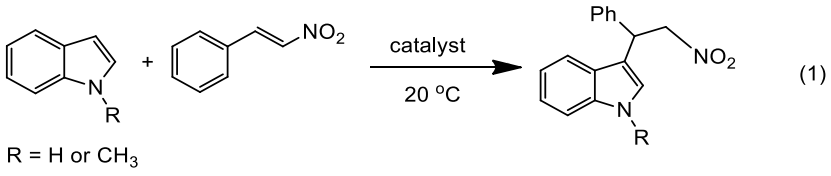

kinetic data displayed second-order behavior as expected. Rate constants, and background corrected half-lives and relative rates under the different conditions that were employed are summarized in Table 1. In the absence of a catalyst, neither indole nor *N*-methylindole reacts with *β*-nitrostyrene in CD_2Cl_2 or $CDCl_3$ for all practical purposes. That is, the reaction half-lives were estimated to be 9 months or more (see Tables S1 and S2 for the kinetic data); a control experiment in which CH_2Cl_2 was washed with H_2SO_4 as done in the preparation of **1** and **2** had no impact on the background rate of the reaction with indole. These transformations are accelerated by 10 mol % of DPP, but it is an ineffective catalyst in that it takes between 3 and 48 weeks for half of the starting material to be converted to product depending upon the reaction conditions. Incorporation of an electron-withdrawing nitro group in DPP

at the 3-position of both phenyl rings [(3-$O_2NC_6H_4O)_2P(O)OH$, DPP*] has a modest accelerating effect corresponding to a factor of 4.5. Monocharged phosphoric acid derivative **1**, however, speeds up the reactions of indole and *N*-methylindole relative to DPP by factors of 12 and 210 in CD_2Cl_2 (entries 4 and 14) and 7.2 and 78 in $CDCl_3$ (entries 10 and 20). These differences can be enhanced by 1 order of magnitude if a second charged center is incorporated into the catalyst. That is, k_2/k_{DPP} = 120 and 2100

Table 1. Kinetic data of Friedel-Crafts reactions.[a]

entry	solvent	R	cat.	mol %	k (M^{-1} h^{-1})	$t_{1/2}$ (h)[b]	k_{rel}[b]
1	CD_2Cl_2	H	-	-	0.000544	19400	-
2	CD_2Cl_2	H	DPP	10	0.0185	587	1.0
3	CD_2Cl_2	H	DPP*	10	0.0813	131	4.5
4	CD_2Cl_2	H	**1**	10	0.215	49.2	12
5	CD_2Cl_2	H	**2**	10	2.06	5.12	120
6	CD_2Cl_2	H	**2**	5.0	0.904	11.7	100[c]
7	CD_2Cl_2	H	**2**	2.0	0.367	28.8	100[c]
8	$CDCl_3$	H	-	-	0.000396	26600	-
9	$CDCl_3$	H	DPP	5.0	0.0203	530	1.0
10	$CDCl_3$	H	**1**	5.0	0.143	74.0	7.2
11	$CDCl_3$	H	**2**	5.0	0.750	14.1	38
12	CD_2Cl_2	Me	-	-	0.000324	32600	-
13	CD_2Cl_2	Me	DPP	10	0.00176	7350	1.0
14	CD_2Cl_2	Me	**1**	10	0.297	35.6	210
15	CD_2Cl_2	Me	**2**	10	3.06	3.45	2100
16	CD_2Cl_2	Me	**2**	5.0	1.39	7.59	1900[c]
17	CD_2Cl_2	Me	**2**	2.5	0.771	13.7	2200[c]
18	$CDCl_3$	Me	-	-	0.00156	6760	-
19	$CDCl_3$	Me	DPP	5.0	0.00286	8110	1.0
20	$CDCl_3$	Me	**1**	5.0	0.103	104	78
21	$CDCl_3$	Me	**2**	5.0	1.13	9.35	870

[a]Both reactant concentrations were 94.8 mM. [b]Background corrected half-lives and relative rates. [c]Linearly corrected for the amount of catalyst.

for indole and *N*-methylindole in CD_2Cl_2 (entries 5 and 15) and 38 and 870, respectively, in $CDCl_3$ (entries 11 and 21). As a result, the half-lives for these reactions are reduced to as little as 3.5 h.

Bifunctional activation brought about by phosphoric acid derivatives has been invoked previously[1,9a,10,22] and would involve a N-H···O=P hydrogen bond when indole is used as the reactant (Scheme S1). With *N*-methylindole, this interaction is absent, and consequently, one might expect this latter transformation to proceed more slowly. This is the case for the DPP-catalyzed reactions where $k_{indole}/k_{N\text{-}methylindole}$ = 13-15 in CD_2Cl_2 and $CDCl_3$. When **1** and **2** were used, $k_{N\text{-}methylindole}/k_{indole}$ = 1.4−1.5 except for when the former catalyst is used in $CDCl_3$, then $k_{indole}/k_{N\text{-}methylindole}$ = 1.4. These results are consistent with bifunctional activation being involved in the rate-determining step when DPP is used, but it is unclear if this is important with the charge-containing phosphoric acids. These species undoubtedly are more acidic than DPP, and thus, their N-H···O=P hydrogen bonds should be weaker. However, *N*-methylindole is more nucleophilic than indole, and this could counterbalance the loss of the hydrogen bond when **1** and **2** are used.

A small solvent effect (≤∼2) is observed for the Friedel-Crafts reactions when CD_2Cl_2 and $CDCl_3$ are used. If DPP is the catalyst, the background corrected rate constants are ∼2 times larger in the latter solvent upon making a 2-fold linear correction for the catalyst loading (i.e., 5 vs 10 mol %). In contrast, this transformation takes place 1.2-1.5 times faster in the former medium when **1** and **2** are employed, except for when **1** is used in the reaction with indole and then k_{CDCl3}/k_{CD2Cl2} = 1.3. Presumably the more polar solvent tends to lead to faster reactions with the charged catalysts, as observed with charged thioureas,[17] because it stabilizes the polar transition state. Lack of solubility under the reaction conditions prevented toluene from being explored, but **2** was found to be unreactive in THF-d_8 since it is a hydrogen bond acceptor and a more polar solvent. Chlorobenzene is also a poorer solvent for this reaction than CD_2Cl_2 and $CDCl_3$ even though it is less polar by some measures.[23,24]

Catalyst loading was examined with **2** in CD_2Cl_2 (entries 5-7 and 15-17), and smaller amounts of it led to slower transformations with both indole and *N*-methylindole. Linear relationships between the mol % of **2** and the background-corrected reaction rate constants are observed in both cases (Figure S1). This indicates that these Friedel-Crafts reactions are first order in catalyst, which contrasts with the

second-order behavior reported for a charged thiourea.[17]

To examine the catalytic abilities of **1** and **2** further, Diels-Alder reactions between 1,3-cyclopentadiene and methyl vinyl ketone (MVK) or acrylonitrile (AN) were carried out (eq 2).

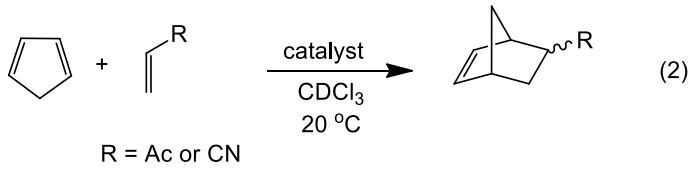

(2)

These reactions were monitored by ^{1}H NMR to obtain the reactant and product concentrations at different times (Table S3). Both transformations displayed second-order behavior, and the resulting data are summarized in Table 2. For the reaction with MVK, 1.0 mol % of DPP was found to be a very poor catalyst as the rate constant is only 25% larger than for the noncatalyzed transformation (entries 1 and 2). DPP* is almost 20 times more reactive (entry 3), but the *endo*/*exo* selectivity for these three processes is the same. Our monocharged phosphoric acid, however, is 1000 times more active than DPP (entry 4) and reduces the reaction half-life to under 5 min. It also increases the *endo*/*exo* ratio from 81:19 to 88:12 as commonly observed with Lewis acids.[25] The doubly charged derivative is even better in that it is 2500 times more reactive than DPP and $t_{1/2}$ = 1.5 min without any loss in the diastereoselectivity relative to **1** (entry 5). Moreover, a reduced catalyst loading of 0.1 mol % still leads to a very efficient transformation (i.e., $t_{1/2}$ = 17 min) without any falloff in the selectivity.

Similar results were obtained for the Diels-Alder reaction between 1,3-cyclopentadiene and acrylonitrile, but all three catalysts (DPP, **1** and **2**) are less effective. Diphenyl phosphate only enhances the reaction rate of the noncatalyzed process by 7% (entries 7 and 8), and this difference is well within the experimental uncertainties of the two measurements; we estimate the errors in the rate constants to be ±10%. There is also no change in the observed *endo*/*exo* ratio of 65:35, and thus, 1 mol % of DPP has little, if any, effect on this reaction. An equivalent amount of **1** does speed up the transformation and

Table 2. Kinetic data of Diels-Alder reactions.[a]

entry	R	cat.	mol %	k (M^{-1} h^{-1})	$t_{1/2}$ (h)[b]	*endo*/*exo*	k_{rel}[b]
1	Ac	-	-	0.660	15.2	81:19	-
2	Ac	DPP	1.0	0.823	61.3	81:19	1.0
3	Ac	DPP*	1.0	3.89	3.26	82:18	19
4	Ac	**1**	1.0	163	3.7 min	88:12	1000
5	Ac	**2**	1.0	412	1.5 min	88:12	2500
6	Ac	**2**	0.10	35.9	17 min	87:13	-
7	CN	-	-	0.0689	143	65:35	-
8	CN	DPP	1.0	0.0744	2170	65:35	1.0
9	CN	**1**	1.0	0.119	203	70:30	11
10[a]	CN	**2**	1.0	0.302	43	75:25	50
11[a]	CN	**2**	5.0	1.58	6.6	76:24	-

[a]Both reactant concentrations were 100 mM. [b]Background corrected half-lives and relative rates.

improves the diastereoselectivity, but the reaction is still slow with an observed nonbackground corrected half-life of 84 h and an *endo*/*exo* ratio of 70:30 (entry 9). This kinetic acceleration, however, does correspond to a factor of 11 compared to DPP. A further improvement is found with the doubly charged catalyst **2** in terms of the rate (k_2/k_{DPP} = 50) and the product selectivity (*endo*/*exo* = 75:25, entry 10). The apparent half-life for this reaction is 33 h, but this is for a 1 mol % loading, and when 5 mol % is employed (entry 11) this decreases to 6.6 h.

A ring-opening polymerization of δ-valerolactone with benzyl alcohol as the initiator in four different solvents was examined (eq 3) since this is an important process in which DPP is commonly used.[13,26]

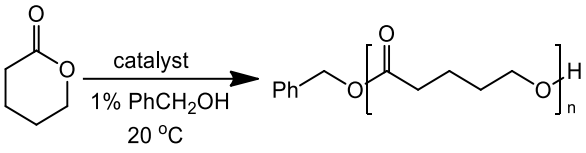

(3)

The conversion of the monomer in these living polymerizations was followed by ^{1}H NMR (Table S4), and the data can be fit using a first-order kinetic model.[13,27,28] No conversion was observed over the

course of one month in the absence of a catalyst, whereas the ring-opening polymerization is facile when 0.5 mol % of DPP or **2** is used. Rate constants for the propagation stage are provided along with reaction half-lives and relative rates in Table 3. In all four solvents, our doubly charged catalyst outperforms DPP by a factor of about two. The actual reaction rates vary by a factor of 12 regardless of the catalysts with the faster processes occurring in benzene-d_6 and toluene-d_8 and the slower ones taking place in CD_2Cl_2 and $CDCl_3$. When smaller concentrations of the monomer are used, the polymerization takes longer but k_{rel} increases. This was also observed for the Friedel-Crafts and Diels-Alder reactions presumably because the reactants are more polar than the solvent and enhance the polarity of the medium.

The effects of the two catalysts on the number-average molecular weights ($M_{n,NMR}$) of the polymers at different conversions were also investigated by ^{1}H NMR. In all four solvents, $M_{n,NMR}$ was found to be similar at equivalent conversions of the monomer regardless of the catalyst (Figure S2).

Table 3. Kinetic data of polymerizations.[a]

entry	solvent	cat.	k (h^{-1})	$t_{1/2}$ (h)	k_{rel}
1	$C_6D_5CD_3$	DPP	0.444	1.6	1.0
2	$C_6D_5CD_3$	**2**	0.833	0.8	1.9
3	C_6D_6	DPP	0.325	2.1	1.0
4	C_6D_6	**2**	0.574	1.2	1.8
5	CD_2Cl_2	DPP	0.0380	18	1.0
6	CD_2Cl_2	**2**	0.0759	9.1	2.0
7	$CDCl_3$	DPP	0.0460	15	1.0
8	$CDCl_3$	**2**	0.108	6.4	2.3

[a]Experiments performed with 0.5 M δ-valerolactone, 1.0 mol % of $PhCH_2OH$, and 0.5 mol % of the catalyst.

2.3. Conclusion

In summary, we successfully designed and synthesized two electrostatically enhanced phosphoric acid derivatives (**1** and **2**). To the best of our knowledge, these compounds are the first examples of phosphoric acids with positively charged centers incorporated to enhance their acidities and catalytic

abilities in nonpolar media. This was evaluated by investigating a series of acid-catalyzed processes and comparing the catalytic efficiencies of **1** and **2** with diphenyl phosphate (DPP) and di(3-nitrophenyl) phosphate (DPP*), their noncharged analogues. Impressively, both charged phosphoric acid derivatives out-performed DPP and DPP* in all of the reactions that were examined, in some cases by more than 3 orders of magnitude. Extension of this strategy to other Brønsted acid catalysts such as chiral phosphoric acid derivatives is a promising research avenue and currently is the focus of ongoing efforts in our group.

2.4. Experimental Section

2.4.1. General Information

Reactions were carried out in 120 ˚C oven-dried glassware including nuclear magnetic resonance (NMR) tubes. Chemical reagents were used as supplied unless otherwise noted and came from Sigma-Aldrich except for sodium tetrakis(3,5-bis(trifluoromethyl)phenyl)borate which was obtained from Matrix Scientific. Deuterated solvents were purchased from Cambridge Isotope Laboratories except for tetrahydrofuran-d_8 which was supplied by Sigma-Aldrich. Flash chromatography purifications were performed with a CombiFlash® Rf automated flash chromatography system equipped with RediSep Rf gold® normal-phase 40 g silica gel columns manufactured by Teledyne Isco. Inc. A standard flow rate of 40 mL min^{-1} was employed and linear gradients were used in switching from one solvent to another; when two times are given the first is the duration of the linear gradient and the second is the length of time that the eluent was used. Proton, carbon, fluorine and phosphorous nuclear magnetic resonance spectra were recorded with Varian Inova 500 MHz and Bruker Avance III HD Nanobay 400 MHz instruments. Chemical shifts are reported in ppm (δ) and were referenced as follows: ^{1}H spectra, $CDCl_3$ (7.27 δ), CD_2Cl_2 (5.32 δ), C_6D_6 (7.16 δ), $C_6D_5CD_3$ (7.09 δ) and THF-d_8 (3.58 δ); ^{13}C spectra, $CDCl_3$ (77.0 δ), CD_2Cl_2 (54.0 δ) and DMSO-d_6 (39.5 δ); ^{19}F spectra, CF_3COOH (-76.55 δ, external calibrant); ^{31}P spectra, 85% H_3PO_4 in H_2O (0.00 δ, external calibrant). IR spectra were obtained with an attenuated total reflectance (ATR) source using a Nicolet iS5 Fourier transform infrared (FT-IR) spectrometer. High-resolution electrospray ionization mass spectra (HRMS-ESI) were recorded with a Bruker ESI-BioTOF mass spectrometer from methanolic solutions containing polyethylene glycol as an internal

standard.

2.4.2. Synthesis Procedures

*N-Octyl-3-hydroxypyridinium iodide (**3**).* 3-Hydroxypyridine (1.00 g, 10.5 mmol) was transferred into a 250 mL round bottomed flask under a dry nitrogen atmosphere and 30 mL isopropanol was added with stirring. The resulting suspension was heated to 40 ˚C with an oil bath and when the solid dissolved, 1.90 mL (2.53 g, 10.5 mmol) of 1-iodooctane was quickly added via syringe and the temperature was increased to 110 ˚C. After refluxing the reaction mixture for 8 h it was allowed to cool to room temperature and the solvent was removed with a rotary evaporator to afford an orange oil. Purification by medium pressure liquid chromatography (MPLC) was carried out with CH_2Cl_2 (10 min), EtOAc (2 and 10 min) and 1 : 1 EtOAc/MeOH (15 and 5 min) to afford 2.32 g (66%) of the title compound as a viscous yellow oil. ^{1}H NMR (500 MHz, CD_2Cl_2) δ 8.58 (s, 1H), 8.11 (d, *J* = 5.9 Hz, 1H), 8.01 (d, *J* = 8.3 Hz, 1H), 7.72 (dd, *J* = 5.9 and 8.8 Hz, 1H), 4.48 (t, *J* = 7.8 Hz, 2H), 2.00 (m, 2H), 1.29 (m, 11H), 0.87 (t, *J* = 6.4 Hz, 3H). ^{13}C NMR (100 MHz, CD_2Cl_2) δ 161.2, 133.3, 133.2, 132.8, 128.7, 62.8, 32.2, 31.9, 29.5, 29.4, 26.6, 23.1, 14.3. HRMS-ESI: calcd for $C_{13}H_{22}NO^+$ $(M - I^-)^+$ 208.1696, found 208.1685.

*Phenyl 1,3-N-octylpyridinium phosphate iodide/chloride (**4**).* *N*-Octyl-3-hydroxypyridinium iodide (1.00 g, 2.98 mmol) was added into a 250 mL round bottomed flask under a dry nitrogen atmosphere and dissolved in 30 mL of anhydrous acetonitrile with stirring. When the resulting solution became homogeneous, 490 µL of phenyl dichlorophosphate (0.692 g, 3.28 mmol) was slowly added via syringe. After gentle reflux for 10 h the reaction mixture was allowed to cool to room temperature and quenched with 5 mL of H_2O. The resulting solution was stirred for 15 min and concentrated under reduced pressure to afford a yellowish oil. It was then dissolved in 30 mL of CH_2Cl_2 and extracted with H_2O (30 mL) and brine (30 mL) before being dried over Na_2SO_4. Purification by MPLC using EtOAc (10 min) and 1 : 1 EtOAc/MeOH (15 and 5 min) gave 0.96 g (72%, assuming a 1 : 1 Cl^-/I^- ratio) of **4** as a white solid (mp 117 - 120 ˚C). ^{1}H NMR (500 MHz, CD_2Cl_2) δ 9.03 (s, 1H), 8.34 (d, *J* = 7.8 Hz, 1H), 8.24 (d, *J* = 5.4 Hz, 1H), 7.80 (dd, *J* = 5.9 and 8.3 Hz, 1H), 7.23 (t, *J* = 7.9 Hz, 2H), 7.18 (d, *J* = 7.8 Hz, 2H), 7.03 (t, *J* = 7.3 Hz, 1H), 4.51 (t, *J* = 7.9 Hz, 2H), 2.39 (bs, 1H, OH), 1.91 (m, 2H), 1.27 (m, 10H), 0.86 (t, *J* = 6.8 Hz,

3H). ^{13}C NMR (100 MHz, CD_2Cl_2) δ 155.0, 153.6, 137.7, 137.5, 136.5, 129.7, 128.8, 123.9, 120.9, 62.8, 32.2, 32.1, 29.50, 29.46, 26.6, 23.1, 14.3. ^{31}P NMR (162 MHz, CD_2Cl_2) δ -11.04. HRMS-ESI: calcd for $C_{19}H_{27}NO_4P^+$ $(M - X^-)^+$ 364.1672, found 364.1663.

*Phenyl 1,3-N-octylpyridinium phosphate tetrakis(3,5-bis(trifluoromethyl)phenyl)borate (**1**).* Phenyl 1,3-*N*-octylpyridinium phosphate iodide/chloride (0.100 g, 0.208 - 0.250 mmol) and sodium tetrakis(3,5-bis(trifluoromethyl)phenyl)borate (0.221 g, 0.250 mmol) were mixed together in a 20 mL vial and dissolved in 8 mL of anhydrous CH_2Cl_2. Molecular sieves (4 Å, 0.2 g) that had been activated at 300 ˚C overnight were added and the resulting solution was stirred at 20 ˚C for 3 h. A sodium halide precipitate formed and was filtered through a syringe containing a 0.45 µm polytetrafluorethylene (PTFE) membrane. The reaction mixture was subsequently washed 3 times with 8 mL portions of 2.0 M H_2SO_4 and then with H_2O until the aqueous layer became pH neutral. Sodium sulfate was used to dry the CH_2Cl_2 and then it was concentrated under reduced pressure to afford 0.24 g (85%) of **1** as a yellow solid (mp 63 - 66 ˚C). ^{1}H NMR (500 MHz, CD_2Cl_2) δ 8.64 (s, 1H), 8.28 (d, *J* = 8.3 Hz, 1H), 8.18 (d, *J* = 5.9 Hz, 1H), 7.85 (dd, *J* = 6.4 and 8.3 Hz, 1H), 7.72 (s, 8H), 7.55 (s, 4H), 7.31 (t, *J* = 7.3 Hz, 2H), 7.20 (t, *J* = 7.4 Hz, 1H), 7.16 (d, *J* = 7.8 Hz, 2H), 4.66 (bs, 1H, OH), 4.41 (t, *J* = 7.8 Hz, 2H), 1.93 (m, 2H), 1.24 (m, 10H), 0.85 (t, *J* = 6.9 Hz, 3H). ^{13}C NMR (100 MHz, CD_2Cl_2): δ 162.3 (q, $^1J_{B\text{-}C}$ = 49.6 Hz), 152.6, 150.8, 139.4, 138.0, 137.4, 135.4, 130.7, 130.0, 129.4 (qq, $^3J_{B\text{-}C}$ = 2.9 Hz, $^2J_{F\text{-}C}$ = 31.4 Hz), 126.6, 125.2 (q, $^1J_{F\text{-}C}$ = 270 Hz), 120.4, 118.1 (septet, $^3J_{F\text{-}C}$ = 3.3 Hz), 64.1, 32.1, 31.9, 29.4, 29.2, 26.5, 23.0, 14.2. ^{19}F NMR (376 MHz, CD_2Cl_2) δ -62.77. ^{31}P NMR (162 MHz, CD_2Cl_2) δ -13.13. HRMS-ESI: calcd for $C_{19}H_{27}NO_4P^+$ $(M - BArF_4^-)^+$ 364.1672, found 364.1663, calcd for $C_{32}H_{12}BF_{24}^-$ ($BAr^F{}_4^-$) 863.0654, found: 863.0693.

*Di(1,3-N-octylpyridinium) phosphate iodide/chloride (**5**).* *N*-Octyl-3-hydroxypyridinium iodide (1.00 g, 2.98 mmol) was added into a 250 mL round bottomed flask under N_2 and mixed with 30 mL of anhydrous acetonitrile. When the salt dissolved into this stirred solution, 130 µL of phosphorus oxychloride (0.214 g, 1.39 mmol) was injected in one portion into the flask and the reaction mixture was heated to 100 - 105 ˚C and refluxed for 10 h. Upon cooling to room temperature, 5 mL of H_2O was added and the resulting solution was stirred for an additional 15 min. It was subsequently concentrated

with a rotary evaporator to give a sticky brown oil which was dissolved in 30 mL of CH_2Cl_2, washed with H_2O (30 mL) and brine (30 mL), dried over Na_2SO_4 and concentrated under reduced pressure. Purification by MPLC using CH_2Cl_2 (10 min), EtOAc (2 and 5 min) and then 1 : 1 EtOAc/MeOH (15 and 5 min) afforded 0.55 g (62% assuming a 1 : 1 Cl^-/I^- ratio) of a light yellow solid (mp 61 - 63 ˚C). ^{1}H NMR (500 MHz, $CDCl_3$) δ 9.36 (s, 2H), 8.59 (d, *J* = 8.8 Hz, 2H), 8.35 (d, *J* = 5.9 Hz, 2H), 7.95 (dd, *J* = 5.9 and 8.3 Hz, 2H), 4.78 (t, *J* = 7.3 Hz, 4H), 2.60 (bs, 1H, OH), 2.01 (m, 4H), 1.29 (m, 20H), 0.87 (t, *J* = 6.9 Hz, 6H). ^{13}C NMR (100 MHz, $CDCl_3$) δ 152.9, 138.3, 137.5, 136.9, 128.7, 62.5, 31.52, 31.50, 28.9, 28.8, 26.0, 22.4, 13.9. ^{31}P NMR (162 MHz, $CDCl_3$) δ -12.88. HRMS-ESI: calcd for $C_{26}H_{42}N_2O_4P^+$ $(M - H^+ - 2X^-$, X = Cl and I$)^+$ 477.2877, found 477.2886.

*Di(1,3-N-octylpyridinium) phosphate tetrakis(3,5-bis(trifluoromethyl)phenyl)borate (**2**).* In a 20 mL vial, di(1,3-*N*-octylpyridinium) phosphate iodide/chloride (0.100 g, 0.137 - 0.182 mmol) and sodium tetrakis(3,5-bis(trifluoromethyl)phenyl)borate (0.323 g, 0.364 mmol) were mixed together and dissolved in 8 mL of anhydrous CH_2Cl_2. Activated 4 Å molecular sieves that had been dried at 300 ˚C overnight were added and the reaction mixture was stirred at room temperature for 3 h. During this time the sodium halide salt precipitated and then the white solid was filtered away by passing the CH_2Cl_2 solution through a syringe with a 0.45 µm PTFE membrane. The organic material was washed 3 times with 8 mL of 2.0 M sulfuric acid followed by water until the aqueous phase became pH neutral. It was then dried with Na_2SO_4 and concentrated under reduced pressure to give 0.30 g (86%) of a yellow solid (mp 48 - 50 ˚C). ^{1}H NMR (500 MHz, CD_2Cl_2) δ 8.62 (s, 2H), 8.26 (d, *J* = 8.3 Hz, 2H), 8.13 (d, *J* = 5.9 Hz, 2H), 7.76 (dd, *J* = 5.9 and 8.3 Hz, 2H), 7.71 (s, 16H), 7.55 (s, 8H), 4.40 (t, *J* = 7.8 Hz, 4H), 2.15 (bs, OH), 1.94 (m, 4H), 1.26 (m, 20H), 0.85 (t, *J* = 6.9 Hz, 6H). ^{13}C NMR (100 MHz, DMSO-d_6) δ 160.9 (q, $^1J_{B\text{-}C}$ = 49.6 Hz), 152.5, 139.2, 137.3, 136.1, 136.0, 134.0, 128.3 (qq, $^3J_{B\text{-}C}$ = 2.9 Hz, $^2J_{F\text{-}C}$ = 31.4 Hz), 124.0 (q, $^1J_{F\text{-}C}$ = 270 Hz), 117.6 (septet, $^3J_{F\text{-}C}$ = 3.3 Hz), 61.0, 31.1, 30.7, 28.4, 28.3, 25.4, 22.0, 13.8. ^{19}F NMR (376 MHz, CD_2Cl_2) δ -62.74. ^{31}P NMR (162 MHz, CD_2Cl_2) δ -13.28. ATR-IR: 2936, 2862, 1610, 1501, 1353, 1272, 1108, 838, 681 cm^{-1}. HRMS-ESI: calcd for $C_{26}H_{42}N_2O_4P^+$ $(M - H^+ - 2BAr^F{}_4^-)^+$ 477.2877, found 477.2899. calcd for $C_{32}H_{12}BF_{24}^-$ ($BAr^F{}_4^-$) 863.0654, found 863.0622.

Di(3-nitrophenyl) phosphate (DPP).* 3-Nitrophenol (0.500 g, 3.59 mmol) was dissolved in 25 mL of

anhydrous acetonitrile in a 100 mL round bottomed flask under a dry nitrogen atmosphere. Pyridine (0.87 mL, 0.854 g, 10.8 mmol) was injected into the flask in one portion, followed by the rapid addition of phosphorus oxychloride (0.17 mL, 0.276 g, 1.80 mmol). The resulting solution was gently refluxed for 14 h and then the volatile material was removed with a rotary evaporator. Extraction of the residue with 30 mL of CH_2Cl_2 resulted in an organic solution that was washed with 30 mL of water, 30 mL of brine, and then dried over Na_2SO_4. Purification of the concentrated residue was carried out by MPLC with 1:1 hexanes/CH_2Cl_2 (1 min) and CH_2Cl_2 (10 min and 10 min). Upon rotary evaporation, the desired material was dissolved in 3 mL of $CHCl_3$ in a 18 × 23 mm vial and 3 mL of 2 M H_2SO_4 was added. This solution was heated to 50 ˚C and stirred for 4 h, after which the organic layer was separated, washed with water until the aqueous layer became pH neutral, and dried over Na_2SO_4. Concentration under reduced pressure afforded 0.19 g (31%) of a white solid (mp 105 - 107 ˚C). ^{1}H NMR (500 MHz, CD_2Cl_2): δ 8.16 (d, *J* = 7.8 Hz, 2H), 8.13 (s, 2H), 7.67 (d, *J* = 8.3 Hz, 2H), 7.64 (t, *J* = 7.8 Hz, 2H), 1.61 (s, OH). ^{13}C NMR (100 MHz, CD_2Cl_2) : δ 150.7, 150.6, 131.7, 126.9, 121.8, 116.2. ^{31}P NMR (162 MHz, CD_2Cl_2): δ -18.53. HRMS-ESI: calcd for $C_{12}H_8N_2O_8P^-$ $(M - H^+)^-$ 339.0024, found 339.0026.

2.4.3. Kinetic Studies

Preparation of 20 mM Catalyst Stock Solutions. Catalysts **1** (0.1280 g, 0.1043 mmol) and **2** (0.1443 g, 0.06547 mmol) were placed in separate 23 × 85 mm vials and dissolved in 5.22 and 3.27 mL of CH_2Cl_2, respectively. The vials were capped, sealed with parafilm and stored in a freezer at –20 ˚C until needed.

General Procedure for Friedel-Crafts Kinetic Studies. In a dry 15 × 45 mm vial, 427 µL (for a 10 mol % catalyst loading) of a 20 mM catalyst solution was added and the solvent (CH_2Cl_2) was removed under vacuum. A second dry 15 × 45 mm vial was filled with 10.0 mg (0.0854 mmol)of indole or 11.2 mg (0.0854 mmol) of *N*-methylindole and 12.8 mg (0.0854 mmol) of *trans-β*-nitrostyrene and was dissolved in 900 µL of CD_2Cl_2, $CDCl_3$, THF-d_8 or C_6H_5Cl to afford 94.8 mM solutions; smaller amounts of the reactants were used to produce lower concentrations. After stirring for 30 s and upon complete dissolution of the reactants, this material was transferred via syringe to the catalyst-containing vial. The

resulting solution was vigorously shaken to ensure good mixing and the starting time was recorded. This material was transferred to an oven-dried NMR tube for kinetic measurements and the reaction progress was monitored by ^{1}H NMR using the relative integration of the signals at 6.58 (indole), 6.51 (*N*-methylindole) and 4.96 (both products) δ; in THF-d_8 these resonances are at 6.39 (indole) and 5.08 (products). The one exception was for the chlorobenzene experiments in which the solvent was changed for the kinetic measurements to $CDCl_3$. For slow reactions taking ≥ 24 h, additional solvent was added at 24 h intervals to maintain the total volume at 900 µL due to small changes caused by evaporation.

General Procedure of Kinetic Studies of Diels-Alder Reactions. Cyclopentadiene was freshly prepared by cracking dicyclopentadiene at 190 ˚C and fractionally distilling it between 37 - 45 ˚C; the purity was verified by ^{1}H NMR and found to be ≥ 99.8 %. In a dry 15 × 45 mm vial, 63.5 mg (80.8 µL and 0.960 mmol) of cyclopentadiene was measured out with a microliter syringe, the vial was immediately capped and 2400 µL of $CDCl_3$ was added. In another dry 15 × 45 mm vial, 67.2 mg (79.9 µL and 0.960 mmol) of methyl vinyl ketone or 51.0 mg (63.0 µL and 0.960 mmol) of acrylonitrile was weighed out and immediately dissolved into 2400 µL of $CDCl_3$. To a third vial of the same size, 400 µL of the 20 mM catalyst stock solution was added for a 1.0 mol % loading and the solvent was removed under vacuum. The catalyst was redissolved in 400 µL of $CDCl_3$ and added to a NMR tube containing 200 µL of the cyclopentadiene solution and an equal volume of the methyl vinyl ketone or acrylonitrile solution (this affords 100 mM reactant concentrations) with vigorous mixing for ~5 - 10 sec. The initial time was recorded and the reaction progress was monitored by ^{1}H NMR. For the reaction with methyl vinyl ketone, the reaction progress was determined by integrating the signals at 6.47 (cyclopentadiene) and 5.86 (product) δ and the *endo*:*exo* ratio was obtained using the product resonances at 2.22 (*exo*) and 2.14 (*endo*) δ. For the transformation with acrylonitrile, the signals at 5.67 (acyrlonitrile) and 3.24 (product) δ were used to measure the rate constants and the absorptions at 3.24 (*endo* and *exo*) and 2.85 (*endo*) δ were used to obtain the *endo*:*exo* ratios.

General Procedure of Kinetic Studies of Ring-opening Polymerizations. In a dry 15 × 45 mm vial, 800 mg (8.00 mmol) of *δ*-valerolactone was weighed out and 8.4 µL (8.7 mg, 0.080 mmol) of benzyl alcohol was added via a 10 µL syringe. This mixture was stirred for 10 min at room temperature and

then 40 mg portions were weighed out into four 15 × 45 mm vials and 800 µL of a deuterated solvent was added in each case in order to afford 0.50 M monomer solutions; more or less of the lactone solution was used to produce different concentrations. Four different 15 × 45 mm vials were each charged with 100 µL portions of the 20 mM stock solution of the catalyst and the solvent was removed under reduced pressure. The monomer containing solutions were then transferred into these vials, these mixtures were shaken for 10 s and then transferred into NMR tubes. Each reaction was monitored by 1H NMR using the δ-valerolactone signals at 3.64 (toluene-d_8), 3.60 (benzene-d_6), 4.28 (CD_2Cl_2) and 4.32 ($CDCl_3$) δ and polymer resonances at 3.93 & 3.42 (toluene-d_8), 3.94 & 3.42 (benzene-d_6), 4.03 & 3.58 (CD_2Cl_2) and 4.05 & 3.62 ($CDCl_3$) δ, where the first chemical shift is for the polymer chain CH_2's excluding the end group and the latter one is for the CH_2 end group. The number-average molecular weights were determined using the polymer signals just noted and the initiator (benzyl alcohol) resonances at 4.95 (toluene-d_8), 4.99 (benzene-d_6), 5.07 (CD_2Cl_2) and 5.09 ($CDCl_3$) δ.

2.4.4. Catalyst Titration

A NaOH pellet (0.198 g, 4.95 mmol) was weighed in a 23 × 85 mm vial and dissolved in 5.0 mL of deionized water. It was then diluted with 9.9 mL of methanol and stirred to afford the titrant solution. Catalyst **2** (0.735 g, 0.333 mmol) was placed in a second vial and 1.0 mL of methanol was added with stirring. The titrant was added to the catalyst solution in 0.05 mL portions using a 1.0 mL syringe and the pH was measured after each addition using pH paper. The endpoint was observed after adding 0.95–1.00 mL of the titrant indicating that the phosphoric acid was 95–100% protonated.

Chapter 3: Asymmetric Arylation of 2,2,2-Trifluoroacetophenones Catalyzed by Chiral Electrostatically-Enhanced Phosphoric Acids*

3.1. Background

Indoles are among the most important type of nitrogen-containing heterocyclic scaffolds, as they are widely found in natural products,[1] pharmaceuticals[2] and synthetic chemicals.[3] Most of these indole-based compounds possess special chemical properties as well as bioactivities, and thus, they have attracted widespread attention.[4] Fluorinated species are another important class of organic materials since the small size and high electronegativity of a fluorine atom lead to compounds with remarkably different properties than their fluorine-free analogues.[5] A combination of fluorine substituents on indole frameworks leading to novel bioactivities and pharmaceutical properties made the synthesis of such compounds inviting targets.[6,7]

A number of strategies have been devised to incorporate fluorine atoms into indole derivatives.[7c,8] Given the electron-rich nature and the enhanced reactivity in electrophilic alkylations (especially at the C-3 position) of this heterocycle,[9] one of the most straightforward methods for synthesizing these derivatives is to carry out a Friedel-Crafts alkylation with an indole and a fluorine-containing electrophile.[10] This type of transformation is also a powerful method for the formation of carbon-carbon bonds that can be applied to construct optically active compounds.[11] In general, these reactions proceed in good yields and high enantioselectivities with suitable catalysts. For the specific case of Friedel-Crafts alkylations of indole derivatives with 2,2,2-trifluoromethyl aryl ketones, inorganic bases,[12] cinchona alkaloids,[13] guanidine,[14] trifluoromethanesulfonic acid,[15] and phosphoric acids[16] were reported to be successful catalysts. Most of these studies, however, focused on either racemic products or bis-coupled adducts. There are only a few reports on asymmetric alkylations, and these required either long reaction times (i.e., up to 96 h)[16] or harsh reaction conditions (i.e., up to 9 kbar pressure)[13] presumably

---

*Reprinted adapted with permission from: Ma, J.; Kass, S. R. *Org. Lett.* **2018**, *20*, 2689–2692. Copyright 2018 American Chemical Society.

because it is a challenge to trigger the alkylation and terminate it at the monoarylated stage.[15,16] More effective enantioselective catalysts, consequently, are still needed for this transformation.

In general, there is a good correlation between reactivity and the acidity of related organocatalysts.[17] For this reason, electron-withdrawing substituents such as trifluoromethyl or nitro groups are sometimes incorporated into phenyl rings at the 3 and 3' positions of BINOL-derived phosphoric acids.[18,19] In previous studies from our laboratory, positively charged ion centers were found to enhance the catalytic reactivities of phenols,[20] thioureas[21] and phosphoric acids[22] by orders of magnitude. This approach was also used to obtain good to excellent enantioselectivities for the alkylation of indoles with *trans*-*β*-nitrostyrene derivatives using chiral thioureas.[23] As a result, we decided to develop a series of BINOL-based phosphoric acid catalysts possessing 3,3'-phosphonium ion substituents (Figure 1) that were prepared using reported synthetic methods.[24] These large groups provide needed steric bulk and two acidity-enhancing positively charged ion centers. Their performance in the Friedel-Crafts reactions of indole derivatives with 2,2,2-trifluoromethyl aryl ketones are reported herein.

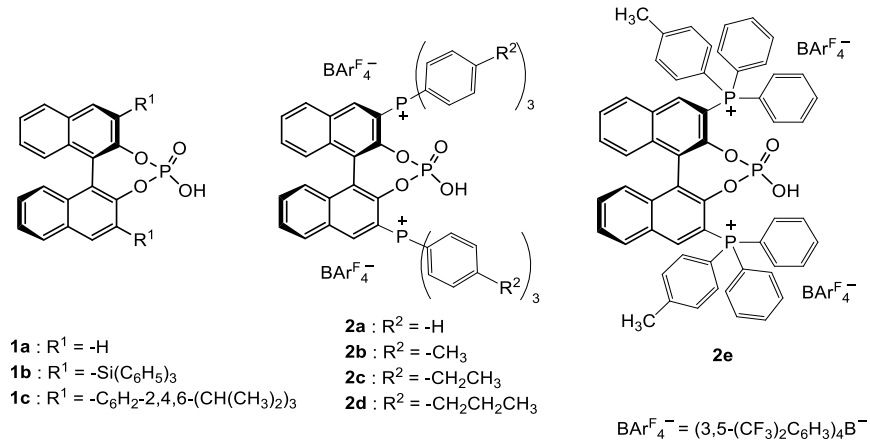

Figure 1. Catalysts involved in this work.

3.2. Results and Discussion

This investigation was initiated by examining the reaction of indole (**3a**) with 2,2,2-trifluoroacetophenone (**4a**) using the tri(*p*-tolyl)phosphonium ion containing phosphoric acid at the 3,3'-

positions of the (*R*)-BINOL backbone (i.e., **2b**) along with the noncoordinating tetrakis(3,5-bis(trifluoromethyl)phenyl)borate ($BAr^F{}_4^-$) counterion; more common and interacting anions lead to less active catalysts.[20-22] At room temperature in CH_2Cl_2 with a 5 mol % catalyst loading, both the desired and undesired mono- and bis-coupled products (**5a** and **6**, respectively) were formed, respectively (eq 1). This led to a loss of yield for the former species, as previously has been reported with other strong acid catalysts,[12,15] and the enantioselectivity was also poor (Table 1, entry 1).

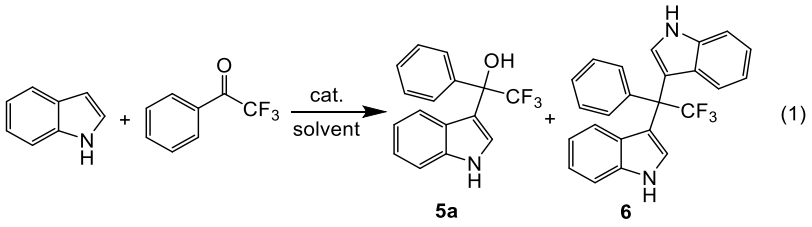

To our delight, when the reaction temperature was reduced to 0 °C, the formation of the bis-coupled byproduct was nearly eliminated and a dramatic increase in the ee from 17% to 85% was observed (entry 2). A further decrease to -30 °C only led to a 1% increase in the ee at the expense of a much longer reaction time (entry 3), and this result was surpassed by adding 3 Å molecular sieves (MS) at 0 °C (i.e., 87% ee, entry 4). Other MS (4 Å, 5 Å and 13X) decreased both the yield and the enantioselectivity (entries 5-7). Attempts to improve this transformation with inorganic salts (Na_2SO_4, NaCl, $MgSO_4$ and $CaCl_2$) as drying agents also led to poorer results (entries 8-11). An increase in the catalyst loading to 10 mol % did not improve the enantioselectivity further (entry 12) so the other phosphonium ion containing species were screened with 5 mol % catalyst at 0 °C in the presence of 3 Å MS. The triphenylphosphonium containing derivative **2a** gave a much lower yield (30%) and selectivity (77% ee) (entry 13), while the tri(*p*-ethylphenyl) and tri(*p*-propylphenyl)phosphonium derivatives **2c** and **2d** gave similar results to **2b** (entries 14-15). Interestingly, the diphenyl(*p*-tolyl)phosphonium ion tagged catalyst **2e**, which is sterically similar to **2a** and electronically in between **2a** and **2b**, afforded the product with a reduced yield and ee relative to **2b** of 68% and 84%, respectively. These results suggest that the large difference between **2a** and **2b** is due to electronic effects brought

about by replacing a hydrogen atom with a methyl group on each of the phenyl rings attached to the phosphorous atom. A lower temperature experiment at -30 °C was also performed with 3 Å MS and a 3% increase in ee to 90% was observed (entry 17). A further drop in the temperature to -50 °C was impractical due to reduced catalyst solubility.

Table 1. Optimization of reaction conditions.[a]

entry	cat.	*t* (°C)	additive	time (h)	yield **5a** (%)[b]	ee (%)[c]
1	**2b**	20	-	5	48	17
2	**2b**	0	-	22	90	85
3	**2b**	-30	-	96	87	86
4[d]	**2b**	0	3 Å MS	22	92	87
5[d]	**2b**	0	4 Å MS	22	87	66
6[d]	**2b**	0	5 Å MS	21	79	80
7[d]	**2b**	0	13X MS	21	58	85
8[e]	**2b**	0	Na_2SO_4	20	81	83
9[e]	**2b**	0	NaCl	20	86	80
10[e]	**2b**	0	$MgSO_4$	20	83	80
11[e]	**2b**	0	$CaCl_2$	20	81	80
12[d,f]	**2b**	0	3 Å MS	20	87	87
13[d]	**2a**	0	3 Å MS	22	30[g]	77
14[d]	**2c**	0	3 Å MS	22	91	86
15[d]	**2d**	0	3 Å MS	22	86	86
16[d]	**2e**	0	3 Å MS	22	68[g]	84
17[d]	**2b**	-30	3 Å MS	40	85	90

[a]Experiments performed with 0.140 mmol indole, 0.168 mmol 2,2,2-trifluoroacetophenone, 0.007 mmol catalyst in 0.25 mL CH_2Cl_2. [b]Isolated yield. [c]Determined by chiral HPLC. [d]5 mg of MS were used. [e]1.0 equiv of salt was used. [f]0.014 mmol catalyst was employed. [g]Starting material was present.

Reaction media were examined next with catalyst **2b** and the results are summarized in Table 2. Solvents were found to have a large influence on the reactivity and enantioselectivity. For example,

$CHCl_3$ (entry 2) led to both a lower yield and enantioselectivity than CH_2Cl_2 (entry 1). Chlorobenzene (entry 3) and 1,2-dichloroethane (DCE, entry 4) gave similar results (91% and 89% yields along with 62% and 63% ee), neither of which is as good as CH_2Cl_2. Several mixtures using CH_2Cl_2 and aromatic solvents (i.e., benzene, toluene, *m*-xylene) or CCl_4 were also tested (entries 5-8). None of these screenings led to better results than when CH_2Cl_2 was used.

Table 2. Screening of reaction solvents.[a]

entry	solvent	time (h)	yield **5a** (%)[b]	ee (%)[c]
1	CH_2Cl_2	22	92	87
2	$CHCl_3$	22	37	67
3	C_6H_5Cl	22	91	62
4	DCE	22	89	63
5	1:1 CH_2Cl_2/C_6H_6	20	86	84
6	1:1 $CH_2Cl_2/C_6H_5CH_3$	20	81	83
7	1:1 CH_2Cl_2/1,3-$(CH_3)_2C_6H_4$	20	88	83
8	1:1 CH_2Cl_2/CCl_4	20	89	85

[a]Experiments performed with 0.140 mmol indole, 0.168 mmol 2,2,2-trifluoroacetophenone, 0.007 mmol catalyst **2b** and 5 mg of 3 Å MS in 0.25 mL of solvent at 0 °C. [b]Isolated yield. [c]Determined by chiral HPLC.

The scope of this transformation was examined at 0 °C using 5 mol % **2b**, CH_2Cl_2 as the solvent and 3 Å MS as a drying agent (eq 2). As summarized in Table 3, a wide variety of substituents including electron-withdrawing and electron-donating groups on either reactant were tolerated. With a few exceptions, excellent yields (82-94%) and good enantioselectivities (79-91% ee) were obtained at 0 °C (entry 1-19). Halide substituents at the 5-positon of indole did not affect the selectivity (85-87% ee) (entries 1-2) relative to the parent compound (i.e., R^3, R^4 = H) whereas electron-donating groups at the 5- and 6-positions led to reduced enantioselectivities of 79% and 48% ee (entries 3-4). Interestingly,

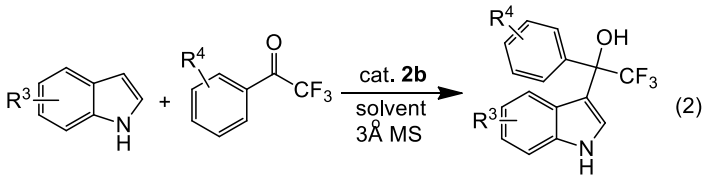

(2)

3a: R^3 = H-
3b: R^3 = 5-F-
3c: R^3 = 5-Br-
3d: R^3 = 5-MeO-
3e: R^3 = 6-Me-
3f : R^3 = 7-Cl-
3g: R^3 = 7-Br-
3h: R^3 = 7-Me-
3i : R^3 = 7-Et-

4a: R^4 = H-
4b: R^4 = 4-F-
4c: R^4 = 4-Cl-
4d: R^4 = 4-Br-
4e: R^4 = 4-Me-
4f : R^4 = 4-CF_3-
4g: R^4 = 3-Cl-
4h: R^4 = 3,5-F_2-
4i : R^4 = 3,5-Cl-F-
4j : R^4 = 3,5-Cl_2-
4k: R^4 = 2,3,4,5,6-F_5-
4l : $PhCOCF_2Cl$

5a: R^3 = H-, R^4 = H-
5b: R^3 = 5-F-, R^4 = H-
5c: R^3 = 5-Br-, R^4 = H-
5d: R^3 = 5-MeO-, R^4 = H-
5e: R^3 = 6-Me-, R^4 = H-
5f : R^3 = 7-Cl-, R^4 = H-
5g: R^3 = 7-Br-, R^4 = H-
5h: R^3 = 7-Me-, R^4 = H-
5i : R^3 = 7-Et-, R^4 = H-
5j : R^3 = H-, R^4 = 4-F-
5k: R^3 = H-, R^4 = 4-Cl-
5l : R^3 = H-, R^4 = 4-Br-
5m: R^3 = H-, R^4 = 4-Me-
5n: R^3 = H-, R^4 = 4-CF_3-
5o: R^3 = H-, R^4 = 3-Cl-
5p: R^3 = H-, R^4 = 3,5-F_2-
5q: R^3 = H-, R^4 = 3,5-Cl-F-
5r : R^3 = H-, R^4 = 3,5-Cl_2-
5s: R^3 = H-, R^4 = 2,3,4,5,6-F_5-
5t : 3-(CPh(OH)(CF_2Cl))-indole

while 6-methylindole (**3e**) gave the worst product enantiomeric purity (48% ee), its isomer 7-methylindole (**3h**) provided the highest enantioselectivity (91% ee, entry 7). This difference should be quite helpful in developing computational models for the mechanism of this reaction. Other substituents at the 7-position of indole (Cl, Br, Et) had no impact on the enantiomeric excess (entries 5-6 and 8), but 7-bromoindole (**3g**) slowed the reaction leading to approximately half the yield over the same time period. Introduction of electron-withdrawing groups (F, Cl, Br and CF_3) to the para position of 2,2,2-trifluoroacetophenone gave slight improvements of 1-3% in the ee (entries 9-11 and 13), whereas an electron-donating methyl group at the same location lowered the enantioselectivity by an equivalent amount (entry 12). Halogen substituents at one or both of the meta positions in 2,2,2-trifluoroacetophenone had little, if any, impact on the reaction outcome (entries 14-17). Perfluoroacetophenone (**4k**) was found to give both a low yield (28%) and ee (64%, entry 18) while 2-chloro-2,2-difluoroacetophenone (**4l**) also gave a low yield (36%) but without much difference in the enantioselectivity (i.e., an 84% ee was observed, entry 19). For the two reactions that gave ≥ 90% ee at

0 °C (entries 7 and 9), a decrease in temperature to -30 °C resulted in improved selectivities of 95% and 93% ee (entries 20-21). The former transformation was further examined with a decreased catalyst loading of 1.5 mol %, and the enantioselectivity was preserved with a measured ee of 96% (entry 22).

Table 3. Reaction scope.[a]

entry	substrate	adduct	time (h)	yield (%)[b]	ee (%)[c]
1	**3b + 4a**	**5b**	26	85	85
2	**3c + 4a**	**5c**	26	82	87
3	**3d + 4a**	**5d**	20	84	79
4	**3e + 4a**	**5e**	20	83	48
5	**3f + 4a**	**5f**	28	87	87
6	**3g + 4a**	**5g**	28	41	88
7	**3h + 4a**	**5h**	14	92	91
8	**3i + 4a**	**5i**	20	85	88
9	**3a + 4b**	**5j**	20	92	90
10	**3a + 4c**	**5k**	20	88	89
11	**3a + 4d**	**5l**	20	94	89
12	**3a + 4e**	**5m**	28	86	85
13	**3a + 4f**	**5n**	20	90	88
14	**3a + 4g**	**5o**	20	89	85
15	**3a + 4h**	**5p**	20	91	86
16	**3a + 4i**	**5q**	20	85	86
17	**3a + 4j**	**5r**	20	88	88
18	**3a + 4k**	**5s**	24	28	64
19	**3a + 4l**	**5t**	28	36	84
20[d]	**3h + 4a**	**5h**	18	96	95
21[d]	**3a + 4b**	**5j**	42	91	93
22[d,e]	**3h + 4a**	**5h**	65	93	96
23[f]	**3h + 4a**	**5h**	70	96	96

[a]Experiments performed with 0.140 mmol indole, 0.168 mmol 2,2,2-trifluoroacetophenone, 5 mol % **2b** and 5 mg of 3 Å MS in 0.25 mL of CH_2Cl_2 at 0 °C. [b]Isolated yield. [c]Determined by chiral HPLC. [d]Reaction run at -30 °C with 10 mg 3 Å MS. [e]1.5 mol % catalyst. [f]Larger scale reaction with 0.840 mmol 7-methylindole, 1.008 mmol 2,2,2-trifluoroacetophenone, 1.5 mol % **2b** and 30 mg 3 Å MS in 1.50 mL of CH_2Cl_2 at -30 °C; 247.5 mg of product was produced.

A larger scale reaction was also performed with six times more material and reactant weights in excess of 100 mg along with a catalyst loading of 1.5 mol %. This led to similar results to the small-scale transformation and afforded a 96% yield and a 96% ee (entry 23).

To compare the reactivity and enantioselectivity of our charged BINOL phosphoric acid derivative **2b** with noncharged analogues, three different structures (**1a**-**1c**) were used. These species included the unsubstituted BINOL phosphoric acid (**1a**), a sterically similar structure with triphenylsilyl substituents at the 3 and 3'-positions (**1b**), and 3,3'-bis(2,4,6-triisopropylphenyl)-BINOL phosphoric acid (**1c**). The last of these derivatives is known as TRIP and is one of the most successful phosphoric acid catalysts that has been reported.[25] 7-Methylindole (**3h**) and 2,2,2-trifluoroacetophenone (**4a**) in CH_2Cl_2 at -30 °C with a 1.5 mol % catalyst loading was used as the test reaction, and the results after 65 h are given in Table 4. The least sterically hindered parent structure with hydrogen atoms at the 3 and 3'-positions (**1a**) was ineffective. Only a 1% yield was obtained and this material was essentially racemic (i.e., 1% ee, entry 1). The catalyst **1b** with two triphenylsilyl substituents only gave a yield of 9%, but this product was formed in 93% ee (entry 2). TRIP is more reactive, but only resulted in a 43% yield. The observed ee of 97%, however, is quite impressive (entry 3). Our charged phosphonium ion tagged phosphoric acid catalyst **2b** proved to be superior in that an excellent yield of 93% was obtained along with a 96% ee (entry 4). Assuming second-order kinetics for these processes,[26] one can estimate that **2b** is more

Table 4. Catalyst comparisons.[a]

entry	catalyst	yield (%)[b]	ee (%)[c]
1	**1a**	1	1
2	**1b**	9	93
3	**1c**	43	97
4	**2b**	93	96

[a]Experiments performed with 0.140 mmol 7-methylindole, 0.168 mmol 2,2,2-trifluoroacetophenone, 1.5 mol% of the desired catalyst and 10 mg of 3Å MS in 0.25 mL of CH_2Cl_2 at -30 °C. [b]Isolated yield after 65 h. [c]Determined by chiral HPLC.

reactive than **1a**-**1c** by factors of 690, 70, and 10, respectively, but still is as selective as the best of these noncharged species.

To investigate the role of hydrogen bonding between the phosphoryl oxygen and indole substrate, a reaction lacking this interaction was performed with 1-methylindole and 2,2,2-trifluoroacetophe-none at 0 °C (eq 3). The yield after 18 h was 71% and the product was formed with a 24% ee. These results

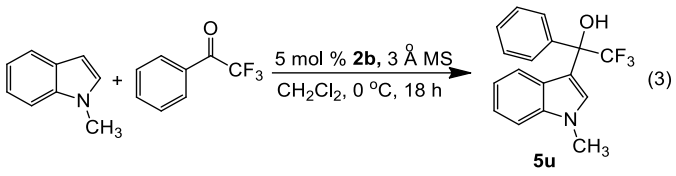

(3)

show that the selectivity is significantly lower and the yield is worse than when indole is used (92% yield and 87% ee in 22 h). These findings indicate that indole reacts 2.6 times faster than *N*-methylindole even though the latter compound is a better nucleophile. This suggests that the P=O••H–N hydrogen bond is important both in terms of the reaction rate and the enantioselectivity as previously reported.[27]

3.3. Conclusion

In summary, we demonstrated a successful application of chiral electrostatically enhanced phosphoric acids to a Friedel-Crafts alkylation to generate fluorinated indole derivatives. A wide scope of substrates is tolerated, giving the corresponding products in good yields and enantioselectivities. A larger synthetic scale reaction affording 250 mg of product was carried out with little, if any, change in the performance of the reaction. Our charged catalyst **2b** was also found to outperform noncharged analogues in terms of reaction rates by orders of magnitude, yet still gave as good or better enantioselectivities.

3.4. Experimental Section

3.4.1. General Information

Unless otherwise noted, all reagents involved in this work were commercially available and used without further purification. Organic solvents used in reactions were dried over 3 Å molecular sieves

that had been activated in an oven overnight. Flash chromatography purifications were performed with a CombiFlash® Rf automated system installed with RediSep Rf gold® 4 gram or 40 gram silica gel columns manufactured by Teledyne Isco Inc. Nuclear magnetic resonance (NMR) spectra were recorded with Varian Inova 500 MHz and Bruker Avance III HD Nanobay 400 MHz instruments. Chemical shifts are reported in ppm (δ) using the following reference signals: ^{1}H and ^{13}C NMR: 7.26 and 77.0 δ ($CDCl_3$), and 5.32 and 54.0 δ (CD_2Cl_2); ^{19}F NMR: -76.55 δ, external calibrant (CF_3COOH); ^{31}P NMR: 0.00 δ, external calibrant (85% H_3PO_4 in H_2O). High-resolution electrospray ionization mass spectra (HRMS-ESI) data were obtained with a Bruker ESI-BioTOF instrument using methanol solutions and polyethylene glycol (PEG) or polypropylene glycol (PPG) as an internal standard. Chiral HPLC analyses were carried out with an Agilent system equipped with RegisCell and RegisPack columns.

3.4.2. General Procedure for the Friedel-Crafts Reaction

Catalyst (1.5–10 mol %) and 3 Å molecular sieves (5–10 mg) were added to a 17 × 60 mm vial and purged for 30 s with dry nitrogen to remove oxygen and moisture. The vial was sealed and cooled to the designated reaction temperature using a cooling bath (or left at room temperature in a few cases). The indole and 2,2,2-trifluoromethyl aryl ketone were weighed in separate vials and 250 μL of CH_2Cl_2 was added to the indole container. After mixing for 5 s, the solution was transferred to the vial with the 2,2,2-trifluoromethyl aryl ketone and vigorously mixed for 10 s. Immediately thereafter this solution was added to the vial with the catalyst and molecular sieves, and swirled for 20–30 s until the solution became homogeneous. After the elapsed reaction time, the reaction mixture was directly loaded onto a 4 gram silica gel column followed by an injection of 0.2–0.3 mL of CH_2Cl_2 that had been used to rinse the vial and molecular sieves. A 1 min wash with hexanes was followed by a linear gradient of hexanes to CH_2Cl_2 over a 7 min period and then the latter solvent was used until the end of the purification. Racemic reference products were obtained at room temperature using diphenyl phosphate as the catalyst and the same purification method as when chiral catalysts were used.

3.4.3. Synthesis Procedures

BINOL phosphoric acids. The parent compound **1a** was purchased from Oakwood Chemical while **1b** and **1c** were synthesized as previously described.[28]

*Tris(p-alkylphenyl)phosphine (**7c-7d**):* In a flame dried 100 mL two-necked round bottomed flask equipped with dropping funnel and septum, anhydrous Et_2O (10 mL) was injected, followed by the addition of ground magnesium turning (0.315 g, 13.0 mmol). The desired *p*-alkylphenyl bromide (10.8 mmol) and Et_2O (10 mL) were mixed and then 5-10 drops were slowly added under an argon atmosphere to initiate Grignard reagent formation. After bubbles were observed, the rest of the solution was added dropwise over a 20 min period under reflux. After 1 h at room temperature this solution was transferred via syringe to a flame-dried 250 mL round bottomed flask and cooled to 0 °C with an ice-water bath. A solution of PCl_3 (0.41 g, 2.70 mmol) in anhydrous THF (10 mL) was slowly added over 10 minutes, and then the reaction mixture was allowed to warm up to room temperature overnight before being quenched with 10 mL of water. The volatiles were evaporated under vacuum and CH_2Cl_2 (50 mL) was added to extract the product. The resulting organic material was washed with water (30 mL) and brine (30 mL), and dried over Na_2SO_4. Concentration with a rotary evaporator afforded a viscous oil which was purified by medium pressure liquid chromatography (MPLC) using hexanes as the eluent.

*Tris(p-ethylphenyl)phosphine (**7c**).* This material was formed as a white solid (0.60 g, mp 98 - 102 °C) in a 64% yield. ^{1}H NMR (500 MHz, CD_2Cl_2): δ 7.24 (t, *J* = 7.4 Hz, 6H), 7.19 (d, *J* = 6.9 Hz, 6H), 2.66 (q, *J* = 7.8 Hz, 6H), 1.24 (t, *J* = 7.3 Hz, 9H). ^{13}C NMR (100 MHz, CD_2Cl_2): δ 145.6, 135.2 (d, *J* = 10.2 Hz), 134.2 (d, *J* = 19.7 Hz), 128.6 (d, *J* = 7.3 Hz), 29.2, 15.8. ^{31}P NMR (162 MHz, CD_2Cl_2): δ -7.96. HRMS-ESI: Calc for $C_{24}H_{28}P^+$ $(M + H^+)^+$ 347.1923, found 347.1936.

*Tris(p-n-propylphenyl)phosphine (**7d**).* A white solid (0.51 g, mp 55 - 57 °C) was formed in a 49% yield. ^{1}H NMR (500 MHz, $CDCl_3$): δ 7.22 (t, *J* = 7.8 Hz, 6H), 7.14 (d, *J* = 7.9 Hz, 6H), 2.58 (t, *J* = 7.5 Hz, 6H), 1.71-1.60 (m, 6H), 0.94 (t, *J* = 7.3 Hz, 9H). ^{13}C NMR (100 MHz, $CDCl_3$): δ 143.2, 134.4 (d, *J* = 8.8 Hz), 133.6 (d, *J* = 19.7 Hz), 128.6 (d, *J* = 7.3 Hz), 37.8, 24.4, 13.9. ^{31}P NMR (162 MHz, CD_2Cl_2): δ -7.73. HRMS-ESI: Calc for $C_{27}H_{34}P^+$ $(M + H^+)^+$ 389.2398, found 389.2399.

*General procedure for synthesis of **9a-9e**.* Starting material **8** was synthesized as previously

described[29] while triphenylphosphine (**7a**), tri(*p*-tolyl)phosphine (**7b**) and diphenyl(*p*-tolyl)phosphine (**7e**) were obtained from Sigma-Aldrich. In a 23 × 85 mm glass vial equipped with a balloon, **8** (0.538 g, 1.0 mmol), $Pd_2(dba)_3$ (0.055 g, 0.060 mmol) and triarylphosphine (3.0 mmol) were mixed. After degassing this mixture for 10 minutes, 0.30 mL of ethylene glycol was added. The resulting mixture was heated to 130 °C for 16 h with stirring. Upon cooling the reaction mixture to room temperature, it was diluted with 30 mL of CH_2Cl_2, washed with water (2 × 20 mL), and dried over Na_2SO_4. The product was dried under vacuum and redissolved into 4 mL of CH_2Cl_2 before being slowly added in 100 mL of Et_2O with stirring. The resulting yellow precipitate was filtered and collected. If the resulting product displayed more than one spot upon thin layer chromatography (TLC) with a 4:1 EtOAc/MeOH mixture, then it was purified by MPLC using a 2-min wash with EtOAc followed by a linear gradient to 4:1 EtOAc/MeOH mixture over a 5 min time frame. The desired product was then concentrated with a rotary evaporator.

*(R)-(2,2'-Dihydroxy-[1,1'-binaphthalene]-3,3'-diyl)bis(triphenylphosphonium) iodide (**9a**).* A yellow solid (0.88 g, mp 222 - 230 °C) was obtained in an 83% yield. ^{1}H NMR (500 MHz, $CDCl_3$): δ 7.79-7.72 (m, 6H), 7.72-7.62 (m, 14H), 7.62-7.50 (m, 14H), 7.32 (d, *J* = 8.5 Hz, 2H), 7.27 (t, *J* = 7.4 Hz, 2H), 7.20 (d, *J* = 7.6 Hz, 2H), 4.31 (bs, OH, 2H). ^{13}C NMR (100 MHz, $CDCl_3$): δ 161.9 (d, *J* = 3.7 Hz), 138.7 (d, *J* = 9.8 Hz), 138.5 (d, *J* = 1.9 Hz), 134.1 (d, *J* = 3.0 Hz), 134.0 (d, *J* = 10.2 Hz), 129.7 (d, *J* = 12.9 Hz), 129.5, 128.7, 126.5, 126.3, 122.6, 120.6 (d, *J* = 7.0 Hz), 120.3 (d, *J* = 91.4 Hz), 111.0 (d, *J* = 94.9 Hz). ^{31}P NMR (162 MHz, $CDCl_3$): δ 22.15. HRMS-ESI: Calc for $C_{56}H_{41}O_2P_2^+$ $(M - H^+ - 2I^-)^+$ 807.2576, found 807.2604.

*(R)-(2,2'-Dihydroxy-[1,1'-binaphthalene]-3,3'-diyl)bis(tri-p-tolylphosphonium) iodide (**9b**).* A yellow solid (0.90 g, mp 210 - 215 °C) was obtained in a 78% yield. ^{1}H NMR (500 MHz, CD_2Cl_2): δ 7.74-7.49 (m, 16H), 7.48-7.34 (m, 12H), 7.29-7.16 (m, 6H), 5.33 (s, OH, 2H), 2.46 (s, 18H). ^{13}C NMR (100 MHz, $CDCl_3$): δ 162.0 (d, *J* = 3.8 Hz), 145.0 (d, *J* = 3.0 Hz), 138.6 (d, *J* = 10.0 Hz), 138.4, 134.0 (d, *J* = 10.6 Hz), 133.5 (d, *J* = 10.6 Hz), 131.0 (d, *J* = 13.0 Hz), 130.4 (d, *J* = 13.3 Hz), 129.4, 128.6, 126.4 (d, *J* = 14.4 Hz), 122.4, 117.3 (d, *J* = 93.9 Hz), 111.6 (d, *J* = 94.6 Hz), 21.8. ^{31}P NMR (162 MHz, CD_2Cl_2): δ 21.62. HRMS-ESI: Calc for $C_{62}H_{53}O_2P_2^+$ $(M - H^+ - 2I^-)^+$ 891.3515, found 891.3493.

*(R)-(2,2'-Dihydroxy-[1,1'-binaphthalene]-3,3'-diyl)bis(tris(4-ethylphenyl)phosphonium) iodide (**9c**).* A yellow solid (1.05 g, mp 194 - 202 °C) was obtained in an 85% yield. ^{1}H NMR (500 MHz, CD_2Cl_2): δ 7.69-7.62 (m, 4H), 7.61-7.53 (m, 12H), 7.50-7.34 (m, 12H), 7.28-7.17 (m, 6H), 5.33 (s, OH, 2H), 2.76 (q, *J* = 7.6 Hz, 12H), 1.27 (t, *J* = 7.6 Hz, 18H). ^{13}C NMR (100 MHz, CD_2Cl_2): δ 162.8 (d, *J* = 3.9 Hz), 151.8 (d, *J* = 2.9 Hz), 139.4 (d, *J* = 9.9 Hz), 139.0, 134.7 (d, *J* =10.6 Hz), 134.3 (d, *J* = 10.6 Hz), 129.9, 129.7 (d, *J* =13.2 Hz), 129.0, 126.8 (d, *J* = 16.0 Hz), 122.9, 120.8 (d, *J* =8.5 Hz), 118.0 (d, *J* = 93.8 Hz), 112.1 (d, *J* = 94.6 Hz), 29.4, 15.2. ^{31}P NMR (162 MHz, CD_2Cl_2): δ 21.61. HRMS-ESI: Calc for $C_{68}H_{65}O_2P_2^+$ (M - H^+ - $2I^-$)$^+$ 975.4454, found 975.4451.

*(R)-(2,2'-Dihydroxy-[1,1'-binaphthalene]-3,3'-diyl)bis(tris(4-propylphenyl)phosphonium) iodide (**9d**).* A yellow solid (0.91 g, mp 147 - 152 °C) was obtained in a 69% yield. ^{1}H NMR (500 MHz, CD_2Cl_2): δ 7.67-7.50 (m, 16H), 7.49-7.33 (m, 12H), 7.30-7.15 (m, 6H), 5.33 (bs, OH, 2H), 2.69 (t, *J* = 8.3 Hz, 12H), 1.75-1.60 (m, 12H), 0.95 (t, *J* = 7.4 Hz, 18H). ^{13}C NMR (100 MHz, CD_2Cl_2): δ 162.8 (d, *J* = 3.9 Hz), 150.3 (d, *J* = 3.0 Hz), 139.5 (d, *J* = 9.9 Hz), 139.0, 134.6 (d, *J* = 10.6 Hz), 134.2 (d, *J* = 10.6 Hz), 130.8 (d, *J* = 13.0 Hz), 130.3 (d, *J* = 13.2 Hz), 129.9, 129.0, 126.8 (d, *J* = 15.7 Hz), 122.9, 118.1 (d, *J* = 93.7 Hz), 112.3 (d, *J* = 94.7 Hz), 38.5, 24.6, 14.1. ^{19}F NMR (376 MHz, CD_2Cl_2): δ -62.84. ^{31}P NMR (162 MHz, CD_2Cl_2): δ 21.45. HRMS-ESI: Calc for $C_{74}H_{77}O_2P_2^+$ (M - H^+ - $2I^-$)$^+$ 1059.5393, found 1059.5376.

*(R)-(2,2'-Dihydroxy-[1,1'-binaphthalene]-3,3'-diyl)bis(diphenyl(p-tolyl)phosphonium) iodide (**9e**).* A yellow solid (0.762 g, mp 208 - 216 °C) was obtained in a 70% yield. ^{1}H NMR (500 MHz, $CDCl_3$): δ 7.70 (t, *J* = 7.2 Hz, 4H), 7.67-7.58 (m, 10H), 7.58-7.44 (m, 14H), 7.39-7.32 (m, 4H), 7.28 (d, *J* = 8.6 Hz, 2H), 7.25-7.20 (m, 2H), 7.17 (t, *J* = 7.3 Hz, 2H), 6.83 (bs, OH, 2H), 2.44 (s, 6H). ^{13}C NMR (100 MHz, $CDCl_3$): δ 161.8 (d, *J* = 3.8 Hz), 145.2 (d, *J* = 3.0 Hz), 138.6 (d, *J* = 10.2 Hz), 138.3 (d, *J* = 1.9 Hz), 134.1 (d, *J* = 10.6 Hz), 133.932, 133.927 (d, *J* = 6.4 Hz), 133.8 (d, *J* = 3.8 Hz), 130.4 (d, *J* = 13.3 Hz), 129.6 (d, *J* = 12.9 Hz), 129.4, 128.6, 126.4, 122.5, 120.51 (d, *J* = 91.4 Hz), 120.46 (d, *J* = 6.2 Hz), 116.6 (d, *J* = 93.8 Hz), 111.1 (d, *J* = 94.8 Hz), 21.7. ^{31}P NMR (162 MHz, $CDCl_3$): δ 22.01. HRMS-ESI: Calc for $C_{58}H_{45}O_2P_2^+$ (M - H^+ - $2I^-$)$^+$ 835.2889, found 835.2905.

*General procedure for synthesis of **10a-10e**.* In a balloon equipped 23 × 85 mm glass vial filled with

dry N_2, 0.500 mmol of the desired iodide **9a**-**9e** was dissolved in 5 mL of pyridine and then 0.28 mL of $POCl_3$ (0.46 g, 3.00 mmol) was added over a 3 min period with stirring. It was then heated to 85 °C for 20 h and slowly quenched with 1 mL of water after being cooled down to room temperature. The reaction mixture was subsequently heated to 85 °C for 1 h, allowed to cool back down to room temperature, and concentrated with a rotary evaporator. The residue was dissolved in 30 mL of CH_2Cl_2, washed with 30 mL of water and 30 mL of brine, and then dried with Na_2SO_4 and concentrated under reduced pressure. Purification of the product was achieved by dissolving it in 4 mL of CH_2Cl_2 and adding this solution dropwise into 100 mL of Et_2O to afford a precipitate that was subsequently collected and dried.

*(R)-(4-Hydroxy-4-oxidodinaphtho[2,1-d:1',2'-f][1,3,2]dioxaphosphepine-2,6-diyl)bis(triphenyl-phosphonium) chloride (**10a**).* This material was obtained in an 81% yield (0.38 g) as a yellow solid (mp 244 - 250 °C). ^{1}H NMR (500 MHz, $CDCl_3$): δ 8.00 (d, *J* = 16.4 Hz, 2H), 7.88 (d, *J* = 8.7 Hz, 2H), 7.83-7.72 (m, 18H), 7.72-7.64 (m, 12H), 7.61-7.52 (m, 4H), 7.29 (d, *J* = 8.3 Hz, 2H), 1.87 (bs, OH, 1H). ^{13}C NMR (100 MHz, CD_2Cl_2): δ 141.6 (d, *J* = 8.5 Hz), 136.7, 135.7 (d, *J* = 10.5 Hz), 135.4 (d, *J* = 3.0 Hz), 131.2, 130.9 (d, *J* = 12.9 Hz), 130.3 (d, *J* = 13.1 Hz), 130.2, 129.8 (d, *J* = 14.4 Hz), 127.4, 127.0, 125.4 (d, *J* = 8.2 Hz), 119.8 (d, *J* = 90.4 Hz), 111.4 (d, *J* = 93.8 Hz). ^{31}P NMR (162 MHz, $CDCl_3$): δ 23.01, 0.89. HRMS-ESI: Calc for $C_{56}H_{40}O_4P_3^+$ $(M - H - 2Cl^-)^+$ 869.2134, found 869.2135.

*(R)-(4-Hydroxy-4-oxidodinaphtho[2,1-d:1',2'-f][1,3,2]dioxaphosphepine-2,6-diyl)bis(tri-p-tolylphosphonium) chloride (**10b**).* This material was obtained in a 90% yield (0.46 g) as a yellow solid (mp 241 - 245 °C). ^{1}H NMR (500 MHz, CD_2Cl_2): δ 8.05 (d, *J* = 16.1 Hz, 2H), 7.88 (d, *J* = 8.0 Hz, 2H), 7.75-7.59 (m, 12H), 7.57 (t, *J* = 7.3 Hz, 2H), 7.54-7.40 (m, 14H), 7.31 (d, *J* = 8.3 Hz, 2H), 2.48 (s, 18H), 2.03 (bs, OH, 1H). ^{13}C NMR (100 MHz, CD_2Cl_2): δ 151.6 (d, *J* = 3.4 Hz), 146.8 (d, *J* = 3.0 Hz), 141.5 (d, *J* = 8.5 Hz), 136.6, 135.5 (d, *J* = 10.8 Hz), 131.00 (d, *J* = 13.5 Hz), 130.98, 130.1, 129.7 (d, *J* = 14.1 Hz), 127.2, 127.0, 125.2 (d, *J* = 7.1 Hz), 116.6 (d, *J* = 93.3 Hz), 112.3 (d, *J* = 91.3 Hz), 22.1. ^{31}P NMR (162 MHz, CD_2Cl_2): δ 22.24, 1.59. HRMS-ESI: Calc for $C_{62}H_{52}O_4P_3^+$ $(M - H^+ - 2Cl^-)^+$ 953.3073, found 953.3081.

*(R)-(4-Hydroxy-4-oxidodinaphtho[2,1-d:1',2'-f][1,3,2]dioxaphosphepine-2,6-diyl)bis(tris(4-ethylphenyl)phosphonium) chloride (**10c**).* This material was obtained in a 71% yield (0.39 g) as a

yellow solid (mp 201 - 207 °C). ^{1}H NMR (500 MHz, CD_2Cl_2): δ 8.07 (d, *J* = 16.1 Hz, 2H), 7.89 (d, *J* = 8.1 Hz, 2H), 7.76-7.61 (m, 12H), 7.57 (t, *J* = 7.2 Hz, 2H), 7.54-7.40 (m, 14H), 7.33 (d, *J* = 8.5 Hz, 2H), 2.79 (q, *J* = 7.6 Hz, 12H), 2.18 (s, OH, 1H), 1.28 (t, *J* = 7.7 Hz, 18H). ^{13}C NMR (100 MHz, CD_2Cl_2): δ 152.6 (d, *J* = 3.0 Hz), 141.4 (d, *J* = 8.2 Hz), 136.6, 135.6 (d, *J* = 10.8 Hz), 130.9, 130.1, 129.8 (d, *J* = 13.5 Hz), 129.5 (d, *J* = 15.8 Hz), 128.5 (d, *J* = 12.3 Hz), 127.2, 127.0, 125.2 (d, *J* = 7.0 Hz), 116.8 (d, *J* = 93.0 Hz), 112.3 (d, *J* = 91.0 Hz), 29.4, 15.1. ^{31}P NMR (162 MHz, CD_2Cl_2): δ 22.01, 1.57. HRMS-ESI: Calc for $C_{68}H_{64}O_4P_3^+$ $(M - H^+ - 2Cl^-)^+$ 1037.4012, found 1037.3991.

*(R)-(4-Hydroxy-4-oxidodinaphtho[2,1-d:1',2'-f][1,3,2]dioxaphosphepine-2,6-diyl)bis(tris(4-propylphenyl)phosphonium) chloride (**10d**).* This material was obtained in an 85% yield (0.51 g) as a yellow solid (mp 161 - 166 °C). ^{1}H NMR (500 MHz, $CDCl_3$): δ 7.93 (d, *J* = 16.3 Hz, 2H), 7.82 (d, *J* = 7.8 Hz, 2H), 7.65-7.57 (m, 12H), 7.57-7.46 (m, 6H), 7.44-7.38 (m, 10H), 7.23 (d, *J* = 8.3 Hz, 2H), 2.67 (t, *J* = 7.2 Hz, 13H), 1.71-1.62 (m, 12H), 0.95 (t, *J* = 7.4 Hz, 18H). ^{13}C NMR (100 MHz, $CDCl_3$): δ 150.4 (d, *J* = 3.0 Hz), 140.7 (d, J = 8.6 Hz), 136.2, 134.9 (d, *J* = 10.8 Hz), 132.0 (d, *J* = 10.2 Hz), 130.7, 130.0 (d, *J* = 13.5 Hz), 129.6, 129.0 (d, *J* = 14.3 Hz), 128.5 (d, *J* = 12.3 Hz), 126.7, 126.4, 116.0 (d, *J* = 93.0 Hz), 111.8 (d, *J* = 90.6 Hz), 38.0, 23.8, 13.8. ^{31}P NMR (162 MHz, CD_2Cl_2): δ 22.44, 1.08. HRMS-ESI: Calc for $C_{74}H_{76}O_4P_3^+$ $(M - H^+ - 2Cl^-)^+$ 1121.4951, found 1121.4983.

*(R)-(4-Hydroxy-4-oxidodinaphtho[2,1-d:1',2'-f][1,3,2]dioxaphosphepine-2,6-diyl)bis-(diphenyl(p-tolyl)phosphonium) chloride (**10e**).* This material was obtained in an 89% yield (0.433 g) as a yellow solid (mp 234 - 240 °C). ^{1}H NMR (500 MHz, $CDCl_3$): δ 7.98 (d, *J* = 16.3 Hz, 2H), 7.86 (d, *J* = 7.7 Hz, 2H), 7.80-7.69 (m, 12H), 7.68-7.58 (m, 12H), 7.57-7.49 (m, 4H), 7.48-7.40 (m, 4H), 7.27 (d, *J* = 8.2 Hz, 2H), 2.47 (s, 6H), 2.06 (bs, OH, 1H). ^{13}C NMR (100 MHz, $CDCl_3$): δ 150.8 (d, *J* = 3.6 Hz), 146.4 (d, *J* = 3.1 Hz), 140.9 (d, *J* = 8.6 Hz), 136.2, 134.94 (d, *J* = 10.6 Hz), 134.93 (d, *J* = 3.1 Hz), 130.93, 130.90 (d, *J* = 13.5 Hz), 129.98 (d, *J* = 13.1 Hz), 129.96 (d, *J* = 13.1 Hz), 129.2 (d, *J* = 14.0 Hz), 126.9, 126.5, 119.2 (d, *J* = 90.6 Hz), 119.1 (d, *J* = 90.7 Hz), 115.2 (d, *J* = 92.9 Hz), 111.05 (d, *J* = 91.2 Hz), 111.02 (d, *J* = 91.1 Hz), 21.9. ^{31}P NMR (162 MHz, $CDCl_3$): δ 22.90, 0.89. HRMS-ESI: Calc for $C_{58}H_{44}O_4P_3^+$ $(M - H^+ - 2Cl^-)^+$ 897.2447, found 897.2424.

*General procedure for synthesis of **2a-2e**.* In a 23 × 85 mm vial, one of the chlorides **10a-10e** (0.200

mmol), sodium tetrakis[3,5-bis(trifluoromethyl)phenyl]borate (0.372 g, 0.420 mmol) and 3 Å molecular sieves (0.05 g) were mixed along with 8 mL of CH_2Cl_2. The solution was stirred at room temperature for 3 h and then filtered through a syringe equipped with a 0.45 μm PTFE membrane. It was subsequently washed twice with 8 mL of 2.0 M H_2SO_4 and three times with 8 mL of water before being dried over Na_2SO_4. Removal of the solvent with a rotary evaporator afforded the desired $BAr^F{}_4$ salt.

*(R)-(4-Hydroxy-4-oxidodinaphtho[2,1-d:1',2'-f][1,3,2]dioxaphosphepine-2,6-diyl)bis(triphenyl-phosphonium) tetrakis[3,5-bis(trifluoromethyl)phenyl]borate (**2a**).* A yellow solid (0.493 g, mp 85 - 89 °C) was obtained in a 95% yield. ^{1}H NMR (500 MHz, CD_2Cl_2): δ 8.15 (d, *J* = 16.5 Hz, 2H), 7.96 (d, *J* = 8.1 Hz, 2H), 7.81-7.76 (m, 4H), 7.74-7.69 (s, 18H), 7.69-7.59 (m, 24H), 7.59-7.54 (m, 4H), 7.52 (s, 8H), 7.26 (d, *J* = 8.4 Hz, 2H), 3.56 (bs, OH, 1H). ^{13}C NMR (100 MHz, CD_2Cl_2): δ 162.4 (q, *J* = 49.6 Hz), 147.0 (d, *J* = 3.0 Hz), 143.4 (d, *J* = 6.9 Hz), 136.4, 136.3, 135.4, 135.2 (d, *J* = 10.5 Hz), 132.9, 131.3 (d, *J* = 13.4 Hz), 131.0 (d, *J* = 13.2 Hz), 130.8 (d, *J* = 11.8 Hz), 129.8, 129.5 (qq, *J* = 2.92 and 31.4 Hz), 127.2, 125.2 (q, *J* = 271 Hz), 124.1 (d, *J* = 6.4 Hz), 118.09 (septet, *J* = 3.64 Hz), 118.05 (d, *J* = 90.6 Hz), 110.3 (d, *J* = 90.8 Hz). ^{19}F NMR (376 MHz, CD_2Cl_2): δ -62.83. ^{31}P NMR (162 MHz, CD_2Cl_2): δ 22.37, -2.97. HRMS-ESI: Calc for $C_{56}H_{40}O_4P_3{}^+$ (M - H^+ - 2$BAr^F{}_4^-$)$^+$ 869.2134, found 869.2180.

*(R)-(4-Hydroxy-4-oxidodinaphtho[2,1-d:1',2'-f][1,3,2]dioxaphosphepine-2,6-diyl)bis(tri-p-tolylphosphonium) tetrakis[3,5-bis(trifluoromethyl)phenyl]borate (**2b**).* A yellow solid (0.491 g, mp 108 - 115 °C) was obtained in a 92% yield. ^{1}H NMR (500 MHz, CD_2Cl_2): δ 8.14 (d, *J* = 16.0 Hz, 2H), 7.96 (d, *J* = 8.1 Hz, 2H), 7.73 (s, 16H), 7.69-7.47 (m, 26H), 7.47-7.37 (m, 10H), 7.24 (d, *J* = 8.4 Hz, 2H), 4.07 (bs, OH, 1H), 2.42 (s, 18H). ^{13}C NMR (100 MHz, CD_2Cl_2): δ 162.3 (q, *J* = 49.6 Hz), 148.1 (d, *J* = 3.7 Hz), 143.3 (d, *J* = 10.4 Hz), 136.2, 135.4, 135.0 (d, *J* = 10.9 Hz), 132.7, 131.7 (d, *J* = 13.5 Hz), 130.7 (d, *J* = 6.9 Hz), 130.4 (d, *J* = 13.8 Hz), 129.44 (qq, *J* = 2.92 and 31.4 Hz), 129.36, 128.5 (d, *J* = 13.4 Hz), 127.5, 127.1, 125.1 (q, *J* = 270 Hz), 118.0 (septet, *J* = 3.64 Hz), 114.7 (d, *J* = 92.9 Hz), 111.2 (d, *J* = 91.6 Hz), 22.1. ^{19}F NMR (376 MHz, CD_2Cl_2): δ -62.82. ^{31}P NMR (162 MHz, CD_2Cl_2): δ 21.75, -3.23. HRMS-ESI: Calc for $C_{62}H_{52}O_4P_3{}^+$ (M - H^+ - 2$BAr^F{}_4^-$)$^+$ 953.3073, found 953.3098.

*(R)-(4-Hydroxy-4-oxidodinaphtho[2,1-d:1',2'-f][1,3,2]dioxaphosphepine-2,6-diyl)bis(tris(4-ethylphenyl)phosphonium) tetrakis[3,5-bis(trifluoromethyl)phenyl]borate (**2c**).* A yellow solid (0.494 g,

mp 106 - 112 °C) was obtained in an 89% yield. ^{1}H NMR (500 MHz, CD_2Cl_2): δ 8.15 (d, *J* = 16.2 Hz, 2H), 7.96 (d, *J* = 8.2 Hz, 2H), 7.71 (s, 16H), 7.64 (t, *J* = 7.5 Hz, 2H), 7.60-7.54 (m, 14H), 7.53 (s, 8H), 7.50-7.40 (m, 12H), 7.25 (d, *J* = 8.6 Hz, 2H), 3.19 (s, OH, 1H), 2.74 (q, *J* = 7.5 Hz, 12H), 1.23 (t, *J* = 7.6 Hz, 18H). ^{13}C NMR (100 MHz, CD_2Cl_2): δ 162.3 (q, *J* = 49.6 Hz), 153.9 (d, *J* = 3.6 Hz), 143.2 (d, *J* = 8.8 Hz), 136.2, 135.4, 135.2 (d, *J* = 10.9 Hz), 132.6, 131.2 (d, *J* = 12.9 Hz), 130.8 (d, *J* = 15.8 Hz), 130.5 (d, *J* = 13.6 Hz), 129.4 (qq, *J* = 2.92 and 31.4 Hz), 129.2, 128.6 (d, *J* = 12.7 Hz), 127.2, 127.1, 125.1 (q, *J* = 270 Hz), 118.0 (septet, *J* = 3.64 Hz), 115.1 (d, *J* = 93.5 Hz), 111.3 (d, *J* = 90.6 Hz), 29.5, 15.1. ^{19}F NMR (376 MHz, CD_2Cl_2): δ -62.84. ^{31}P NMR (162 MHz, CD_2Cl_2): δ 21.45, -2.65. HRMS-ESI: Calc for $C_{68}H_{64}O_4P_3^+$ $(M - H^+ - 2BAr^F{}_4^-)^+$ 1037.4012, found 1037.4038.

*(R)-(4-Hydroxy-4-oxidodinaphtho[2,1-d:1',2'-f][1,3,2]dioxaphosphepine-2,6-diyl)bis(tris(4-propylphenyl)phosphonium) tetrakis[3,5-bis(trifluoromethyl)phenyl]borate (**2d**).* A yellow solid (0.455 g, mp 92 - 96 °C) was obtained in an 80% yield. ^{1}H NMR (500 MHz, CD_2Cl_2): δ 8.15 (d, *J* = 16.2 Hz, 2H), 7.96 (d, *J* = 8.3 Hz, 2H), 7.75-7.69 (m, 18H), 7.64 (t, *J* = 7.4 Hz, 2H), 7.60-7.51 (m, 22H), 7.48-7.43 (m, 10H), 7.24 (d, *J* = 8.5 Hz, 2H), 3.23 (bs, OH, 1H), 2.68 (t, *J* = 7.5 Hz, 12H), 1.71-1.58 (m, 12H), 0.93 (t, *J* = 7.3 Hz, 18H). ^{13}C NMR (100 MHz, CD_2Cl_2): δ 162.3 (q, *J* = 49.6 Hz), 152.6 (d, *J* = 2.9 Hz), 143.3 (d, *J* = 7.6 Hz), 136.2, 135.4, 135.1 (d, *J* = 10.9 Hz), 132.7, 131.1 (d, *J* = 13.6 Hz), 130.9 (d, *J* = 13.6 Hz), 130.8 (d, *J* = 12.7 Hz), 129.5 (qq, *J* = 2.92 and 31.4 Hz), 129.4, 128.2 (d, *J* = 9.6 Hz), 127.18, 127.15, 125.2 (q, *J* = 270 Hz), 118.1 (septet, *J* = 3.64 Hz), 115.0 (d, *J* = 93.2 Hz), 111.3 (d, *J* = 94.0 Hz), 38.5, 24.6, 14.0. ^{19}F NMR (376 MHz, CD_2Cl_2): δ -62.81. ^{31}P NMR (162 MHz, CD_2Cl_2): δ 21.40, -3.15. HRMS-ESI: Calc for $C_{74}H_{76}O_4P_3^+$ $(M - H^+ - 2BAr^F{}_4^-)^+$ 1121.4951, found 1121.4986.

*(R)-(4-Hydroxy-4-oxidodinaphtho[2,1-d:1',2'f][1,3,2]dioxaphosphepine-2,6-diyl)bis(diphen-yl(p-tolyl)phosphonium) tetrakis[3,5-bis(trifluoromethyl)phenyl]borate (**2e**).* A red solid (0.477 g, mp 104 - 108 °C) was obtained in a 91% yield. ^{1}H NMR (500 MHz, CD_2Cl_2): δ 8.16 (d, *J* = 16.3 Hz, 2H), 7.97 (d, *J* = 8.1 Hz, 2H), 7.83-7.76 (m, 4H), 7.72 (s, 16H), 7.70-7.59 (m, 18H), 7.58-7.51 (m, 14H), 7.48-7.43 (m, 4H), 7.25 (d, *J* = 8.6 Hz, 2H), 3.55 (bs, OH, 1H) 2.44 (s, 6H). ^{13}C NMR (100 MHz, CD_2Cl_2): δ 162.4 (q, *J* = 49.65 Hz), 148.5 (d, *J* = 3.1 Hz), 143.5 (d, *J* = 7.8 Hz), 136.2 (d, *J* = 7.7 Hz), 135.4, 135.15 (d, *J* = 2.8 Hz), 135.05 (d, *J* = 10.5 Hz), 135.0 (d, *J* = 3.2 Hz), 132.9, 131.9 (d, *J* = 13.7 Hz),

131.0 (d, *J* = 13.2 Hz), 130.9 (d, *J* = 13.2 Hz), 129.8 (d, *J* = 11.5 Hz), 129.5, 129.4 (qq, *J* = 2.76 and 31.3 Hz), 127.2, 125.1 (q, *J* = 271 Hz), 118.2 (d, *J* = 90.8 Hz), 118.1 (d, *J* = 90.6 Hz), 118.05 (septet, *J* = 3.89 Hz), 113.9 (d, *J* = 93.3 Hz), 110.6 (d, *J* = 90.5 Hz), 110.5 (d, *J* = 90.7 Hz), 22.1. ^{19}F NMR (376 MHz, CD_2Cl_2): δ -62.82. ^{31}P NMR (162 MHz, CD_2Cl_2): δ 22.14, -3.60. HRMS-ESI: Calc for $C_{58}H_{45}O_4P_3^{2+}$ $(M - 2BAr^F{}_4^-)^{2+}$ 449.1260, found 449.1288.

3.4.4. Characterizations of Friedel-Crafts Adducts from Reactions Run at 0 ˚C

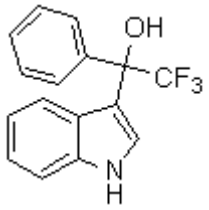

*2,2,2-Trifluoro-1-(1H-indole-3-yl)-1-phenylethanol (**5a**)*. A white solid (37.6 mg) was isolated. ^{1}H NMR (500 MHz, $CDCl_3$): δ 8.25 (bs, NH, 1H), 7.64-7.55 (m, 2H), 7.50-7.44 (m, 1H), 7.41-7.32 (m, 4H), 7.21-7.12 (m, 2H), 6.96 (t, *J* = 7.3 Hz, 1H), 2.89 (bs, OH, 1H). ^{13}C NMR (100 MHz, $CDCl_3$): δ 137.6, 136.2, 128.5, 127.9, 127.6 (d, *J* = 0.8 Hz), 125.3 (q, *J* = 284.3 Hz), 125.1, 123.2 (q, *J* = 3.0 Hz), 122.7, 120.9, 120.3, 114.1, 111.2, 77.0 (q, *J* = 29.6 Hz). ^{19}F NMR (376 MHz, $CDCl_3$): δ -76.75. HRMS-ESI: calc for $C_{16}H_{11}F_3NO^-$ $(M - H^+)^-$ 290.0798, found 290.0812.

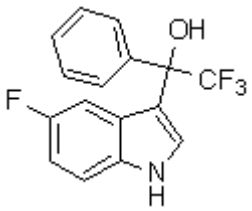

*2,2,2-trifluoro-1-(5-fluoro-1H-indole-3-yl)-1-phenylethanol (**5b**)*. A white solid (36.9 mg) was isolated. ^{1}H NMR (500 MHz, $CDCl_3$): δ 8.26 (bs, NH, 1H), 7.62-7.54 (m, 2H), 7.52-7.46 (m, 1H), 7.40-7.32 (m, 3H), 7.29 (dd, *J* = 4.4 and 8.9 Hz, 1H), 6.96-6.88 (m, 1H), 6.80 (*J* = 2.4 and 9.9 Hz, 1H), 2.64 (bs, OH, 1H). ^{13}C NMR (100 MHz, $CDCl_3$): δ 157.7 (d, *J* = 234.2 Hz), 137.2, 132.7, 128.7, 128.0, 127.5, 125.7 (d, *J* = 10.4 Hz), 125.3 (q, *J* = 284.4 Hz), 124.8 (q, *J* = 3.0 Hz), 114.4 (d, *J* = 4.8 Hz), 111.9 (d, *J* = 9.7 Hz), 111.4 (d, *J* = 26.5 Hz), 106.0 (d, *J* = 24.5 Hz), 77.1 (d, *J* = 26.5 Hz). ^{19}F NMR (376 MHz, $CDCl_3$): δ -76.78, -122.91. HRMS-ESI: calc for $C_{16}H_{10}F_4NO^-$ $(M - H^+)^-$ 308.0704, found 308.0689.

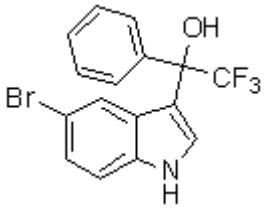

*2,2,2-Trifluoro-1-(5-bromo-1H-indole-3-yl)-1-phenylethanol (**5c**)*. A white solid (42.6 mg) was isolated. ^{1}H NMR (500 MHz, $CDCl_3$): δ 8.29 (bs, NH, 1H), 7.60-7.52 (m, 2H), 7.47-7.41 (m, 1H), 7.40-7.31 (m, 4H), 7.27-7.22 (m, 2H), 2.85 (bs, OH, 1H). ^{13}C NMR (100 MHz, $CDCl_3$): δ 137.2, 134.9, 128.8, 128.1, 127.4 (d, *J* = 3.3 Hz), 126.9, 125.2 (q, *J* = 284.5 Hz), 125.8, 124.3 (q, *J* = 3.0 Hz), 123.5, 113.9, 113.6, 112.6, 76.9 (q, *J* = 29.5 Hz). ^{19}F NMR (376 MHz, $CDCl_3$): δ -76.86. HRMS-ESI: calc for $C_{16}H_{10}BrF_3NO^-$ $(M - H^+)^-$ 367.9903 and 369.9883, found 367.9901 and 369.9876.

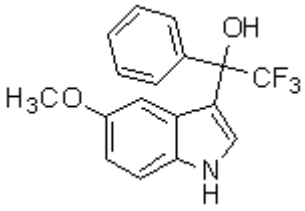

*2,2,2-Trifluoro-1-(5-methoxyl-1H-indole-3-yl)-1-phenylethanol (**5d**)*. A white solid (37.6 mg) was isolated. ^{1}H NMR (500 MHz, $CDCl_3$): δ 8.19 (bs, NH, 1H), 7.64-7.56 (m, 2H), 7.46-7.39 (m, 1H), 7.38-7.32 (m, 3H), 7.26-7.22 (m, 2H), 3.56 (s, 3H), 2.40 (bs, OH, 1H). ^{13}C NMR (100 MHz, $CDCl_3$): δ 154.0, 137.6, 131.3, 128.4, 127.9 (d, *J* = 0.4 Hz), 127.6, 125.7, 125.4 (q, *J* = 284.4 Hz), 123.7 (q, *J* = 3.0 Hz), 113.8, 113.0, 111.9, 102.5, 76.9 (q, *J* = 29.6 Hz), 55.5. ^{19}F NMR (376 MHz, $CDCl_3$): δ -76.75. HRMS-ESI: calc for $C_{17}H_{13}F_3NO_2^-$ $(M - H^+)^-$ 320.0904, found 320.0902.

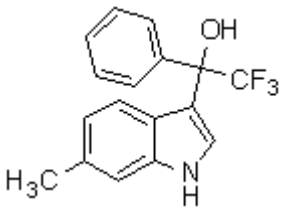

*2,2,2-Trifluoro-1-(6-methyl-1H-indole-3-yl)-1-phenylethanol (**5e**)*. A white solid (35.5 mg) was isolated. **1**H NMR (500 MHz, $CDCl_3$): δ 8.10 (bs, NH, 1H), 7.64-7.56 (m, 2H), 7.51-7.30 (m, 4H), 7.17 (s, 1H), 7.02 (d, *J* = 8.3 Hz, 1H), 6.80 (d, *J* = 8.2 Hz, 1H), 2.86 (bs, OH, 1H), 2.42 (s, 3H). ^{13}C NMR (100 MHz,

$CDCl_3$): δ 137.7, 136.7, 132.7, 128.4, 127.9, 127.6 (d, *J* = 0.6 Hz), 125.3 (q, *J* = 284.3 Hz), 122.9, 122.6 (q, *J* = 2.9 Hz), 122.1, 120.5, 113.9, 111.1, 77.0 (q, *J* = 29.5 Hz), 21.5. ^{19}F NMR (376 MHz, $CDCl_3$): δ -76.79. HRMS-ESI: calc for $C_{17}H_{13}F_3NO^-$ $(M - H^+)^-$ 304.0955, found 304.0941.

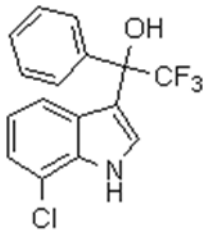

*2,2,2-Trifluoro-1-(7-chloro-1H-indole-3-yl)-1-phenylethanol (**5f**)*. A white solid (39.5 mg) was isolated. ^1H NMR (500 MHz, $CDCl_3$): δ 8.47 (bs, NH, 1H), 7.62-7.54 (m, 2H), 7.51 (s, 1H), 7.40-7.32 (m, 3H), 7.17 (d, *J* = 7.7 Hz, 1H), 7.06 (d, *J* = 8.1 Hz, 1H), 6.88 (t, *J* = 8.0 Hz, 1H), 2.86 (bs, OH, 1H). ^{13}C NMR (100 MHz, $CDCl_3$): δ 137.3, 133.6, 128.7, 128.0, 127.5 (d, *J* = 1.0 Hz), 126.6, 125.2 (q, *J* = 284.5 Hz), 123.7 (q, *J* = 3.0 Hz), 122.1, 121.1, 119.7, 116.7, 115.4, 76.9 (q, *J* = 29.7 Hz). ^{19}F NMR (376 MHz, $CDCl_3$): δ -76.84. HRMS-ESI: Calc for $C_{16}H_{10}ClF_3NO^-$ $(M - H^+)^-$ 324.0408 and 326.0379, found 324.0400 and 326.0379.

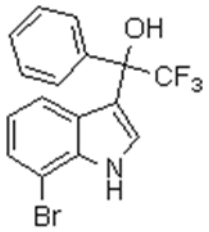

*2,2,2-Trifluoro-1-(7-bromo-1H-indole-3-yl)-1-phenylethanol (**5g**)*. A white solid (21.0 mg) was isolated. ^1H NMR (500 MHz, $CDCl_3$): δ 8.43 (bs, NH, 1H), 7.62-7.55 (m, 2H), 7.52 (s, 1H), 7.40-7.28 (m, 4H), 7.10 (d, *J* = 8.1 Hz, 1H), 6.83 (t, *J* = 8.0 Hz, 1H), 2.85 (bs, OH, 1H). ^{13}C NMR (100 MHz, $CDCl_3$): δ 137.3, 135.0, 128.7, 128.0, 127.5 (d, *J* = 1.0 Hz), 126.4, 125.2 (q, *J* = 284.5 Hz), 125.1, 123.6 (q, *J* = 2.9 Hz), 121.5, 120.3, 115.5, 104.7, 77.0 (q, *J* = 29.6 Hz). ^{19}F NMR (376 MHz, $CDCl_3$): δ -76.79. HRMS-ESI: calc for $C_{16}H_{10}BrF_3NO^-$ $(M - H^+)^-$ 367.9903 and 369.9883, found 367.9918 and 369.9892.

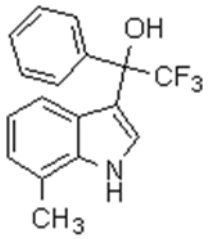

*2,2,2-Trifluoro-1-(7-methyl-1H-indole-3-yl)-1-phenylethanol (**5h**)*. A white solid (39.4 mg) was isolated. ^{1}H NMR (500 MHz, $CDCl_3$): δ 8.14 (bs, NH, 1H), 7.64-7.55 (m, 2H), 7.50-7.43 (m, 1H), 7.38-7.31 (m, 3H), 7.03-6.96 (m, 2H), 6.88 (t, *J* = 7.6 Hz, 1H), 2.89 (bs, OH, 1H), 2.50 (s, 3H). ^{13}C NMR (100 MHz, $CDCl_3$): δ 137.7, 135.8, 128.4, 127.9, 127.6 (d, *J* = 0.5 Hz), 125.3 (q, *J* = 284.3 Hz), 124.6, 123.2, 122.9 (q, *J* = 3.0 Hz), 120.5, 120.4, 118.6, 114.6, 77.0 (q, *J* = 29.5 Hz), 16.5. ^{19}F NMR (376 MHz, $CDCl_3$): δ -76.74. HRMS-ESI: calc for $C_{17}H_{13}F_3NO^-$ $(M - H^+)^-$ 304.0955, found 304.0950.

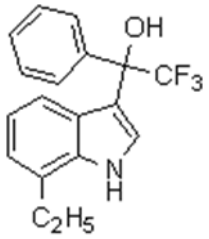

*2,2,2-Trifluoro-1-(7-ethyl-1H-indole-3-yl)-1-phenylethanol (**5i**)*. A white solid (38.1 mg) was isolated. ^{1}H NMR (500 MHz, $CDCl_3$): δ 8.22 (bs, NH, 1H), 7.65-7.57 (m, 2H), 7.49-7.43 (m, 1H), 7.38-7.32 (m, 3H), 7.06-6.98 (m, 2H), 6.96 (t, *J* = 8.0 Hz, 1H), 2.92-2.84 (m, 3H), 1.39 (t, *J* = 7.6 Hz, 3H). ^{13}C NMR (100 MHz, $CDCl_3$): δ 137.7, 135.2, 128.4, 127.9, 127.6 (d, *J* = 1.0 Hz), 126.6, 125.3 (q, *J* = 284.4 Hz), 124.9, 122.8 (q, *J* = 3.0 Hz), 121.2, 120.5, 118.6, 114.5, 77.0 (q, *J* = 29.4 Hz), 23.9, 13.7. ^{19}F NMR (376 MHz, $CDCl_3$): δ -76.78. HRMS-ESI: Calc for $C_{18}H_{15}F_3NO^-$ $(M - H^+)^-$ 318.1111, found 318.1113.

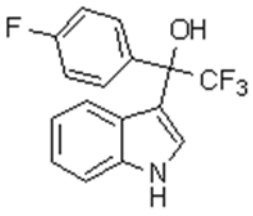

*2,2,2-Trifluoro-1-(4-fluorophenyl)-1-(1H-indole-3-yl)ethanol (**5j**)*. A white solid (40.0 mg) was isolated. ^{1}H NMR (500 MHz, $CDCl_3$): δ 8.27 (bs, NH, 1H), 7.60-7.50 (m, 2H), 7.47 (s, 1H), 7.39 (d, *J* = 8.2 Hz, 1H), 7.20 (t, *J* = 7.7 Hz, 1H), 7.13 (d, *J* = 7.9 Hz, 1H), 7.06-6.92 (t, *J* = 7.6 Hz, 3H), 2.89 (bs, OH, 1H).

^{13}C NMR (100 MHz, $CDCl_3$): δ 162.8 (d, *J* = 245.9 Hz), 136.3, 133.4 (d, *J* = 3.2 Hz), 129.7 (d, *J* = 8.3 Hz), 125.2 (q, *J* = 284.0 Hz), 125.0, 123.1 (q, *J* = 3.0 Hz), 122.9, 120.8, 120.4, 114.8 (d, *J* = 21.5 Hz), 113.8, 111.3, 76.6 (q, *J* = 29.8 Hz), ^{19}F NMR (376 MHz, $CDCl_3$): δ -77.08, -113.82. HRMS-ESI: calc for $C_{16}H_{10}F_4NO^-$ $(M - H^+)^-$ 308.0704, found 308.0708.

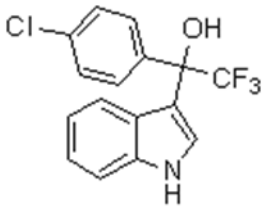

*1-(4-Chlorophenyl)-2,2,2-trifluoro-1-(1H-indole-3-yl)ethanol (**5k**)*. A white solid (40.0 mg) was isolated. ^{1}H NMR (500 MHz, $CDCl_3$): δ 8.27 (bs, NH, 1H), 7.53 (d, *J* = 8.5 Hz, 2H), 7.49-7.44 (m, 1H), 7.39 (d, *J* = 8.2 Hz, 1H), 7.34-7.28 (m, 2H), 7.23-7.17 (m, 1H), 7.13 (d, *J* = 8.1 Hz, 1H), 6.98 (t, *J* = 8.0 Hz, 1H), 2.89 (bs, OH, 1H). ^{13}C NMR (100 MHz, $CDCl_3$): δ 136.24, 136.20, 134.6, 129.2, 128.1, 125.1 (q, *J* = 284.3 Hz), 124.9, 123.1 (q, *J* = 3.1 Hz), 122.9, 120.8, 120.4, 113.5, 111.3, 76.6 (q, *J* = 29.8 Hz). ^{19}F NMR (376 MHz, $CDCl_3$): δ -77.02. HRMS-ESI: calc for $C_{16}H_{10}ClF_3NO^-$ $(M - H^+)^-$ 324.0408 and 326.0379, found 324.0394 and 326.0373.

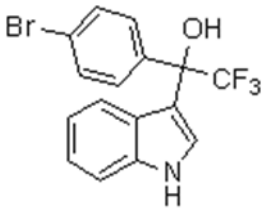

*1-(4-Bromophenyl)-2,2,2-trifluoro-1-(1H-indole-3-yl)ethanol (**5l**)*. A white solid (48.7 mg) was isolated. ^{1}H NMR (500 MHz, $CDCl_3$): δ 8.28 (bs, NH, 1H), 7.51-7.42 (m, 5H), 7.39 (d, *J* = 8.2 Hz, 1H), 7.23-7.17 (m, 1H), 7.13 (d, *J* = 8.0 Hz, 1H), 6.98 (t, *J* = 8.05 Hz, 1H), 2.89 (bs, OH, 1H). ^{13}C NMR (100 MHz, $CDCl_3$): δ 136.7, 136.2, 131.1, 129.5 (d, *J* = 0.5 Hz), 127.9, 125.0 (q, *J* = 284.4 Hz), 124.9, 123.1 (q, *J* = 3.1 Hz), 123.0, 121.8, 120.4, 113.4, 111.3, 76.7 (q, *J* = 29.7 Hz). ^{19}F NMR (376 MHz, $CDCl_3$): δ -76.77. HRMS-ESI: calc for $C_{16}H_{10}BrF_3NO^-$ $(M - H^+)^-$ 367.9903 and 369.9883, found 367.9905 and 369.9884.

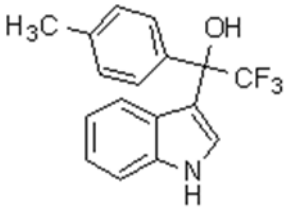

*2,2,2-Trifluoro-1-(1H-indole-3-yl)-1-p-tolylethanol (**5m**)*. A white solid (36.7 mg) was isolated. ^{1}H NMR (500 MHz, $CDCl_3$): δ 8.24 (bs, NH, 1H), 7.48 (d, *J* = 8.1 Hz, 2H), 7.46-7.42 (m, 1H), 7.38 (d, *J* = 7.9 Hz, 1H), 7.19 (d, *J* = 7.6 Hz, 2H), 7.16 (d, *J* = 8.5 Hz, 2H), 6.97 (t, *J* = 7.4 Hz, 1H), 2.87 (bs, OH, 1H), 2.36 (s, 3H). ^{13}C NMR (100 MHz, $CDCl_3$): δ 138.3, 136.2, 134.7, 128.7, 127.5 (d, *J* = 0.6 Hz), 125.4 (q, *J* = 284.3 Hz), 125.2, 123.1 (q, *J* = 3.0 Hz), 122.7, 121.0, 120.2, 114.2, 111.2, 76.9 (q, *J* = 29.4 Hz), 21.1. ^{19}F NMR (376 MHz, $CDCl_3$): δ -76.88. HRMS-ESI: calc for $C_{17}H_{13}F_3NO^-$ $(M - H^+)^-$ 304.0955, found 304.0955.

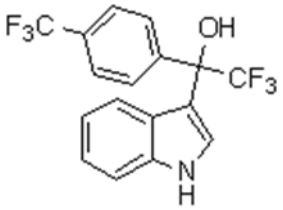

*2,2,2-Trifluoro-1-(4-trifluoromethylphenyl)-1-(1H-indole-3-yl)ethanol (**5n**)*. A white solid (45.1 mg) was isolated. ^{1}H NMR (500 MHz, $CDCl_3$): δ 8.30 (bs, NH, 1H), 7.73 (d, *J* = 8.2 Hz, 2H), 7.61 (d, *J* = 8.3 Hz, 2H), 7.54-7.48 (m, 1H), 7.41 (d, *J* = 8.3 Hz, 1H), 7.21 (t, *J* = 7.3 Hz, 1H), 7.11 (d, *J* = 8.1 Hz, 1H), 6.98 (t, *J* = 7.3 Hz, 1H), 2.96 (bs, OH, 1H). ^{13}C NMR (100 MHz, $CDCl_3$): δ 141.5, 136.3, 130.7 (d, *J* = 32.3 Hz), 128.2, 125.0 (q, *J* = 284.4 Hz), 124.9 (q, *J* = 3.7 Hz), 124.8, 124.0 (q, *J* = 270.5 Hz), 123.2 (d, *J* = 3.1 Hz), 123.1, 120.6, 120.5, 113.3, 111.4, 76.8 (q, *J* = 30.0 Hz). ^{19}F NMR (376 MHz, $CDCl_3$): δ -62.62, -76.84. HRMS-ESI: calc for $C_{17}H_{10}F_6NO^-$ $(M - H^+)^-$ 358.0672, found 358.0687.

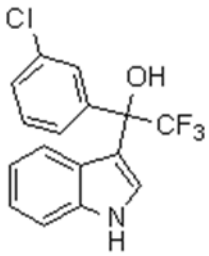

*1-(3-Chlorophenyl)-2,2,2-trifluoro-1-(1H-indole-3-yl)ethanol (**5o**)*. A white solid (40.8 mg) was isolated. ^{1}H NMR (500 MHz, $CDCl_3$): δ 8.29 (bs, NH, 1H), 7.66 (s, 1H), 7.51-7.46 (m, 1H), 7.43 (d, *J* = 7.8 Hz, 1H), 7.39 (d, *J* = 8.2 Hz, 1H), 7.33 (d, *J* = 8.0 Hz, 1H), 7.26 (t, *J* = 8.0 Hz, 1H), 7.21 (d, *J* = 7.8 Hz, 1H), 7.17 (d, *J* = 8.2 Hz, 1H), 6.98 (r, *J* = 7.8 Hz, 1H), 2.57 (bs, OH, 1H). ^{13}C NMR (100 MHz, $CDCl_3$): δ 139.7, 136.2, 134.0, 129.2, 128.8, 127.8 (d, *J* = 1.0 Hz), 126.0, 125.0 (q, *J* = 284.5 Hz), 124.9, 123.1 (q, *J* = 3.0 Hz), 122.9, 120.8, 120.5, 113.4, 111.3, 76.6 (q, *J* = 29.8 Hz). ^{19}F NMR (376 MHz, $CDCl_3$): δ -76.84. HRMS-ESI: calc for $C_{16}H_{10}ClF_3NO^-$ $(M - H^+)^-$ 324.0408 and 326.0379, found 324.0417 and 326.0394.

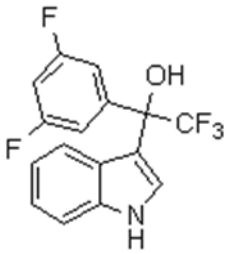

*2,2,2-Trifluoro-1-(1H-indole-3-yl)-1-3,5-difluorophenylethanol (**5p**)*. A white solid (41.5 mg) was isolated. ^{1}H NMR (500 MHz, $CDCl_3$): δ 8.31 (bs, NH, 1H), 7.51-7.46 (m, 1H), 7.41 (d, *J* = 8.2 Hz, 1H) 7.24-7.17 (m, 2H), 7.14 (d, *J* = 6.7 Hz, 2H), 7.04-6.96 (m, 1H), 6.85-6.74 (m, 1H), 2.95 (bs, OH, 1H). ^{13}C NMR (100 MHz, $CDCl_3$): δ 162.6 (dd, *J* = 12.3 and 246.4 Hz), 141.7 (t, *J* = 8.9 Hz), 136.2, 124.8 (q, *J* = 284.5 Hz), 124.7, 123.11, 123.06 (q, *J* = 3.1 Hz), 120.6 (d, *J* = 11.5 Hz), 112.9, 111.4, 111.099 (d, *J* = 26.4 Hz), 111.098 (d, *J* = 11.2 Hz), 104.1 (t, *J* = 25.2 Hz), 76.5 (q, *J* = 29.9 Hz). ^{19}F NMR (376 MHz, $CDCl_3$): δ -76.93, -109.72. HRMS-ESI: calc for $C_{16}H_9F_5NO^-$ $(M - H^+)^-$ 326.0610, found 326.0626.

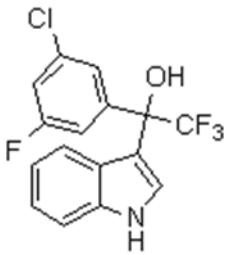

*1-(3-Chloro-5-fluorophenyl)-2,2,2-trifluoro-1-(1H-indole-3-yl)ethanol (**5q**).* A white solid (40.8 mg) was isolated. ^{1}H NMR (500 MHz, $CDCl_3$): δ 8.29 (bs, NH, 1H), 7.52-7.46 (m, 1H), 7.45-7.38 (m, 2H), 7.25-7.16 (m, 3H), 7.12-7.06 (m, 1H), 7.02 (t, *J* = 8.0 Hz, 1H), 2.93 (bs, OH, 1H). ^{13}C NMR (100 MHz,

$CDCl_3$): δ 162.3 (d, *J* = 247.5 Hz), 141.5 (d, *J* = 8.1 Hz), 136.2, 134.7 (d, *J* = 10.4 Hz), 124.8 (q, *J* = 284.5 Hz), 124.7, 123.9 (d, *J* = 1.7 Hz), 123.13, 123.09 (q, *J* = 3.1 Hz), 120.6 (d, *J* = 15.3 Hz), 116.5 (d, *J* = 24.6 Hz), 113.8 (d, *J* = 23.5 Hz), 112.8, 111.4, 76.8 (q, *J* = 29.4 Hz). ^{19}F NMR (376 MHz, $CDCl_3$): δ -76.92, -110.91. HRMS-ESI: calc for $C_{16}H_9ClF_4NO^-$ $(M - H^+)^-$ 342.0314 and 344.0285, found 342.0322 and 344.0300.

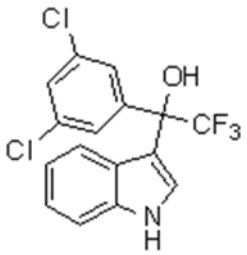

*1-(3.5-Dichlorophenyl)-2,2,2-trifluoro-1-(1H-indole-3-yl)ethanol (**5r**).* A white solid (44.6 mg) was isolated. ^1H NMR (500 MHz, $CDCl_3$): δ 8.30 (bs, NH, 1H), 7.53-7.45 (m, 3H), 7.41 (d, *J* = 8.2 Hz, 1H), 7.35 (t, *J* = 1.9 Hz, 1H), 7.25-7.17 (m, 2H), 7.02 (t, *J* = 7.3 Hz, 1H), 2.92 (bs, OH, 1H). ^{13}C NMR (100 MHz, $CDCl_3$): δ 141.1, 136.2, 134.7, 128.9, 126.4 (d, *J* = 1.1 Hz), 124.8 (q, *J* = 284.6 Hz), 124.6, 123.2, 123.1 (q, *J* = 3.1 Hz), 120.7, 120.5, 112.7, 111.4, 76.7 (q, *J* = 30.1 Hz). ^{19}F NMR (376 MHz, $CDCl_3$): δ -76.87. HRMS-ESI: calc for $C_{16}H_9Cl_2F_3NO^-$ $(M - H^+)^-$ 358.0019 ($^{35}Cl/^{35}Cl$) and 359.9989 ($^{35}Cl/^{37}Cl$), found 358.0005 and 359.9989.

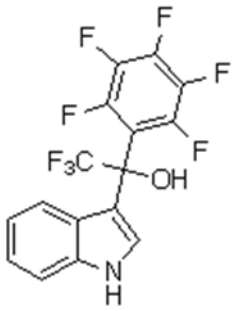

*2,2,2-Trifluoro-1-(1H-indole-3-yl)-1-2,3,4,5,6-pentafluorophenylethanol (**5s**).* A white solid (14.8 mg) was isolated. ^1H NMR (500 MHz, $CDCl_3$): δ 8.32 (bs, NH, 1H), 7.46-7.38 (m, 2H), 7.28 (t, *J* = 8.1 Hz, 1H), 7.25 (t, *J* = 7.8 Hz, 1H), 7.06 (t, *J* = 7.8 Hz, 1H), 3.32 (bs, OH, 1H). ^{13}C NMR (100 MHz, $CDCl_3$): δ 144.8 (dm, *J* = 253.9 Hz), 141.6 (dm, *J* = 255.3 Hz), 137.9 (dm, *J* = 251.7 Hz), 136.0, 128.8, 126.0, 124.7, 123.2, 122.3 (m), 120.7, 119.2, 111.9 (t, *J* = 1.9 Hz), 111.7, 76.7 (q, *J* = 33.5 Hz). ^{19}F NMR (376

MHz, $CDCl_3$): δ -78.18 (t, *J* = 8.8 Hz), -136.48 (ddq, *J* = 4.3, 17.7 and 24.4 Hz), -151.82 (tt, *J* = 4.8 and 21.8 Hz), -161.19 (m). HRMS-ESI: calc for $C_{16}H_6F_8NO^-$ $(M - H^+)^-$ 380.0327, found 380.0334.

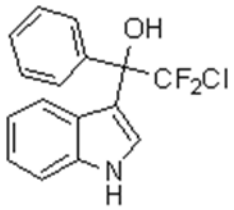

*2-Chloro-2,2-difluoro-1-(1H-indole-3-yl)-1-phenylethanol (**5t**).* A white solid (15.5 mg) was isolated. ^1H NMR (500 MHz, $CDCl_3$): δ 8.24 (bs, NH, 1H), 7.65-7.58 (m, 2H), 7.54-7.50 (m, 1H), 7.38 (d, *J* = 8.2 Hz, 1H), 7.36-7.30 (m, 3H), 7.23 (d, *J* = 8.0 Hz, 1H), 7.20-7.14 (m, 1H), 6.98-6.91 (m, 1H), 3.06 (bs, OH, 1H). ^{13}C NMR (100 MHz, $CDCl_3$): δ 138.1, 136.1, 131.4 (t, *J* = 300.5 Hz), 128.4, 128.0, 127.7, 125.5, 123.2 (t, *J* = 3.7 Hz), 122.7, 131.1, 120.2, 114.6, 111.1, 80.6 (t, *J* = 25.2 Hz). ^{19}F NMR (376 MHz, $CDCl_3$): δ -60.54. HRMS-ESI: calc for $C_{16}H_{11}ClF_2NO^-$ $(M - H^+)^-$ 306.0503 and 308.0473, found 306.0487 and 308.0506.

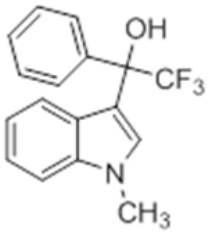

*2,2,2-Trifluoro-1-(1-methyl-indole-3-yl)-1-phenylethanol (**5u**).* A white solid (30.4 mg) was isolated. ^1H NMR (500 MHz, $CDCl_3$): δ 7.65-7.58 (m, 2H), 7.38-7.30 (m, 5H), 7.22 (t, *J* = 7.2 Hz, 1H), 7.14 (d, *J* = 8.0 Hz, 1H), 6.96 (t, *J* = 7.3 Hz, 1H), 3.85 (s, 3H), 2.83 (bs, OH, 1H). ^{13}C NMR (100 MHz, $CDCl_3$): δ 137.8, 137.1, 128.4, 127.9, 127.8 (d, *J* = 2.8 Hz), 127.7, 125.7, 125.3 (q, *J* = 284.4 Hz), 122.3, 121.0, 119.8, 112.4, 109.4, 77.0 (q, *J* = 29.4 Hz), 33.0. ^{19}F NMR (376 MHz, $CDCl_3$): δ -76.73. HRMS-ESI: calc for $C_{17}H_{13}F_3NO^-$ $(M - H^+)^-$ 304.0955, found 304.0962.

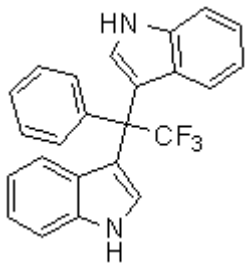

*3-(2,2,2-Trifluoro-1-(1H-indole-3-yl)-1-phenylyl)-1H-indole (**6**).* ^{1}H NMR (500 MHz, $CDCl_3$): δ 8.08 (bs, NH, 2H), 7.54 (d, *J* = 6.90 Hz, 2H), 7.37 (d, *J* = 8.2 Hz, 2H), 7.34-7.27 (m, 3H), 7.20 (d, *J* = 8.3 Hz, 2H), 7.16 (t, *J* = 8.0 Hz, 2H), 6.97-6.91 (m, 2H), 6.88 (d, *J* = 2.6 Hz, 2H). ^{13}C NMR (100 MHz, $CDCl_3$): δ 139.3, 136.7, 129.6 (d, *J* = 2.0 Hz), 127.9, 127.5, 126.7, 126.4, 126.3, 122.3 (q, *J* = 3.3 Hz), 122.0, 119.7, 115.5, 111.1, 55.8. ^{19}F NMR (376 MHz, $CDCl_3$): δ -62.55. HRMS-ESI: calc for $C_{24}H_{16}F_3N_2^-$ $(M - H^+)^-$ 389.1271, found 389.1259.

Chapter 4: Electrostatically Enhanced Phosphoric Acids and Their Applications in Asymmetric Friedel-Crafts Alkylations

4.1. Introduction

Over the past decade or so a large body of novel Brønsted acids have emerged as effective organocatalysts for a variety of organic transformations.[1] These species are excellent alternatives to metal-containing catalysts as they typically are moisture and air tolerant, and are considered to be environmentally friendlier in nature.[2] Among these Brønsted acid catalysts, phosphoric acids bearing a 1,1'-bi-2-naphthol (BINOL) backbone have been extensively investigated. Hundreds of derivatives have been prepared as they provide a means for carrying out enantioselective acid-catalyzed processes.[3] This includes asymmetric carbon-carbon bond forming transformations[4] which are extremely valuable, but can be synthetically challenging to carry out.[5]

BINOL-derived phosphoric acids are generally more active catalysts than other chiral Brønsted acids such as BINOL derivatives,[6] thioureas,[7] and α,α,α,α-tetraaryl-1,3-dioxolane-4,5-dimethanols (TADDOLs)[8] due to their greater acidities.[9] To broaden their scope and develop more reactive derivatives, several strategies have been employed. These include introducing electron withdrawing groups into the catalyst backbone,[10] modifying the phosphate functional group (e.g., to phosphoramides),[11] and employing acidic achiral additives.[12]

More recently, incorporation of positively charged pyridinium ion centers without the introduction of new hydrogen bond donating sites were found to improve the catalytic abilities of phenols,[13] thioureas,[14] and phosphoric acids[15] by orders of magnitude. In addition, several chiral charge-activated thioureas were reported and found to display excellent reactivities and good enantioselectivities in Friedel-Crafts alkylations of indoles with *trans*-*β*-nitrostyrenes.[16] Chiral phosphonium ion-containing (R)-BINOL-derived phosphoric acids were also recently reported and found to give good to excellent enantioselectivities in the reactions of indoles with 2,2,2-trifluoroacetophenones.[17] To build upon these efforts a number of new derivatives are reported, and both charged and noncharged catalysts were investigated using the reaction illustrated in eq. 1 as a well-studied test platform (Figure 1).

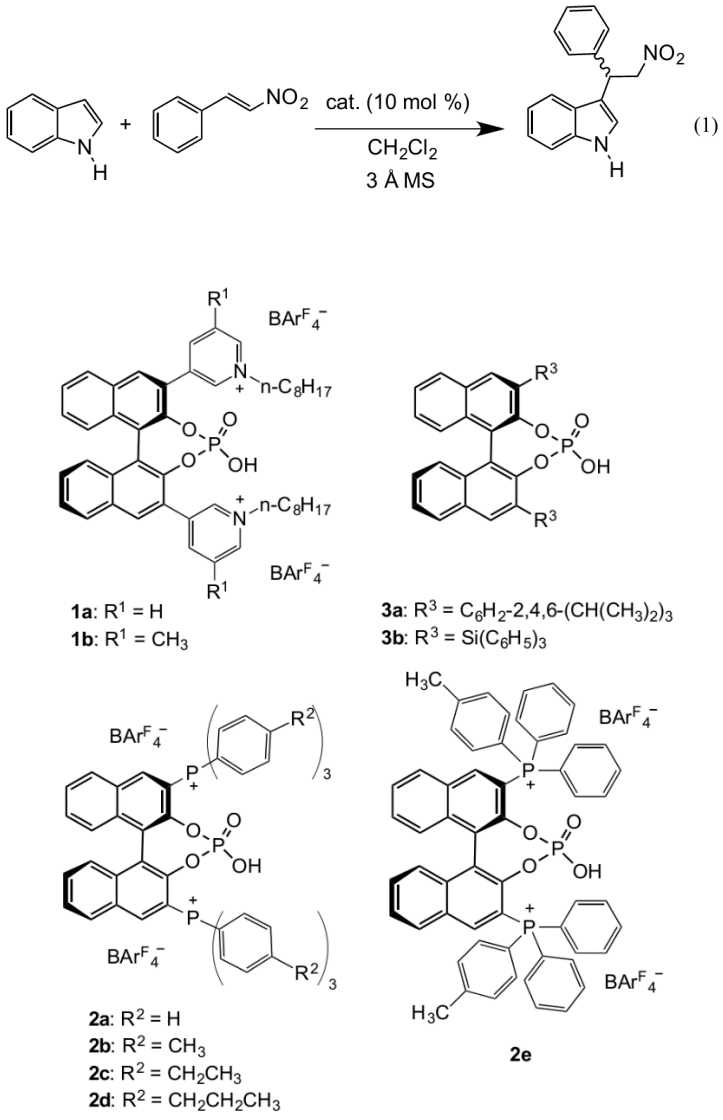

Figure 1. Catalysts used in this work; different counteranions for **2a** were also studied.

4.2. Results and Discussion

Our study was initiated by synthesizing **1a** and **1b**, two (*R*)-BINOL derived phosphoric acids with *N*-octylpyridinium groups at the 3,3'-backbone positions. A noncoordinating tetrakis[3,5-bis(trifluoromethyl)phenyl]borate anion ($BAr^F_4^-$) was incorporated as the counterion because it enhances reactivity and solubility in nonpolar media.[15,18] Catalytic activities for the Friedel-Crafts alkylation of indole with *trans-β*-nitrostyrene were examined at different temperatures in CH_2Cl_2 with

a 10 mol % catalyst loading and 3 Å molecular sieves (MS) to remove adventitious moisture (Table 1). Disappointingly, the enantioselectivities were poor with the best results of only 21% and 16% ee at -30 ˚C for **1a** and **1b**, respectively (entries 1-6). These findings led us to examine bulky triaryl phosphonium ion derivatives **2a-2e** as conveniently prepared alternatives.[17,19]

Table 1. Optimizations of catalysts and reaction conditions.[a]

entry	cat.	T (˚C)	time (h)	yield (%)[b]	ee (%)[c]
1	**1a**	20	24	70	-14
2	**1a**	0	48	58	-16
3	**1a**	-30	73	26	-21
4	**1b**	20	24	70	-12
5	**1b**	0	48	64	-13
6	**1b**	-30	73	30	-16
7	**2a**	20	8	59	35
8	**2a**	0	24	50	36
9	**2a**	-30	46	38	40
10	**2b**	20	5	68	50
11	**2b**	0	24	75	59
12	**2b**	-30	46	81	70
13	**2c**	20	5	67	36
14	**2c**	0	24	71	46
15	**2c**	-30	46	83	61
16	**2d**	20	5	69	34
17	**2d**	0	24	73	46
18	**2d**	-30	46	85	61
19	**2e**	20	5	73	47
20	**2e**	0	24	63	51
21	**2e**	-30	46	60	57

[a]Reactions were performed with 0.1 mmol indole, 0.2 mmol *trans-β*-nitrostyrene, 0.01 mmol catalyst and 10 mg of 3 Å MS in 0.5 mL of CH_2Cl_2. [b]Isolated yield. [c]Determined by chiral HPLC.

To our delight, the preliminary screening results for the phosphonium ion-tagged phosphoric acids (entries 7-21) revealed that they are both more reactive and enantioselective than their pyridinium ion-containing analogues; intriguingly they also led to a reversal in the preferred enantiomer. The parent

derivative **2a** only gave an ee of 35-40% at temperatures ranging from 20 to -30 ˚C (entries 7-9), but incorporation of *p*-methyl substituents on to each phenyl group led to significant improvements in the reaction conversions and stereoselectivities (entries 10-12). That is, over the same time period at -30 ˚C, the isolated yield increased from 38% to 81% and the ee improved from 40% to 70%. A further decrease in temperature to -50 ˚C was not practical in that less than a 10% conversion was observed after 48 hours. Replacement of the *p*-methyl groups by larger ethyl or *n*-propyl substituents had little impact on the product yield, but led to ~10-15% lower ee values over the studied temperature range (entries 13-18).

To address whether the improvement in the stereoselectivity brought about by the *p*-methyl groups is due to steric or electronic effects, the diphenyl(*p*-tolyl)phosphonium ion-tagged BINOL phosphoric acid **2e** was prepared and investigated. Its steric requirements should be very similar to those of the unsubstituted phosphoric acid **2a** because the Ar_3P group can rotate readily enabling any unfavorable interactions brought about by the methyl group to be minimized. Electronically, **2e** should be intermediate in behavior to **2a** and **2b** since these compounds have 2, 0 and 6 methyl groups, respectively. The observed enantioselectivities with **2e** at 20, 0 and -30 ˚C (entries 19-21) are between the results for **2a** and **2b**. This indicates that the larger ee values for **2b** compared to **2a** are primarily due to the electron donating effects of the six methyl groups in the former compound.

The effect of the counterion was examined next by taking the chloride anion precursor to **1a** and converting it to the BF_4^-, PF_6^- and $B(C_6F_5)_4^-$ salts **2f**-**2h** (eq. 2). These species were compared to the

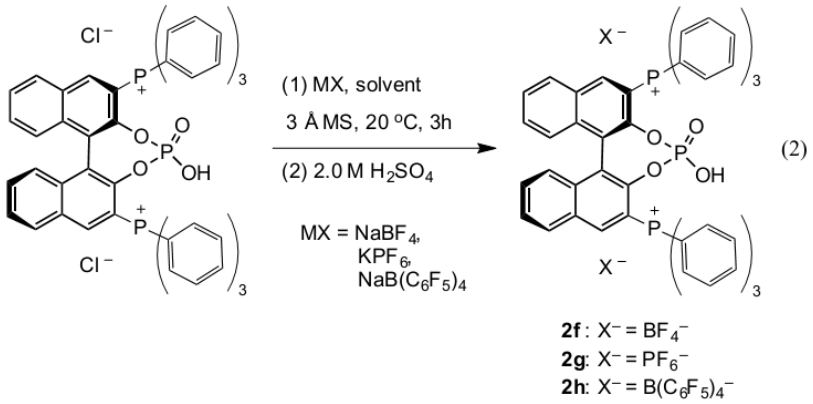

$BAr^F{}_4^-$ salt **2a** at -30 ˚C and their reactivity order is as follows: $BF_4^- < PF_6^- < B(C_6F_5)_4^- < BAr^F{}_4^-$ (Table 2). The resulting enantioselectivities also seem to track with this order and is as follows: $BF_4^- \approx PF_6^- < B(C_6F_5)_4^- < BAr^F{}_4^-$. Consequently, all of the remaining experiments were carried out with $BAr^F{}_4^-$ salts.

Table 2. Counteranion screening results.[a]

entry	cat.	time (h)	yield (%)[b]	ee (%)[c]
1	**2f**	48	18	<1
2	**2g**	48	23	<1
3	**2h**	48	33	33
4	**2a**	46	38	40

[a]Reactions were performed at -30 ˚C with 0.1 mmol indole, 0.2 mmol *trans*-*β*-nitrostyrene, 0.01 mmol of the indicated catalyst and 10 mg of 3 Å MS in 0.5 mL of CH_2Cl_2. [b]Isolated yield. [c]Determined by chiral HPLC.

Reaction additives and media were explored next at -30 ˚C with **2b** as the catalyst (Table 3). Lower yields and enantioselectivities were found for the reactions carried out without MS or with additives other than 3 Å MS (entries 2-5). Of the single component solvents that were examined with 3 Å MS (entries 1 and 6-11), CH_2Cl_2 gave both the highest yield and ee; 81% and 70%, respectively. 1,2-Dichloroethane (DCE) and chlorobenzene are somewhat worse media for this transformation in terms of both the yield and enantioselectivity, but the results in $CHCl_3$ surprisingly are much poorer (i.e., a 54% yield and an ee of 41% were obtained; entries 1 and 6-8). Hydrogen bond accepting solvents such as EtOAc and THF completely deactivate the catalyst shutting down product formation (entries 9-10). Benzonitrile, a weaker hydrogen bond acceptor than the two oxygen-containing solvents, does not retard the catalyst as strongly (entry 11). It still is a very ineffective medium, and affords the product with a 7% lower ee than in CH_2Cl_2.

In an attempt to improve these results, a number of binary solvent mixtures with a less polar component (i.e., benzene, toluene, *m*-xylene, and carbon tetrachloride) were tested (entries 12-17). A 1:1 (v/v) combination of CH_2Cl_2 and C_6H_6 led to a 5% reduction in yield but a 1% increase in ee relative

Table 3. Reaction medium screening.[a]

entry	solvent	time (h)	yield (%)[b]	ee (%)[c]
1	CH_2Cl_2	46	81	70
2[d]	CH_2Cl_2	47	54	67
3[e]	CH_2Cl_2	48	73	57
4[f]	CH_2Cl_2	48	62	57
5[g]	CH_2Cl_2	48	61	62
6	DCE[h]	46	73	63
7	C_6H_5Cl	45	77	64
8	$CHCl_3$	45	54	41
9	EtOAc	164	trace	–
10	THF	164	trace	–
11	C_6H_5CN	140	43	63
12	CH_2Cl_2/C_6H_6 1:1	46	76	71
13	$CH_2Cl_2/C_6H_5CH_3$ 1:1	47	83	66
14	CH_2Cl_2/*m*-xylene 1:1	47	76	63
15	CH_2Cl_2/CCl_4 1:1	48	86	70
16	CH_2Cl_2/C_6H_6 1:2	50	88	72
17	1,2-DCE/C_6H_6 1:1	45	77	65

[a]Reactions were performed at -30 ˚C with 0.1 mmol indole, 0.2 mmol *trans*-*β*-nitrostyrene, 0.01 mmol of **2b** and 10 mg of 3 Å MS (unless otherwise noted) in 0.5 mL of the specified solvent; mixtures are on a volume to volume basis. [b]Isolated yield. [c]Determined by chiral HPLC. [d]No MS were used. [e]10 mg of 4 Å MS were used. [f]10 mg of 5 Å MS were used. [g]10 mg of 13X MS were used. [h]DCE = 1,2-dichloroethane.

to the former solvent (entry 12). The opposite trend was observed with a 1:1 CH_2Cl_2/toluene mixture in that the yield was 2% higher but the ee dropped 4% (entry 13). Unfortunately, *m*-xylene was ineffective as a cosolvent in both regards and led to a ~6% decrease in the yield and ee (entry 14). Carbon tetrachloride and dichloromethane in a 1:1 ratio gave an improved yield (86%) without affecting the ee (entry 15). Higher proportions of benzene were also investigated since it is the only cosolvent that led to a higher observed ee. A 1:2 CH_2Cl_2/C_6H_6 mixture afforded our best result, an 88% isolated yield and a 72% ee (entry 16). A further increase in benzene to a 1:3 solvent combination is not feasible because the catalyst does not dissolve in this medium. Finally, a previously reported 1:1 DCE/C_6H_6 solvent combination was examined,[20] but it led to a reduction in both the yield and enantioselectivity (entry 17).

Under our optimal conditions, the reactivity of charged catalyst **2b** was compared to two similar and well-established noncharged analogues, (*R*)-3,3'-bis(2,4,6-triisopropylphenyl)-BINOL phosphoric acid (TRIP, **3a**)[21] and (*R*)-3,3'-bis(triphenylsilyl)-BINOL phosphoric acid (**3b**, Figure 1).[22] The reactions of indole with *trans*-*β*-nitrostyrene were followed at the same three time points by ^{1}H NMR spectroscopy, and enantioselectivies were measured by chiral HPLC. Second-order rate constants and the resulting ee values are given in Table 4. Both TRIP and its 3,3'-bis(triphenylsilyl) analogue are equally effective in this transformation with $k = 0.030 \pm 0.003$ M^{-1} h^{-1} and ee values of 49% and 48%, respectively (entries 1 and 2). The charged triarylphosphonium ion-containing catalyst **2b** was found to be ~5 times more reactive and significantly more selective with an ee of 72% (entry 3).

Table 4. Comparison of charged and noncharged catalysts.[a]

entry	cat.	k (M^{-1} h^{-1})[b]	ee (%)[c]
1	**3a**	2.7 x 10^{-2}	49
2	**3b**	3.3 x 10^{-2}	48
3	**2b**	1.6 x 10^{-1}	72

[a]Reactions were carried out at -30 ˚C with 0.1 mmol indole, 0.2 mmol *trans*-*β*-nitrostyrene, 0.01 mmol of **2b** and 10 mg of 3 Å MS in 0.5 mL of a 1:2 CH_2Cl_2/C_6H_6 mixture. [b]Determined by ^{1}H NMR. [c]Measured by chiral HPLC.

The scope of this reaction was also addressed (eq 3), and the results are summarized in Table 5. A wide range of indoles (**4a**-**4k**) and *trans*-*β*-nitrostyrenes (**5a**-**5f**) bearing electron-donating and electron-withdrawing groups are tolerated and afford high conversions (75 - >99%) with enantiomeric excesses ranging from 60-90%. Indoles **4b**-**4d** and **4f** with an electron-withdrawing halogen atom at the 5- or 6-position react more slowly than the parent compound (i.e., **4a**) and afforded ~10% lower conversions after an ~33% longer time period, but had little impact upon the ee (i.e., the values ranged from 69-73%, entries 1-4 and 6). A chlorine atom at the 7-position (**4e**) behaved differently in that it had a bigger influence on the rate of the reaction and the enantioselectivity. That is, significantly more time was

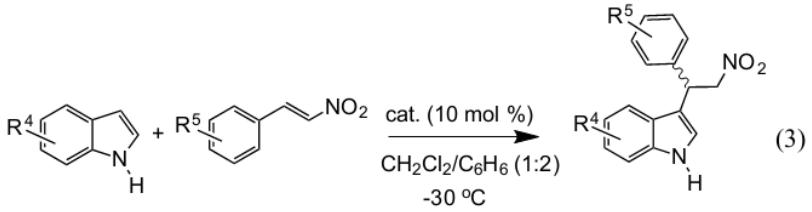

(3)

4a: R^4 = H
4b: R^4 = 5-F
4c: R^4 = 5-Cl
4d: R^4 = 6-Cl
4e: R^4 = 7-Cl
4f: R^4 = 5-Br
4g: R^4 = 5-MeO
4h: R^4 = 6-MeO
4i: R^4 = 6-Me
4j: R^4 = 7-Me
4k: R^4 = 7-Et

5a: R^5 = H
5b: R^5 = 4-F
5c: R^5 = 2-Cl
5d: R^5 = 3-Br
5e: R^5 = 4-Br
5f: R^5 = 4-MeO

6a: R^4 = H, R^5 = H
6b: R^4 = 5-F, R^5 = H
6c: R^4 = 5-Cl, R^5 = H
6d: R^4 = 6-Cl, R^5 = H
6e: R^4 = 7-Cl, R^5 = H
6f: R^4 = 5-Br, R^5 = H
6g: R^4 = 5-MeO, R^5 = H
6h: R^4 = 6-MeO, R^5 = H
6i: R^4 = 6-Me, R^5 = H
6j: R^4 = 7-Me, R^5 = H
6k: R^4 = 7-Et, R^5 = H
6l: R^4 = H, R^5 = 4-F
6m: R^4 = H, R^5 = 2-Cl
6n: R^4 = H, R^5 = 3-Br
6o: R^4 = H, R^5 = 4-Br
6p: R^4 = H, R^5 = 4-MeO

needed to produce the product but it also was formed with an increased ee of 83%. An electron donating methoxy substituent at the 5- or 6-position (**4g** and **4h**) accelerated the transformation as expected, led to high conversions of 97 and 96%, respectively in shorter time periods, and had little effect (± 4%) on the observed ee (entries 7 and 8). Alkyl groups at the 6- and 7-positions (**4i**-**4k**) also led to very efficient transformations but had little impact on the speed of the transformation (entries 9-11). A methyl group, however, was found to have the largest influence on the enantioselectivity of all the substituents that were studied. 6-Methylindole (**4i**) gave the smallest ee (60%) in the reaction with *trans*-*β*-nitrostyrene whereas its 7-methyl isomer (**4j**) afforded the highest value (90% ee). 7-Ethylindole (**4k**) also displayed good enantioselectivity (85% ee), but it is not as large as when the smaller methyl-containing indole was used. These results indicate that subtle changes in the location and size of an indole substituent can influence the product selectivity, and that incorporation of a chlorine, methyl or ethyl group at the 7-position is particularly favorable from a stereochemical point of view. Incorporation of electron-withdrawing halogen atoms or an electron-donating methoxy group into the aromatic ring of *trans*-*β*-nitrostyrene led to a few solubility issues, but in all cases excellent conversions were obtained (entries

Table 5. Substrate scope.[a]

entry	reactants	pdt	time (h)	conv. (%)[b]	ee (%)[c]
1	**4a + 5a**	**6a**	50	88	72
2	**4b + 5a**	**6b**	68	81	72
3	**4c + 5a**	**6c**	66	75	73
4	**4d + 5a**	**6d**	66	79	70
5	**4e + 5a**	**6e**	114	88	83
6	**4f + 5a**	**6f**	68	78	69
7	**4g + 5a**	**6g**	40	97	68
8	**4h + 5a**	**6h**	39	96	76
9	**4i + 5a**	**6i**	47	92	60
10	**4j + 5a**	**6j**	58	99	90
11	**4k + 5a**	**6k**	58	98	85
12[d,f]	**4a + 5b**	**6l**	64	>99	74
13	**4a + 5c**	**6m**	39	>99	65
14	**4a + 5d**	**6n**	39	>99	74
15[e,g]	**4a + 5e**	**6o**	64	>99	70
16[d]	**4a + 5f**	**6p**	68	91	79
17[h]	**4j + 5a**	**6j**	64	>99	90

[a]Reactions were carried out at -30 ˚C with 0.1 mmol of the indole, 0.2 mmol of the *trans-β*-nitrostyrene, 0.01 mmol of **2b** and 10 mg of 3 Å MS in 0.5 mL of a 1:2 CH_2Cl_2/C_6H_6 mixture. [b]Determined by ^{1}H NMR. [c]Measured by chiral HPLC. [d]A 1:1 CH_2Cl_2/C_6H_6 mixture was used as the solvent. [e]A 2:1 CH_2Cl_2/C_6H_6 mixture was used as the solvent. [f]This reaction was run at half of the typical concentrations. [g]This reaction was run at 2/3 of the usual concentrations in 1 mL of solvent and with 20 mg of 3 Å MS. [h]This reaction was scaled up by a factor of 10.

12-16). The products were formed with moderate ee ranging from 70-79% except for **5c,** which led to a lower value of 65%, presumably because of the ortho chlorine atom. The reaction of **4j** with **5a** was also scaled up by a factor of 10 (entry 17) to afford >250 mg of product without any loss in the yield or ee.

1-Methylindole (**4l**) was explored to investigate the role of the N–H •• O=P hydrogen bond in the reaction of indole with *trans-β*-nitrostyrene since this interaction is blocked in this case. This change resulted in a reduction in the yield from 81% to 5% and in the ee from 70% to 30% under the same

reaction conditions.[23] These results indicate that the hydrogen bond between indole and the phosphoryl oxygen of the phosphoric acid is important both in terms of the reaction efficiency and stereoselectivity. A kinetic study with catalytic loadings of **2b** ranging from 5-20 mol % was also carried out. A plot of the second-order rate constants vs. the mol % of the catalyst is linear indicating a first-order dependence on the catalyst concentration (Figure 2). Alternatively, the same conclusion is reached by carrying out a normalized time scale analysis.[24] Interestingly, even though the background process is not competitive, the ee was found to correlate with the catalyst loading. That is, when 5, 10 and 20 mol % of **2b**, were used, ee values of 60%, 70% and 73% were observed. This may be due to the changes in the medium arising from differences in the catalyst concentration since it is a soluble salt. These results, nevertheless, suggest that the operating mechanism is analogous to noncharged phosphoric acid derivatives,[20b] and that a pair of hydrogen bond interactions play a key role in the efficiency and stereoselectivity of this transformation (Figure 3), which is consistent with previous reports of other phosphoric acid catalysts.[25]

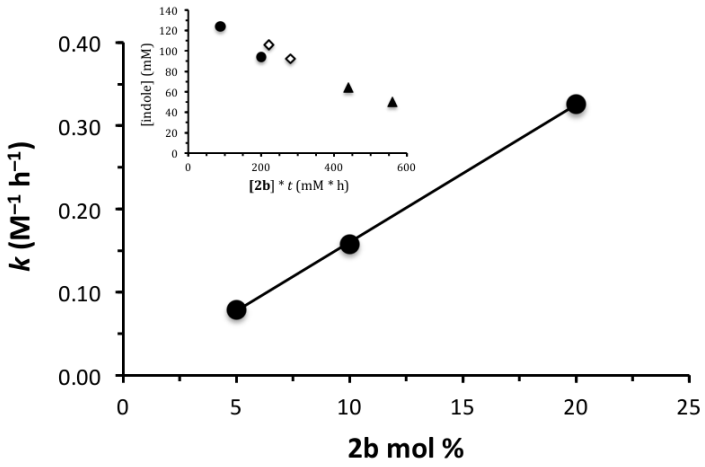

Figure 2. Linear least squares fit of second-order rate constants vs the catalyst (**2b**) mol %; k (M^{-1} h^{-1}) = 0.016 x **2b** mol % – 0.0040, r^2 = 1.00. Inset is for the normalized time scale analysis.

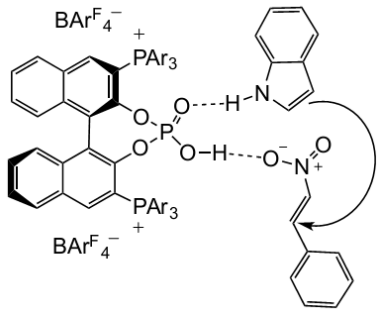

Figure 3. Proposed Friedel-Crafts alkylation transition state.

4.3. Conclusion

In summary, we demonstrated the successful synthesis of a series of electrostatically enhanced pyridinium-containing and phosphonium ion-tagged phosphoric acids, and studied their catalytic performance in the Friedel-Crafts alkylation of indoles with *trans-β*-nitrostyrenes. Unfortunately, the pyridinium-containing phosphoric acids failed to afford high stereoselectivity. On the other hand, the phosphonium ion-containing phosphoric acids are good catalysts for a wide range of substrates, promoting higher reactivities and enantioselectivities than their noncharged analogues. Charge activated organocatalysts consequently continue to show promise in the development of new hydrogen bond and Brønsted acid catalysts.

4.4. Experimental

4.4.1. Materials and General Methods

All the reagents used in this work were obtained from commercial sources and used without further purification. Reaction solvents were dried with oven-activated 3 Å molecular sieves. Proton and carbon chemical shifts are reported in ppm (δ) based upon internal reference signals from the solvent: $CDCl_3$ (7.26 and 77.0 δ) and CD_2Cl_2 (5.32 and 54.0 δ). For ^{19}F and ^{31}P, external calibrants were used as follows: CF_3COOH (-76.55 δ) and 85% aqueous H_3PO_4 (0.00 δ). High-resolution electrospray ionization mass spectra (HRMS-ESI) were obtained with a time of flight (TOF) instrument using methanol solutions and polyethylene glycol (PEG) or polypropylene glycol (PPG) as an internal standard. HPLC analyses

were carried out on chiral RegisCell and RegisPack columns.

4.4.2. Synthesis Procedures.

*(R)-2,2'-Bis(ethoxymethoxy)-1,1'-binaphthyl (**7**).*[26] (*R*)-1,1'-Bi-2-naphthol (0.50 g, 1.75 mmol) was transferred into a 250 mL round-bottomed flask under a dry nitrogen atmosphere, and 20 mL of anhydrous THF was added via syringe. The resulting solution was stirred and cooled to -20 ˚C before adding 0.43 g (3.83 mmol) of potassium *tert*-butoxide in one portion. This mixture was stirred for 15 min before 0.35 mL (0.356 g, 3.83 mmol) chloromethyl ethyl ether was syringed in over 5 min. The resulting solution was allowed to warm to room temperature and stirred for 1 hour, after which brine (30 mL) was added to quench the reaction and the solvent was removed under vacuum. Ethyl acetate (30 mL x 3) was used to extract the crude product and the combined organic material was washed with water (30 mL x 2) and brine (30 mL), dried over $MgSO_4$, and concentrated to give a yellow oil. Purification by MPLC was carried out using the following protocol: a hexanes wash with a flow rate of 40 mL min^{-1} was carried out for 5 min, then the eluent was switched via a linear gradient over the course of 5 min to 1:1 hexanes/CH_2Cl_2 and maintained for 20 min. The last fraction was concentrated to afford 0.47 g (67%) of the product as a colorless viscous oil. ^{1}H NMR (500 MHz, CD_2Cl_2) δ 8.01 (d, *J* = 9.0 Hz, 2H), 7.94 (d, *J* = 8.2 Hz, 2H), 7.68 (d, *J* = 9.1 Hz, 2H), 7.40 (t, *J* = 7.8 Hz, 2H), 7.28 (t, *J* = 7.6 Hz, 2H), 7.23 (d, *J* = 8.5 Hz, 2H), 5.21 (d, *J* = 7.0 Hz, 2H), 5.09 (d, *J* = 7.0 Hz, 2H), 3.51-3.36 (m, 4H), 1.07 (t, *J* = 7.1 Hz, 2H). ^{13}C NMR (100 MHz, $CDCl_3$) δ 152.8, 134.0, 129.8, 129.3, 127.8, 126.2, 125.5, 123.9, 121.2, 117.4, 93.8, 63.9, 14.8. HRMS-ESI: calc for $C_{26}H_{26}O_4Na^+$ $(M + Na^+)^+$ 425.1729, found 425.1748.

*(R)-3,3'-dibromo-2,2'-bis(ethoxymethoxy)-1,1'-binaphthyl (**8**).* (*R*)-2,2'-Bis(ethoxymethoxy)-1,1'-binaphthyl (**7**, 3.10 g, 7.70 mmol) was dissolved into 50 mL of diethyl ether in a 250 mL round-bottomed flask under a dry nitrogen atmosphere, after which n-butyllithium (9.25 mL, 2.5 M in hexane, 23.1 mmol) was added dropwise at room temperature. The resulting solution was stirred for 2 h before being cooled to -20 ˚C and slowly adding 1,2-dibromotetrachloroethane (7.52 g, 23.1 mmol) in THF (30 mL). Upon warming to room temperature and stirring overnight, the reaction was quenched with 30 mL of

brine. Removal of the solvents with a rotary evaporator afforded a residue which was extracted with EtOAc (30 mL x 3). The combined organic material was washed with 30 mL of water and 30 mL of brine, and then dried over $MgSO_4$. Evaporation of the solvent under vacuum gave a yellow solid which was purified by MPLC; hexanes were used for 2 min. then a linear gradient to a 9:1 hexanes/EtOAc mixture was applied over a 3 min period, and this binary solution was maintained until the product eluted off the column. It was concentrated under reduced pressure to afford 3.88 g (90%) of a white solid (mp 107 – 113 ˚C). ^{1}H NMR (500 MHz, $CDCl_3$) δ 8.27 (s, 2H), 7.81 (d, *J* = 8.2 Hz, 2H), 7.43 (t, J = 7.7 Hz, 2H), 7.30 (t, J = 8.2 Hz, 2H), 7.17 (d, *J* = 8.5 Hz, 2H), 4.91 (d, *J* = 5.9 Hz, 2H), 4.84 (d, *J* = 5.9 Hz, 2H), 3.08-2.98 (m, 2H), 2.72-2.62 (m, 2H), 0.60 (t, *J* = 7.1 Hz, 6H). ^{13}C NMR (100 MHz, $CDCl_3$) δ 150.2, 133.0, 132.9, 131.5, 127.2, 127.0, 126.9, 126.5, 126.0, 117.5, 97.9, 64.8, 14.3. HRMS-ESI: calc for $C_{26}H_{24}O_4Br_2Na^+$ $(M + Na^+)^+$ 582.9919, found 582.9899.

General procedure for the synthesis of ***9a-9b***. (*R*)-3,3'-Dibromo-2,2'-bis(ethoxymethoxy)-1,1'-binaphthyl (**8**) (0.70 g, 1.25 mmol), 3-pyridinylboronic acid (0.54 g, 4.37 mmol) [or 5-methylpyridine-3-boronic acid (0.60 g, 4.37 mmol)] and tetrakis(triphenylphosphine)palladium (0.14 g, 0.13 mmol) were mixed together in a 250 mL round-bottomed flask and then dissolved in degassed 1,2-dimethoxylethane (8 mL), after which 3.3 mL of a 2.0 M aqueous Na_2CO_3 solution was added. The resulting mixture was refluxed at 93 ˚C with stirring for 16 h and upon cooling to room temperature the volatiles were removed with a rotary evaporator. Dichloromethane (30 mL x 3) was used to extract the resulting residue and the combined organic solutions were washed with 30 mL of saturated NH_4Cl and 30 mL of brine before being dried over Na_2SO_4. Concentration of this material under vacuum gave a yellow oil that was purified by MPLC using EtOAc as the eluent. The resulting white solid was dissolved in 5 mL of ethanol and then 1.5 mL of 6.0 M HCl was added dropwise over 5 min with stirring. After 3 h at room temperature a white precipitate had formed and the reaction was quenched with 30 mL of aqueous $NaHCO_3$. A rotary evaporator was used to remove the ethanol and the remaining material was extracted with EtOAc (50 mL x 2). The combined organic layers were washed with water and brine, and then dried over Na_2SO_4. Concentration of this solution afforded a viscous yellow liquid that was purified by MPLC with EtOAc as the eluent.

*(R)-3,3'-Di(3-pyridyl)-2,2'-dihydroxyl-1,1'-binaphthyl (**9a**)*. This compound was obtained as a white solid (0.40 g) in a 73% yield (mp 206 - 212 ˚C). ^{1}H NMR (500 MHz, CD_2Cl_2) δ 11.42 (s, 2H), 9.10 (s, 2H), 7.72 (d, *J* = 7.8 Hz, 2H), 7.58 (d, *J* = 7.1 Hz, 2H), 7.35-7.25 (m, 4H), 7.23-7.15 (m, 4H), 6.77 (dd, *J* = 5.0 and 7.6 Hz, 2H), 6.58 (d, *J* = 4.3 Hz, 2H). ^{13}C NMR (100 MHz, CD_2Cl_2) δ 152.7, 150.2, 144.8, 135.7, 135.6, 134.6, 130.5, 129.6, 129.4, 128.9, 127.2, 125.1, 123.5, 123.3, 116.1. HRMS-ESI: calc for $C_{30}H_{21}N_2O_2^+$ $(M + H^+)^+$ 441.1603, found 441.1588.

*(R)-3,3'-Di[3-(5-methyl)pyridyl]-2,2'-dihydroxyl-1,1'-binaphthyl (**9b**)*. This species was obtained as a white solid (0.42 g) in a 72% yield (mp 201 - 208 ˚C). ^{1}H NMR (500 MHz, CD_2Cl_2) δ 11.68 (s, 2H), 8.89 (s, 2H), 7.59 (d, *J* = 8.8 Hz, 2H), 7.52 (s, 2H), 7.33-7.26 (m, 4H), 7.19 (d, *J* = 9.3 Hz, 2H), 7.17 (s, 2H), 6.30 (s, 2H), 2.03 (s, 6H). ^{13}C NMR (100 MHz, CD_2Cl_2) δ 152.9, 147.7, 145.2, 136.0, 135.6, 134.0, 132.7, 130.2, 129.8, 129.7, 128.5, 127.0, 125.1, 123.2, 116.0, 18.7. HRMS-ESI: calc for $C_{32}H_{25}N_2O_2^+$ $(M + H^+)^+$ 469.1916, found 469.1933.

*General procedure for the synthesis of **10a-10b***. Compound **9a** or **9b** (0.227 mmol) was added into a 100 mL round-bottomed flask under an atmosphere of dry nitrogen and then was dissolved in 15 mL of anhydrous acetonitrile. After stirring for 5 min, 0.164 mL of 1-iodooctane (0.218 g, 0.908 mmol) was syringed into the flask in one portion and the solution was heated to 100 ˚C and refluxed overnight. Upon cooling to room temperature, the reaction mixture was concentrated under vacuum. The crude product was dissolved in 5 mL of CH_2Cl_2 and triturated by adding it dropwise to 100 mL of hexanes. Filtration of the resulting precipitate and a subsequent wash with hexanes gave the desired product.

*(R)-3,3'-Di(3-N-octylpyridinium)-2,2'-dihydroxyl-1,1'-binaphthyl iodide (**10a**).* A yellow solid (0.16 g) was obtained in a 77% yield (mp 278 - 282 ˚C). ^{1}H NMR (500 MHz, CD_2Cl_2) δ 9.98 (s, 2H), 8.86-8.77 (m, 4H), 8.34 (s, 2H), 8.10-8.01 (m, 4H), 7.43 (t, *J* = 7.2 Hz, 2H), 7.33 (t, *J* = 7.4 Hz, 2H), 7.14 (d, *J* = 8.5 Hz, 2H), 4.80-4.65 (m, 4H), 2.09-1.98 (m, 4H), 1.40-1.18 (m, 22H), 0.82 (t, *J* = 6.6 Hz, 6H). ^{13}C NMR (100 MHz, CD_2Cl_2) δ 149.7, 146.4, 145.6, 145.5, 142.0, 139.6, 135.0, 132.6, 130.1, 129.5, 128.9, 128.5, 125.6, 125.1, 118.6, 62.7, 32.3, 32.2, 29.50, 29.48, 26.5, 23.1, 14.4. HRMS-ESI: calc for $C_{46}H_{53}N_2O_2^+$ $(M - H^+ - 2I^-)^+$ 665.4107, found 665.4139.

*(R)-3,3'-Di(3-(N-octyl-5-methyl)pyridinium)-2,2'-dihydroxyl-1,1'-binaphthyl iodide (**10b**)*. A yellow

solid (0.19 g) was obtained in an 88% yield (mp 265 - 270 ˚C). ^{1}H NMR (500 MHz, CD_2Cl_2) δ 9.86 (s, 2H), 8.71 (s, 2H), 8.65 (s, 2H), 8.30 (s, 2H), 8.04 (d, *J* = 7.9 Hz, 2H), 7.45 (t, *J* = 7.8 Hz, 2H), 7.35 (t, *J* = 8.3 Hz, 2H), 7.14 (d, *J* = 8.3 Hz, 2H), 6.53 (s, 2H), 4.79-4.62 (m, 4H), 2.67 (s, 6H), 2.12-2.00 (m, 4H), 1.42-1.18 (m, 20H), 0.83 (d, *J* = 6.8 Hz, 6H). ^{13}C NMR (100 MHz, CD_2Cl_2) δ 149.5, 146.2, 144.2, 141.3, 139.8, 139.0, 135.0, 132.5, 130.2, 129.5, 128.9, 125.7, 125.3, 125.1, 118.5, 62.5, 32.3, 32.2, 29.53, 29.51, 26.5, 23.1, 19.2, 14.4. HRMS-ESI: calc for $C_{48}H_{57}N_2O_2^+$ (M - H^+ - $2I^-$)$^+$ 693.4420, found 693.4401.

*General procedure for the synthesis of **11a**-**11b***. Iodide salt **10a** or **10b** (0.218 mmol) was dissolved into 20 mL of anhydrous acetonitrile under a N_2 atmosphere and 64 μL (0.10 g, 0.654 mmol) of $POCl_3$ was added with stirring in one portion followed by 44 μL (0.044 g, 0.544 mmol) of anhydrous pyridine. The resulting solution was heated to 90 ˚C and refluxed for 16 h before cooling to room temperature and adding 0.5 mL of water. This material was heated back to 90 ˚C for 1 h and then allowed to return to room temperature. Removal of the solvent under vacuum afforded a residue which was dissolved in 40 mL of CH_2Cl_2 and washed with 2.0 M HCl (15 mL), 15 mL of brine and then dried over Na_2SO_4. Rotary evaporation of this material gave a brown oil that was purified by MPLC. A linear gradient from EtOAc to a 1:1 EtOAc/MeOH mixture over 10 min followed by a 10 min wash with this solution eluted the product. This material was concentrated under reduced pressure to give the desired compound as a yellow solid.

*(R)-3,3'-(4-Hydroxy-4-oxidodinaphtho[2,1-d:1',2'-f][1,3,2]dioxaphosphepine-2,6-diyl)bis(1-octylpyridin-1-ium) chloride (**11a**)*. This compound (0.12 g) was generated in a 69% yield (mp 195 - 202 ˚C). ^{1}H NMR (500 MHz, CD_2Cl_2) δ 10.38 (s, 2H), 9.11 (d, *J* = 5.6 Hz, 2H), 8.82 (d, *J* = 7.7 Hz, 2H), 8.20 (s, 2H), 8.08-7.95 (m, 4H), 7.48 (t, *J* = 7.3 Hz, 2H), 7.30 (t, *J* = 7.9 Hz, 2H), 7.19 (d, *J* = 8.7 Hz, 2H), 4.86-4.60 (m, 4H), 2.19 (bs, OH, 1H) 2.10-1.93 (m, 4H), 1.37-1.15 (m, 20H), 0.82 (t, *J* = 6.7 Hz, 6H). ^{13}C NMR (100 MHz, CD_2Cl_2) δ 155.31, 155.26, 153.64, 153.58, 137.64, 137.58, 137.0, 136.7, 136.6, 129.7, 128.7, 123.9, 123.8, 121.0, 120.9, 63.0, 32.2, 32.1, 29.5, 29.4, 26.6, 23.1, 14.4. ^{31}P NMR (162 MHz, CD_2Cl_2) δ 5.64. HRMS-ESI: calc for $C_{46}H_{52}N_2O_4P^+$ (M - H^+ - $2Cl^-$)$^+$ 727.3665, found 727.3677.

***(**R)-5,5'-(4-Hydroxy-4-oxidodinaphtho[2,1-d:1',2'-f][1,3,2]dioxaphosphepine-2,6-diyl)bis(3-methyl-*

*1-octylpyridin-1-ium) chloride (**11b**)*. This compound (0.15 g) was produced in an 83% yield (mp 194 - 200 ˚C). ^{1}H NMR (500 MHz, CD_2Cl_2) δ 10.25 (s, 2H), 9.19 (s, 2H), 8.62 (s, 2H), 8.20 (s, 2H), 8.02 (d, *J* = 8.2 Hz, 2H), 7.47 (t, *J* = 7.1 Hz, 2H), 7.30 (t, *J* = 8.5 Hz, 2H), 7.21 (d, *J* = 8.6 Hz, 2H), 4.72 (t, *J* = 7.3 Hz, 4H), 2.63 (s, 6H), 2.54 (bs, OH, 1H), 2.15-1.95 (m, 4H), 1.45-1.14 (m, 20H), 0.82 (t, *J* = 6.8 Hz, 6H). ^{13}C NMR (100 MHz, CD_2Cl_2) δ 147.2, 146.5, 144.7, 142.6, 139.7, 138.8, 133.9, 132.5, 131.0, 129.4, 128.1, 127.6, 127.3, 126.4, 124.0, 62.6, 32.3, 32.1, 29.6, 29.5, 26.7, 23.1, 19.0, 14.4. ^{31}P NMR (162 MHz, CD_2Cl_2) δ 6.19. HRMS-ESI: calc for $C_{48}H_{56}N_2O_4P^+$ (M - H^+ - $2Cl^-$)$^+$ 755.3978, found 755.4002.

*General procedure for the synthesis of **1a**-**1b***. Chloride salt **11a** or **11b** (0.0755 mmol), sodium tetrakis[3,5-bis(trifluoromethyl)phenyl]borate (0.141 g, 0.159 mmol) and 3 Å molecular sieves (0.10 g) were mixed in a 23 x 85 mm vial, and then 7 mL of CH_2Cl_2 was added. The resulting solution was stirred at room temperature for 3 h before being filtered through a 0.45 μm polytetrafluoroethylene (PTFE) membrane. The filtered solution was washed with 2.0 M H_2SO_4 (7 mL x 2) and water (7 mL x 3), and then was dried over Na_2SO_4 before being concentrated to afford the product.

*(R)-3,3'-(4-Hydroxy-4-oxidodinaphtho[2,1-d:1',2'-f][1,3,2]dioxaphosphepine-2,6-diyl)bis(1-octylpyridin-1-ium) tetrakis[3,5-bis(trifluoromethyl)phenyl]borate (**1a**)*. A yellow solid (0.17 g) was formed in a 92% yield (mp 77 - 81 ˚C). ^{1}H NMR (500 MHz, CD_2Cl_2) δ 9.54 (s, 2H), 8.90 (d, *J* = 7.8 Hz, 2H), 8.29 (d, *J* = 5.9 Hz, 2H), 8.12 (s, 2H), 8.06 (d, *J* = 8.3 Hz, 2H), 8.00 (dd, *J* = 5.9 and 7.9 Hz, 2H), 7.77 (s, 16H), 7.65-7.57 (m, 10H), 7.47 (t, *J* = 8.3 Hz, 2H), 7.35 (d, *J* = 8.8 Hz, 2H), 4.62-4.44 (m, 4H), 2.60 (bs, OH, 1H) 2.07-1.93 (m, 4H), 1.36-1.21 (m, 20H), 0.84 (t, *J* = 6.9 Hz, 6H). ^{13}C NMR (100 MHz, CD_2Cl_2) δ 162.4 (q, *J* = 48.9 Hz), 147.1, 145.7, 145.4, 141.4, 140.7, 140.5, 135.5, 134.0, 133.1, 131.3, 129.5 (qq, *J* = 2.92 and 31.4 Hz), 128.6, 127.9, 127.7, 127.2, 125.9, 125.2 (q, *J* = 270 Hz), 124.1, 118.2 (septet, *J* = 3.64 Hz), 63.9, 32.1, 32.0, 29.4, 29.3, 26.6, 23.0, 14.2. ^{19}F NMR (376 MHz, CD_2Cl_2) δ -62.68. ^{31}P NMR (162 MHz, CD_2Cl_2) δ 6.76. HRMS-ESI: calc for $C_{46}H_{52}N_2O_4P^+$ (M - H^+ - $2BAr^F{}_4^-$)$^+$ 727.3665, found 727.3679.

*(R)-5,5'-(4-Hydroxy-4-oxidodinaphtho[2,1-d:1',2'-f][1,3,2]dioxaphosphepine-2,6-diyl)bis(3-methyl-1-octylpyridin-1-ium) tetrakis[3,5-bis(trifluoromethyl)phenyl]borate (**1b**)*. A yellow solid (0.17 g) was

generated in a 91% yield (mp 54 - 58 ˚C). ^{1}H NMR (500 MHz, CD_2Cl_2) δ 9.06 (s, 2H), 8.55 (s, 2H), 8.21 (s, 2H), 8.13 (s, 2H), 8.06 (d, *J* = 7.8 Hz, 2H), 7.74 (s, 16H), 7.63 (t, *J* = 7.1 Hz, 2H), 7.56 (s, 8H), 7.48 (t, *J* = 8.5 Hz, 2H), 7.34 (d, *J* = 8.3 Hz, 2H), 4.83 (bs, OH, 1H), 4.45 (t, *J* = 7.3 Hz, 4H), 2.55 (s, 6H), 2.07-1.90 (m, 4H), 1.36-1.17 (m, 20H), 0.82 (t, *J* = 6.8 Hz, 6H). ^{13}C NMR (100 MHz, CD_2Cl_2) δ 162.3 (q, *J* = 49.6 Hz), 147.6, 143.9, 142.5, 141.6, 141.3, 139.0, 135.4, 133.65, 133.63, 131.7, 129.5 (qq, *J* = 2.92 and 31.4 Hz), 128.4, 127.3, 125.47, 125.45, 125.2 (q, *J* = 270 Hz), 123.58, 123.56, 118.1 (septet, *J* = 3.64 Hz), 63.7, 32.1, 32.0, 29.4, 29.3, 26.6, 23.0, 19.1, 14.2. ^{19}F NMR (376 MHz, CD_2Cl_2) δ -62.76. ^{31}P NMR (162 MHz, CD_2Cl_2) δ 5.68. HRMS-ESI: calc for $C_{48}H_{56}N_2O_4P^+$ $(M - H^+ - 2BAr^F{}_4^-)^+$ 755.3978, found 755.3998.

General procedure for the synthesis of ***2f-2g***. In a 23 x 85 mm vial, (*R*)-(4-hydroxy-4-oxidodinaphtho[2,1-d:1',2'-f][1,3,2]dioxaphosphepine-2,6-diyl)bis(triphenylphosphonium) chloride (0.188 g, 0.200 mmol), sodium tetrafluoroborate (0.046 g, 0.420 mmol) or potassium hexafluorophosphate (0.077 g, 0.420 mmol) and 3 Å molecular sieves (0.50 g) were mixed together and then 3 mL of methanol was added. After stirring at room temperature for 2 h, 10 mL of CH_2Cl_2 was added and the reaction was stirred for an additional 1 h before filtering the solution through a 0.45 μm PTFE membrane. The solvent was removed under vacuum and the residue was redissolved in 8 mL of CH_2Cl_2. It was then washed twice with 8 mL of 2.0 M H_2SO_4 and three times with 8 mL of water before being dried over Na_2SO_4. Concentration of the solution under reduced pressure afforded the desired product.

*(R)-(4-Hydroxy-4-oxidodinaphtho[2,1-d:1',2'-f][1,3,2]dioxaphosphepine-2,6-diyl)bis(triphenyl-phosphonium) tetrafluoroborate (****2f****)*. A yellow solid (0.141 g) was afforded in a 67% yield (mp 233 – 236 ˚C). ^{1}H NMR (500 MHz, $CDCl_3$) δ 8.00 (d, *J* = 16.3 Hz, 2H), 7.87 (d, *J* = 7.7 Hz, 2H), 7.83-7.72 (m, 18H), 7.68-7.62 (m, 12H), 7.57-7.48 (m, 4H), 7.28 (d, *J* = 8.3 Hz, 2H), 1.25 (bs, OH, 1H). ^{13}C NMR (100 MHz, $CDCl_3$) δ 150.7 (d, *J* = 9.9 Hz), 141.0 (d, *J* = 8.4 Hz), 136.2 (d, *J* = 2.4 Hz), 135.03, 134.95 (d, *J* = 10.5 Hz), 131.0, 130.0 (d, *J* = 13.1 Hz), 129.8, 129.2 (d, *J* = 14.3 Hz), 127.0, 126.5, 124.5 (d, *J* = 10.1 Hz), 118.9 (d, *J* = 90.4 Hz), 110.8 (d, *J* = 91.0 Hz). ^{19}F NMR (376 MHz, CD_2Cl_2) δ -154.11. ^{31}P NMR (162 MHz, CD_2Cl_2) δ 22.93, 0.87. HRMS-ESI: calc for $C_{56}H_{40}O_4P_3^+$ $(M - H^+ - 2BF_4^-)^+$ 869.2134,

found 869.2103.

*(R)-(4-Hydroxy-4-oxidodinaphtho[2,1-d:1',2'-f][1,3,2]dioxaphosphepine-2,6-diyl)bis(triphenyl-phosphonium) hexafluorophosphate (**2g**)*. A yellow solid (0.177 g) was produced in a 76% yield (mp 225 – 230 ˚C). ^{1}H NMR (500 MHz, $CDCl_3$) δ 8.00 (d, *J* = 16.3 Hz, 2H), 7.88 (d, *J* = 7.7 Hz, 2H), 7.81-7.72 (m, 18H), 7.68-7.62 (m, 12H), 7.58-7.50 (m, 4H), 7.28 (d, *J* = 8.3 Hz, 2H), 2.11 (bs, OH, 1H). ^{13}C NMR (100 MHz, $CDCl_3$) δ 144.7 (d, *J* = 8.6 Hz), 141.0 (d, *J* = 8.4 Hz), 136.2 (d, *J* = 2.9 Hz), 135.1, 135.0 (d, *J* = 10.6 Hz), 131.0, 130.1 (d, *J* = 13.2 Hz), 129.8, 129.2 (d, *J* = 14.4 Hz), 127.0, 126.5, 124.5 (d, *J* = 7.0 Hz), 118.9 (d, *J* = 90.5 Hz), 110.7 (d, *J* = 91.1 Hz). ^{19}F NMR (376 MHz, $CDCl_3$) δ -73.62 (d, *J* = 712 Hz). ^{31}P NMR (162 MHz, $CDCl_3$) δ 22.94, 0.77, -144.43 (septet, *J* = 712 Hz). HRMS-ESI: calc for $C_{56}H_{40}O_4P_3^+$ $(M - H^+ - 2PF_6^-)^+$ 869.2134, found 869.2155.

*(R)-(4-Hydroxy-4-oxidodinaphtho[2,1-d:1',2'-f][1,3,2]dioxaphosphepine-2,6-diyl)bis(triphenyl-phosphonium) tetrakis(pentafluorophenyl)borate (**2h**)*. In a 23 x 85 mm vial, (*R*)-(4-hydroxy-4-oxidodinaphtho[2,1-d:1',2'-f][1,3,2]dioxaphosphepine-2,6-diyl)bis(triphenylphosphonium) chloride (0.188 g, 0.200 mmol), potassium tetrakis(pentafluorophenyl)borate (0.302 g, 0.420 mmol) and 3 Å molecular sieves (0.50 g) were mixed together and then 8 mL of CH_2Cl_2 was added. The solution was stirred at room temperature for 3 h and then filtered through a 0.45 μm PTFE membrane. It was subsequently washed twice with 2.0 M H_2SO_4 and three times with water before being dried over Na_2SO_4. Removal of the CH_2Cl_2 gave **2h** as a yellow solid (0.337 g) in a 76% yield (mp 178 – 182 ˚C). ^{1}H NMR (500 MHz, CD_2Cl_2) δ 8.10 (d, *J* = 16.5 Hz, 2H), 7.91 (d, *J* = 8.1 Hz, 2H), 7.84-7.77 (m, 6H), 7.77-7.69 (m, 12H), 7.69-7.59 (m, 14H), 7.54 (d, *J* = 8.1 Hz, 2H), 7.29 (d, *J* = 8.5 Hz, 2H), 2.20 (bs, OH, 1H). ^{13}C NMR (100 MHz, CD_2Cl_2) δ 149.7 (d, *J* = 9.4 Hz), 148.7 (d, *J* = 236.4 Hz), 142.5 (d, *J* = 8.5 Hz), 138.8 (d, *J* = 242.9 Hz), 136.9 (d, *J* = 231.2 Hz), 135.7 (d, *J* = 3.0 Hz), 136.7, 135.5 (d, *J* = 10.5 Hz), 132.0, 130.6 (d, *J* = 13.1 Hz), 130.5, 130.2 (d, *J* = 14.3 Hz), 128.1, 127.0, 124.7 (d, *J* = 6.9 Hz), 124.2 (m), 119.1 (d, *J* = 90.6 Hz), 110.6 (d, *J* = 91.2 Hz). ^{19}F NMR (376 MHz, CD_2Cl_2) δ -133.12, -163.39 (t, *J* = 20.4 Hz), -167.38 (t, *J* = 17.1 Hz). ^{31}P NMR (162 MHz, CD_2Cl_2) δ 22.81, 0.89. HRMS-ESI: calc for $C_{56}H_{40}O_4P_3^+$ $(M - H^+ - 2B(C_6F_5)_4^-)^+$ 869.2134, found 869.2116.

4.4.3. General Procedure for the Friedel-Crafts Alkylations

A 23 x 85 mm vial was charged with a catalyst (10 mol %) and 3 Å molecular sieves (10 mg), and then was sealed followed by a 1 min purge with dry nitrogen. After adding 250 μL of CH_2Cl_2 via syringe, the resulting solution was cooled if the reaction was being carried out at subambient temperature. Indole (0.100 mmol) and *trans-β*-nitrostyrene (0.200 mmol) were dissolved in 250 μL of CH_2Cl_2 and this solution was then added dropwise over 10-15 s. The reaction mixture was shaken and the transformation was allowed to proceed over the course of 5-164 h. Reaction conversions were determined by removing 1-2 drops of the reaction mixture and dissolving it in 0.5 mL of $CDCl_3$ after flowing dry nitrogen over the sample for ≤ 15 s to evaporate the CH_2Cl_2. Upon completion of reaction, the solution was injected on to a 4 g silica gel column followed by 0.2-0.3 mL of CH_2Cl_2 that had been used to rinse the molecular sieves. MPLC purification was carried out first with hexanes (1 min) followed by a linear gradient to 100% CH_2Cl_2 over the course of 7 min, and then this solvent was maintained until all of the components eluted off the column. Racemic reference materials were obtained in the same way using diphenylphosphate as the reaction catalyst.

4.4.4. Analytical Data for the Friedel-Crafts Products

*3-(2-Nitro-1-phenylethyl)-1H-indole (**6a**)*.[20b] ^{1}H NMR (500 MHz, $CDCl_3$) δ 8.10 (bs, NH, 1H), 7.46 (d, *J* = 8.0 Hz, 1H), 7.39-7.30 (m, 5H), 7.29-7.24 (m, 1H), 7.23-7.18 (m, 1H), 7.12-7.06 (m, 1H), 7.03 (d, *J* = 2.5 Hz, 1H), 5.20 (t, *J* = 8.2 Hz, 1H), 5.07 (dd, *J* = 7.7 Hz and 12.6 Hz, 1H), 4.95 (dd, *J* = 8.4 Hz and 12.5 Hz, 1H). ^{13}C NMR (100 MHz, $CDCl_3$) δ 139.2, 136.5, 128.9, 127.7, 127.5, 126.1, 122.7, 121.6, 119.9, 118.9, 114.4, 111.4, 79.5, 41.5. HRMS-ESI: calc for $C_{16}H_{13}N_2O_2^-$ $(M - H^+)^-$ 265.0977, found 265.0971. Enantiomeric excess was determined with a Regiscell column (75:25 hexanes/iPrOH, 1.0 mL min^{-1}, 20 ˚C, 250 nm, τ_{major} = 17.0 min, τ_{minor} = 20.1 min).

*5-Fluoro-3-(2-nitro-1-phenylethyl)-1H-indole (**6b**)*.[27] Reaction conversion was determined by relative integration of the ^{1}H NMR signals at δ 6.42 (**4b**) and 4.78 (**6b**). Enantiomeric excess was measured with a Regiscell column (92:8 hexanes/iPrOH, 1.0 mL min^{-1}, 20 ˚C, 254 nm, τ_{major} = 56.1 min, τ_{minor} = 48.2 min).

*5-Chloro-3-(2-nitro-1-phenylethyl)-1H-indole (**6c**).*[20b,28] Reaction conversion was determined by relative integration of the ^{1}H NMR signals at δ 6.41 (**4c**) and 4.82 (**6c**). Enantiomeric excess was measured with a Regiscell column (80:20 hexanes/iPrOH, 1.0 mL min^{-1}, 20 ˚C, 250 nm, τ_{major} = 16.8 min, τ_{minor} = 13.8 min).

*6-Chloro-3-(2-nitro-1-phenylethyl)-1H-indole (**6d**).*[29] Reaction conversion was determined by relative integration of the ^{1}H NMR signals at δ 6.43 (**4d**) and 4.82 (**6d**). Enantiomeric excess was measured with a Regiscell column (85:15 hexanes/iPrOH, 1.0 mL min^{-1}, 20 ˚C, 250 nm, τ_{major} = 21.2 min, τ_{minor} = 19.8 min).

*7-Chloro-3-(2-nitro-1-phenylethyl)-1H-indole (**6e**).* A yellow solid was isolated with a mp of 58 - 62 ˚C. ^{1}H NMR (500 MHz, $CDCl_3$) δ 8.32 (bs, NH, 1H), 7.37-7.29 (m, 5H), 7.29-7.26 (m, 1H), 7.20 (d, *J* = 7.6 Hz, 1H), 7.13 (d, *J* = 2.4 Hz, 1H), 7.00 (t, *J* = 7.8 Hz, 1H), 5.17 (t, *J* = 8.0 Hz, 1H), 5.06 (dd, *J* = 8.0 Hz and 12.5 Hz, 1H), 4.95 (dd, *J* = 8.0 Hz and 12.5 Hz, 1H). ^{13}C NMR (100 MHz, $CDCl_3$) δ 138.8, 133.8, 129.0, 127.71, 127.691, 127.688, 127.5, 122.1, 120.8, 117.6, 116.9, 115.6, 79.4, 41.5. HRMS-ESI: calc for $C_{16}H_{12}N_2O_2Cl^-$ $(M - H^+)^-$ 299.0587 and 301.0558, found 299.0577 and 301.0553. Reaction conversion was determined by relative integration of the ^{1}H NMR signals at δ 6.60 (**4e**) and 4.95 (**6e**). Enantiomeric excess was measured with a Regiscell column (75:25 hexanes/iPrOH, 1.0 mL min^{-1}, 20 ˚C, 250 nm, τ_{major} = 34.7 min, τ_{minor} = 39.6 min).

*5-Bromo-3-(2-nitro-1-phenylethyl)-1H-indole (**6f**).*[20b] Reaction conversion was determined by relative integration of the ^{1}H NMR signals at δ 6.40 (**4f**) and 4.82 (**6f**). Enantiomeric excess was measured with a Regiscell column (75:25 hexanes/iPrOH, 1.0 mL min^{-1}, 20 ˚C, 250 nm, τ_{major} = 12.1 min, τ_{minor} = 10.8 min).

*5-Methoxy-3-(2-nitro-1-phenylethyl)-1H-indole (**6g**).*[28] Reaction conversion was determined by relative integration of the ^{1}H NMR signals at δ 6.39 (**4g**) and 4.84 (**6g**). Enantiomeric excess was measured with a Regiscell column (75:25 hexanes/iPrOH, 1.0 mL min^{-1}, 20 ˚C, 250 nm, τ_{major} = 12.9 min, τ_{minor} = 11.4 min).

*6-Methoxy-3-(2-nitro-1-phenylethyl)-1H-indole (**6h**).* A white solid was isolated with a mp of 82 - 85 ˚C.^{1}H NMR (500 MHz, $CDCl_3$) δ 7.96 (bs, NH, 1H), 7.35-7.29 (m, 4H), 7.29-7.24 (m, 2H), 6.92 (dd, *J*

= 0.8 Hz and 2.3 Hz, 1H), 6.83 (d, *J* = 2.2 Hz, 1H), 6.74 (dd, *J* = 2.3 Hz and 8.8 Hz, 1H), 5.14 (t, *J* = 8.1 Hz, 1H), 5.05 (dd, *J* = 7.7 Hz and 12.40 Hz, 1H), 4.92 (dd, *J* = 8.3 Hz and 12.5 Hz, 1H), 3.82 (s, 3H). ^{13}C NMR (100 MHz, $CDCl_3$) δ 156.9, 139.2, 137.3, 128.9, 127.7, 127.5, 120.5, 120.3, 119.6, 114.4, 110.0, 94.7, 79.6, 55.6, 41.6. HRMS-ESI: calc for $C_{17}H_{16}N_2O_3Na^+$ $(M + Na^+)^+$ 319.1059, found 319.1074. Reaction conversion was determined by relative integration of the ^{1}H NMR signals at δ 6.39 (**4h**) and 4.92 (**6h**). Enantiomeric excess was measured with a Regiscell column (75:25 hexanes/iPrOH, 1.0 mL min^{-1}, 20 ˚C, 250 nm, τ_{major} = 20.7 min, τ_{minor} = 16.6 min).

*6-Methyl-3-(2-nitro-1-phenylethyl)-1H-indole (**6i**)*. This compound was isolated as a colorless viscous oil. ^{1}H NMR (500 MHz, $CDCl_3$) δ 7.94 (bs, NH, 1H), 7.41-7.28 (m, 5H), 7.28-7.23 (m, 1H), 7.15 (s, 1H), 6.94 (d, *J* = 2.4 Hz, 1H), 6.92 (d, *J* = 8.1 Hz, 1H), 5.17 (t, *J* = 8.0 Hz, 1H), 5.06 (dd, *J* = 7.7 Hz and 12.5 Hz, 1H), 4.94 (dd, *J* = 8.4 Hz and 12.5 Hz, 1H), 2.44 (s, 3H). ^{13}C NMR (100 MHz, $CDCl_3$) δ 139.2, 136.9, 132.6, 128.9, 127.7, 127.5, 123.9, 121.7, 120.9, 118.5, 114.3, 111.3, 79.5, 41.6, 21.6. HRMS-ESI: calc for $C_{17}H_{15}N_2O_2^-$ $(M - H^+)^-$ 279.1134, found 279.1149. Reaction conversion was determined by relative integration of the ^{1}H NMR signals at δ 6.51 (**4i**) and 4.94 (**6i**). Enantiomeric excess was measured with a Regiscell column (75:25 hexanes/iPrOH, 1.0 mL min^{-1}, 20 ˚C, 250 nm, τ_{major} = 13.1 min, τ_{minor} = 12.0 min).

*7-Methyl-3-(2-nitro-1-phenylethyl)-1H-indole (**6j**)*.[20b] Reaction conversion was determined by relative integration of the ^{1}H NMR signals at δ 6.57 (**4j**) and 4.95 (**6j**). Enantiomeric excess was measured with a Regispack column (97:3 hexanes/iPrOH, 1.0 mL min^{-1}, 20 ˚C, 250 nm, τ_{major} = 40.1 min, τ_{minor} = 35.6 min).

*7-Ethyl-3-(2-nitro-1-phenylethyl)-1H-indole (**6k**)*.[30] Reaction conversion was determined by relative integration of the ^{1}H NMR signals at δ 6.58 (**4k**) and 4.96 (**6k**). Enantiomeric excess was measured with a Regispack column (97:3 hexanes/iPrOH, 1.0 mL min^{-1}, 20 ˚C, 250 nm, τ_{major} = 33.3 min, τ_{minor} = 29.7 min).

*3-(1-(4-Fluorophenyl)-2-nitroethyl)-1H-indole (**6l**)*.[31] Reaction conversion was determined by relative integration of the ^{1}H NMR signals at δ 6.47 (**4a**) and 4.79 (**6l**). Enantiomeric excess was measured with a Regiscell column (75:25 hexanes/iPrOH, 1.0 mL min^{-1}, 20 ˚C, 250 nm, τ_{major} = 18.1

min, τ_{minor} = 22.8 min).

*3-(1-(2-Chlorophenyl)-2-nitroethyl)-1H-indole (**6m**)*.[32] Reaction conversion was determined by relative integration of the ^{1}H NMR signals at δ 6.47 (**4a**) and 5.64 (**6m**). Enantiomeric excess was measured with a Regiscell column (75:25 hexanes/iPrOH, 1.0 mL min^{-1}, 20 ˚C, 250 nm, τ_{major} = 20.5 min, τ_{minor} = 13.3 min).

*3-(1-(3-Bromophenyl)-2-nitroethyl)-1H-indole (**6n**)*.[32] Reaction conversion was determined by relative integration of the ^{1}H NMR signals at δ 6.47 (**4a**) and 4.81 (**6n**). Enantiomeric excess was measured with a Regiscell column (75:25 hexanes/iPrOH, 1.0 mL min^{-1}, 20 ˚C, 250 nm, τ_{major} = 20.2 min, τ_{minor} = 27.7 min).

*3-(1-(4-Bromophenyl)-2-nitroethyl)-1H-indole (**6o**)*.[32] Reaction conversion was determined by relative integration of the ^{1}H NMR signals at δ 6.47 (**4a**) and 4.81 (**6o**). Enantiomeric excess was measured with a Regiscell column (75:25 hexanes/iPrOH, 1.0 mL min^{-1}, 20 ˚C, 250 nm, τ_{major} = 21.7 min, τ_{minor} = 27.0 min).

*3-(1-(4-Methoxylphenyl)-2-nitroethyl)-1H-indole (**6p**)*.[20b] Reaction conversion was determined by relative integration of the ^{1}H NMR signals at δ 6.47 (**4a**) and 4.79 (**6p**). Enantiomeric excess was measured with a Regiscell column (80:20 hexanes/iPrOH, 1.0 mL min^{-1}, 20 ˚C, 250 nm, τ_{major} = 25.3 min, τ_{minor} = 27.9 min).

*3-(2-Nitro-1-phenylethyl)-1-methylindole (**6q**)*.[33] ^{1}H NMR (500 MHz, $CDCl_3$) δ 7.54 (d, *J* = 8.0 Hz, 1H), 7.45-7.27 (m, 7H), 7.16 (t, *J* = 7.0 Hz, 1H), 6.91 (s, 1H), 5.25 (t, *J* = 8.1 Hz, 1H), 5.09 (dd, *J* = 7.6 Hz and 12.6 Hz, 1H), 4.98 (dd, *J* = 8.5 Hz and 12.6 Hz, 1H), 3.75 (s, 3H). ^{13}C NMR (100 MHz, $CDCl_3$) δ 139.3, 137.2, 128.8, 127.6, 127.4, 126.4, 126.2, 122.1, 119.3, 118.9, 112.6, 109.4, 79.4, 41.4, 32.6. HRMS-ESI: calc for $C_{17}H_{16}N_2O_2Na^+$ $(M + Na^+)^+$ 303.1109, found 303.1118. Enantiomeric excess was measured with a Regiscell column (95:5 hexanes/iPrOH, 1.0 mL min^{-1}, 20 ˚C, 250 nm, τ_{major} = 59.6 min, τ_{minor} = 56.6 min).

Bibliography

References for Chapter 1

(1) (a) List, B. *Chem. Rev.* **2007**, *107*, 5413-5415. (b) MacMillan, D. W. C. *Nature* **2008**, *455*, 304-308. (c) Dondoni, A.; Massi, A. *Angew. Chem., Int. Ed.* **2008**, *47*, 4638-4660. (d) Dalko, P. I.; Moisan, L. *Angew. Chem., Int. Ed.* **2004**, *43*, 5138-5175.

(2) (a) Yamada, S.; Otani, G. *Tetrahedron Lett.* **1969**, 4237-4240. (b) Hajos, Z. G.; Parrish, D. R. *J. Org. Chem.* **1974**, *39*, 1615-1621.

(3) (a) Gaunt, M. J.; Johansson, C. C. C.; McNally, A.; Vo, N. T. *Drug Discov. Today* **2007**, *12*, 8-27. (b) Houk, K. N.; List, B. *Acc. Chem. Res.* **2004**, *37*, 487-487.

(4) (a) Hernandez, J. G.; Juaristi, E. *Chem. Commun.* **2012**, *48*, 5396-5409. (b) Schreiner, P. R. *Chem. Soc. Rev.* **2003**, *32*, 289-296. (c) Xi, Y. M.; Shi, X. D. *Chem. Commun.* **2013**, *49*, 8583-8585.

(5) (a) Bae, H. Y.; Some, S.; Lee, J. H.; Kim, J. Y.; Song, M. J.; Lee, S.; Zhang, Y. J.; Song, C. E. *Adv. Synth. Catal.* **2011**, *353*, 3196-3202. (b) Yuan, H. N.; Wang, S.; Nie, J.; Meng, W.; Yao, Q. W.; Ma, J. A. *Angew. Chem., Int. Ed.* **2013**, *52*, 3869-3873. (c) Rossi, S.; Benaglia, M.; Massolo, E.; Raimondi, L. *Catal. Sci. Technol.* **2014**, *4*, 2708-2723.

(6) (a) Balakrishna, B.; Nunez-Rico, J. L.; Vidal-Ferran, A. *Eur. J. Org. Chem.* **2015**, 5293-5303. (b) Forzatti, P.; Lietti, L. *Catal. Today* **1999**, *52*, 165-181.

(7) (a) Erkkila, A.; Majander, I.; Pihko, P. M. *Chem. Rev.* **2007**, *107*, 5416-5470. (b) Mukherjee, S.; Yang, J. W.; Hoffmann, S.; List, B. *Chem. Rev.* **2007**, *107*, 5471-5569. (c) Bertelsen, S.; Marigo, M.; Brandes, S.; Diner, P.; Jorgensen, K. A. *J. Am. Chem. Soc.* **2006**, *128*, 12973-12980.

(8) (a) Flanigan, D. M.; Romanov-Michailidis, F.; White, N. A.; Rovis, T. *Chem. Rev.* **2015**, *115*, 9307-9387. (b) Jen, W. S.; Wiener, J. J. M.; MacMillan, D. W. C. *J. Am. Chem. Soc.* **2000**, *122*, 9874-9875.

(9) (a) Akiyama, T. *Chem. Rev.* **2007**, *107*, 5744-5758. (b) Grondal, C.; Jeanty, M.; Enders, D. *Nat. Chem.* **2010**, *2*, 167-178. (c) Taylor, M. S.; Jacobsen, E. N. *Angew. Chem., Int. Ed.* **2006**, *45*, 1520-1543. (d) Zuend, S. J.; Jacobsen, E. N. *J. Am. Chem. Soc.* **2009**, *131*, 15358-15374.

(10) Seayad, J.; List, B. *Org. Biomol. Chem.* **2005**, *3*, 719-724.

(11) (a) Methot, J. L.; Roush, W. R. *Adv. Synth. Catal.* **2004**, *346*, 1035-1050. (b) Xiao, Y. M.; Sun, Z. H.; Guo, H. C.; Kwon, O. *Beilstein J. Org. Chem.* **2014**, *10*, 2089-2121. (c) Marinetti, A.; Voituriez, A. *Synlett* **2010**, 174-194.

(12) (a) Sulzer-Mosse, S.; Alexakis, A. *Chem. Commun.* **2007**, 3123-3135. (b) Palomo, C.; Oiarbide, M.; Lopez, R. *Chem. Soc. Rev.* **2009**, *38*, 632-653.

(13) (a) Taylor, J. E.; Bull, S. D.; Williams, J. M. J. *Chem. Soc. Rev.* **2012**, *41*, 2109-2121. (b) Leow, D.; Tan, C. H. *Chem. Asian J.* **2009**, *4*, 488-507.

(14) (a) Bryant, L. A.; Fanelli, R.; Cobb, A. J. A. *Beilstein J. Org. Chem.* **2016**, *12*, 429-443. (b) Marcelli, T.; van Maarseveen, J. H.; Hiemstra, H. *Angew. Chem., Int. Ed.* **2006**, *45*, 7496-7504. (c) Zheng, S. Q.; Schienebeck, C. M.; Zhang, W.; Wang, H. Y.; Tang, W. P. *Asian J. Org. Chem.* **2014**, *3*, 366-376.

(15) Samet, M.; Kass, S. R. *J. Org. Chem.* **2015**, *80*, 7727-7731.

(16) Doyle, A. G.; Jacobsen, E. N. *Chem. Rev.* **2007**, *107*, 5713-5743.

(17) Connon, S. J. *Chem. Eur. J.* **2006**, *12*, 5418-5427.

(18) (a) Aleman, J.; Parra, A.; Jiang, H.; Jorgensen, K. A. *Chem. Eur. J.* **2011**, *17*, 6890-6899. (b) Zhao, B. L.; Li, J. H.; Du, D. M. *Chem. Rec.* **2017**, *17*, 994-1018.

(19) Akiyama, T.; Itoh, J.; Fuchibe, K. *Adv. Synth. Catal.* **2006**, *348*, 999-1010.

(20) (a) Parmar, D.; Sugiono, E.; Raja, S.; Rueping, M. *Chem. Rev.* **2014**, *114*, 9047-9153. (b) Zamfir, A.; Schenker, S.; Freund, M.; Tsogoeva, S. B. *Org. Biomol. Chem.* **2010**, *8*, 5262-5276.

(21) (a) Connon, S. J. *Chem. Commun.* **2008**, 2499-2510. (b) Sun, Y. L.; Wei, Y.; Shi, M. *Chemcatchem* **2017**, *9*, 718-727. (c) Chauhan, P.; Mahajan, S.; Kaya, U.; Hack, D.; Enders, D. *Adv. Synth. Catal.* **2015**, *357*, 253-281. (d) Kenny, R.; Liu, F. *Chem. Rec.* **2017**, *17*, 535-553.

(22) Beckett, A. H. *Biochem. Soc. Trans.* **1991**, *19*, 443-446.

(23) (a) Corey, E. J.; Guzman-Perez, A. *Angew. Chem., Int. Ed.* **1998**, *37*, 388-401. (b) Bella, M.; Gasperi, T. *Synthesis* **2009**, 1583-1614. (c) Cozzi, P. G.; Hilgraf, R.; Zimmermann, N. *Eur. J. Org. Chem.* **2007**, 5969-5994.

(24) Ariens, E. J. *Eur. J. Clin. Pharmacol.* **1984**, *26*, 663-668.

(25) Christoffers, J.; Mann, A. *Angew. Chem., Int. Ed.* **2001**, *40*, 4591-4597.

(26) Porter, W. H. *Pure Appl. Chem.* **1991**, *63*, 1119-1122.

(27) Pirkle, W. H.; Pochapsky, T. C. *Chem. Rev.* **1989**, *89*, 347-362.

(28) Brill, Z. G.; Condakes, M. L.; Ting, C. P.; Maimone, T. J. *Chem. Rev.* **2017**, *117*, 11753-11795.

(29) Gnas, Y.; Glorius, F. *Synthesis* **2006**, 1899-1930.

(30) Dalko, P. I.; Moisan, L. *Angew. Chem., Int. Ed.* **2001**, *40*, 3726-3748.

(31) (a) Diner, P.; Nielsen, M.; Marigo, M.; Jorgensen, K. A. *Angew. Chem., Int. Ed.* **2007**, *46*, 1983-1987. (b) Wong, M. W.; Ng, A. M. E. *Aust. J. Chem.* **2014**, *67*, 1100-1109. (c) Peng, Q.; Duarte, F.; Paton, R. S. *Chem. Soc. Rev.* **2016**, *45*, 6093-6107.

(32) Terada, M. *Chem. Commun.* **2008**, 4097-4112.

(33) Serdyuk, O. V.; Heckel, C. M.; Tsogoeva, S. B. *Org. Biomol. Chem.* **2013**, *11*, 7051-7071.

(34) Rueping, M.; Kuenkel, A.; Atodiresei, I. *Chem. Soc. Rev.* **2011**, *40*, 4539-4549.

(35) Cheon, C. H.; Yamamoto, H. *Chem. Commun.* **2011**, *47*, 3043-3056.

(36) Akiyama, T.; Mori, K. *Chem. Rev.* **2015**, *115*, 9277-9306.

(37) (a) Jencks, W. P. *Acc. Chem. Res.* **1976**, *9*, 425-432. (b) Ault, A. *J. Chem. Educ.* **2007**, *84*, 38-39.

(38) Pihko, P. M. *Angew. Chem., Int. Ed.* **2004**, *43*, 2062-2064.

(39) Kenny, R.; Liu, F. *Eur. J. Org. Chem.* **2015**, 5304-5319.

(40) (a) Sohtome, Y.; Hashimoto, Y.; Nagasawa, K. *Adv. Synth. Catal.* **2005**, *347*, 1643-1648. (b) Wei, Y.; Shi, M. *Acc. Chem. Res.* **2010**, *43*, 1005-1018. (c) Ashokkumar, V.; Siva, A. *Org. Biomol. Chem.* **2015**, *13*, 10216-10225.

(41) Denmark, S. E.; Beutner, G. L. *Angew. Chem., Int. Ed.* **2008**, *47*, 1560-1638.

(42) (a) Okino, T.; Hoashi, Y.; Takemoto, Y. *J. Am. Chem. Soc.* **2003**, *125*, 12672-12673. (b) Fang, Y. Q.; Tadross, P. M.; Jacobsen, E. N. *J. Am. Chem. Soc.* **2014**, *136*, 17966-17968. (c) Herrera, R. P.; Sgarzani, V.; Bernardi, L.; Ricci, A. *Angew. Chem., Int. Ed.* **2005**, *44*, 6576-6579.

(43) Terada, M. *Synthesis* **2010**, 1929-1982.

(44) Akiyama, T.; Itoh, J.; Yokota, K.; Fuchibe, K. *Angew. Chem., Int. Ed.* **2004**, *43*, 1566-1568.

(45) Uraguchi, D.; Terada, M. *J. Am. Chem. Soc.* **2004**, *126*, 5356-5357.

(46) Akiyama, T.; Morita, H.; Itoh, J.; Fuchibe, K. *Org. Lett.* **2005**, *7*, 2583-2585.

(47) Hoffmann, S.; Seayad, A. M.; List, B. *Angew. Chem., Int. Ed.* **2005**, *44*, 7424-7427.

(48) (a) Klussmann, M.; Ratjen, L.; Hoffmann, S.; Wakchaure, V.; Goddard, R.; List, B. *Synlett* **2010**, 2189-2192. (b) Reid, J. P.; Goodman, J. M. *Chem. Eur. J.* **2017**, *23*, 14248-14260. (c) Clot-Almenara, L.; Rodriguez-Escrich, C.; Osorio-Planes, L.; Pericas, M. A. *ACS Catal.* **2016**, *6*, 7647-7651.

(49) Storer, R. I.; Carrera, D. E.; Ni, Y.; MacMillan, D. W. C. *J. Am. Chem. Soc.* **2006**, *128*, 84-86.

(50) Chen, X. H.; Xu, X. Y.; Liu, H.; Cun, L. F.; Gong, L. Z. *J. Am. Chem. Soc.* **2006**, *128*, 14802-14803.

(51) (a) Rueping, M.; Sugiono, E.; Theissmann, T.; Kuenkel, A.; Kockritz, A.; Pews-Davtyan, A.; Nemati, N.; Beller, M. *Org. Lett.* **2007**, *9*, 1065-1068. (b) Rueping, M.; Antonchick, A. P. *Angew. Chem., Int. Ed.* **2008**, *47*, 10090-10093. (c) Tang, H. Y.; Lu, A. D.; Zhou, Z. H.; Zhao, G. F.; He, L. N.; Tang, C. C. *Eur. J. Org. Chem.* **2008**, 1406-1410. (d) Guo, Q. X.; Peng, Y. G.; Zhang, J. W.; Song, L.; Feng, Z.; Gong, L. Z. *Org. Lett.* **2009**, *11*, 4620-4623. (e) Liang, T.; Zhang, Z. J.; Antilla, J. C. *Angew. Chem., Int. Ed.* **2010**, *49*, 9734-9736.

(52) Akiyama, T.; Honma, Y.; Itoh, J.; Fuchibe, K. *Adv. Synth. Catal.* **2008**, *350*, 399-402.

(53) Harada, S.; Kuwano, S.; Yamaoka, Y.; Yamada, K.; Takasu, K. *Angew. Chem., Int. Ed.* **2013**, *52*, 10227-10230.

(54) Hermeke, J.; Toy, P. H. *Tetrahedron* **2011**, *67*, 4103-4109.

(55) Kashikura, W.; Mori, K.; Akiyama, T. *Org. Lett.* **2011**, *13*, 1860-1863.

(56) Rowland, G. B.; Zhang, H. L.; Rowland, E. B.; Chennamadhavuni, S.; Wang, Y.; Antilla, J. C. *J. Am. Chem. Soc.* **2005**, *127*, 15696-15697.

(57) Muller, S.; Webber, M. J.; List, B. *J. Am. Chem. Soc.* **2011**, *133*, 18534-18537.

(58) Akiyama, T.; Saitoh, Y.; Morita, H.; Fuchibe, K. *Adv. Synth. Catal.* **2005**, *347*, 1523-1526.

(59) Chen, X. H.; Zhang, W. Q.; Gong, L. Z. *J. Am. Chem. Soc.* **2008**, *130*, 5652-5653.

(60) He, L.; Chen, X. H.; Wang, D. N.; Luo, S. W.; Zhang, W. Q.; Yu, J.; Ren, L.; Gong, L. Z. *J. Am. Chem. Soc.* **2011**, *133*, 13504-13518.

(61) Momiyama, N.; Konno, T.; Furiya, Y.; Iwamoto, T.; Terada, M. *J. Am. Chem. Soc.* **2011**, *133*, 19294-19297.

(62) Zhou, F. T.; Yamamoto, H. *Angew. Chem., Int. Ed.* **2016**, *55*, 8970-8974.

(63) (a) Fan, T.; Zhang, H. H.; Li, C.; Shen, Y.; Shi, F. *Adv. Synth. Catal.* **2016**, *358*, 2017-2031. (b) Gridnev, I. D.; Kouchi, M.; Sorimachi, K.; Terada, M. *Tetrahedron Lett.* **2007**, *48*, 497-500.

(64) (a) Mori, K.; Wakazawa, M.; Akiyama, T. *Chem. Sci.* **2014**, *5*, 1799-1803. (b) Akiyanza, T.; Katoh, T.; Mori, K. *Angew. Chem., Int. Ed.* **2009**, *48*, 4226-4228. (c) Wang, Y.; Tu, M. S.; Shi, F.; Tu, S. J. *Adv. Synth. Catal.* **2014**, *356*, 2009-2019.

(65) Kaupmees, K.; Tolstoluzhsky, N.; Raja, S.; Rueping, M.; Leito, I. *Angew. Chem., Int. Ed.* **2013**, *52*, 11569-11572.

(66) Lee, S.; Kim, S. *Tetrahedron Lett.* **2009**, *50*, 3345-3348.

(67) Wang, Y. Z.; Liu, W.; Ren, W. L.; Shi, Y. *Org. Lett.* **2015**, *17*, 4976-4979.

(68) Hatano, M.; Goto, Y.; Izumiseki, A.; Akakura, M.; Ishihara, K. *J. Am. Chem. Soc.* **2015**, *137*, 13472-13475.

(69) Samet, M.; Buhle, J.; Zhou, Y. W.; Kass, S. R. *J. Am. Chem. Soc.* **2015**, *137*, 4678-4680.

(70) Fan, Y.; Kass, S. R. *Org. Lett.* **2016**, *18*, 188-191.

(71) (a) Bartmess, J. E. *NIST Chemistry WebBook, NIST Standard Reference Database Number 6*. (b) Mallard, W. G.; Lustrum, P. J., Eds.; National Institute of Standards and Technology: Gaithersburg, M.

(72) Fan, Y.; Kass, S. R. *J. Org. Chem.* **2017**, *82*, 13288-13296.

(73) Reid, J. P.; Simon, L.; Goodman, J. M. *Acc. Chem. Res.* **2016**, *49*, 1029-1041.

(74) (a) Wen, W.; Zeng, Y.; Peng, L. Y.; Fu, L. N.; Guo, Q. X. *Org. Lett.* **2015**, *17*, 3922-3925. (b) Baudequin, C.; Zamfir, A.; Tsogoeva, S. B. *Chem. Commun.* **2008**, 4637-4639.

(75) (a) Feng, J. C.; Yan, W. J.; Wang, D.; Li, P.; Sun, Q. T.; Wang, R. *Chem. Commun.* **2012**, *48*, 8003-8005. (b) Momiyama, N.; Tabuse, H.; Terada, M. *J. Am. Chem. Soc.* **2009**, *131*, 12882-12883. (c) Akiyama, T.; Suzuki, T.; Mori, K. *Org. Lett.* **2009**, *11*, 2445-2447.

(76) Reid, J. P.; Goodman, J. M. *J. Am. Chem. Soc.* **2016**, *138*, 7910-7917.

(77) Connon, S. J. *Angew. Chem., Int. Ed.* **2006**, *45*, 3909-3912.

(78) Itoh, J.; Fuchibe, K.; Akiyama, T. *Angew. Chem., Int. Ed.* **2008**, *47*, 4016-4018.

(79) Hatano, M.; Moriyama, K.; Maki, T.; Ishihara, K. *Angew. Chem., Int. Ed.* **2010**, *49*, 3823-3826.

References for Chapter 2

(1) Akiyama, T. *Chem. Rev.* **2007**, *107*, 5744-5758.

(2) Yu, J.; Shi, F.; Gong, L. Z. *Acc. Chem. Res.* **2011**, *44*, 1156-1171.

(3) Rueping, M.; Koenigs, R. M.; Atodiresei, I. *Chem. - Eur. J.* **2010**, *16*, 9350-9365.

(4) Parmar, D.; Sugiono, E.; Raja, S.; Rueping, M. *Chem. Rev.* **2014**, *114*, 9047-9135.

(5) Liao, H. H.; Chatupheeraphat, A.; Hsiao, C. C.; Atodiresei, I.; Rueping, M. *Angew. Chem., Int. Ed.* **2015**, *54*, 15540-15544.

(6) Takemoto, Y. *Org. Biomol. Chem.* **2005**, *3*, 4299-4306.

(7) (a) Seebach, D.; Beck, A. K.; Heckel, A. *Angew. Chem., Int. Ed.* **2001**, *40*, 92-138. (b) Huang, Y.; Unni, A. K.; Thadani, A. N.; Rawal, V. H. *Nature* **2003**, *424*, 146. (c) Rueping, M.; Sugiono, E.; Moreth, S. A. *Adv. Synth. Catal.* **2007**, *349*, 759-764.

(8) (a) Matsui, K.; Takizawa, S.; Sasai, H. *J. Am. Chem. Soc.* **2005**, *127*, 3680-3681. (b) Wieting, J. M.; Fisher, T. J.; Schafer, A. G.; Visco, M. D.; Gallucci, J. C.; Mattson, A. E. *Eur. J. Org. Chem.* **2015**, *2015*, 525-533. (c) Zhang, Y. D.; Li, N.; Qu, B.; Ma, S. L.; Lee, H.; Gonnella, N. C.; Gao, J.; Li, W. J.; Tan, Z. L.; Reeves, J. T.; Wang, J.; Lorenz, J. C.; Li, G. S.; Reeves, D. C.; Premasiri, A.; Grinberg, N.; Haddad, N.; Lu, B. Z.; Song, J. H. J.; Senanayake, C. H. *Org. Lett.* **2013**, *15*, 1710-1713.

(9) (a) Rueping, M.; Kuenkel, A.; Atodiresei, I. *Chem. Soc. Rev.* **2011**, *40*, 4539-4549. (b) Honjo, T.; Phipps, R. J.; Rauniyar, V.; Toste, F. D. *Angew. Chem., Int. Ed.* **2012**, *51*, 9684-9688. (c) Held, F. E.; Grau, D.; Tsogoeva, S. B. *Molecules* **2015**, *20*, 16103-16126.

(10) Akiyama, T.; Itoh, J.; Fuchibe, K. *Adv. Synth. Catal.* **2006**, *348*, 999-1010.

(11) Wang, B. L.; Zhang, J. X.; Li, N. K.; Liu, G. G.; Shen, Q.; Wang, X. W. *Tetrahedron Lett.* **2011**, *52*, 4671-4674.

(12) Takagi, R.; Kondo, A.; Ohkata, K. *J. Mol. Catal. A: Chem.* **2007**, *278*, 120-126.

(13) Makiguchi, K.; Ogasawara, Y.; Kikuchi, S.; Satoh, T.; Kakuchi, T. *Macromolecules* **2013**, *46*, 1772-1782.

(14) Li, Y. H.; Lu, L. Q.; Das, S.; Pisiewicz, S.; Junge, K.; Beller, M. *J. Am. Chem. Soc.* **2012**, 134, 18325-18329.

(15) Kaupmees, K.; Tolstoluzhsky, N.; Raja, S.; Rueping, M.; Leito, I. *Angew. Chem., Int. Ed.* **2013**, *52*, 11569-11572.

(16) Samet, M.; Buhle, J.; Zhou, Y. W.; Kass, S. R. *J. Am. Chem. Soc.* **2015**, *137*, 4678-4680.

(17) Fan, Y.; Kass, S. R. *Org. Lett.* **2016**, *18*, 188-191.

(18) Only small reactivity differences are expected for 4-*N*-alkylpyridinium ion DPP derivatives since the negative charge in their conjugate bases is not delocalized onto the aromatic rings.

(19) Nishida, H.; Takada, N.; Yoshimura, M.; Sonoda, T.; Kobayashi, H. *Bull. Chem. Soc. Jpn.* **1984**, *57*, 2600-2604.

(20) Rosokha, S. V.; Stern, C. L.; Ritzert, J. T. *CrystEngComm* **2013**, *15*, 10638-10647.

(21) Scherer, A.; Mukherjee, T.; Hampel, F.; Gladysz, J. A. *Organometallics* **2014**, *33*, 6709-6722.

(22) (a) Simon, L.; Goodman, J. M. *J. Am. Chem. Soc.* **2008**, *130*, 8741-8747. (b) Marcelli, T.; Hammar, P.; Himo, F. *Chem. - Eur. J.* **2008**, *14*, 8562-8571. (c) Yamanaka, M.; Hirata, T. J. *Org. Chem.* **2009**, *74*, 3266-3271.

(23) Reichardt, C., Welton, T. *Solvents and Solvent Effects in Organic Chemistry*, 4th ed.; Wiley-VCH: Weinheim, 2010.

(24) *Burdick & Jackson Solvent Guide*, 3rd ed.; Burdick & Jackson Laboratories: Muskegon, MI, 1990.

(25) Nie, J.; Kobayashi, H.; Sonoda, T. *Catal. Today* **1997**, *36*, 81-84.

(26) Makiguchi, K.; Satoh, T.; Kakuchi, T. *Macromolecules* **2011**, *44*, 1999-2005.

(27) Kan, S. L.; Jin, Y.; He, X. J.; Chen, J.; Wu, H.; Ouyang, P. K.; Guo, K.; Li, Z. J. *Polym. Chem.* **2013**, *4*, 5432-5439.

(28) Chen, J.; Kan, S. L.; Xia, H. D.; Zhou, F.; Chen, X.; Jiang, X. Q.; Guo, K.; Li, Z. J. *Polymer* **2013**, *54*, 4177-4182.

References for Chapter 3

(1) (a) Dixon, R. A. *Nature* **2001**, *411*, 843-847. (b) Li, S. M. *Nat. Prod. Rep.* **2010**, *27*, 57-78.

(2) (a) Kochanowska-Karamyan, A. J.; Hamann, M. T. *Chem. Rev.* **2010**, *110*, 4489-4497. (b) Zhang, M. Z.; Chen, Q.; Yang, G. F. *Eur. J. Med. Chem.* **2015**, *89*, 421-441.

(3) (a) Taber, D. F.; Tirunahari, P. K. *Tetrahedron* **2011**, *67*, 7195-7210. (b) Barluenga, J.; Rodriguez, F.; Fananas, F. J. *Chem. - Asian J.* **2009**, *4*, 1036-1048.

(4) (a) Melander, R. J.; Minvielle, M. J.; Melander, C. *Tetrahedron* **2014**, *70*, 6363-6372. (b) Rani, P.; Srivastava, V. K.; Kumar, A. *Eur. J. Med. Chem.* **2004**, *39*, 449-452. (c) Zhang, H. C.; Ye, H.; Moretto, A. F.; Brumfield, K. K.; Maryanoff, B. E. *Org. Lett.* **2000**, *2*, 89-92. (d) Du, Y. F.; Liu, R. H.; Linn, G.; Zhao, K. *Org. Lett.* **2006**, *8*, 5919-5922. (e) Radwan, M. A. A.; Ragab, E. A.; Sabry, N. M.; El-Shenawy, S. M. *Bioorgan. Med. Chem.* **2007**, *15*, 3832-3841. (f) Agarwal, A.; Srivastava, K.; Puri, S. K.; Chauhan, P. M. S. *Bioorg. Med. Chem. Lett.* **2005**, *15*, 3133-3136. (g) Chen, J.-B.; Jia, Y.-X. *Org. Biomol. Chem.* **2017**, *15*, 3550-3567.

(5) (a) Muller, K.; Faeh, C.; Diederich, F. *Science* **2007**, *317*, 1881-1886. (b) Biffinger, J. C.; Kim, H. W.; DiMagno, S. G. *ChemBioChem* **2004**, *5*, 622-627. (c) Mikami, K.; Itoh, Y.; Yamanaka, M. *Chem. Rev.* **2004**, *104*, 1-16.

(6) (a) Chae, J.; Konno, T.; Ishihara, T.; Yamanaka, H. *Chem. Lett.* **2004**, *33*, 314-315. (b) Lin, R. Y.; Ding, S. T.; Shi, Z. Z.; Jiao, N. *Org. Lett.* **2011**, *13*, 4498-4501.

(7) (a) Shimizu, R.; Egami, H.; Nagi, T.; Chae, J.; Hamashima, Y.; Sodeoka, M. *Tetrahedron Lett.* **2010**, *51*, 5947-5949. (b) Yin, B.; Wang, L. H.; Inagi, S.; Fuchigami, T. *Tetrahedron* **2010**, *66*, 6820-6825. (c) Dolensky, B.; Nam, G.; Deng, W. P.; Narayanan, J.; Fan, J. F.; Kirk, K. L. *J. Fluorine Chem.* **2004**, *125*, 501-508.

(8) (a) Ferry, A.; Billard, T.; Bacque, E.; Langlois, B. R. *J. Fluorine Chem.* **2012**, *134*, 160-163. (b) Baudoux, J.; Salit, A. F.; Cahard, D.; Plaquevent, J. C. *Tetrahedron Lett.* **2002**, *43*, 6573-6574.

(9) Lakhdar, S.; Westermaier, M.; Terrier, F.; Goumont, R.; Boubaker, T.; Ofial, A. R.; Mayr, H. *J. Org. Chem.* **2006**, *71*, 9088-9095.

(10) (a) Wen, L. L.; Shen, Q. L.; Wan, X. L.; Lu, L. *J. Org. Chem.* **2011**, *76*, 2282-2285. (b) Blay, G.; Fernandez, I.; Munoz, M. C.; Pedro, J. R.; Vila, C. *Chem. - Eur. J.* **2010**, *16*, 9117-9122. (c) Shevchenko, N. E.; Shmatova, O. I.; Balenkova, E. S.; Roschenthaler, G. V.; Nenajdenko, V. G. *Eur. J. Org. Chem.* **2013**, 2237-2245.

(11) (a) Parmar, D.; Sugiono, E.; Raja, S.; Rueping, M. *Chem. Rev.* **2014**, *114*, 9047-9153. (b) You, S.

L.; Cai, Q.; Zeng, M. *Chem. Soc. Rev.* **2009**, *38*, 2190-2201. (c) Poulsen, T. B.; Jorgensen, K. A. *Chem. Rev.* **2008**, *108*, 2903-2915. (d) Uraguchi, D.; Terada, M. *J. Am. Chem. Soc.* **2004**, *126*, 5356-5357.

(12) Liu, X. D.; Wang, Y.; Ma, H. Y.; Xing, C. H.; Yuan, Y.; Lu, L. Tetrahedron 2017, 73, 2283-2289.

(13) (a) Kasztelan, A.; Biedrzycki, M.; Kwiatkowski, P. *Adv. Synth. Catal.* **2016**, *358*, 2962-2969. (b) Biedrzycki, M.; Kasztelan, A.; Kwiatkowski, P. *ChemCatChem* **2017**, *9*, 2453-2456.

(14) Bandini, M.; Sinisi, R. *Org. Lett.* **2009**, *11*, 2093-2096.

(15) Wang, Y.; Yuan, Y.; Xing, C. H.; Lu, L. *Tetrahedron Lett.* **2014**, *55*, 1045-1048.

(16) (a) Nie, J.; Zhang, G. W.; Wang, L.; Fu, A. P.; Zheng, Y.; Ma, J. A. *Chem. Commun.* **2009**, 2356-2358. (b) Wang, T.; Zhang, G.-W.; Teng, Y.; Nie, J.; Zheng, Y.; Ma, J.-A. *Adv. Synth. Catal.* **2010**, *352*, 2773-2777.

(17) Kaupmees, K.; Tolstoluzhsky, N.; Raja, S.; Rueping, M.; Leito, I. *Angew. Chem., Int. Ed.* **2013**, *52*, 11569-11572.

(18) Akiyama, T.; Morita, H.; Itoh, J.; Fuchibe, K. *Org. Lett.* **2005**, *7*, 2583-2585.

(19) (a) Akiyama, T.; Itoh, J.; Yokota, K.; Fuchibe, K. *Angew. Chem., Int. Ed.* **2004**, *43*, 1566-1568. (b) Zhou, F. T.; Yamamoto, H. *Angew. Chem., Int. Ed.* **2016**, *55*, 8970-8974.

(20) Samet, M.; Buhle, J.; Zhou, Y. W.; Kass, S. R. *J. Am. Chem. Soc.* **2015**, *137*, 4678-4680.

(21) Fan, Y.; Kass, S. R. *Org. Lett.* **2016**, *18*, 188-191.

(22) Ma, J.; Kass, S. R. *Org. Lett.* **2016**, *18*, 5812-5815.

(23) Fan, Y.; Kass, S. R. *J. Org. Chem.* **2017**, *82*, 13288-13296.

(24) Hermeke, J.; Toy, P. H. *Tetrahedron* **2011**, *67*, 4103-4109.

(25) (a) Clot-Almenara, L.; Rodriguez-Escrich, C.; Osorio-Planes, L.; Pericas, M. A. *ACS Catal.* **2016**, *6*, 7647-7651. (b) Reid, J. P.; Goodman, J. M. *Chem. - Eur. J.* **2017**, *23*, 14248-14260.

(26) Wang, Y. Z.; Liu, W.; Ren, W. L.; Shi, Y. *Org. Lett.* **2015**, *17*, 4976-4979.

(27) Fu, A.; Meng, W.; Li, H.; Nie, J.; Ma, J. A. *Org. Biomol. Chem.* **2014**, *12*, 1908-1918.

(28) (a) Storer, R. I.; Carrera, D. E.; Ni, Y.; MacMillan, D. W. C. *J. Am. Chem. Soc.* **2006**, *128*, 84-86. (b) Klussmann, M.; Ratjen, L.; Hoffmann, S.; Wakchaure, V.; Goddard, R.; List, B. *Synlett* **2010**, 2189-2192.

(29) (a) Romanov-Michailidis, F.; Guenee, L.; Alexakis, A. *Angew. Chem., Int. Ed.* **2013**, *52*, 9266-9270. (b) Meng, Y.; Slaven, W. T.; Wang, D.; Liu, T. J.; Chow, H. F.; Li, C. J. *Tetrahedron: Asymmetry* **1998**, *9*, 3693-3707. (c) Hua, J.; Lin, W. B. *Org. Lett.* **2004**, *6*, 861-864.

References for Chapter 4

(1) (a) Akiyama, T. *Chem. Rev.* **2007**, *107*, 5744-5758. (b) Akiyama, T.; Mori, K. *Chem. Rev*. **2015**, *115*, 9277-9306.

(2) (a) Palomo, C.; Landa, A.; Mielgo, A.; Oiarbide, M.; Puente, A.; Vera, S. *Angew. Chem., Int. Ed.* **2007**, *46*, 8431-8435. (b) Calogero, S.; Lanari, D.; Orru, M.; Piermatti, O.; Pizzo, F.; Vaccaro, L. *J. Catal.* **2011**, *282*, 112-119. (c) Ramachary, D. B.; Chowdari, N. S.; Barbas, C. F. *Angew. Chem., Int. Ed.* **2003**, *42*, 4233-4237.

(3) Parmar, D.; Sugiono, E.; Raja, S.; Rueping, M. *Chem. Rev.* **2014**, *114*, 9047-9153.

(4) (a) Terada, M. *Chem. Commun.* **2008**, 4097-4112. (b) Zamfir, A.; Schenker, S.; Freund, M.; Tsogoeva, S. B. *Org. Biomol. Chem.* **2010**, 8, 5262-5276.

(5) (a) Kaib, P. S. J.; Schreyer, L.; Lee, S.; Properzi, R.; List, B. *Angew. Chem., Int. Ed.* **2016**, *55*, 13200-13203. (b) Bandar, J. S.; Ascic, E.; Buchwald, S. L. *J. Am. Chem. Soc.* **2016**, *138*, 5821-5824.

(6) (a) Matsui, K.; Takizawa, S.; Sasai, H. *J. Am. Chem. Soc.* **2005**, *127*, 3680-3681. (b) Wieting, J. M.; Fisher, T. J.; Schafer, A. G.; Visco, M. D.; Gallucci, J. C.; Mattson, A. E. *Eur. J. Org. Chem.* **2015**, 525-533.

(7) (a) Takemoto, Y. *Org. Biomol. Chem.* **2005**, *3*, 4299-4306. (b) Ji, N.; Yuan, J. N.; Xue, S. S.; Zhang, J. N.; He, W. *Tetrahedron* **2016**, *72*, 512-517.

(8) (a) Seebach, D.; Beck, A. K.; Heckel, A. *Angew. Chem., Int. Ed.* **2001**, *40*, 92-138. (b) Rueping, M.; Sugiono, E.; Moreth, S. A. *Adv. Synth. Catal.* **2007**, *349*, 759-764.

(9) (a) Phillips, A. M. F.; Pombeiro, A. J. L. *Org. Biomol. Chem.* **2017**, *15*, 2307-2340. (b) Min, C.; Seidel, D. *Chem. Soc. Rev.* **2017**, *46*, 5889-5902.

(10) (a) Akiyama, T.; Itoh, J.; Yokota, K.; Fuchibe, K. *Angew. Chem., Int. Ed.* **2004**, *43*, 1566-1568. (b) Sun, F. L.; Zheng, X. J.; Gu, Q.; He, Q. L.; You, S. L. *Eur. J. Org. Chem.* **2010**, 47-50. (c) Akiyama, T.; Morita, H.; Itoh, J.; Fuchibe, K. *Org. Lett.* **2005**, *7*, 2583-2585.

(11) (a) Jiao, P.; Nakashima, D.; Yamamoto, H. *Angew. Chem., Int. Ed.* **2008**, *47*, 2411-2413. (b) Rueping, M.; Nachtsheim, B. J. *Synlett* **2010**, 119-122. (c) Vellalath, S.; Coric, I.; List, B. *Angew. Chem., Int. Ed.* **2010**, *49*, 9749-9752.

(12) Li, G. L.; Antilla, J. C. *Org. Lett.* **2009**, *11*, 1075-1078.

(13) Samet, M.; Buhle, J.; Zhou, Y. W.; Kass, S. R. *J. Am. Chem. Soc.* **2015**, *137*, 4678-4680.

(14) Fan, Y.; Kass, S. R. *Org. Lett.* **2016**, *18*, 188-191.

(15) Ma, J.; Kass, S. R. *Org. Lett.* **2016**, *18*, 5812-5815.

(16) Fan, Y.; Kass, S. R. *J. Org. Chem.* **2017**, *82*, 13288-13296.

(17) Ma, J.; Kass, S. R. *Org. Lett.* **2018**, *20*, 2689–2692.

(18) (a) Nishida, H.; Takada, N.; Yoshimura, M.; Sonoda, T.; Kobayashi, H. *Bull. Chem. Soc. Jpn.* **1984**, *57*, 2600-2604. (b) Blight, B. A.; Hunter, C. A.; Leigh, D. A.; Mcnab, H.; Thomson, P. I. T. *Nat. Chem.* **2011**, *3*, 244-248.

(19) (a) Hermeke, J.; Toy, P. H. *Tetrahedron* **2011**, *67*, 4103-4109. (b) Reid, J. P.; Goodman, J. M. *J. Am. Chem. Soc.* **2016**, *138*, 7910-7917.

(20) (a) Hong, L.; Sun, W. S.; Yang, D. X.; Li, G. F.; Wang, R. *Chem. Rev.* **2016**, *116*, 4006-4123. (b) Itoh, J.; Fuchibe, K.; Akiyama, T. *Angew. Chem., Int. Ed.* **2008**, *47*, 4016-4018.

(21) (a) Clot-Almenara, L.; Rodriguez-Escrich, C.; Osorio-Planes, L.; Pericas, M. A. *ACS Catal.* **2016**, *6*, 7647-7651. (b) Reid, J. P.; Simon, L.; Goodman, J. M. *Acc. Chem. Res.* **2016**, *49*, 1029–1041.

(22) Reid, J. P.; Goodman, J. M. *Chem. Eur. J.* **2017**, *23*, 14248-14260.

(23) The low conversion due to slow rate was observed with **4l** and is the reason for the low isolated yield.

(24) Bures, J. *Angew. Chem., Int. Ed.* **2016**, *55*, 2028-2031.

(25) (a) Klussmann, M.; Ratjen, L.; Hoffmann, S.; Wakchaure, V.; Goddard, R.; List, B. *Synlett* **2010**, 2189-2192. (b) Storer, R. I.; Carrera, D. E.; Ni, Y.; MacMillan, D. W. C. *J. Am. Chem. Soc.* **2006**, *128*, 84-86.

(26) Park, Y. S.; Grove, C. I.; Gonzalez-Lopez, M.; Urgaonkar, S.; Fettinger, J. C.; Shaw, J. T. *Angew. Chem., Int. Ed*. **2011**, *50*, 3730-3733.

(27) Marques-Lopez, E.; Alcaine, A.; Tejero, T.; Herrera, R. P. *Eur. J. Org. Chem.* **2011**, 3700-3705.

(28) Herrera, R. P.; Sgarzani, V.; Bernardi, L.; Ricci, A. *Angew. Chem., Int. Ed.* **2005**, *44*, 6576-6579.

(29) Jeganathan, M.; Kanagaraj, K.; Dhakshinamoorthy, A.; Pitchumani, K. *Tetrahedron Lett.* **2014**, *55*, 2061-2064.

(30) Babu, K. S.; Rao, V. R. S.; Sunitha, P.; Babu, S. S.; Rao, J. M. *Synthetic Commun.* **2008**, *38*, 1784-1791.

(31) Kumar, A. V.; Rao, K. R. *Tetrahedron Lett.* **2011**, *52*, 5188-5191.

(32) Ganesh, M.; Seidel, D. *J. Am. Chem. Soc.* **2008**, *130*, 16464-16465.

(33) Lu, S. F.; Du, D. M.; Xu, J. X. *Org. Lett.* **2006**, *8*, 2115-2118.

Appendices

Appendix for Chapter 2

Scheme S1. Plausible transition states for the Friedel-Crafts reaction of *β*-nitrostyrene with indole and *N*-methylindole.

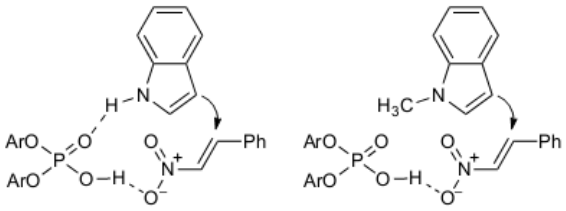

Table S1. Kinetic data of Friedel-Crafts reactions of indole and *β*-nitrostyrene.

$[indole]_0 = [\beta\text{-nitrostyrene}]_0 = 94.8$ mM			
catalyst, solvent	time (h)	conversion (%)	[reactants], mM
no catalyst, CD_2Cl_2	99.0	0.24	94.6
	165.5	0.45	94.4
	336.0	1.41	93.5
10% DPP, CD_2Cl_2	24.5	6.50	88.6
	47.5	10.54	84.8
	54.0	11.66	83.7
	121.0	19.60	76.2
	145.0	22.20	73.8
10% DPP*, CD_2Cl_2	10.5	7.48	87.7
10% **1**, CD_2Cl_2	2.0	5.00	90.1
	5.0	12.71	82.8
	26.3	35.24	61.4
	71.5	59.70	38.2
10% **2**, CD_2Cl_2	1.0	17.53	78.2
	2.0	29.19	67.1
	4.0	44.68	52.4
	6.0	54.24	43.4
	8.0	61.33	36.7

Continued Table S1.

5% **2**, CD_2Cl_2	2.0	15.46	80.1
	4.0	30.45	65.9
	6.0	38.18	58.6
	8.0	43.49	53.6
	24.0	67.91	30.4
2% **2**, CD_2Cl_2	1.0	4.17	90.8
	2.0	7.13	88.0
	4.0	13.45	82.0
	6.0	18.13	77.6
	8.0	22.15	73.8
no catalyst, $CDCl_3$	220.0	0.19	94.6
	267.0	0.35	94.5
	336.0	0.62	94.2
5% DPP, $CDCl_3$	21.3	2.78	92.2
	46.0	6.32	88.8
	69.0	10.88	84.5
	99.0	14.93	80.6
	165.5	23.23	72.8
5% **1**, $CDCl_3$	2.0	4.28	90.7
	5.0	8.55	86.7
	26.3	26.58	69.6
	71.5	49.68	47.7
5% **2**, $CDCl_3$	1.0	8.37	86.9
	2.3	16.20	79.4
	3.0	20.20	75.7
	4.0	24.57	71.5
	5.0	29.30	67.0
	21.3	60.69	37.3
5% DPP, C_6H_5Cl	24.0	3.50	91.5
	30.5	6.11	89.0
	47.5	9.78	85.5
	55.0	11.45	83.9
5% **2**, C_6H_5Cl	0.50	3.06	91.9
	2.0	5.52	89.6
	6.0	17.05	78.6
	24.0	45.34	51.8

Continued Table S1.

5% DPP, THF-d_8	96.0	1.13	93.7
5% **2**, THF-d_8	96.0	1.15	93.7

Table S2. Kinetic data of Friedel-Crafts reactions of *N*-methylindole and *β*-nitrostyrene.

[*N*-methylindole]$_0$ = [*β*-nitrostyrene]$_0$ = 94.8 mM			
catalyst, solvent	time (h)	conversion (%)	[reactants], mM
no catalyst, CD_2Cl_2	99.0	0.02	94.8
	169.5	0.17	94.6
	220.0	0.36	94.5
	267.0	0.53	94.3
10% DPP, CD_2Cl_2	121.0	2.10	92.8
	169.5	3.11	91.9
	222.0	3.85	91.2
	289.0	4.76	90.3
10% **1**, CD_2Cl_2	2.0	1.98	92.9
	5.0	8.65	86.6
	26.3	38.44	58.4
	71.5	66.39	31.9
10% **2**, CD_2Cl_2	1.0	25.20	70.9
	2.0	39.63	57.2
	4.0	54.51	43.1
	6.0	64.30	33.8
5% **2**, CD_2Cl_2	2.0	17.39	78.3
	4.0	29.98	66.4
	7.0	43.60	53.5
	20.5	72.45	26.1
2.5% **2**, CD_2Cl_2	2.0	10.60	84.8
	4.0	19.92	75.9
	6.0	28.72	67.6
	7.0	31.41	65.0
	20.5	59.39	38.5
no catalyst, $CDCl_3$	99.0	0.69	94.1
	165.3	1.63	93.3
	220.0	2.40	92.5

Continued Table S2.

	267.0	3.09	91.9
5% DPP, $CDCl_3$	69.0	0.14	94.7
	99.0	1.01	93.8
	165.5	2.78	92.2
	220.0	4.06	91.0
5% **1**, $CDCl_3$	5.0	1.82	93.1
	26.5	21.06	74.8
	71.5	40.73	56.2
	76.0	43.22	53.8
5% **2**, $CDCl_3$	1.0	8.37	86.9
	2.3	16.20	79.4
	3.0	20.20	75.7
	4.0	24.57	71.5
	5.0	29.30	67.0
	21.3	60.69	37.3

Table S3. Kinetic data of Diels-Alder reactions.

$[cyclopentadiene]_0 = [methyl\ vinyl\ ketone]_0 = 100$ mM in $CDCl_3$			
catalyst	time (h)	conversion (%)	[reactants], mM
no catalyst	1.00	7.30	92.7
	2.58	15.96	84.0
	3.50	19.73	80.3
	5.33	26.79	73.2
1% DPP	0.95	9.87	90.1
	2.67	20.37	79.6
	3.50	24.30	75.7
	5.33	32.01	68.0
1% DPP*	1.50	36.83	63.2
1% **1**	0.0333 (120 s)	29.85	70.2
	0.0667 (240 s)	47.89	52.1
	0.100 (360 s)	59.25	40.8
	0.133 (480 s)	67.27	32.7
1% **2**	0.0306 (110 s)	62.00	38.0
	0.0417 (151 s)	68.62	31.4

Continued Table S3.

	0.0500 (180 s)	72.94	27.1
	0.0633 (228 s)	77.67	22.3
	0.0778 (280 s)	81.16	18.8
0.1% **2**	0.20 (12 min)	58.82	41.2
	0.28 (17 min)	63.90	36.1
	0.35 (21 min)	67.26	32.7
	0.55 (33 min)	74.89	25.1
	0.82 (49 min)	81.21	18.8
$[cyclopentadiene]_0 = [acrylonitrile]_0 = 100$ mM in $CDCl_3$			
no catalyst	5.0	4.61	95.4
	24.0	15.62	84.4
	48.8	25.49	74.5
	72.0	33.96	66.0
	77.5	35.88	64.1
1% DPP	5.0	4.16	95.8
	23.0	15.86	84.1
	47.8	26.15	73.9
	71.0	34.76	65.2
	76.5	36.89	63.1
1% **1**	2.0	7.11	92.9
	19.0	24.02	76.0
	26.0	28.13	71.9
	44.0	36.68	63.3
1% **2**	1.0	8.66	91.3
	3.0	14.27	85.7
	6.5	23.17	76.8
	24.3	44.72	55.3
5% **2**	0.38 (23 min)	5.94	94.1
	0.58 (35 min)	10.15	89.9
	0.92 (55 min)	13.11	86.9
	1.50 (90 min)	19.78	80.2
$[cyclopentadiene]_0 = [methyl\ vinyl\ ketone]_0 = 10.0$ mM in $CDCl_3$			
no catalyst	3.50	4.02	96.0
	22.50	9.53	90.5
	27.00	10.64	89.4
	44.00	14.38	85.6

Continued Table S3.

1% DPP	5.33	2.79	97.2
	24.00	8.48	91.5
	28.75	9.77	90.2
	45.50	14.67	85.3
1% **2**	0.100 (360 s)	14.90	85.1
	0.200 (720 s)	25.05	75.0
	0.300 (1080 s)	32.97	67.0
	0.450 (1620 s)	40.10	59.9

Table S4. Kinetic data of polymerizations.

[δ-valerolactone]$_0$ = 0.50 M, [monomer]$_0$: [initiator]$_0$: [cat.]$_0$ = 100 : 1.0 : 0.50			
solvent, catalyst	time (h)	conversion (%)	$M_{n,\,NMR}$ (Da)
toluene-d_8, DPP	0.5	20.83	3096
	1.0	39.83	6352
	2.0	64.48	10120
	3.0	78.36	13124
	4.0	85.51	-
	5.0	88.71	-
benzene-d_6, DPP	0.5	16.92	2295
	1.0	30.70	4393
	2.0	51.52	7776
	3.0	65.61	10220
	4.0	74.72	-
	5.0	80.36	-
CD_2Cl_2, DPP	0.5	3.55	909
	1.0	5.47	1162
	2.0	8.85	1483
	3.0	12.58	2167
	4.0	16.21	2588
	5.0	18.33	2824
$CDCl_3$, DPP	0.5	2.95	903
	1.0	6.47	1237
	2.0	11.11	1888
	3.0	14.78	2295

Continued Table S4.

	4.0	18.15	2852
	5.0	22.14	3335
	6.0	25.36	-
	7.0	28.64	-
toluene-d_8, **2**	0.100	13.12	2079
	0.250	24.36	3912
	0.383	34.40	5915
	0.567	45.18	7266
	0.717	52.82	9095
	0.883	59.42	10019
	1.02	64.27	-
	2.33	86.49	-
benzene-d_6, **2**	0.150	12.99	3212
	0.283	22.85	4212
	0.433	30.88	5414
	0.600	39.20	6519
	0.767	44.87	6928
	0.933	50.95	7717
	1.05	54.39	8218
	2.33	75.62	-
CD_2Cl_2, **2**	0.5	7.75	1352
	1.0	11.33	1726
	2.0	19.71	2828
	3.0	25.92	3640
	4.0	30.18	4257
	5.0	34.09	4723
$CDCl_3$, **2**	0.5	9.49	1411
	1.0	14.61	2210
	2.0	26.74	3511
	3.0	36.41	4413
	4.0	42.57	4988
	5.0	47.21	-
	6.0	49.84	-
	7.0	52.62	-

Continued Table S4.

solvent = CD_2Cl_2, $[monomer]_0 : [initiator]_0 : [cat.]_0 = 100 : 1.0 : 1.0$			
$[monomer]_0$ (M)	catalyst	time (h)	conversion (%)
1.0	DPP	0.5	20.37
		1.0	35.21
		1.5	46.50
		2.0	52.79
	2	0.5	28.51
		1.0	44.70
		1.5	52.98
		2.0	58.33
0.50	DPP	1.0	12.66
		2.0	25.80
		3.0	32.15
		4.0	37.39
	2	1.0	20.28
		2.0	35.09
		3.0	43.47
		4.0	48.81
0.25	DPP	1.0	3.70
		2.0	5.33
		3.0	6.19
		4.0	6.95
	2	1.0	6.76
		2.0	9.05
		3.0	11.11
		4.0	12.56

Figure S1. Observed rate constants versus catalyst mol % loadings for the Friedel-Crafts reactions of *β*-nitrostyrene with indole (top) and *N*-methylindole (bottom).

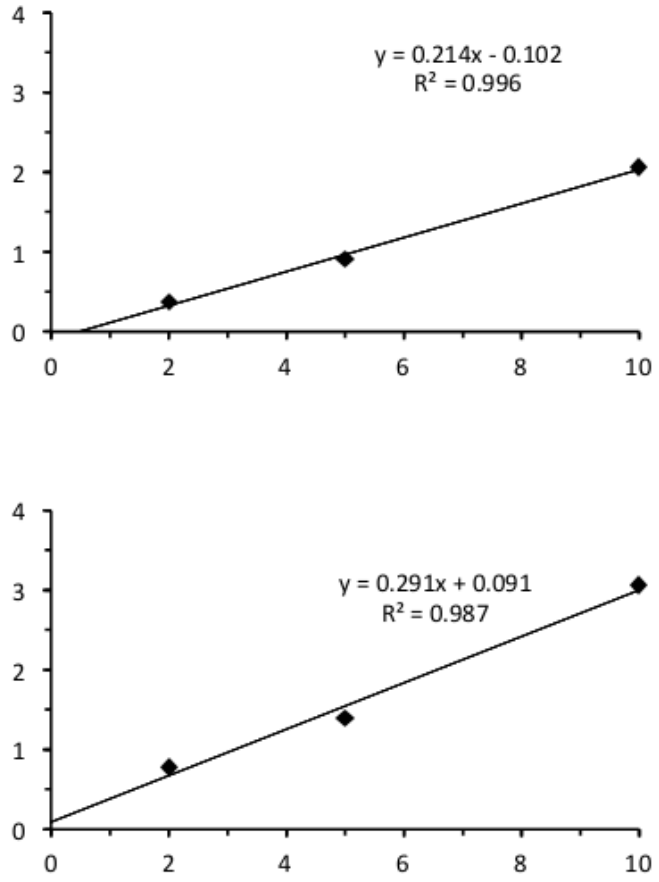

Figure S2. Number-average molecular weight ($M_{n,NMR}$) versus conversion plots in toluene-d_8 (a), benzene-d_6 (b), CD_2Cl_2 (c) and $CDCl_3$ (d).

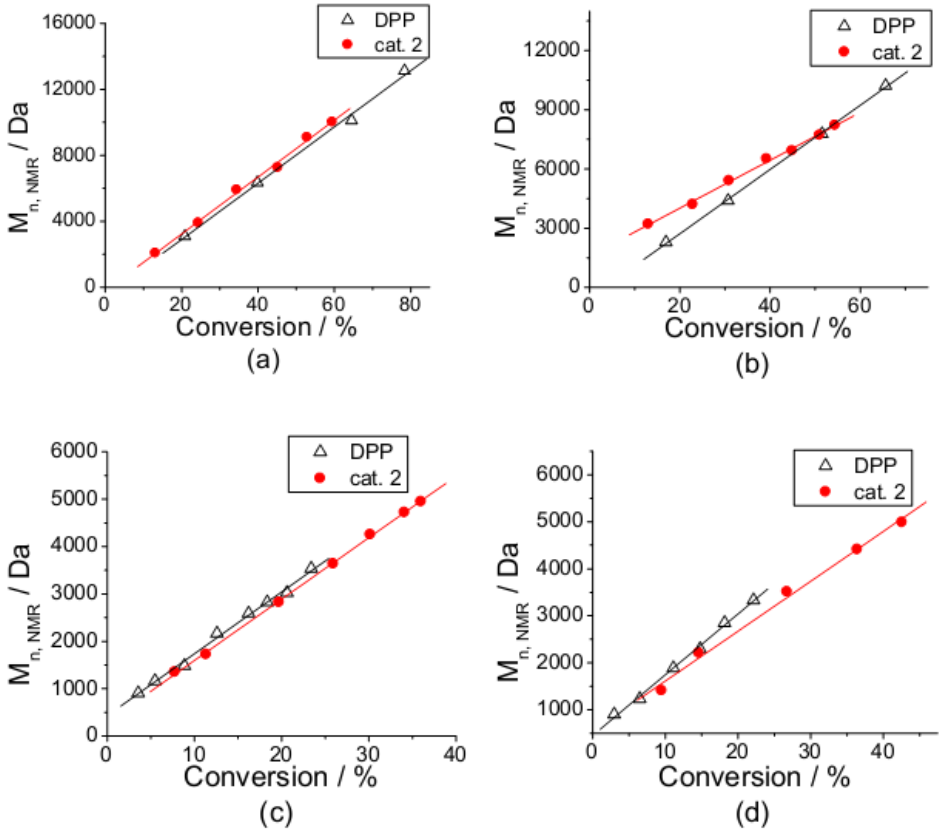

Figure S3. ^{1}H and ^{13}C NMR spectra of **3**.

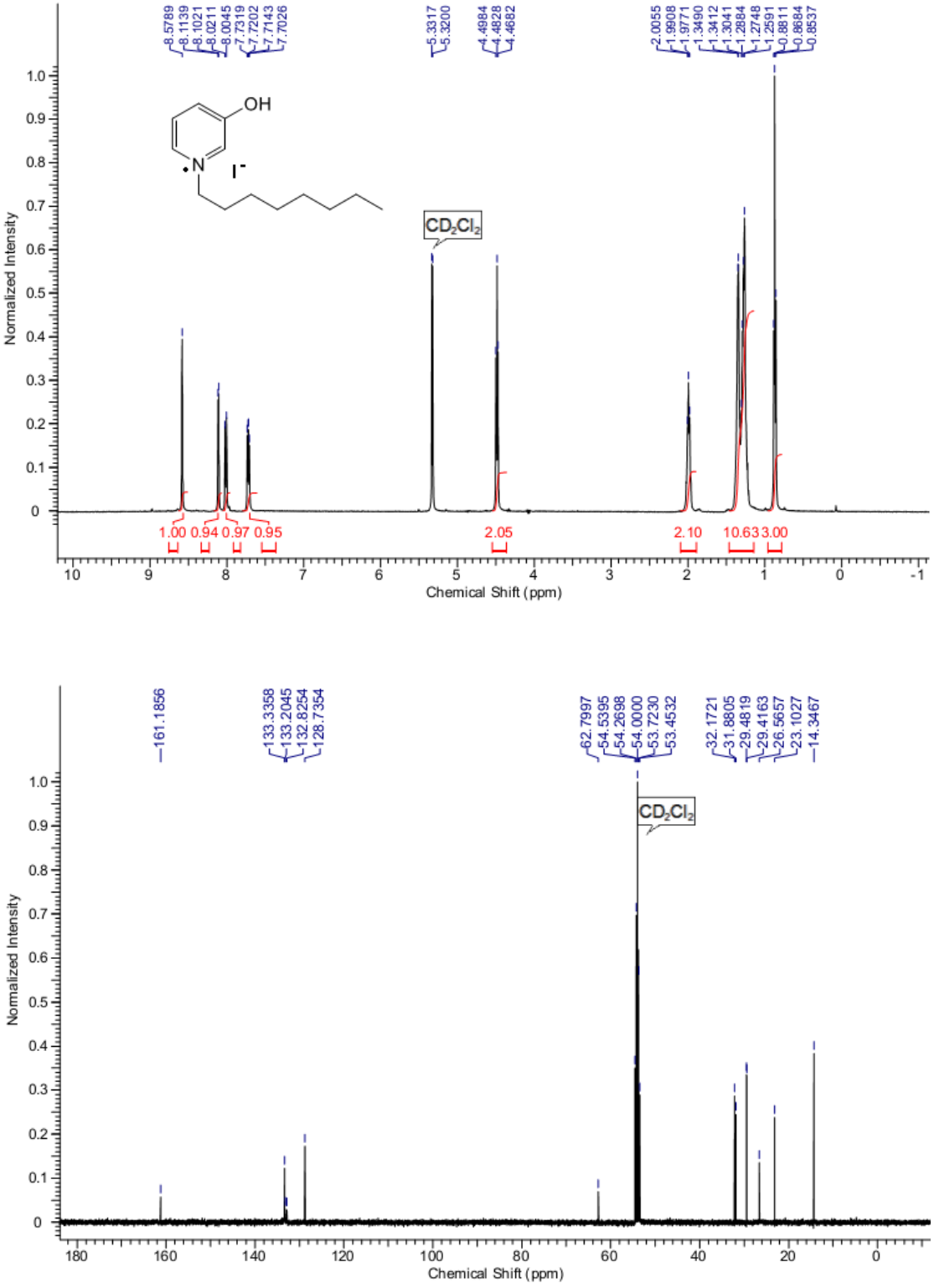

Figure S4. ^{1}H, ^{13}C and ^{31}P NMR spectra of **4**.

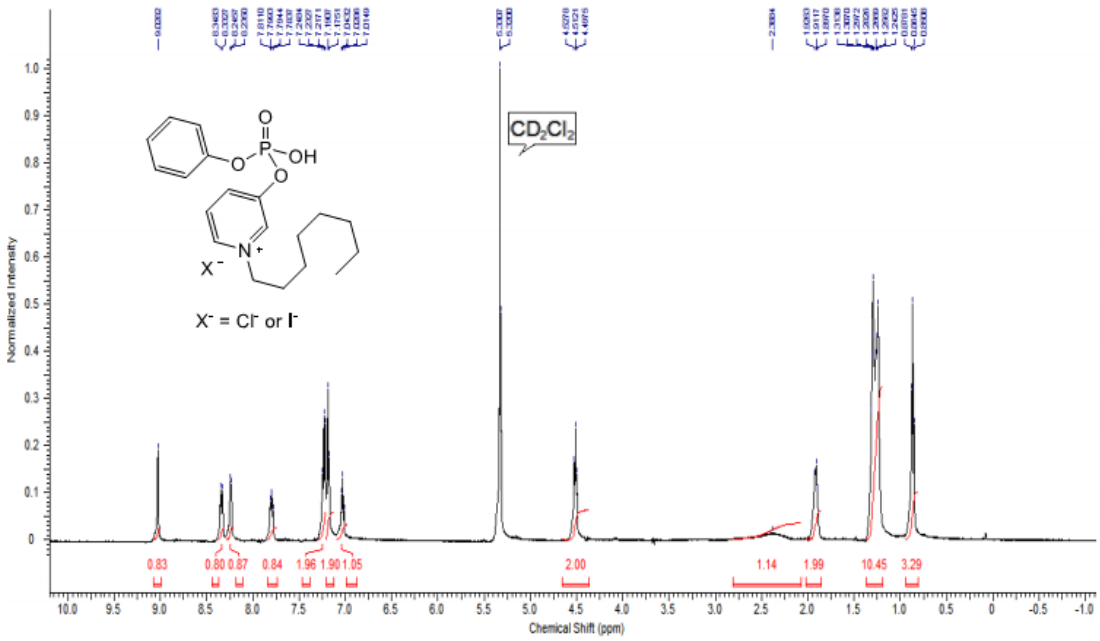

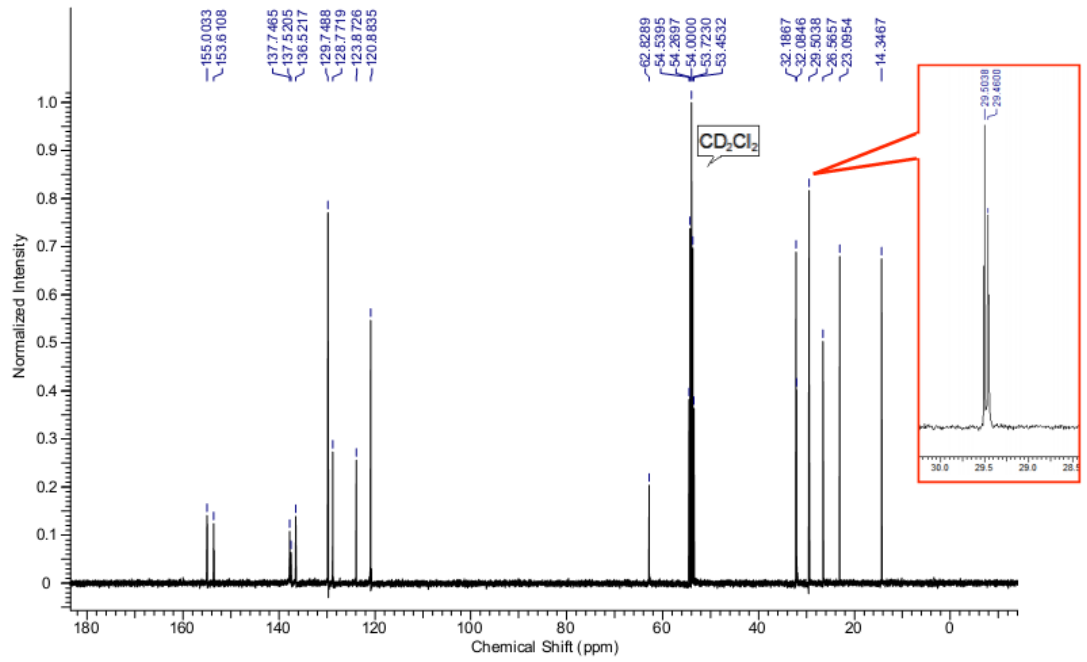

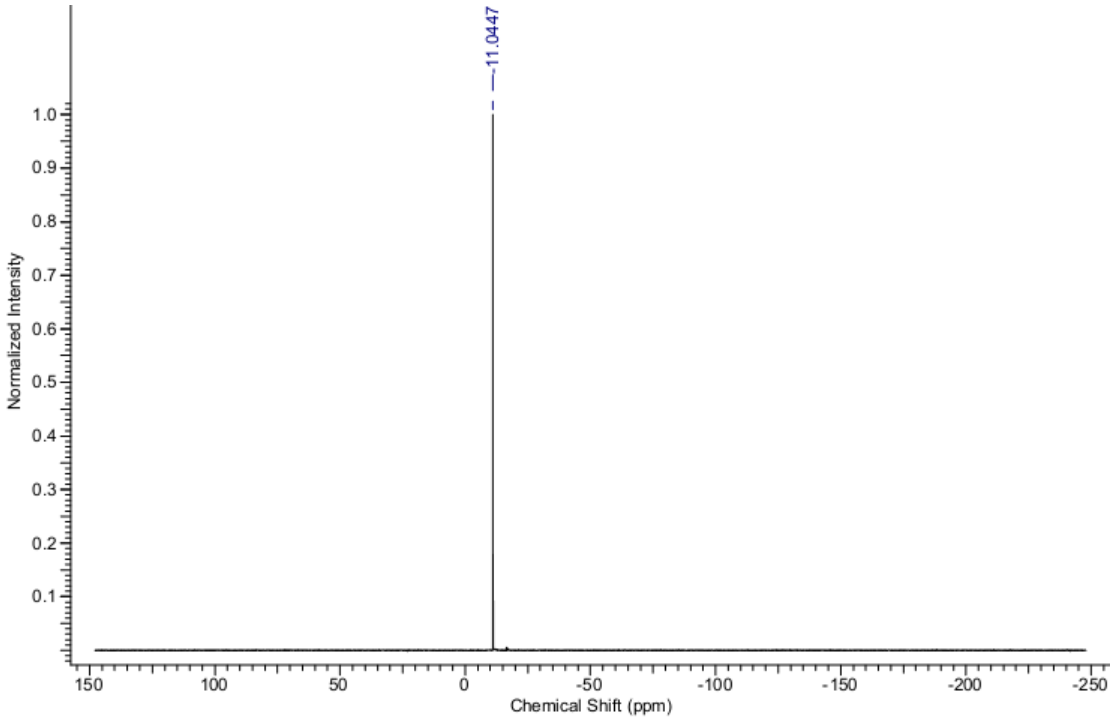

Figure S5. ^{1}H, ^{13}C, ^{19}F and ^{31}P NMR spectra of **1**.

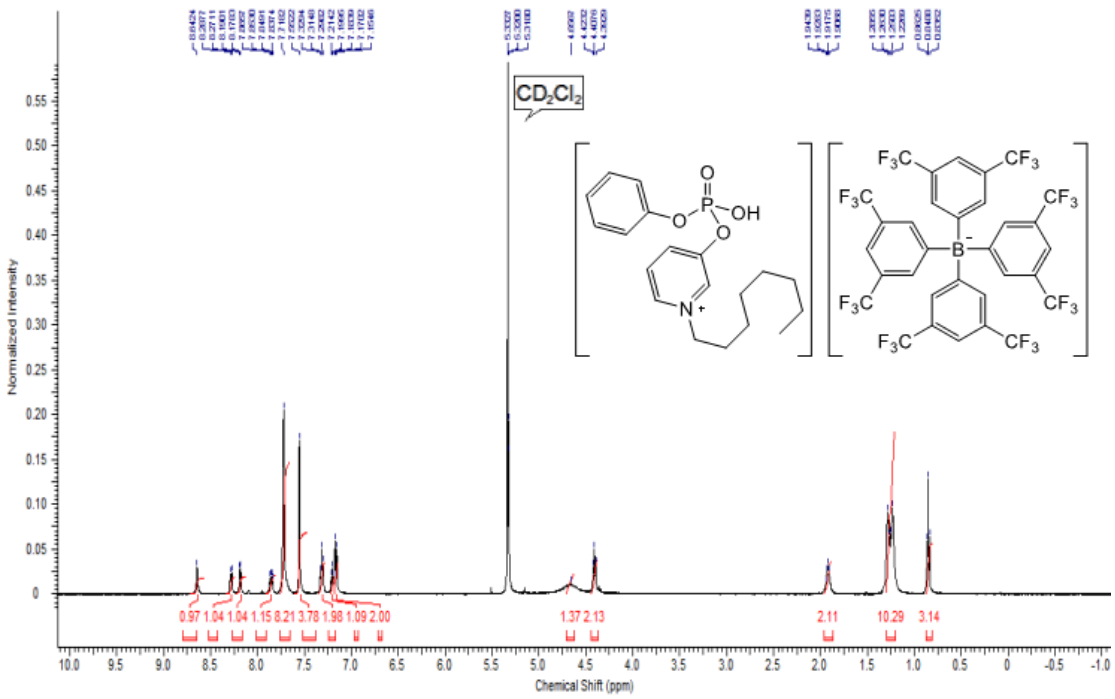

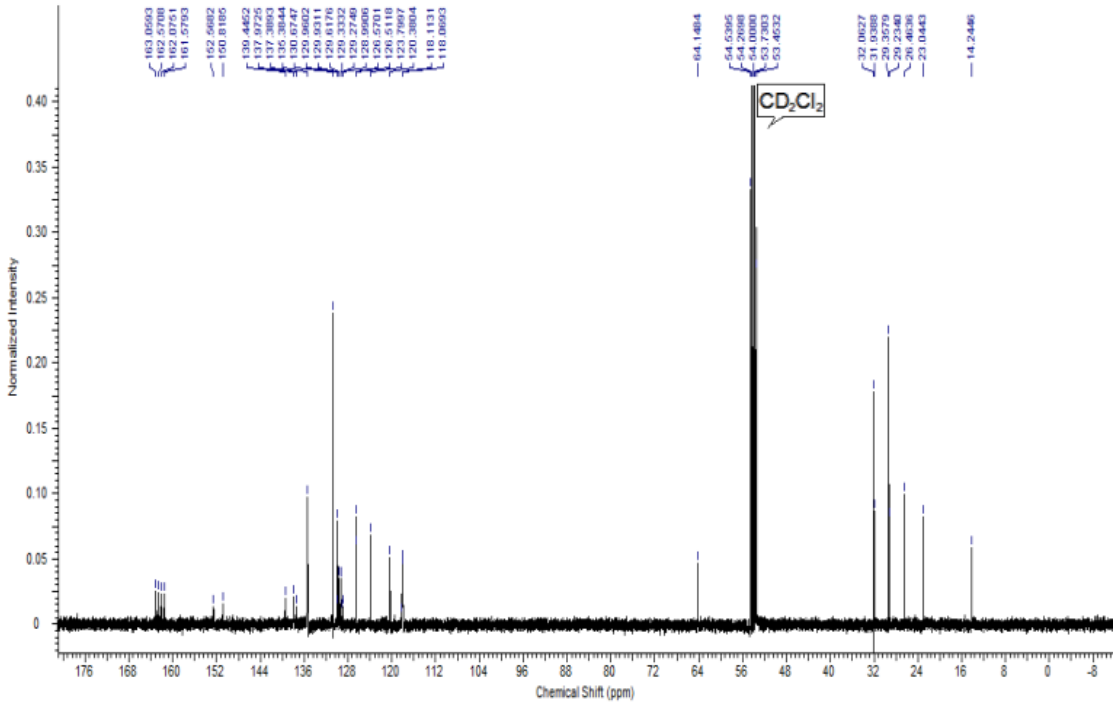
163.0993
162.5708
162.0751
161.5793
152.5682
150.8185
139.4452
137.9725
137.3893
135.3844
130.6747
129.9922
129.9311
129.6176
129.3332
129.2749
128.9906
126.5701
126.5118
123.7997
120.3864
118.1131
118.0693
64.1484
54.5395
54.2698
54.0000
53.7303
53.4632
32.0627
31.9388
29.3579
29.2340
26.4636
23.0443
14.2446
CD2Cl2
Normalized Intensity
Chemical Shift (ppm)

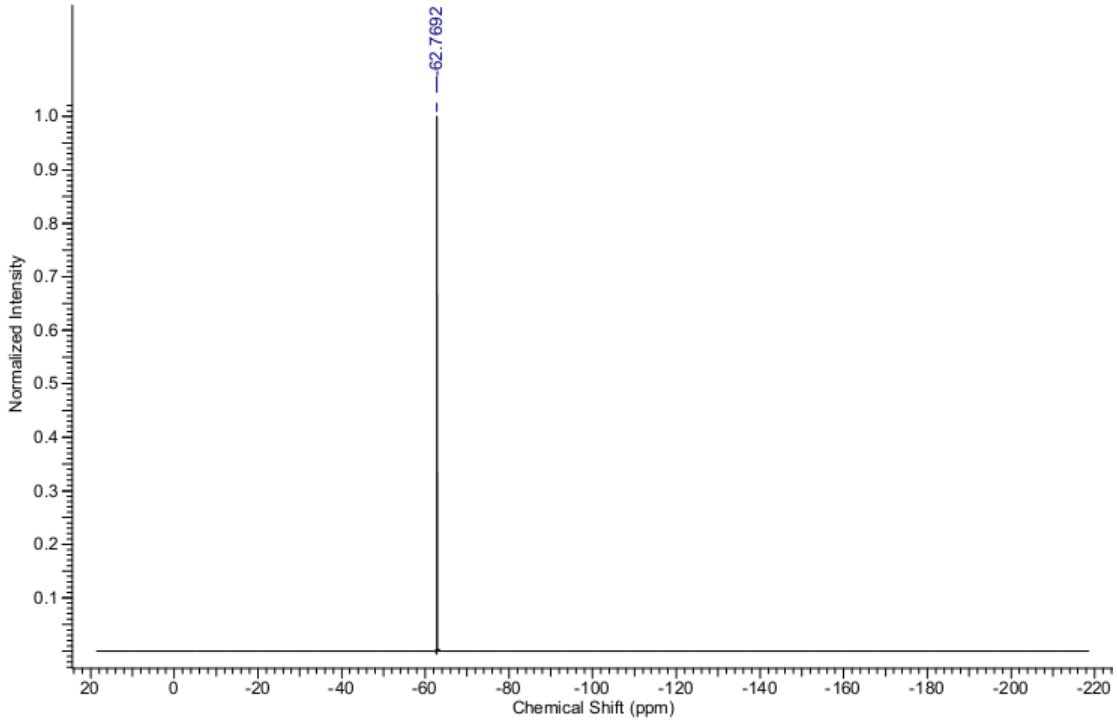
62.7692
Normalized Intensity
Chemical Shift (ppm)

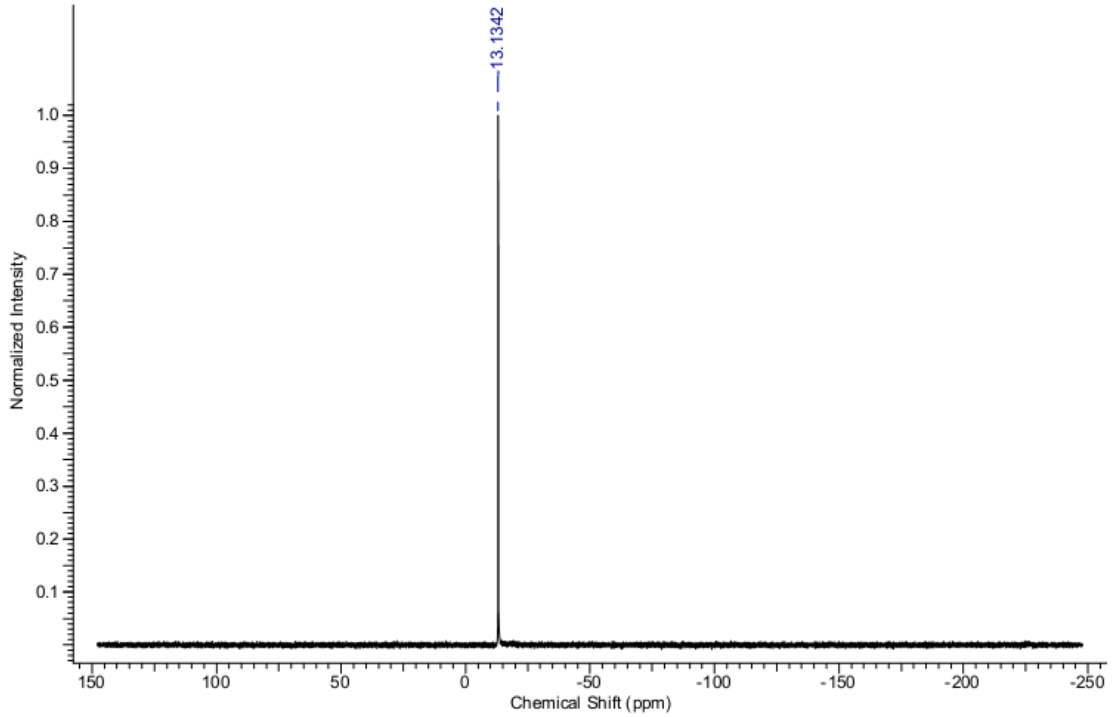

Figure S6. ^{1}H, ^{13}C and ^{31}P NMR spectra of **5**.

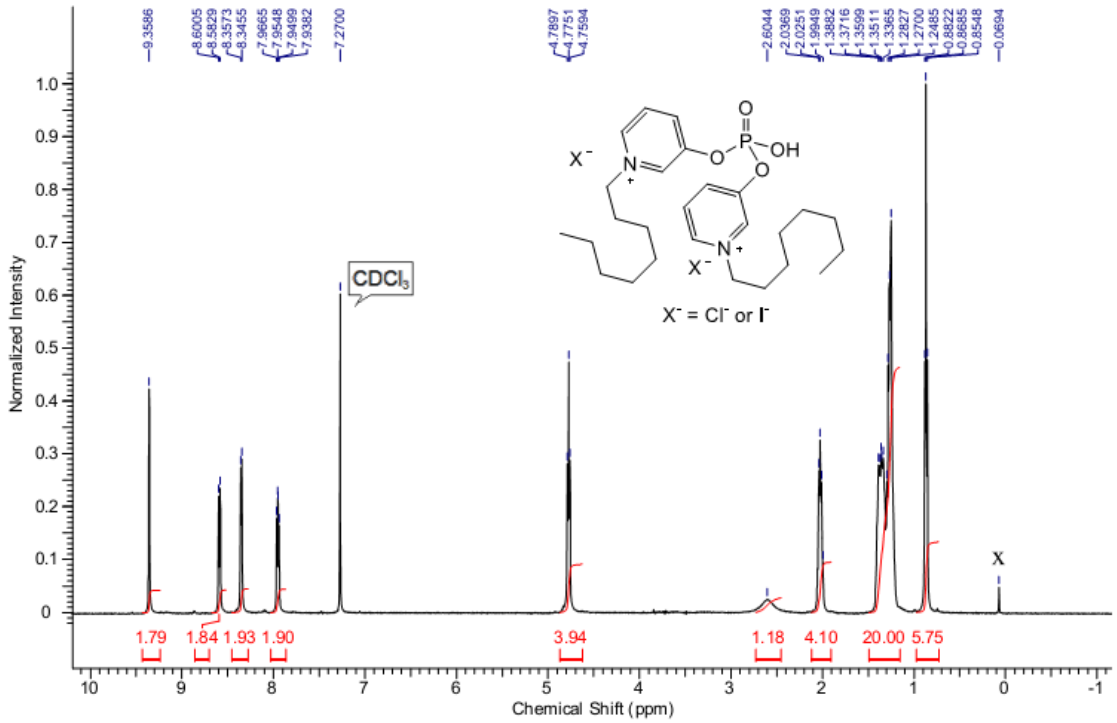

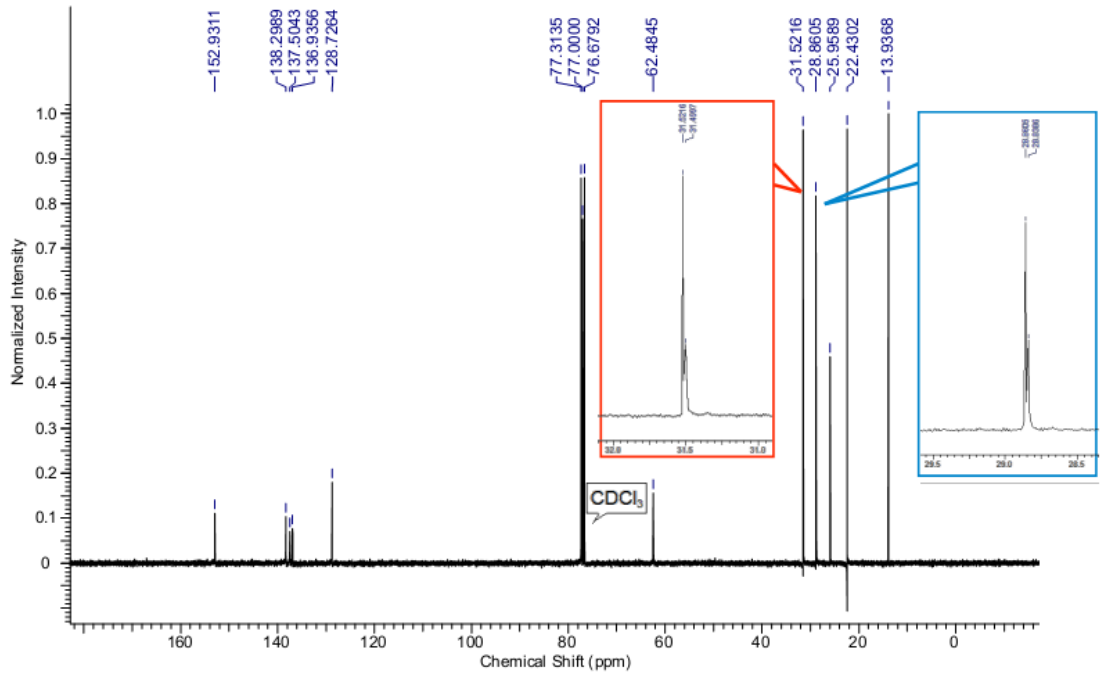
152.9311
138.2989
137.5043
136.9356
128.7264
77.3135
77.0000
76.6792
62.4845
31.5216
28.8605
25.9589
22.4302
13.9368
CDCl3
Normalized Intensity
Chemical Shift (ppm)

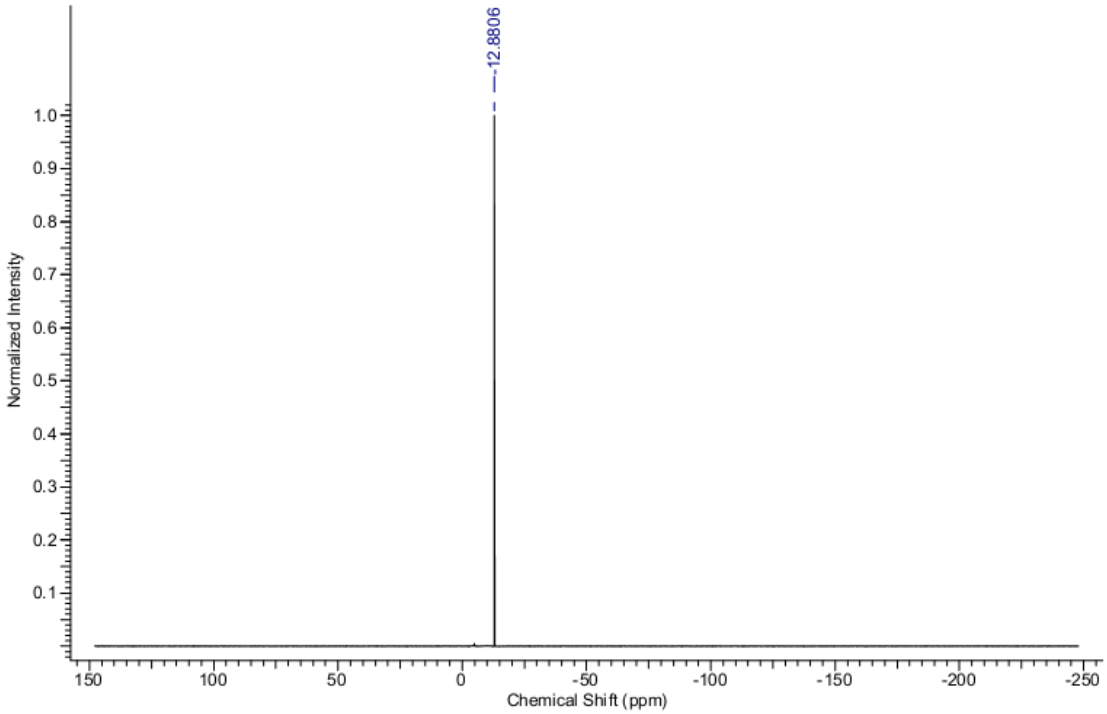
12.8806
Normalized Intensity
Chemical Shift (ppm)

Figure S7. ^{1}H, ^{13}C, ^{19}F and ^{31}P NMR spectra of **2**.

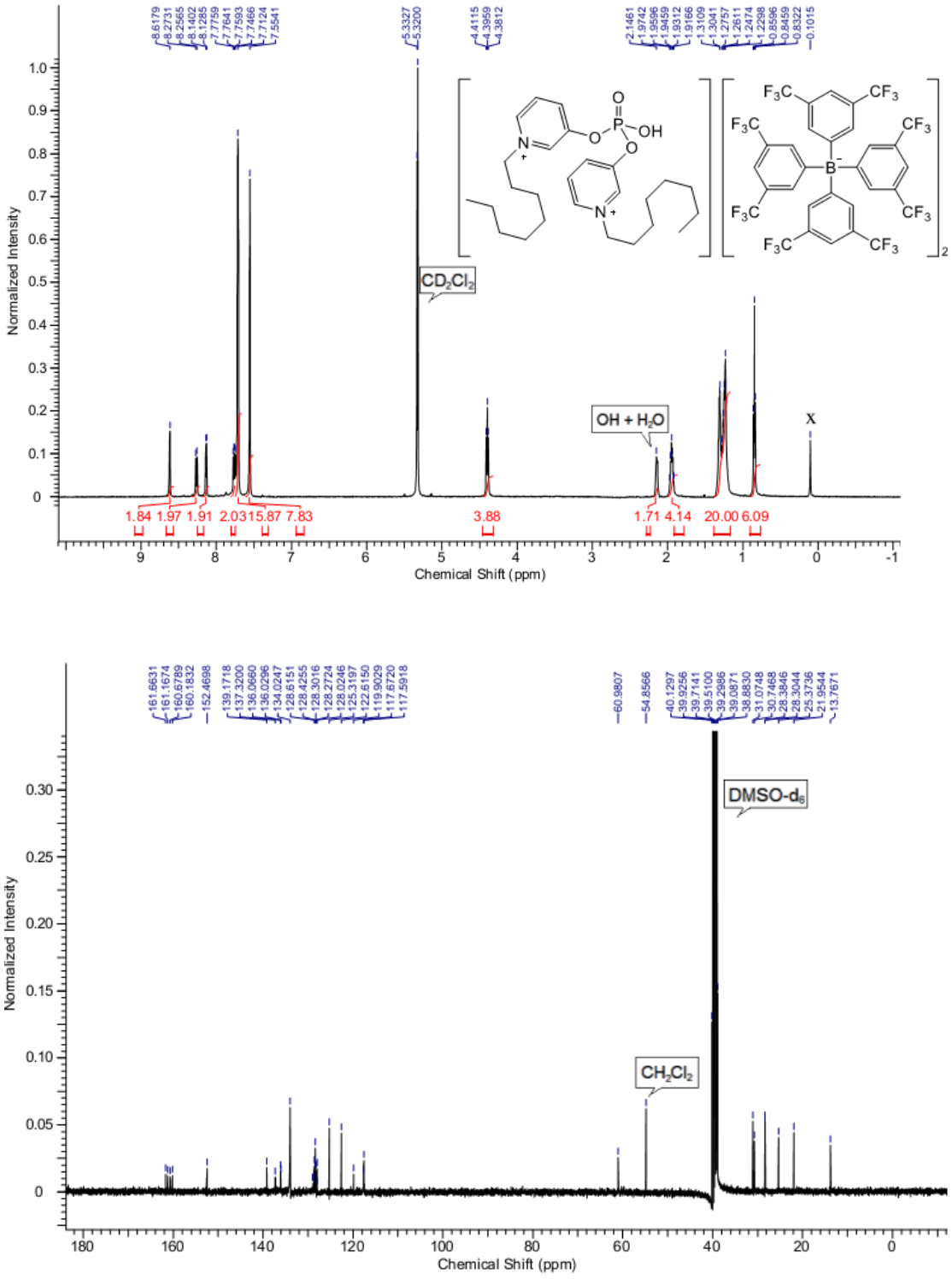

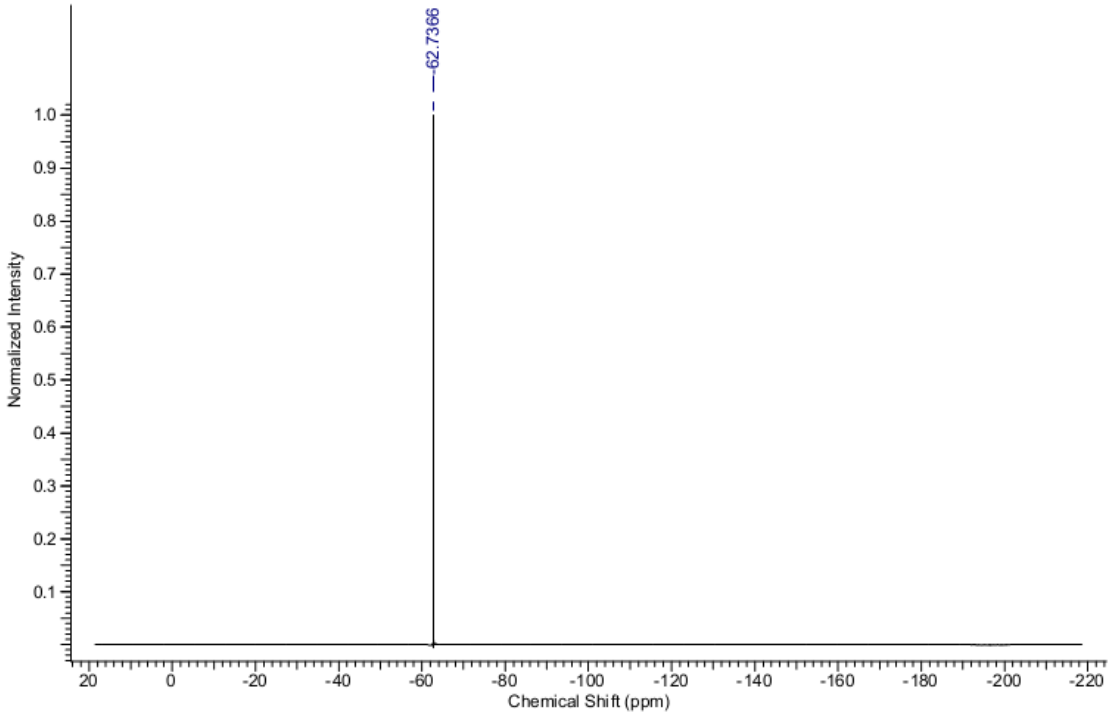
62.7366
Normalized Intensity
1.0
0.9
0.8
0.7
0.6
0.5
0.4
0.3
0.2
0.1
20
0
-20
-40
-60
-80
-100
-120
-140
-160
-180
-200
-220
Chemical Shift (ppm)

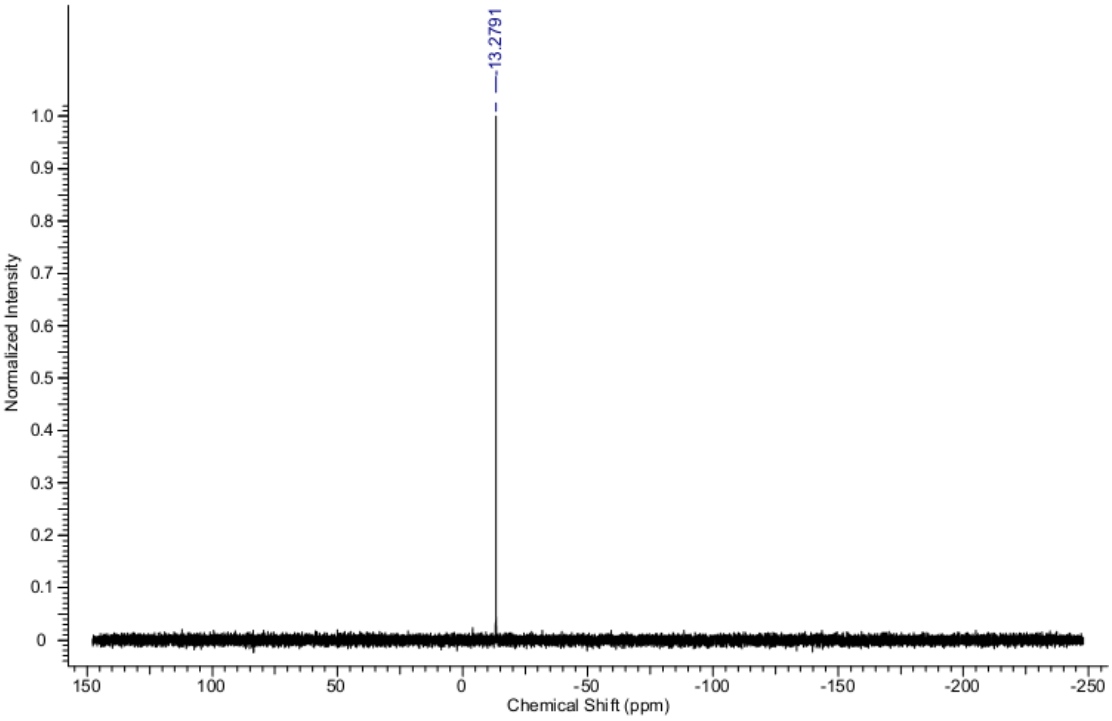
13.2791
Normalized Intensity
1.0
0.9
0.8
0.7
0.6
0.5
0.4
0.3
0.2
0.1
0
150
100
50
0
-50
-100
-150
-200
-250
Chemical Shift (ppm)

Figure S8. ^{1}H, ^{13}C and ^{31}P NMR spectra of di(3-nitrophenyl)phosphate (DPP*).

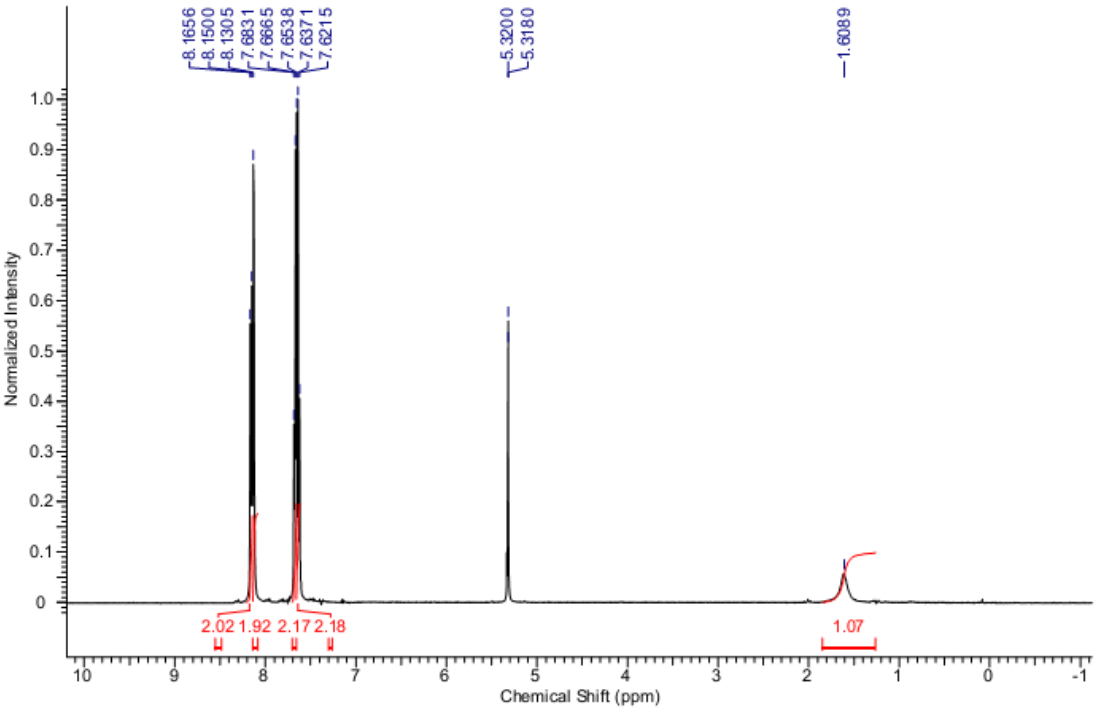

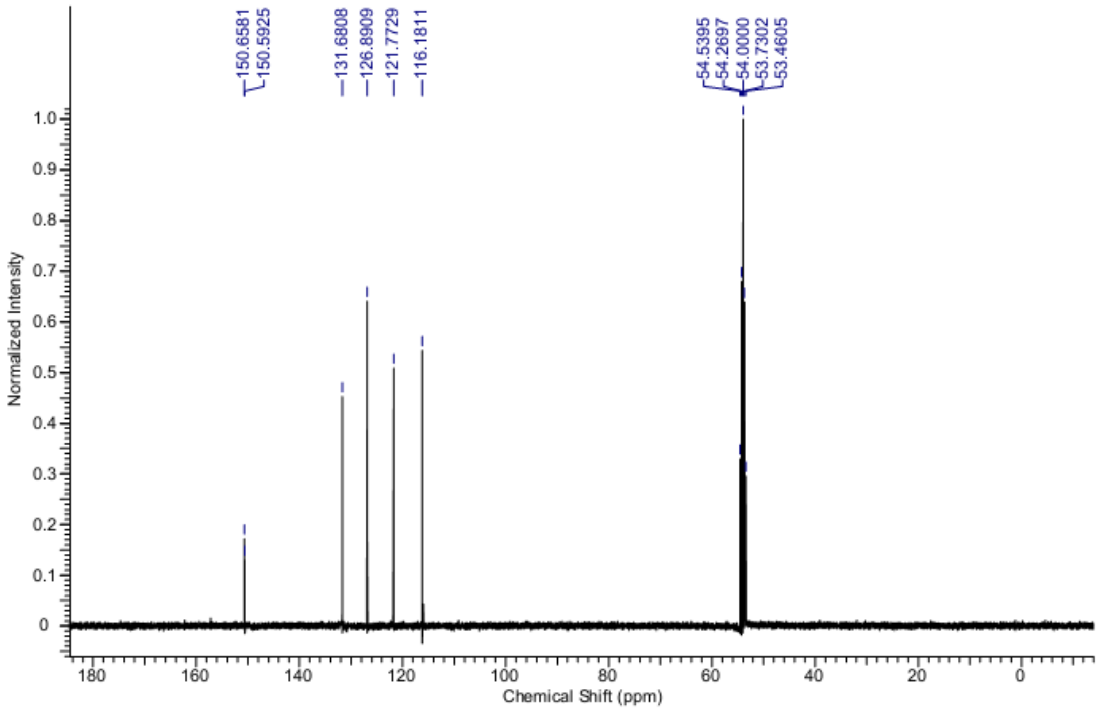

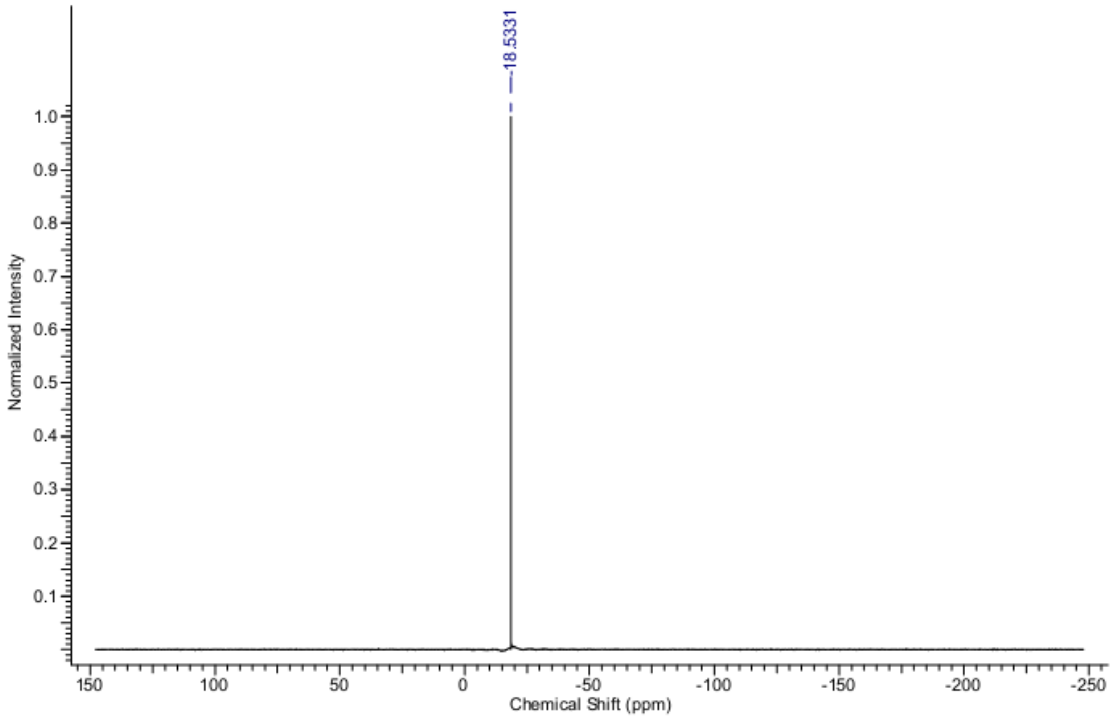
18.5331
Normalized Intensity
1.0
0.9
0.8
0.7
0.6
0.5
0.4
0.3
0.2
0.1
150
100
50
0
-50
-100
-150
-200
-250
Chemical Shift (ppm)

Appendix for Chapter 3

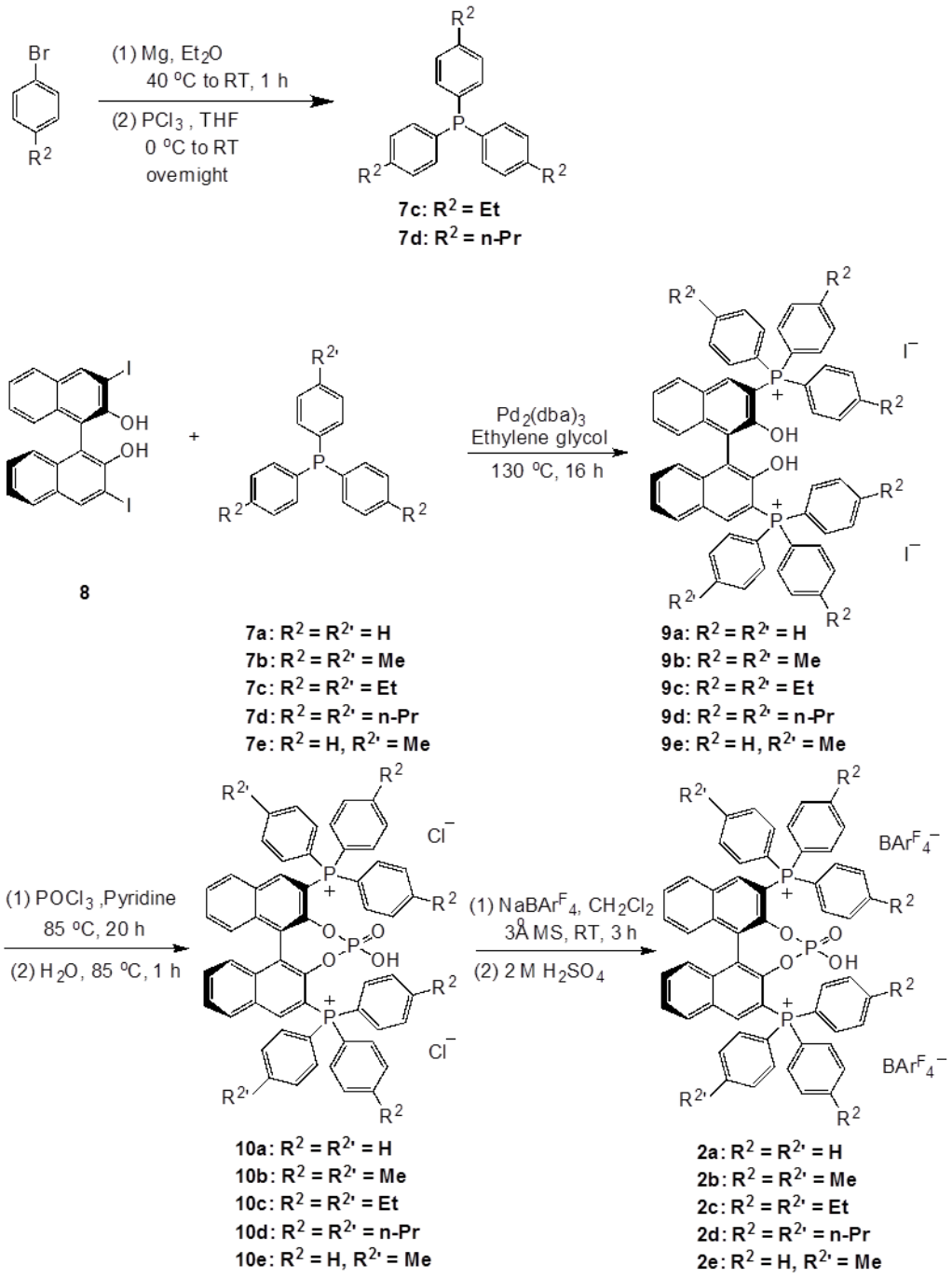

Scheme S1. Synthetic scheme of **2a-2e**.

I. NMR Spectra

Figure S1. ^{1}H, ^{13}C and ^{31}P NMR of tris(*p*-ethylphenyl)phosphine (**7c**).

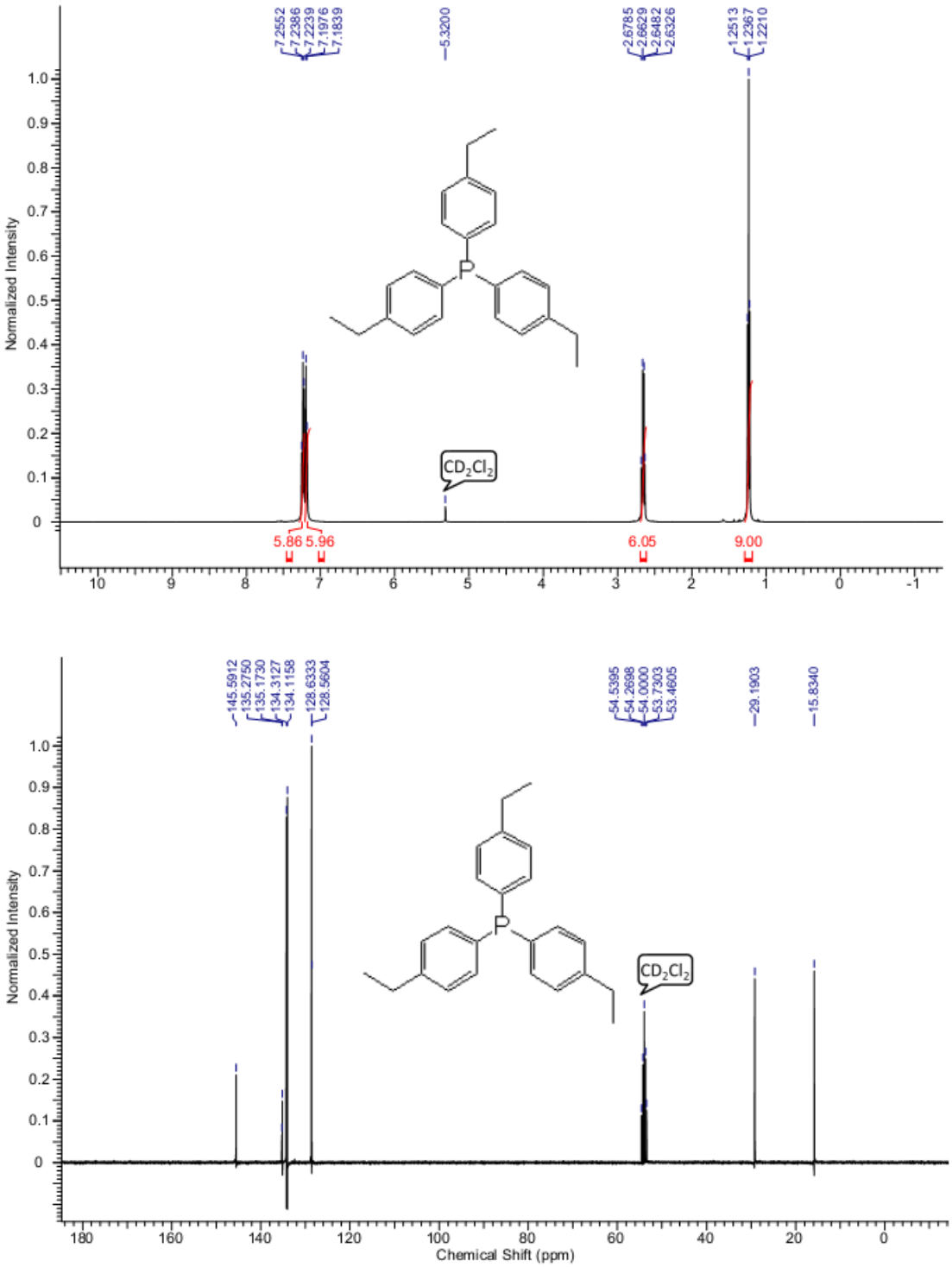

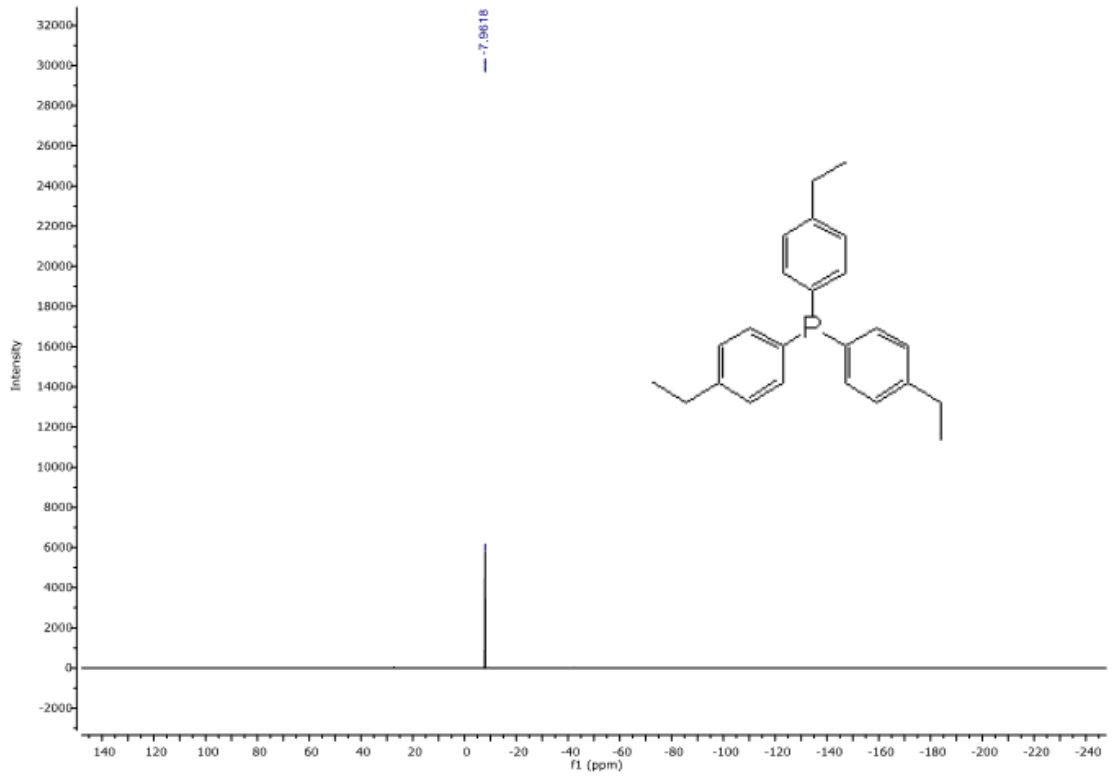

Figure S2. ^{1}H, ^{13}C and ^{31}P NMR of tris(*p*-n-propylphenyl)phosphine (**7d**).

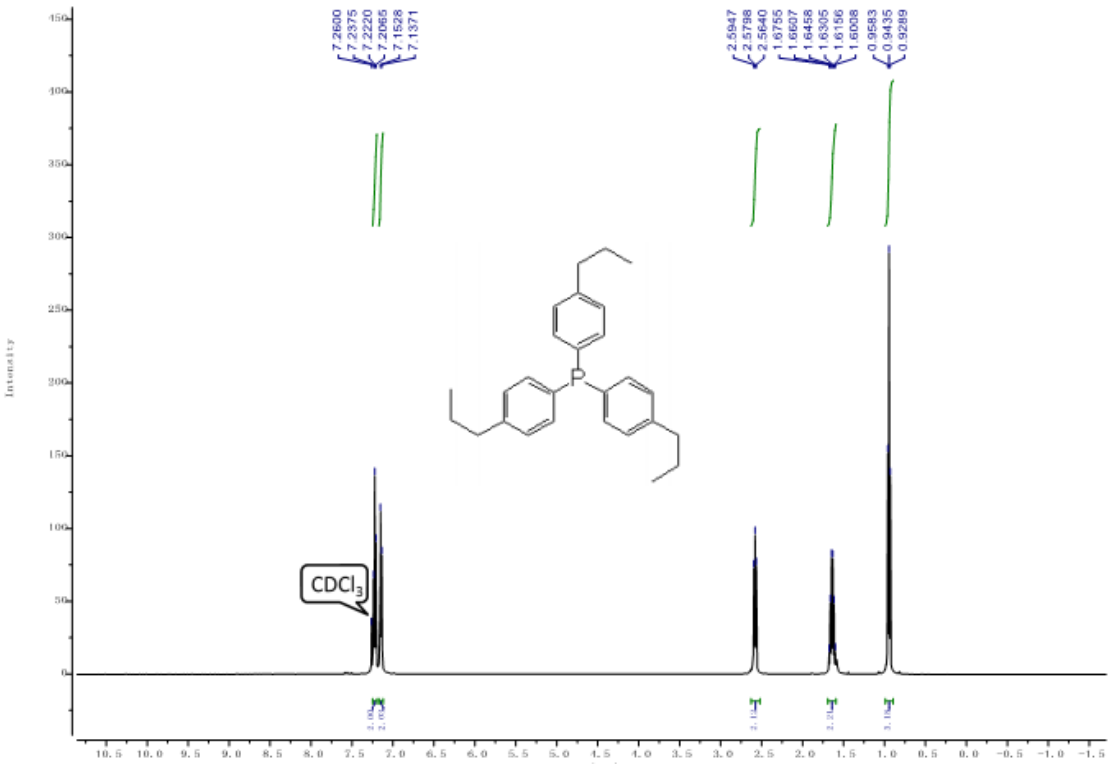

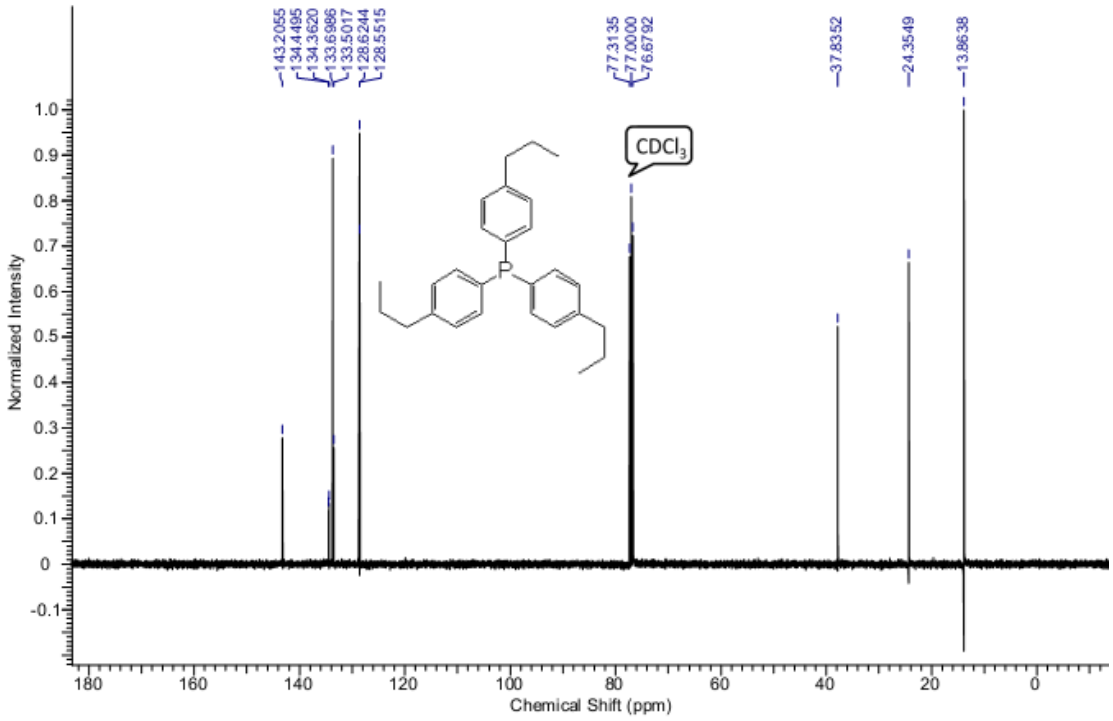
143.2055
134.4495
134.3620
133.6986
133.5017
128.6244
128.5515
77.3135
77.0000
76.6792
37.8352
24.3549
13.8638
CDCl3
Normalized Intensity
Chemical Shift (ppm)

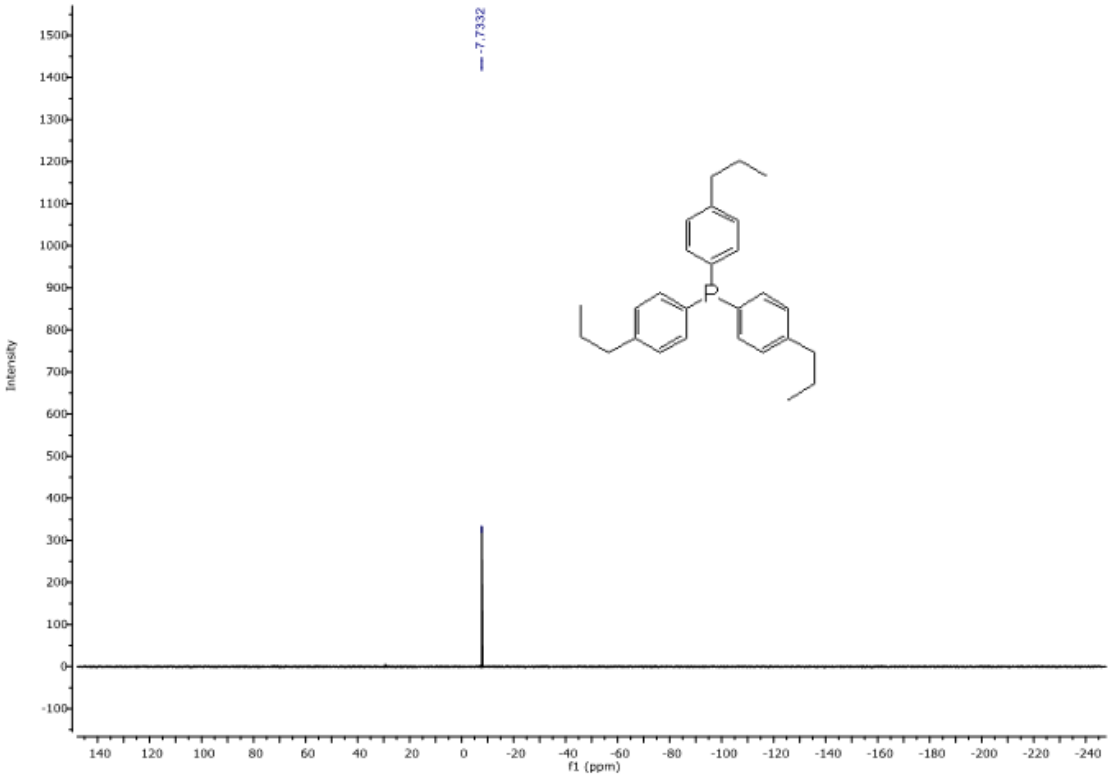
-7.7332
Intensity
f1 (ppm)

Figure S3. ^{1}H, ^{13}C and ^{31}P NMR of (*R*)-(2,2'-dihydroxy-[1,1'-binaphthalene]-3,3'-diyl)bis(triphenylphosphonium) iodide (**9a**).

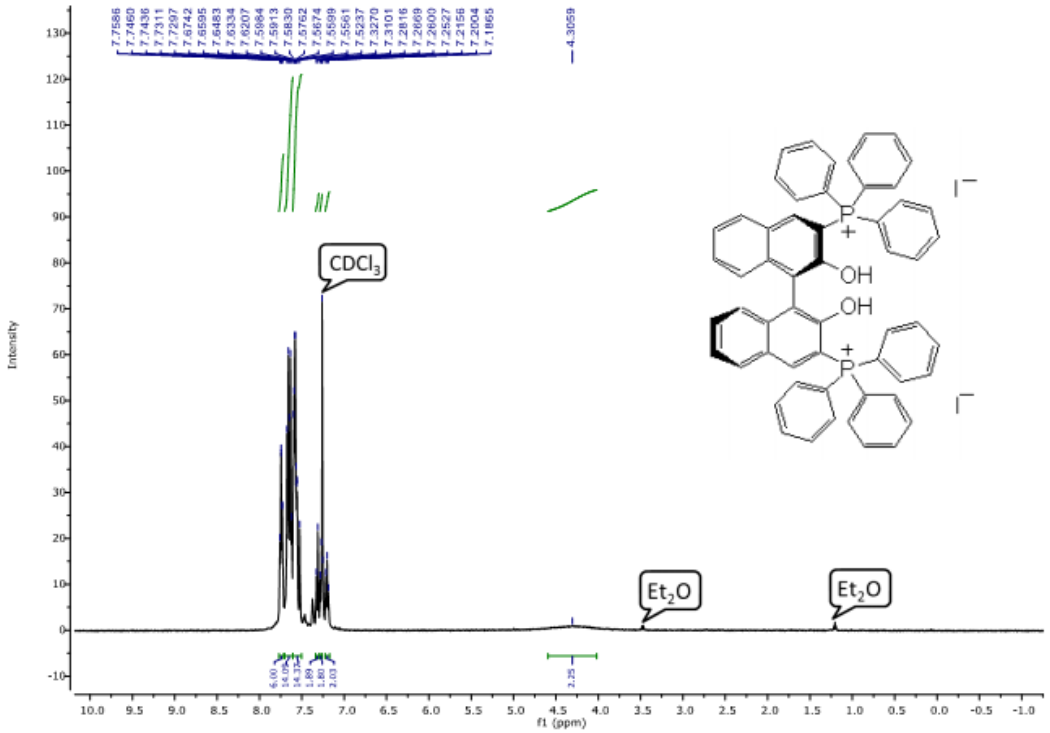

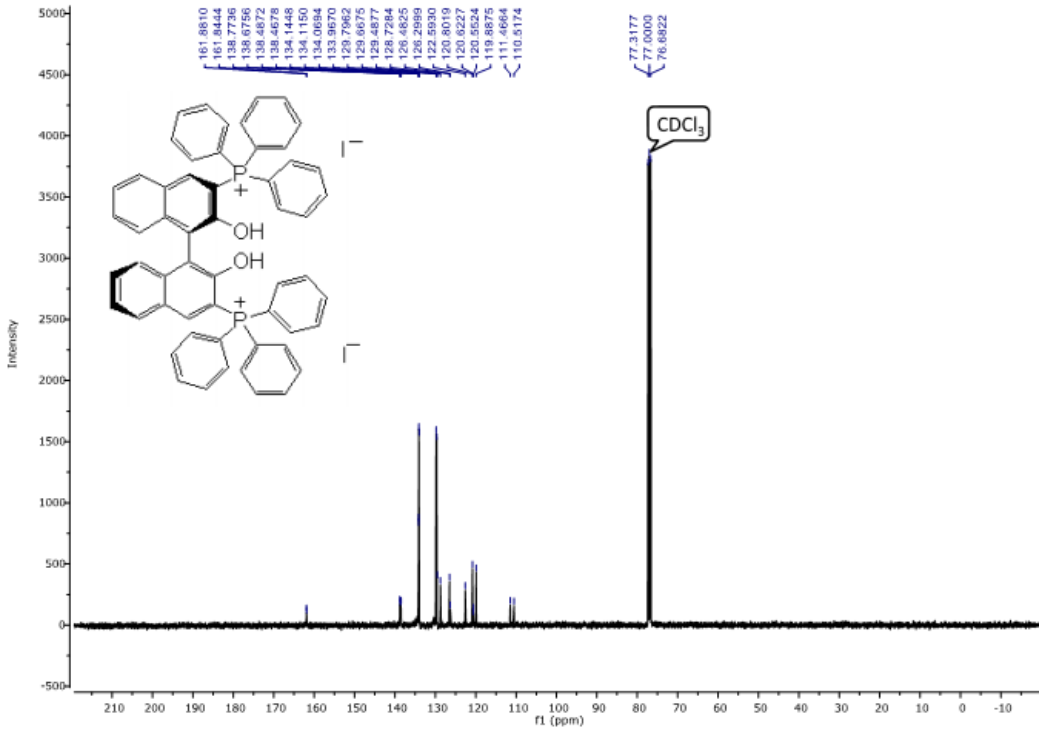

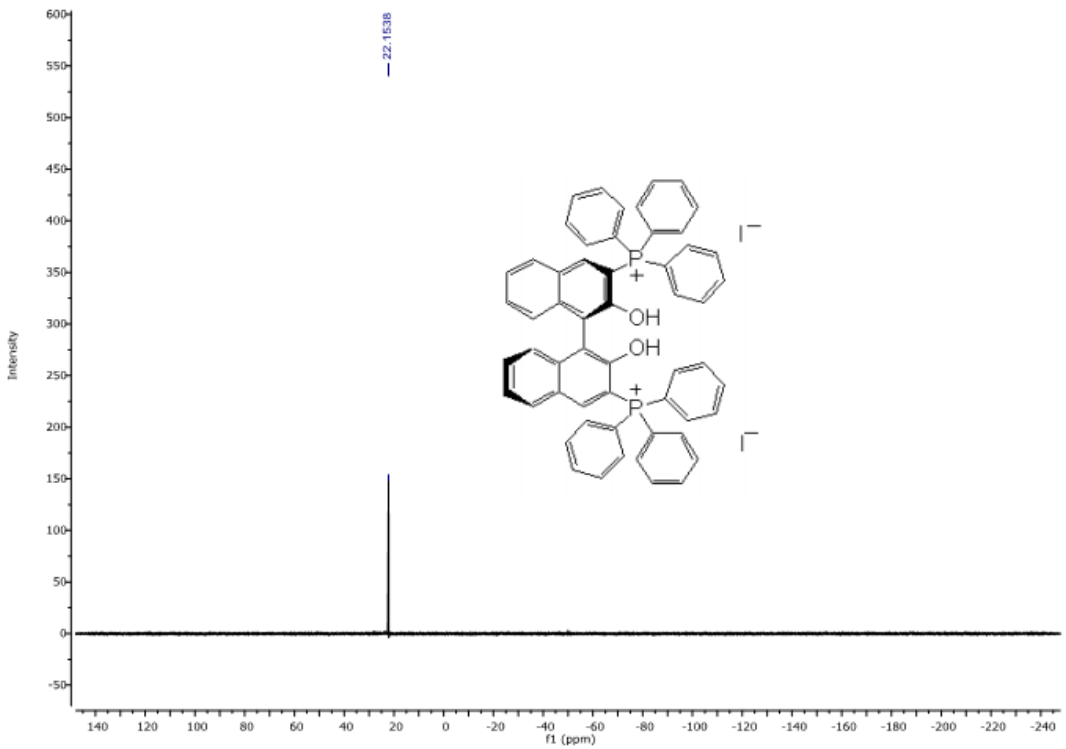

Figure S4. ^{1}H, ^{13}C and ^{31}P NMR of (*R*)-(2,2'-dihydroxy-[1,1'-binaphthalene]-3,3'-diyl)bis(tri-*p*-tolylphosphonium) iodide (**9b**).

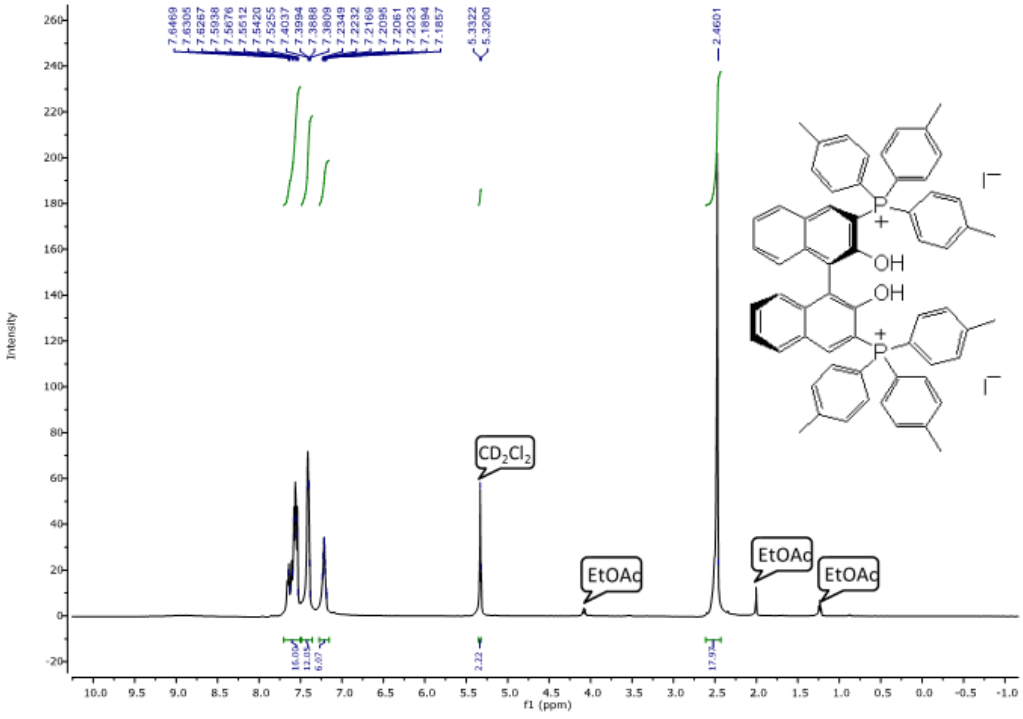

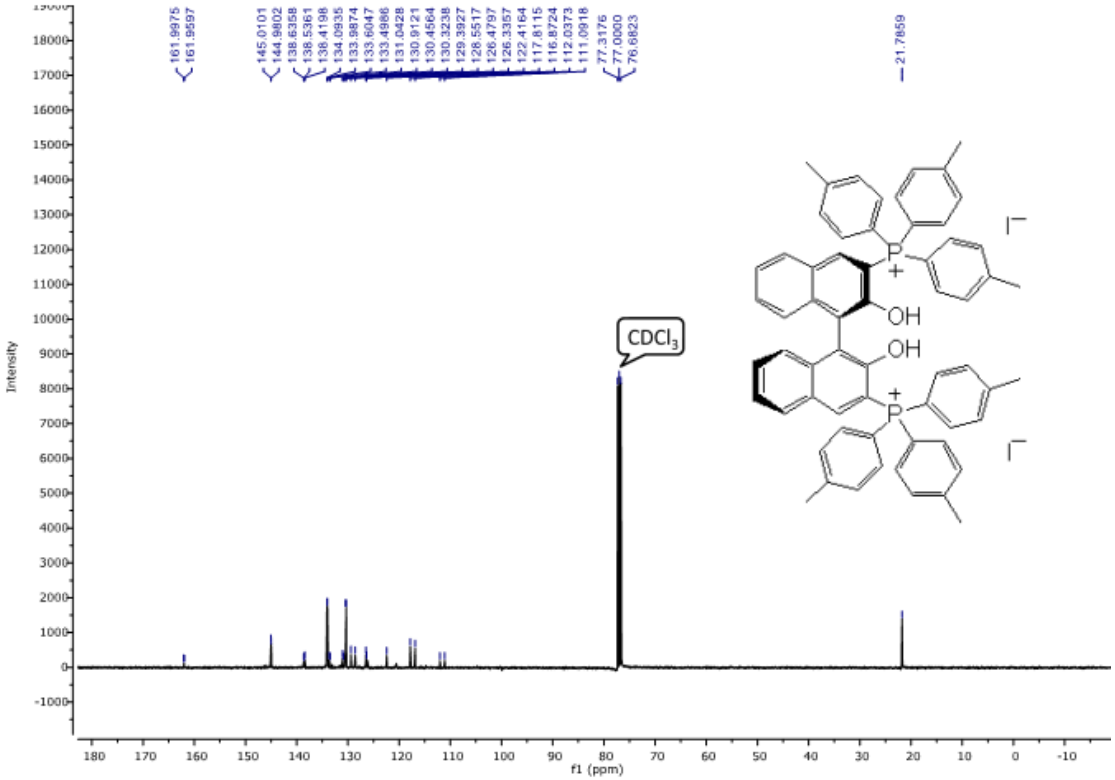
161.9975
161.9597
145.0101
144.9802
138.6358
138.5361
138.4198
134.0935
133.9874
133.6047
133.4986
131.0428
130.9121
130.4564
130.3238
129.3927
128.5517
126.4797
126.3357
122.4164
117.8115
116.8724
112.0373
111.0918
77.3176
77.0000
76.6823
21.7859
CDCl3
OH
OH
I⁻
I⁻
Intensity
f1 (ppm)

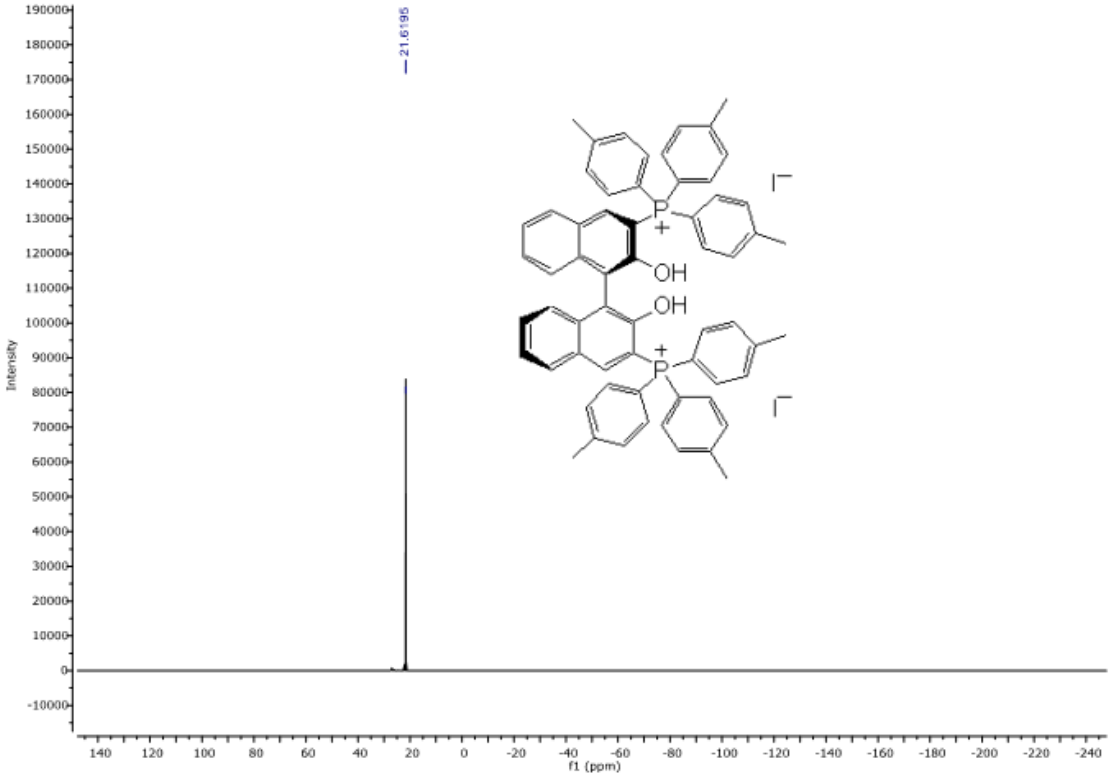
21.6196
OH
OH
I⁻
I⁻
Intensity
f1 (ppm)

Figure S5. ^{1}H, ^{13}C and ^{31}P NMR of (*R*)-(2,2'-dihydroxy-[1,1'-binaphthalene]-3,3'-diyl)bis(tris(4-ethylphenyl)phosphonium) iodide (**9c**).

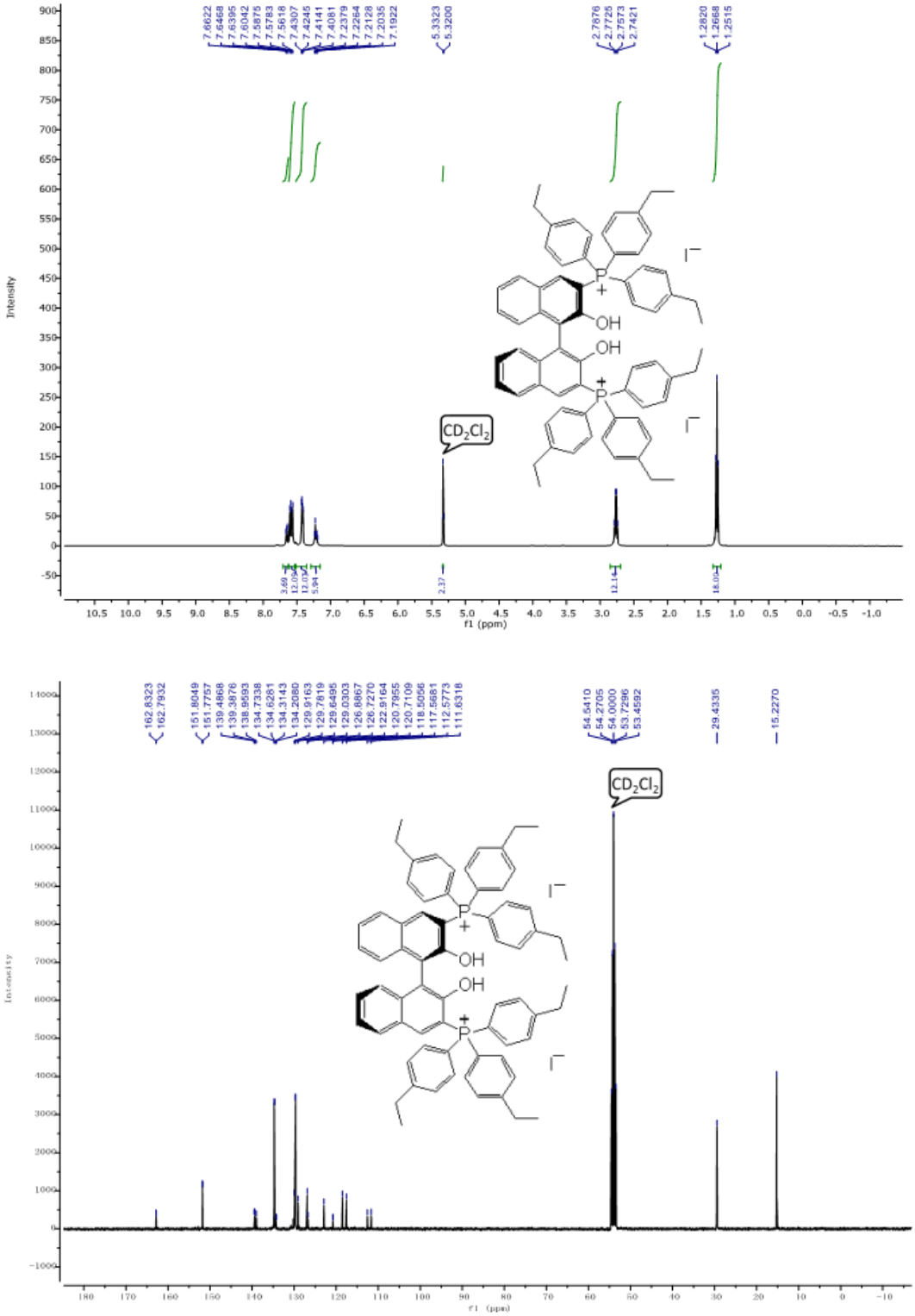

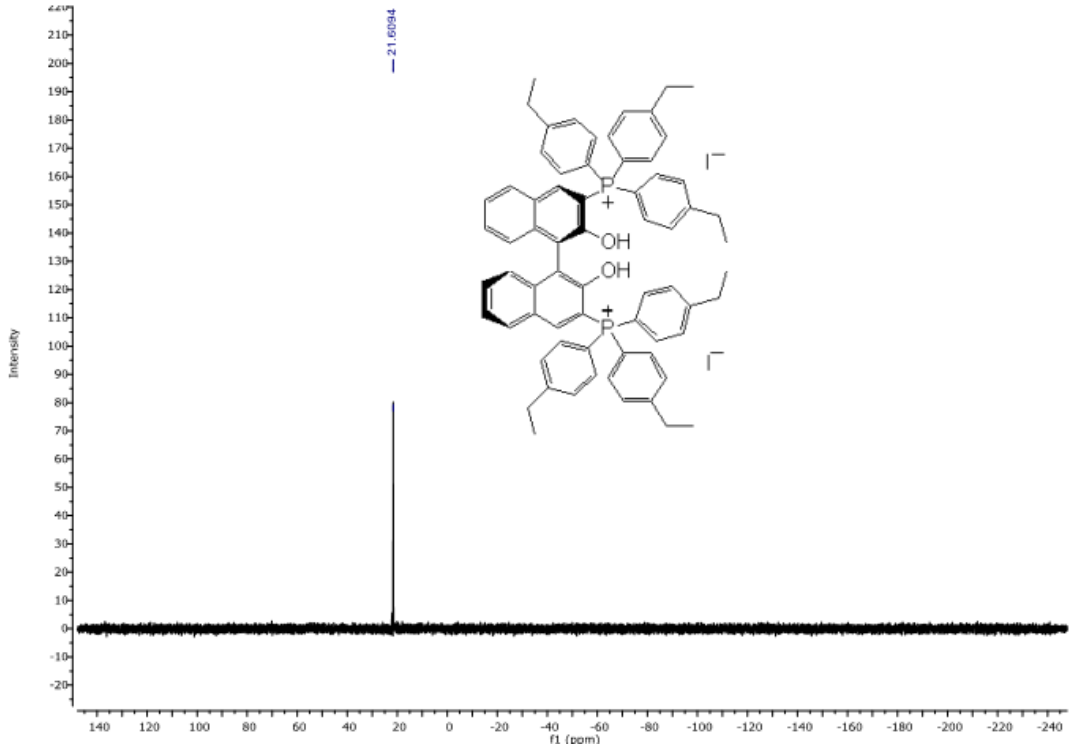

Figure S6. ^{1}H, ^{13}C and ^{31}P NMR of (*R*)-(2,2'-dihydroxy-[1,1'-binaphthalene]-3,3'-diyl)bis(tris(4-propylphenyl)phosphonium) iodide (**9d**).

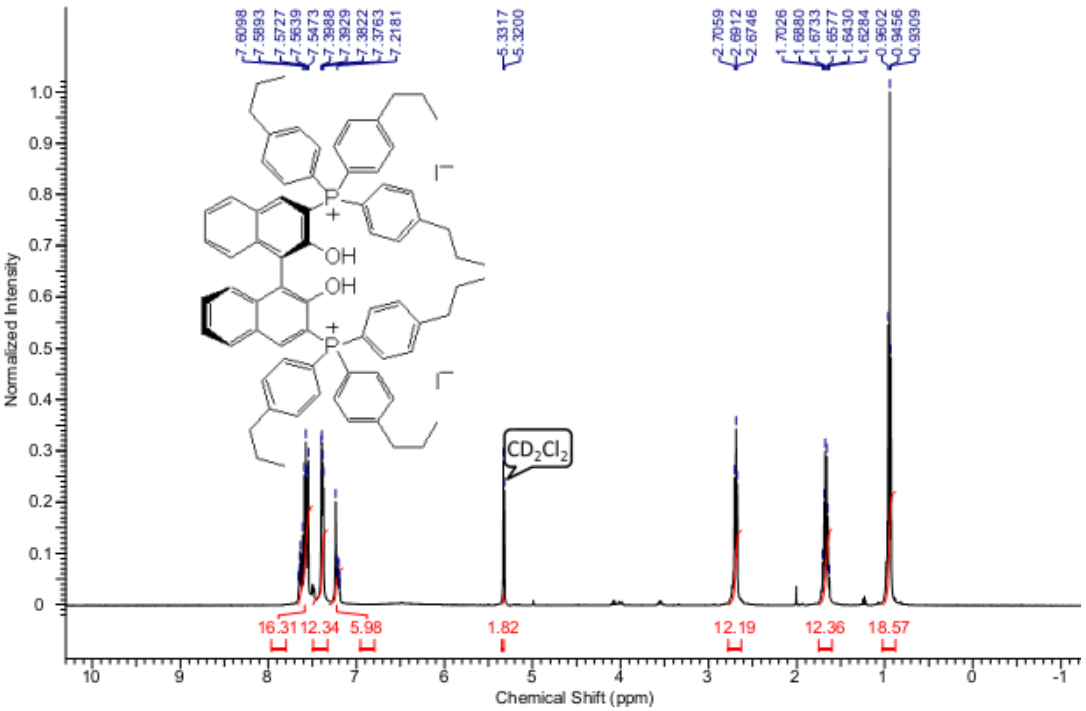

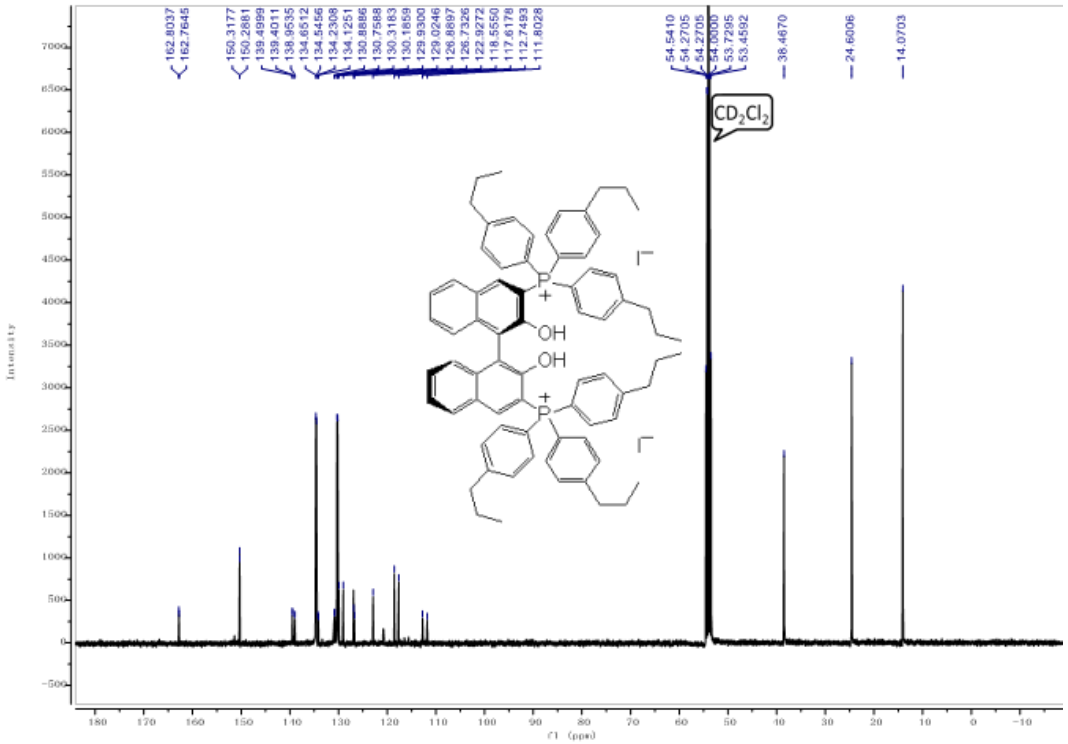
162.8037
162.7645
150.3177
150.2881
139.4999
139.4011
138.9535
134.6512
134.5456
134.2308
134.1251
130.8886
130.7588
130.3183
130.1859
129.9300
129.0246
126.8897
126.7326
122.9272
118.5550
117.6178
112.7493
111.8028
54.5410
54.2705
54.2705
54.0000
53.7295
53.4592
38.4670
24.6006
14.0703
CD2Cl2
Intensity
f1 (ppm)

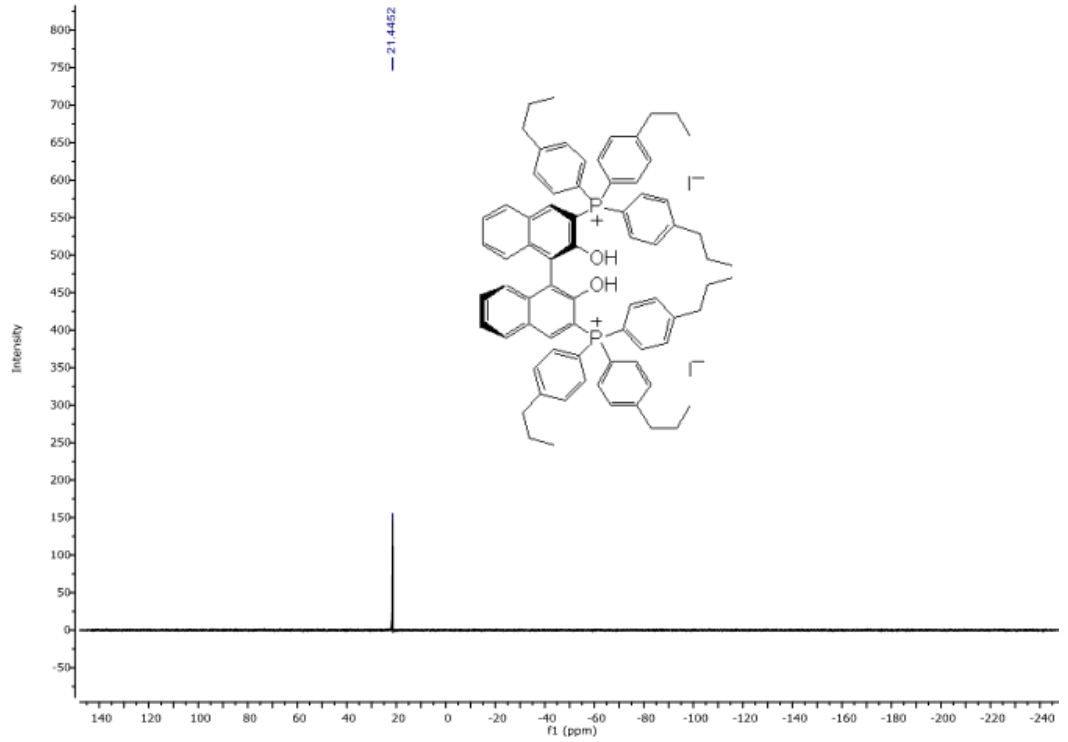
21.4452
Intensity
f1 (ppm)

Figure S7. ^{1}H, ^{13}C and ^{31}P NMR of (*R*)-(2,2'-dihydroxy-[1,1'-binaphthalene]-3,3'-diyl)bis(di-phenyl(*p*-tolyl)phosphonium) iodide (**9e**).

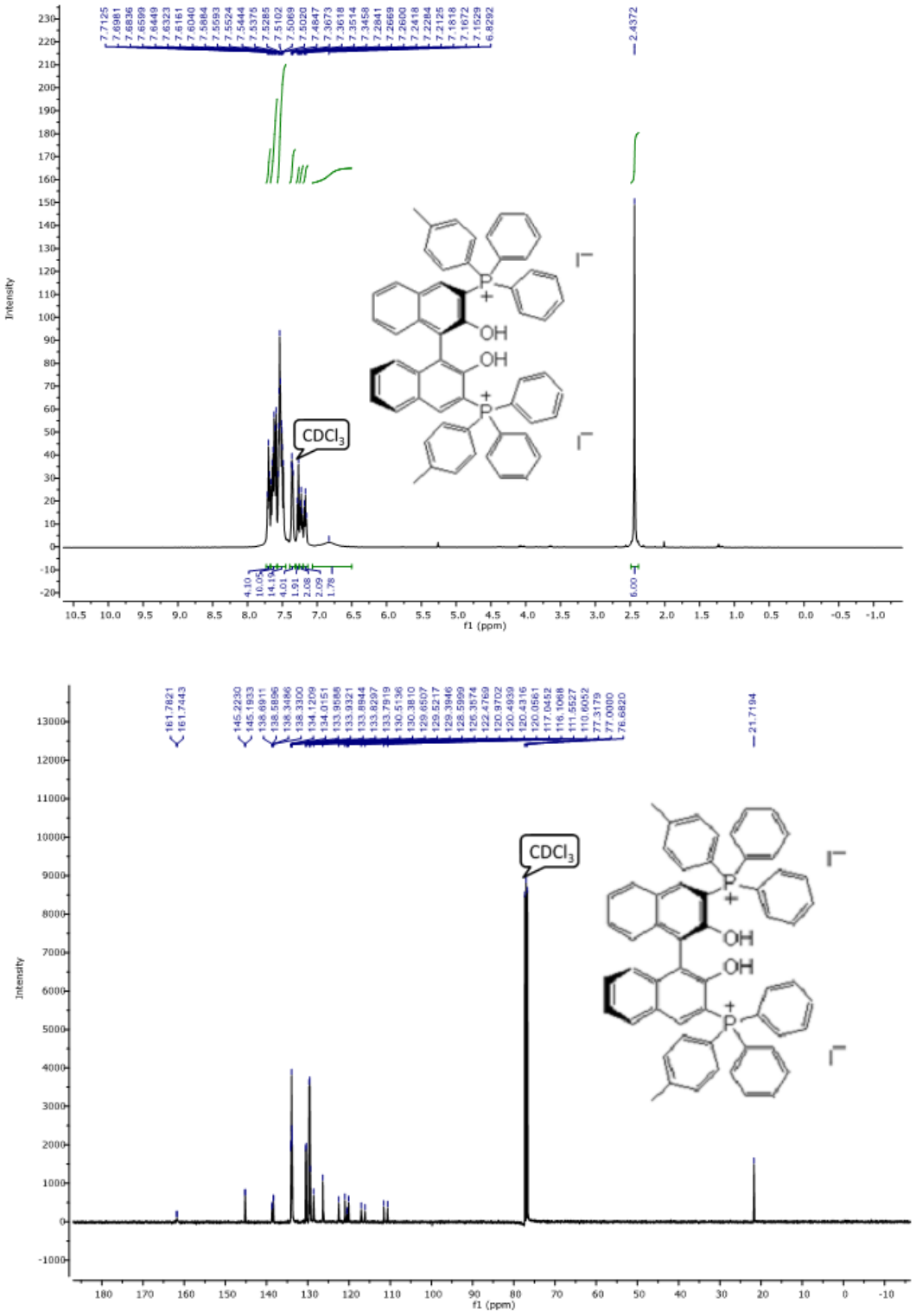

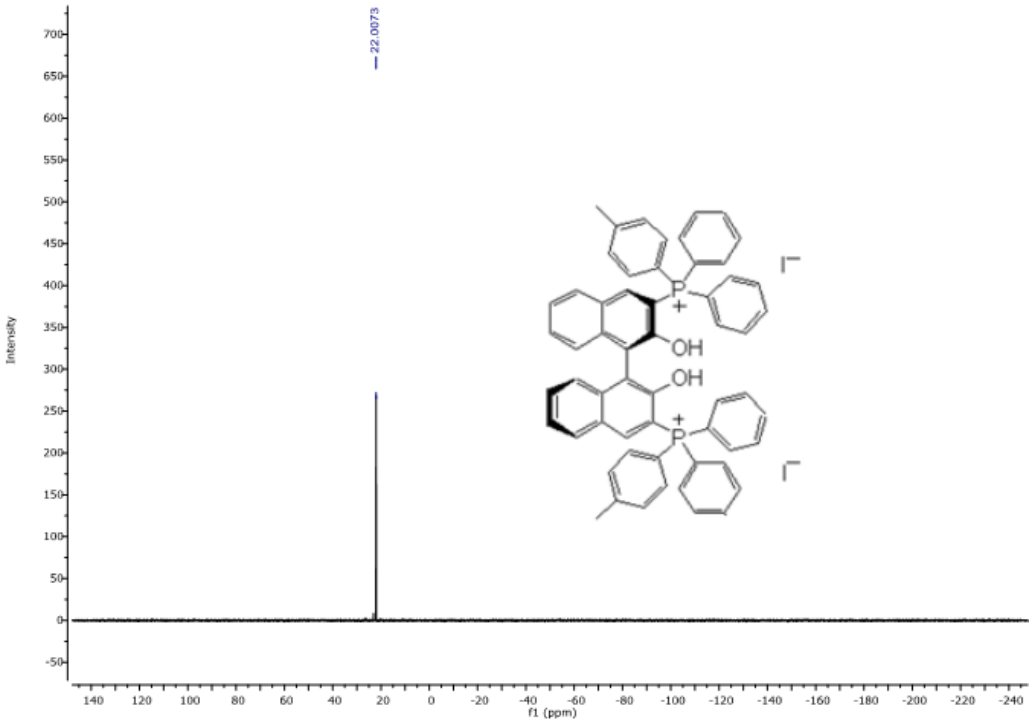

Figure S8. ^{1}H, ^{13}C and ^{31}P NMR of (*R*)-(4-hydroxy-4-oxidodinaphtho[2,1-*d*:1',2'-*f*][1,3,2]dioxaphosphepine-2,6-diyl)bis(triphenylphosphonium) chloride (**10a**).

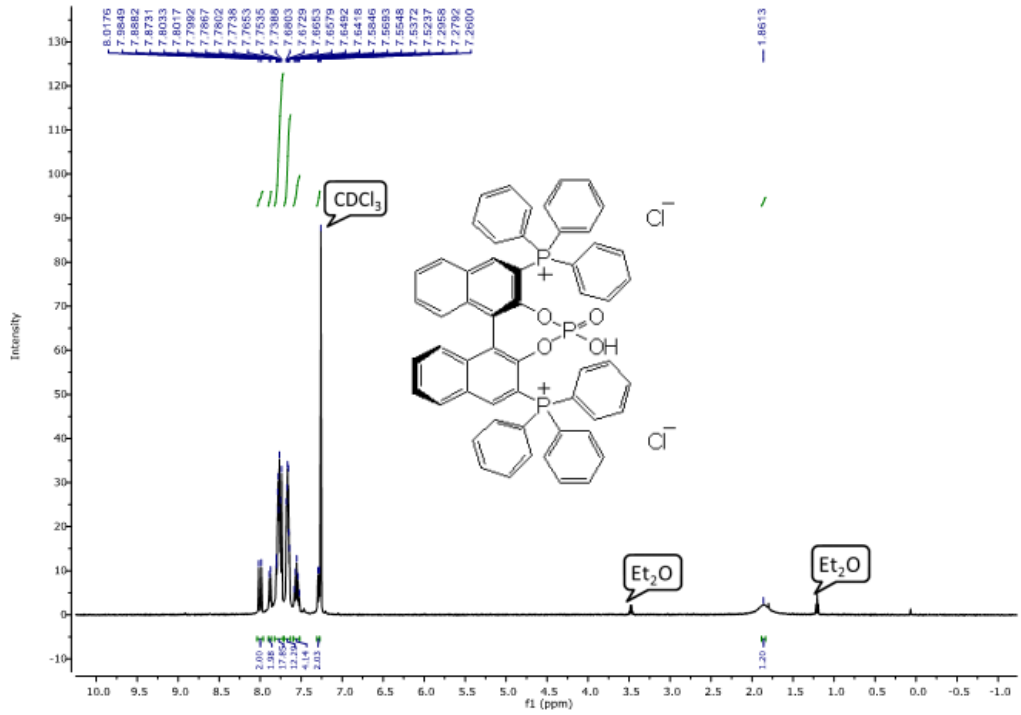

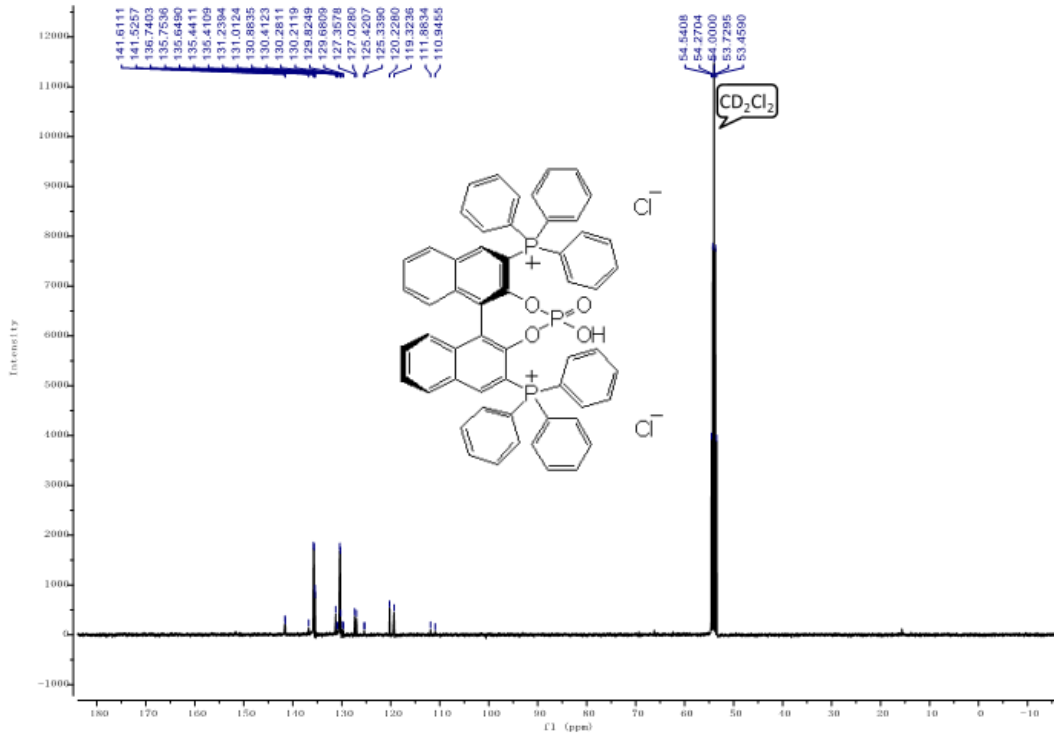
141.6111
141.5257
136.7403
135.7536
135.6490
135.4411
135.4109
131.2384
131.0124
130.8835
130.4123
130.2811
130.2119
129.8249
129.6809
127.3578
127.0280
125.4207
125.3390
120.2280
119.3236
111.8834
110.9455
54.5408
54.2704
54.0000
53.7295
53.4590
CD2Cl2
Cl⁻
Cl⁻
OH
Intensity
f1 (ppm)

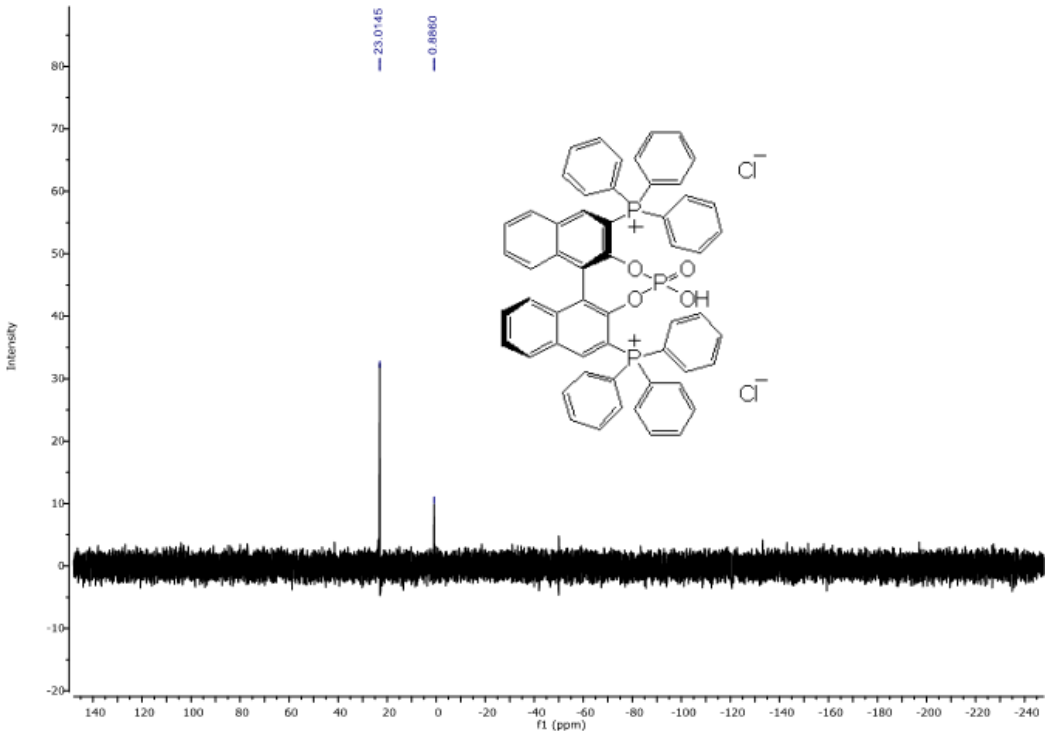
23.0145
0.8860
Cl⁻
Cl⁻
OH
Intensity
f1 (ppm)

Figure S9. ^{1}H, ^{13}C and ^{31}P NMR of (*R*)-(4-hydroxy-4-oxidodinaphtho[2,1-*d*:1',2'-*f*][1,3,2]dioxaphosphepine-2,6-diyl)bis(tri-*p*-tolylphosphonium) chloride (**10b**).

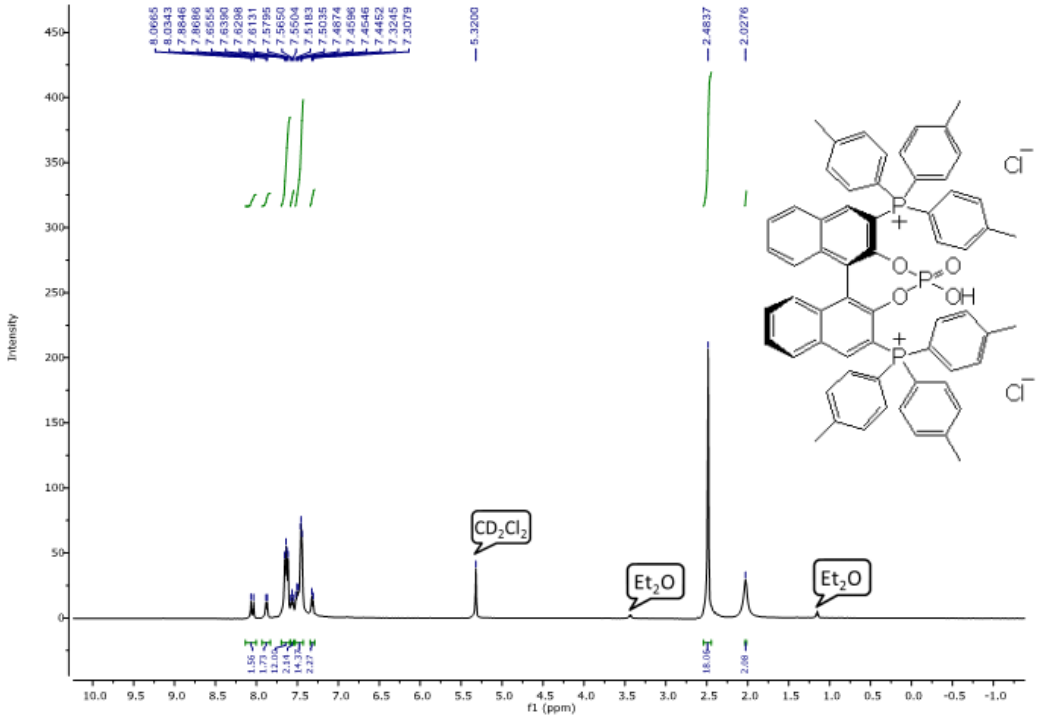

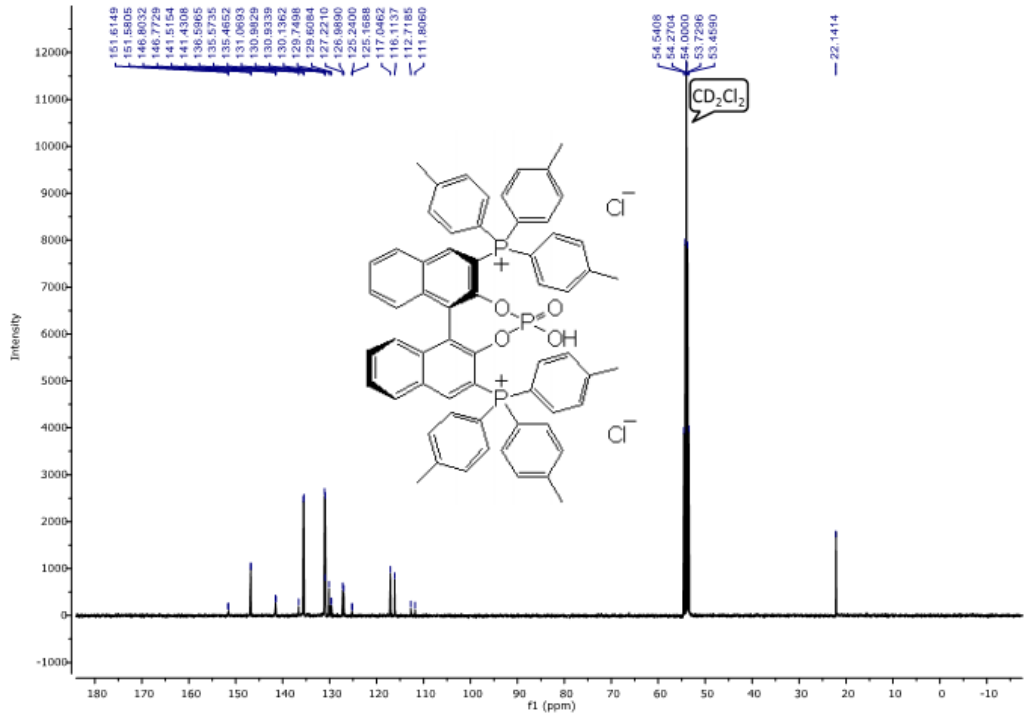

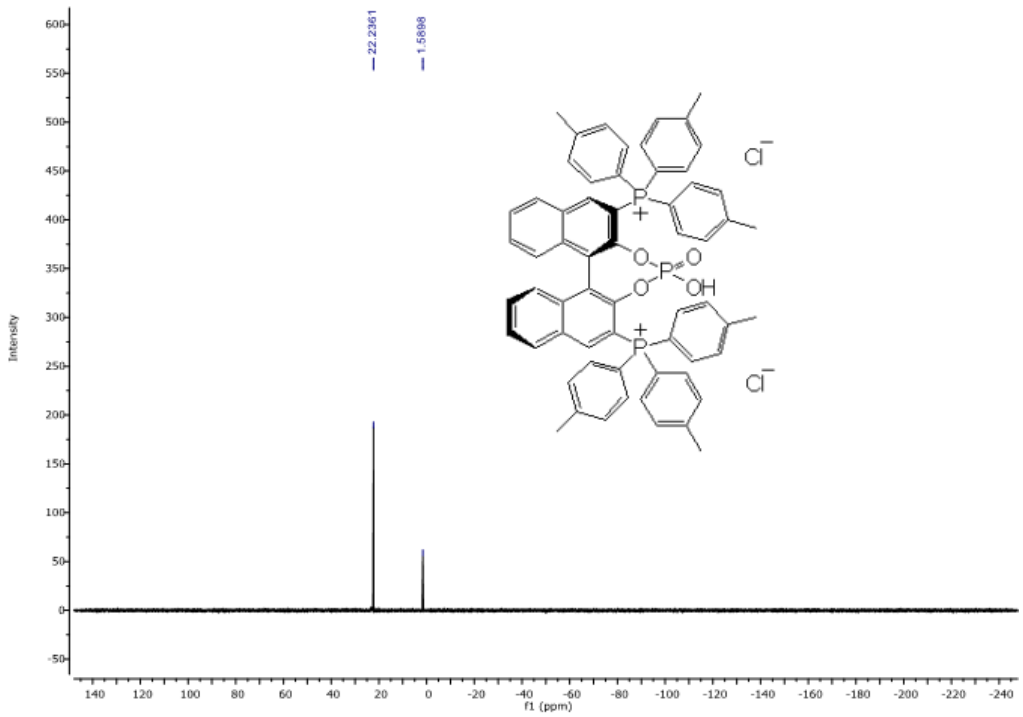

Figure S10. ^{1}H, ^{13}C and ^{31}P NMR of (*R*)-(4-hydroxy-4-oxidodinaphtho[2,1-*d*:1',2'-*f*][1,3,2]dioxaphosphepine-2,6-diyl)bis(tris(4-ethylphenyl)phosphonium) chloride (**10c**).

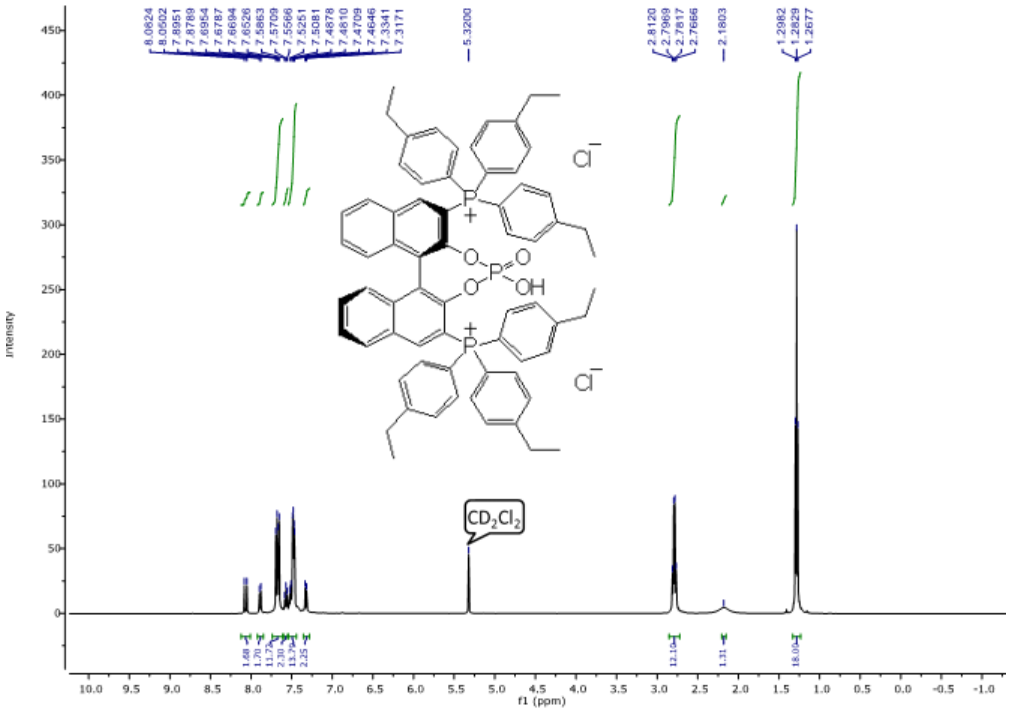

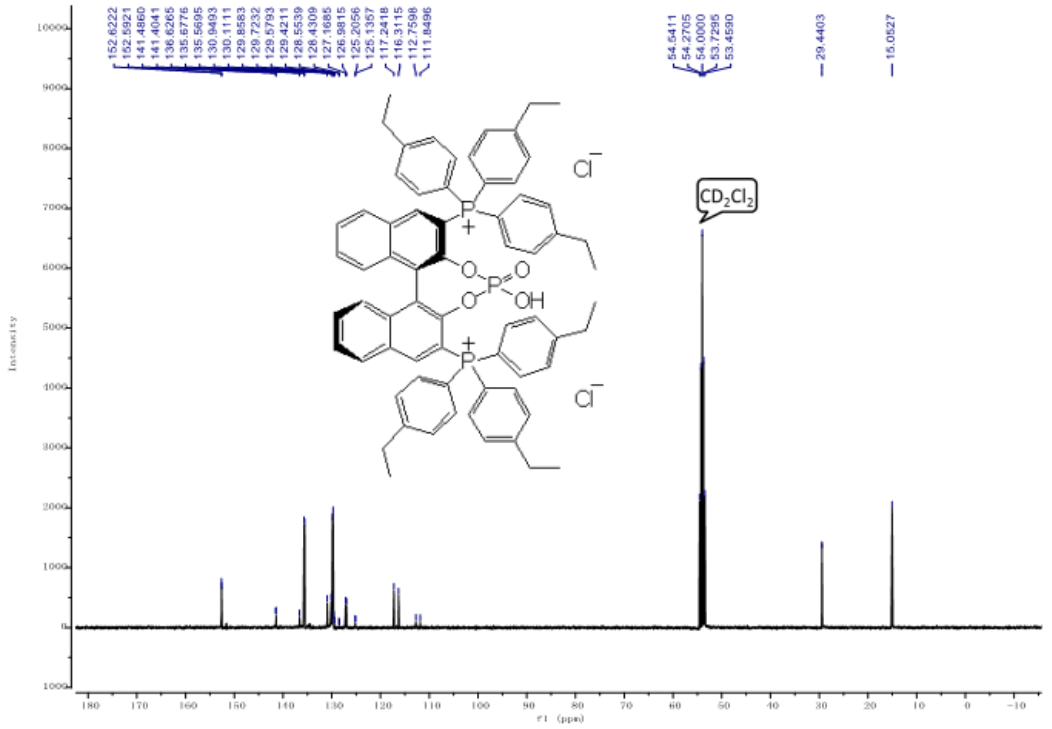
152.6222
152.5921
141.4860
141.4041
136.6265
135.6776
135.5695
130.9493
130.1111
129.8583
129.7232
129.5793
129.4211
128.5539
128.4309
127.1685
126.9815
125.2056
125.1357
117.2418
116.3115
112.7598
111.8496
54.5411
54.2705
54.0000
53.7295
53.4590
29.4403
15.0527
CD2Cl2
Cl⁻
Cl⁻
OH
Intensity
f1 (ppm)

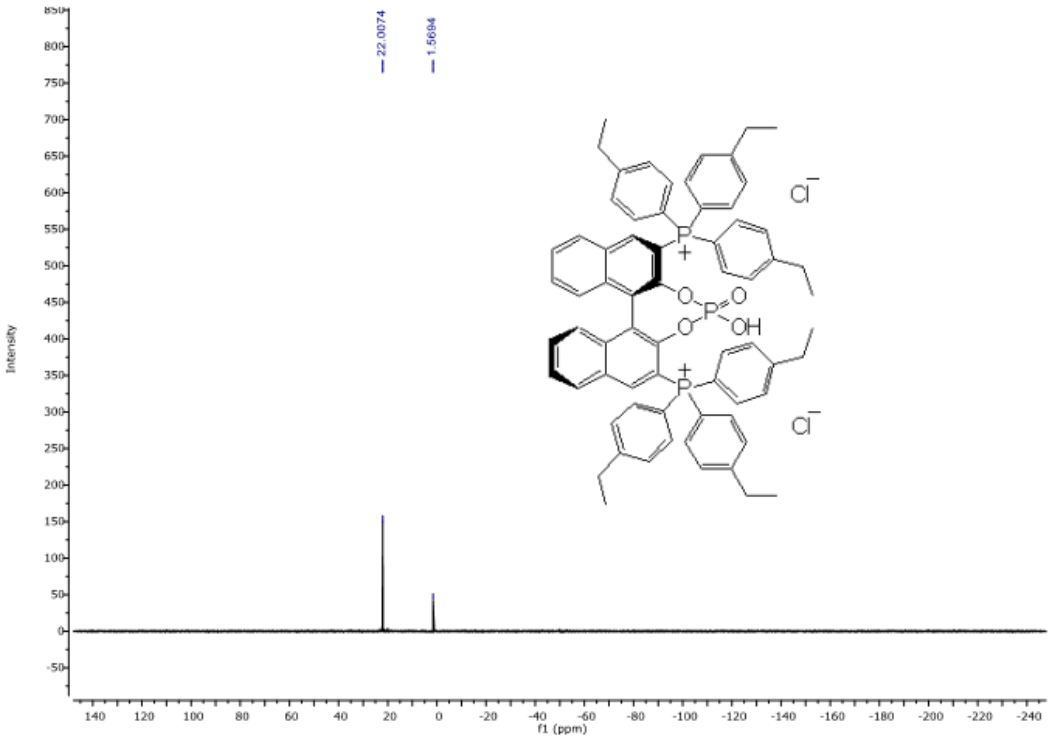
22.0074
1.5684
Cl⁻
Cl⁻
OH
Intensity
f1 (ppm)

Figure S11. ^{1}H, ^{13}C and ^{31}P NMR of (*R*)-(4-hydroxy-4-oxidodinaphtho[2,1-*d*:1',2'-*f*][1,3,2]dioxaphosphepine-2,6-diyl)bis(tris(4-propylphenyl)phosphonium) chloride (**10d**).

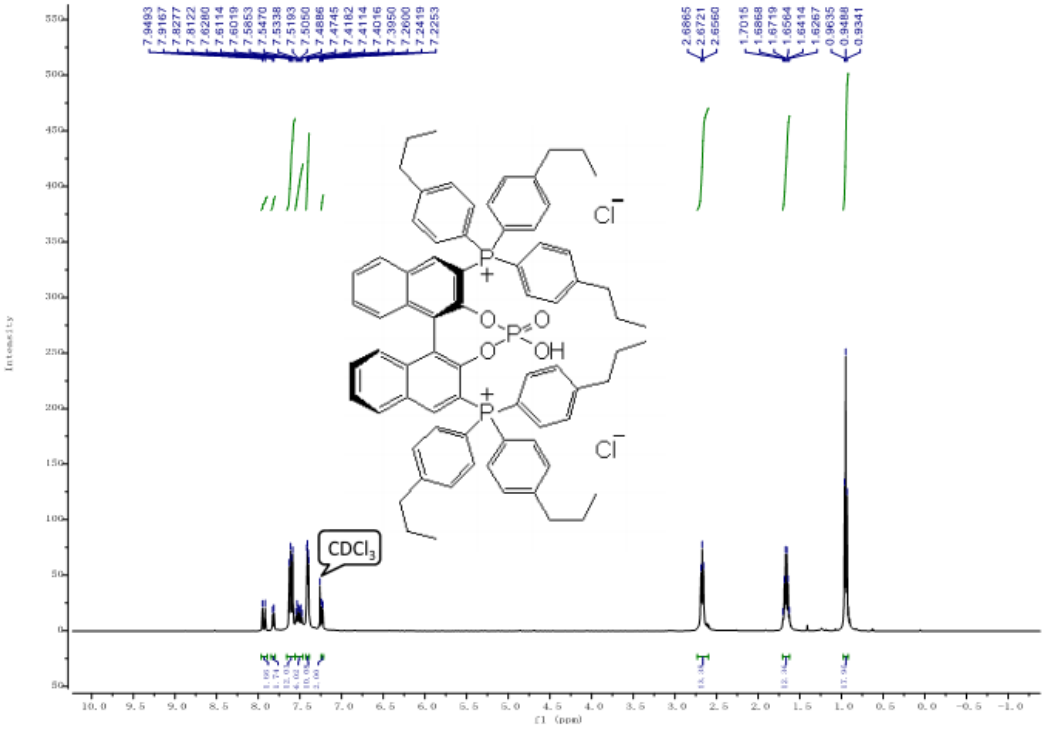

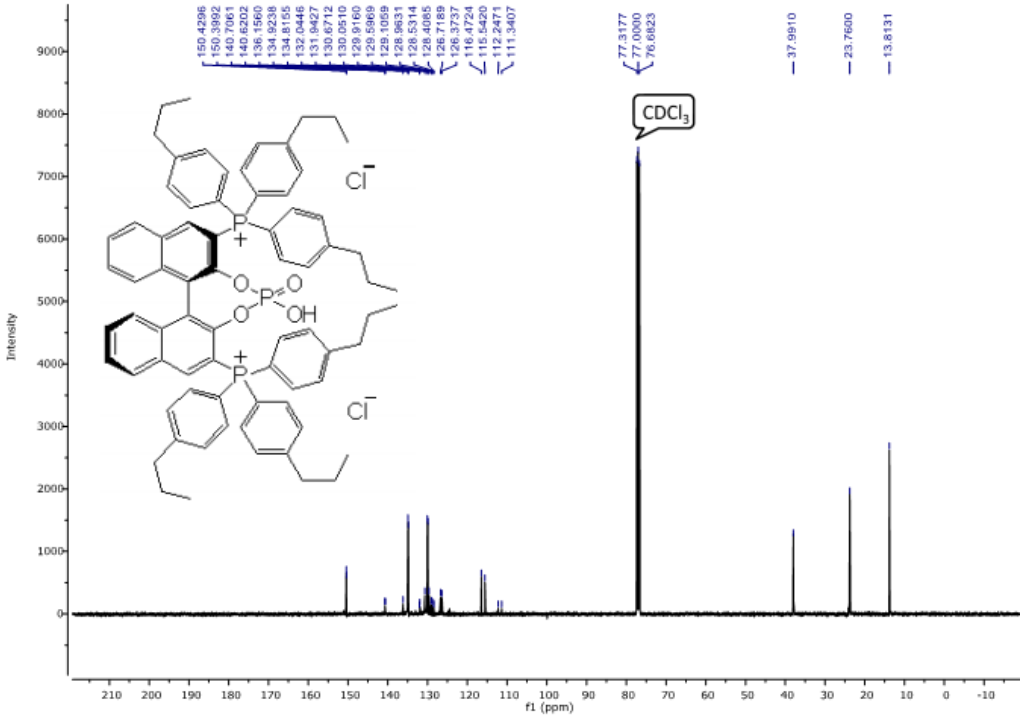

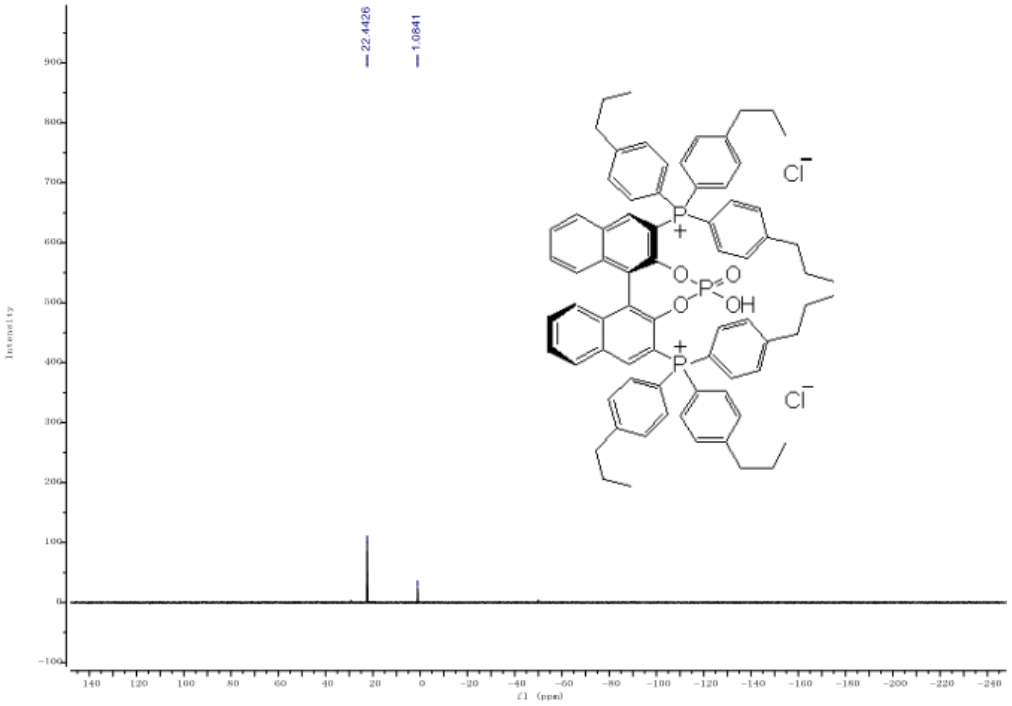

Figure S12. ^{1}H, ^{13}C and ^{31}P NMR of (*R*)-(4-hydroxy-4-oxidodinaphtho[2,1-*d*:1',2'-*f*][1,3,2]dioxaphosphepine-2,6-diyl)bis(diphenyl(*p*-tolyl)phosphonium) chloride (**10e**).

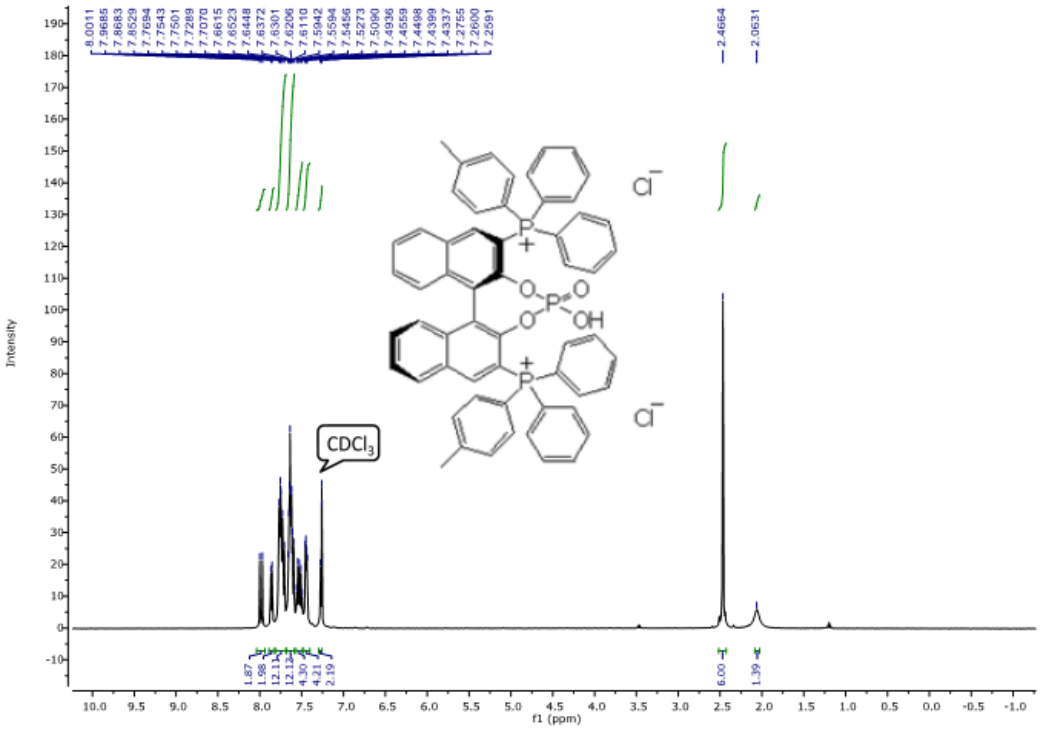

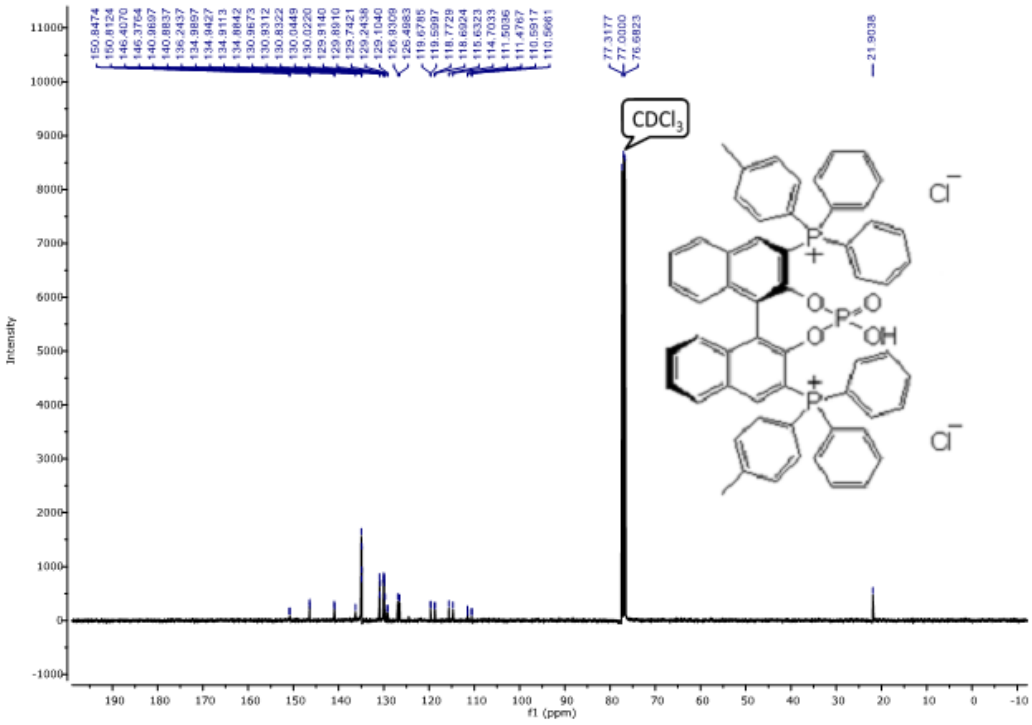
CDCl3
Cl⁻
Cl⁻
Intensity
f1 (ppm)

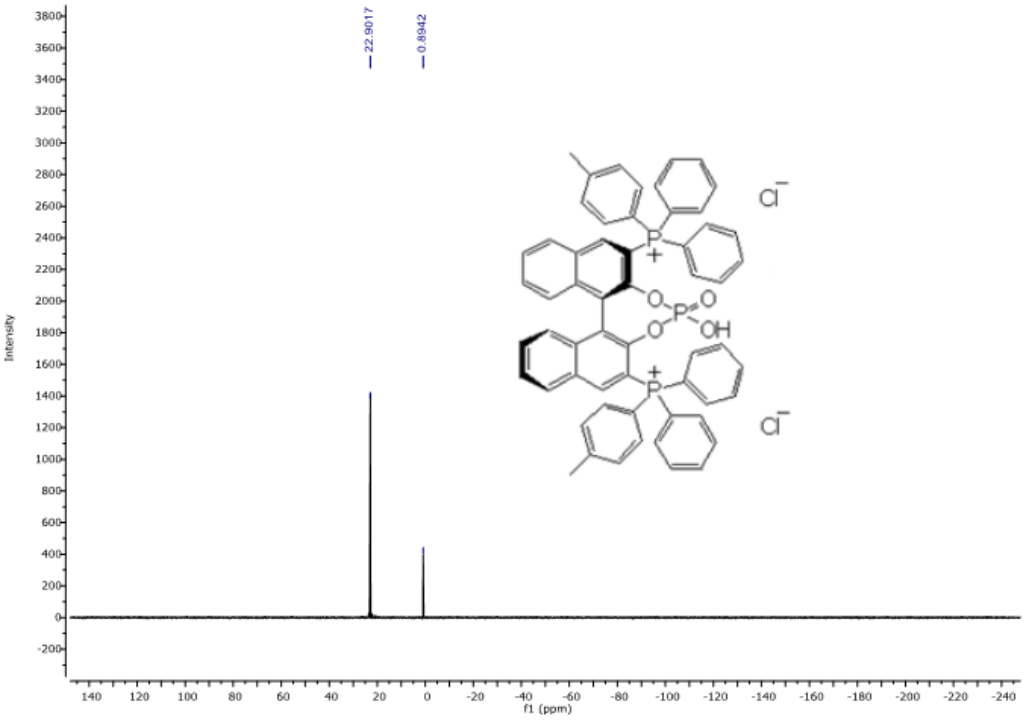
22.9017
0.8942
Cl⁻
Cl⁻
Intensity
f1 (ppm)

Figure S13. ^{1}H, ^{13}C, ^{19}F and ^{31}P NMR of (*R*)-(4-hydroxy-4-oxidodinaphtho[2,1-*d*:1',2'-*f*][1,3,2]dioxaphosphepine-2,6-diyl)bis(triphenylphosphonium) tetrakis[3,5-bis(trifluoromethyl)phenyl]-borate (**2a**).

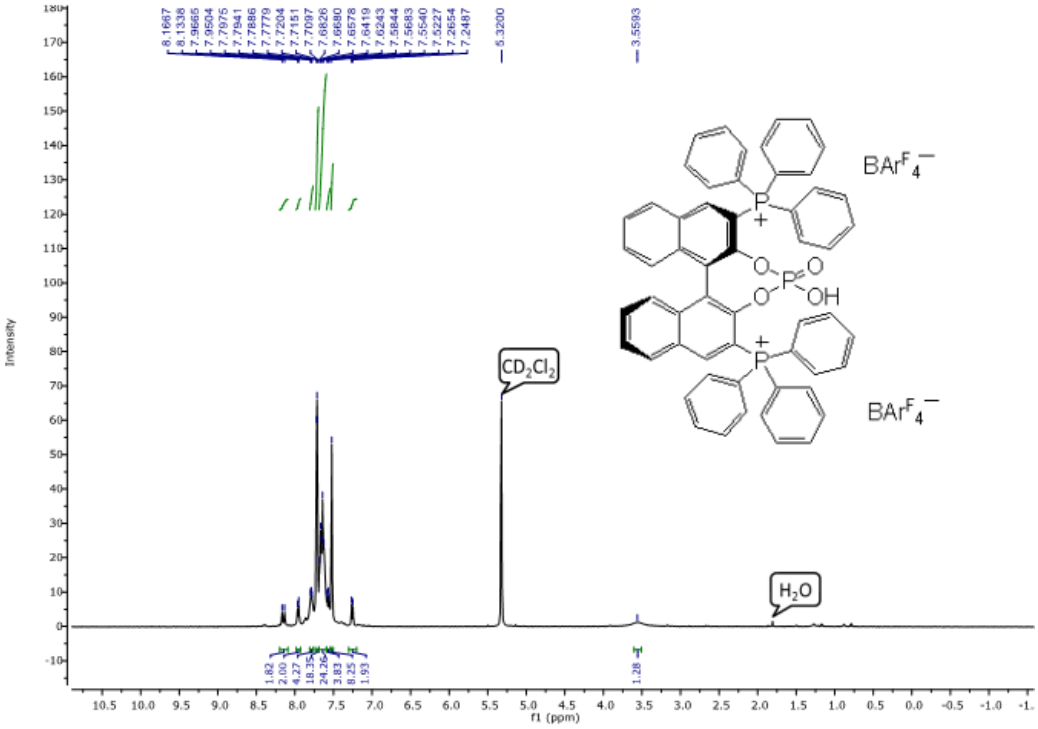

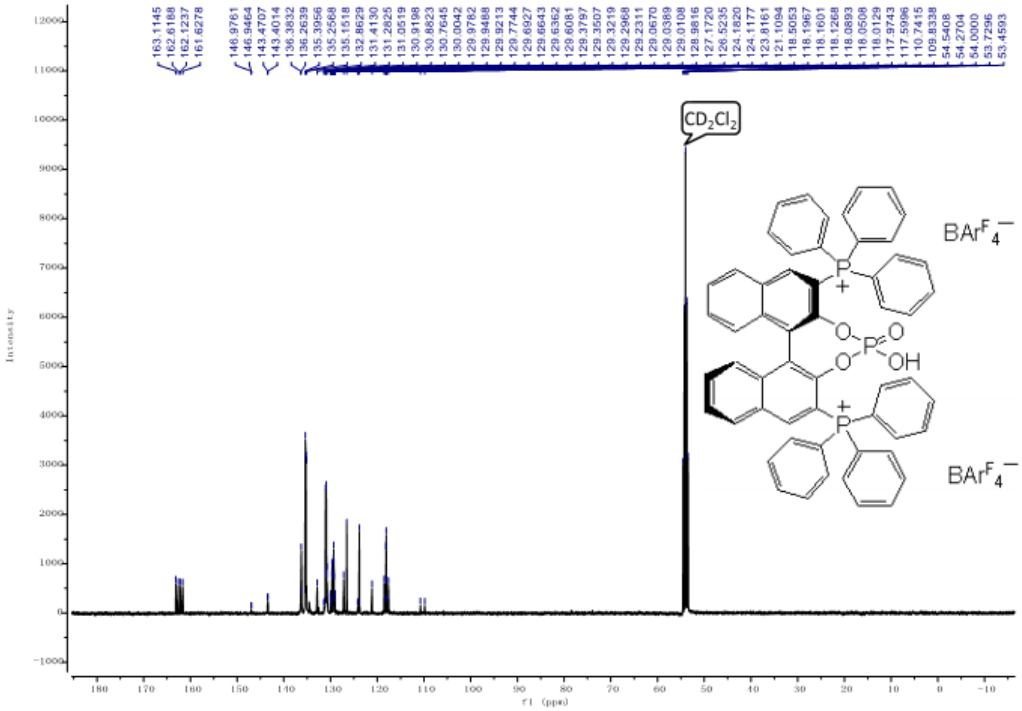

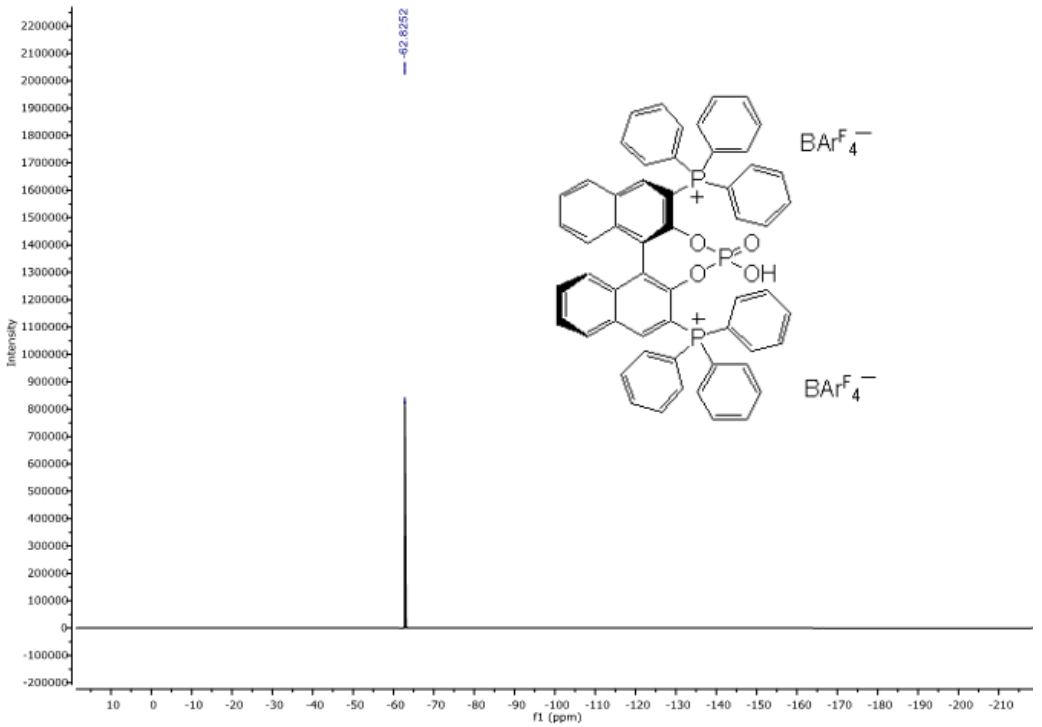
-62.8252
Intensity
f1 (ppm)
BAr$^{F}_{4}$$^{-}$
BAr$^{F}_{4}$$^{-}$

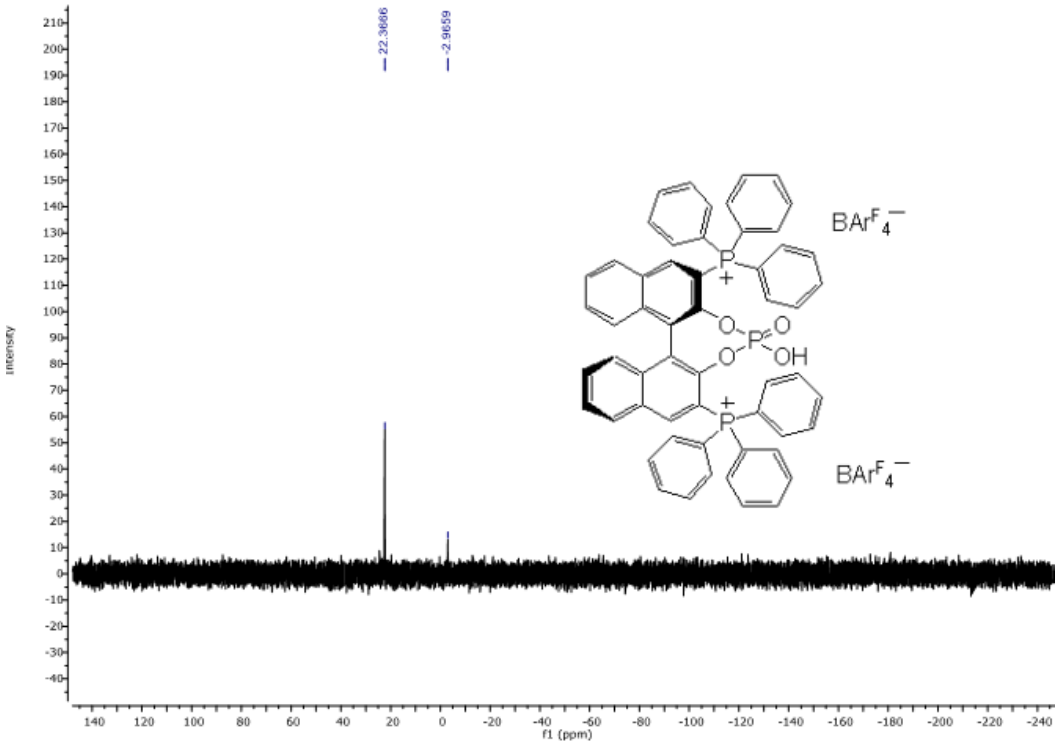
22.3686
2.9659
Intensity
f1 (ppm)
BAr$^{F}_{4}$$^{-}$
BAr$^{F}_{4}$$^{-}$

Figure S14. ^{1}H, ^{13}C, ^{19}F and ^{31}P NMR of (*R*)-(4-hydroxy-4-oxidodinaphtho[2,1-*d*:1',2'-*f*][1,3,2]dioxaphosphepine-2,6-diyl)bis(tri-*p*-tolylphosphonium) tetrakis[3,5-bis(trifluoromethyl)phenyl]-borate (**2b**).

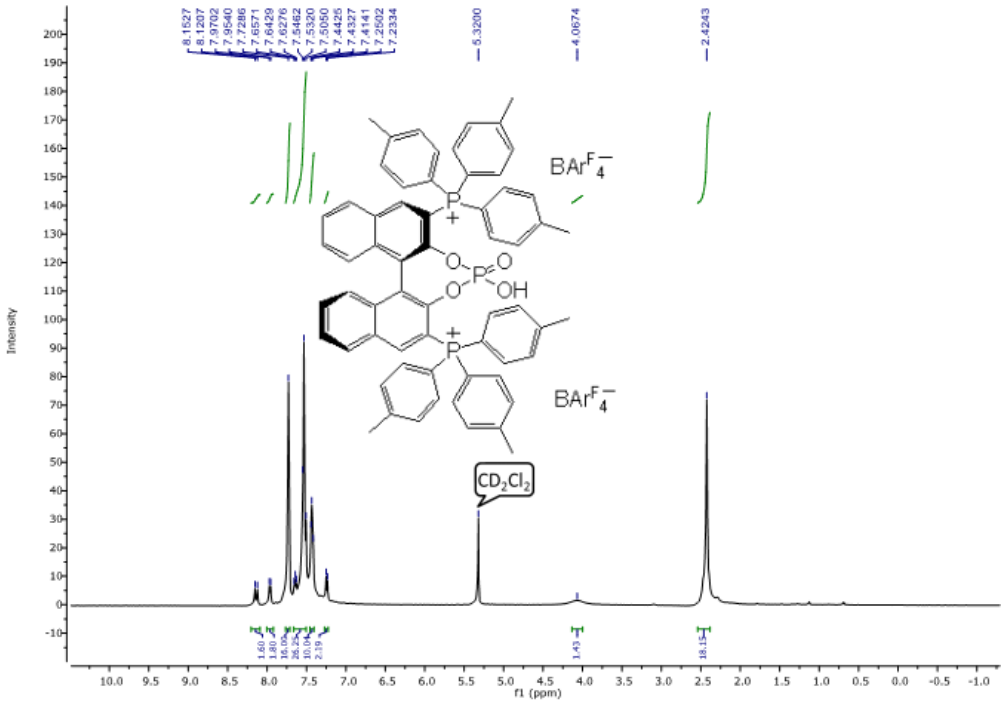

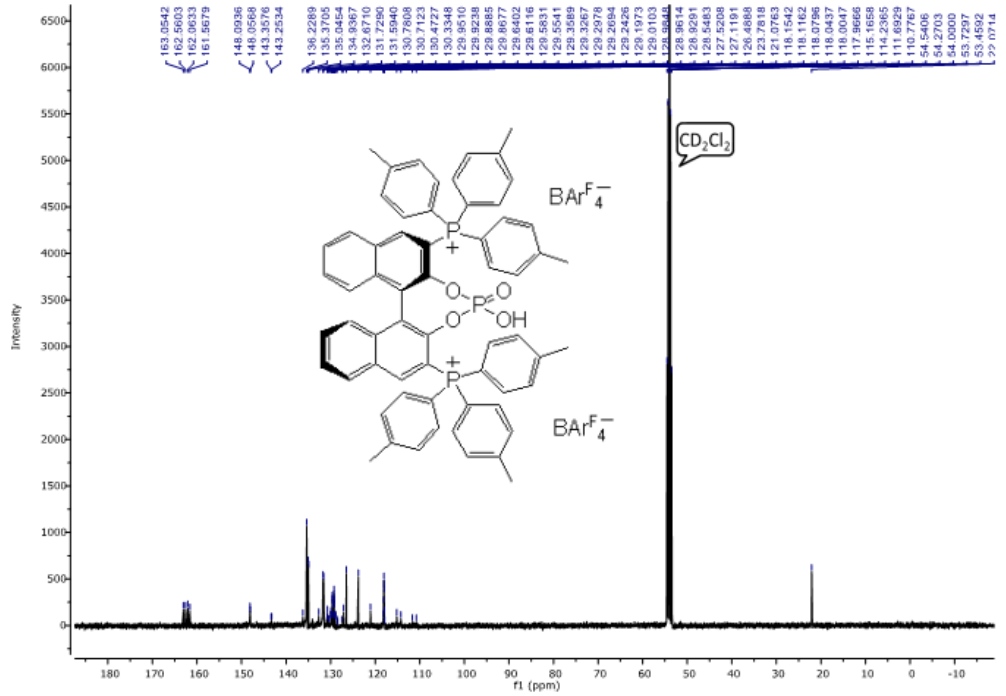

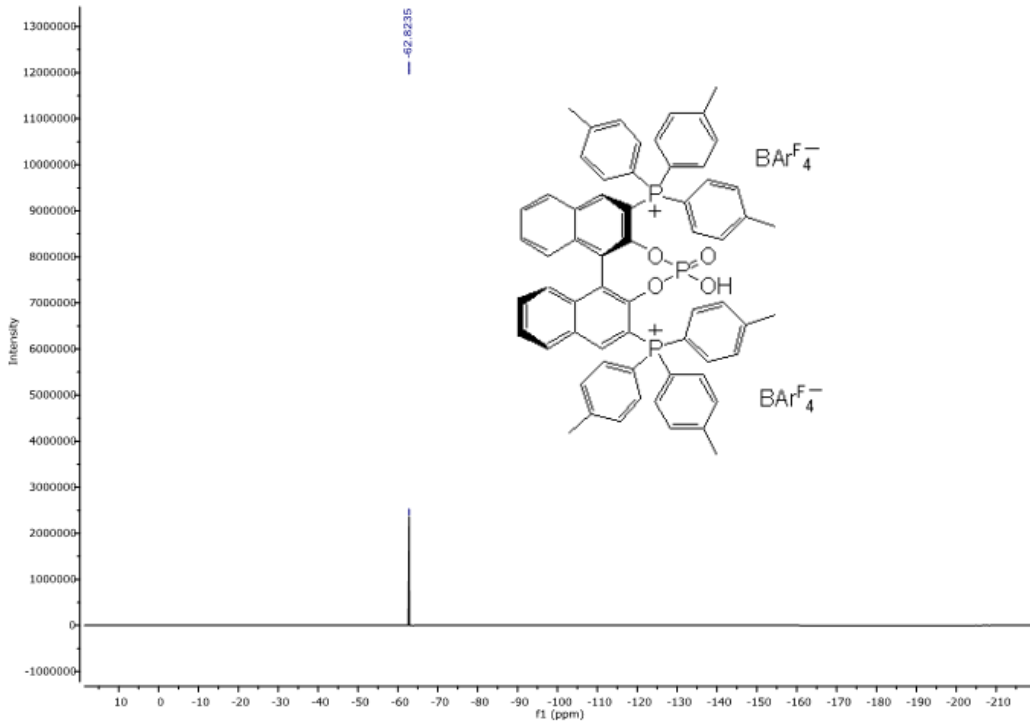
-62.8235
Intensity
f1 (ppm)
BAr$^{F}_{4}$$^{-}$
BAr$^{F}_{4}$$^{-}$
OH

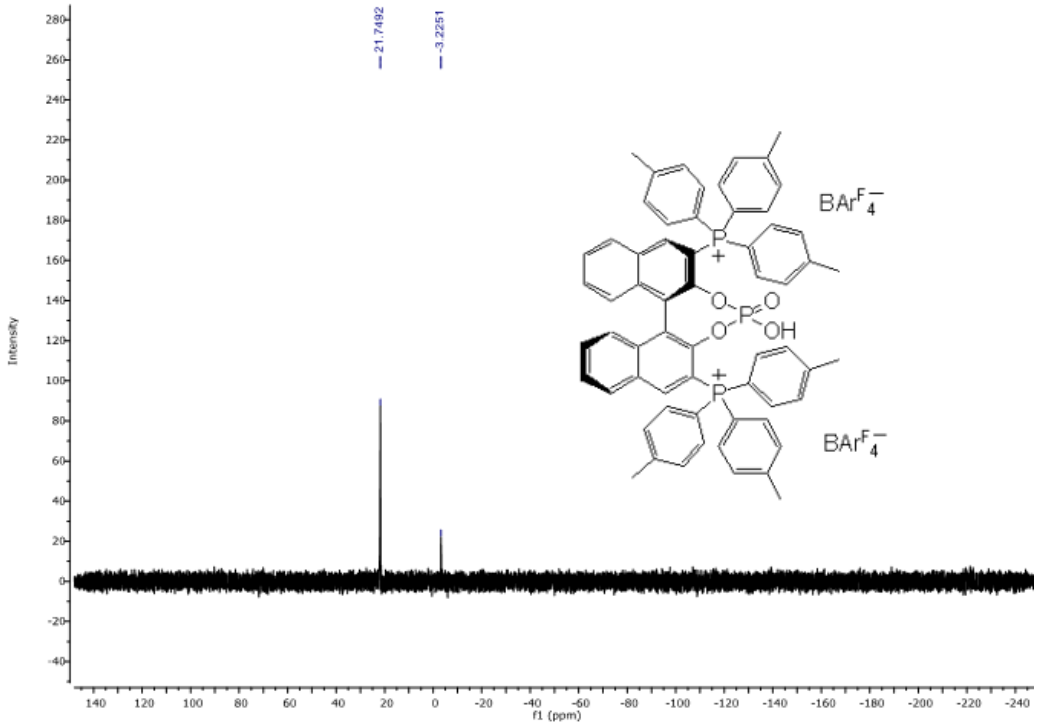
-21.7492
-3.2251
Intensity
f1 (ppm)
BAr$^{F}_{4}$$^{-}$
BAr$^{F}_{4}$$^{-}$
OH

Figure S15. ^{1}H, ^{13}C, ^{19}F and ^{31}P NMR of (*R*)-(4-hydroxy-4-oxidodinaphtho[2,1-*d*:1',2'-*f*][1,3,2]dioxaphosphepine-2,6-diyl)bis(tris(4-ethylphenyl)phosphonium) tetrakis[3,5-bis(trifluoromethyl)-phenyl]borate (**2c**).

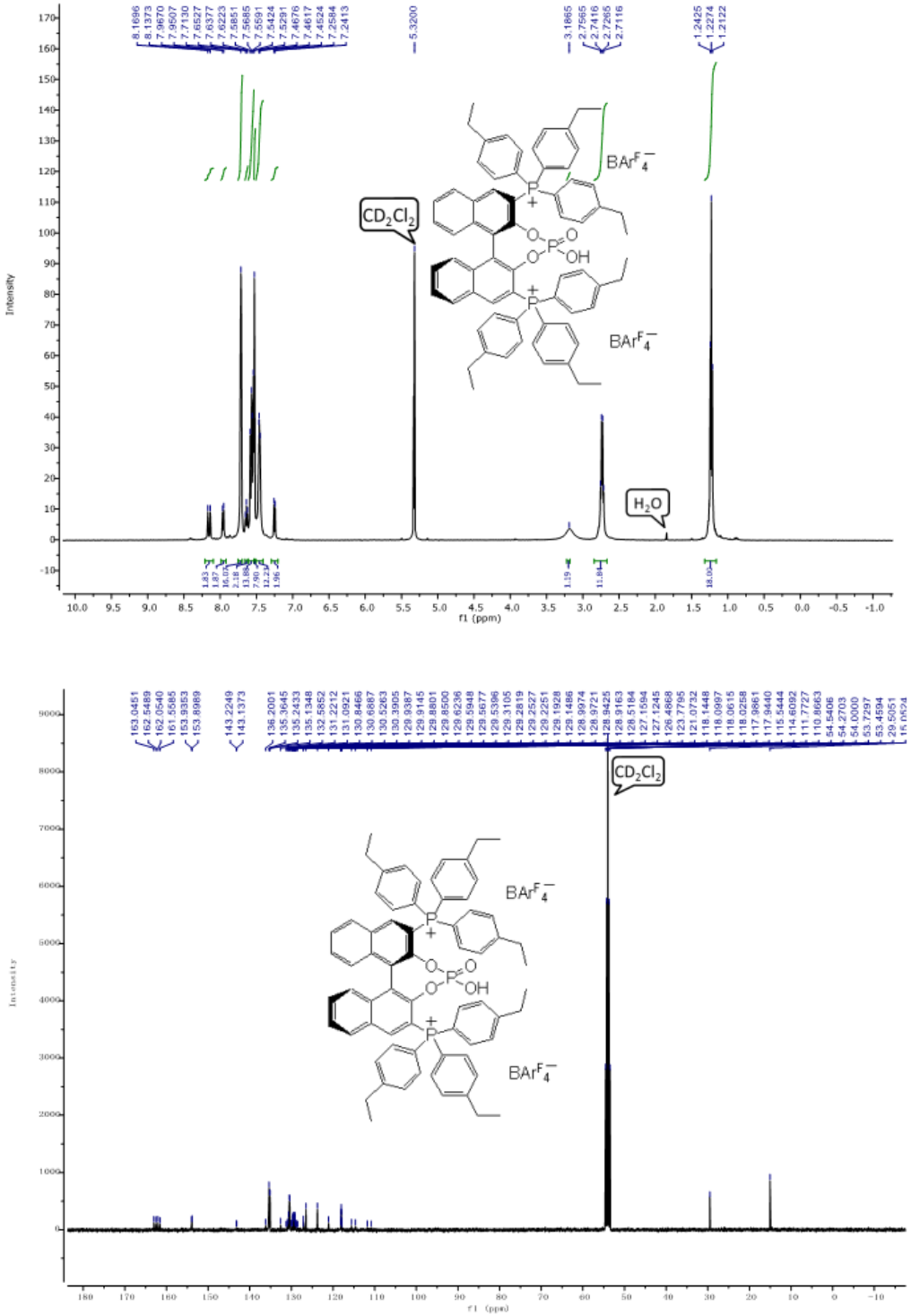

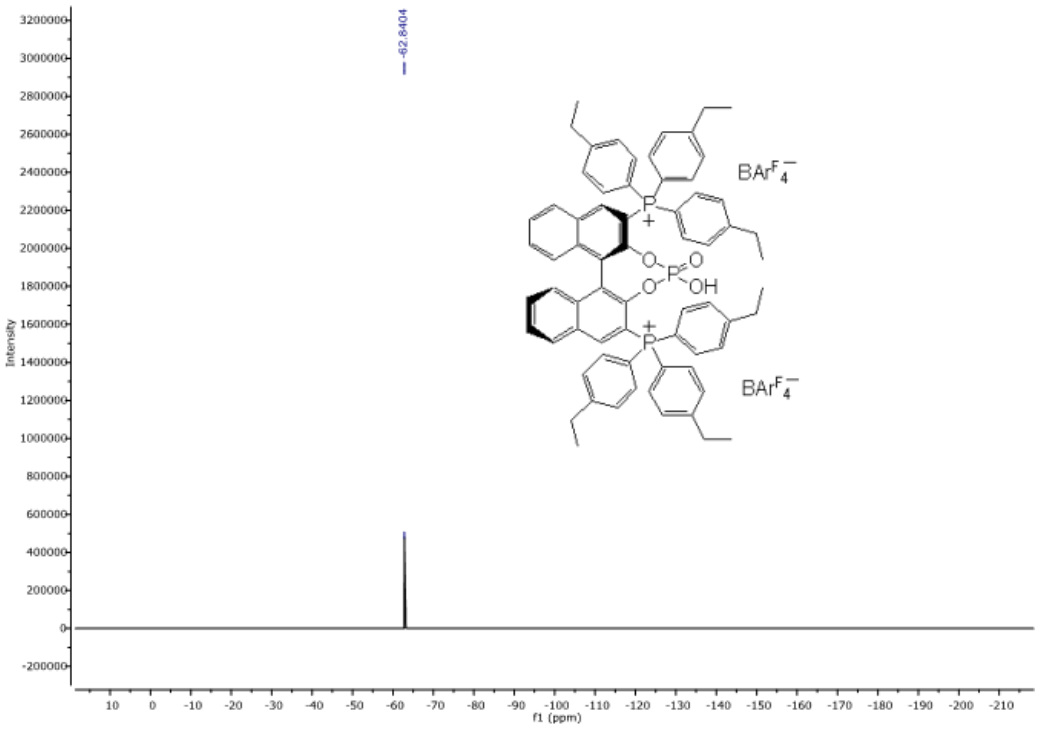
-62.8404
Intensity
f1 (ppm)
BAr$^{F}_{4}$
BAr$^{F}_{4}$

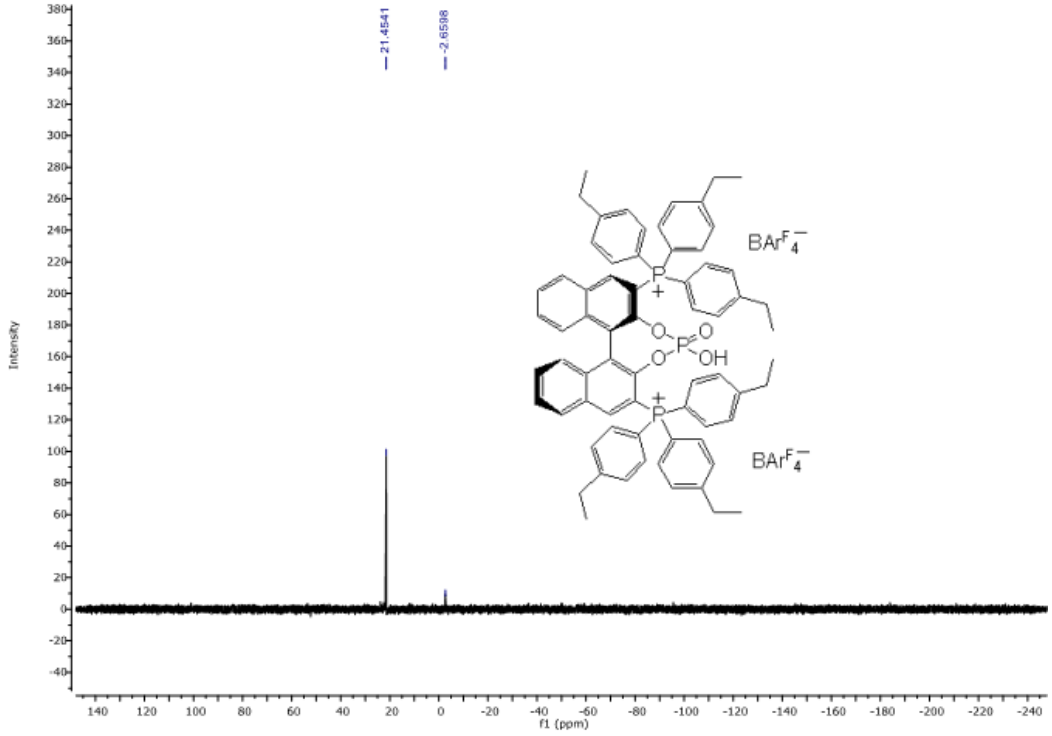
-21.4541
-2.6598
Intensity
f1 (ppm)
BAr$^{F}_{4}$
BAr$^{F}_{4}$

Figure S16. ^{1}H, ^{13}C, ^{19}F and ^{31}P NMR of (*R*)-(4-hydroxy-4-oxidodinaphtho[2,1-*d*:1',2'-*f*][1,3,2]dioxaphosphepine-2,6-diyl)bis(tris(4-propylphenyl)phosphonium) tetrakis[3,5-bis(trifluoromethyl)-phenyl]borate (**2d**).

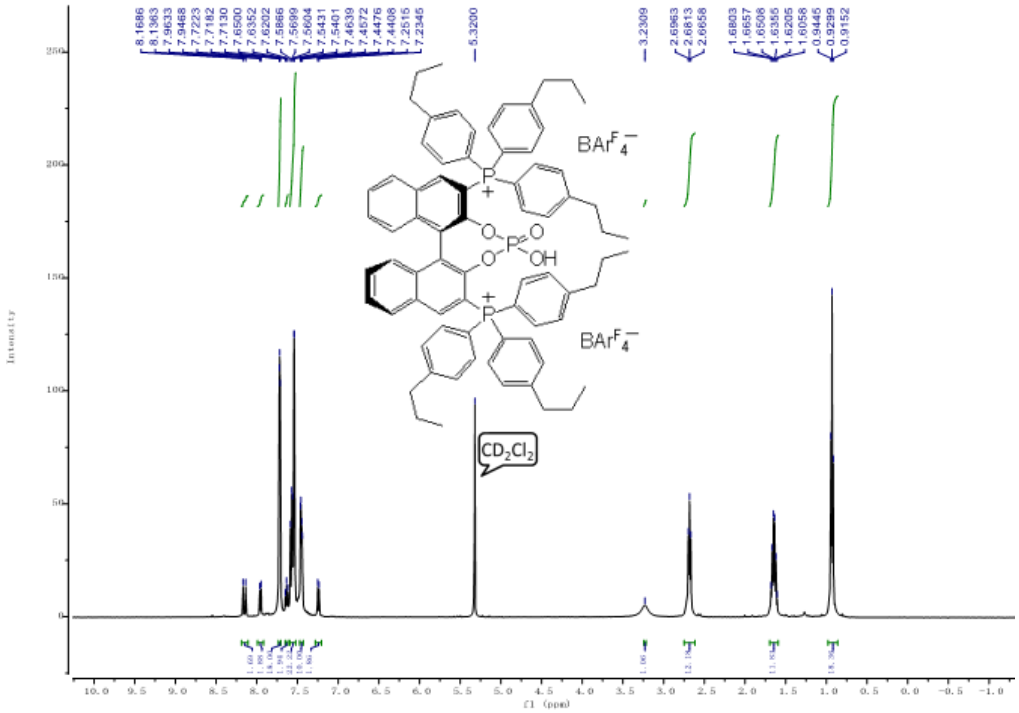

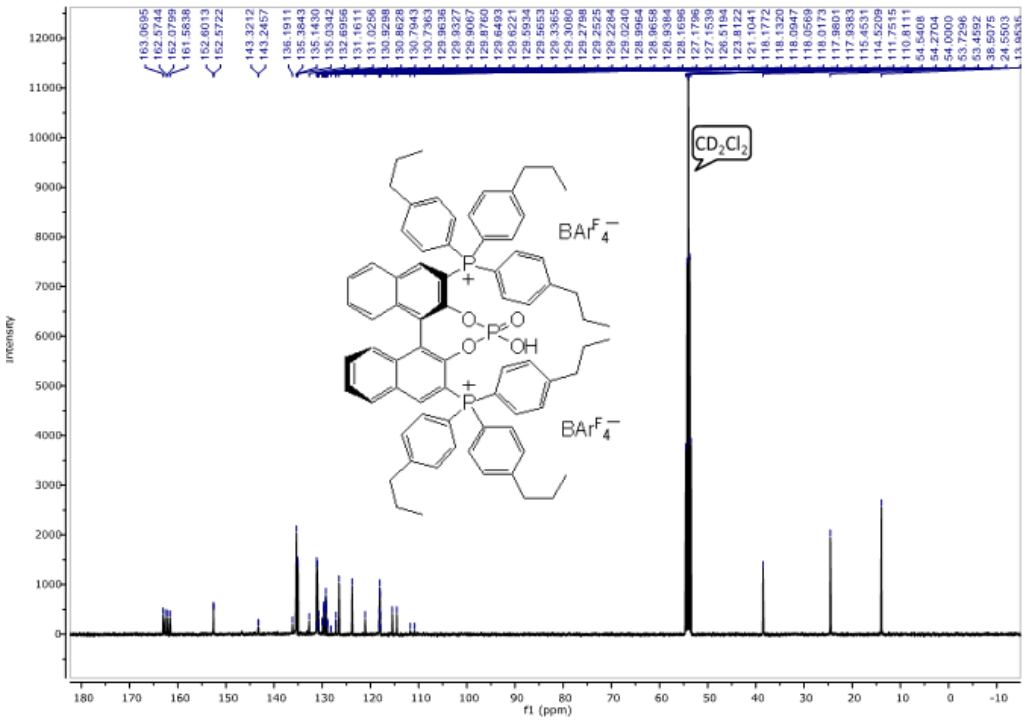

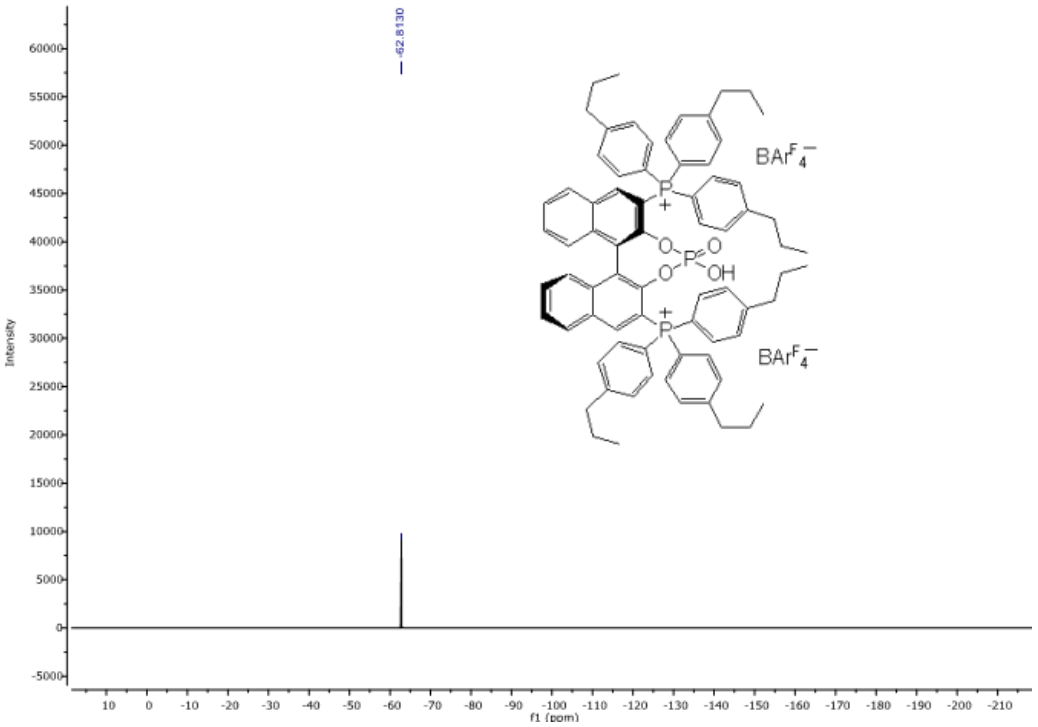
-62.8130
Intensity
f1 (ppm)
BAr$^{F}_{4}$$^{-}$
BAr$^{F}_{4}$$^{-}$
OH

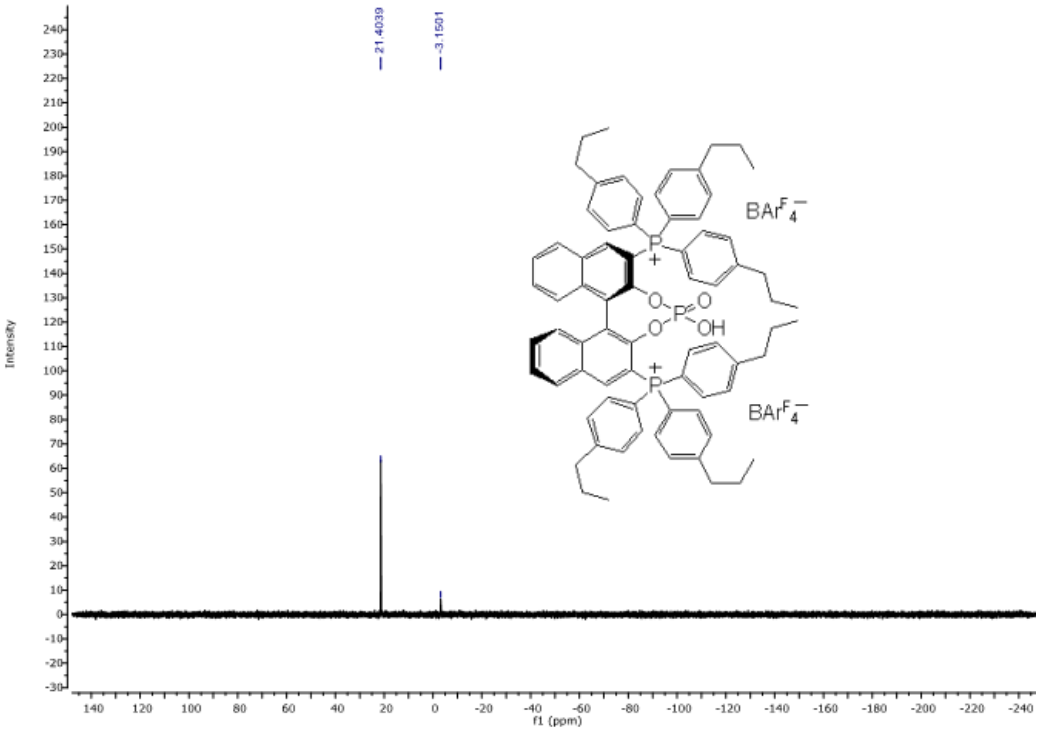
21.4039
-3.1501
Intensity
f1 (ppm)
BAr$^{F}_{4}$$^{-}$
BAr$^{F}_{4}$$^{-}$
OH

Figure S17. ^{1}H, ^{13}C, ^{19}F and ^{31}P NMR of (*R*)-(4-hydroxy-4-oxidodinaphtho[2,1-*d*:1',2'-*f*][1,3,2]dioxaphosphepine-2,6-diyl)bis(diphenyl(*p*-tolyl)phosphonium) tetrakis[3,5-bis(trifluoromethyl)-phenyl]borate (**2e**).

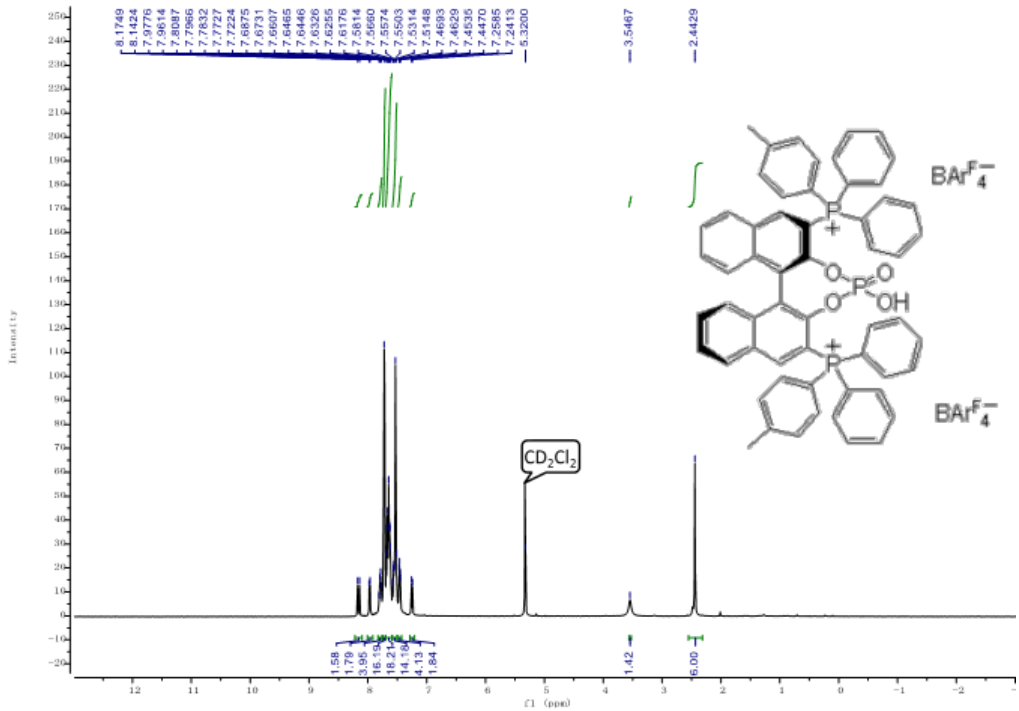

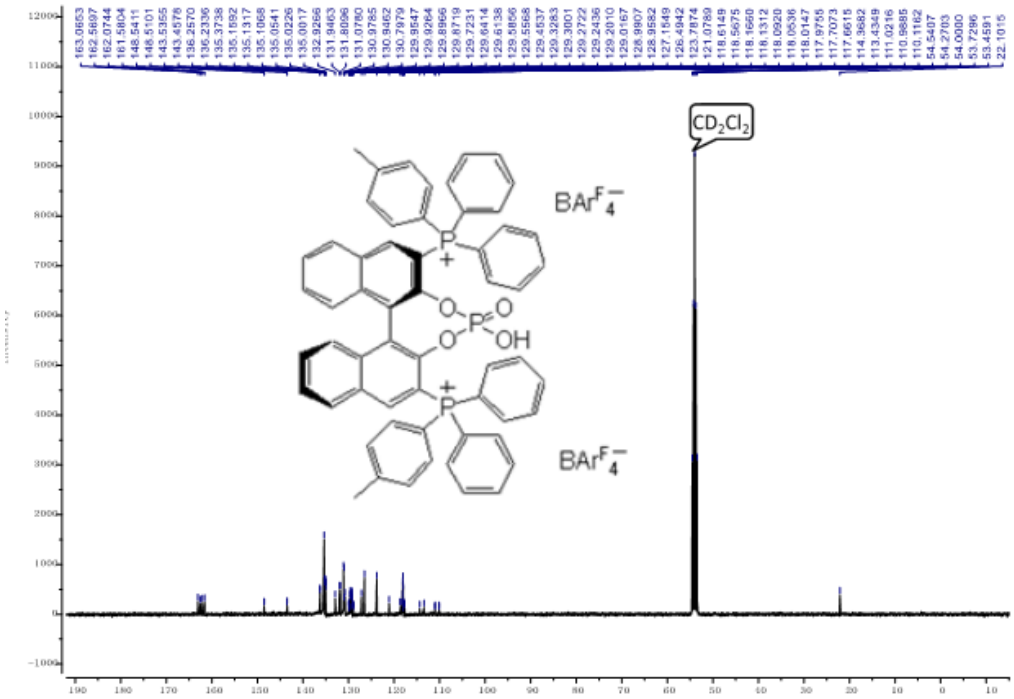

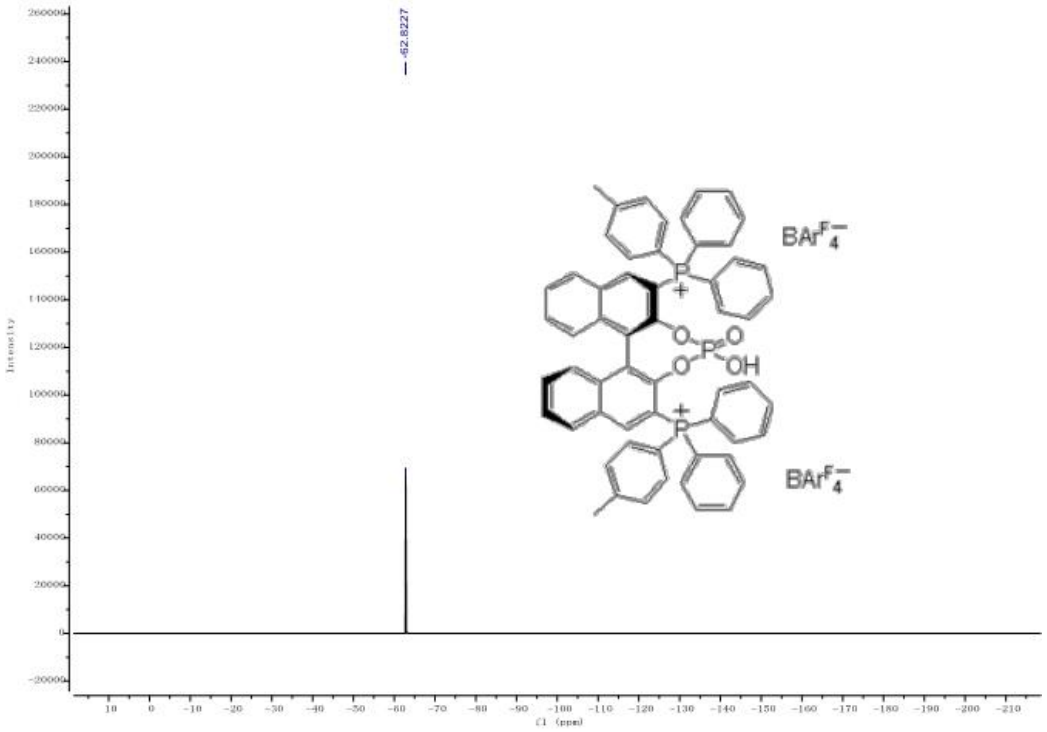
-62.8227
Intensity
f1 (ppm)
BAr$^{F}_{4}^{-}$
BAr$^{F}_{4}^{-}$
OH

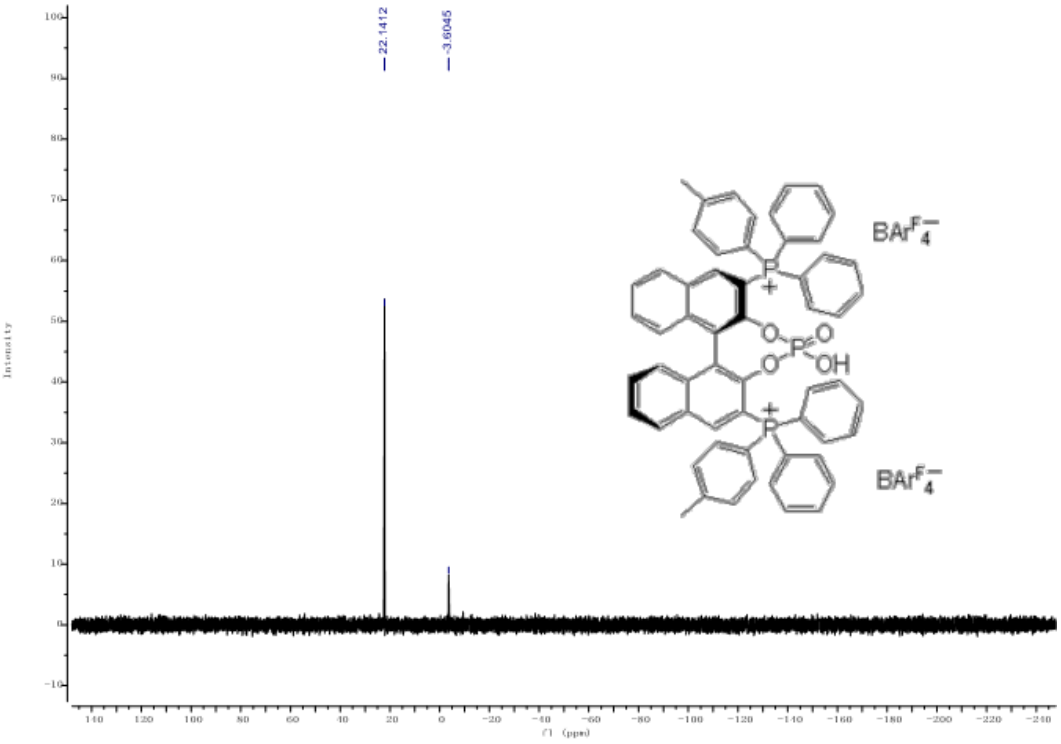
22.1412
-3.6045
Intensity
f1 (ppm)
BAr$^{F}_{4}^{-}$
BAr$^{F}_{4}^{-}$
OH

Figure S18. ^{1}H, ^{13}C and ^{19}F NMR of 2,2,2-trifluoro-1-(1H-indole-3-yl)-1-phenylethanol (**5a**).

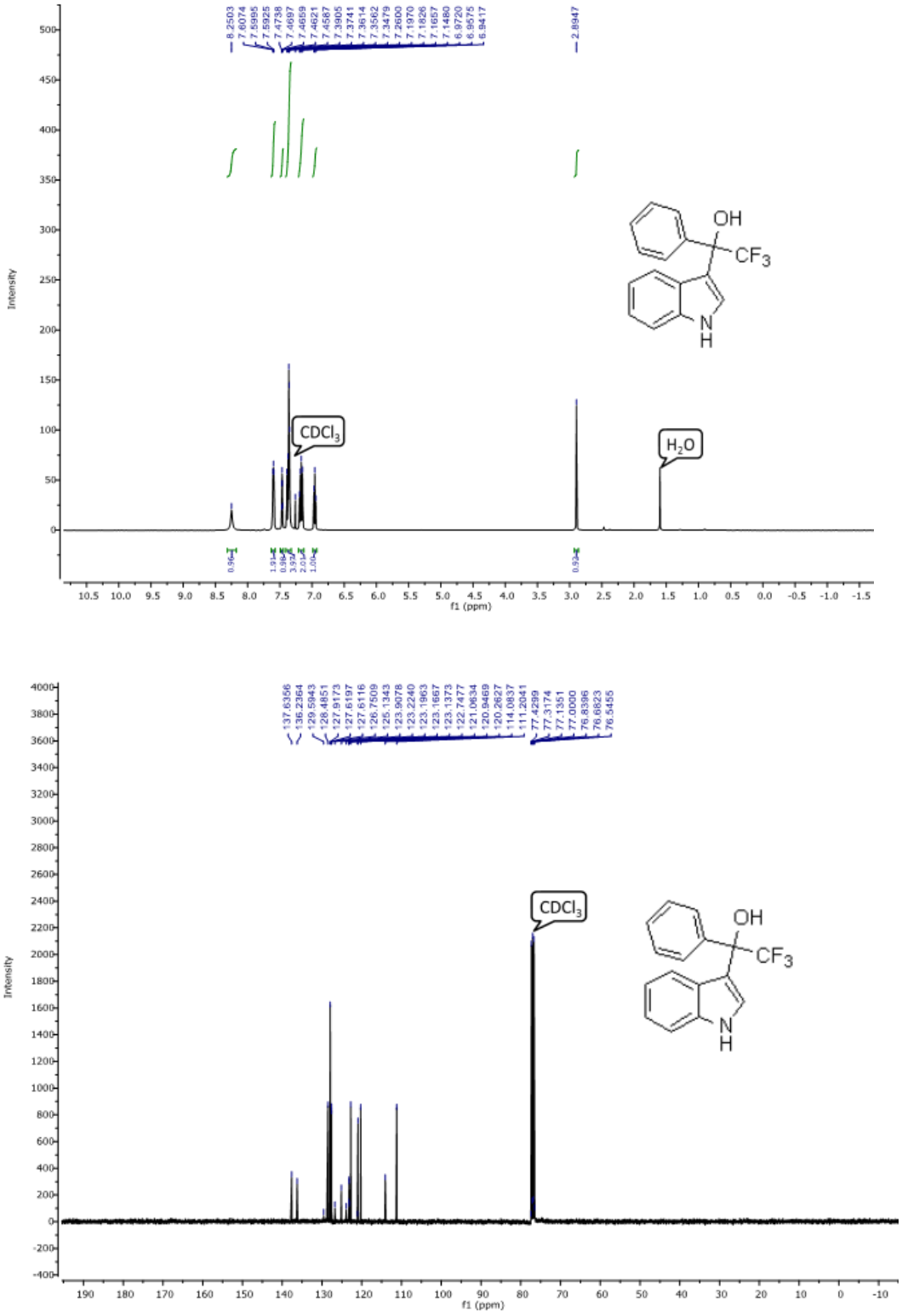

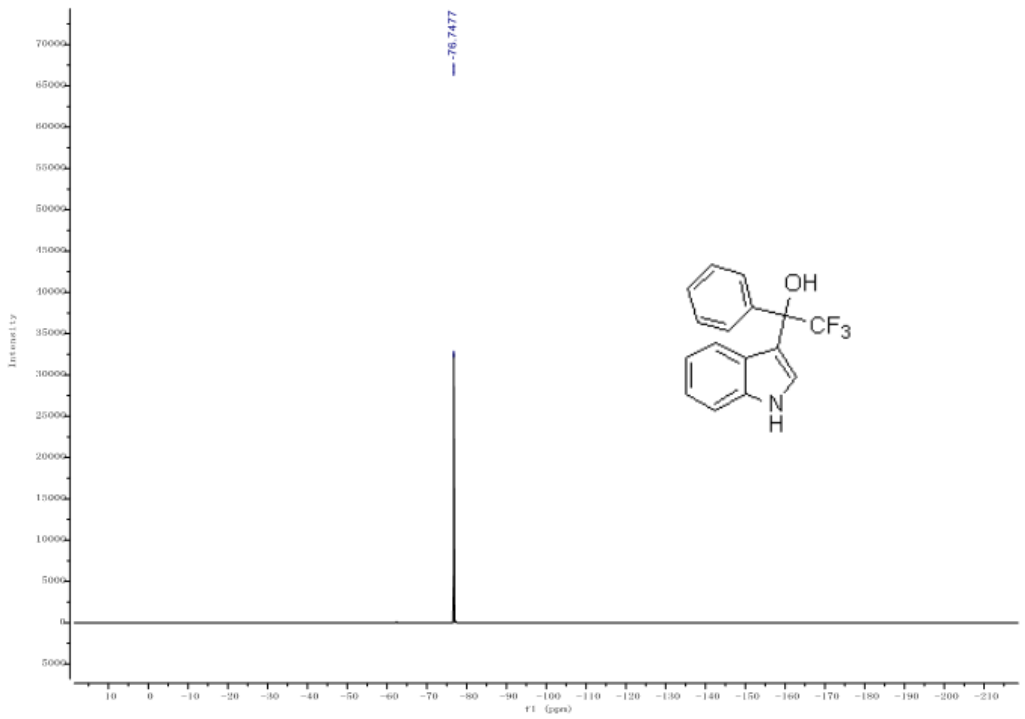

Figure S19. ^{1}H, ^{13}C and ^{19}F NMR of 3-(2,2,2-trifluoro-1-(1H-indole-3-yl)-1-phenylyl)-1H-indole (**6**).

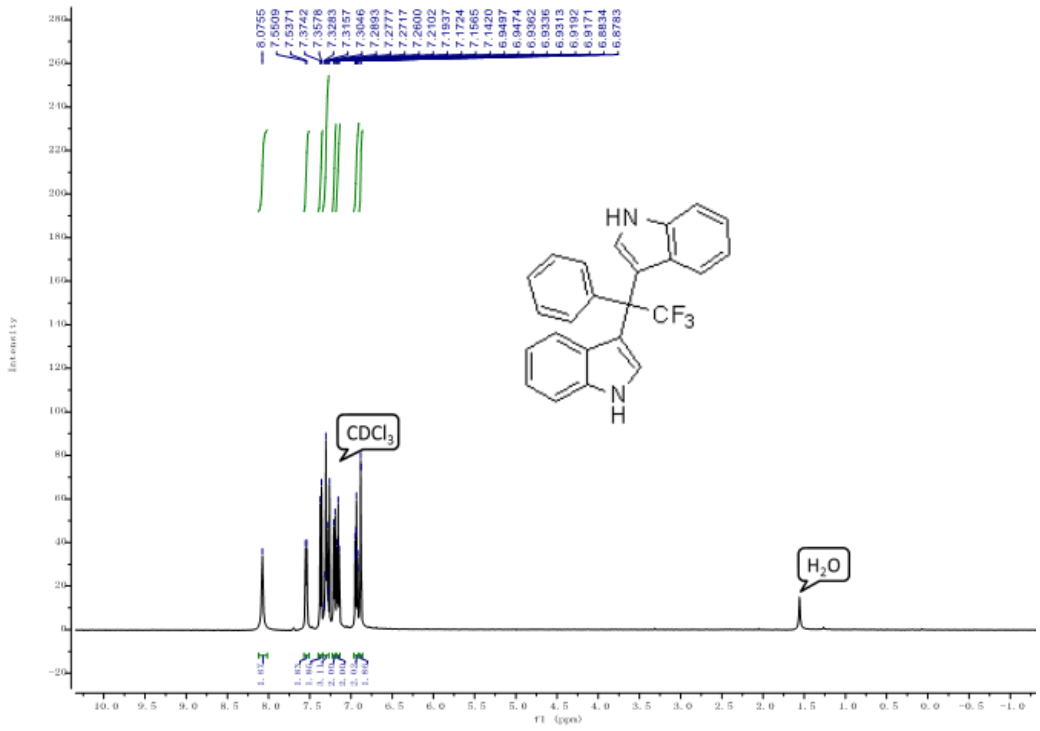

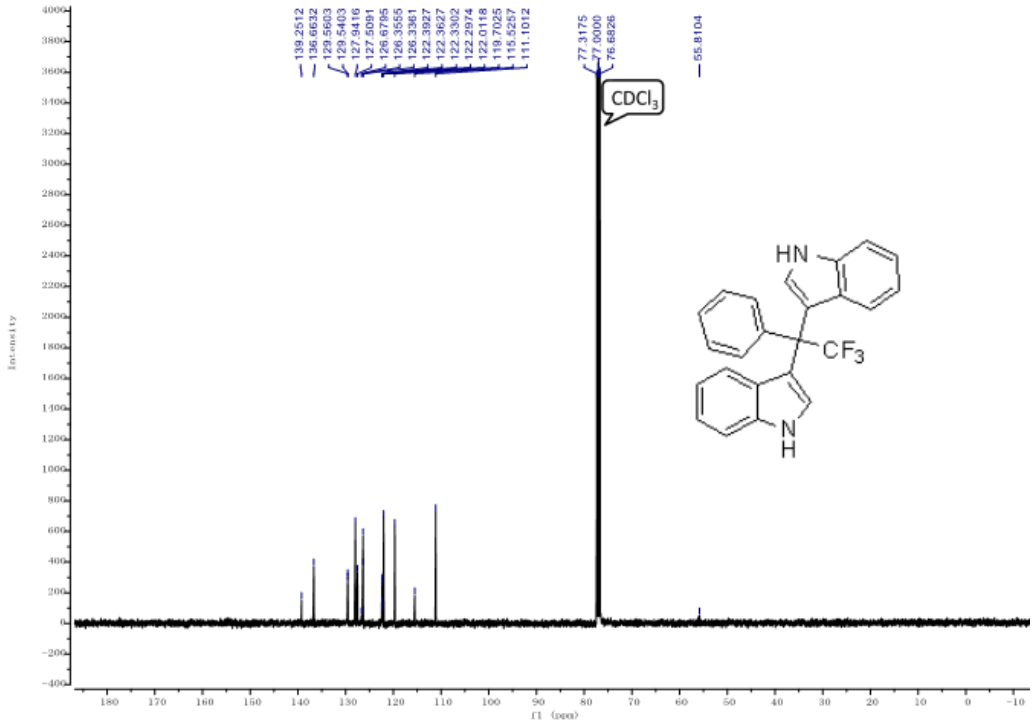
139.2512
136.6632
129.5603
129.5403
127.9416
127.5091
126.6795
126.3555
126.3361
122.3927
122.3627
122.3392
122.2974
122.0118
119.7025
115.5257
111.1012
77.3175
77.0000
76.6826
55.8104
CDCl3
HN
CF3
N
H
Intensity
f1 (ppm)

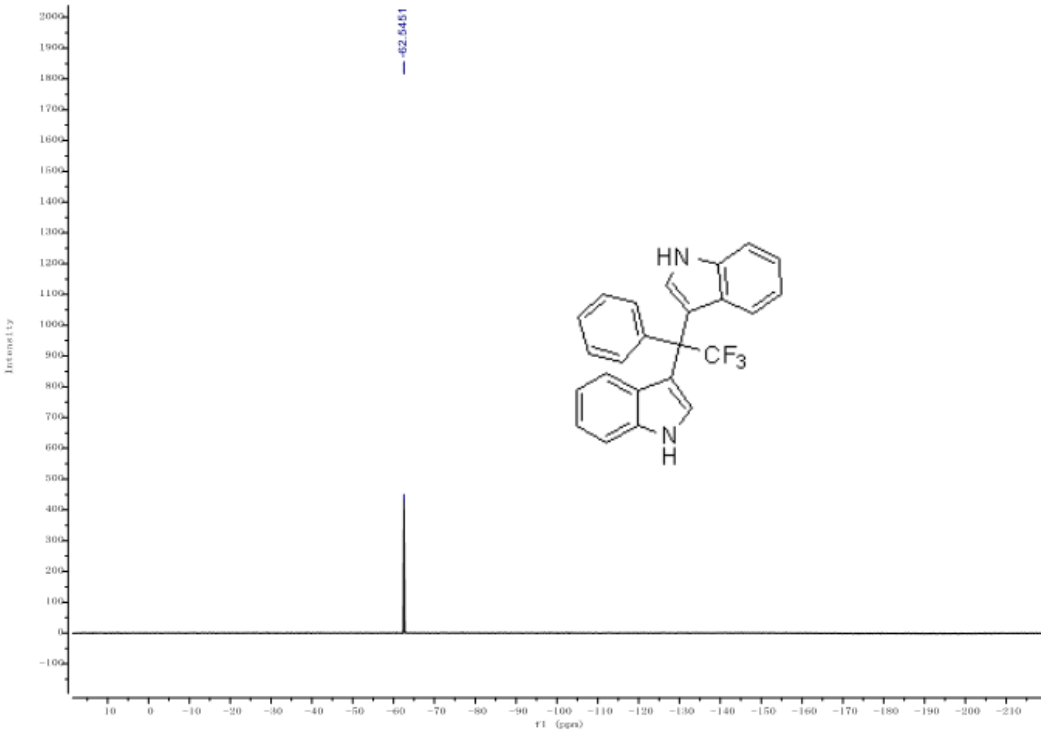
-62.5451
HN
CF3
N
H
Intensity
f1 (ppm)

Figure S20. ^{1}H, ^{13}C and ^{19}F NMR of 2,2,2-trifluoro-1-(5-fluoro-1H-indole-3-yl)-1-phenylethanol (**5b**).

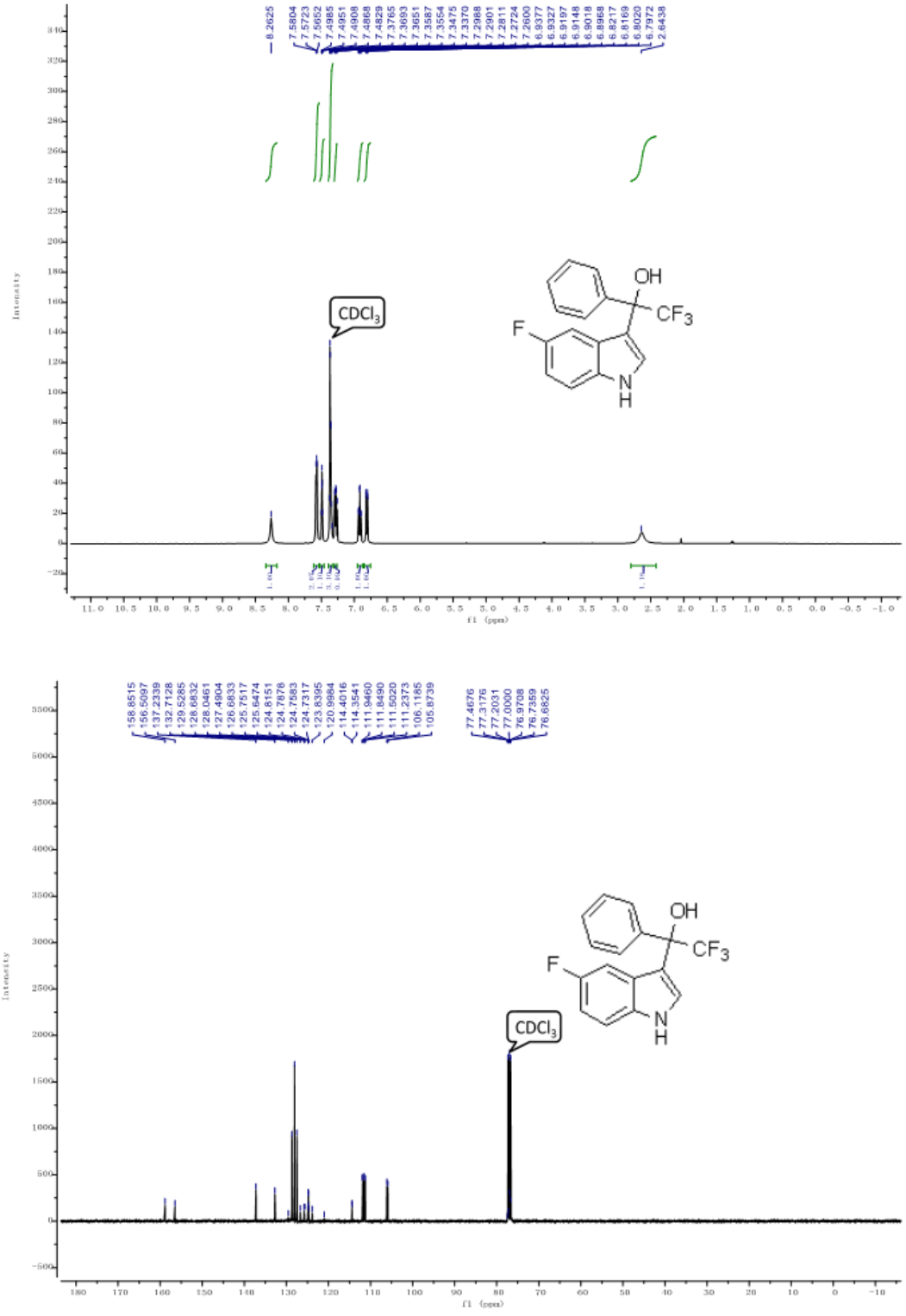

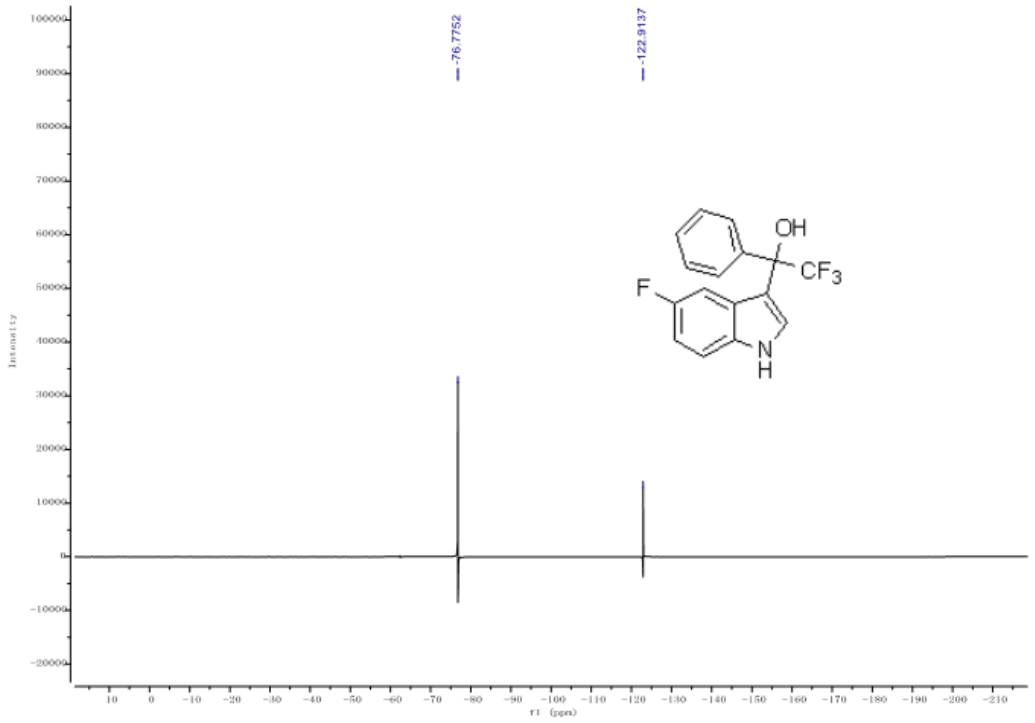

Figure S21. ^{1}H, ^{13}C and ^{19}F NMR of 2,2,2-trifluoro-1-(5-bromo-1H-indole-3-yl)-1-phenylethanol (**5c**).

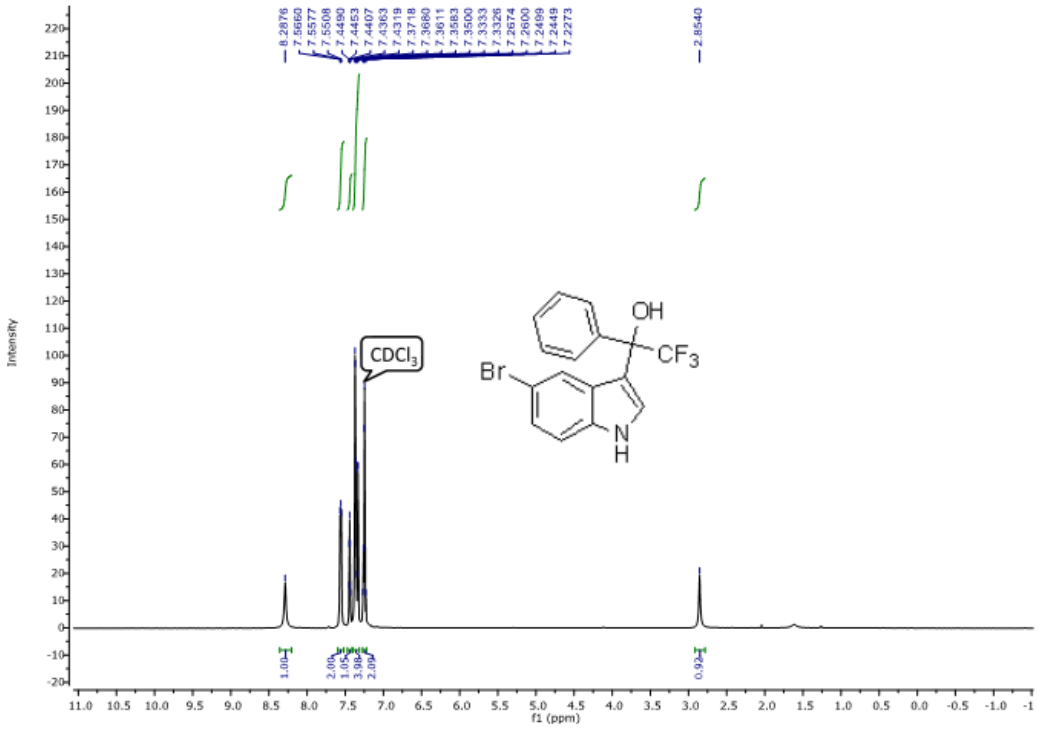

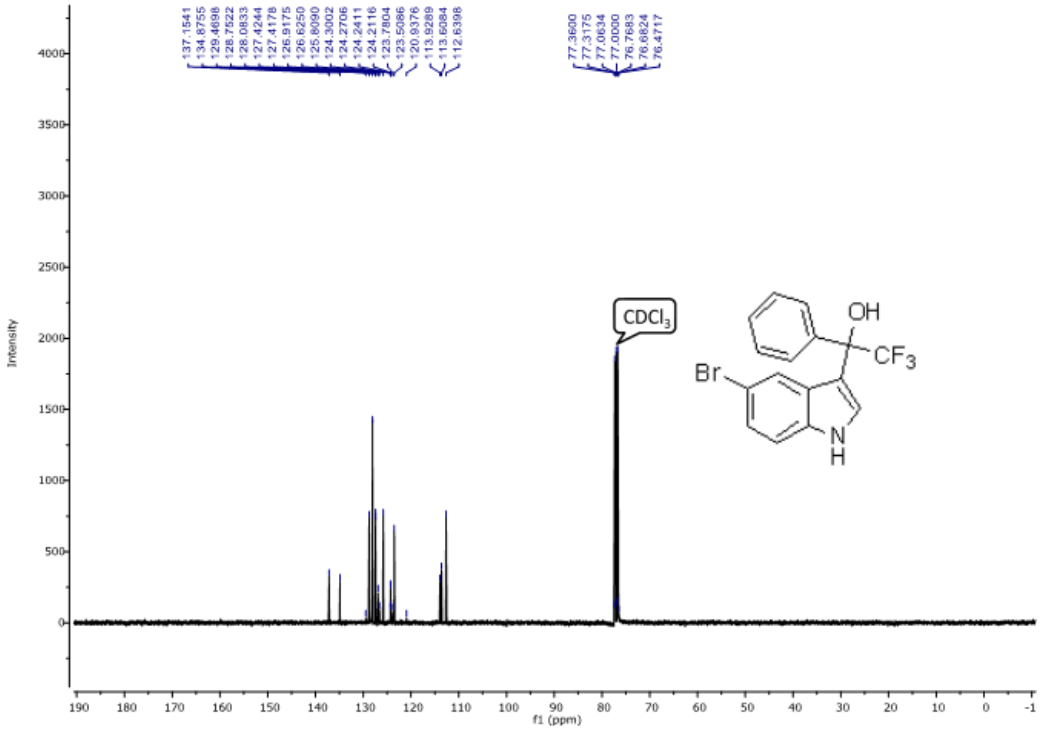
137.1541
134.8755
129.4698
128.7522
128.0833
127.4244
127.4178
126.9175
126.6250
125.8090
124.3002
124.2706
124.2411
124.2116
123.7804
123.5086
120.9376
113.9289
113.6084
112.6398
77.3600
77.3175
77.0634
77.0000
76.7683
76.6824
76.4717
CDCl3
OH
CF3
Br
N
H
Intensity
f1 (ppm)

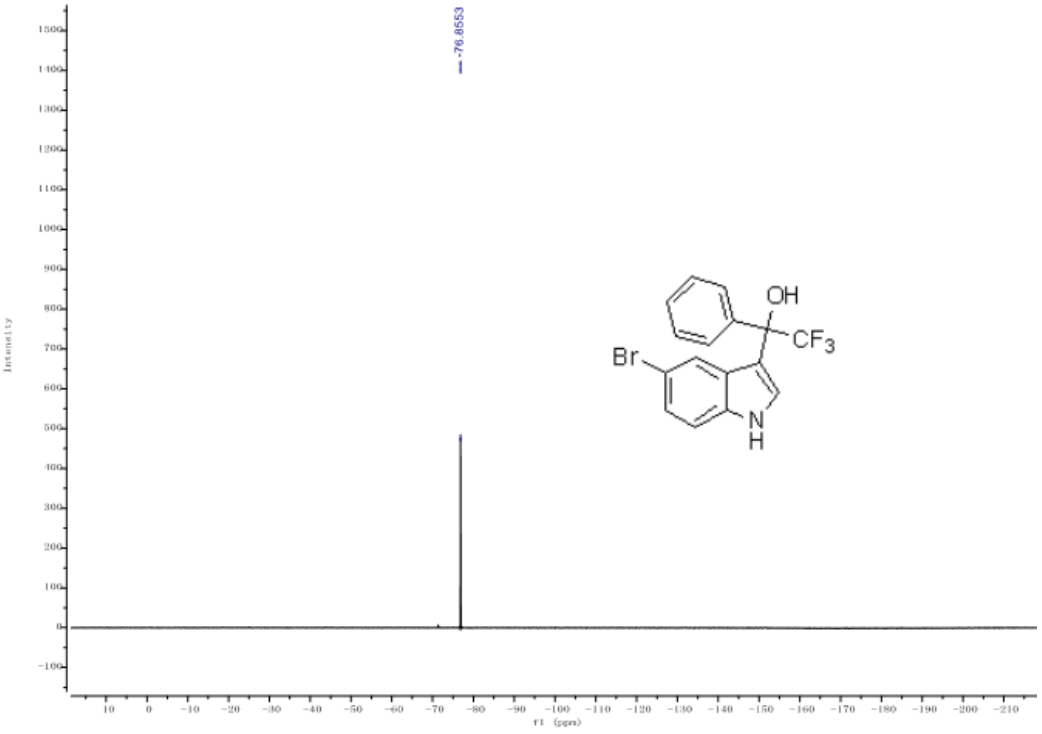
-76.8553
OH
CF3
Br
N
H
Intensity
f1 (ppm)

Figure S22. ^{1}H, ^{13}C and ^{19}F NMR of 2,2,2-trifluoro-1-(5-methoxyl-1H-indole-3-yl)-1-phenyl-ethanol (**5d**).

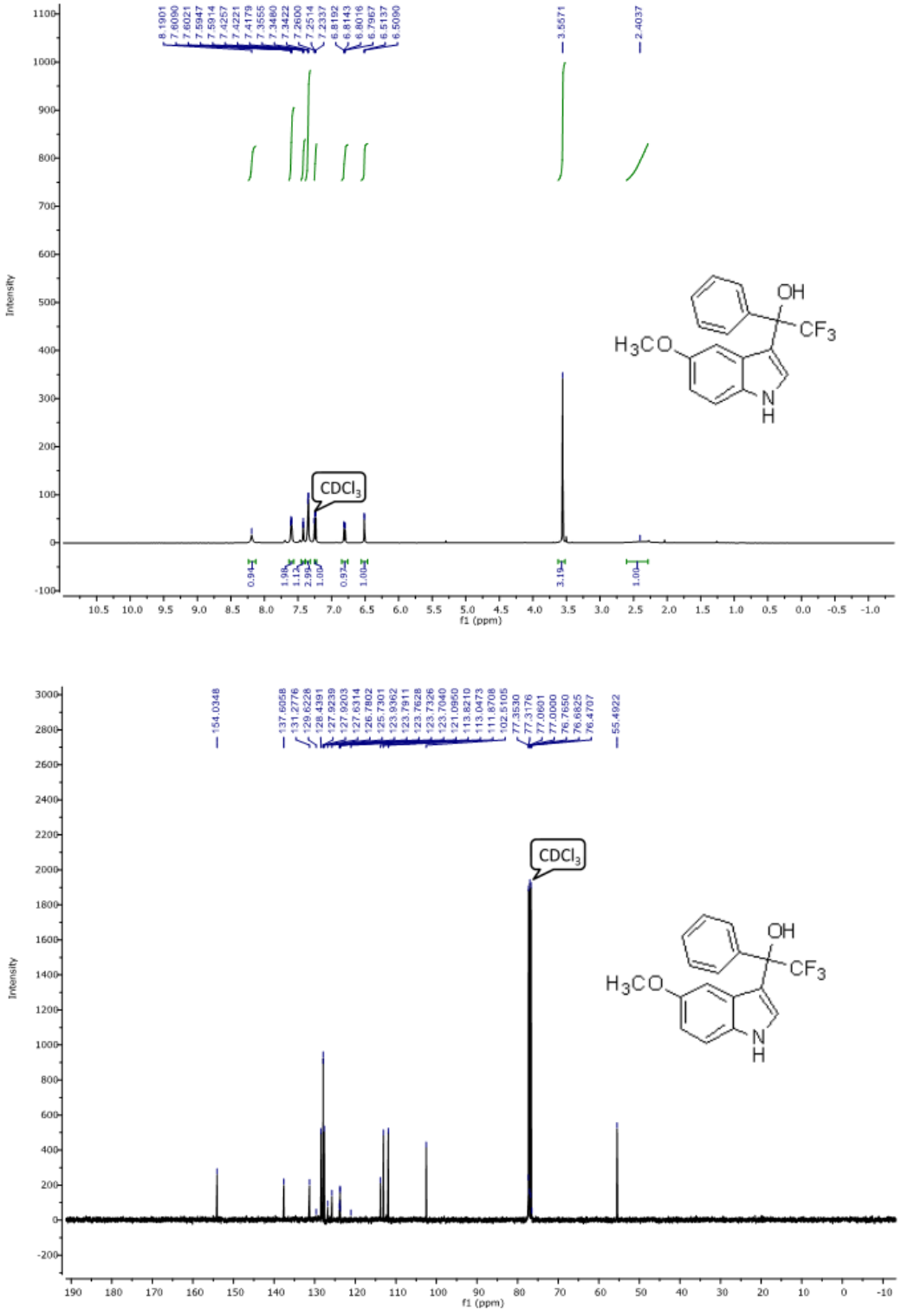

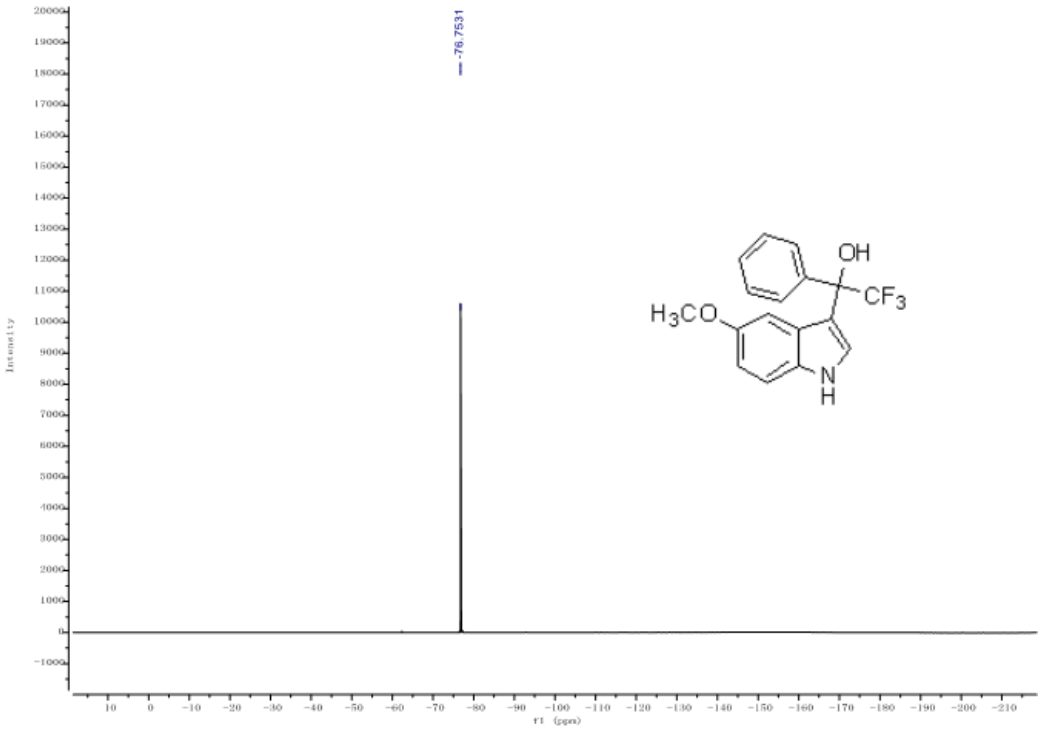

Figure S23. ^{1}H, ^{13}C and ^{19}F NMR of 2,2,2-trifluoro-1-(6-methyl-1H-indole-3-yl)-1-phenylethanol (**5e**).

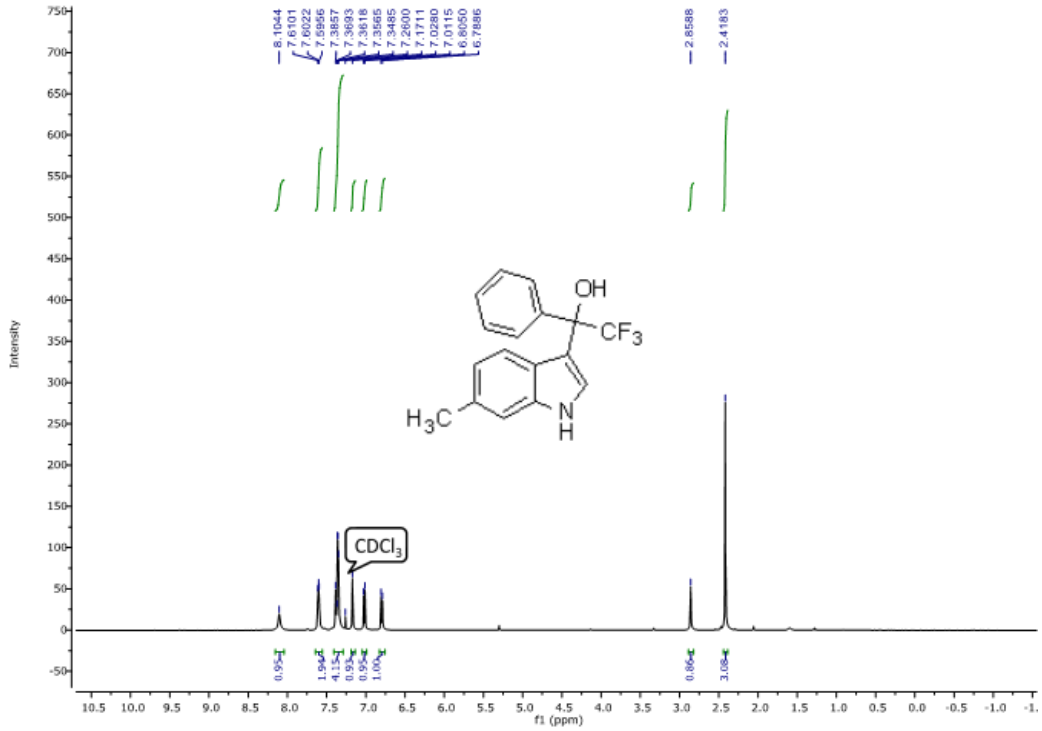

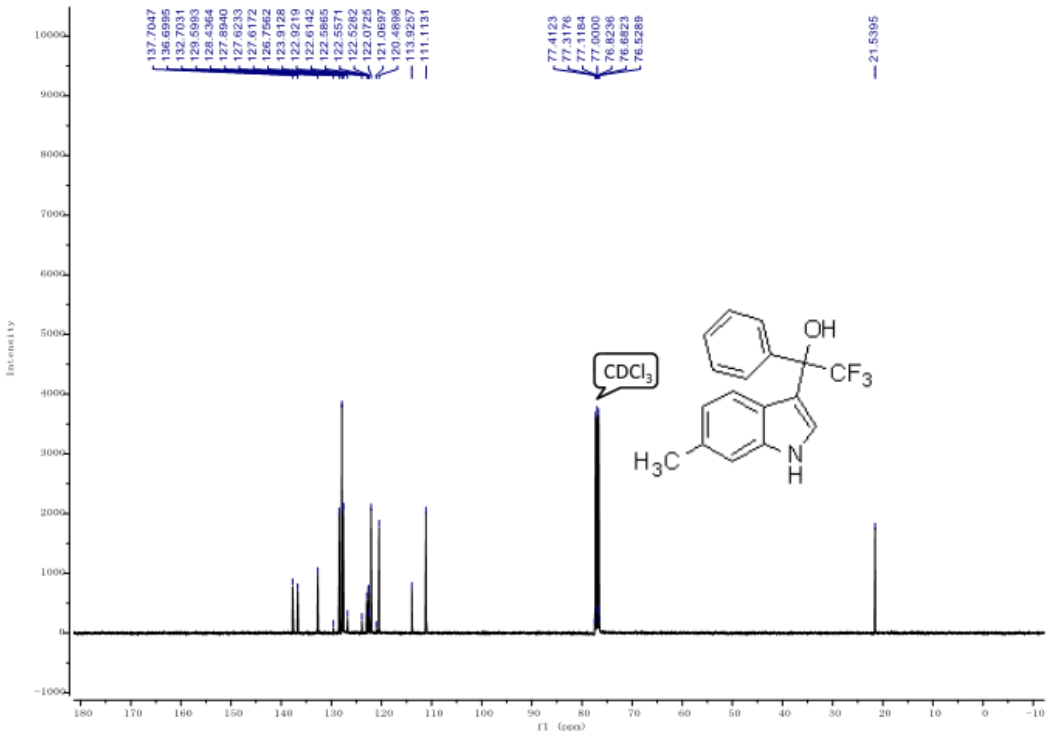
137.7047
136.6995
132.7031
129.5993
128.4364
127.8940
127.6233
127.6172
126.7562
123.9128
122.9219
122.6142
122.5865
122.5571
122.5262
122.0725
121.0697
120.4898
113.9257
111.1131
77.4123
77.3176
77.1184
77.0000
76.8236
76.6923
76.5289
21.5395
CDCl3
OH
CF3
H3C
N
H
Intensity
f1 (ppm)

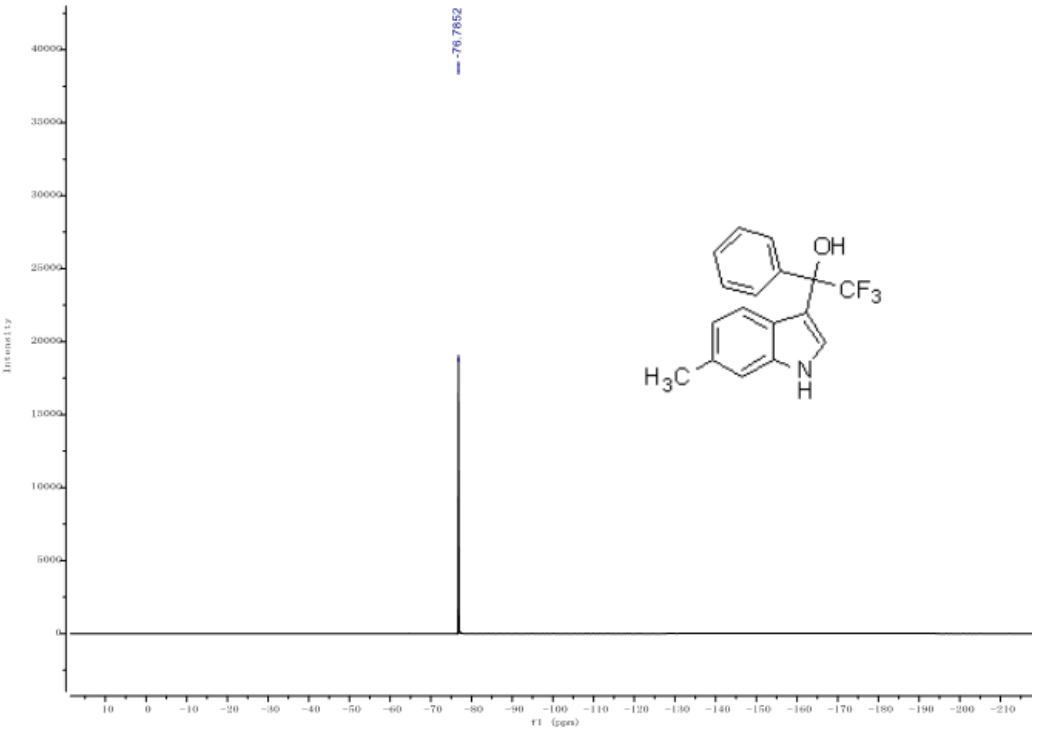
-76.7852
OH
CF3
H3C
N
H
Intensity
f1 (ppm)

Figure S24. ^{1}H, ^{13}C and ^{19}F NMR of 2,2,2-trifluoro-1-(7-chloro-1H-indole-3-yl)-1-phenylethanol (**5f**).

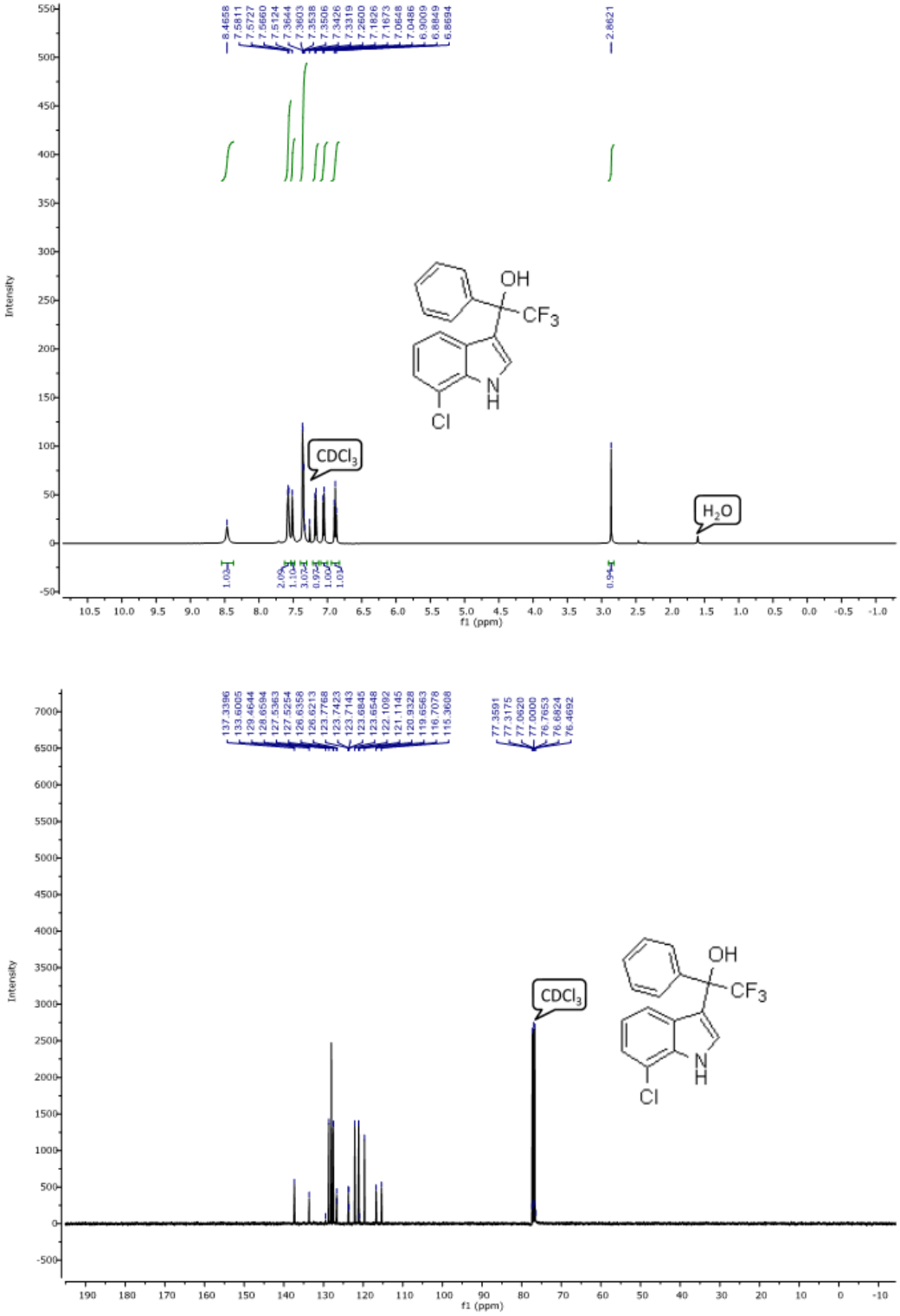

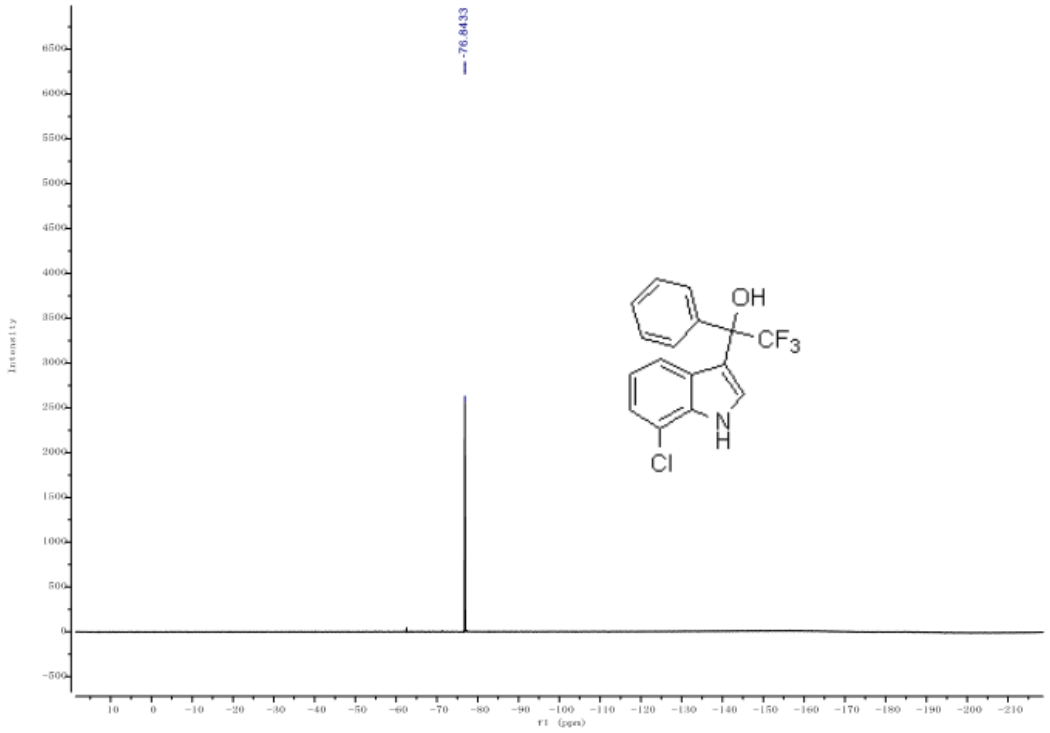

Figure S25. ^{1}H, ^{13}C and ^{19}F NMR of 2,2,2-trifluoro-1-(7-bromo-1H-indole-3-yl)-1-phenylethanol (**5g**).

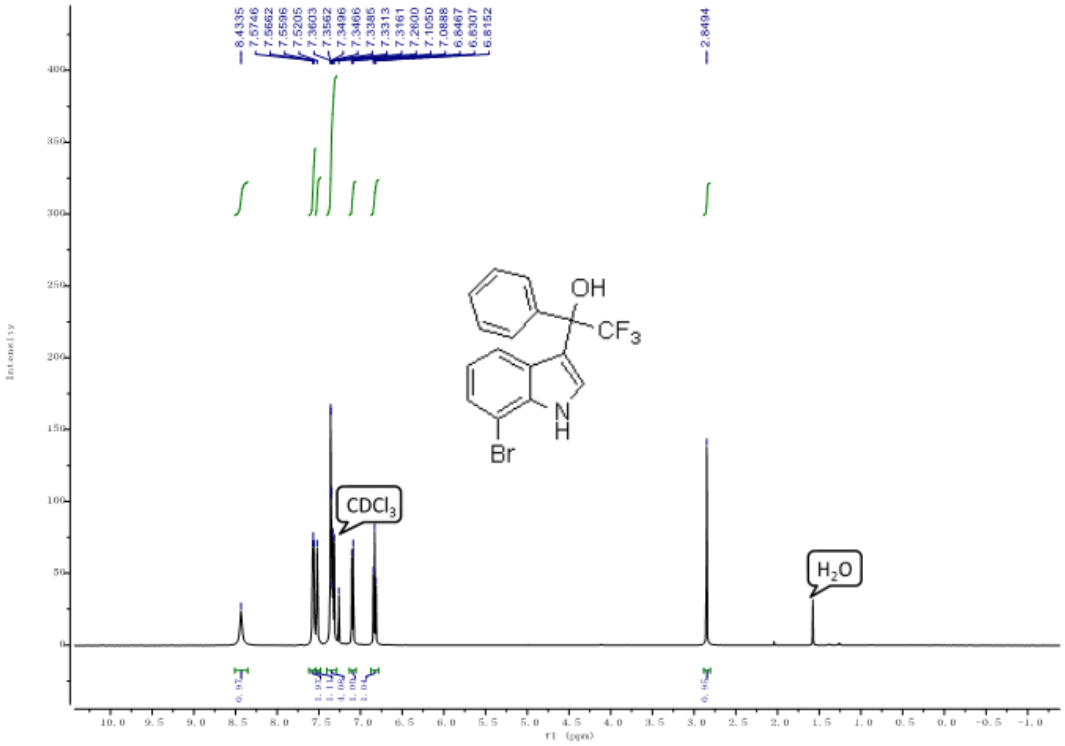

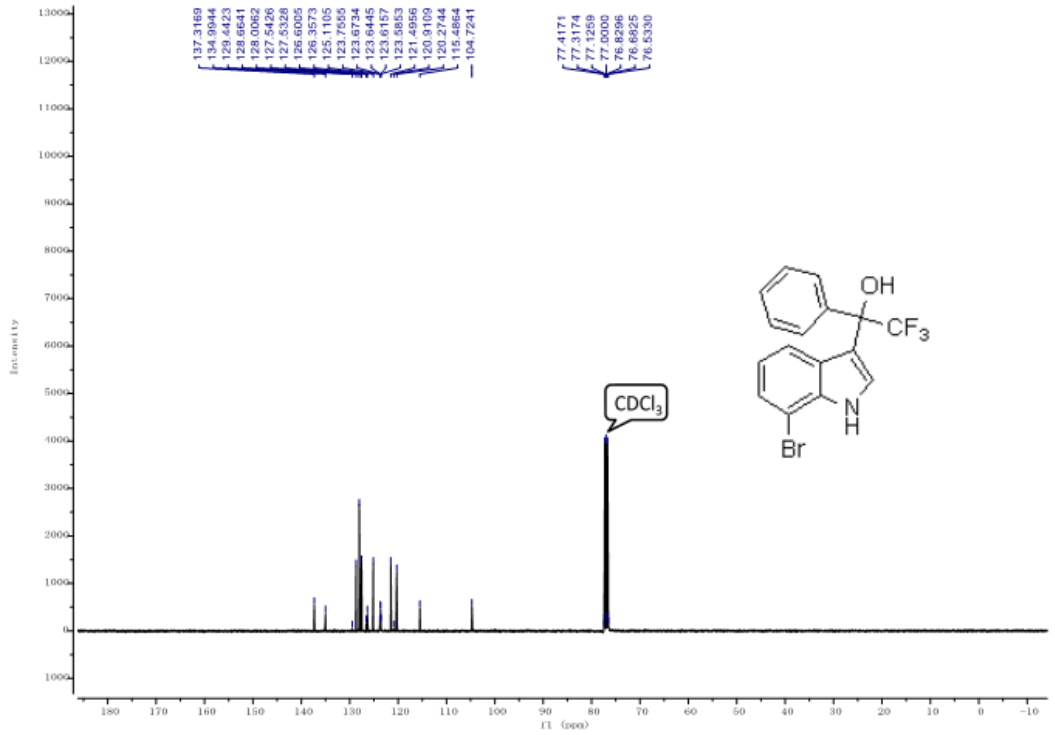
137.3169
134.9944
129.4423
128.6641
128.0062
127.5426
127.5328
126.6005
126.3573
125.1105
123.7555
123.6734
123.6445
123.6157
123.5853
121.4956
120.9109
120.2744
115.4864
104.7241
77.4171
77.3174
77.1259
77.0000
76.8296
76.6825
76.5330
CDCl3
OH
CF3
N
H
Br
Intensity
f1 (ppm)

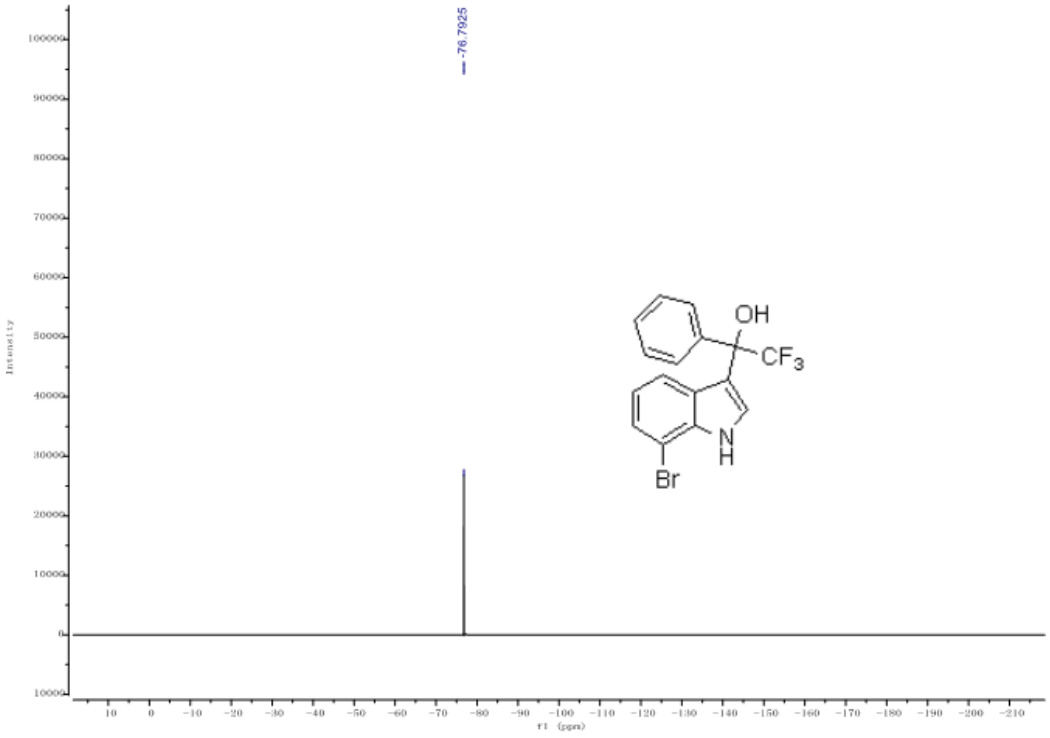
-76.7925
OH
CF3
N
H
Br
Intensity
f1 (ppm)

Figure S26. ^{1}H, ^{13}C and ^{19}F NMR of 2,2,2-trifluoro-1-(7-methyl-1H-indole-3-yl)-1-phenylethanol (**5h**).

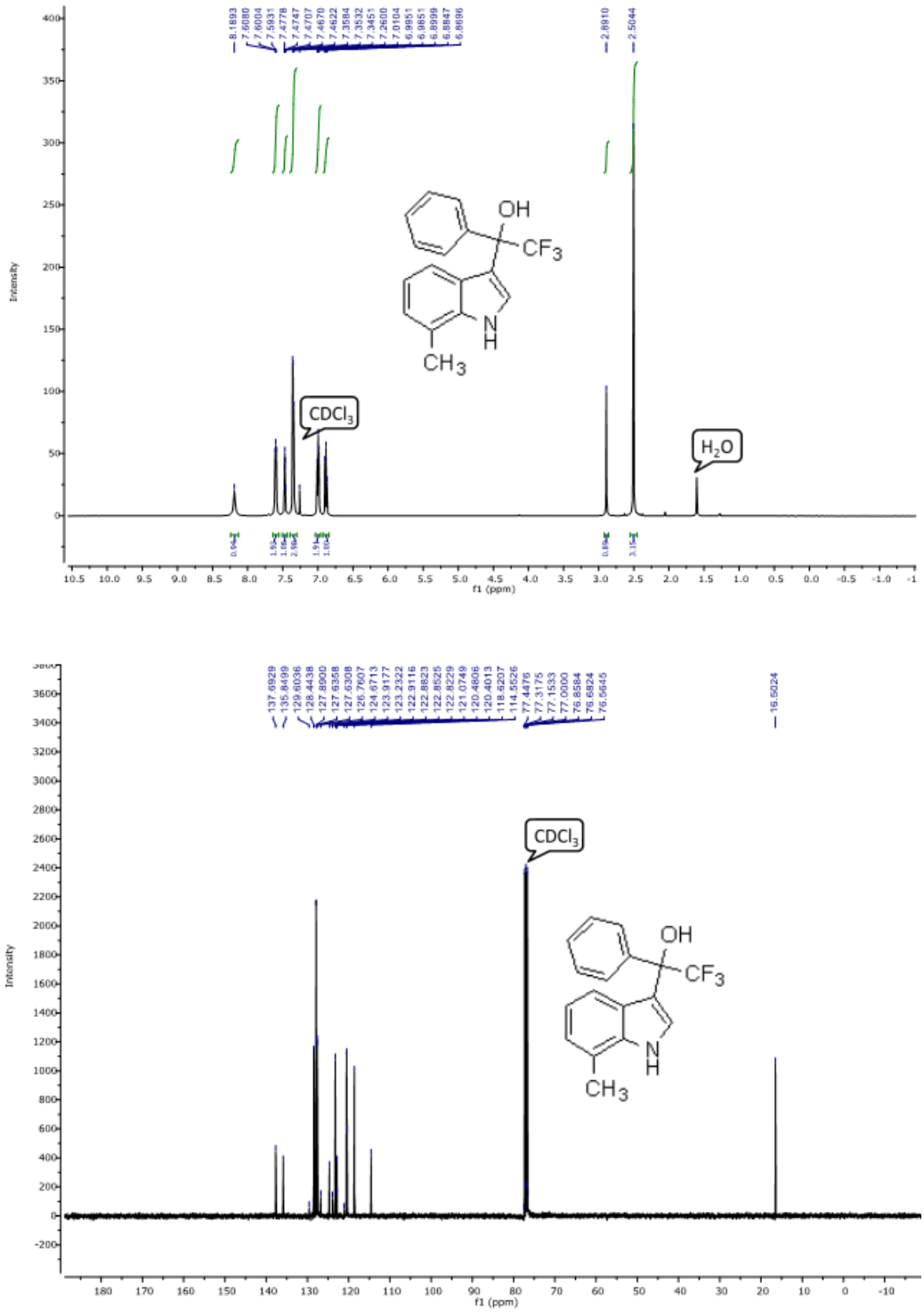

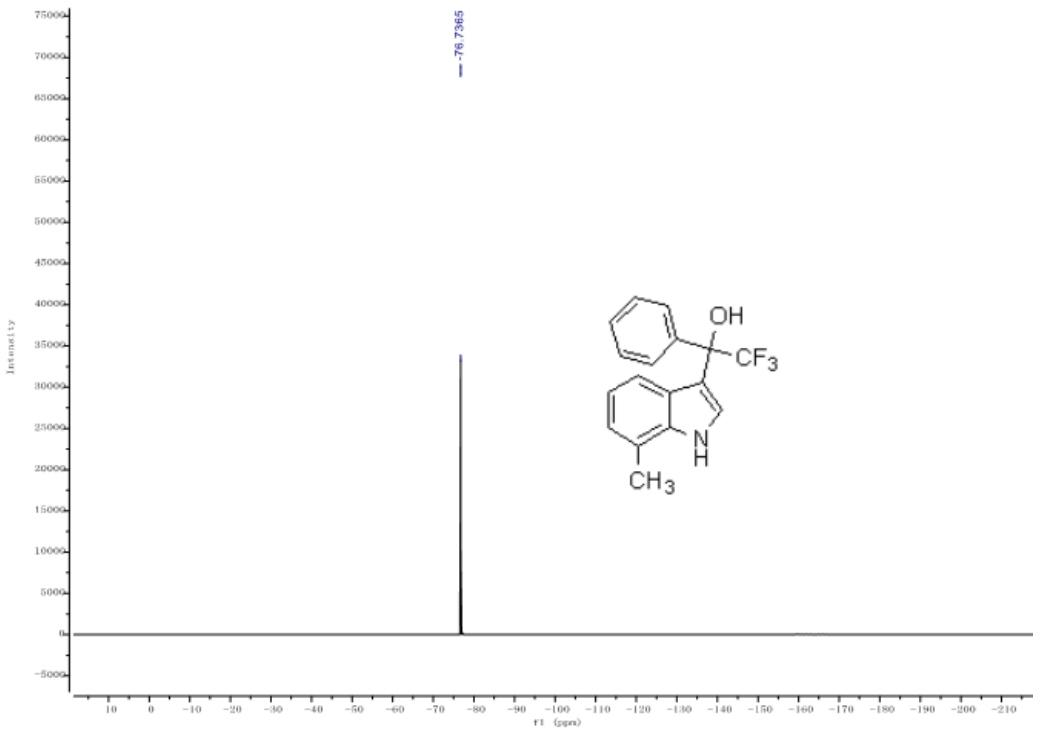

Figure S27. ^{1}H, ^{13}C and ^{19}F NMR of 2,2,2-trifluoro-1-(7-ethyl-1H-indole-3-yl)-1-phenylethanol (**5i**).

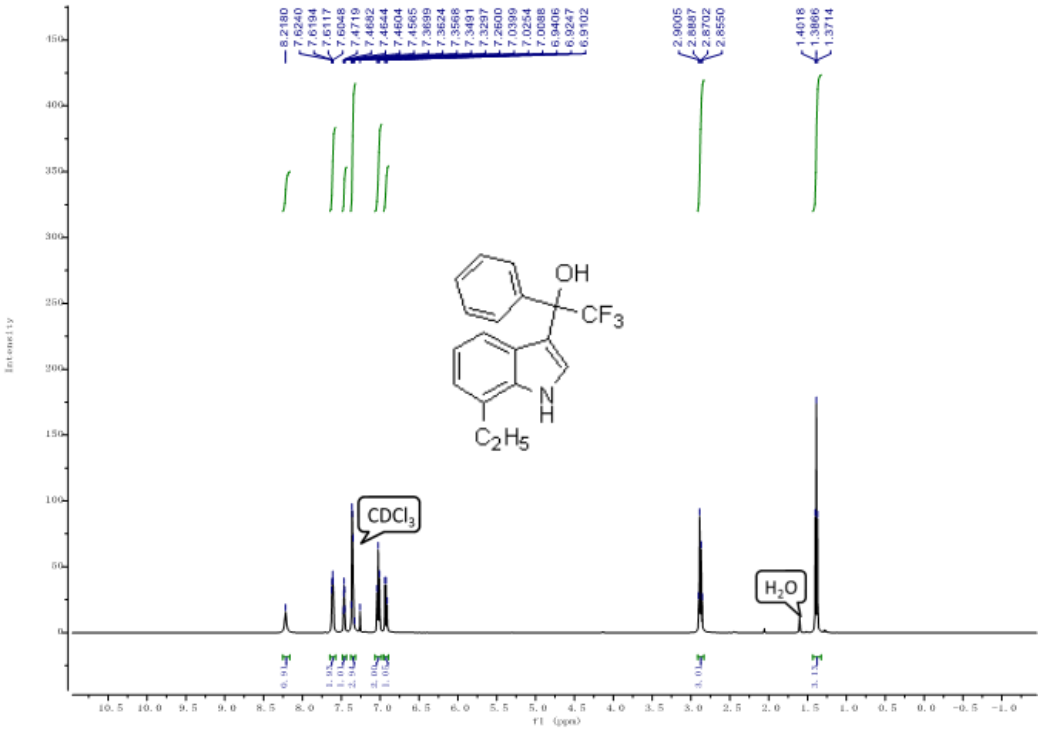

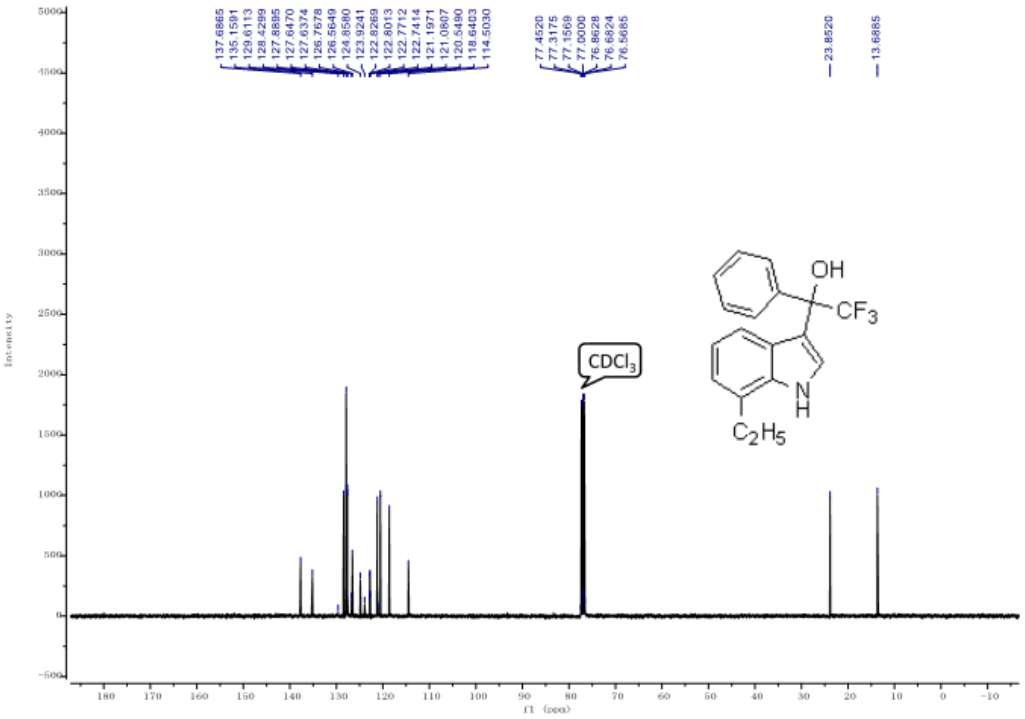
137.6865
135.1591
129.6113
128.4299
127.8885
127.6470
127.6374
126.7678
126.5649
124.8580
123.9241
122.8269
122.8013
122.7712
122.7414
121.1971
121.0807
120.5490
118.6403
114.5030
77.4520
77.3175
77.1569
77.0000
76.8628
76.6824
76.5685
23.8520
13.6885
CDCl3
OH
CF3
N
H
C2H5
Intensity
f1 (ppm)

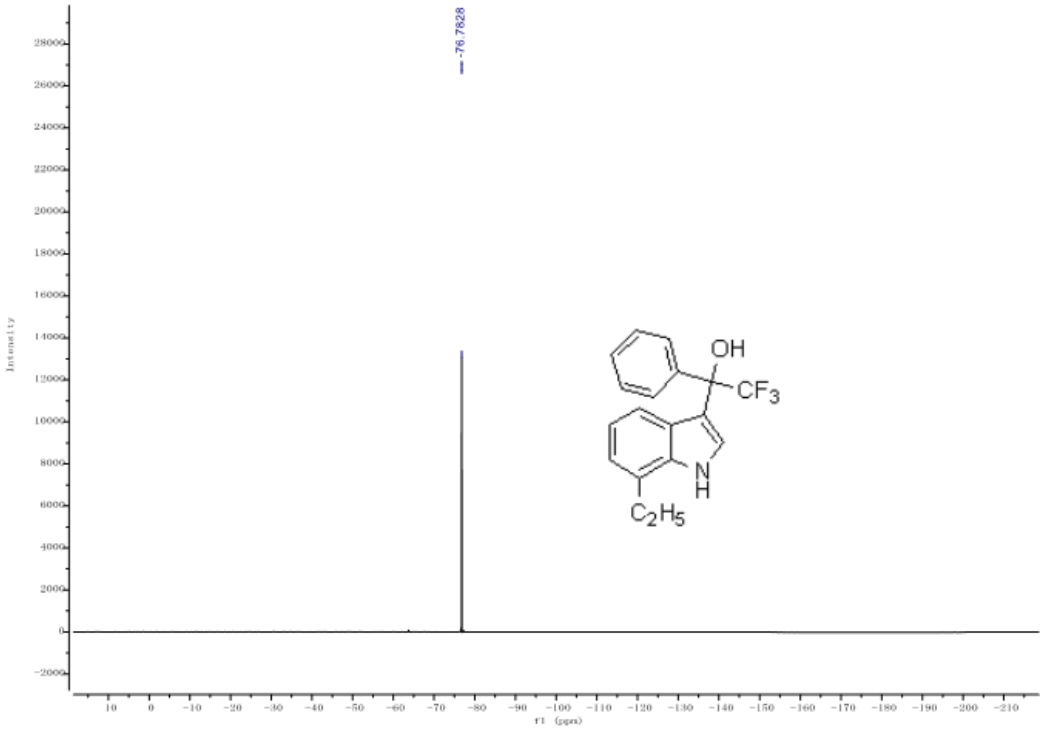
-76.7828
OH
CF3
N
H
C2H5
Intensity
f1 (ppm)

Figure S28. ^{1}H, ^{13}C and ^{19}F NMR of 2,2,2-trifluoro-1-(4-fluorophenyl)-1-(1H-indole-3-yl)ethanol (**5j**).

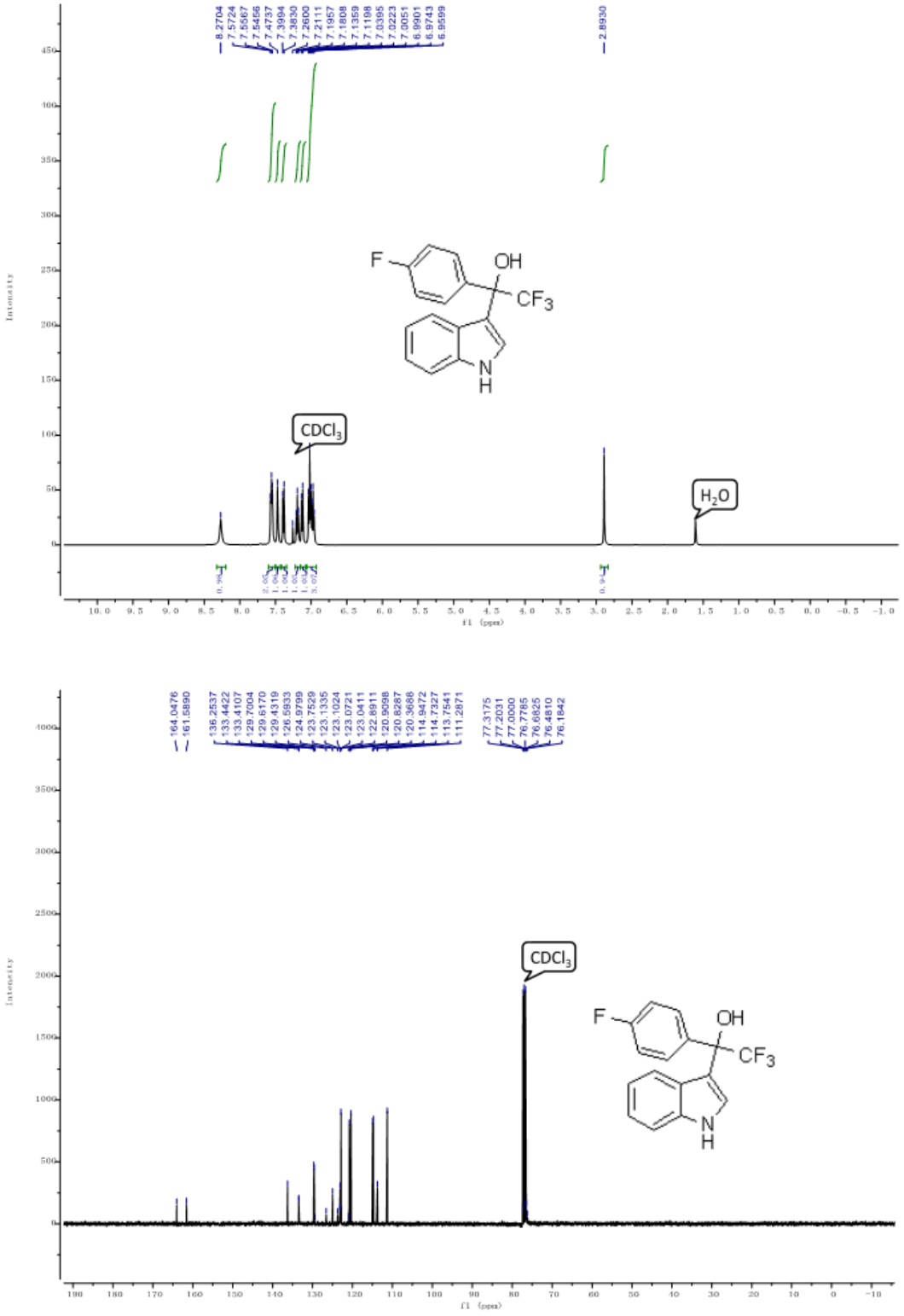

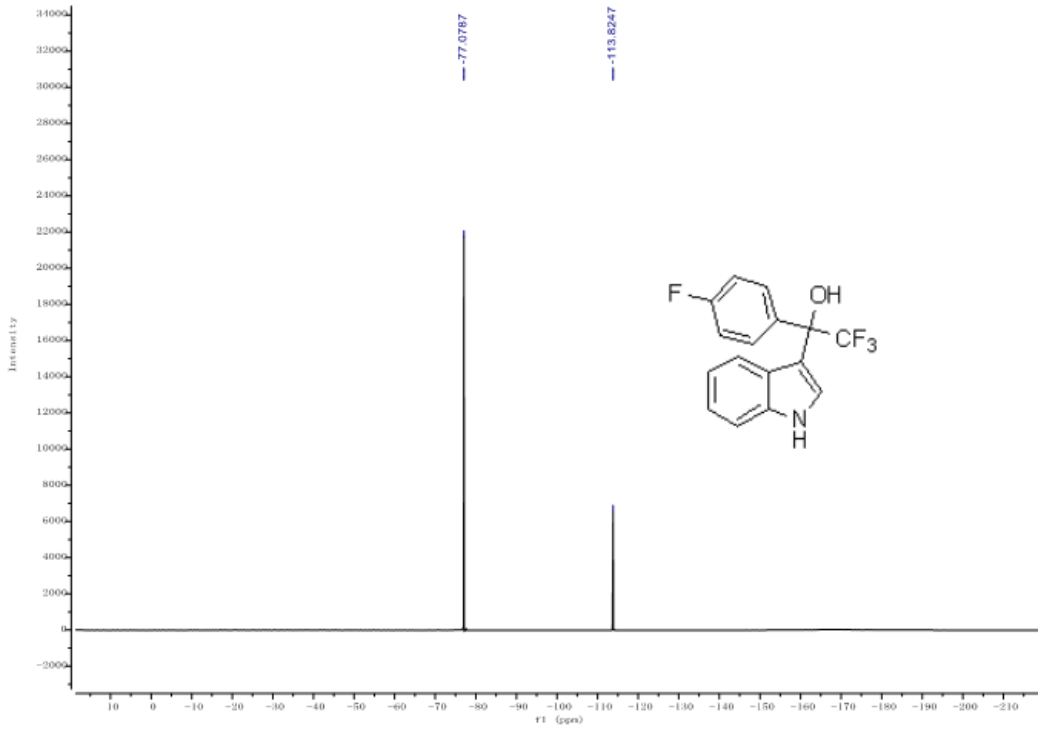

Figure S29. ^{1}H, ^{13}C and ^{19}F NMR of 1-(4-chlorophenyl)-2,2,2-trifluoro-1-(1H-indole-3-yl)ethanol (**5k**).

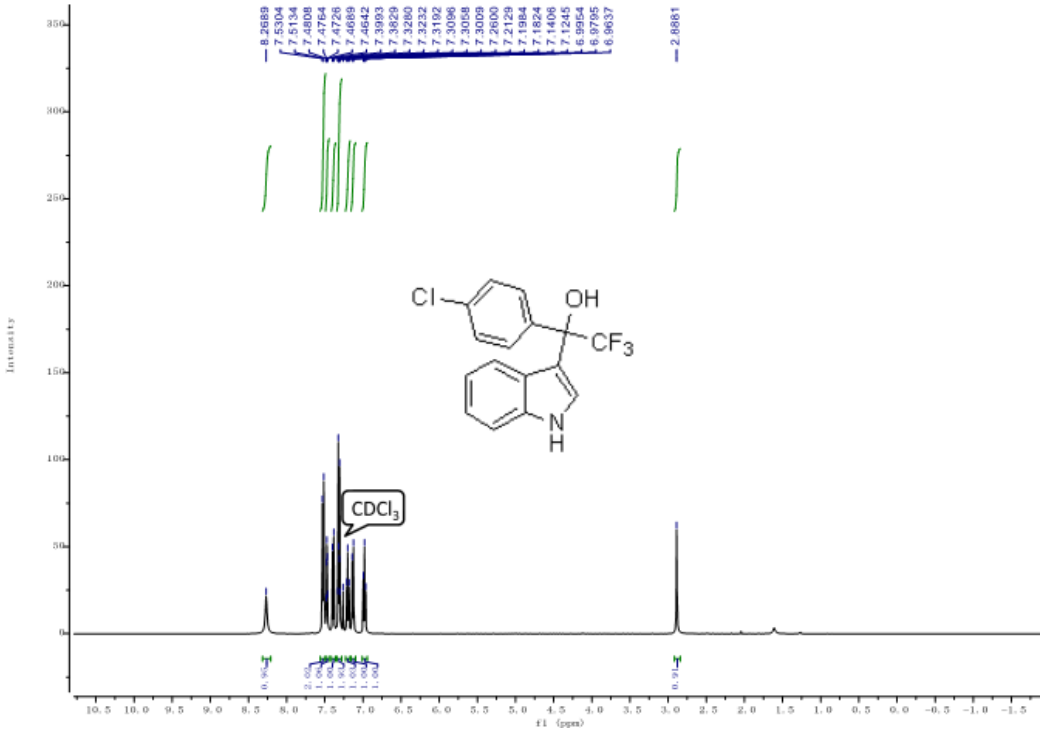

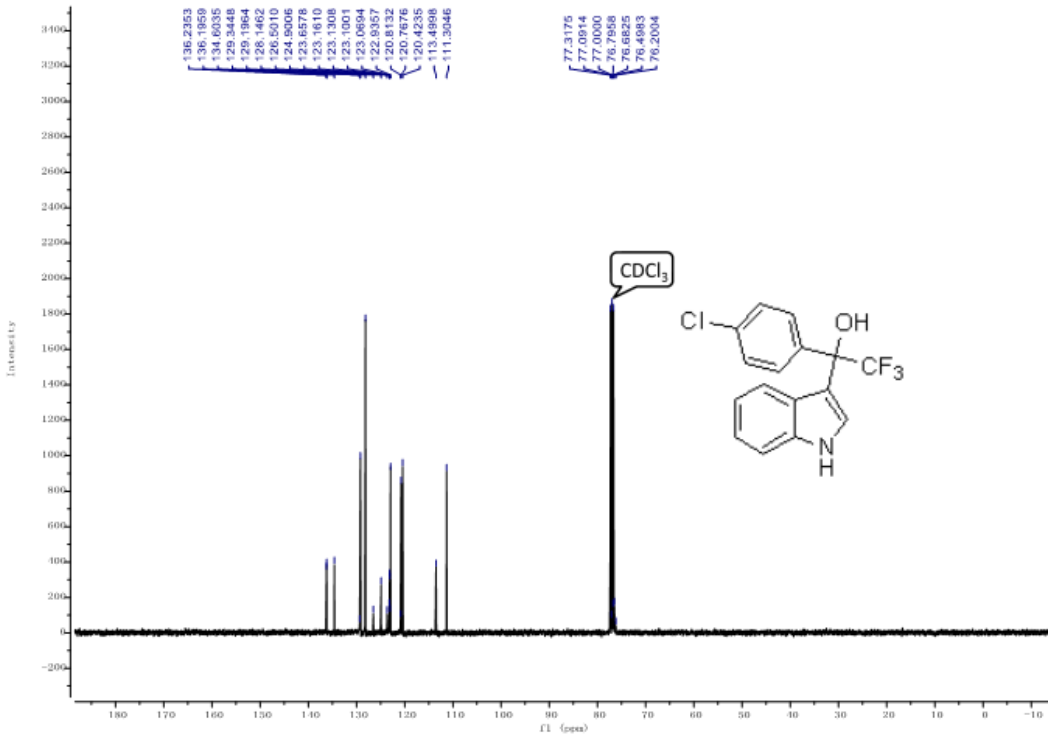
136.2353
136.1959
134.6035
129.3448
129.1964
128.1462
126.5010
124.9006
123.6578
123.1610
123.1308
123.1001
123.0694
122.9357
120.8132
120.7676
120.4235
113.4998
111.3046
77.3175
77.0914
77.0000
76.7958
76.6825
76.4983
76.2004
CDCl3
Cl
OH
CF3
N
H
Intensity
f1 (ppm)

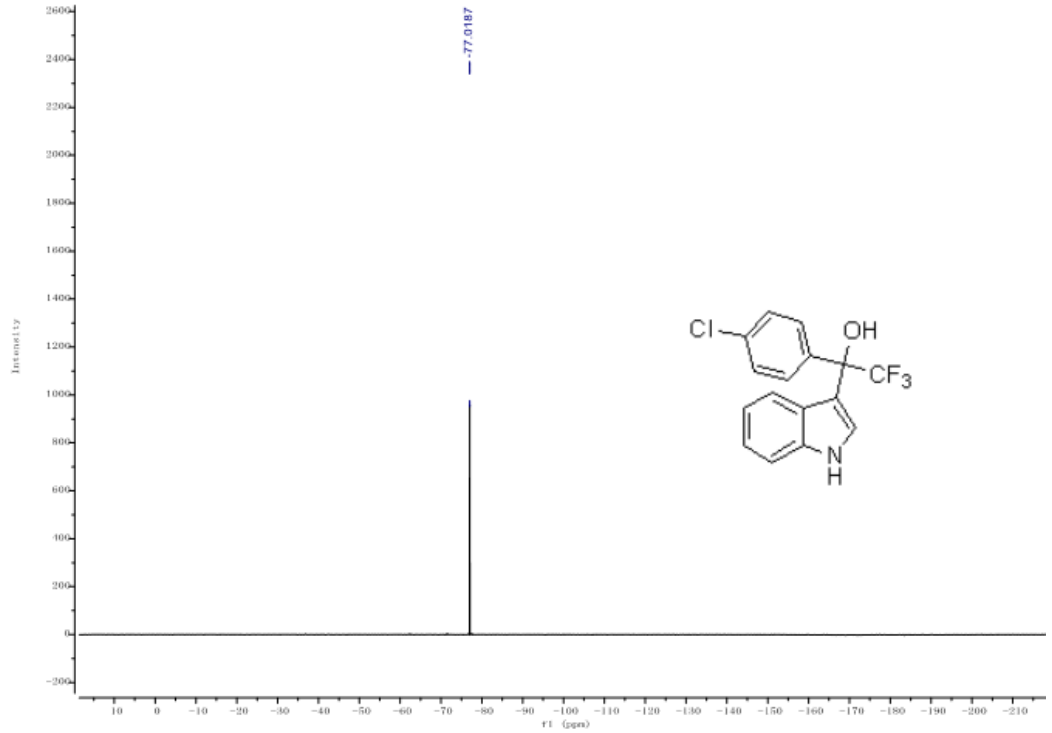
-77.0187
Cl
OH
CF3
N
H
Intensity
f1 (ppm)

Figure S30. ^{1}H, ^{13}C and ^{19}F NMR of 1-(4-bromophenyl)-2,2,2-trifluoro-1-(1H-indole-3-yl)ethanol (**5l**).

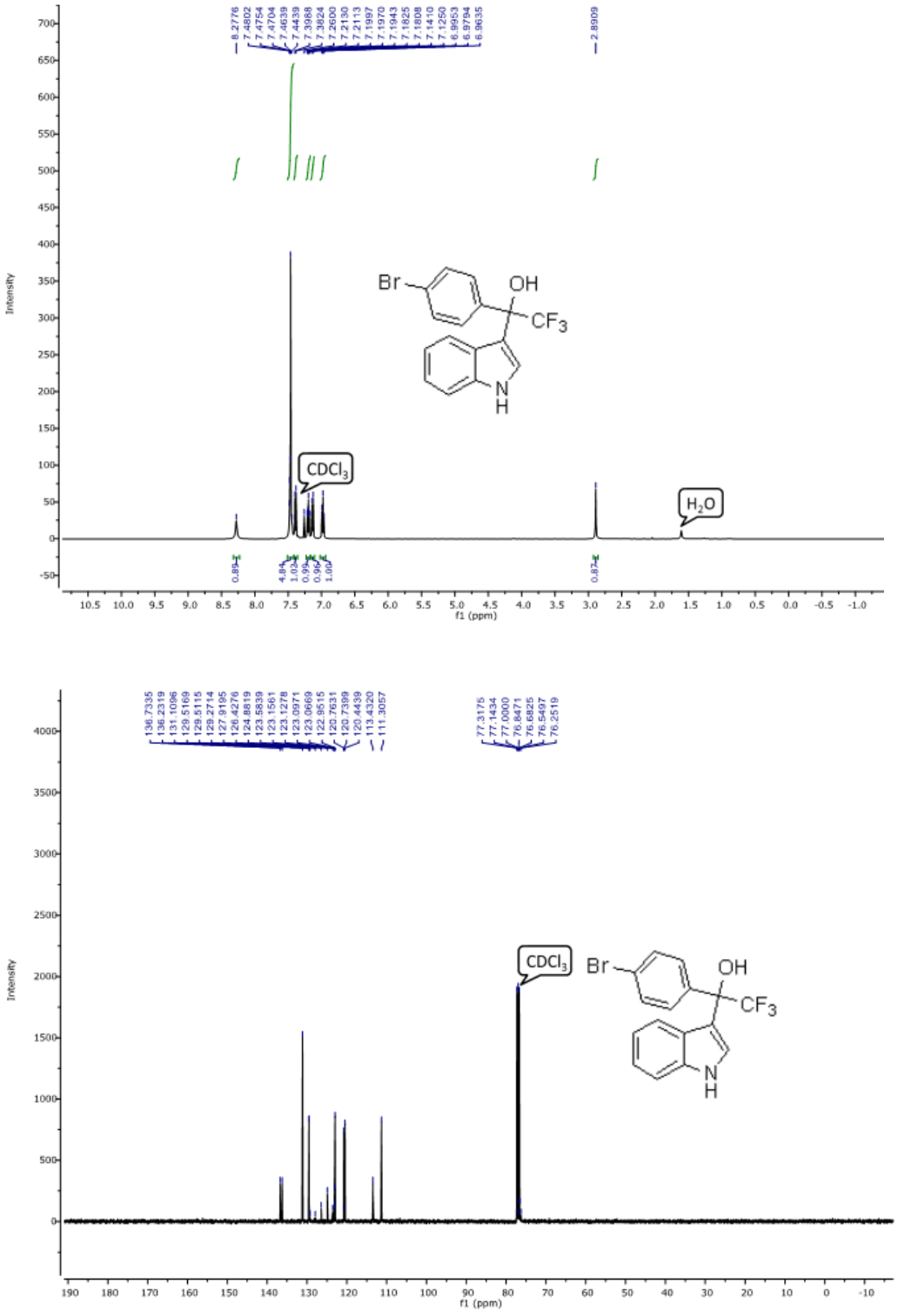

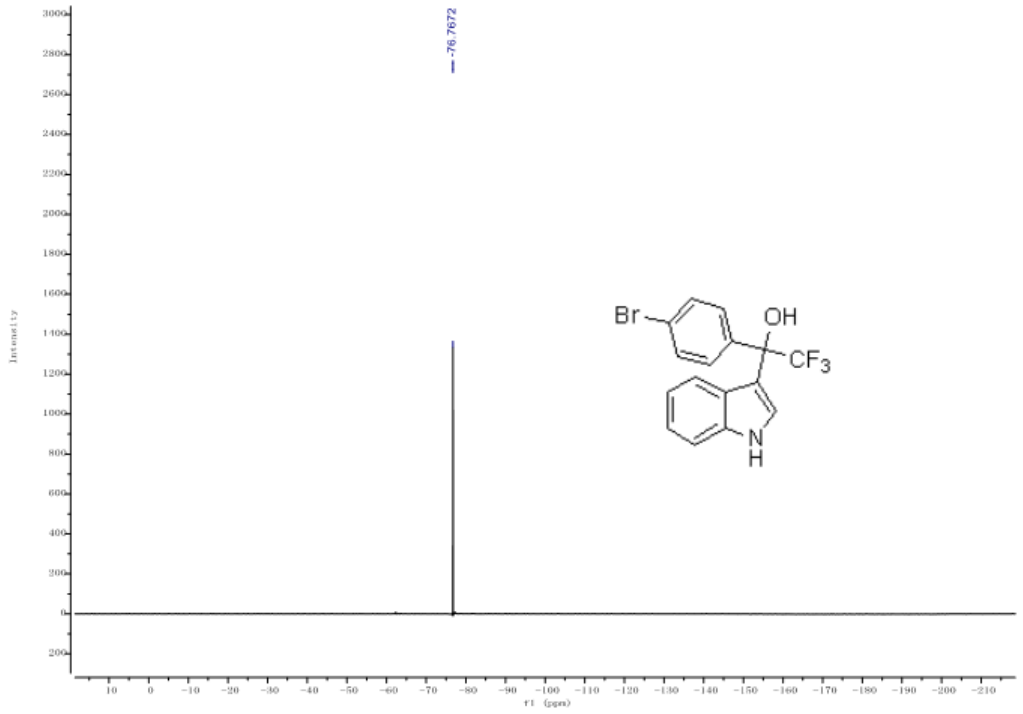

Figure S31. ^{1}H, ^{13}C and ^{19}F NMR of 2,2,2-trifluoro-1-(1H-indole-3-yl)-1-*p*-tolylethanol (**5m**).

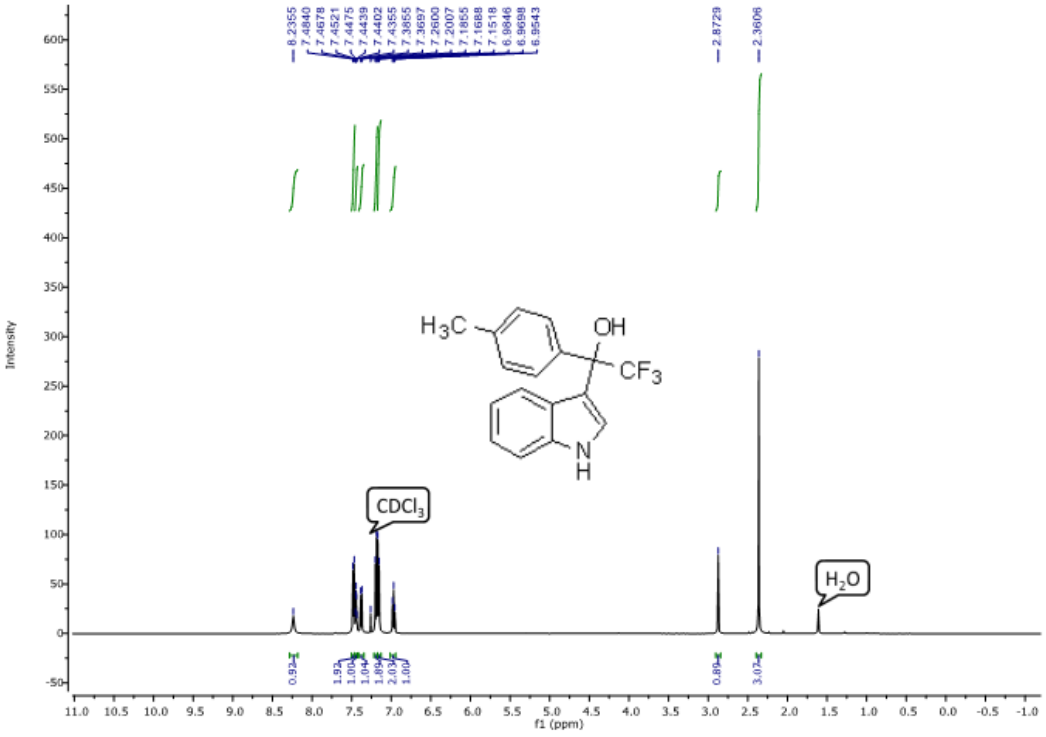

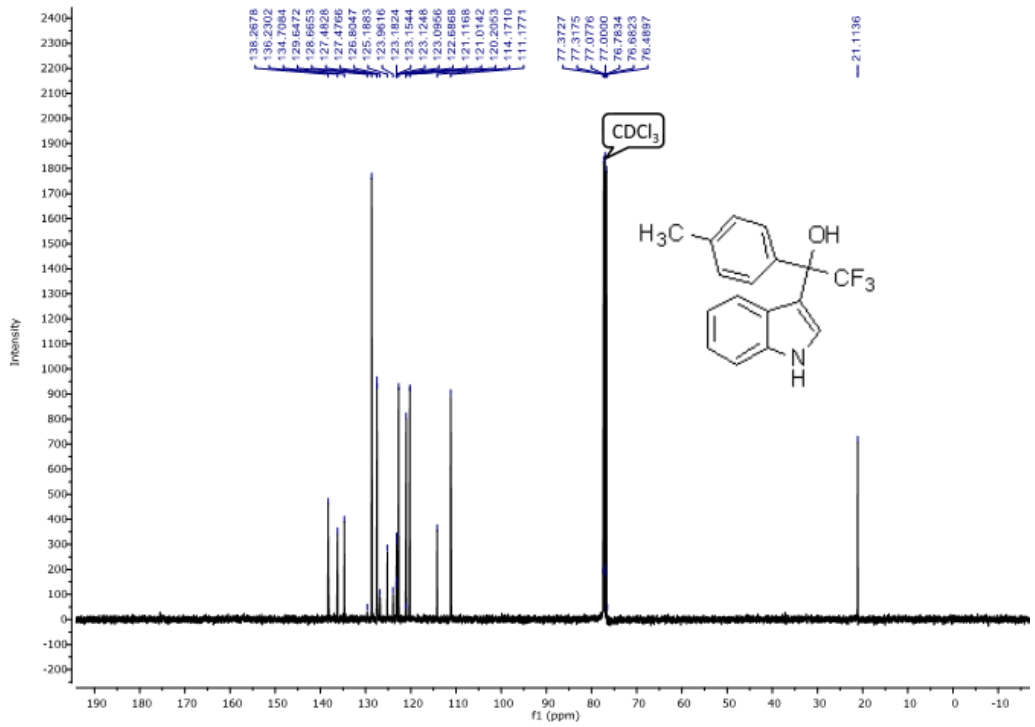
138.2678
136.2302
134.7084
129.6472
128.6653
127.4826
127.4766
126.8047
125.1883
123.9616
123.1824
123.1544
123.1248
123.0956
122.6868
121.1168
121.0142
120.2063
114.1710
111.1771
77.3727
77.3175
77.0776
77.0000
76.7834
76.6823
76.4897
21.1136
CDCl3
H3C
OH
CF3
N
H
Intensity
f1 (ppm)

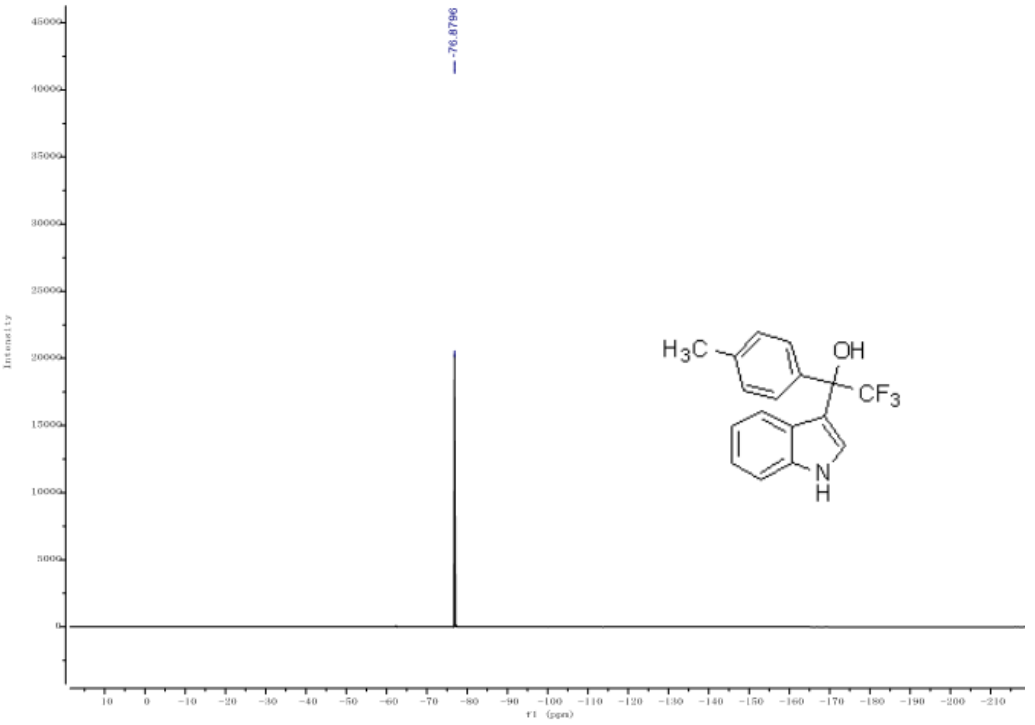
-76.8796
H3C
OH
CF3
N
H
Intensity
f1 (ppm)

Figure S32. ^{1}H, ^{13}C and ^{19}F NMR of 2,2,2-trifluoro-1-(4-trifluoromethylphenyl)-1-(1H-indole-3-yl)ethanol (**5n**).

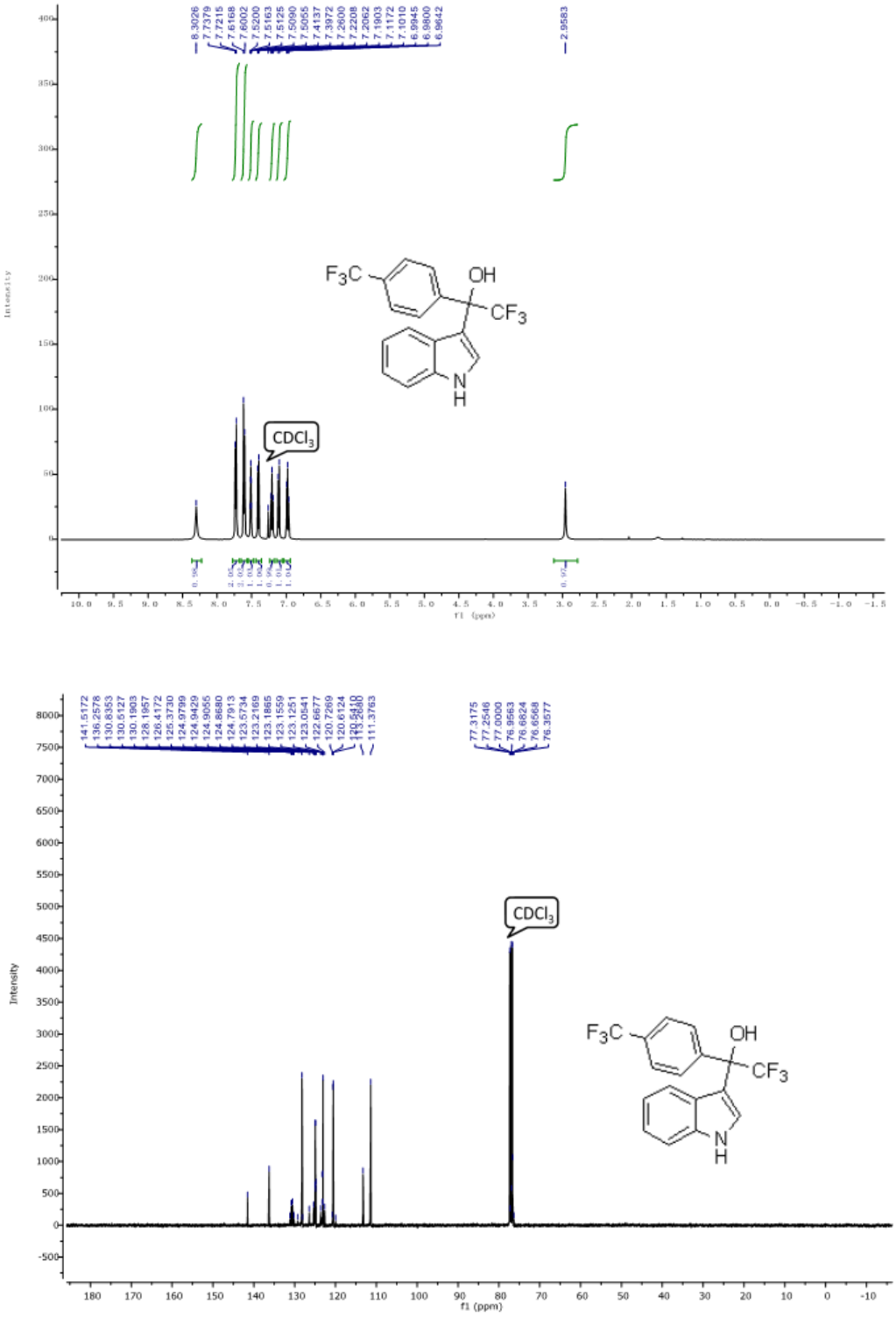

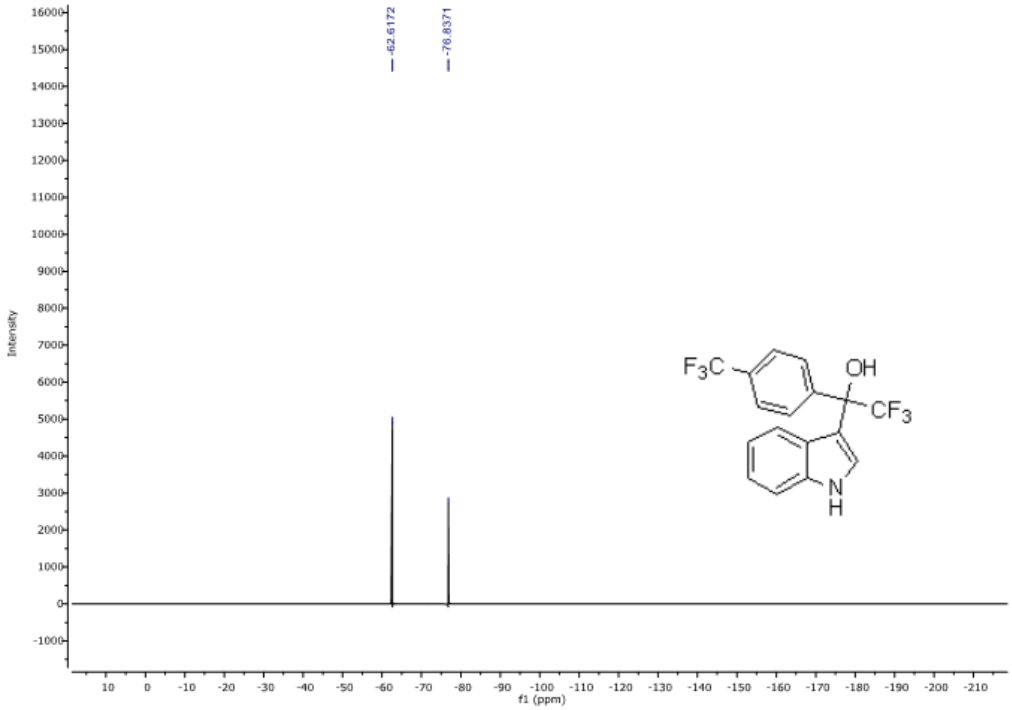

Figure S33. ^{1}H, ^{13}C and ^{19}F NMR of 1-(3-chlorophenyl)-2,2,2-trifluoro-1-(1H-indole-3-yl)ethanol (**5o**).

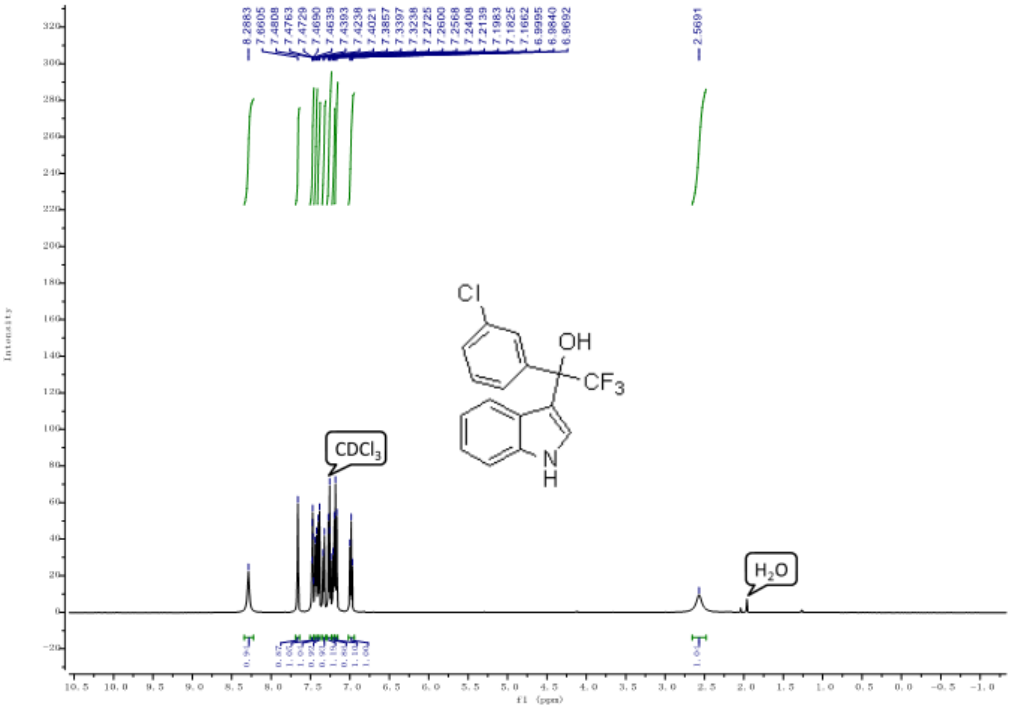

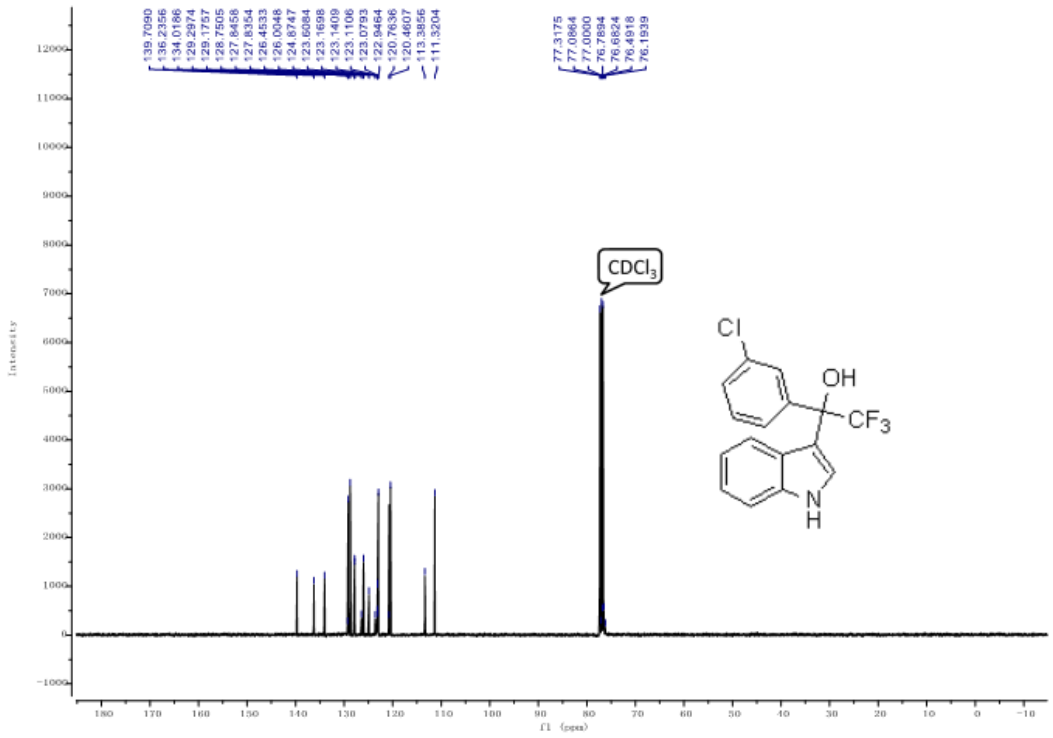
139.7090
136.2356
134.0186
129.2974
129.1757
128.7505
127.8458
127.8354
126.4533
126.0048
124.8747
123.6884
123.1698
123.1409
123.1106
123.0793
122.9464
120.7636
120.4607
113.3856
111.3204
77.3175
77.0864
77.0000
76.7894
76.6624
76.4918
76.1939
CDCl3
Cl
OH
CF3
N
H
Intensity
f1 (ppm)

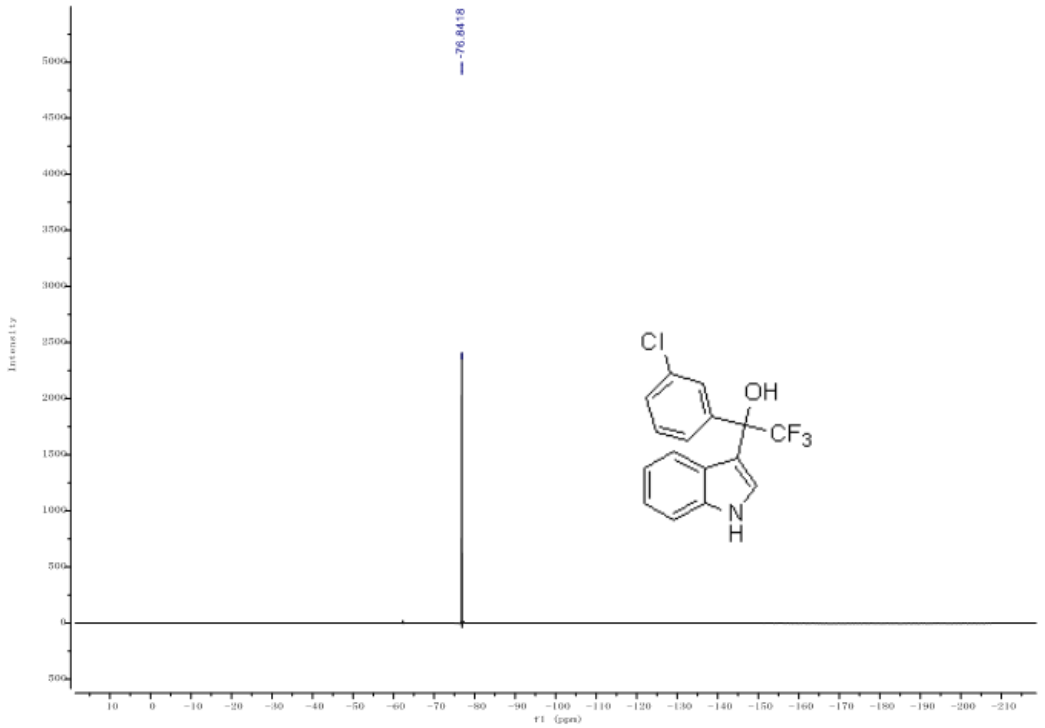
-76.8418
Cl
OH
CF3
N
H
Intensity
f1 (ppm)

Figure S34. ^{1}H, ^{13}C and ^{19}F NMR of 2,2,2-trifluoro-1-(1H-indole-3-yl)-1-3,5-difluorophenyl-ethanol (**5p**).

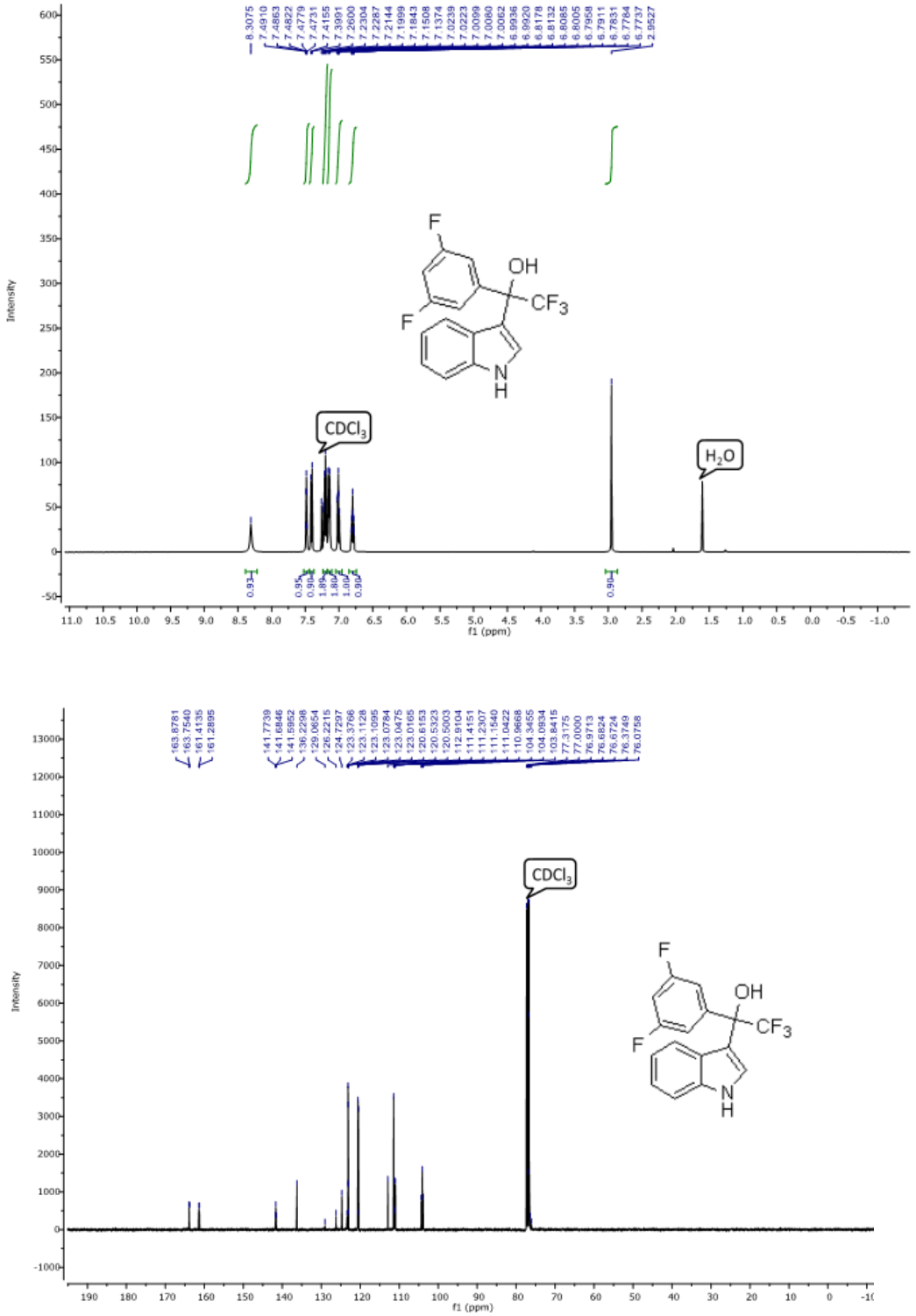

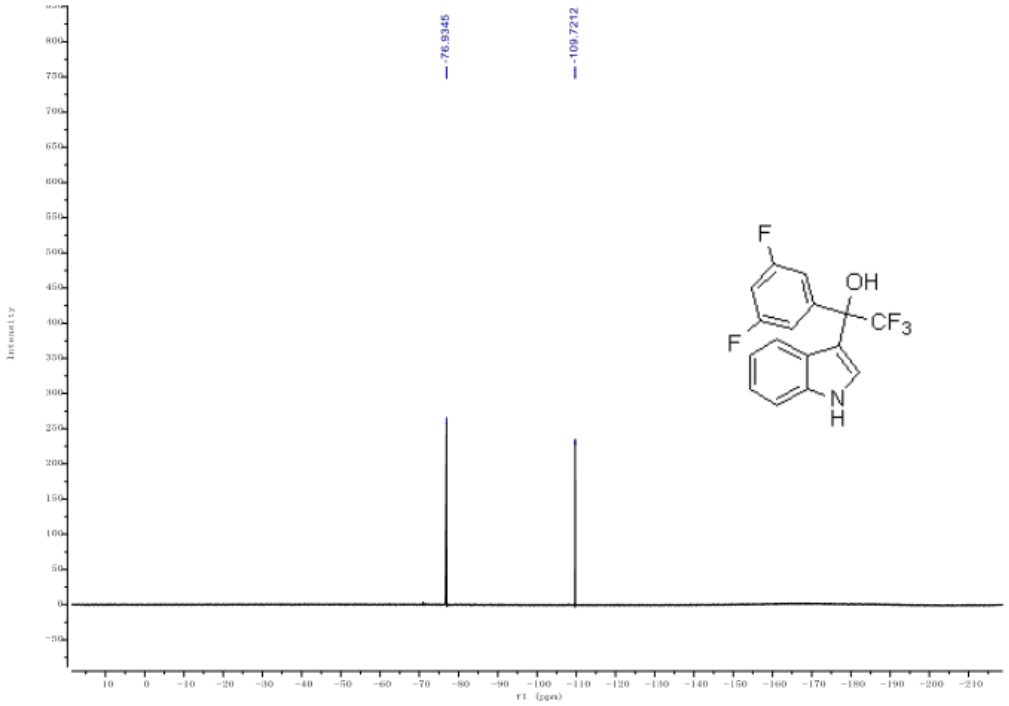

Figure S35. ^{1}H, ^{13}C and ^{19}F NMR of 1-(3-chloro-5-fluorophenyl)-2,2,2-trifluoro-1-(1H-indole-3-yl)ethanol (**5q**).

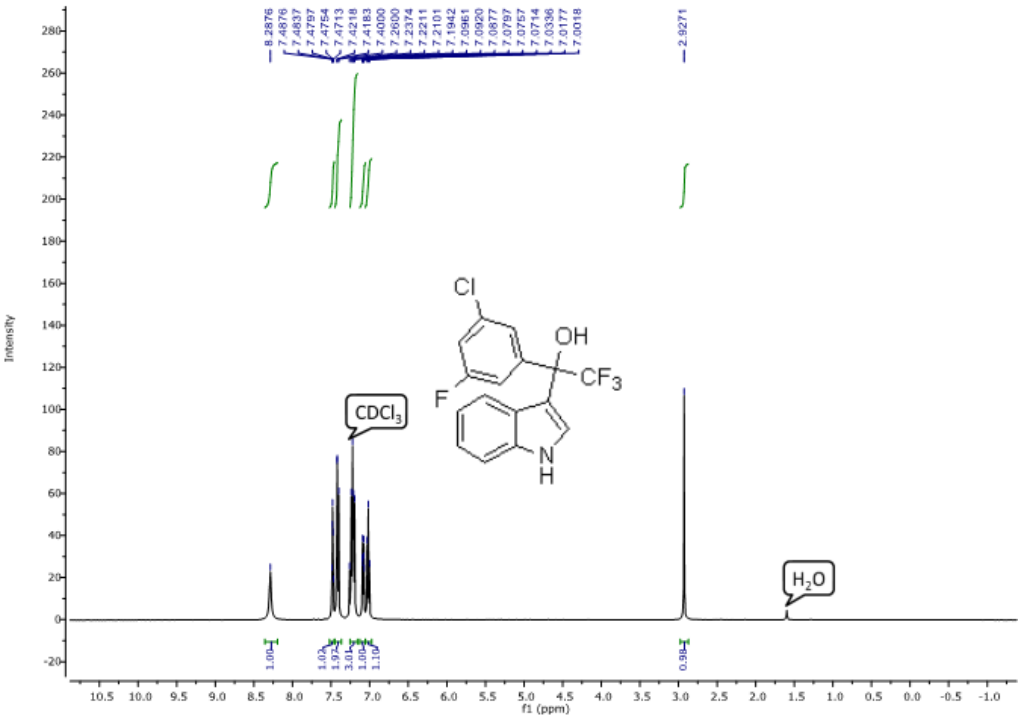

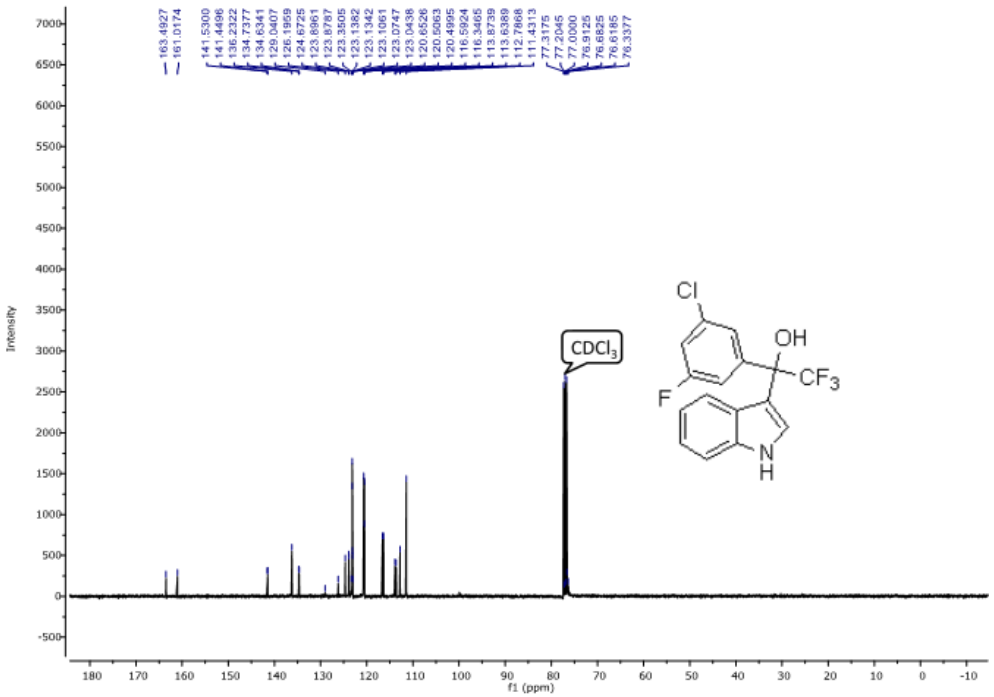
163.4927
161.0174
141.5300
141.4496
136.2322
134.7377
134.6341
129.0407
126.1959
124.6725
123.8961
123.8787
123.3505
123.1362
123.1342
123.1061
123.0747
123.0438
120.6526
120.5863
120.4995
116.5924
116.4665
113.8739
113.6389
112.7868
111.4313
77.3175
77.2045
77.0000
76.9125
76.6825
76.6185
76.3377
CDCl3
Cl
OH
CF3
F
N
H
Intensity
f1 (ppm)

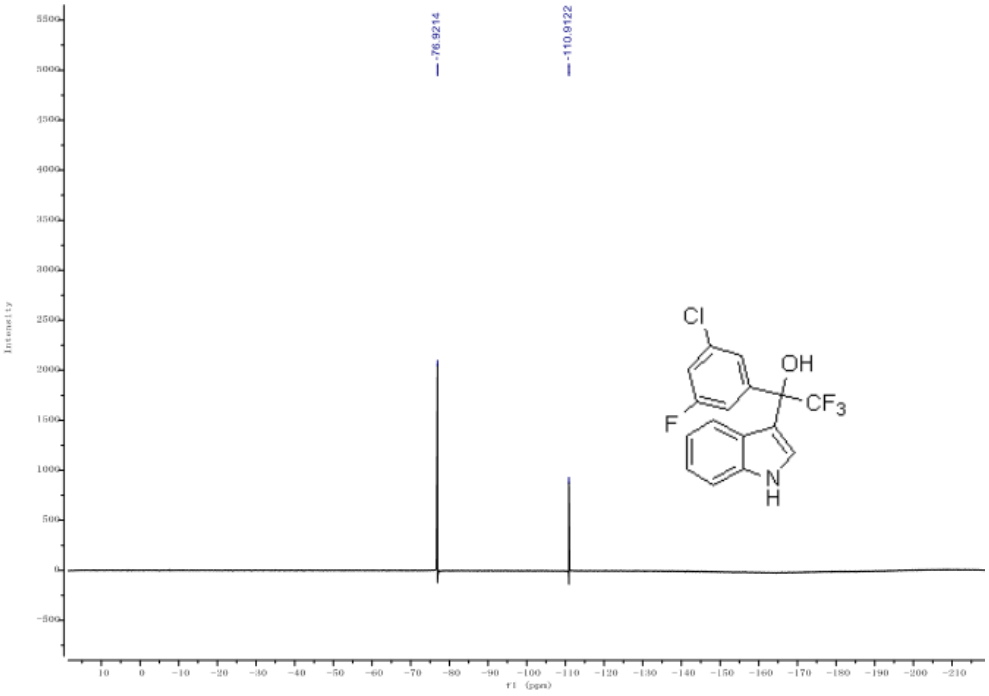
-76.9214
-110.9122
Cl
OH
CF3
F
N
H
f1 (ppm)

Figure S36. ^{1}H, ^{13}C and ^{19}F NMR of 1-(3.5-dichlorophenyl)-2,2,2-trifluoro-1-(1H-indole-3-yl)ethanol (**5r**).

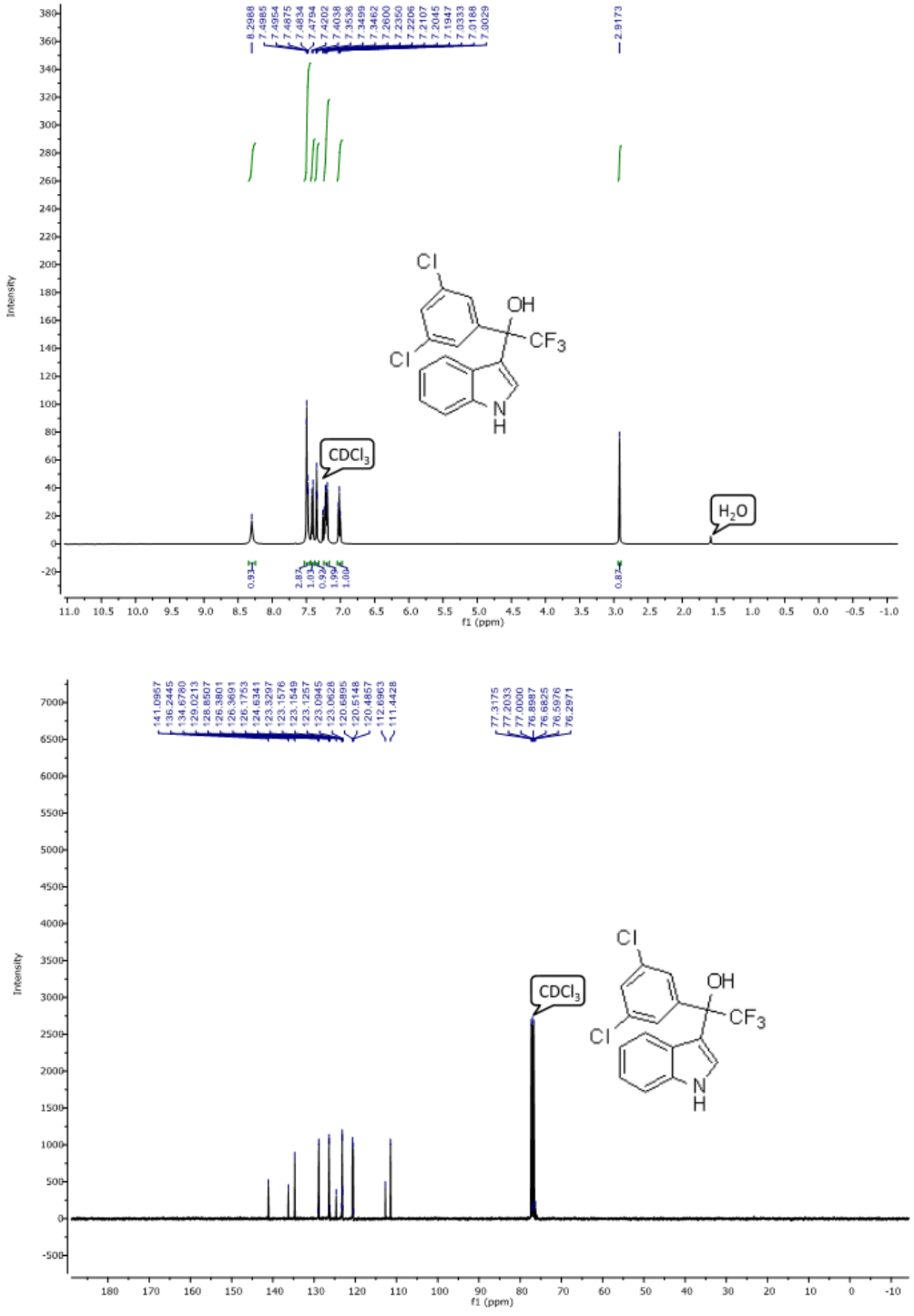

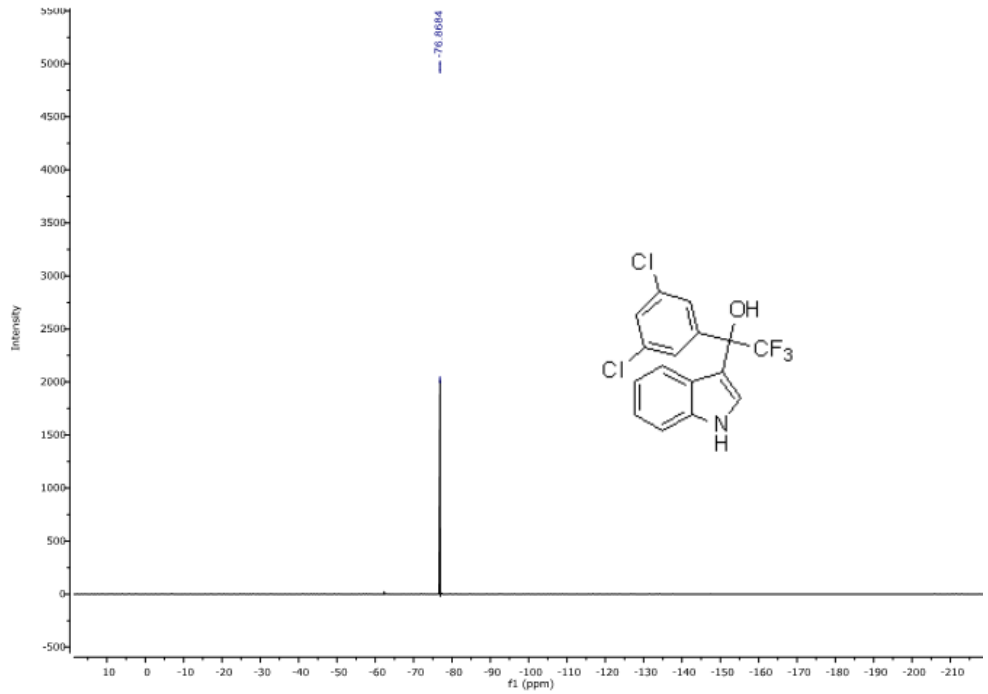

Figure S37. ^{1}H, ^{13}C and ^{19}F NMR of 2,2,2-trifluoro-1-(1H-indole-3-yl)-1-2,3,4,5,6-pentafluoro-phenylethanol (**5s**).

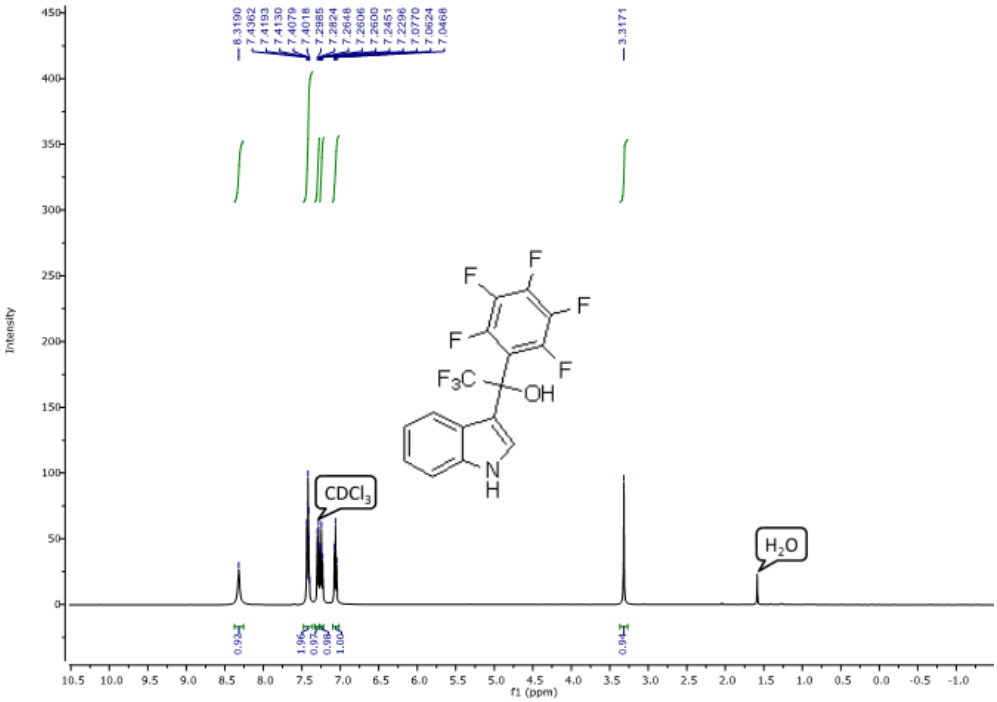

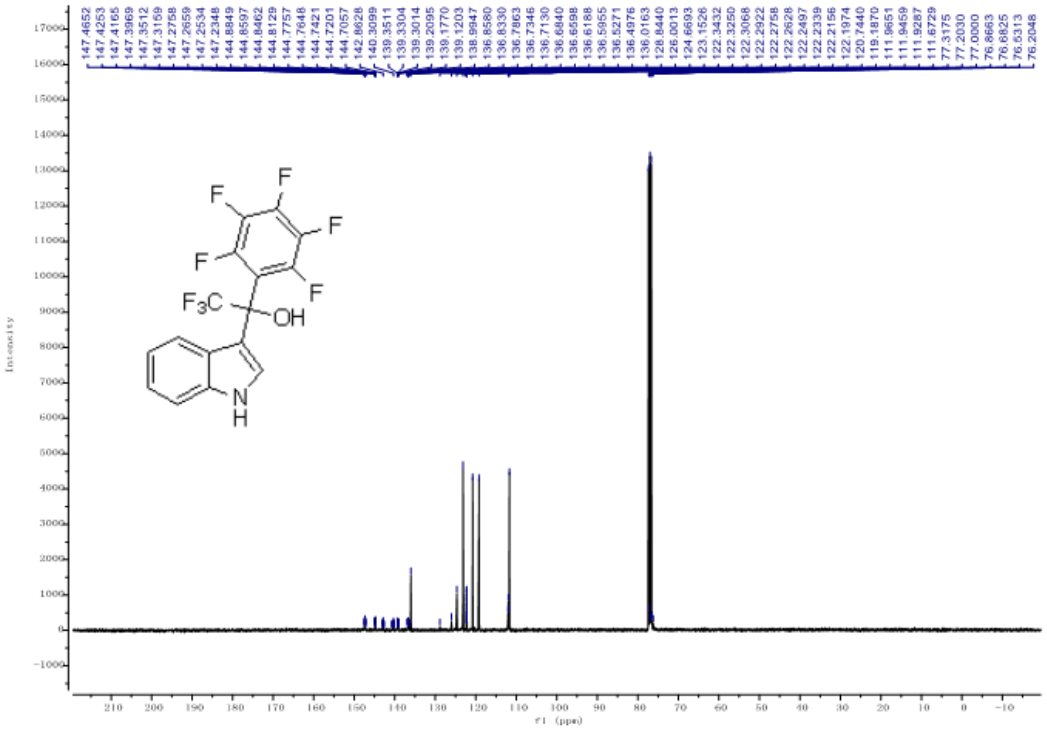
F
F
F
F
F
F3C
OH
N
H
Intensity
f1 (ppm)

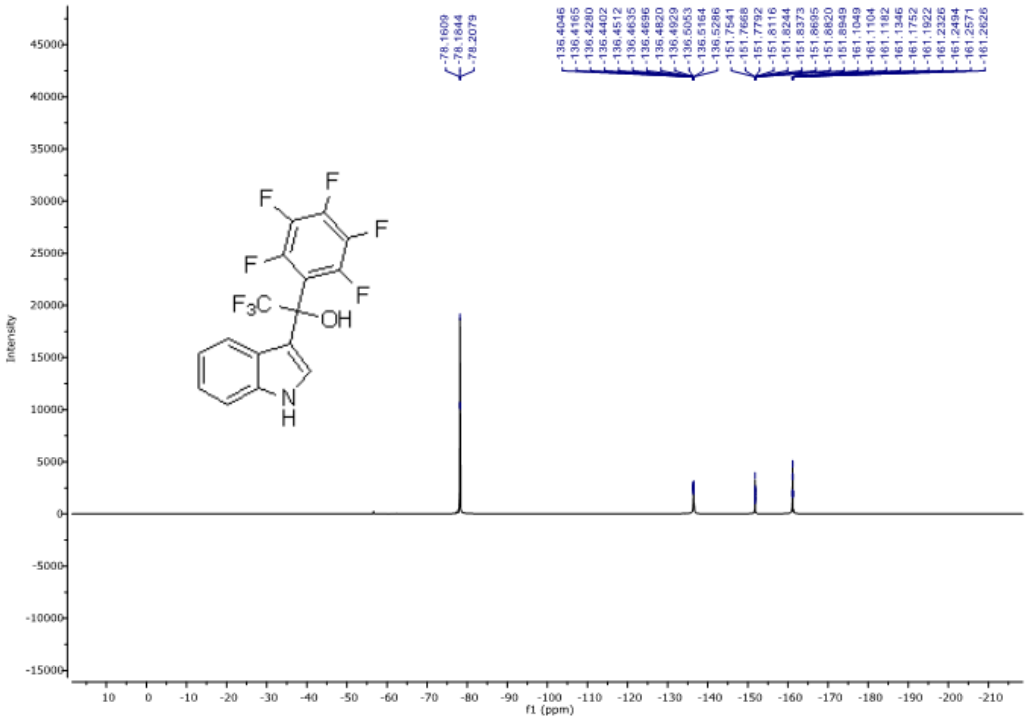
F
F
F
F
F
F3C
OH
N
H
Intensity
f1 (ppm)

Figure S38. ^{1}H, ^{13}C and ^{19}F NMR of 2-chloro-2,2-difluoro-1-(1H-indole-3-yl)-1-phenylethanol (**5t**).

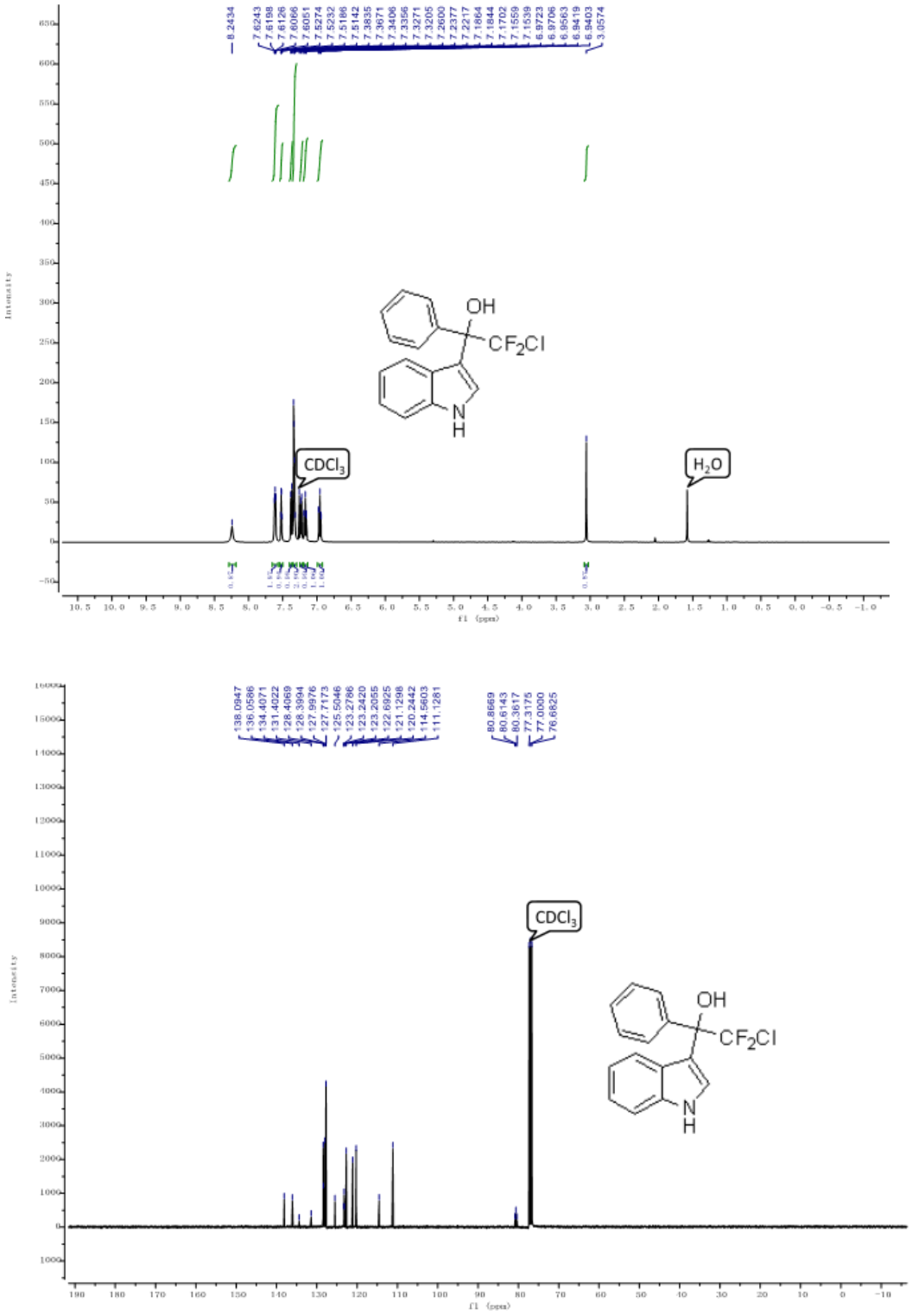

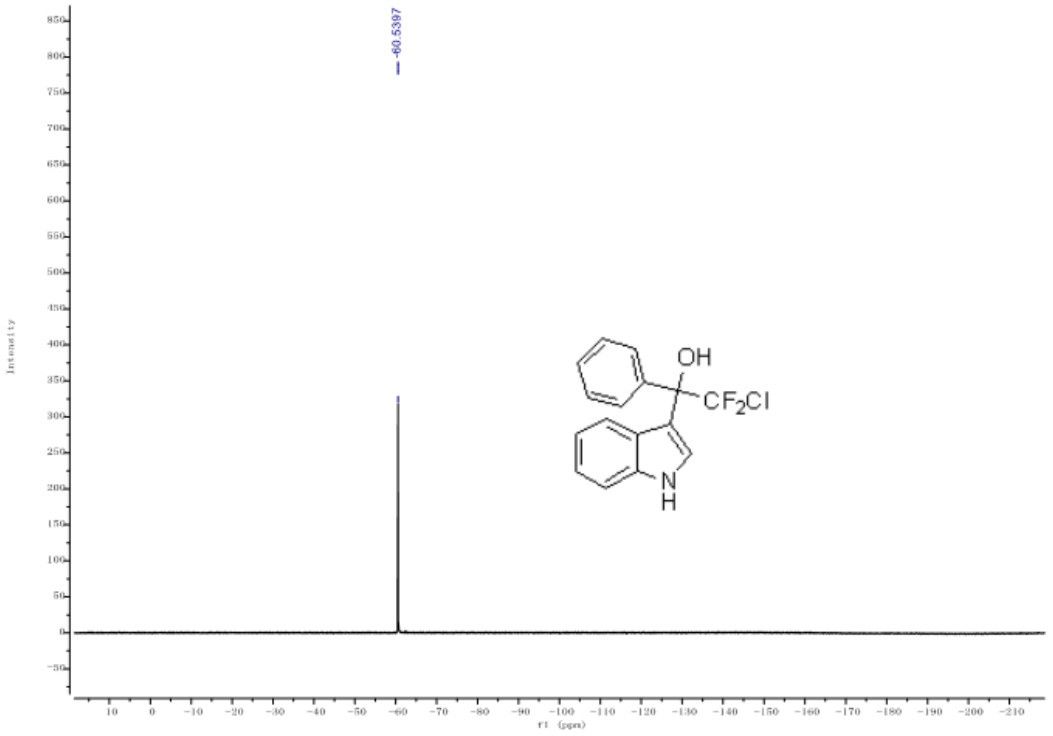

Figure S39. ^{1}H, ^{13}C and ^{19}F NMR of 2,2,2-trifluoro-1-(1-methyl-indole-3-yl)-1-phenylethanol (**5u**).

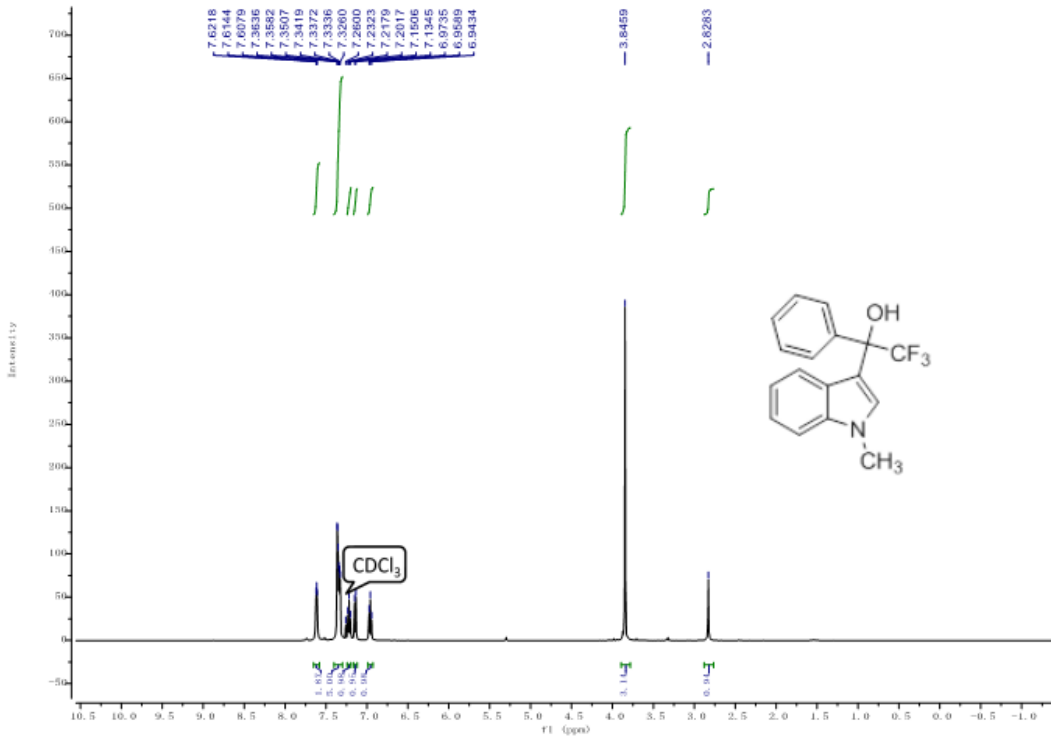

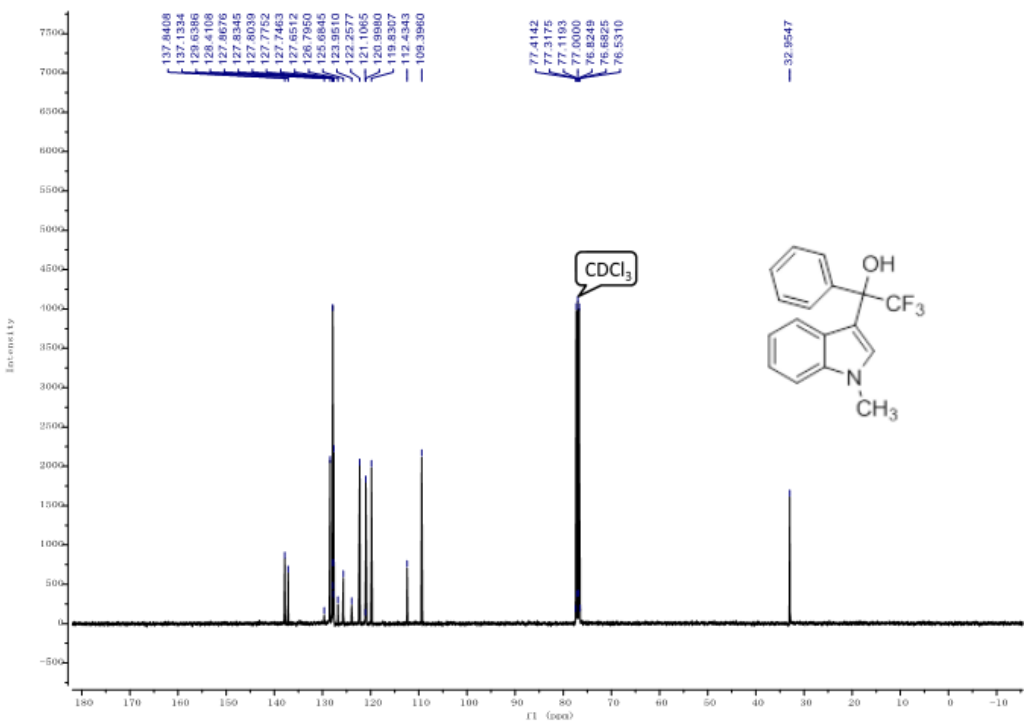
137.8408
137.1334
129.6386
128.4108
128.4676
127.8676
127.8345
127.8059
127.7752
127.7463
127.6572
126.7950
125.6845
123.9510
122.2577
121.1065
120.9980
119.8307
112.4343
109.3960
77.4142
77.3175
77.1193
77.0000
76.8249
76.6825
76.5310
32.9547
CDCl3
OH
CF3
N
CH3
Intensity
f1 (ppm)

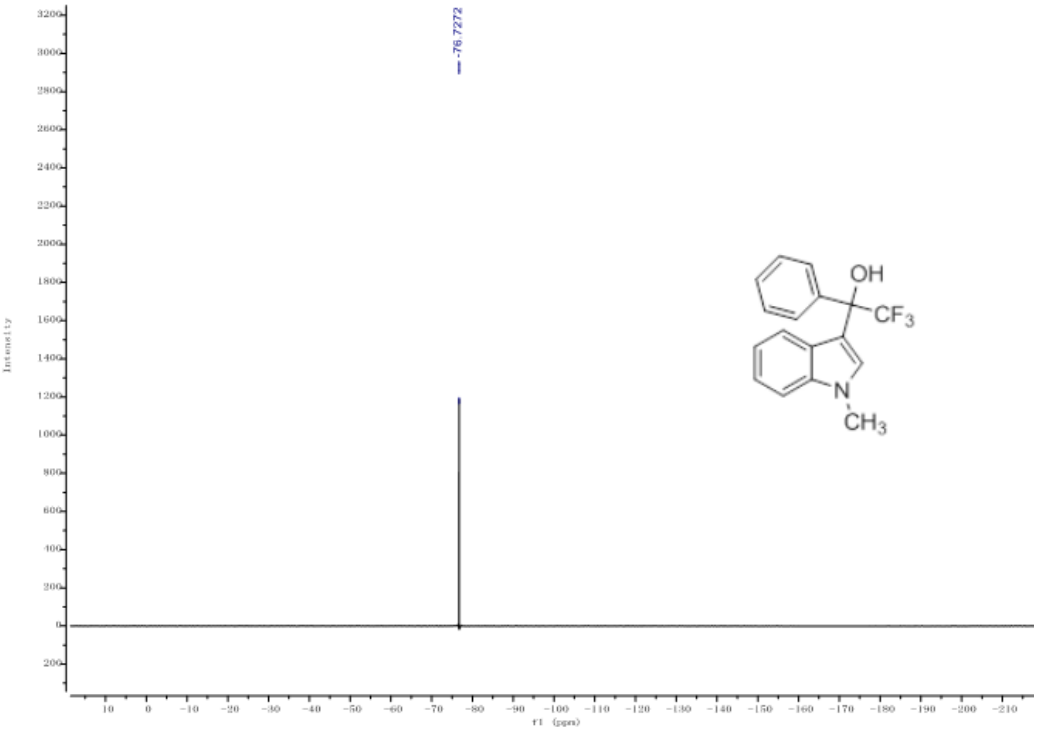
-76.7272
OH
CF3
N
CH3
Intensity
f1 (ppm)

II. HPLC traces

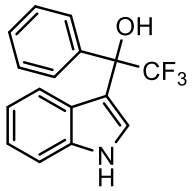

5a: RegisCell column (Hexanes/iPrOH=75/25, 1.0 mL/min, 20 °C, 250 nm)

Racemic:

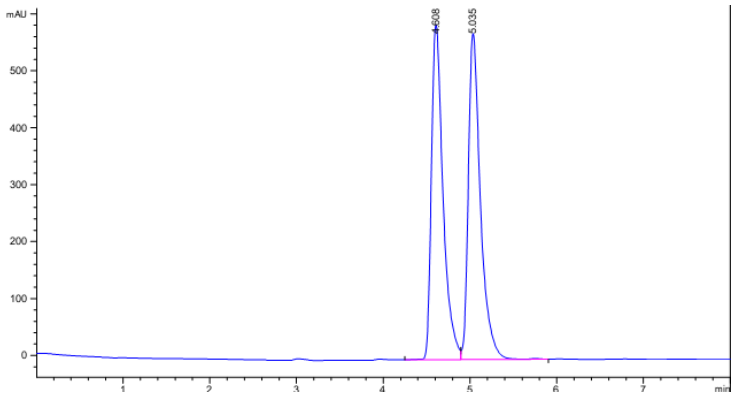

Peak #	RetTime [min]	Type	Width [min]	Area [mAU*s]	Height [mAU]	Area %
1	4.608	BV	0.1405	5471.92822	588.13062	49.6144
2	5.035	VV R	0.1450	5556.97412	572.82330	50.3856
Totals :				1.10289e4	1160.95392	

An example of the enantiomeric enriched product (Table 1, entry 17):

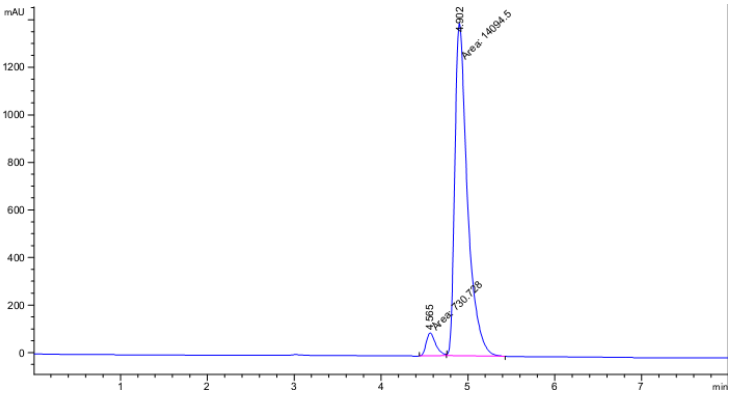

Peak #	RetTime [min]	Type	Width [min]	Area [mAU*s]	Height [mAU]	Area %
1	4.565	MM	0.1272	730.72803	95.72878	4.9290
2	4.902	MM	0.1678	1.40945e4	1399.77283	95.0710
Totals :				1.48252e4	1495.50160	

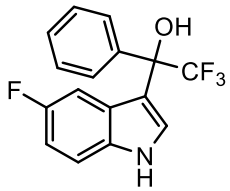

5b: RegisCell column (Hexanes/iPrOH=99.2/0.8, 1.0 mL/min, 20 °C, 250 nm)

Racemic:

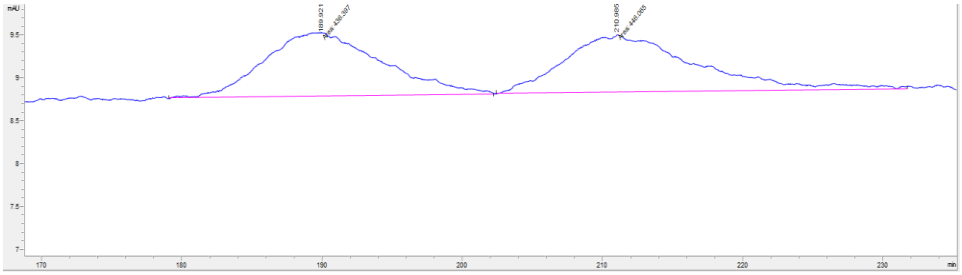

Peak #	RetTime [min]	Type	Width [min]	Area [mAU*s]	Height [mAU]	Area %
1	189.921	MM	9.7324	436.39682	7.47329e-1	49.4522
2	210.985	MM	11.0088	446.06525	6.75317e-1	50.5478
Totals :				882.46207	1.42265	

Table 3, entry 1:

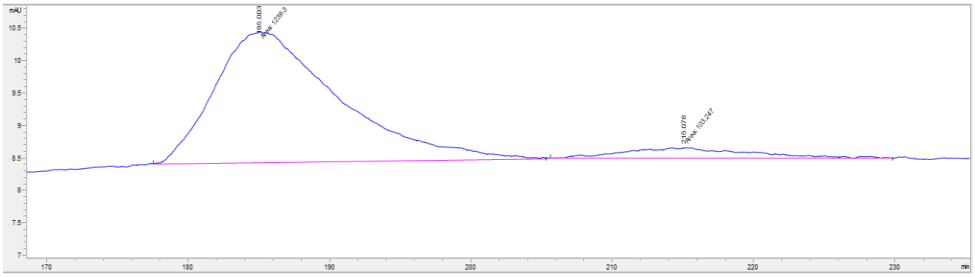

Peak #	RetTime [min]	Type	Width [min]	Area [mAU*s]	Height [mAU]	Area %
1	185.003	MM	10.2187	1239.30054	2.02129	92.3096
2	215.078	MM	10.3928	103.24681	1.65574e-1	7.6904
Totals :				1342.54735	2.18687	

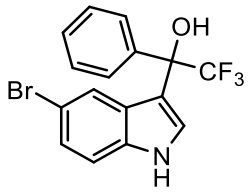

5c: RegisPack column (Hexanes/iPrOH=96/4, 1.0 mL/min, 20 °C, 250 nm)

Racemic:

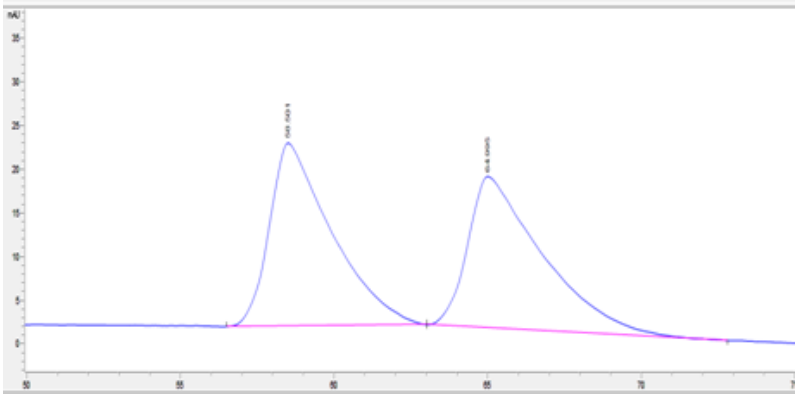

Peak #	RetTime [min]	Type	Width [min]	Area [mAU*s]	Height [mAU]	Area %
1	58.501	BB	1.7806	2936.19702	20.90520	50.1483
2	64.995	BB	2.0603	2918.83472	17.30062	49.8517
Totals :				5855.03174	38.20581	

Table 3, entry 2:

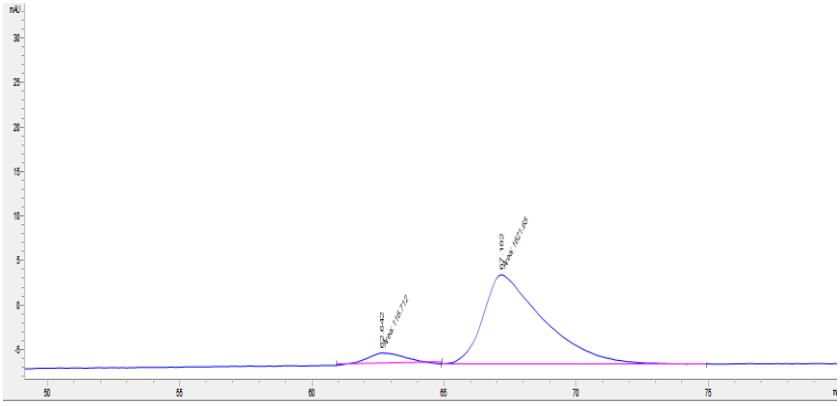

Peak #	RetTime [min]	Type	Width [min]	Area [mAU*s]	Height [mAU]	Area %
1	62.642	MM	1.6082	116.71169	1.20952	6.7139
2	67.182	MM	2.6874	1621.65112	10.05717	93.2861
Totals :				1738.36281	11.26670	

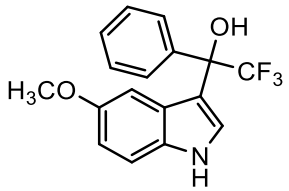

5d: RegisCell column (Hexanes/iPrOH=85/15, 1.0 mL/min, 20 °C, 250 nm)

Racemic:

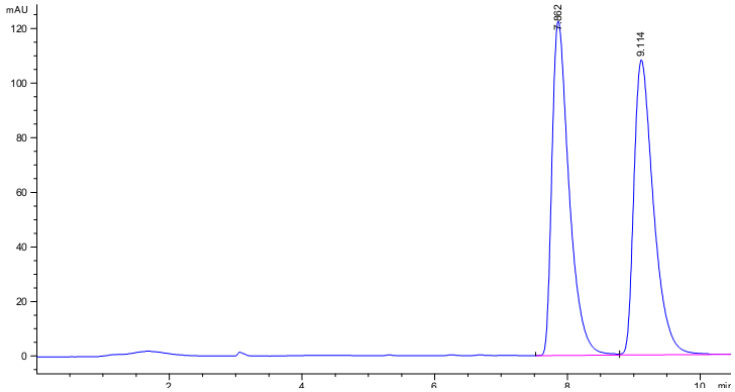

Peak #	RetTime [min]	Type	Width [min]	Area [mAU*s]	Height [mAU]	Area %
1	7.862	BV	0.2717	2200.07642	122.42687	49.8621
2	9.114	VBA	0.3109	2212.24756	108.05466	50.1379
Totals :				4412.32397	230.48153	

Table 3, entry 3:

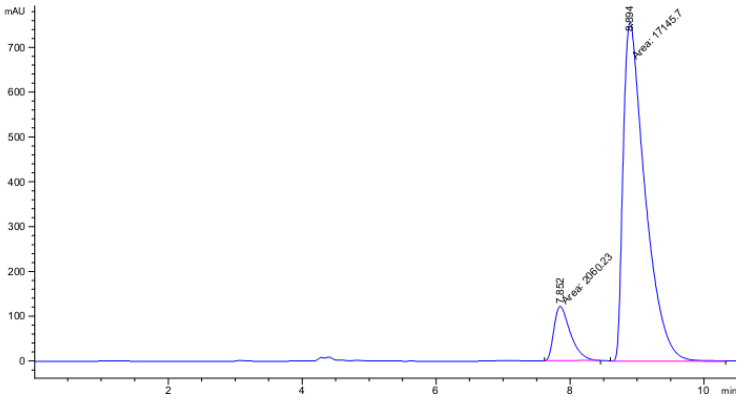

Peak #	RetTime [min]	Type	Width [min]	Area [mAU*s]	Height [mAU]	Area %
1	7.852	MM	0.2838	2060.23218	120.98914	10.7271
2	8.894	MM	0.3781	1.71457e4	755.76947	89.2729
Totals :				1.92059e4	876.75861	

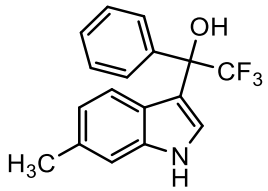

5e: RegisCell column (Hexanes/iPrOH=95/5, 1.0 mL/min, 20 °C, 250 nm)

Racemic:

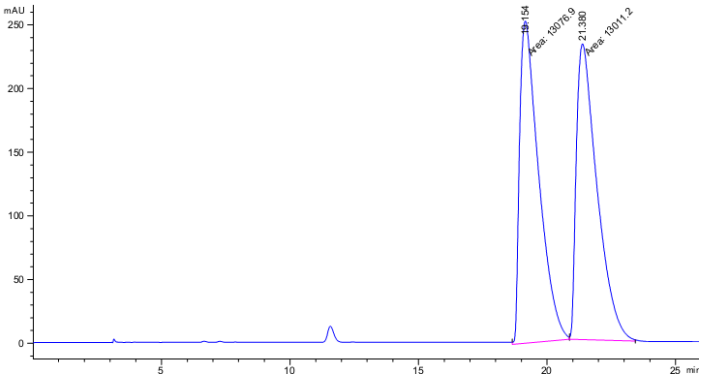

Peak #	RetTime [min]	Type	Width [min]	Area [mAU*s]	Height [mAU]	Area %
1	19.154	MM	0.8615	1.30769e4	252.97937	50.1261
2	21.380	MM	0.9340	1.30112e4	232.16554	49.8739
Totals :				2.60881e4	485.14491	

Table 3, entry 4:

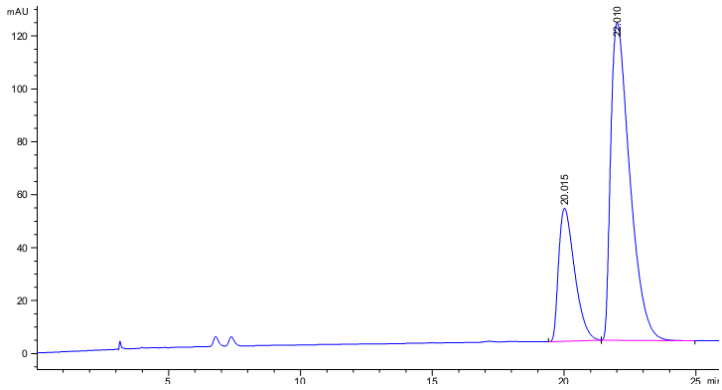

Peak #	RetTime [min]	Type	Width [min]	Area [mAU*s]	Height [mAU]	Area %
1	20.015	BB	0.6446	2113.07593	50.24733	25.9750
2	22.010	BB	0.7652	6021.96436	120.05927	74.0250
Totals :				8135.04028	170.30659	

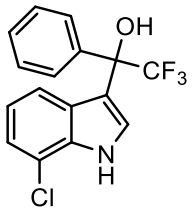

5f: RegisCell column (Hexanes/iPrOH=75/25, 1.0 mL/min, 20 °C, 250 nm)

Racemic:

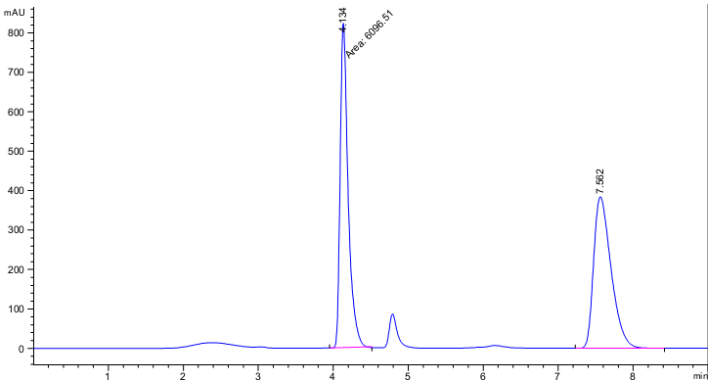

Peak #	RetTime [min]	Type	Width [min]	Area [mAU*s]	Height [mAU]	Area %
1	4.134	MM	0.1234	6096.50830	823.56335	49.5643
2	7.562	BB	0.2483	6203.68701	384.34109	50.4357
Totals :				1.23002e4	1207.90445	

Table 3, entry 5:

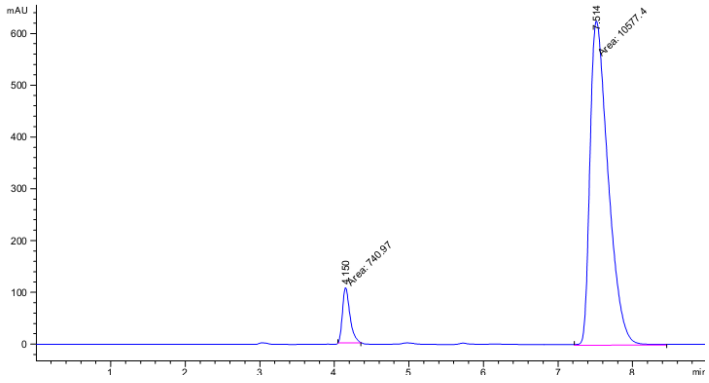

Peak #	RetTime [min]	Type	Width [min]	Area [mAU*s]	Height [mAU]	Area %
1	4.150	MM	0.1157	740.96960	106.71207	6.5466
2	7.514	MM	0.2817	1.05774e4	625.77478	93.4534
Totals :				1.13184e4	732.48685	

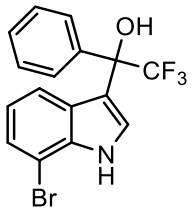

5g: RegisCell column (Hexanes/iPrOH=75/25, 1.0 mL/min, 20 °C, 250 nm)

Racemic:

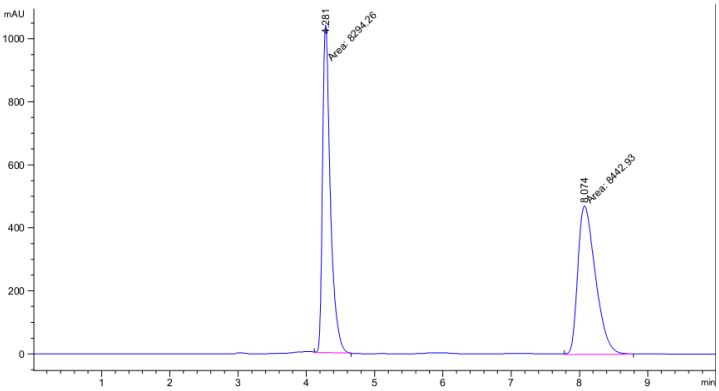

Peak #	RetTime [min]	Type	Width [min]	Area [mAU*s]	Height [mAU]	Area %
1	4.281	MM	0.1328	8294.25977	1040.95947	49.5559
2	8.074	MM	0.2986	8442.93066	471.24802	50.4441
Totals :				1.67372e4	1512.20749	

Table 3, entry 6:

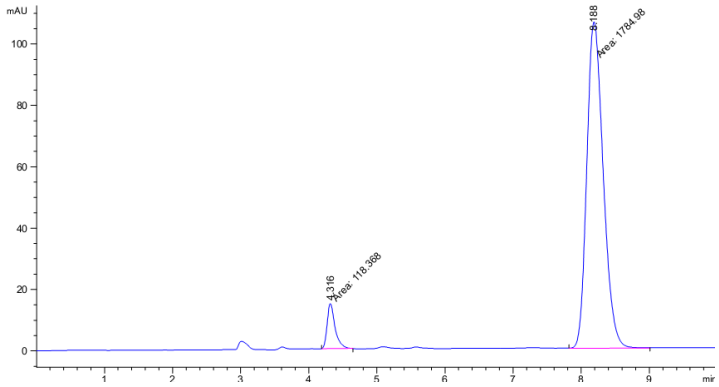

Peak #	RetTime [min]	Type	Width [min]	Area [mAU*s]	Height [mAU]	Area %
1	4.316	MM	0.1340	118.36771	14.72718	6.2189
2	8.188	MM	0.2797	1784.97839	106.37480	93.7811
Totals :				1903.34611	121.10198	

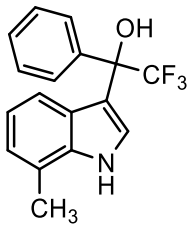

5h: RegisCell column (Hexanes/iPrOH=75/25, 1.0 mL/min, 20 °C, 250 nm)

Racemic:

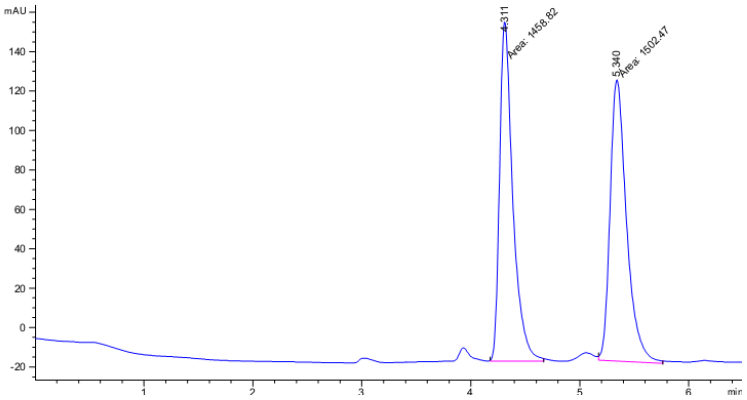

Peak #	RetTime [min]	Type	Width [min]	Area [mAU*s]	Height [mAU]	Area %
1	4.311	MM	0.1410	1458.82031	172.49506	49.2629
2	5.340	MM	0.1752	1502.47314	142.91119	50.7371
Totals :				2961.29346	315.40625	

Table 3, entry 7:

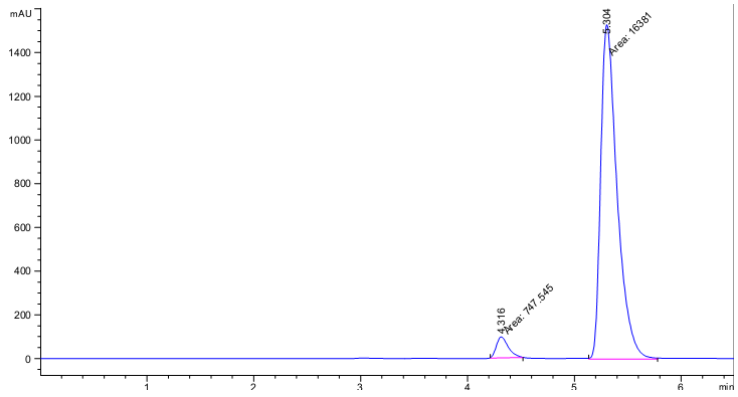

Peak #	RetTime [min]	Type	Width [min]	Area [mAU*s]	Height [mAU]	Area %
1	4.316	MM	0.1294	747.54486	96.29123	4.3643
2	5.304	MM	0.1784	1.63810e4	1530.51147	95.6357
Totals :				1.71286e4	1626.80270	

Table 3, entry 20:

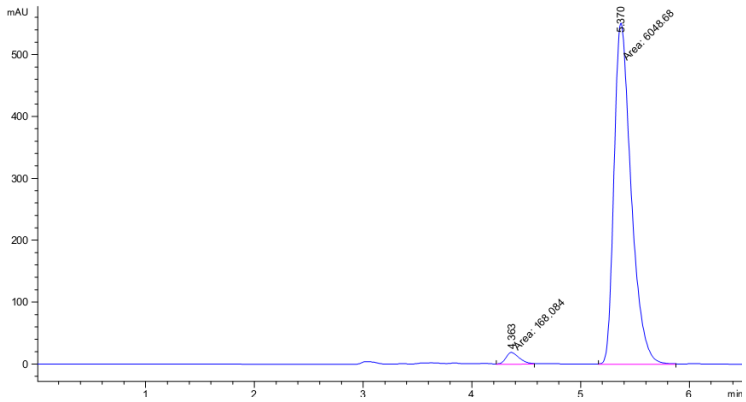

Peak #	RetTime [min]	Type	Width [min]	Area [mAU*s]	Height [mAU]	Area %
1	4.363	MM	0.1467	168.08415	19.09901	2.7037
2	5.370	MM	0.1827	6048.67627	551.87000	97.2963
Totals :				6216.76042	570.96900	

Table 3, entry 22:

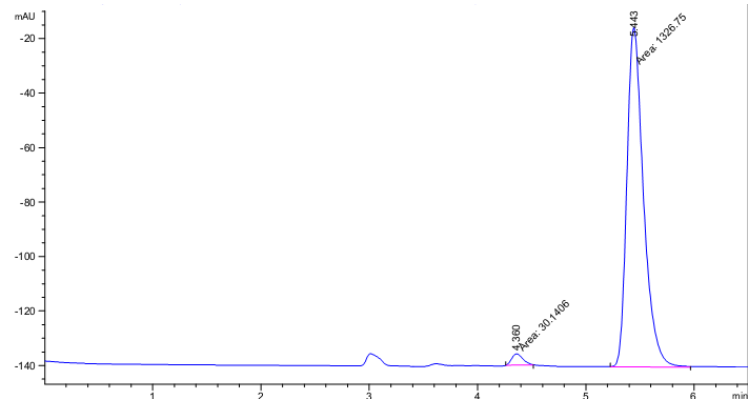

Peak #	RetTime [min]	Type	Width [min]	Area [mAU*s]	Height [mAU]	Area %
1	4.360	MM	0.1201	30.14058	4.18265	2.2213
2	5.443	MM	0.1775	1326.75330	124.55093	97.7787
Totals :				1356.89387	128.73359	

Table 3, entry 23:

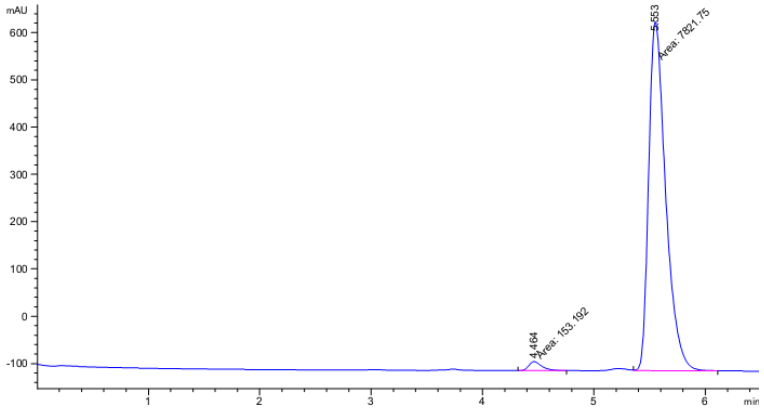

Peak #	RetTime [min]	Type	Width [min]	Area [mAU*s]	Height [mAU]	Area %
1	4.464	MM	0.1337	153.19191	19.09194	1.9209
2	5.553	MM	0.1751	7821.74707	744.37439	98.0791
Totals :				7974.93898	763.46633	

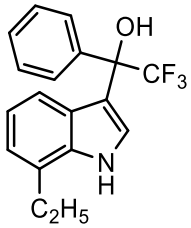

5i: RegisCell column (Hexanes/iPrOH=75/25, 1.0 mL/min, 20 °C, 250 nm)

Racemic:

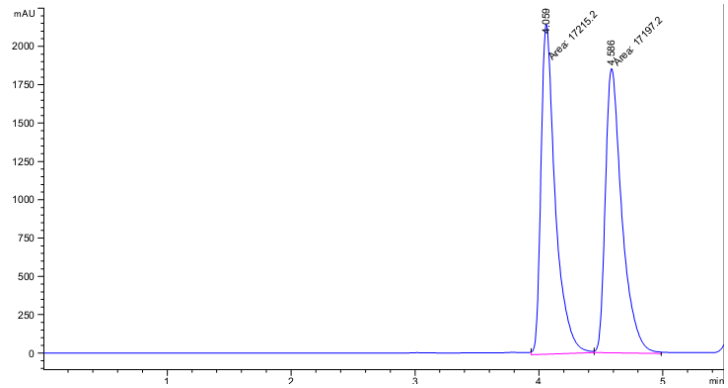

Peak #	RetTime [min]	Type	Width [min]	Area [mAU*s]	Height [mAU]	Area %
1	4.059	MM	0.1330	1.72152e4	2156.92920	50.0261
2	4.586	MM	0.1544	1.71972e4	1856.35815	49.9739
Totals :				3.44124e4	4013.28735	

Table 3, entry 8:

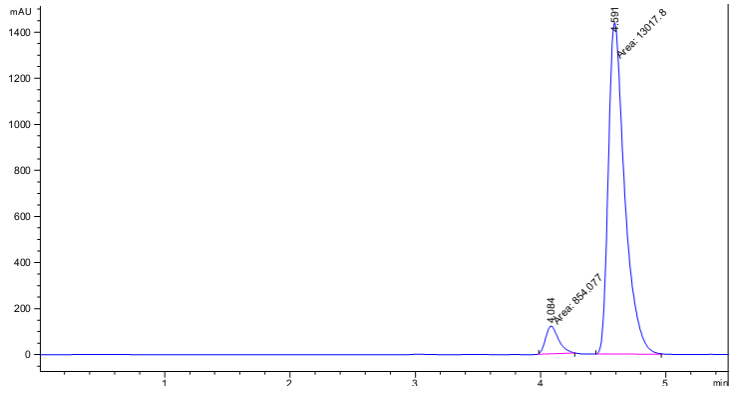

Peak #	RetTime [min]	Type	Width [min]	Area [mAU*s]	Height [mAU]	Area %
1	4.084	MM	0.1184	854.07721	120.23866	6.1569
2	4.591	MM	0.1507	1.30178e4	1439.52380	93.8431
Totals :				1.38719e4	1559.76247	

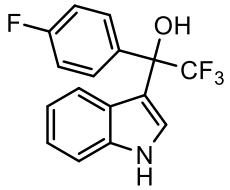

5j: RegisCell column (Hexanes/iPrOH=75/25, 1.0 mL/min, 20 °C, 250 nm)

Racemic:

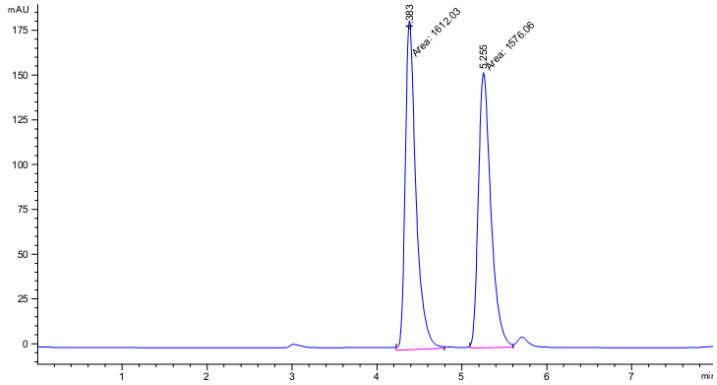

Peak #	RetTime [min]	Type	Width [min]	Area [mAU*s]	Height [mAU]	Area %
1	4.383	MM	0.1462	1612.02576	183.79695	50.5640
2	5.255	MM	0.1709	1576.06177	153.73180	49.4360
Totals :				3188.08752	337.52875	

Table 3, entry 9:

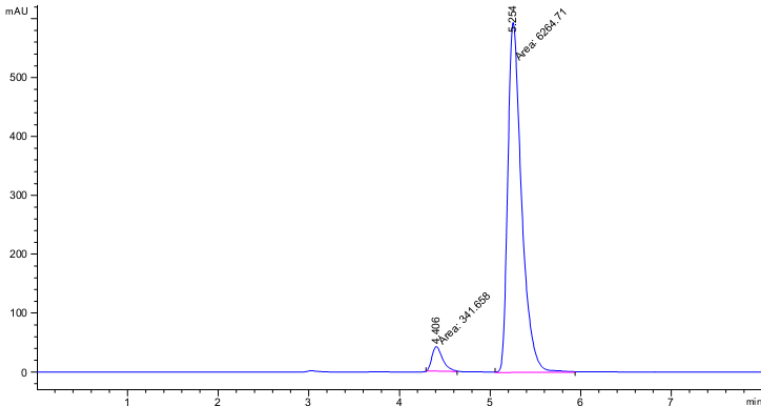

Peak #	RetTime [min]	Type	Width [min]	Area [mAU*s]	Height [mAU]	Area %
1	4.406	MM	0.1367	341.65793	41.66687	5.1716
2	5.254	MM	0.1756	6264.71191	594.73444	94.8284
Totals :				6606.36984	636.40131	

Table 3, entry 21:

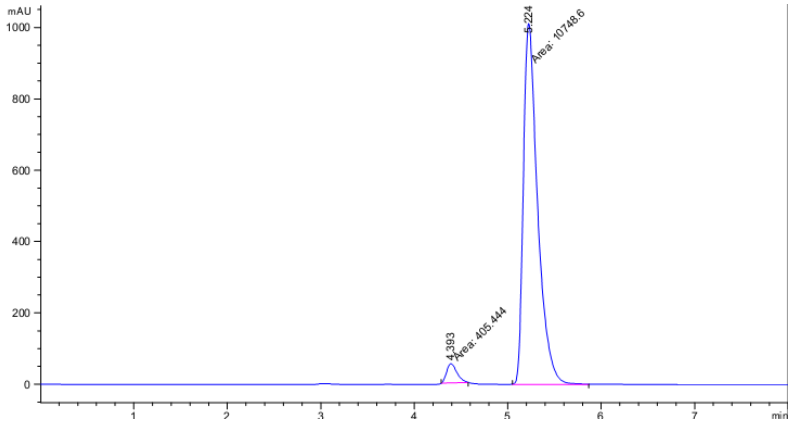

Peak #	RetTime [min]	Type	Width [min]	Area [mAU*s]	Height [mAU]	Area %
1	4.393	MM	0.1257	405.44449	53.75917	3.6349
2	5.224	MM	0.1769	1.07486e4	1012.60431	96.3651
Totals :				1.11541e4	1066.36348	

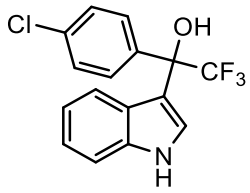

5k: RegisCell column (Hexanes/iPrOH=75/25, 1.0 mL/min, 20 °C, 250 nm)

Racemic:

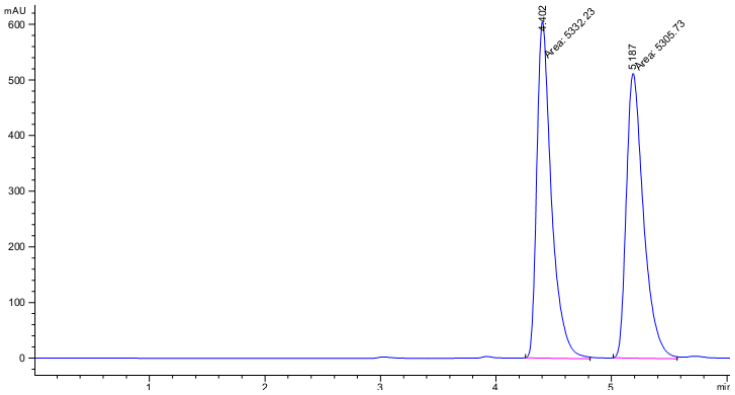

Peak #	RetTime [min]	Type	Width [min]	Area [mAU*s]	Height [mAU]	Area %
1	4.402	MM	0.1469	5332.22705	605.04913	50.1245
2	5.187	MM	0.1727	5305.73340	511.89703	49.8755
Totals :				1.06380e4	1116.94617	

Table 3, entry 10:

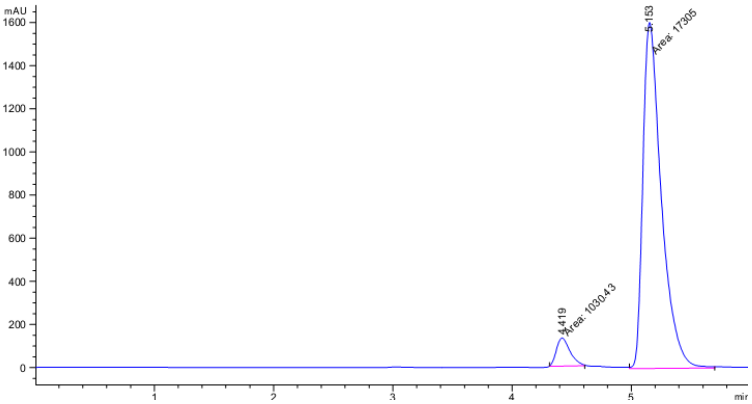

Peak #	RetTime [min]	Type	Width [min]	Area [mAU*s]	Height [mAU]	Area %
1	4.419	MM	0.1322	1030.42578	129.91055	5.6199
2	5.153	MM	0.1795	1.73050e4	1606.83118	94.3801
Totals :				1.83354e4	1736.74173	

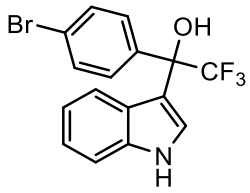

5l: RegisCell column (Hexanes/iPrOH=75/25, 1.0 mL/min, 20 °C, 250 nm)

Racemic:

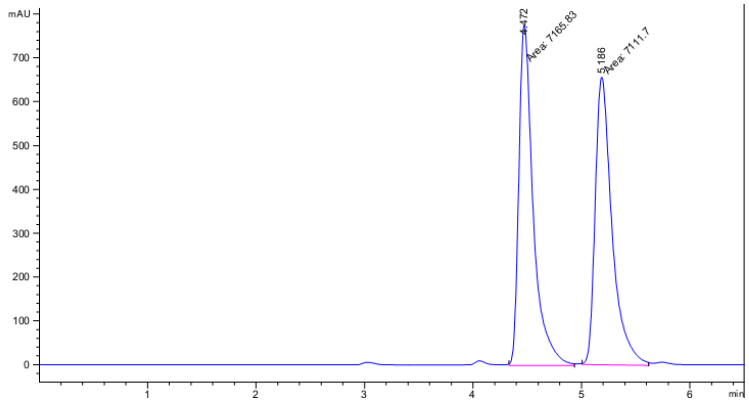

Peak #	RetTime [min]	Type	Width [min]	Area [mAU*s]	Height [mAU]	Area %
1	4.472	MM	0.1535	7165.83301	777.95685	50.1896
2	5.186	MM	0.1804	7111.70361	657.00336	49.8104
Totals :				1.42775e4	1434.96021	

Table 3, entry 11:

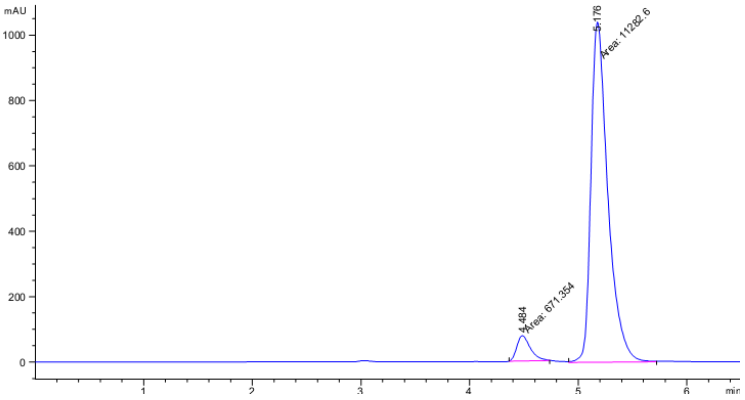

Peak #	RetTime [min]	Type	Width [min]	Area [mAU*s]	Height [mAU]	Area %
1	4.484	MM	0.1437	671.35400	77.88982	5.6162
2	5.176	MM	0.1806	1.12826e4	1040.94006	94.3838
Totals :				1.19539e4	1118.82989	

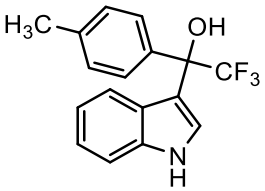

5m: RegisCell column (Hexanes/iPrOH=85/15, 1.0 mL/min, 20 °C, 250 nm)

Racemic:

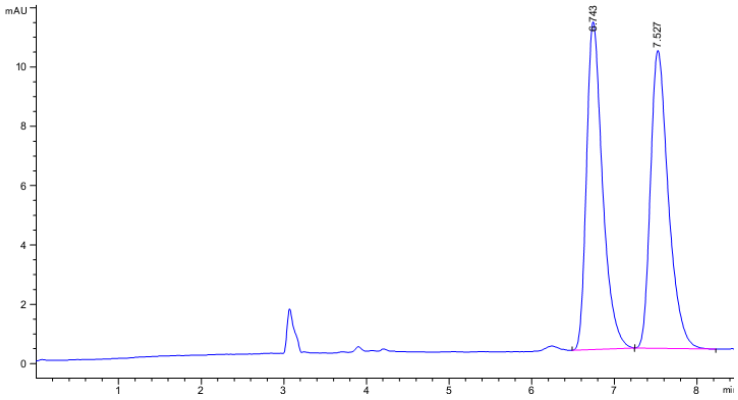

Peak #	RetTime [min]	Type	Width [min]	Area [mAU*s]	Height [mAU]	Area %
1	6.743	BB	0.2030	148.66405	11.04791	49.6152
2	7.527	BB	0.2273	150.96988	10.04676	50.3848
Totals :				299.63393	21.09467	

Table 3, entry 12:

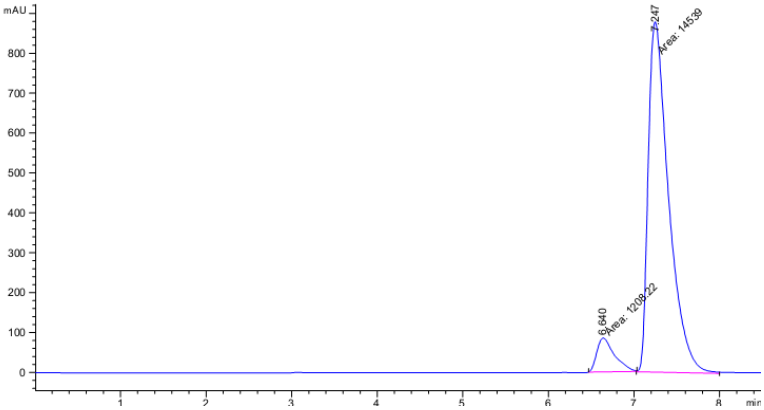

Peak #	RetTime [min]	Type	Width [min]	Area [mAU*s]	Height [mAU]	Area %
1	6.640	MM	0.2379	1208.22437	84.64909	7.6726
2	7.247	MM	0.2759	1.45390e4	878.33447	92.3274
Totals :				1.57472e4	962.98356	

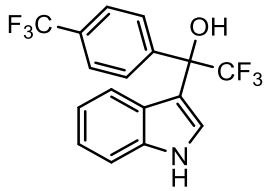

5n: RegisCell column (Hexanes/iPrOH=75/25, 1.0 mL/min, 20 °C, 250 nm)

Racemic:

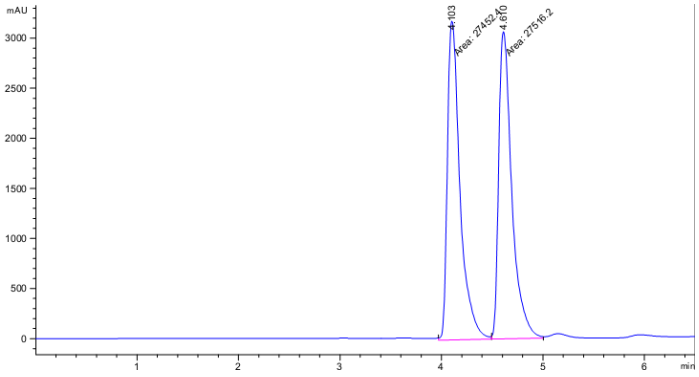

Peak #	RetTime [min]	Type	Width [min]	Area [mAU*s]	Height [mAU]	Area %
1	4.103	MM	0.1437	2.74524e4	3184.66699	49.9420
2	4.610	MM	0.1494	2.75162e4	3070.35303	50.0580
Totals :				5.49686e4	6255.02002	

Table 3, entry 13:

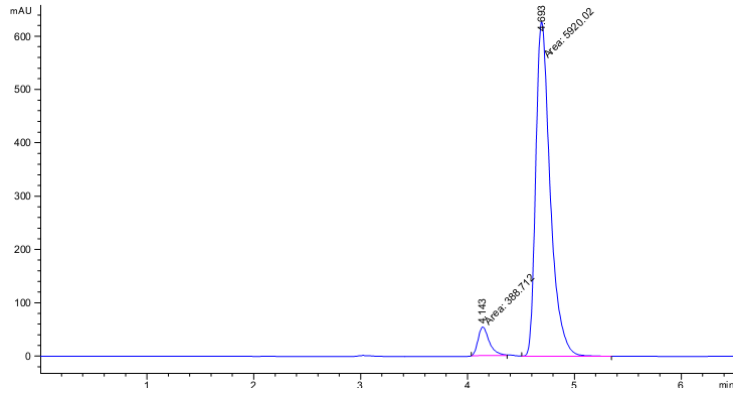

Peak #	RetTime [min]	Type	Width [min]	Area [mAU*s]	Height [mAU]	Area %
1	4.143	MM	0.1207	388.71179	53.69274	6.1615
2	4.693	MM	0.1570	5920.01904	628.39514	93.8385
Totals :				6308.73083	682.08788	

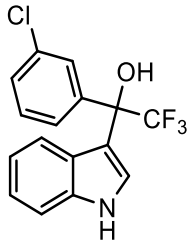

5o: RegisCell column (Hexanes/iPrOH=85/15, 1.0 mL/min, 20 °C, 250 nm)

Racemic:

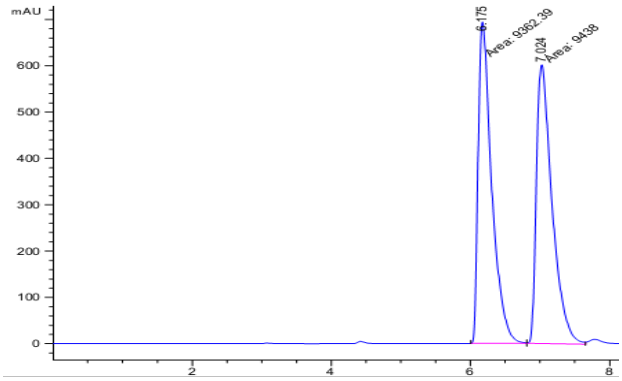

Peak #	RetTime [min]	Type	Width [min]	Area [mAU*s]	Height [mAU]	Area %
1	6.175	MM	0.2250	9362.38867	693.58905	49.7989
2	7.024	MM	0.2613	9437.99902	602.09595	50.2011
Totals :				1.88004e4	1295.68500	

Table 3, entry 14:

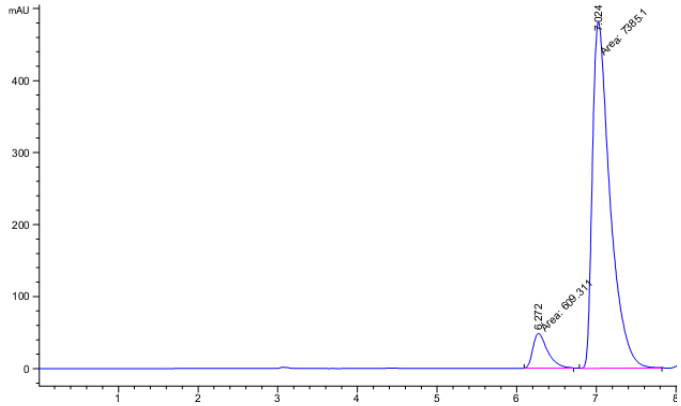

Peak #	RetTime [min]	Type	Width [min]	Area [mAU*s]	Height [mAU]	Area %
1	6.272	MM	0.2112	609.31140	48.07935	7.6217
2	7.024	MM	0.2559	7385.10107	481.04327	92.3783
Totals :				7994.41248	529.12262	

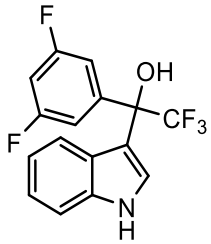

5p: RegisCell column (Hexanes/iPrOH=75/25, 1.0 mL/min, 20 °C, 250 nm)

Racemic:

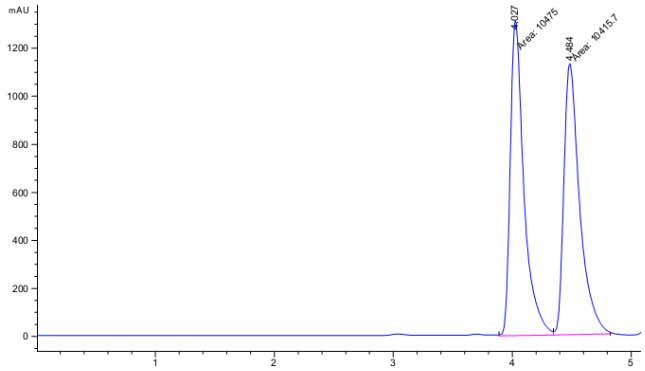

Peak #	RetTime [min]	Type	Width [min]	Area [mAU*s]	Height [mAU]	Area %
1	4.027	MM	0.1329	1.04750e4	1313.63367	50.1419
2	4.484	MM	0.1537	1.04157e4	1129.72607	49.8581
Totals :				2.08907e4	2443.35974	

Table 3, entry 15:

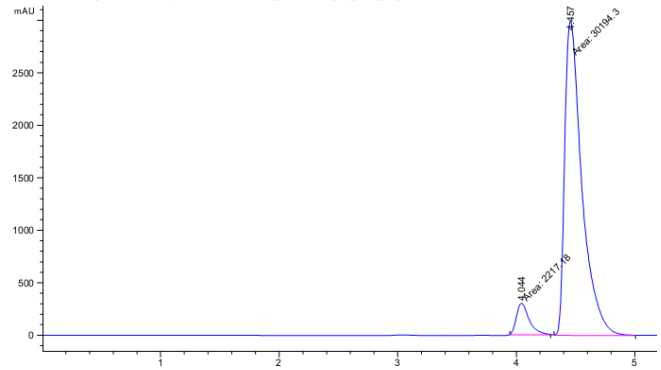

Peak #	RetTime [min]	Type	Width [min]	Area [mAU*s]	Height [mAU]	Area %
1	4.044	MM	0.1234	2217.17944	299.46216	6.8407
2	4.457	MM	0.1680	3.01943e4	2994.62646	93.1593
Totals :				3.24115e4	3294.08862	

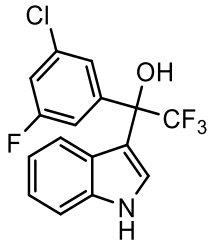

5q: RegisCell column (Hexanes/iPrOH=85/15, 1.0 mL/min, 20 °C, 250 nm)

Racemic:

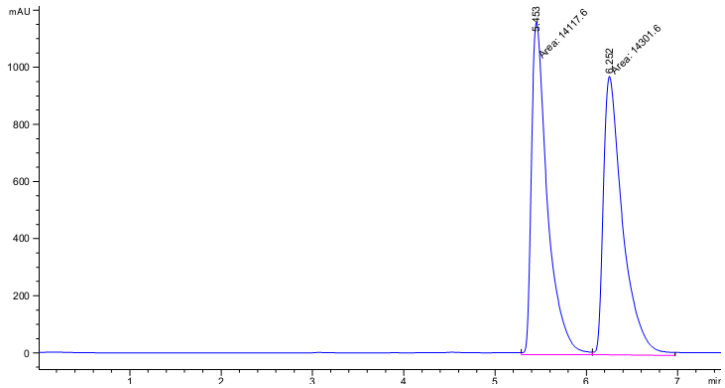

Peak #	RetTime [min]	Type	Width [min]	Area [mAU*s]	Height [mAU]	Area %
1	5.453	MM	0.2023	1.41176e4	1162.95129	49.6762
2	6.252	MM	0.2444	1.43016e4	975.09045	50.3238
Totals :				2.84192e4	2138.04175	

Table 3, entry 16:

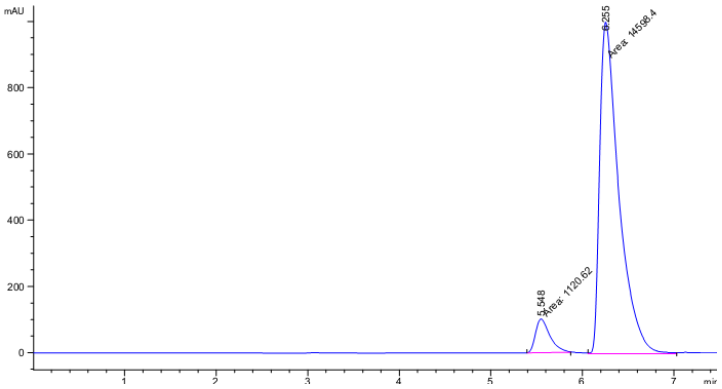

Peak #	RetTime [min]	Type	Width [min]	Area [mAU*s]	Height [mAU]	Area %
1	5.548	MM	0.1820	1120.62219	102.61222	7.1291
2	6.255	MM	0.2426	1.45984e4	1002.84320	92.8709
Totals :				1.57190e4	1105.45542	

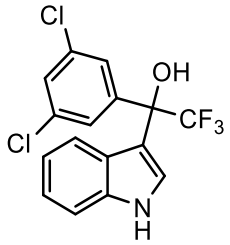

5r: RegisCell column (Hexanes/iPrOH=95/5, 1.0 mL/min, 20 °C, 250 nm)

Racemic:

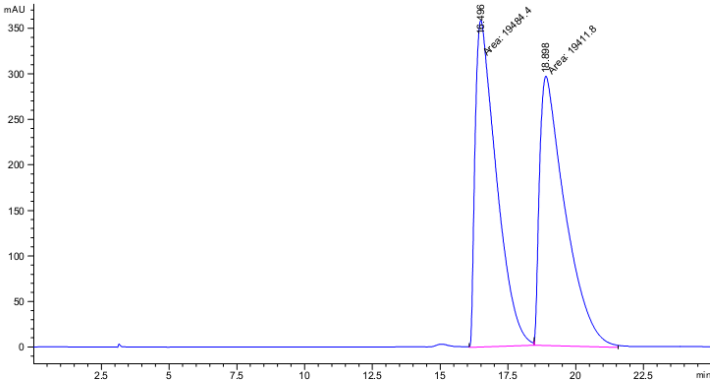

Peak #	RetTime [min]	Type	Width [min]	Area [mAU*s]	Height [mAU]	Area %
1	16.496	MM	0.9055	1.94844e4	358.62350	50.0934
2	18.898	MM	1.0946	1.94118e4	295.55917	49.9066
Totals :				3.88962e4	654.18268	

Table 3, entry 17:

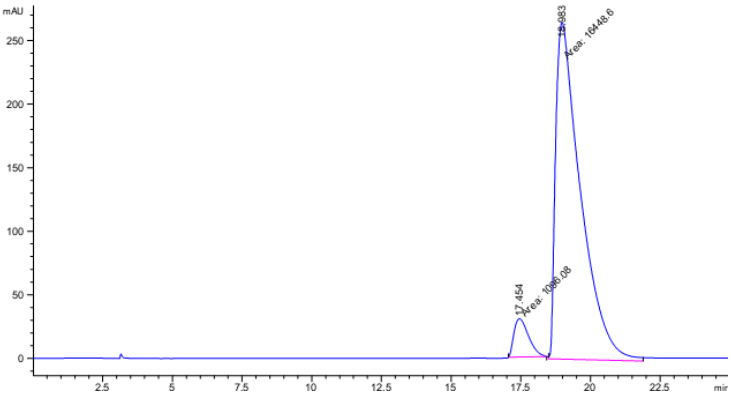

Peak #	RetTime [min]	Type	Width [min]	Area [mAU*s]	Height [mAU]	Area %
1	17.454	MM	0.6084	1096.08350	30.02746	6.2474
2	18.983	MM	1.0358	1.64486e4	264.66965	93.7526
Totals :				1.75447e4	294.69711	

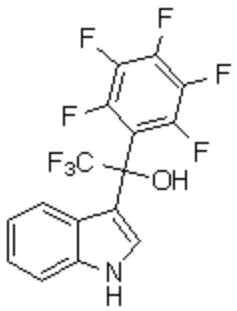

5s: RegisCell column (Hexanes/iPrOH=85/15, 1.0 mL/min, 20 °C, 250 nm)

Racemic:

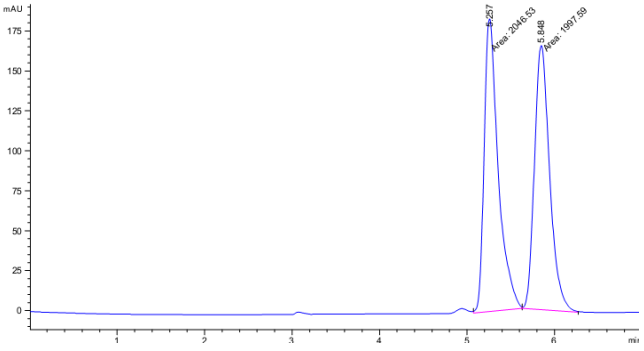

Peak #	RetTime [min]	Type	Width [min]	Area [mAU*s]	Height [mAU]	Area %
1	5.257	MM	0.1861	2046.53394	183.29889	50.6052
2	5.848	MM	0.2012	1997.58752	165.48781	49.3948
Totals :				4044.12146	348.78670	

Table 3, entry 18:

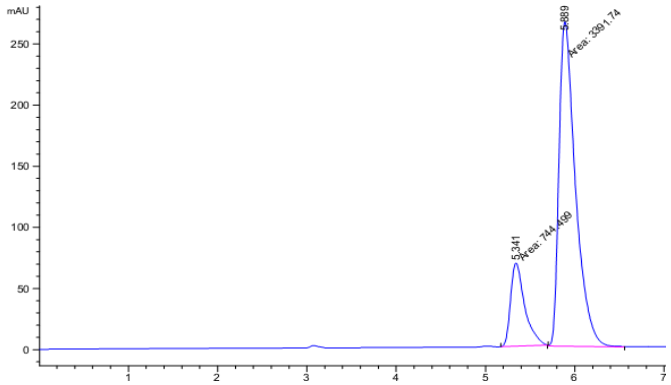

Peak #	RetTime [min]	Type	Width [min]	Area [mAU*s]	Height [mAU]	Area %
1	5.341	MM	0.1825	744.49884	67.98394	17.9994
2	5.889	MM	0.2129	3391.74487	265.56802	82.0006
Totals :				4136.24371	333.55196	

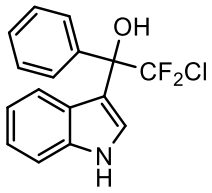

5t: RegisCell column (Hexanes/iPrOH=75/25, 1.0 mL/min, 20 °C, 250 nm)

Racemic

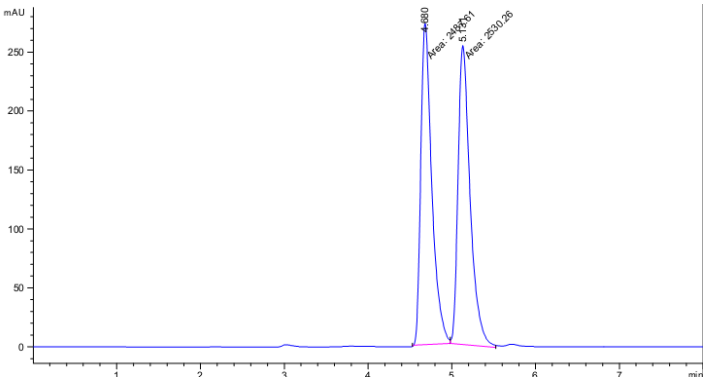

Peak #	RetTime [min]	Type	Width [min]	Area [mAU*s]	Height [mAU]	Area %
1	4.680	MM	0.1521	2487.61304	272.65225	49.5750
2	5.131	MM	0.1662	2530.26196	253.67404	50.4250
Totals :				5017.87500	526.32629	

Table 3, entry 19:

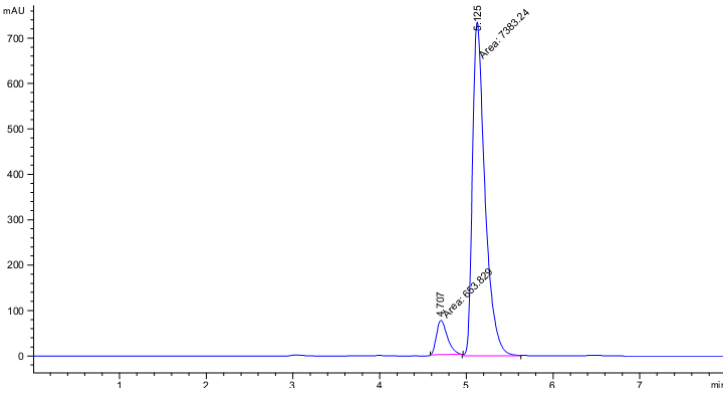

Peak #	RetTime [min]	Type	Width [min]	Area [mAU*s]	Height [mAU]	Area %
1	4.707	MM	0.1434	653.82928	75.99197	8.1352
2	5.125	MM	0.1674	7383.23877	735.28009	91.8648
Totals :				8037.06805	811.27206	

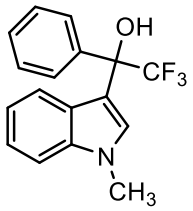

5u: RegisPack column (Hexanes/iPrOH=98/2, 1.0 mL/min, 20 °C, 250 nm)

Racemic:

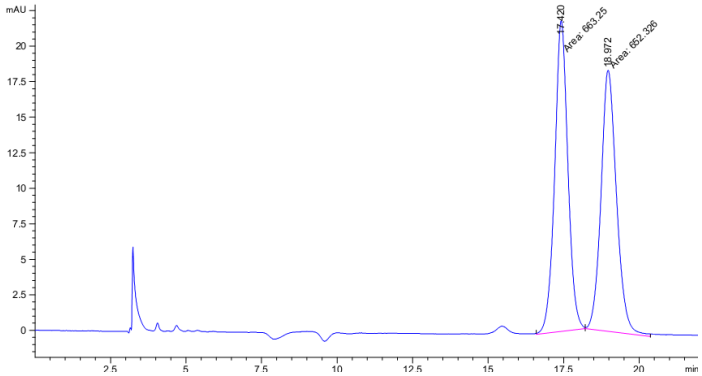

Peak #	RetTime [min]	Type	Width [min]	Area [mAU*s]	Height [mAU]	Area %
1	17.420	MM	0.5056	663.24988	21.86380	50.4152
2	18.972	MM	0.5917	652.32605	18.37514	49.5848
Totals :				1315.57593	40.23894	

Enantiomeric enriched:

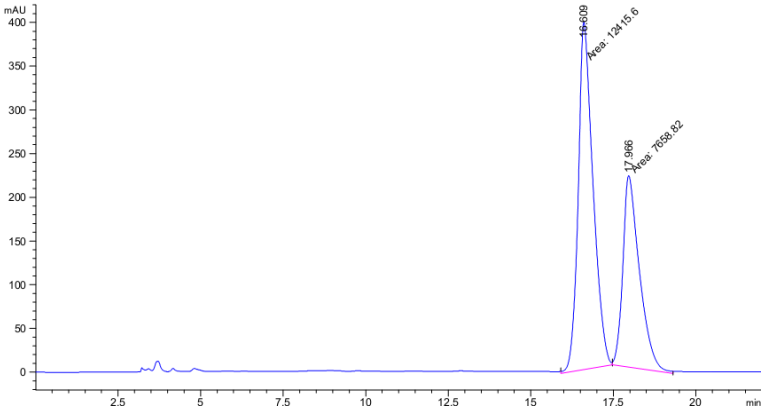

Peak #	RetTime [min]	Type	Width [min]	Area [mAU*s]	Height [mAU]	Area %
1	16.609	MM	0.5206	1.24156e4	397.44159	61.8478
2	17.966	MM	0.5828	7658.81934	219.00726	38.1522
Totals :				2.00744e4	616.44885	

Appendix for Chapter 4

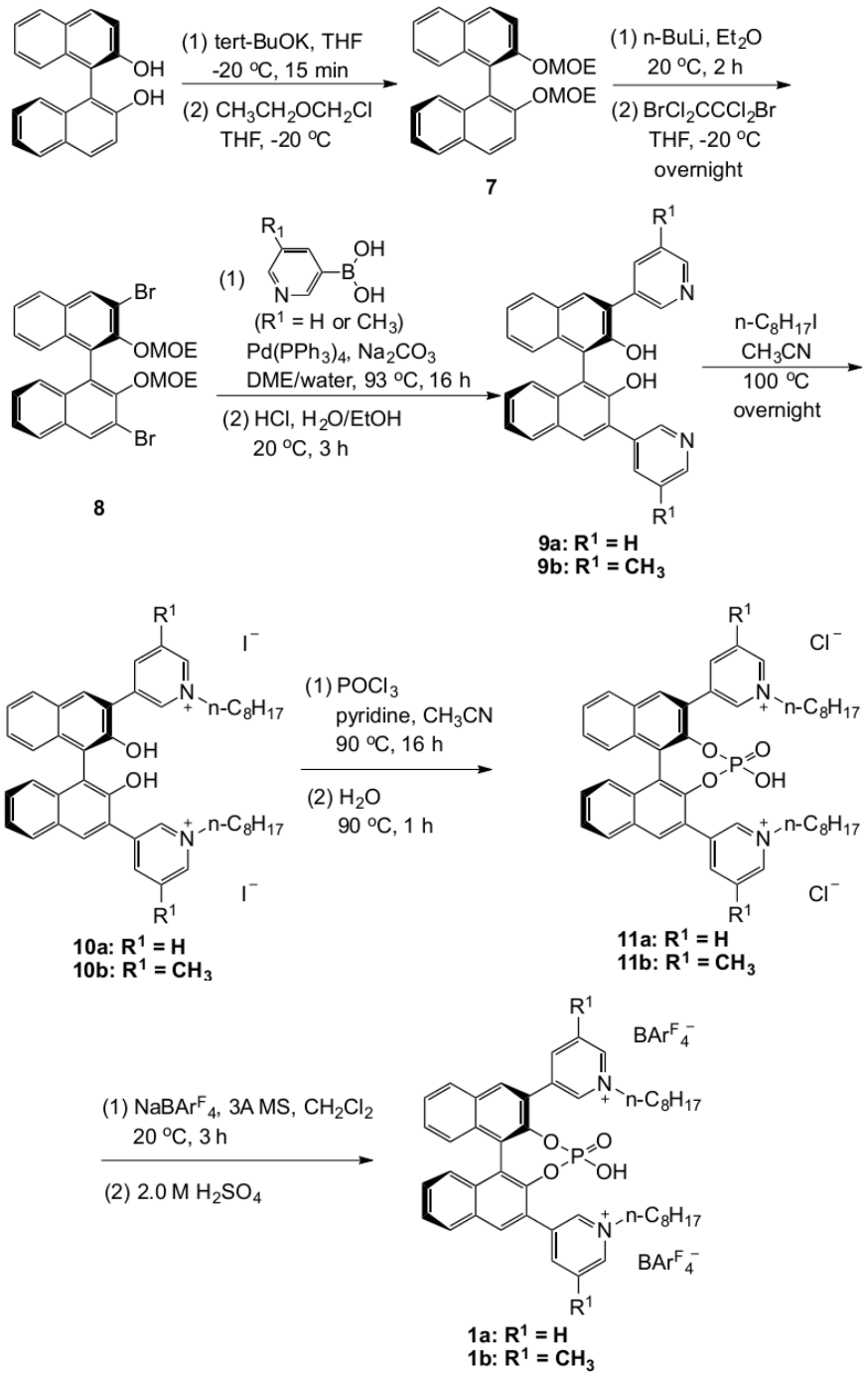

Scheme S1. Synthetic route for pyridinium ion-containing phosphoric acids **1a** and **1b**.

Table S1. Kinetic data for the Friedel-Crafts alkylation of indole with *trans-β*-nitrostyrene.[a]

catalyst, solvent	time (h)	conversion (%)	rate constant (M^{-1} h^{-1})
10% 3a, CH_2Cl_2/C_6H_6 1:2	18.0	17	0.0270
	23.5	23	
	40.5	36	
10% 3b, CH_2Cl_2/C_6H_6 1:2	18.0	17	0.0331
	23.5	22	
	40.5	33	
10% 2b, CH_2Cl_2/C_6H_6 1:2	18.0	61	0.158
	23.5	69	
	40.5	84	
5% 2b, CH_2Cl_2	22.0	47	0.0790[b]
	28.0	54	
10% 2b, CH_2Cl_2	22.0	68	0.158[c]
	28.0	75	
20% 2b, CH_2Cl_2	2.2	38	0.326[d]
	5.0	53	

[a][indole]$_0$ = 200 mM, [*β*-nitrostyrene]$_0$ = 400 mM, T = -30 ˚C. [b]$t_{1/2}$ = 26 h, ee =60%. [c]$t_{1/2}$ = 13 h, ee =70%. [d]$t_{1/2}$ = 6.2 h, ee =73%.

I. NMR Spectra

Figure S1. ^{1}H and ^{13}C NMR of (*R*)-2,2'-bis(ethoxymethoxy)-1,1'-binaphthyl (**7**).

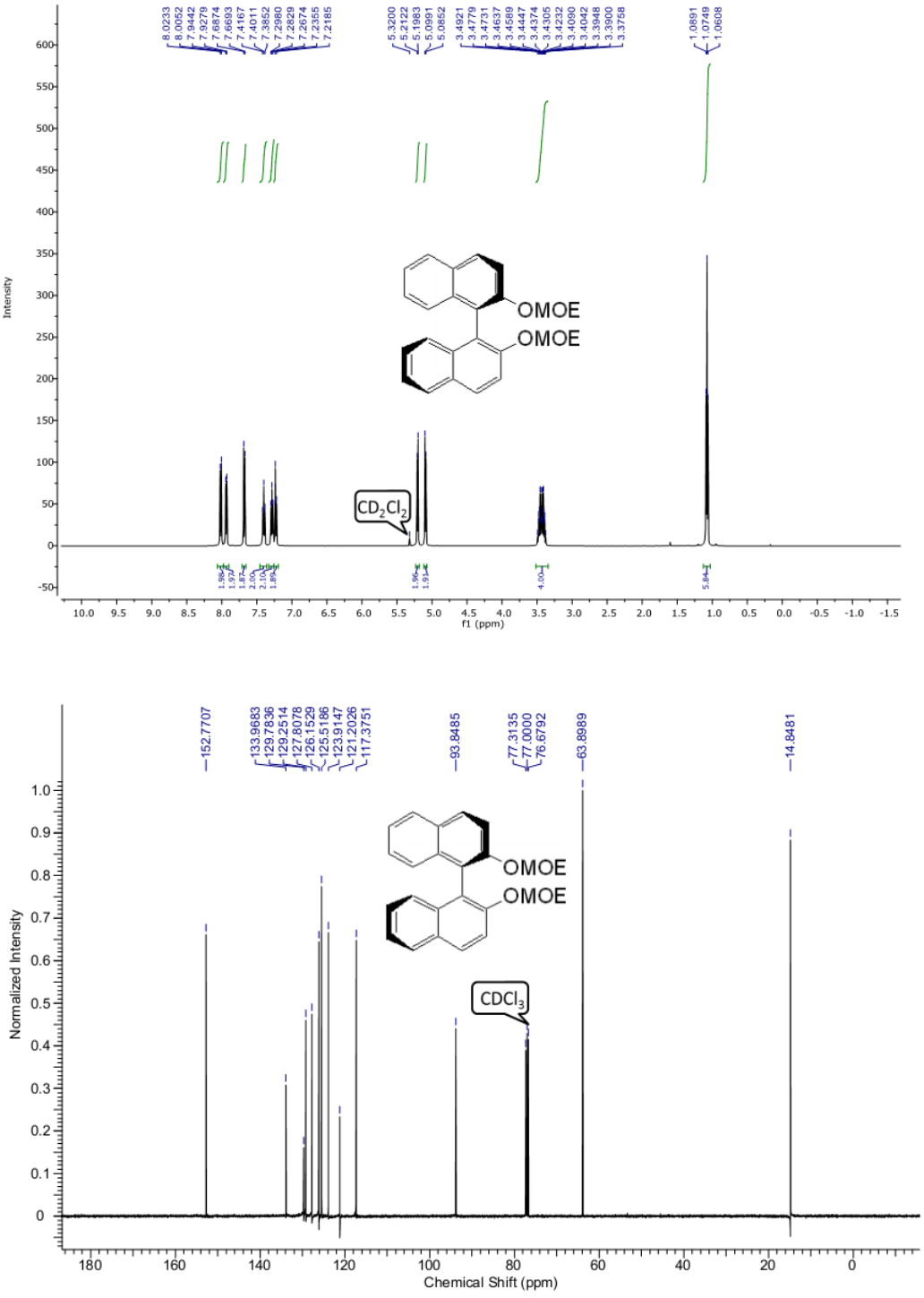

Figure S2. ^{1}H and ^{13}C NMR of (*R*)-3,3'-dibromo-2,2'-bis(ethoxymethoxy)-1,1'-binaphthyl (**8**).

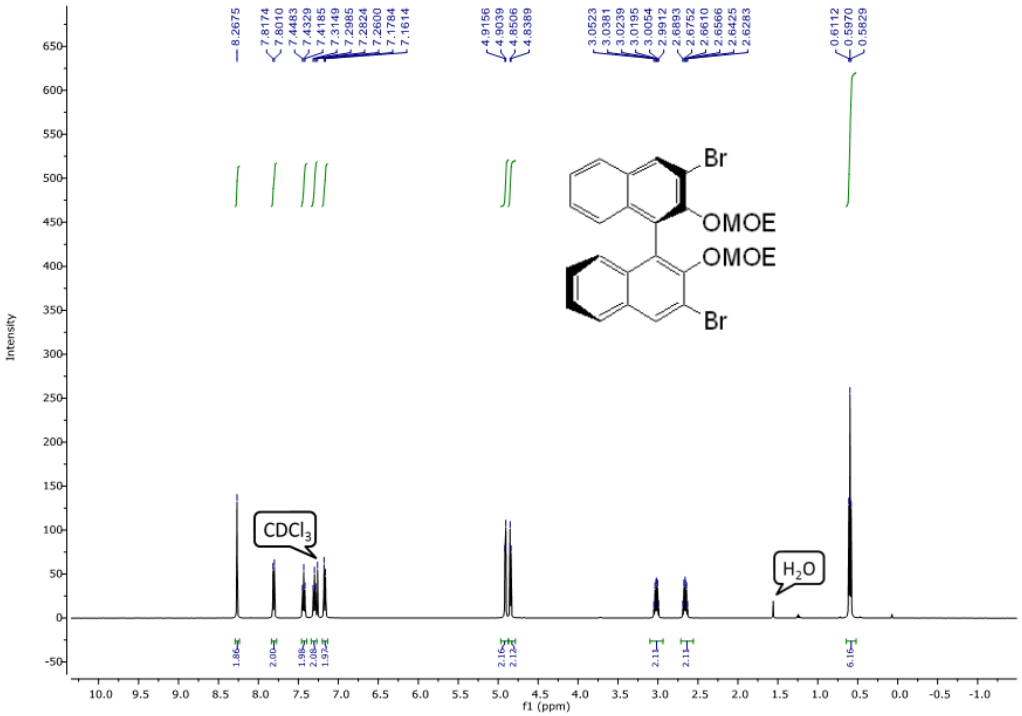

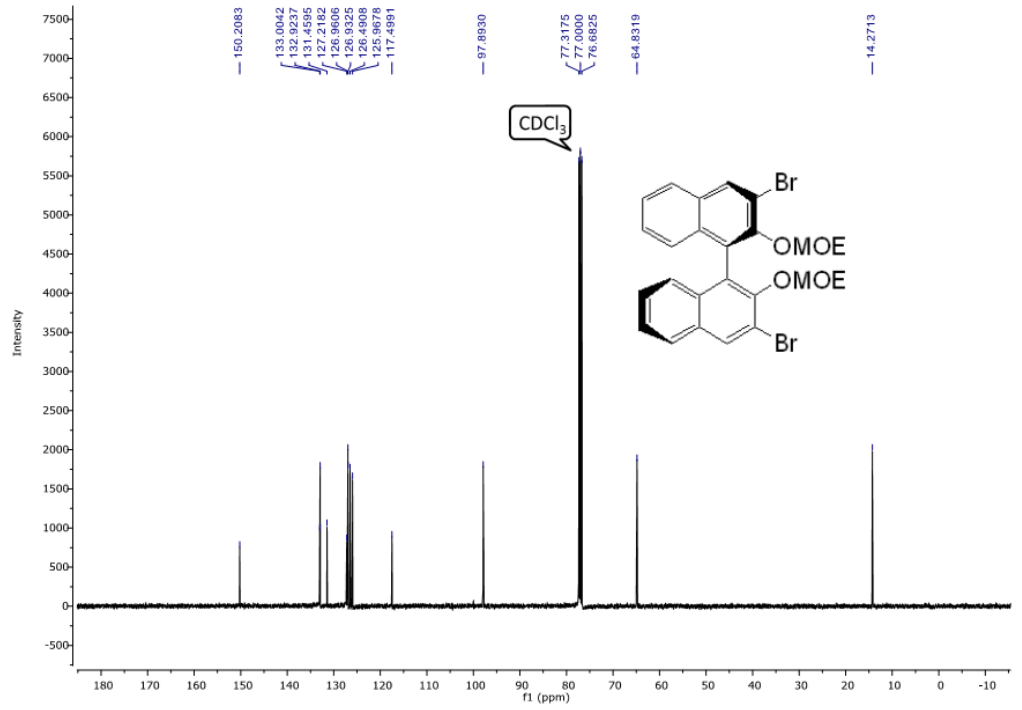

Figure S3. ^{1}H and ^{13}C NMR of (*R*)-3,3'-di(3-pyridyl)-2,2'-di(ethoxymethoxy)-1,1'-binaphthyl (**9a**).

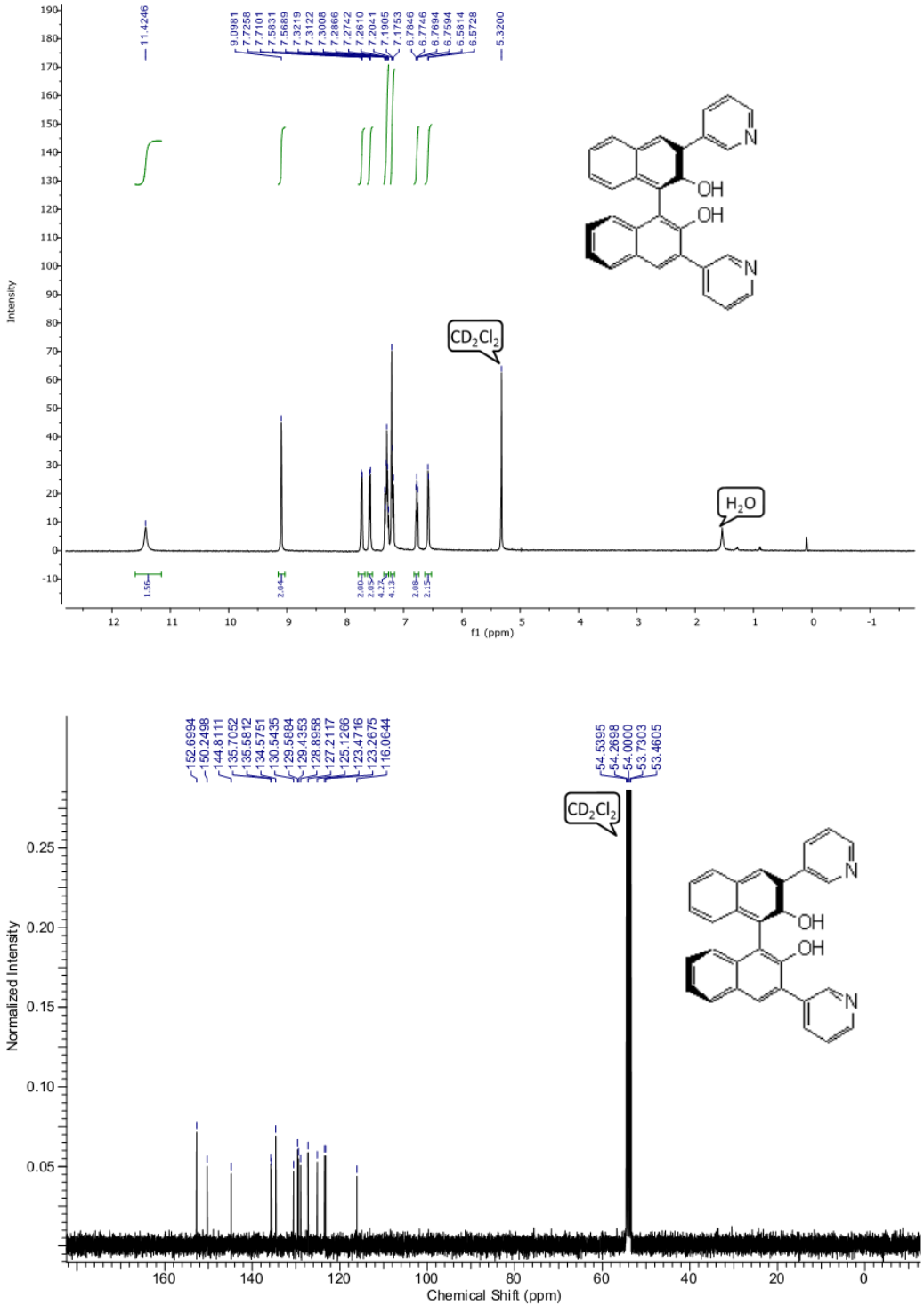

Figure S4. ^{1}H and ^{13}C NMR of (*R*)-3,3'-di[3-(5-methyl)-pyridyl]-2,2'-di(ethoxymethoxy)-1,1'-binaphthyl (**9b**).

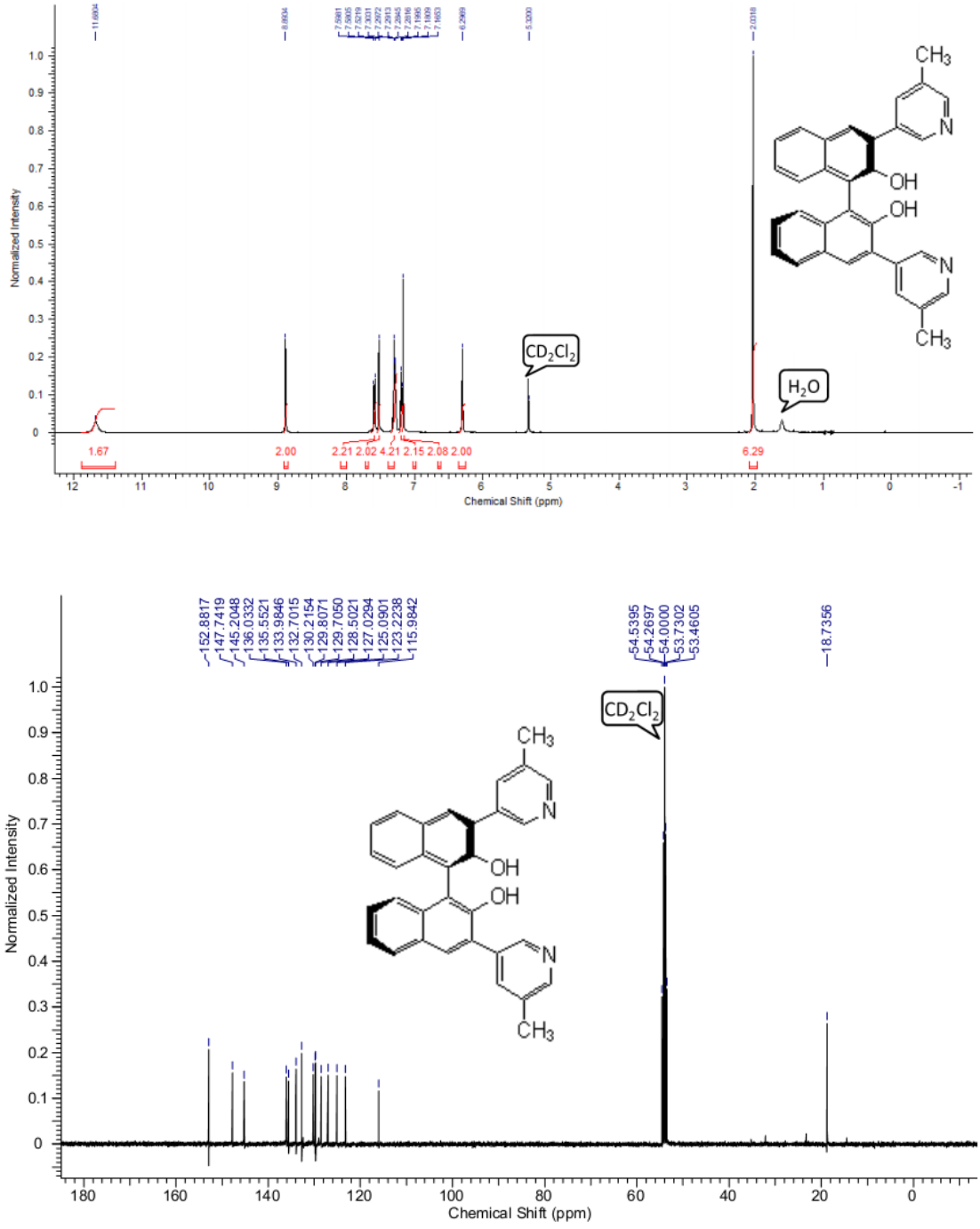

Figure S5. ^{1}H and ^{13}C NMR of (*R*)-3,3'-di(3-*N*-octylpyridinium)-2,2'-dihydroxyl-1,1'-binaphthyl iodide (**10a**).

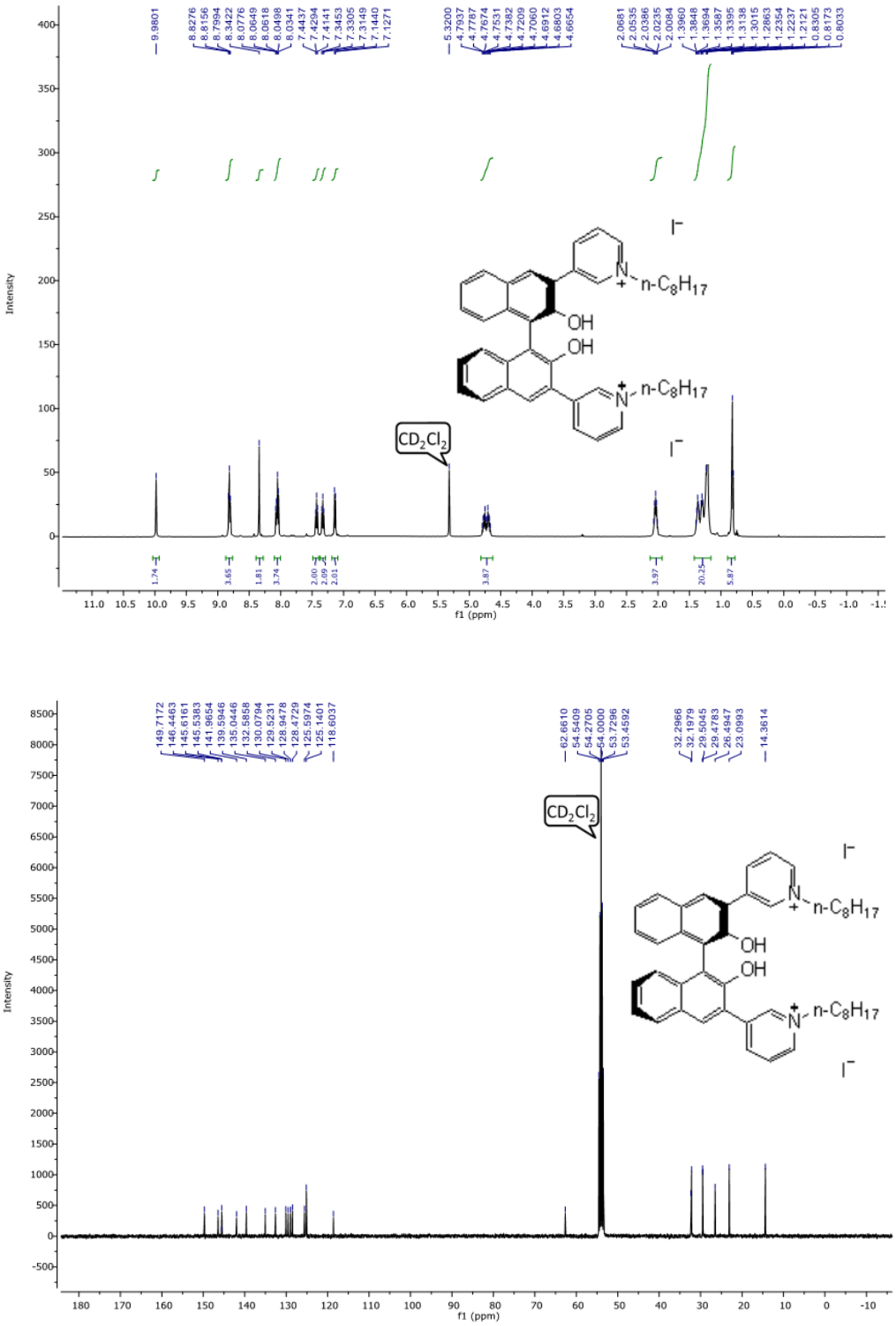

Figure S6. ^{1}H and ^{13}C NMR of (*R*)-3,3'-di(3-(*N*-octyl-5-methyl)pyridinium)-2,2'-dihydroxyl-1,1'-binaphthyl iodide (**10b**).

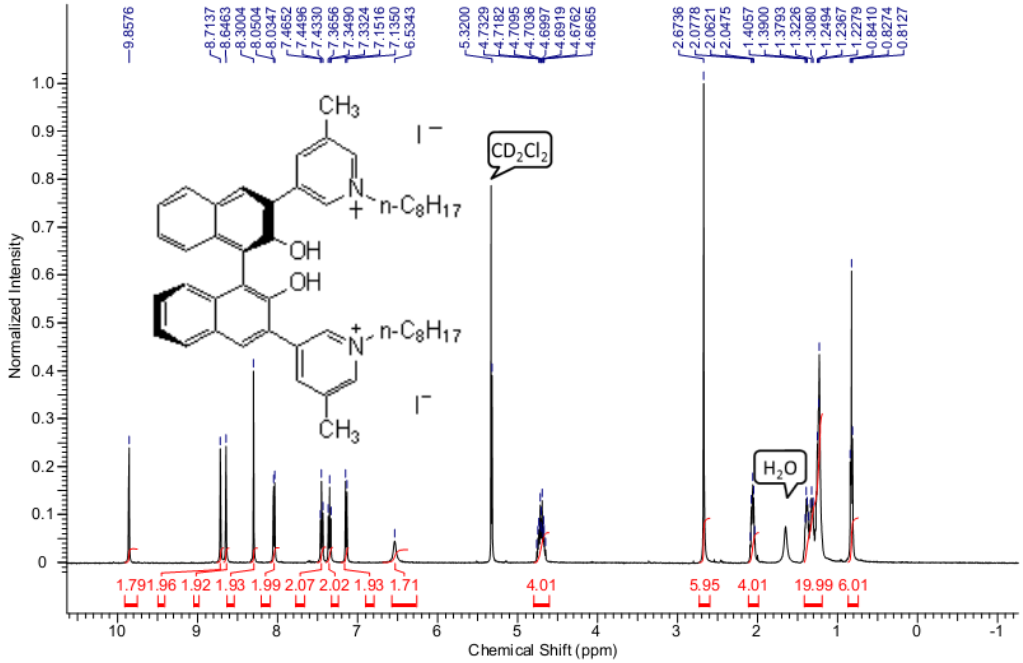

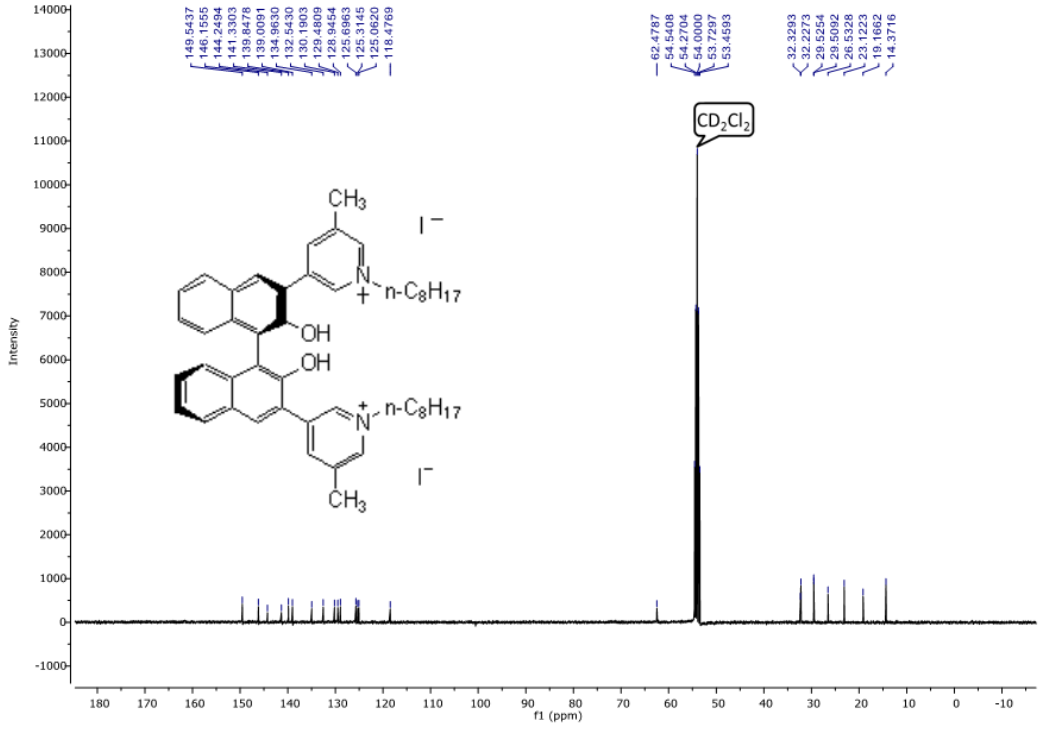

Figure S7. ^{1}H, ^{13}C and ^{31}P NMR of (*R*)-3,3'-(4-hydroxy-4-oxidodinaphtho[2,1-*d*:1',2'-*f*][1,3,2]dioxaphosphepine-2,6-diyl)bis(1-octylpyridin-1-ium) chloride (**11a**).

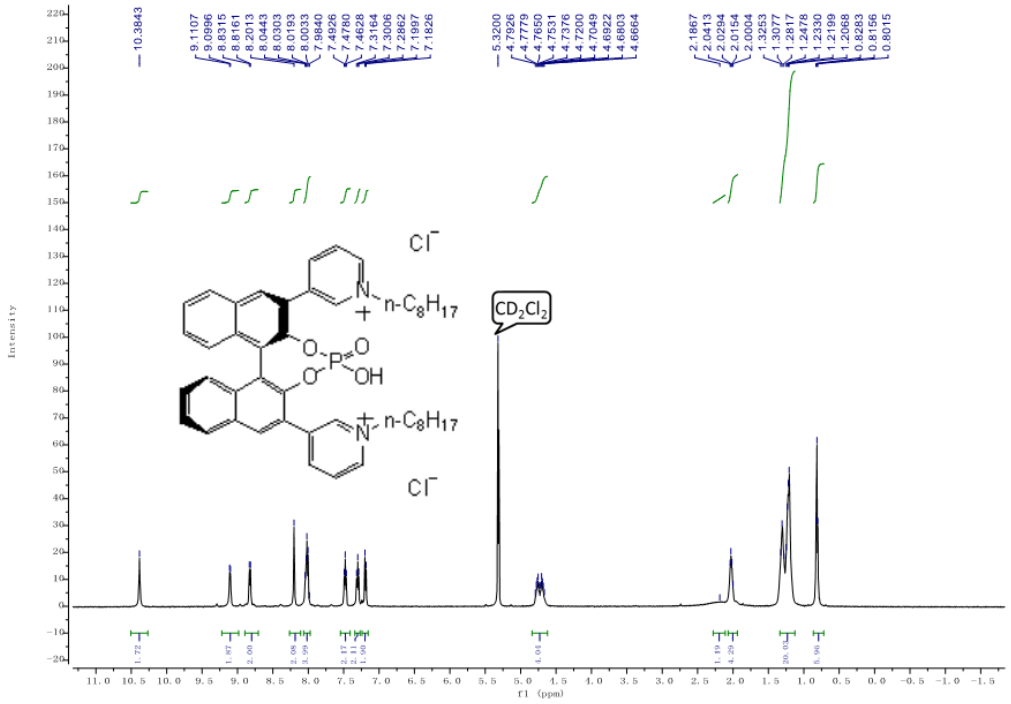

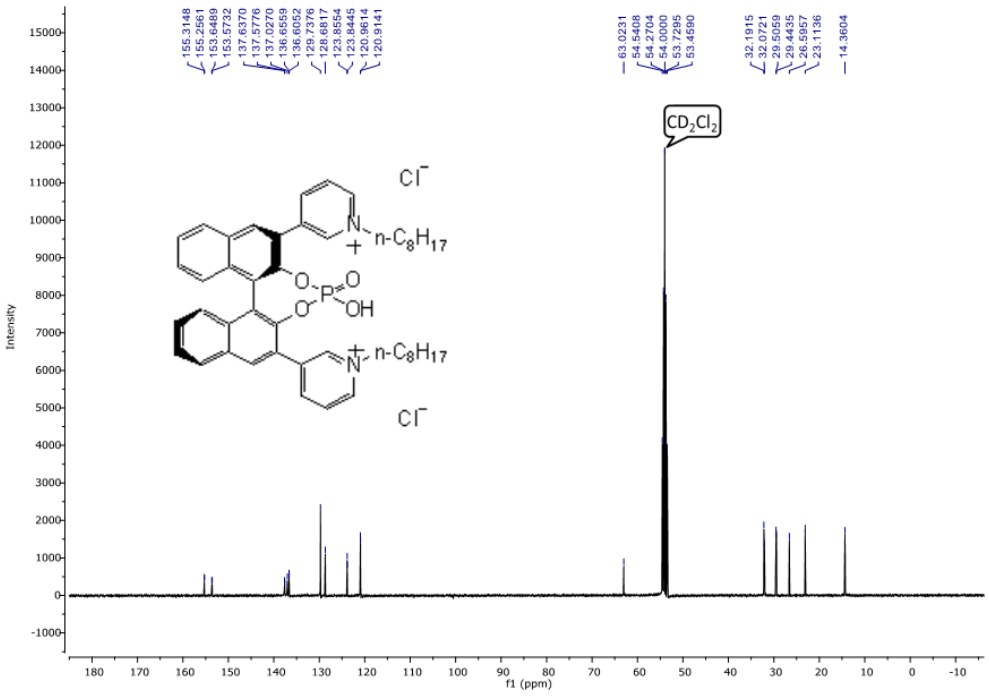

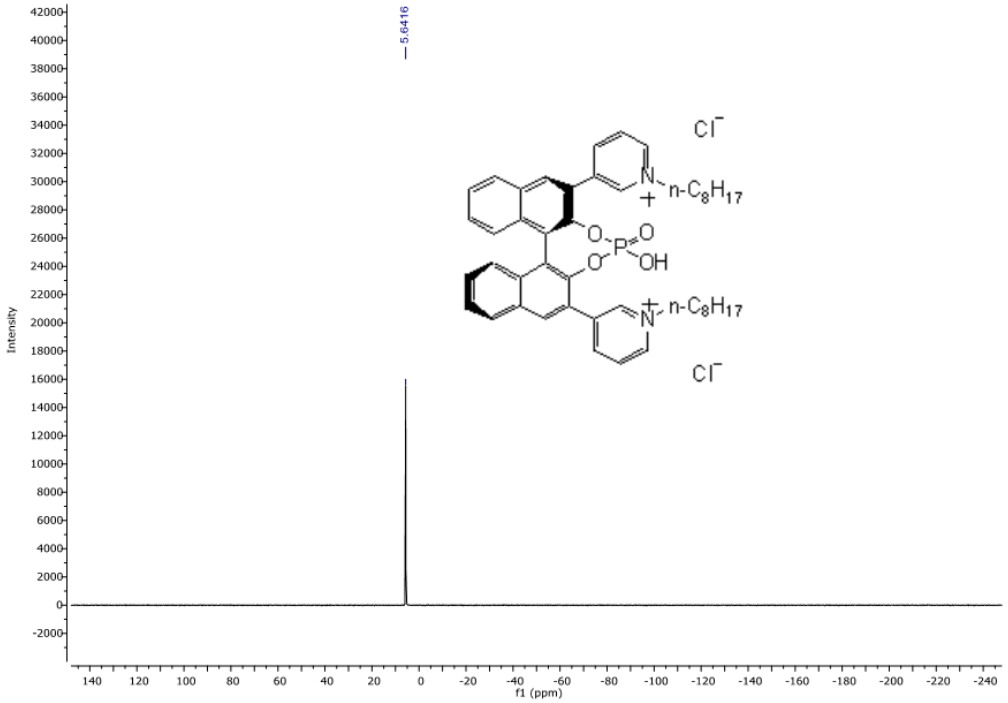

Figure S8. ^{1}H, ^{13}C and ^{31}P NMR of (*R*)-5,5'-(4-hydroxy-4-oxidodinaphtho[2,1-*d*:1',2'-*f*][1,3,2]dioxaphosphepine-2,6-diyl)bis(3-methyl-1-octylpyridin-1-ium) chloride (**11b**).

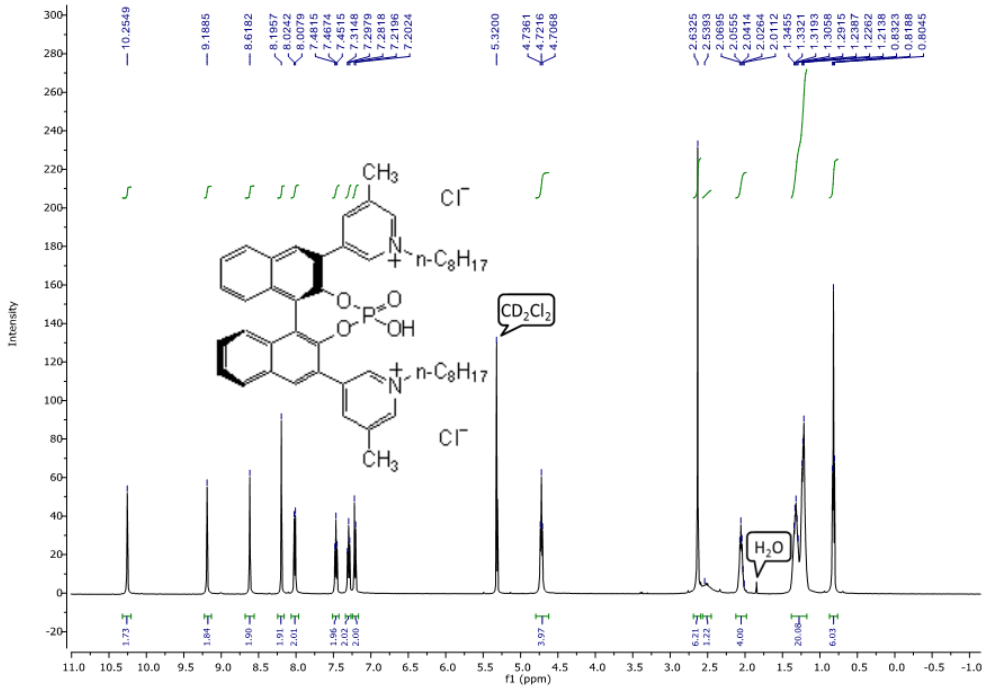

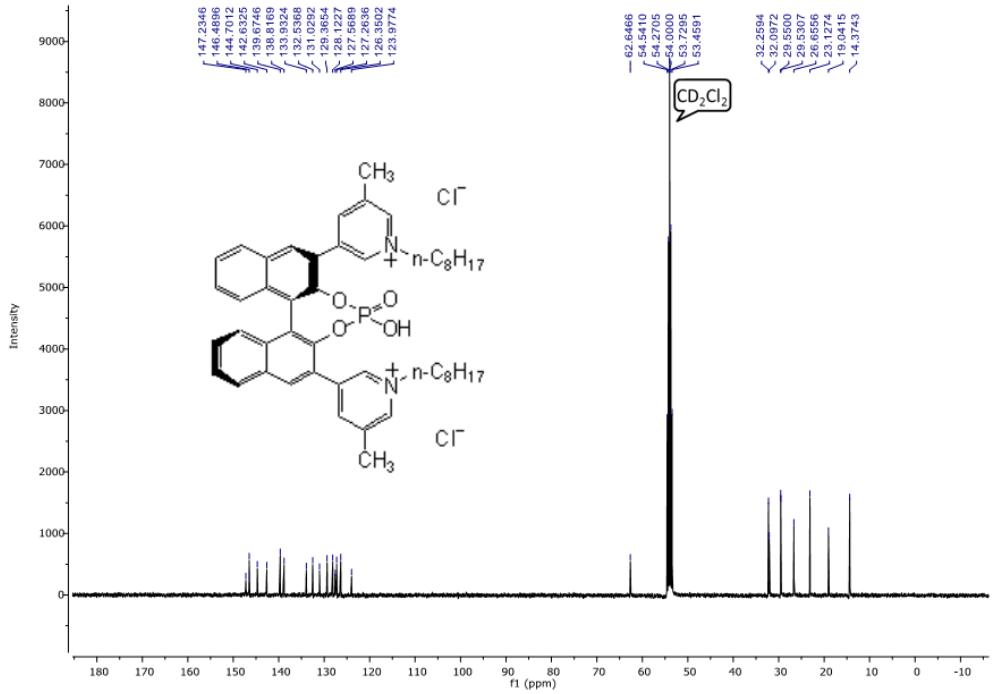
147.2346
146.4896
144.7012
142.6325
139.6746
138.8169
133.9324
132.5368
131.0292
129.3654
128.1227
127.5689
127.2636
126.3502
123.9774
62.6466
54.5410
54.2705
54.0000
53.7295
53.4591
32.2594
32.0972
29.5500
29.5307
26.6556
23.1274
19.0415
14.3743
CD2Cl2
Intensity
f1 (ppm)

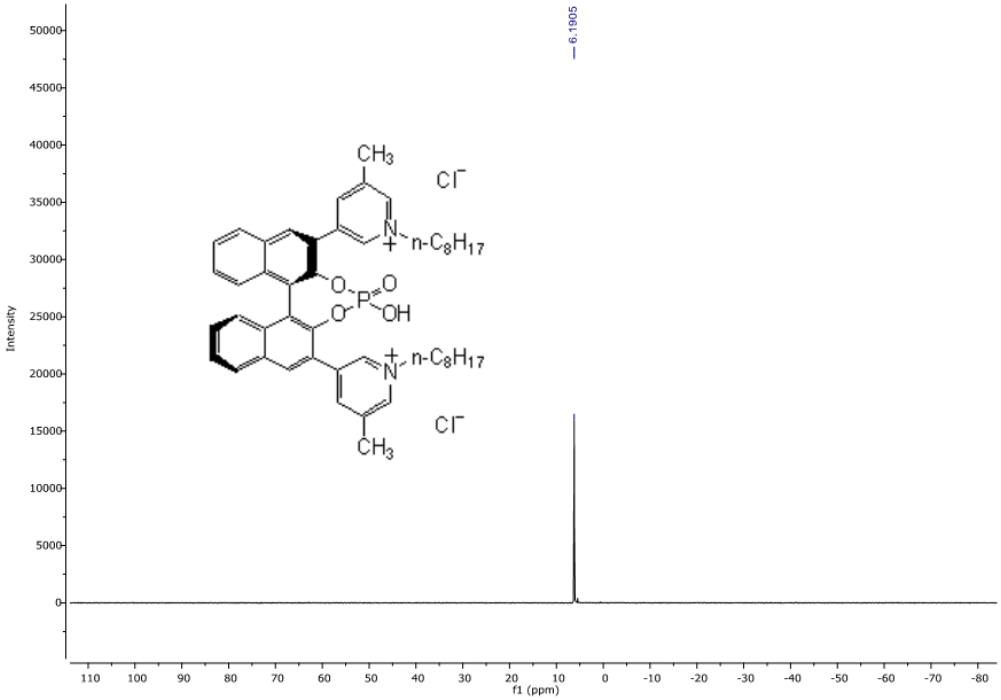
6.1905
Intensity
f1 (ppm)

Figure S9. ^{1}H, ^{13}C, ^{19}F and ^{31}P NMR of (*R*)-3,3'-(4-hydroxy-4-oxidodinaphtho[2,1-*d*:1',2'-*f*][1,3,2]dioxaphosphepine-2,6-diyl)bis(1-octylpyridin-1-ium) tetrakis[3,5-bis(trifluoromethyl)phenyl]borate (**1a**).

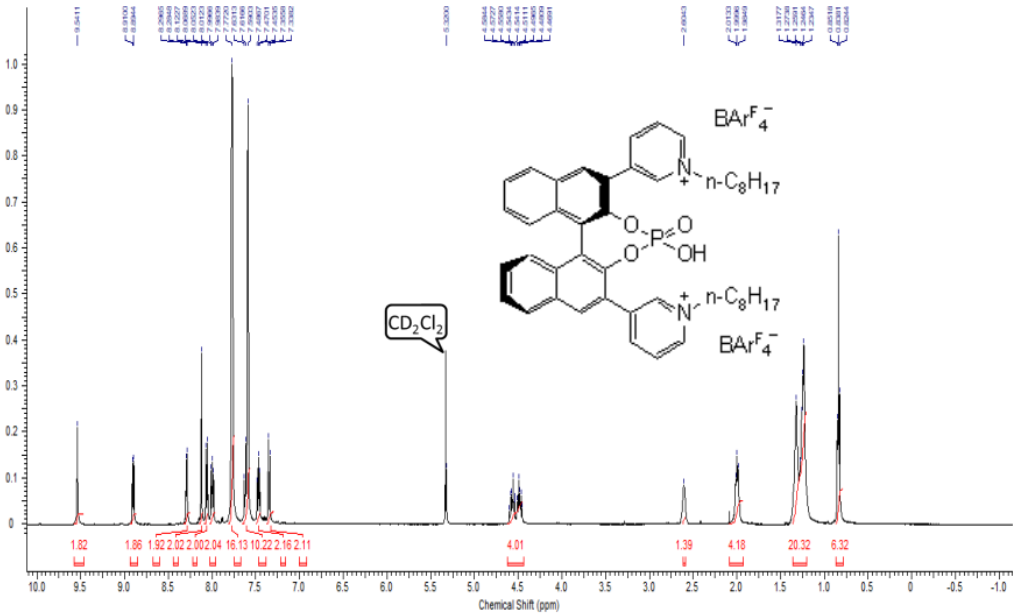

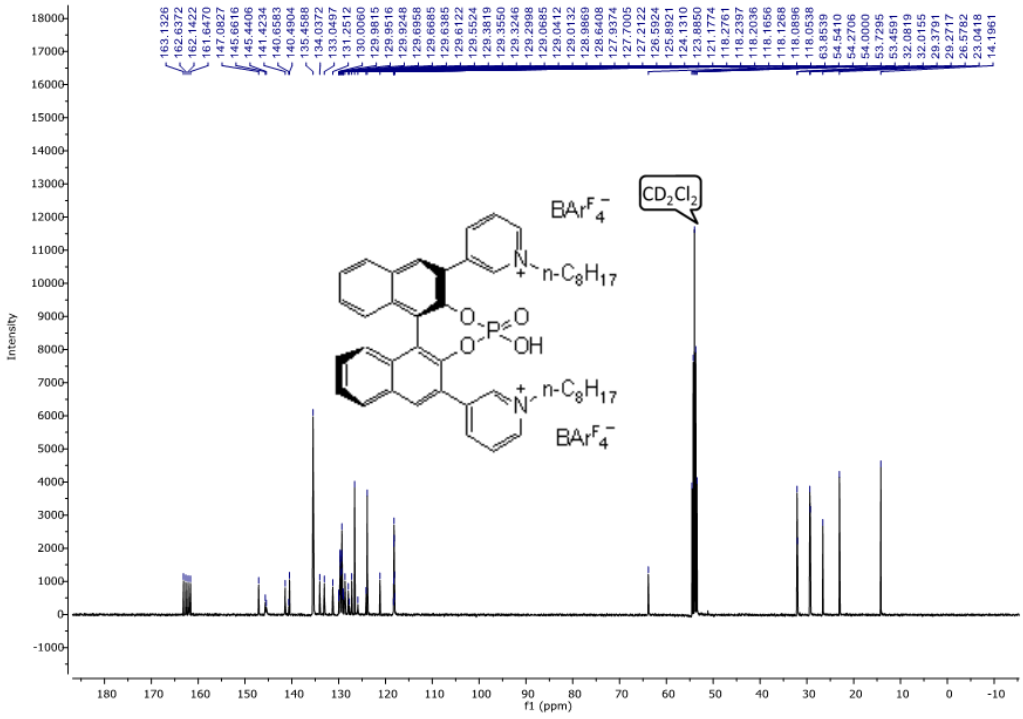

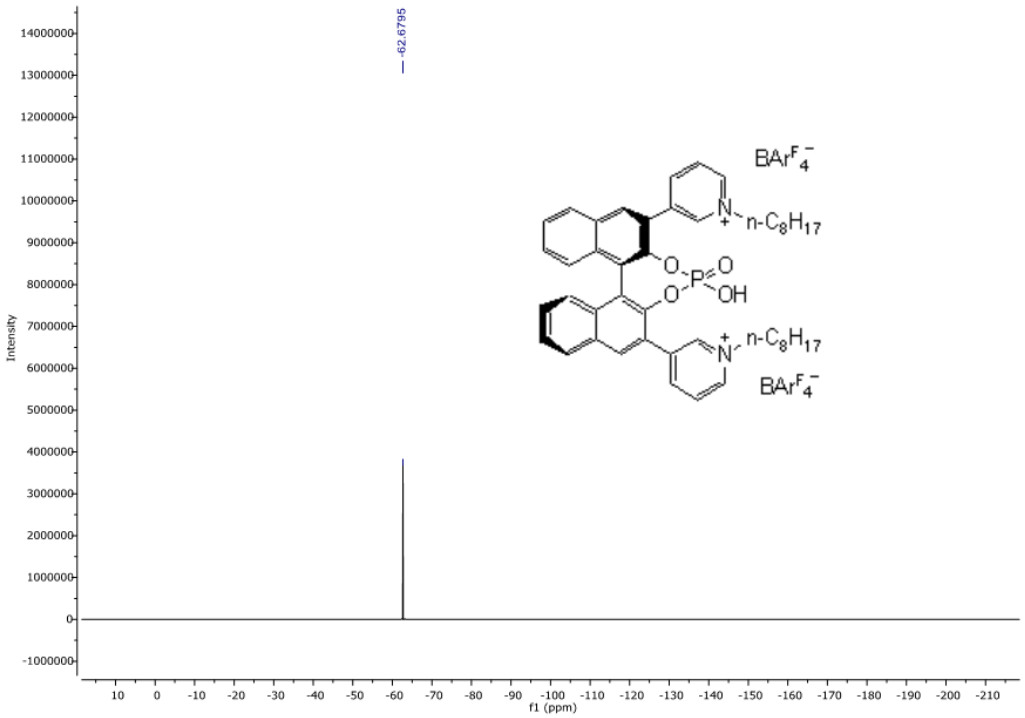
-62.6795
Intensity
f1 (ppm)
BAr$^{F}_{4}^{-}$
n-C$_8$H$_{17}$
O
P
OH
n-C$_8$H$_{17}$
BAr$^{F}_{4}^{-}$

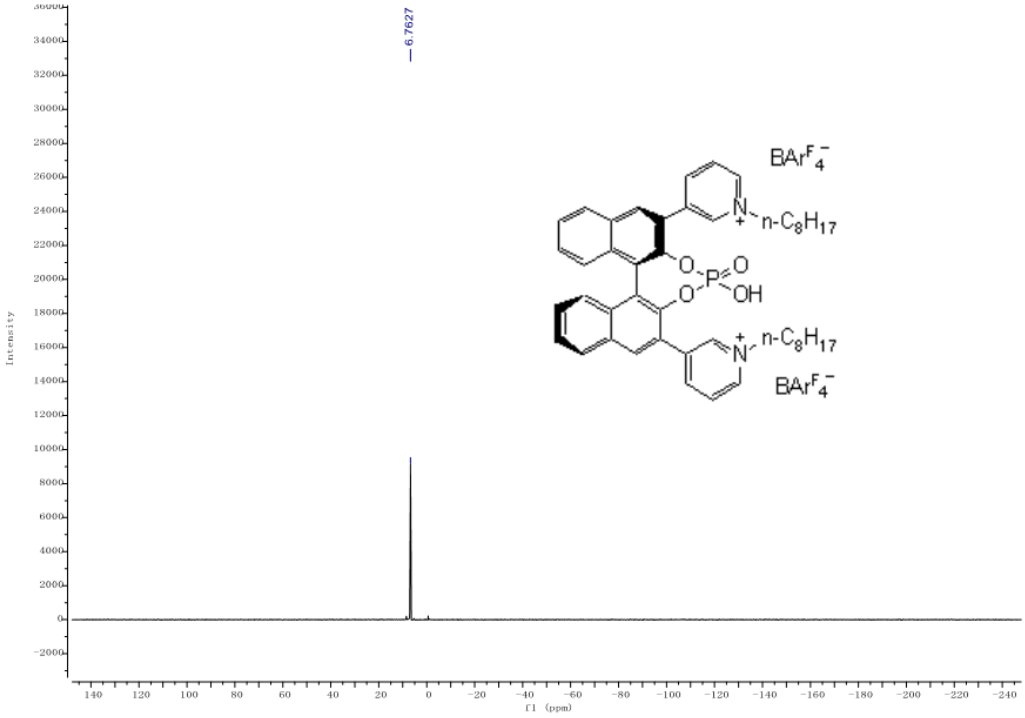
-6.7627
Intensity
f1 (ppm)
BAr$^{F}_{4}^{-}$
n-C$_8$H$_{17}$
O
P
OH
n-C$_8$H$_{17}$
BAr$^{F}_{4}^{-}$

Figure S10. ^{1}H, ^{13}C, ^{19}F and ^{31}P NMR of (*R*)-5,5'-(4-hydroxy-4-oxidodinaphtho[2,1-*d*:1',2'-*f*][1,3,2]dioxaphosphepine-2,6-diyl)bis(3-methyl-1-octylpyridin-1-ium) tetrakis[3,5-bis(trifluoromethyl)phenyl]borate (**1b**).

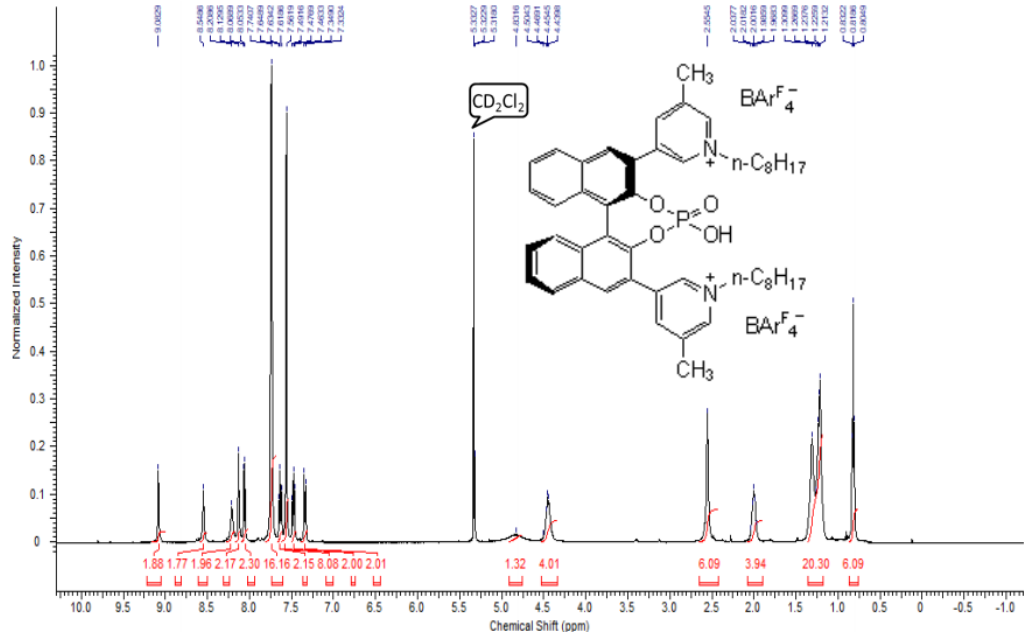

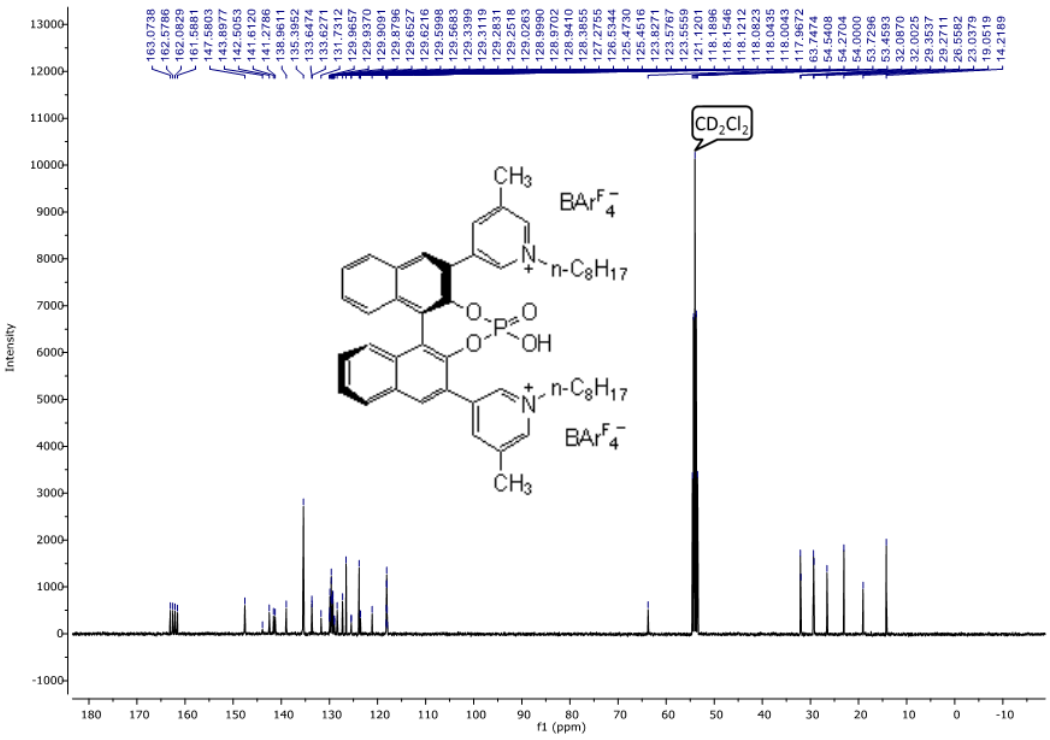

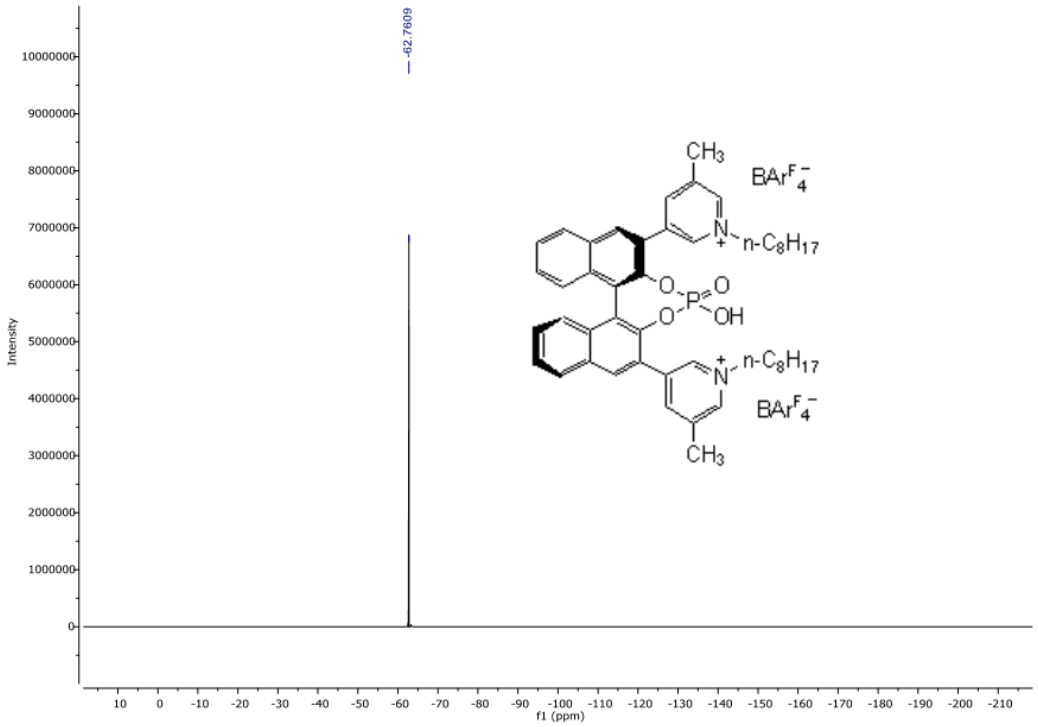
-62.7609
Intensity
f1 (ppm)
CH3
BArF4−
n-C8H17
O
P
OH

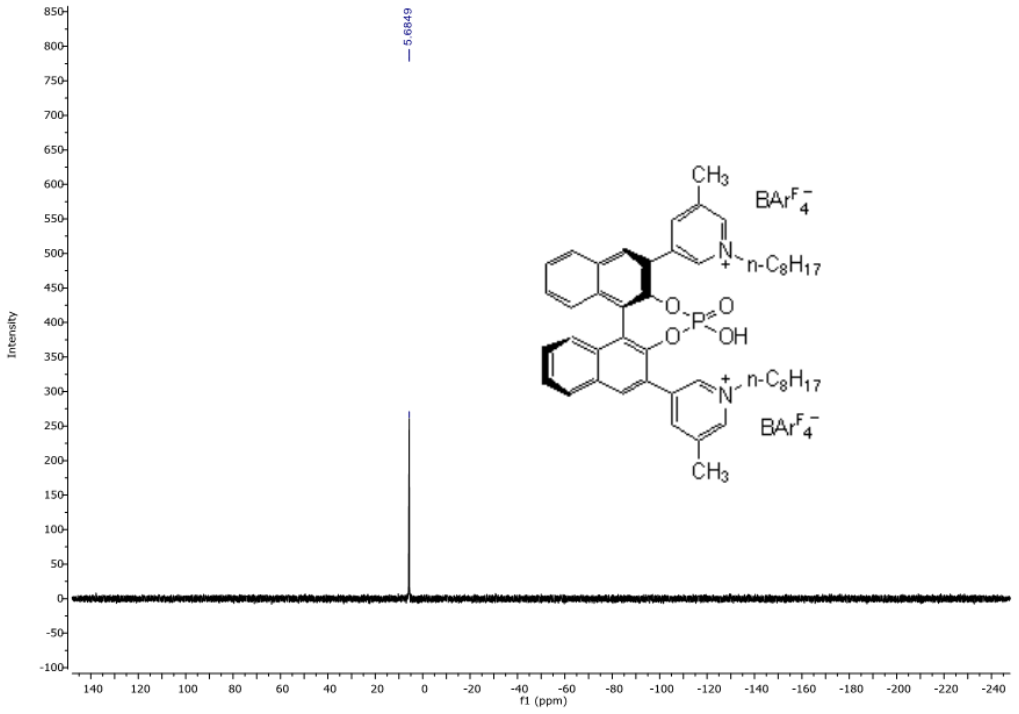
5.6849
Intensity
f1 (ppm)
CH3
BArF4−
n-C8H17
O
P
OH

Figure S11. ^{1}H, ^{13}C, ^{19}F and ^{31}P NMR of (*R*)-(4-hydroxy-4-oxidodinaphtho[2,1-d:1',2'-f][1,3,2]dioxaphosphepine-2,6-diyl)bis(triphenylphosphonium) tetrafluoroborate (**2f**).

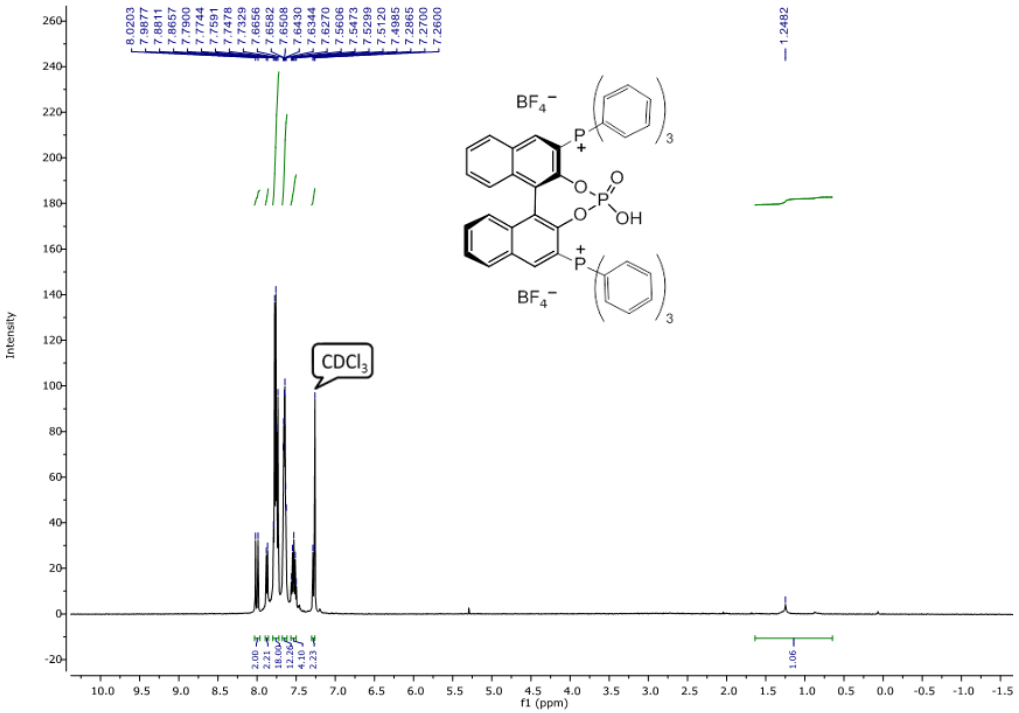

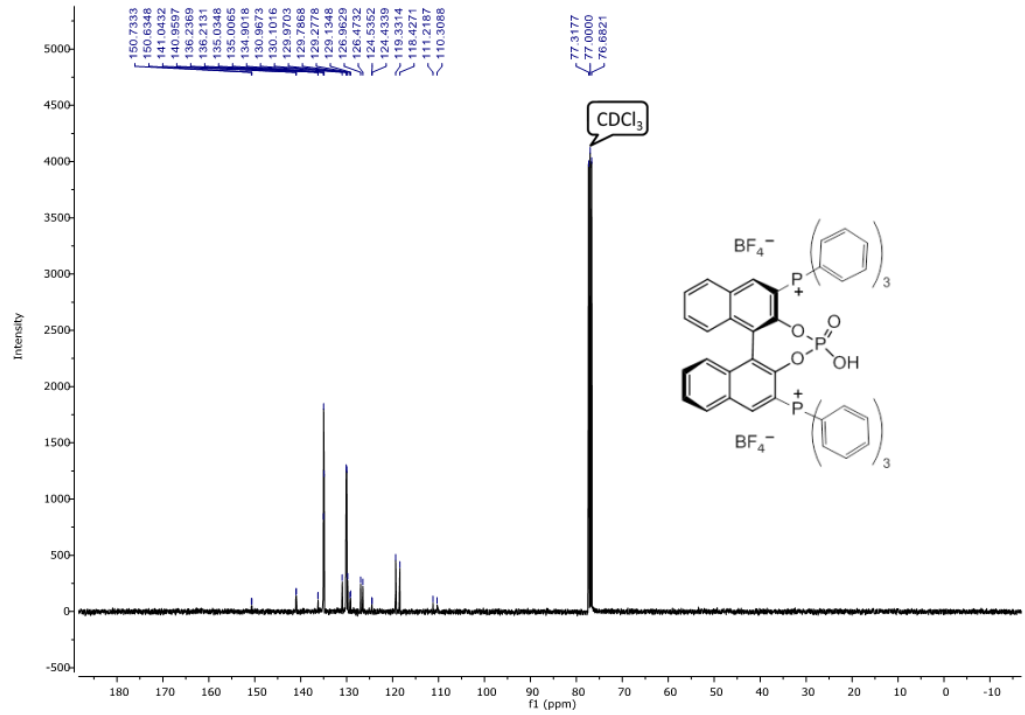

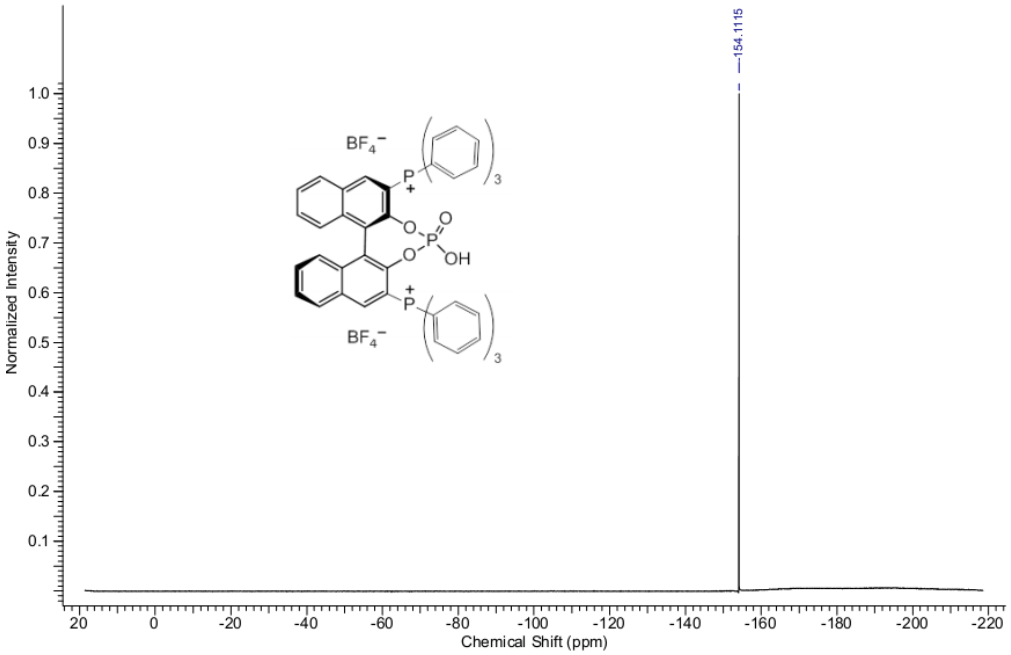
154.1115
Normalized Intensity
Chemical Shift (ppm)
BF4−
OH

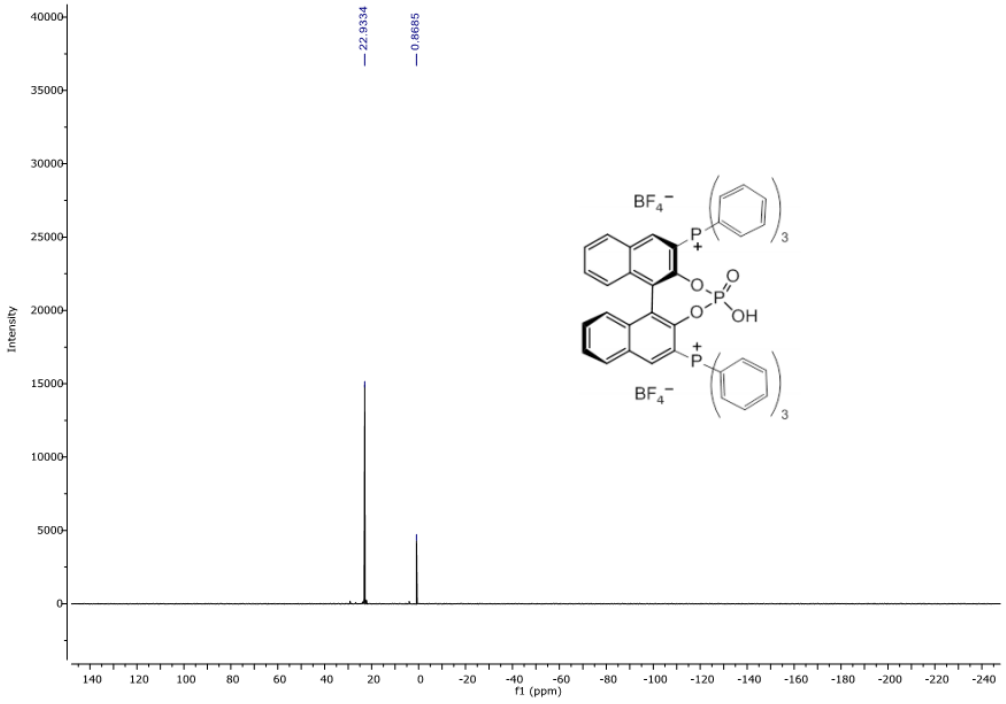
22.9334
0.8685
Intensity
f1 (ppm)
BF4−
OH

Figure S12. ^{1}H, ^{13}C, ^{19}F and ^{31}P NMR of (*R*)-(4-hydroxy-4-oxidodinaphtho[2,1-d:1',2'-f][1,3,2]dioxaphosphepine-2,6-diyl)bis(triphenylphosphonium) hexafluorophosphate (**2g**).

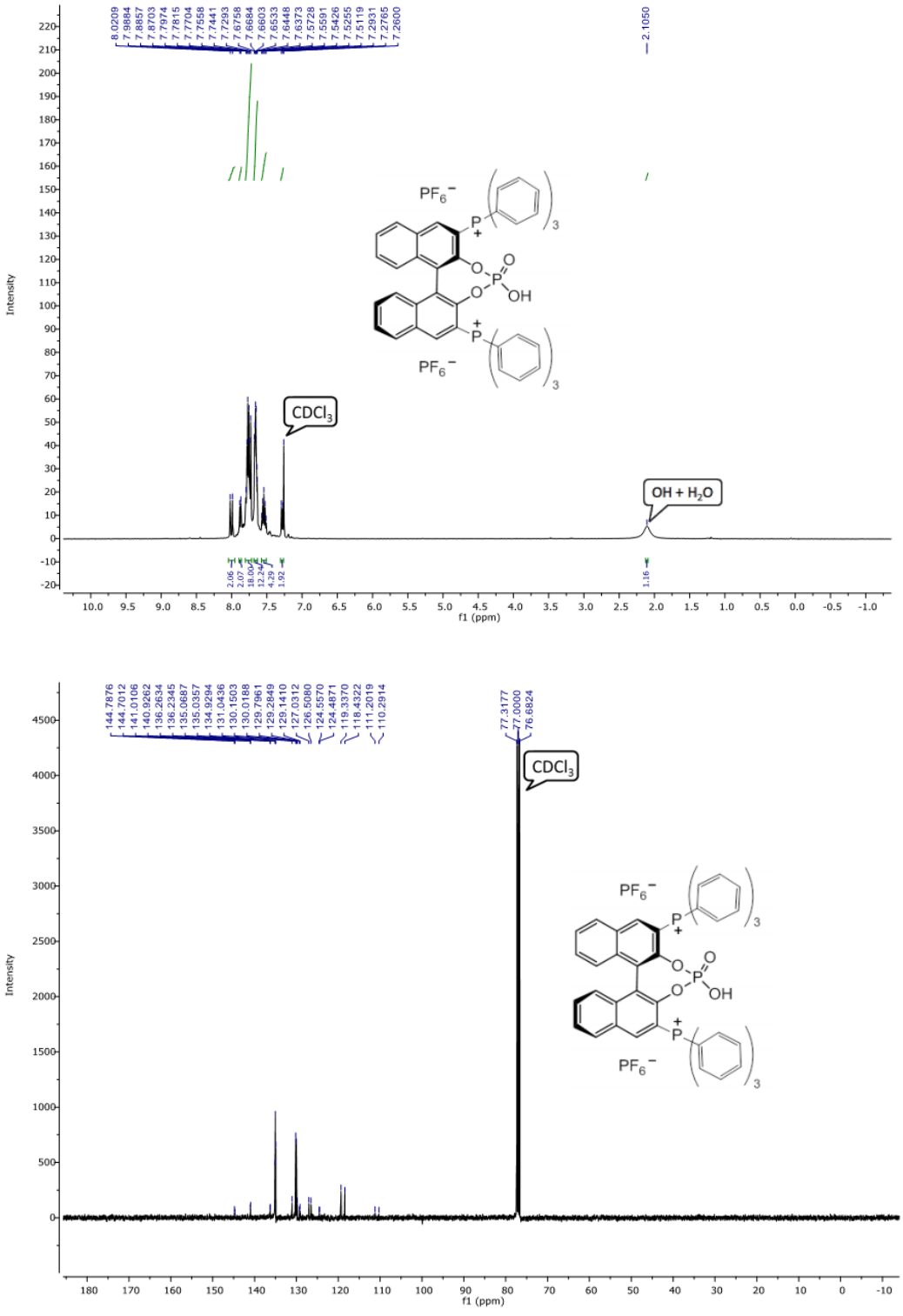

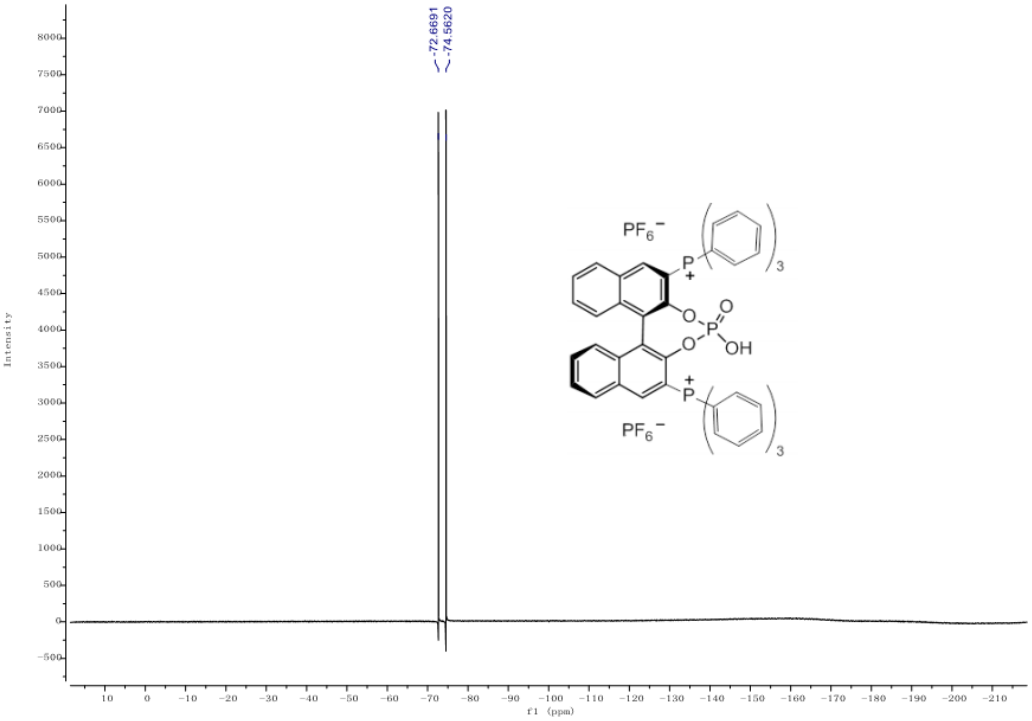
-72.6691
-74.5620
Intensity
f1 (ppm)
PF6−
PF6−
OH

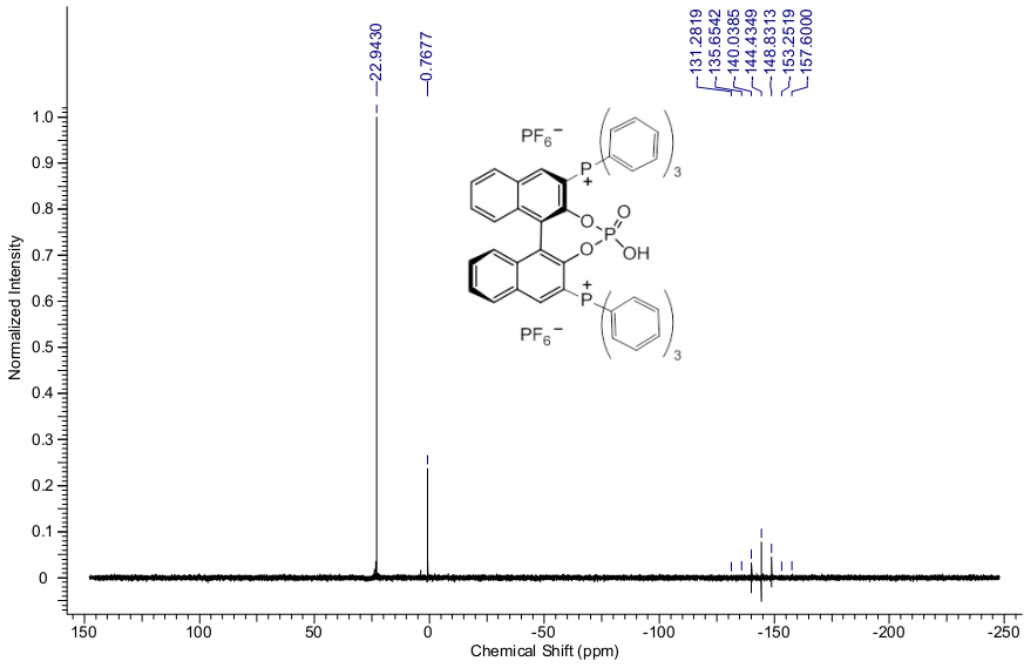
22.9430
0.7677
131.2819
135.6542
140.0385
144.4349
148.8313
153.2519
157.6000
Normalized Intensity
Chemical Shift (ppm)
PF6−
PF6−
OH

Figure S13. ^{1}H, ^{13}C, ^{19}F and ^{31}P NMR of (*R*)-(4-hydroxy-4-oxidodinaphtho[2,1-d:1',2'-f][1,3,2]dioxaphosphepine-2,6-diyl)bis(triphenylphosphonium) tetrakis(pentafluorophenyl)borate (**2h**).

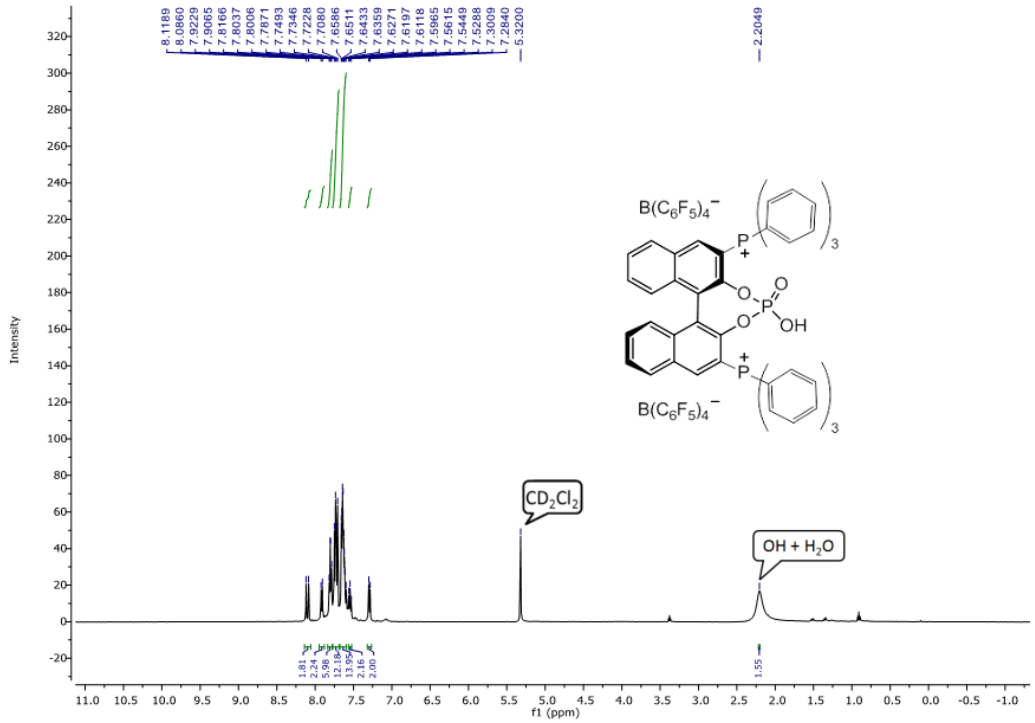

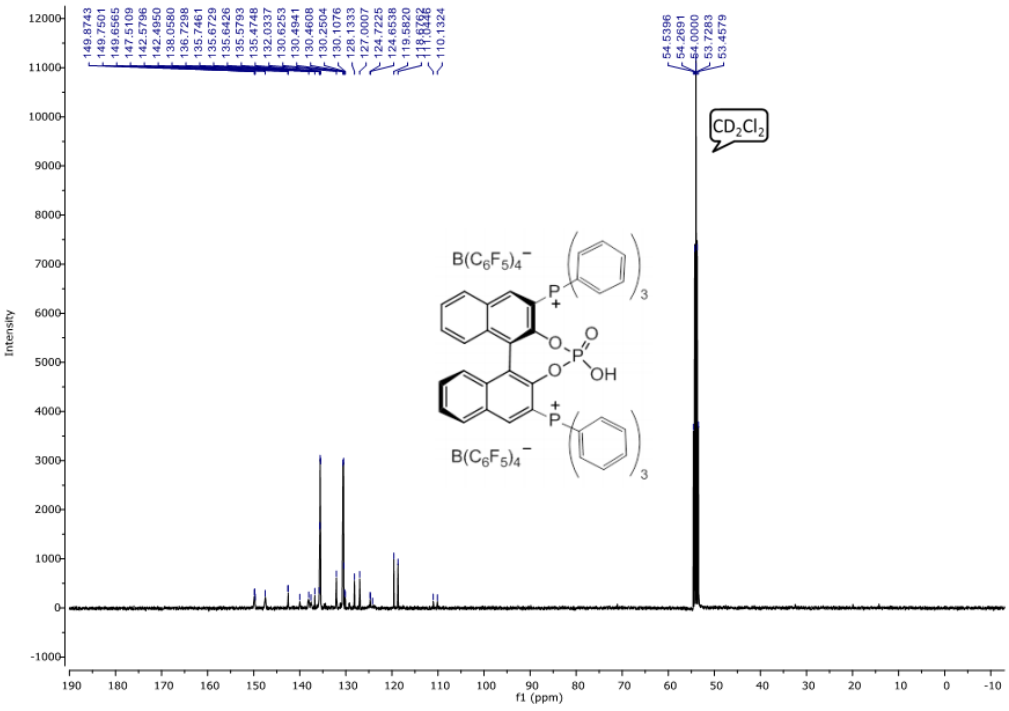

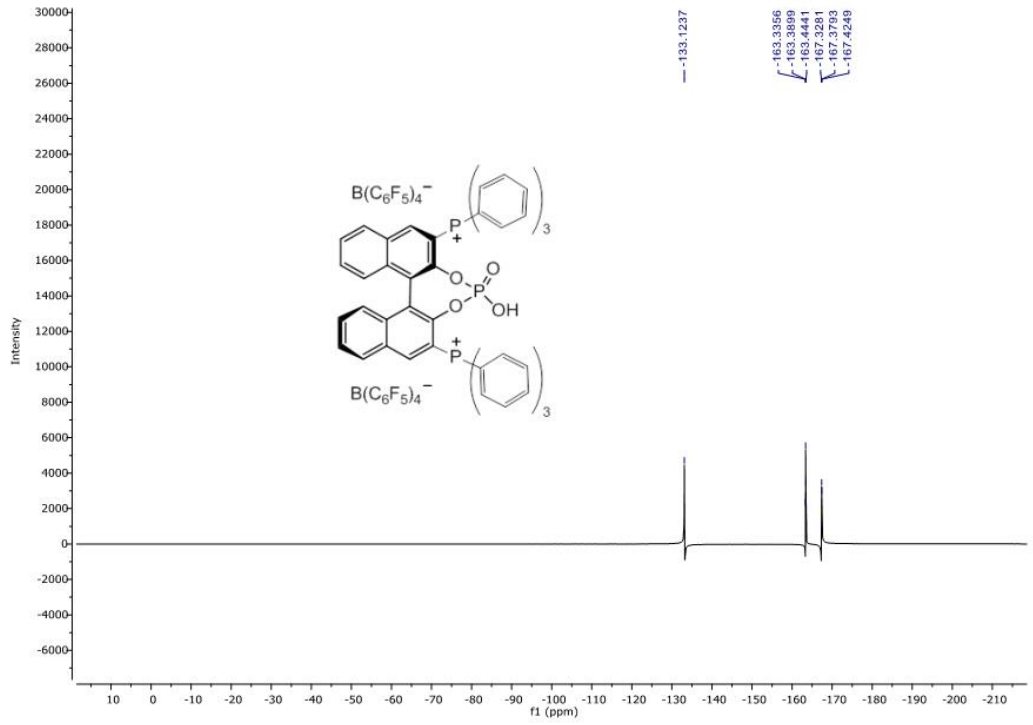
-133.1237
-163.3356
-163.3899
-163.4441
-167.3281
-167.3793
-167.4249
Intensity
f1 (ppm)
B(C6F5)4−
OH

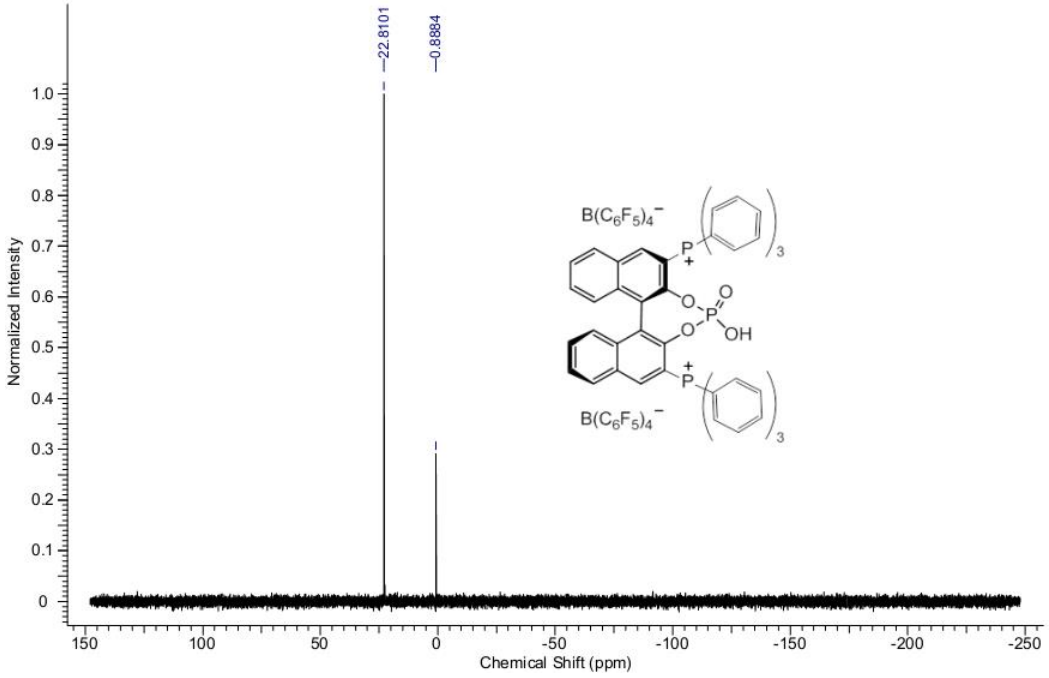
-22.8101
-0.8884
Normalized Intensity
Chemical Shift (ppm)
B(C6F5)4−
OH

Figure S14. ^{1}H and ^{13}C NMR of 3-(2-nitro-1-phenylethyl)-1H-indole (**6a**).

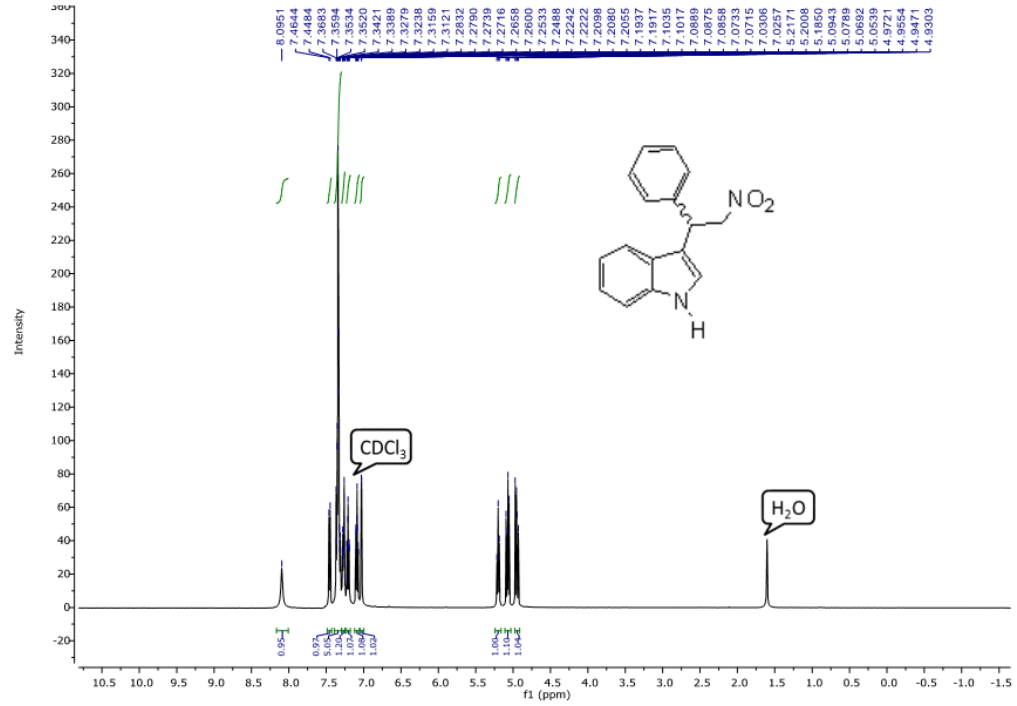

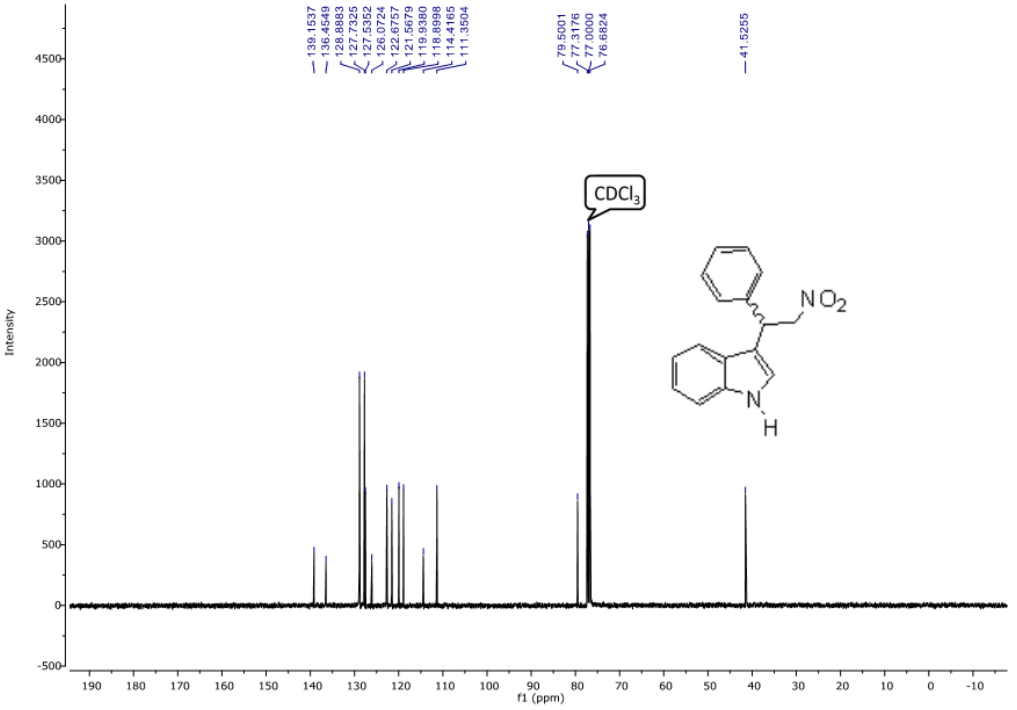

Figure S15. ^{1}H and ^{13}C NMR of 7-chloro-3-(2-nitro-1-phenylethyl)-1H-indole (**6e**).

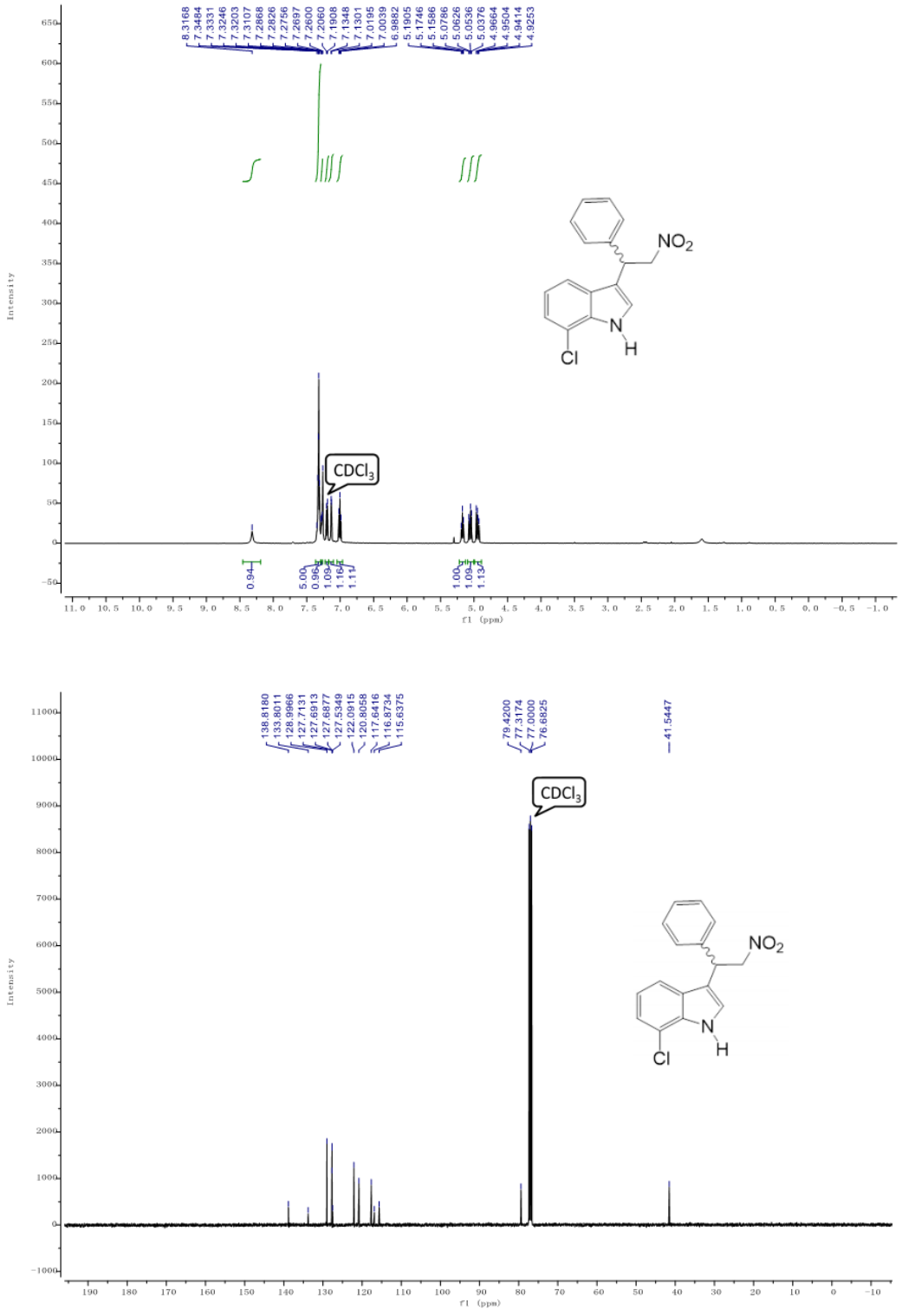

Figure S16. ^{1}H and ^{13}C NMR of 6-methoxy-3-(2-nitro-1-phenylethyl)-1H-indole (**6h**).

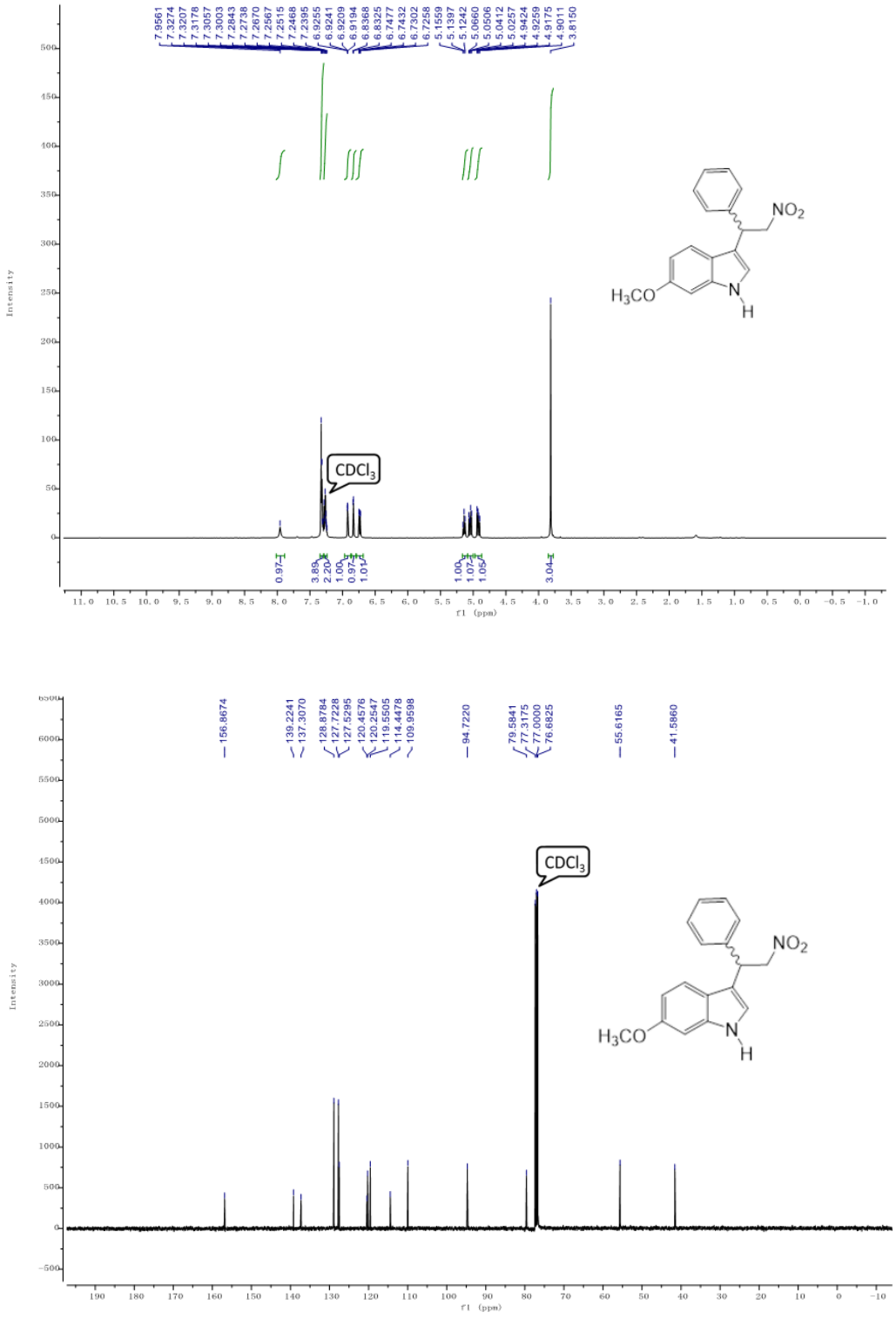

Figure S17. ^{1}H and ^{13}C NMR of 6-methyl-3-(2-nitro-1-phenylethyl)-1H-indole (**6i**).

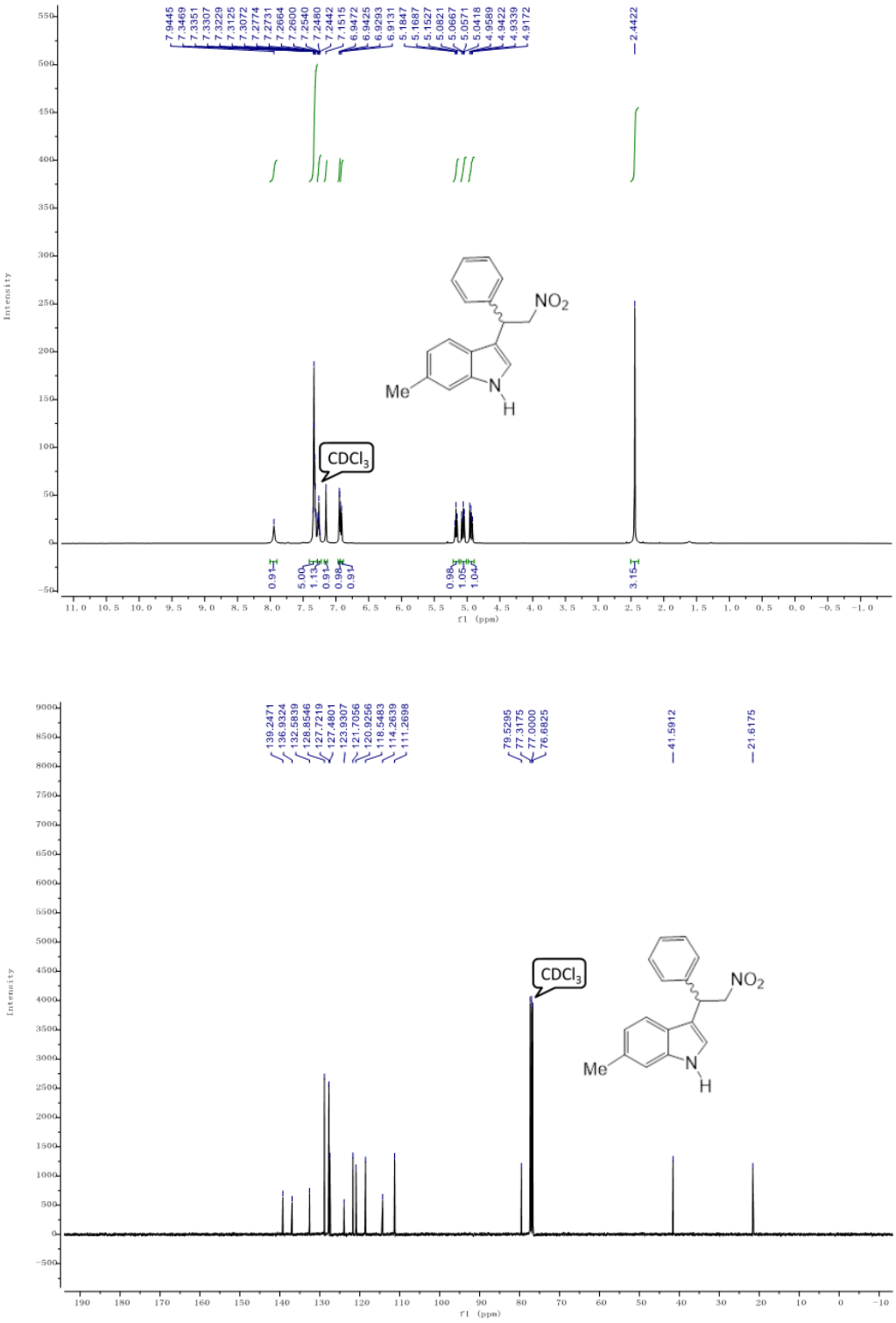

Figure S18. ^{1}H and ^{13}C NMR of 3-(2-nitro-1-phenylethyl)-1-methyl-indole (**6q**).

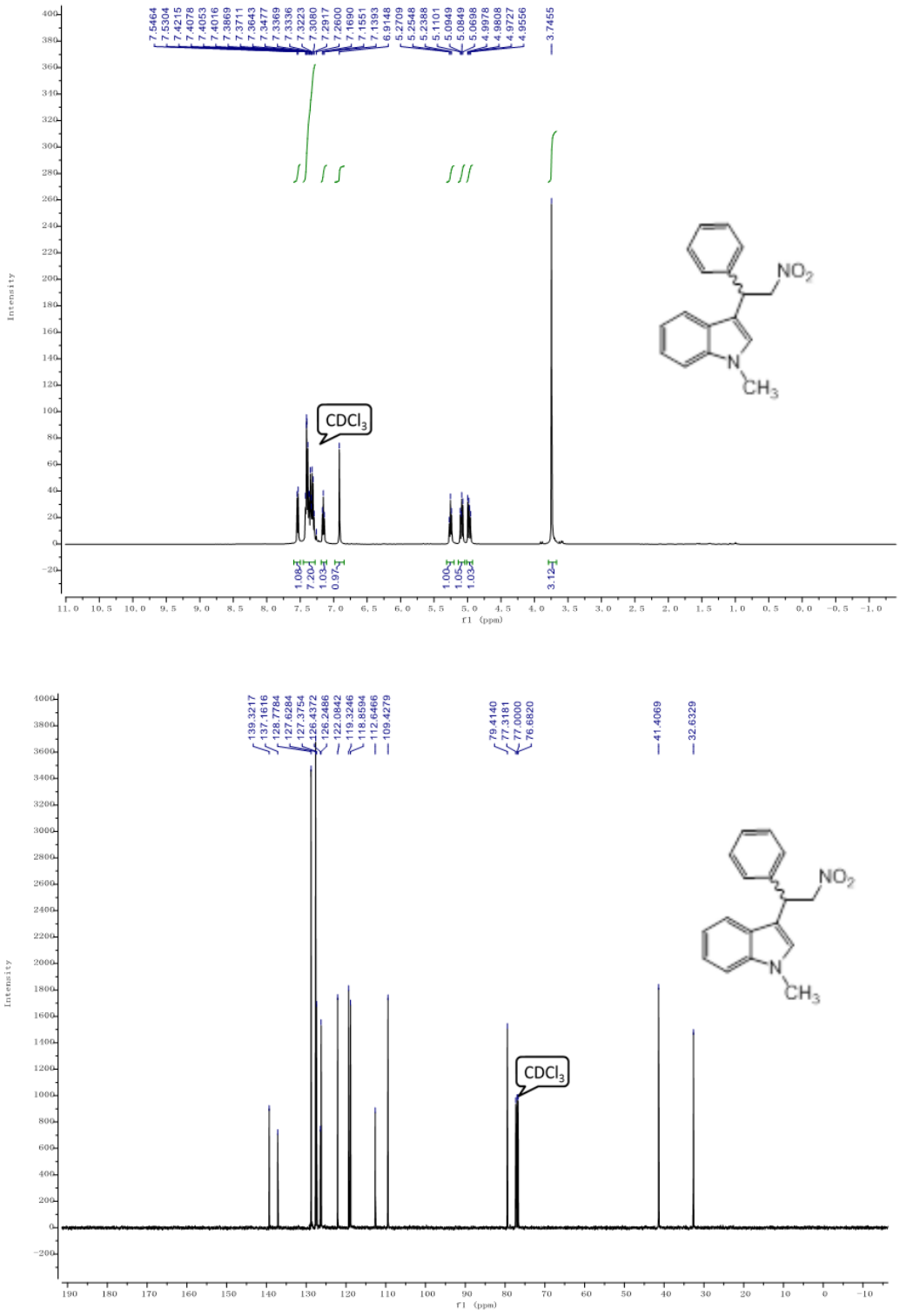

II. HPLC traces of the Friedel-Crafts products

3-(2-Nitro-1-phenylethyl)-1H-indole (6a)

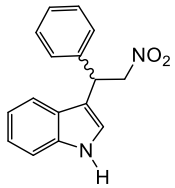

Racemic:

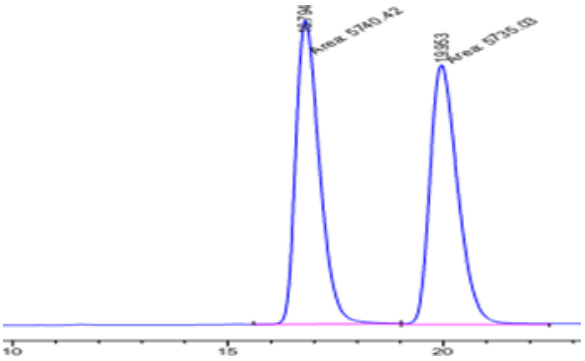

Peak #	RetTime [min]	Type	Width [min]	Area [mAU*s]	Height [mAU]	Area %
1	16.794	MM	0.6391	5740.41943	149.69276	50.0235
2	19.953	MM	0.7476	5735.03125	127.85993	49.9765
Totals :				1.14755e4	277.55270	

Enantiomeric enriched:

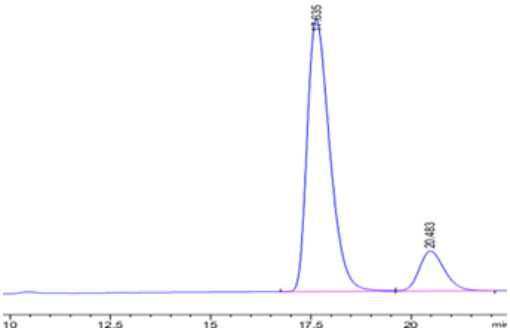

Peak #	RetTime [min]	Type	Width [min]	Area [mAU*s]	Height [mAU]	Area %
1	17.635	BV	0.6038	3517.77881	90.04215	85.8160
2	20.483	VV	0.6805	581.43268	13.23504	14.1840
Totals :				4099.21149	103.27719	

5-Fluoro-3-(2-nitro-1-phenylethyl)-1H-indole (6b)

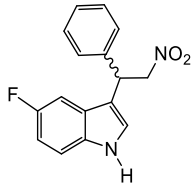

Racemic:

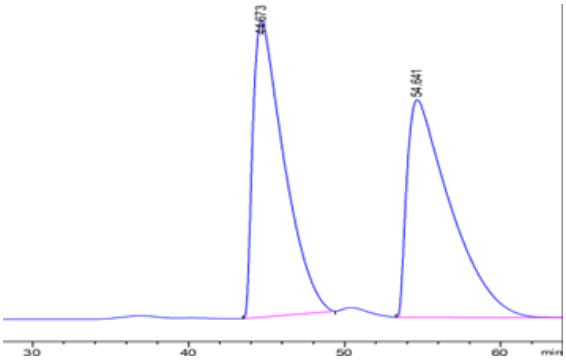

Peak #	RetTime [min]	Type	Width [min]	Area [mAU*s]	Height [mAU]	Area %
1	44.673	BB	1.9525	3.00181e4	216.11565	49.4346
2	54.641	BBA	2.6160	3.07047e4	158.50781	50.5654
Totals :				6.07228e4	374.62346	

Enantiomeric enriched:

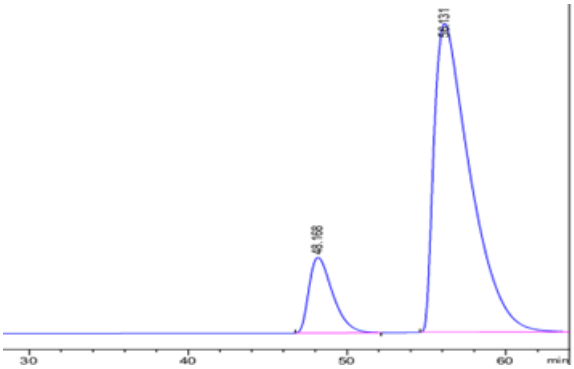

Peak #	RetTime [min]	Type	Width [min]	Area [mAU*s]	Height [mAU]	Area %
1	48.168	BB	1.3614	1481.70105	14.31721	13.8250
2	56.131	BBA	2.2083	9235.84375	58.48797	86.1750
Totals :				1.07175e4	72.80518	

5-Chloro-3-(2-nitro-1-phenylethyl)-1H-indole (6c)

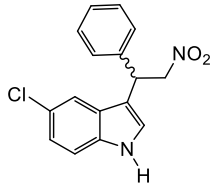

Racemic:

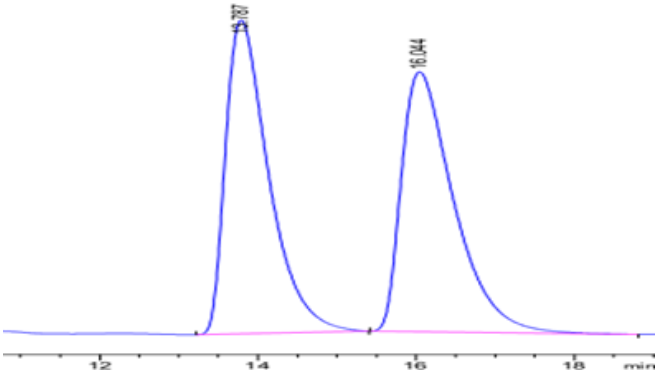

Peak #	RetTime [min]	Type	Width [min]	Area [mAU*s]	Height [mAU]	Area %
1	13.787	BB	0.5772	6596.67773	173.66838	49.9277
2	16.044	BBA	0.7001	6615.78711	143.96646	50.0723
Totals :				1.32125e4	317.63484	

Enantiomeric enriched:

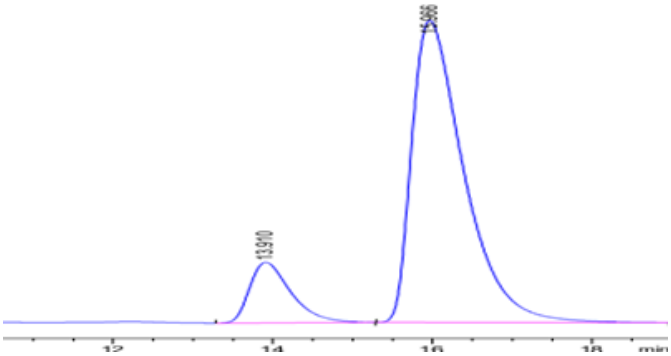

Peak #	RetTime [min]	Type	Width [min]	Area [mAU*s]	Height [mAU]	Area %
1	13.910	BB	0.5491	1051.39026	29.26641	13.6951
2	15.966	BBA	0.6915	6625.73730	145.99371	86.3049
Totals :				7677.12756	175.26012	

6-Chloro-3-(2-nitro-1-phenylethyl)-1H-indole (6d)

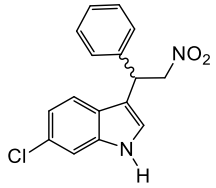

Racemic:

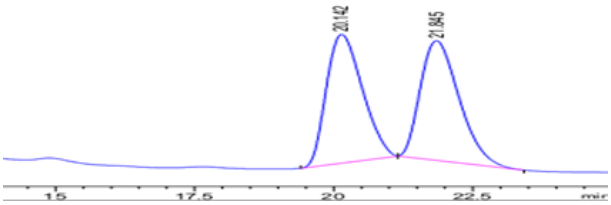

Peak #	RetTime [min]	Type	Width [min]	Area [mAU*s]	Height [mAU]	Area %
1	20.142	BB	0.6989	794.26648	17.65273	49.9351
2	21.845	BB	0.7527	796.33044	16.39360	50.0649
Totals :				1590.59692	34.04633	

Enantiomeric enriched:

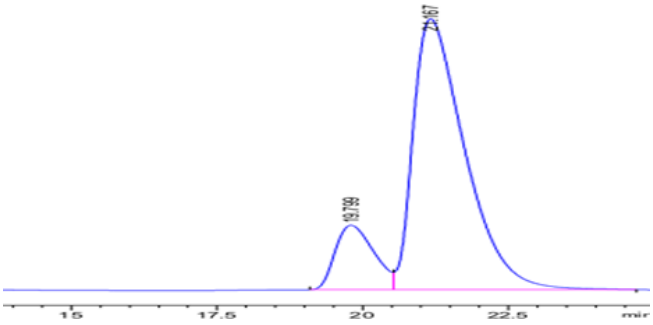

Peak #	RetTime [min]	Type	Width [min]	Area [mAU*s]	Height [mAU]	Area %
1	19.799	BV	0.7167	1551.34448	33.59811	15.0981
2	21.167	VBA	0.9381	8723.78125	141.34546	84.9019
Totals :				1.02751e4	174.94357	

7-Chloro-3-(2-nitro-1-phenylethyl)-1H-indole (6e)

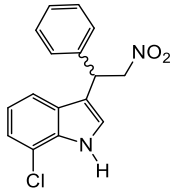

Racemic:

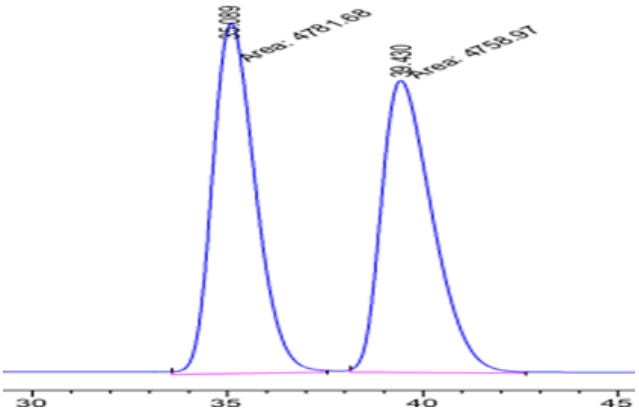

Peak #	RetTime [min]	Type	Width [min]	Area [mAU*s]	Height [mAU]	Area %
1	35.089	MM	1.2707	4781.68213	62.71548	50.1190
2	39.430	MM	1.5164	4758.97217	52.30559	49.8810
Totals :				9540.65430	115.02107	

Enantiomeric enriched:

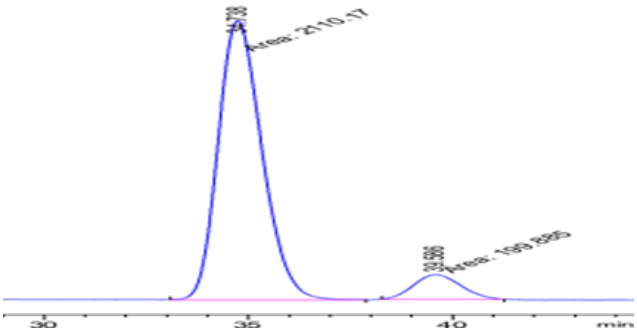

Peak #	RetTime [min]	Type	Width [min]	Area [mAU*s]	Height [mAU]	Area %
1	34.738	MM	1.2419	2110.16577	28.31836	91.3472
2	39.586	MM	1.3345	199.88469	2.49638	8.6528
Totals :				2310.05046	30.81474	

5-Bromo-3-(2-nitro-1-phenylethyl)-1H-indole (6f)

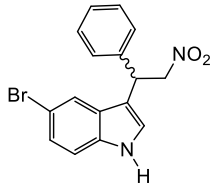

Racemic:

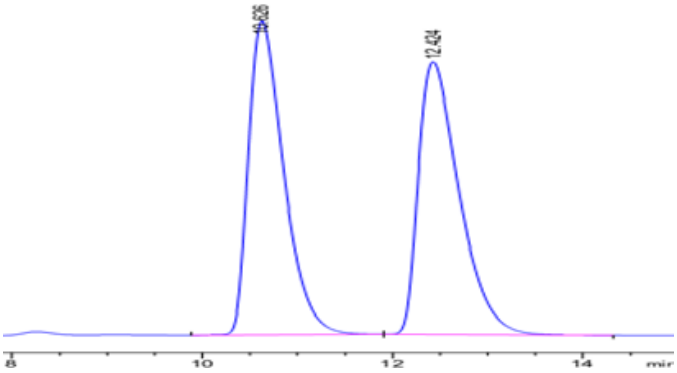

Peak #	RetTime [min]	Type	Width [min]	Area [mAU*s]	Height [mAU]	Area %
1	10.626	BB	0.3959	1.28737e4	500.73447	49.8426
2	12.424	BBA	0.4580	1.29550e4	434.32193	50.1574
Totals :				2.58287e4	935.05640	

Enantiomeric enriched:

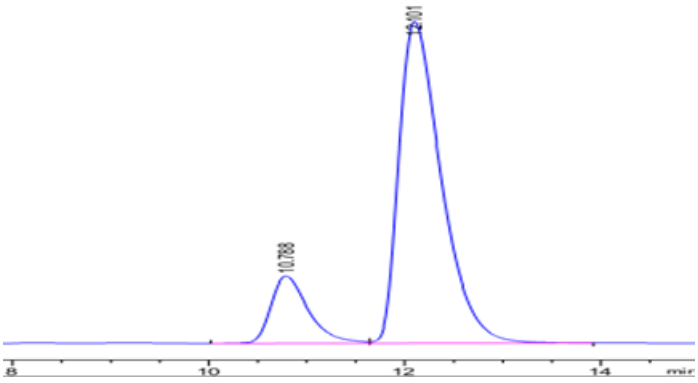

Peak #	RetTime [min]	Type	Width [min]	Area [mAU*s]	Height [mAU]	Area %
1	10.788	BV	0.4026	1473.39026	55.70464	15.5582
2	12.101	VB	0.4623	7996.78613	266.33301	84.4418
Totals :				9470.17639	322.03764	

5-Methoxy-3-(2-nitro-1-phenylethyl)-1H-indole (6g)

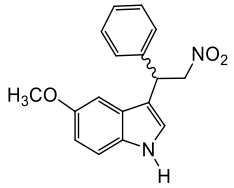

Racemic:

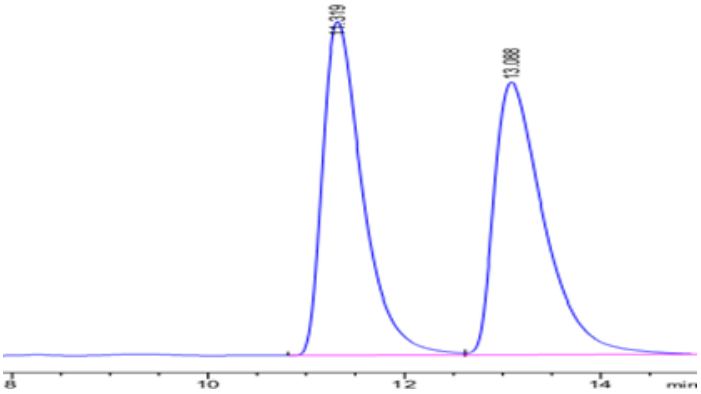

Peak #	RetTime [min]	Type	Width [min]	Area [mAU*s]	Height [mAU]	Area %
1	11.319	BV	0.4297	1.02455e4	362.52960	49.6582
2	13.088	VBA	0.5333	1.03865e4	296.08017	50.3418
Totals :				2.06320e4	658.60977	

Enantiomeric enriched:

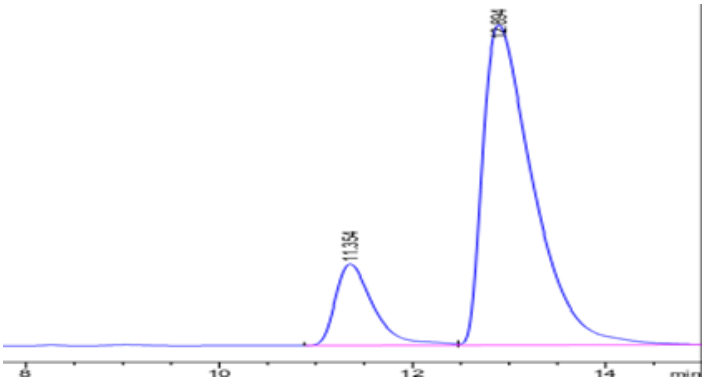

Peak #	RetTime [min]	Type	Width [min]	Area [mAU*s]	Height [mAU]	Area %
1	11.354	BV	0.4143	4092.59595	149.98643	16.1242
2	12.894	VBA	0.5447	2.12891e4	590.32178	83.8758
Totals :				2.53817e4	740.30821	

6-Methoxy-3-(2-nitro-1-phenylethyl)-1H-indole (6h)

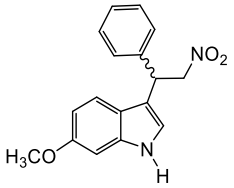

Racemic:

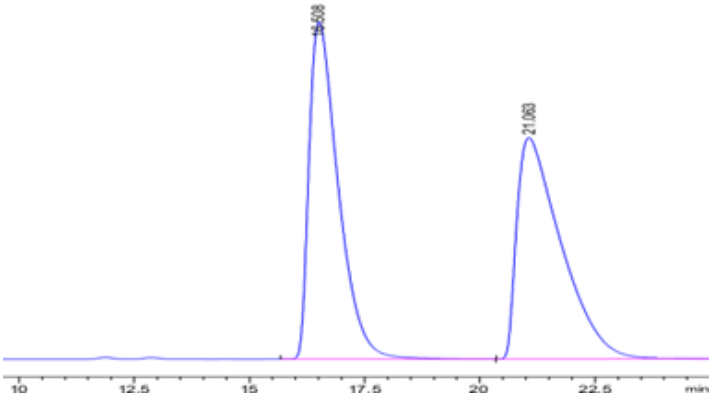

Peak #	RetTime [min]	Type	Width [min]	Area [mAU*s]	Height [mAU]	Area %
1	16.508	BB	0.6724	1.44372e4	327.44815	50.1153
2	21.063	BBA	0.9797	1.43708e4	215.02467	49.8847
Totals :				2.88080e4	542.47282	

Enantiomeric enriched:

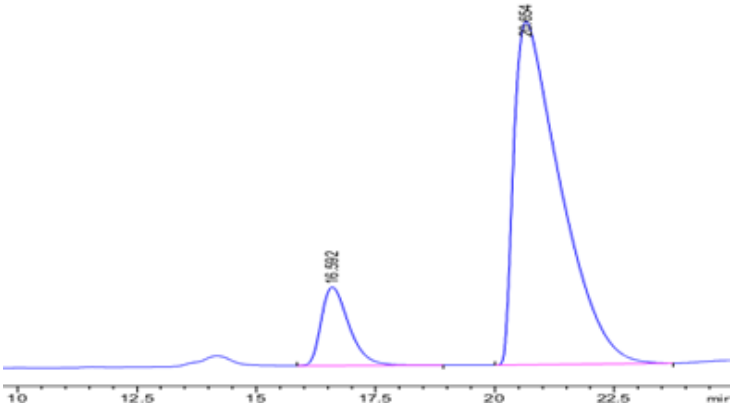

Peak #	RetTime [min]	Type	Width [min]	Area [mAU*s]	Height [mAU]	Area %
1	16.592	BB	0.6220	2421.99292	59.86405	12.0007
2	20.654	BB	1.0022	1.77602e4	261.56509	87.9993
Totals :				2.01821e4	321.42914	

6-Methyl-3-(2-nitro-1-phenylethyl)-1H-indole (6i)

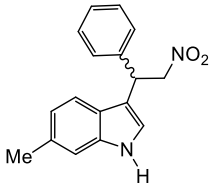

Racemic:

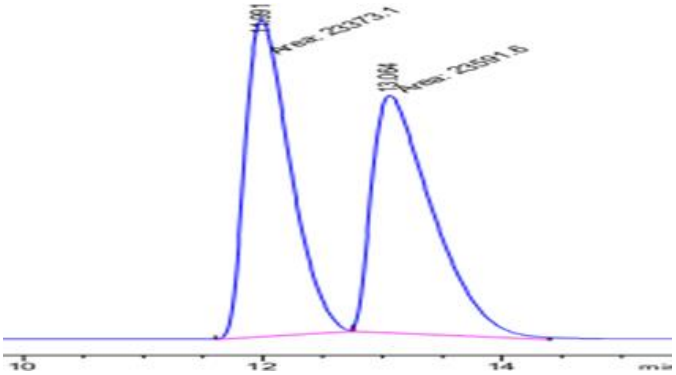

Peak #	RetTime [min]	Type	Width [min]	Area [mAU*s]	Height [mAU]	Area %
1	11.991	MM	0.4358	2.33731e4	893.88239	49.7673
2	13.064	MM	0.5879	2.35916e4	668.75677	50.2327
Totals :				4.69647e4	1562.63916	

Enantiomeric enriched:

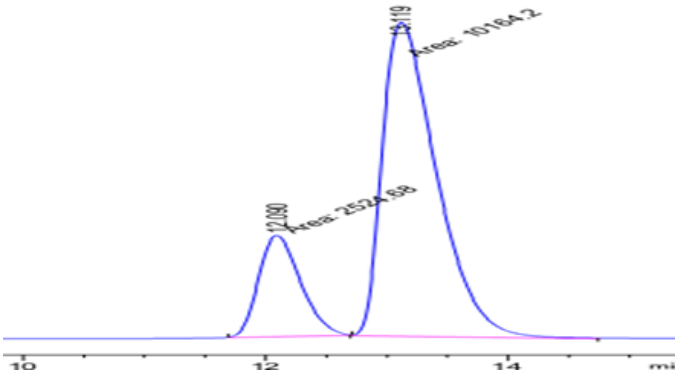

Peak #	RetTime [min]	Type	Width [min]	Area [mAU*s]	Height [mAU]	Area %
1	12.090	MM	0.3997	2524.68433	105.28066	19.8968
2	13.119	MM	0.5183	1.01642e4	326.82126	80.1032
Totals :				1.26889e4	432.10192	

7-Methyl-3-(2-nitro-1-phenylethyl)-1H-indole (6j)

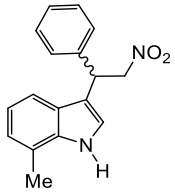

Racemic:

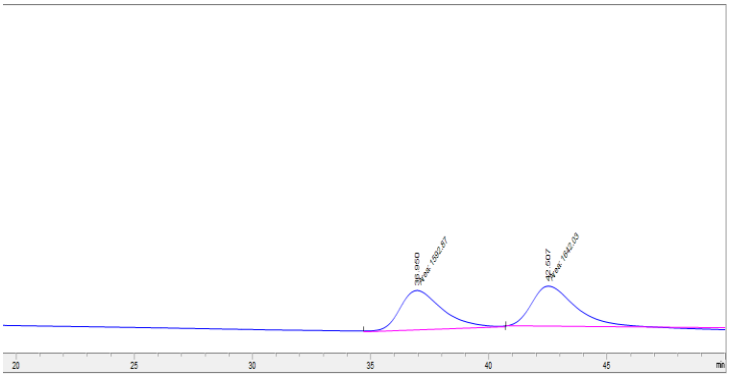

Peak #	RetTime [min]	Type	Width [min]	Area [mAU*s]	Height [mAU]	Area %
1	36.950	MM	2.1401	1592.86719	12.40487	49.2402
2	42.507	MM	2.1926	1642.02771	12.48133	50.7598
Totals :				3234.89490	24.88620	

Enantiomeric enriched:

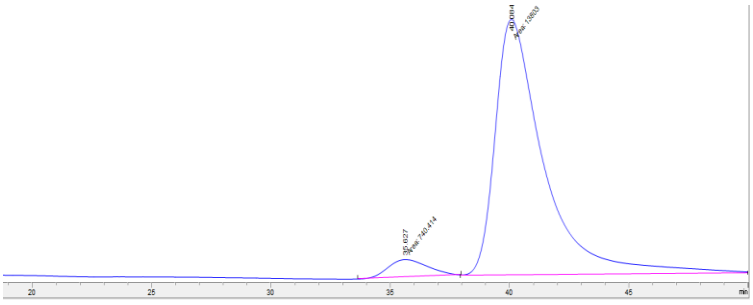

Peak #	RetTime [min]	Type	Width [min]	Area [mAU*s]	Height [mAU]	Area %
1	35.627	MM	1.8958	740.41412	6.50923	5.0910
2	40.084	MM	2.3894	1.38030e4	96.27863	94.9090
Totals :				1.45435e4	102.78786	

7-Ethyl-3-(2-nitro-1-phenylethyl)-1H-indole (6k)

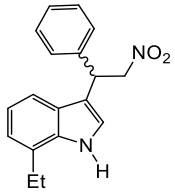

Racemic:

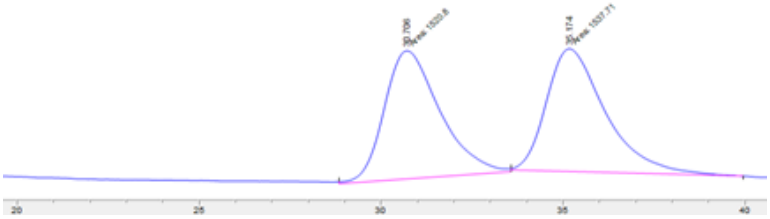

Peak #	RetTime [min]	Type	Width [min]	Area [mAU*s]	Height [mAU]	Area %
1	30.706	MM	1.7810	1520.80310	14.23208	49.7235
2	35.174	MM	1.8845	1537.71484	13.59965	50.2765
Totals :				3058.51794	27.83173	

Enantiomeric enriched:

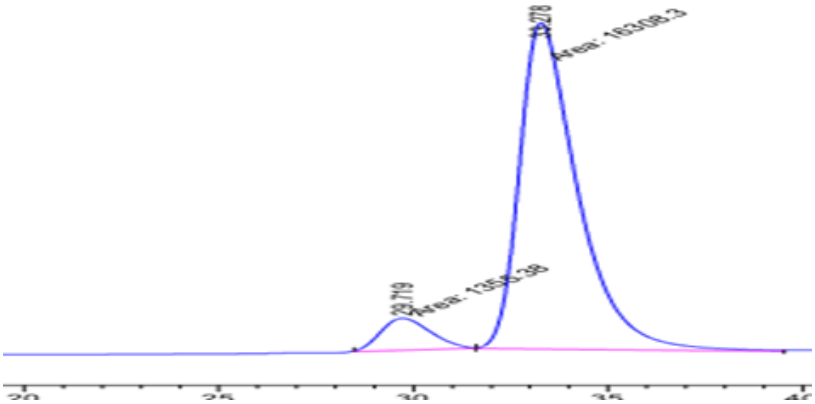

Peak #	RetTime [min]	Type	Width [min]	Area [mAU*s]	Height [mAU]	Area %
1	29.719	MM	1.4697	1355.37805	15.37000	7.6733
2	33.278	MM	1.7337	1.63083e4	156.77618	92.3267
Totals :				1.76637e4	172.14618	

3-(1-(4-Fluorophenyl)-2-nitroethyl)-1H-indole (6l)

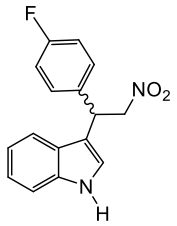

Racemic:

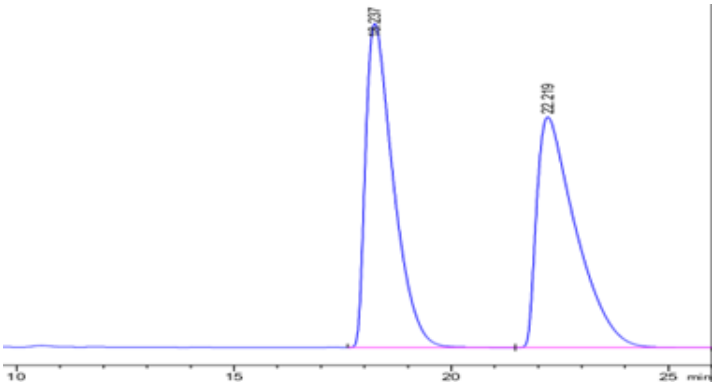

Peak #	RetTime [min]	Type	Width [min]	Area [mAU*s]	Height [mAU]	Area %
1	18.237	BB	0.6689	3.03319e4	684.65778	49.9868
2	22.219	BBA	0.9194	3.03479e4	486.75705	50.0132
Totals :				6.06799e4	1171.41483	

Enantiomeric enriched:

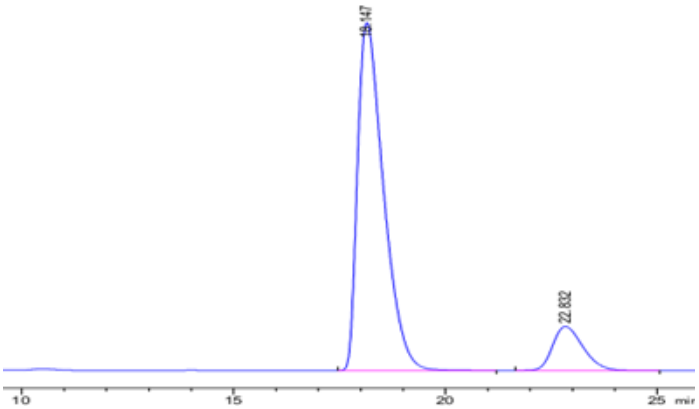

Peak #	RetTime [min]	Type	Width [min]	Area [mAU*s]	Height [mAU]	Area %
1	18.147	BB	0.6503	1.45942e4	343.05911	87.1750
2	22.832	BB	0.7604	2147.06738	43.30700	12.8250
Totals :				1.67412e4	386.36611	

3-(1-(2-Chlorophenyl)-2-nitroethyl)-1H-indole (6m)

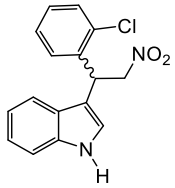

Racemic:

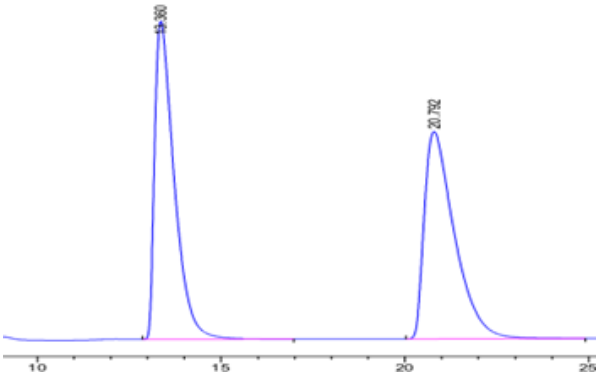

Peak #	RetTime [min]	Type	Width [min]	Area [mAU*s]	Height [mAU]	Area %
1	13.360	BB	0.5555	1.30414e4	352.60681	49.9645
2	20.792	BB	0.8559	1.30599e4	229.49115	50.0355
Totals :				2.61012e4	582.09796	

Enantiomeric enriched:

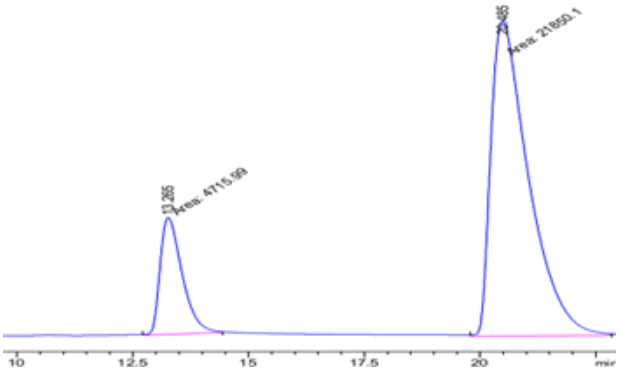

Peak #	RetTime [min]	Type	Width [min]	Area [mAU*s]	Height [mAU]	Area %
1	13.265	MM	0.5503	4715.99219	142.84187	17.7519
2	20.485	MM	0.9454	2.18501e4	385.20233	82.2481
Totals :				2.65661e4	528.04420	

3-(1-(3-Bromophenyl)-2-nitroethyl)-1H-indole (6n)

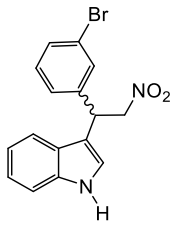

Racemic:

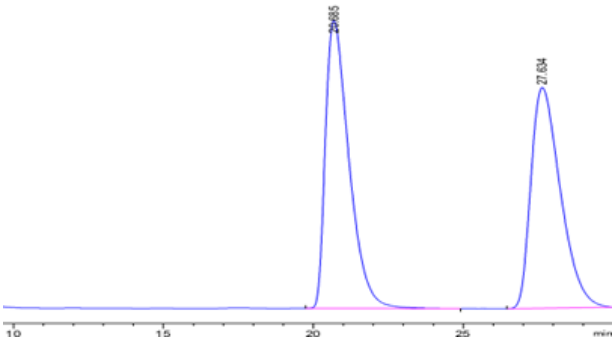

Peak #	RetTime [min]	Type	Width [min]	Area [mAU*s]	Height [mAU]	Area %
1	20.685	BB	0.8391	8882.18262	162.14198	51.1004
2	27.634	BBA	1.0520	8499.63965	124.26053	48.8996
Totals :				1.73818e4	286.40251	

Enantiomeric enriched:

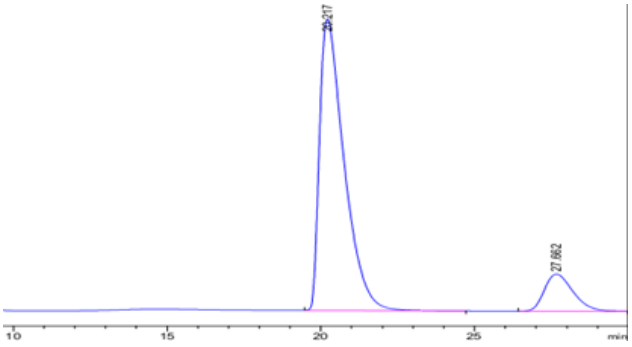

Peak #	RetTime [min]	Type	Width [min]	Area [mAU*s]	Height [mAU]	Area %
1	20.217	BB	0.8339	2.22075e4	401.14774	87.1050
2	27.662	BBA	0.9809	3287.58765	50.94094	12.8950
Totals :				2.54951e4	452.08867	

3-(1-(4-Bromophenyl)-2-nitroethyl)-1H-indole (6o)

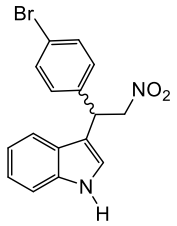

Racemic:

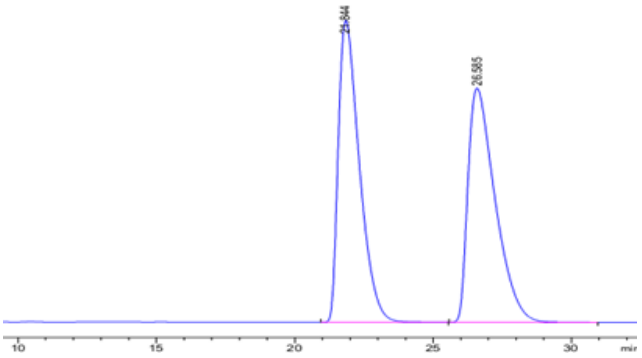

Peak #	RetTime [min]	Type	Width [min]	Area [mAU*s]	Height [mAU]	Area %
1	21.844	BB	0.8113	2.23793e4	422.94650	49.9922
2	26.585	BB	1.0319	2.23862e4	328.16092	50.0078
Totals :				4.47655e4	751.10742	

Enantiomeric enriched:

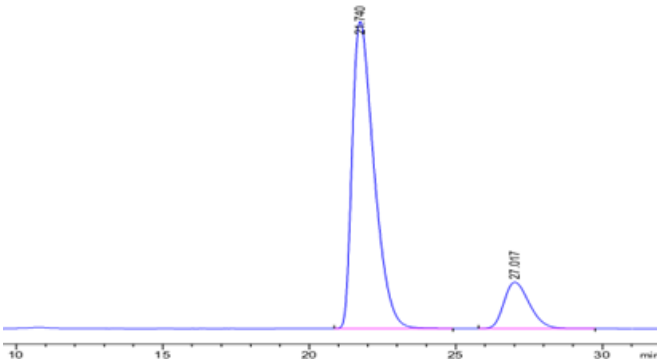

Peak #	RetTime [min]	Type	Width [min]	Area [mAU*s]	Height [mAU]	Area %
1	21.740	BB	0.7916	1.64783e4	319.57516	85.0549
2	27.017	BB	0.9228	2895.42627	48.20235	14.9451
Totals :				1.93737e4	367.77752	

3-(1-(4-Methoxylphenyl)-2-nitroethyl)-1H-indole (6p)

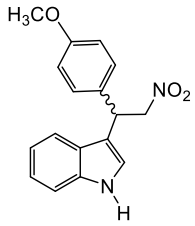

Racemic:

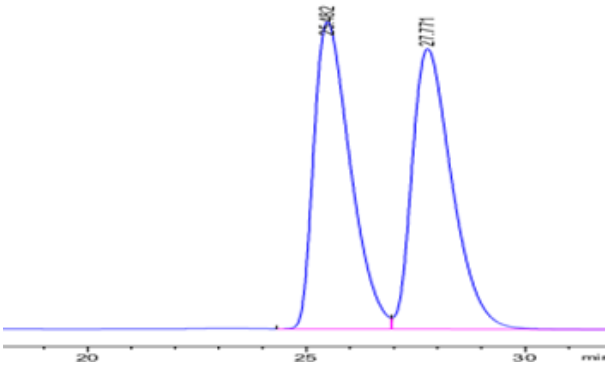

Peak #	RetTime [min]	Type	Width [min]	Area [mAU*s]	Height [mAU]	Area %
1	25.482	BV	0.8899	1.38104e4	238.37424	50.0270
2	27.771	VBA	0.9721	1.37955e4	217.46091	49.9730
Totals :				2.76060e4	455.83514	

Enantiomeric enriched:

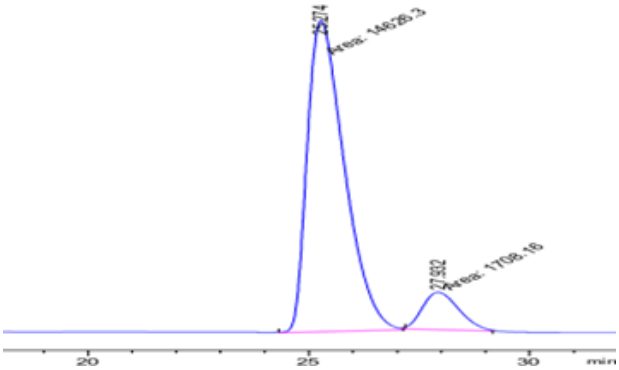

Peak #	RetTime [min]	Type	Width [min]	Area [mAU*s]	Height [mAU]	Area %
1	25.274	MM	0.9768	1.46263e4	249.56046	89.5426
2	27.932	MM	0.9509	1708.15735	29.93939	10.4574
Totals :				1.63344e4	279.49985	

3-(2-Nitro-1-phenylethyl)-1-methyl-indole (6q)

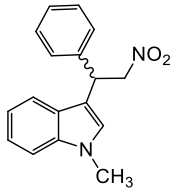

Racemic:

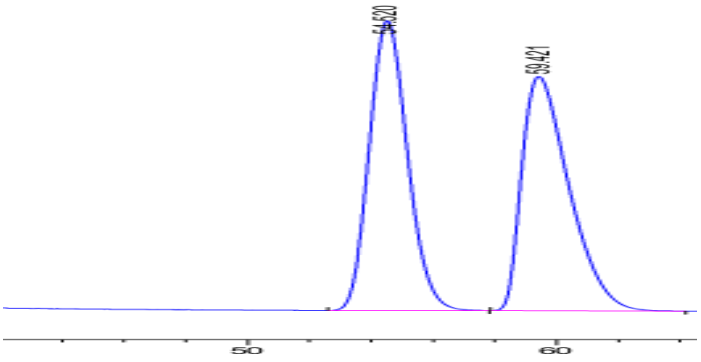

Peak #	RetTime [min]	Type	Width [min]	Area [mAU*s]	Height [mAU]	Area %
1	54.520	BB	1.3420	2792.53711	32.51315	50.0076
2	59.421	BB	1.6239	2791.69263	26.26804	49.9924
Totals :				5584.22974	58.78119	

Enantiomeric enriched:

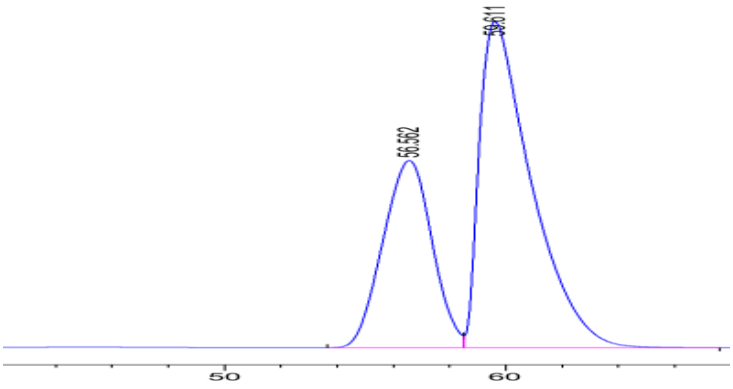

Peak #	RetTime [min]	Type	Width [min]	Area [mAU*s]	Height [mAU]	Area %
1	56.562	BV	1.9205	8487.16895	69.90237	35.1412
2	59.611	VB	1.8653	1.56645e4	121.72903	64.8588
Totals :				2.41516e4	191.63141	